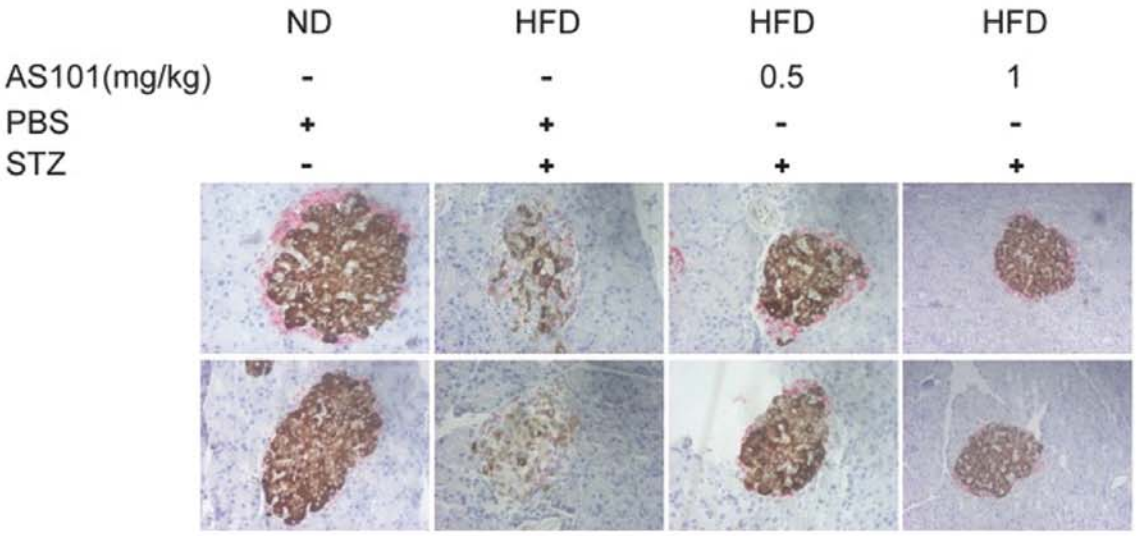

Special Collection on Diabetes

AS101 preserves insulin production in the pancreas, see Halperin-Sheinfeld et al. - "The Tellurium compound, AS101, increases SIRT1 level and activity and prevents type 2 diabetes."

Diabetes | AGING

Editorial and Publishing Office Aging (Albany NY)
6666 E. Quaker Str., Suite 1B
Orchard Park, NY 14127
Phone: 1-800-922-0957, option 1
Fax: 1-716-508-8254
e-Fax: 1-716-608-1380

Submission
Please submit your manuscript on-line at http://aging.msubmit.net

Editorial
For editorial inquiries, please call us or email editors@impactaging.com

Production
For questions related to preparation of your article for publication, please call us or email krasnova@impactaging.com

Indexing
If you have questions about the indexing status of your paper, please email kurenova@impactaging.com

Printing
Each issue or paper can be printed on demand. To make a printing request, please call us or email krasnova@impactaging.com.

Billing/Payments
If you have questions about billing/invoicing or would like to make a payment, please call us or email payment@impactaging.com

Publisher's Office
Aging is published by Impact Journals, LLC
To contact the Publisher's Office, please email: publisher@impactjournals.com, visit www.impactjournals.com, or call 1-800-922-0957, option 5

AGING

EDITORIAL BOARD

Table of Contents

Research Paper

Individualizing treatment targets for elderly patients with type 2 diabetes: factors influencing clinical decision making in the 24-week, randomized INTERVAL study

W. David Strain[1], Abhijit S. Agarwal[2], Päivi M. Paldánius[3]

[1] Diabetes and Vascular Research Centre, University of Exeter Medical School, Exeter EX2 5AX, UK
[2] Novartis Pharmaceuticals Corporation, East Hanover, NJ 07936-1080, USA
[3] Novartis Pharma AG, Postfach, CH-4002 Basel, Switzerland

Correspondence to: W. David Strain; **email:** d.strain@exeter.ac.uk doi:10.18632/aging.101188
Keywords: elderly, individualization, predictors, type 2 diabetes

Received: November 8, 2016 **Accepted:** February 19, 2017 **Published:** March 5, 2017

ABSTRACT

We tested the feasibility of setting individualized glycemic goals and factors influencing targets set in a clinical trial in elderly patients with type 2 diabetes.

A 24-week, randomized, double-blind, placebo-controlled study was conducted in 45 outpatient centers in seven European countries. 278 drug-naïve or inadequately controlled (mean HbA1c 7.9%) patients with type 2 diabetes aged ≥70 years with HbA1c levels ≥7.0% and ≤10.0% were enrolled. Investigator-defined individualized HbA1c targets and the impact of baseline characteristics on individualized treatment targets was evaluated.

The average individualized HbA1c target was set at 7.0%. HbA1c at baseline predicted a target setting such that higher the HbA1c, more aggressive was the target (P<0.001). Men were more likely to be set aggressive targets than women (P=0.026). Frailty status of patients showed a trend towards significance (P=0.068), whereas diabetes duration, age, or polypharmacy did not. There was heterogeneity between countries regarding how baseline factors were viewed.

Despite training and guidance to individualize HbA1c goals, targets were still set in line with conventional values. A strong influence of country-specific guidelines on target setting was observed; confirming the importance of further education to implement new international guidelines in older adults.

INTRODUCTION

Type 2 diabetes is one of the most common chronic diseases in older populations, affecting ~ 20.0% of individuals with age >75 years [1, 2]. A considerable proportion of these older individuals have multiple comorbidities due in part to their longevity [3, 4]. Older individuals with diabetes have significantly increased risk of microvascular and macrovascular disease, cognitive dysfunction, functional impairment, depression, and vision and hearing impairment compared with younger adults [5, 6]. Further, the high prevalence of polypharmacy in elderly patients exposes them to a greater risk of complications and adverse reactions to any new pharmaceutical intervention [6]. However, frailty and multiple comorbidities have led to the exclusion of elderly patients from a majority of clinical trials of glycemic therapeutics until recently [6–9]. The recent global guidelines for the treatment of elderly patients have emphasized on the need of a holistic and individualized approach to patient management and setting appropriate targets for this population [2, 6–10]. However, there is no evidence to date that setting these individualized targets is even feasible, let alone assessing whether they can be achieved or improve outcomes [5, 6, 9, 10].

The INdividualized Treatment targets for ElderRly patients with type 2 diabetes using Vildagliptin Add-on or Lone therapy (INTERVAL) study was the first, and

to date the only, clinical study that pragmatically assessed the feasibility of setting and achieving investigator-defined individualized treatment targets in elderly patients with type 2 diabetes [11]. Despite the guidance to set individualized targets based on patients' comorbidities and baseline characteristics and the training provided to facilitate this endeavor, the mean individualized HbA1c target set was 7.0%, identical to the contemporaneous conventional guidelines.

Current guidelines advocate individualizing goals, yet our investigators, with a particular interest in diabetes in older adults and despite specific training in establishing these targets, deviated only marginally from conventional targets. To understand the factors that may hinder the application of global guidelines to individualize goals, we now review the targets set by these trained investigators, the determinants of those targets and the factors impacting HbA1c reduction.

RESULTS

The study enrolled 278 patients in total. Patients' demographic characteristics have been presented in detail elsewhere [11]. In brief, 152 (54.7%) patients were female, 124 (44.6%) patients were aged ≥75 years and 26 (9.4%) patients reached the stringent criteria for frail (although physicians regarded more of their patients as frail according to general clinical judgement). The mean (standard deviation) age was 74.8 (4.17) years (range, 70–97 years) and body mass index 29.8 (4.34) kg/m^2. The mean (standard deviation; range) HbA1c was 7.9% (0.72; 6.6% to 10.3%), with 173 (62.2%) patients with HbA1c levels of ≤8.0%, despite a mean (standard deviation; range) duration of diabetes of 11.4 years (7.47; 0.3 to 35.0 years). The patients were taking an average of six (range, 1–15) different medications, with a substantially higher tablet burden, before randomization to study drug or placebo.

A summary of the individualized HbA1c targets set by the investigators by countries is provided in Figure 1. The mean overall HbA1c target reduction was −0.9% (range, −4.4% to −0.1%). In patients with HbA1c up to 8.0%, the mean individualized target reduction was less stringent, −0.7% (range, −2.4% to −0.1%), whereas in patients with HbA1c >8.0% the mean individual target reduction was −1.2% (range, −4.4% to −0.2%).

The impact of baseline characteristics on target setting, overall and by country, is summarized in Figure 2a. In the overall study, screening HbA1c was positively associated with the target reduction such that for every 1% increase in the baseline HbA1c, the target reduction

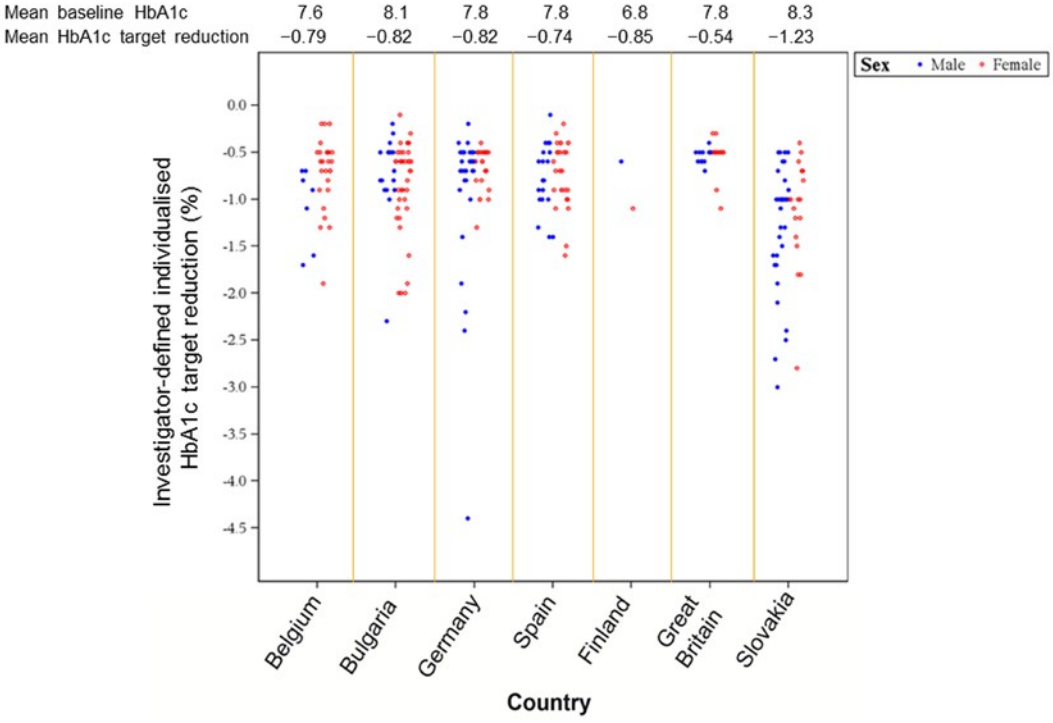

Figure 1. Summary of individualized HbA1c targets set by investigators (by country).

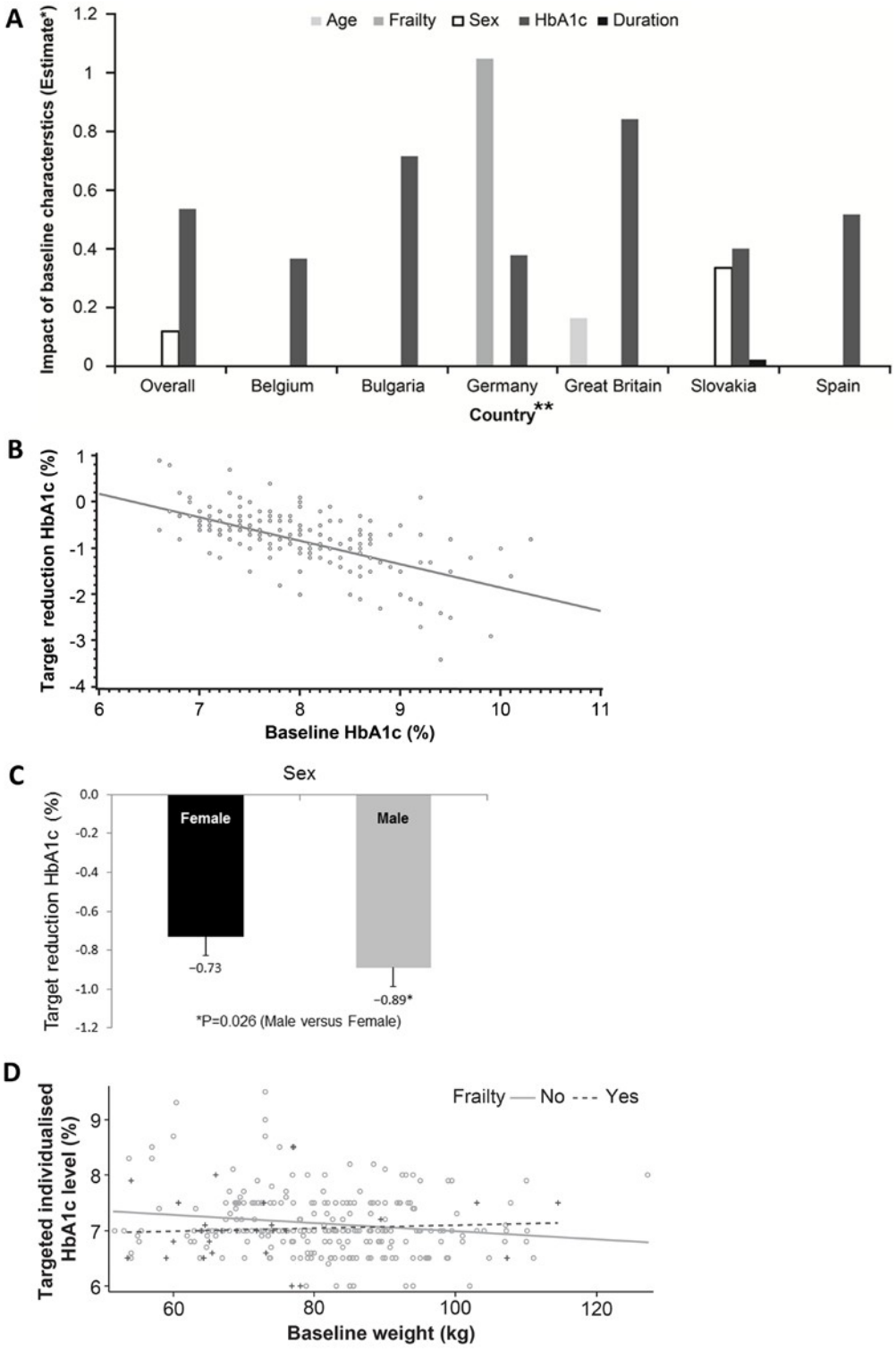

Figure 2. **(A)** Baseline factors affecting target setting (overall and by country). *For categorical covariates, the estimate is the difference between the adjusted means of comparison-reference in the corresponding category. For continuous covariates, the estimate is the change in adjusted means per unit. **Patients from Finland were identified by a single investigator. The figure estimates the difference between adjusted means for different factors potentially driving the individualized target setting and thus no reliable statistics for such a low sample size (n=2) could be generated. Hence, Finland has been removed. **(B)** Baseline HbA1c versus target reduction HbA1c. **(C)** Sex status versus target reduction HbA1c. **(D)** Baseline weight versus targeted individualized HbA1c by frailty status.

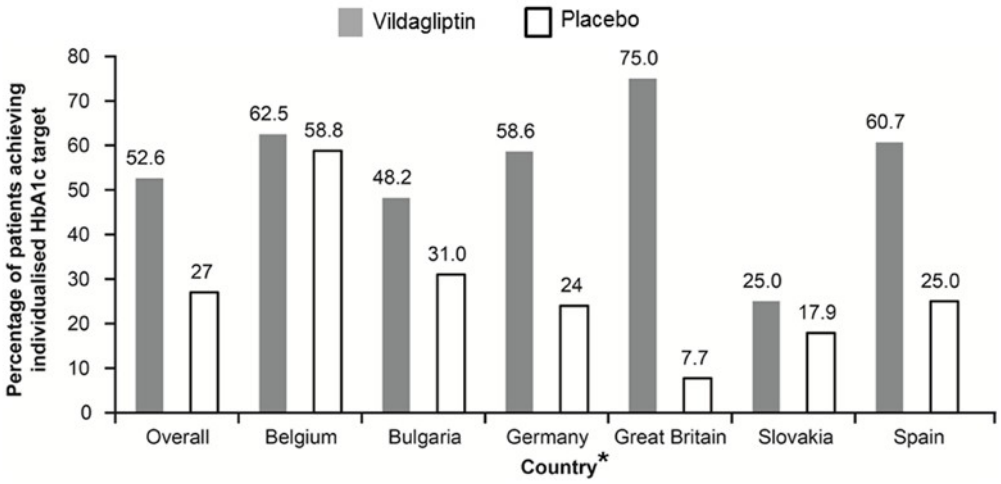

Figure 3. Summary of individualized HbA1c target response (overall and by country). *Patients from Finland were identified by a single investigator. The figure estimates the difference between adjusted means for different factors potentially driving the individualized target setting and thus no reliable statistics for such a low sample size (n=2) could be generated. Hence, Finland has been removed.

was increased by −0.5% (Pearson's correlation −0.6353; P<0.001; Figure 2b). Men were set more aggressive targets than women (P=0.026; Figure 2c), whereas the frailty status only demonstrated a trend towards significance (P=0.068). In non-frail patients, the baseline weight was a predictor of a less aggressive glycemic target setting (P=0.012) such that more obese patients were set more aggressive targets, while in frail patients, a lower body weight did not additionally impact the glycemic target (P=0.725; Figure 2d). Interestingly and unexpectedly, neither age (P=0.510) nor the duration of diabetes (P=0.760) had an impact on the targets set. Hematological and biochemical parameters also did not seem to predict the target established. Physicians did not seem to consider the degree of polypharmacy when setting targets (P=0.301); the addition of the number of concomitant prescriptions and other medications to the analysis model did not significantly alter any of the associations.

When exploring determinants at the country level, screening HbA1c was the only universal factor affecting target setting (P<0.001). Sex was a significant factor in Slovakia (P=0.025) and showed a trend in Germany (P=0.057), similar to the overall study. The frailty status was a significant factor only in Germany (P=0.002), while it also showed a trend in Belgium (P=0.085). Age was a significant factor only in Great Britain (P=0.025), whereas duration of diabetes was a significant factor only in Slovakia (P=0.018).

As previously reported, the adjusted odds ratio of achieving the individualized target in the overall study population was 3.16 (P<0.001) with study drug, vildagliptin, compared to placebo [11]. This was on a background of 37 (27%) participants achieving their target on placebo alone. Great Britain had the highest odds ratio (59.22; 95% confidence interval 3.00 to 1168.96; P=0.007) driven predominantly by the low percentage of patients in the placebo group achieving their individualized targets (7.7%). Belgium, on the other hand, with the highest percentage of patients achieving targets with placebo alone (58.8%), had the least relative benefit by introduction of medication (odds ratio 1.13; 95% confidence interval 0.28 to 4.63; P=0.862) (Figure 3).

DISCUSSION

Although global guidelines for the management of type 2 diabetes advocate individualization of target setting, to date, the INTERVAL study is the first and only clinical study to explore the feasibility of setting such targets, let alone the evaluation of achieving these in a clinical setting. Despite extensive training and guidance to regard local guidelines as a secondary consideration, in our study, physicians maintained the traditional goal of 7.0% for this elderly and frail cohort. Further, this study is the first to explore the independent determinants of the targets that were set and, thereby, determine the specific areas of education that may be required to facilitate more appropriate target setting for elderly adults with type 2 diabetes. Guidelines published by the European Diabetes Working Party for Older People (aged ≥70 years) [9], the Consensus Development Conference on Diabetes and Older Adults

(aged ≥65 years) convened by the American Diabetes Association [6], the Position Statement of the American Diabetes Association and the European Association for the Study of Diabetes [3] and, more recently, the International Diabetes Federation [2], all recommend an HbA1c target of 7.0% to 7.5% for elderly patients with type 2 diabetes without major comorbidities and 7.6% to 8.5% for frail, dependent patients with multiple comorbidities and high risk of hypoglycemia. These recommendations are based on opinions of the respective committees and experts rather than actual clinical evidence [12], indeed, the limited data used for formulating these recommendations were extrapolated from younger patients as most clinical trials exclude frail elderly patients with polypharmacy and multiple comorbidities [2, 6, 9]. Furthermore, these guidelines also suggest a patient-centered approach by providing the patient and caregiver structured education about the disease and treatment options and taking into account their individual medical, social, and cultural circumstances. Each patient should have the opportunity to make an informed decision regarding their treatment targets and therapeutic options including lifestyle modifications and pharmaceutical interventions [7, 8]. This is similar to the guidance and training provided to the investigators in the INTERVAL study, all of whom had special interest in diabetes in the elderly. Therefore, the conventional target of 7.0% that was set here was cause for concern and suggests that significant additional resources will be required to facilitate a change in clinical practice in a wider arena. We suggest that the introduction of guidelines alone may be insufficient to change attitudes and establish individualized care that these guidelines are hoping to achieve.

The physicians in one or more centers in some countries seemed to set rigid, particularly aggressive and uniform HbA1c targets even in these elderly patients with type 2 diabetes. The median and mean target reductions in these countries were similar for all patients suggesting that these aggressive targets were not a response to differing baseline characteristics such as comorbidities and duration of disease but a blanket adherence to more historic, aggressive HbA1c targets.

Unexpectedly, there was a paradoxical association between sex of the participant and individualized target set, with more aggressive targets being set for men compared with women, despite a higher attributable risk of hyperglycemia to the adverse consequences of diabetes in women than men [13–16]. One likely explanation for this finding may be that elderly women with diabetes were potentially perceived to be more prone to falls and fractures [3, 17], and investigators potentially wished to avoid hypoglycemia by setting less stringent targets. Alternatively, this finding could also be attributed to the incorrect assumption that older men have a higher risk of cardiovascular disease and, therefore, require more aggressive treatment [18, 19]. Either way significant education is required here.

The frailty status showed a tendency towards significance in the overall population, but that may be attributed in part to stringency of the modified Fried criteria that were used to define frailty in this study. The lack of association between age or duration of diabetes and targets set may represent the distinction that occurs in older adults compared with younger populations, where chronological age is discounted in preference of biological age. We had no way of capturing this subjective and, often, subconscious assessment by our investigators. However, given the overall aggressive targets that were set, this could represent the direct converse; physicians today disregard age when setting targets for fear of being accused of discriminating against people based on age [20]. This is a significant barrier to optimizing treatment for elderly adults.

Multiple co-morbidities and polypharmacy are other important factors in the management of older adults. Drug-drug interactions, increased risk of side effects particularly in patients with renal impairment, decreased adherence, less clinical benefit from otherwise appropriate medicines, and an increased risk of falling in older patients are all important considerations [6]. The study population was representative of the real world elderly patients with type 2 diabetes with the majority having multiple comorbidities and an average of six and up to 15 co-prescriptions pre-randomization, many with multiple daily dosing, further translating into a higher volume of tablets per person. Unpredictably, the number of medications did not impact individualized target setting in this study. This may be due to the perceived safety profile of the active agent, vildagliptin; however, it was disappointing that the implied multiple co-morbidities that accompany polypharmacy were not a consideration.

Nevertheless, choosing an optimal target is not always easy. Lack of consensus even among internationally acknowledged diabetes experts in weighing appropriateness of factors for setting glycemic targets for individual patients has led to exploration of usefulness of a survey-based algorithm for target setting [21]. The proposed algorithm suggests considering factors, such as life expectancy and risk of hypoglycemia, as main drivers of target setting while resource setting or disease duration *per se* are considered less important [21]. However, despite helpful tools, such as algorithms, assessment of

cognitive function or patient's adherence to therapy remain subjective, confirming that individualized target setting is still an art.

Findings from the Diabetes Prevention Program suggested that adults aged ≥60 years showed better efficacy from lifestyle interventions than younger patients with type 2 diabetes [22]. This could explain the results from the INTERVAL study in which all patients seemed to benefit from the opportunity to interact with their physicians while setting their individualized treatment targets as evidenced in particular by the high percentage of patients (27%) in the placebo arm who reached their individualized targets. However, the proportion of patients in the placebo group achieving their individualized targets varied remarkably across countries. This may be due to variation in the background education provided to older adults. Adequate advice regarding lifestyle, diet and exercise prior to their enrolment into the study would tend to attenuate the placebo effect. In other centers, where the perception may be that elderly adults may not benefit from such advice or a system does not support such education, enrolment into the study would tend to generate an exaggerated efficacy of the patient engagement. We do acknowledge the small sample size of patients from each country limits the application of these results as representative of the entire country; however, they do provide a unique glimpse of the challenges in the synchronization of global guidelines with local clinical practices.

The INTERVAL study introduced a unique endpoint of individualized glycemic treatment targets to guide the "real-life" approach for treatment of elderly patients with type 2 diabetes, and reflected the unmet clinical need to understand the importance of individualized target setting, particularly in a more fragile population. No studies on individualized treatment targets or assessments of tolerability of any individualized treatments have been reported prior to this study. The INTERVAL study was exploratory, and further work will be required to better understand the consequences of such individualization of glycemic targets and the determinants of the glycemic targets set.

In conclusion, INTERVAL was the first study to explore the feasibility of setting individualized targets when managing diabetes in the growing elderly population. In our population of trained and motivated investigators, individualized treatment targets were disappointingly aligned with conventional guideline targets. Therefore, we suggest significant investment in the implementation and adaptation of the ubiquitous global treatment guidelines to personalize medicine in any population will be required before we can truly offer individualized care.

MATERIALS AND METHODS

Study design and patient population

This was a 24-week, randomized, double-blind, placebo-controlled study conducted at 45 outpatient centers in seven European countries (Belgium, Bulgaria, Germany, Finland, Slovakia, Spain, and United Kingdom) between 22 December 2010 and 14 March 2012. Drug-naïve or inadequately controlled patients with type 2 diabetes aged ≥70 years with HbA1c levels ≥7.0% and ≤10.0% at the screening visit were eligible to participate in this study. The frailty status of patients was evaluated using a modified version of the criteria proposed by Fried and colleagues [23]. Patients were considered frail if they met any two of the following three criteria: unintentional weight loss, slow walking speed, and poor grip strength as measured by a dynamometer.

Study investigators were trained in individualizing treatment targets based on their clinical judgement considering characteristics, such as age, frailty, comorbidities, and baseline HbA1c values. During the randomization visit, each patient agreed to an individualized 24-week HbA1c target with the investigator. Patients were provided with information about the meaning of their individualized treatment targets, triggers and symptoms of hypoglycemia, and appropriate treatment for adverse events. However, no formal diabetes education program was engaged, and agreement was sought from participants to maintain their current diet and exercise habits for the duration of the study. Patients were randomized in a 1:1 ratio to receive either vildagliptin (according to the label) or placebo. Study analyses were performed on the full analysis set (FAS), comprising all randomized patients. Further details of the study population and design are described elsewhere [11].

Study assessments and endpoints

We have previously reported the co-primary endpoints of proportion of patients reaching their investigator-defined HbA1c target and reduction in the HbA1c value from baseline to week 24. The a priori secondary analyses presented herein evaluated the individualized HbA1c targets set by the investigators and the impact of baseline characteristics on these targets. Further, the response from baseline of the co-primary study endpoint of meeting the individualized treatment targets was also explored.

Statistical analysis

Logistic regression and descriptive statistics were used to asses: (a) target reductions set by the investigators (overall and by country); (b) impact of baseline characteristics (age, frailty status, sex, screening HbA1c, duration of diabetes, and number of medications at baseline visit) on target setting (overall and by country); and (c) individualized HbA1c target response at endpoint (overall and by country). We also assessed the absolute change in HbA1c by country using a regression model with terms for treatment and centered baseline HbA1c. The odds ratio, defined as the odds of responding in one group divided by the odds of responding in the second group, was also presented. The last observation carried forward method was used to handle missing data because of early discontinuation or data censoring. Continuous data were used, wherever possible, to maximize power.

Abbreviations

FAS, full analysis set; HbA1c, glycated hemoglobin; INTERVAL, INdividualized Treatment targets for ElderRly patients with type 2 diabetes using Vildagliptin Add-on or Lone therapy

ACKNOWLEDGEMENTS

We gratefully acknowledge the INTERVAL study investigators and their staff at 45 participating centers. We also thank Anna Marie Hamann (DATAMAP, GmBH) and Rangan Gupta (Novartis Healthcare Private Limited) for technical and editorial support. WDS would like to acknowledge the support of the National Institute for Health Research (NIHR), Exeter Clinical Research Facility and the NIHR Biomedical Research Centre scheme. WDS is in receipt of a Higher Education Funding Council for the England "New-Blood" Clinical Senior Lectureship award. The views expressed in this publication are those of the authors and not necessarily those of the National Health Service, the NIHR, or the Department of Health. WDS was a member of Peninsula College of Medicine and Dentistry before the demerging of Peninsula into University of Exeter Medical School and Plymouth University Peninsula Schools of Medicine and Dentistry in 2012.

CONFLICTS OF INTEREST

All authors have completed the Unified Competing Interest form at www.icmje.org/coi_disclosure.pdf (available on request from the corresponding author) and declare that WDS reports grants and personal fees from Novartis, during the conduct of the study; personal fees from Novartis, personal fees from Boehringer Ingelheim, personal fees from Pfizer, grants and personal fees from Novo-Nordisk, outside the submitted work. PMP and ASA are employees and shareholders of Novartis. No other potential conflicts of interest relevant to this article were reported.

FUNDING

The study sponsor, Novartis Pharma AG, participated in the study design, data collection, data review, and data analysis. The corresponding author participated in the study design, data collection, and data review; reviewed the trial report (signatory investigator); had full access to all data in the study; and had final responsibility for the decision to submit for publication.

Author contributions

WDS represented the study investigators and participated in the study design, data collection, data review, data interpretation, and overall clinical interpretation. PMP played a crucial part in the study design, overall planning and implementation of the trial, data collection, and data interpretation. ASA participated in data interpretation and drafting of the manuscript. All authors were involved in manuscript revisions and approval of the final manuscript. The authors affirm that this manuscript is an honest, accurate, and transparent account of the study being reported; that no important aspects of the study have been omitted; and that any discrepancies from the study as planned (and, if relevant, registered) have been explained. WDS and PMP are the guarantors.

REFERENCES

1. Narayan KM, Boyle JP, Geiss LS, Saaddine JB, Thompson TJ. Impact of recent increase in incidence on future diabetes burden: U.S., 2005-2050. Diabetes Care. 2006; 29:2114–16. doi: 10.2337/dc06-1136

2. Sinclair A, Dunning T, Colagiuri S. Managing older people with type 2 diabetes: global guideline. International Diabetes Federation 2013.

3. Inzucchi SE, Bergenstal RM, Buse JB, Diamant M, Ferrannini E, Nauck M, Peters AL, Tsapas A, Wender R, Matthews DR. Management of hyperglycemia in type 2 diabetes: a patient-centered approach: position statement of the American Diabetes Association (ADA) and the European Association for the Study of Diabetes (EASD). Diabetes Care. 2015; 38:140–49. doi: 10.2337/dc14-2441

4. Krein SL, Heisler M, Piette JD, Makki F, Kerr EA. The effect of chronic pain on diabetes patients' self-management. Diabetes Care. 2005; 28:65–70. doi: 10.2337/diacare.28.1.65

5. Pratley RE, Gilbert M. Clinical management of elderly patients with type 2 diabetes mellitus. Postgrad Med. 2012; 124:133–43. doi: 10.3810/pgm.2012.01.2526

6. Kirkman MS, Briscoe VJ, Clark N, Florez H, Haas LB, Halter JB, Huang ES, Korytkowski MT, Munshi MN, Odegard PS, Pratley RE, Swift CS. Diabetes in older adults. Diabetes Care. 2012; 35:2650–64. doi: 10.2337/dc12-1801

7. American Geriatrics Society Expert Panel on the Care of Older Adults with Multimorbidity. Patient-centered care for older adults with multiple chronic conditions: a stepwise approach from the American Geriatrics Society: American Geriatrics Society Expert Panel on the Care of Older Adults with Multimorbidity. J Am Geriatr Soc. 2012; 60:1957–68. doi: 10.1111/j.1532-5415.2012.04187.x

8. Guiding principles for the care of older adults with multimorbidity: an approach for clinicians. Guiding principles for the care of older adults with multimorbidity: an approach for clinicians: American Geriatrics Society Expert Panel on the Care of Older Adults with Multimorbidity. J Am Geriatr Soc. 2012; 60:E1–25. doi: 10.1111/j.1532-5415.2012.04188.x

9. Sinclair AJ, Paolisso G, Castro M, Bourdel-Marchasson I, Gadsby R, Rodriguez Mañas L, and European Diabetes Working Party for Older People. European Diabetes Working Party for Older People 2011 clinical guidelines for type 2 diabetes mellitus. Executive summary. Diabetes Metab. 2011 (Suppl 3); 37:S27–38. doi: 10.1016/S1262-3636(11)70962-4

10. Sinclair A, Morley JE, Rodriguez-Mañas L, Paolisso G, Bayer T, Zeyfang A, Bourdel-Marchasson I, Vischer U, Woo J, Chapman I, Dunning T, Meneilly G, Rodriguez-Saldana J, et al. Diabetes mellitus in older people: position statement on behalf of the International Association of Gerontology and Geriatrics (IAGG), the European Diabetes Working Party for Older People (EDWPOP), and the International Task Force of Experts in Diabetes. J Am Med Dir Assoc. 2012; 13:497–502. doi: 10.1016/j.jamda.2012.04.012

11. Strain WD, Lukashevich V, Kothny W, Hoellinger MJ, Paldánius PM. Individualised treatment targets for elderly patients with type 2 diabetes using vildagliptin add-on or lone therapy (INTERVAL): a 24 week, randomised, double-blind, placebo-controlled study. Lancet. 2013; 382:409–16. doi: 10.1016/S0140-6736(13)60995-2

12. Kahn R. Guidelines: we'll always need them, we sometimes dislike them, and we have to make them better. Diabetologia. 2010; 53:2280–84. doi: 10.1007/s00125-010-1885-7

13. Hu G, Jousilahti P, Qiao Q, Katoh S, Tuomilehto J. Sex differences in cardiovascular and total mortality among diabetic and non-diabetic individuals with or without history of myocardial infarction. Diabetologia. 2005; 48:856–61. doi: 10.1007/s00125-005-1730-6

14. Huxley R, Barzi F, Woodward M. Excess risk of fatal coronary heart disease associated with diabetes in men and women: meta-analysis of 37 prospective cohort studies. BMJ. 2006; 332:73–78. doi: 10.1136/bmj.38678.389583.7C

15. Kannel WB, McGee DL. Diabetes and cardiovascular disease. The Framingham study. JAMA. 1979; 241:2035–38. doi: 10.1001/jama.1979.03290450033020

16. Lee C, Joseph L, Colosimo A, Dasgupta K. Mortality in diabetes compared with previous cardiovascular disease: a gender-specific meta-analysis. Diabetes Metab. 2012; 38:420–27. doi: 10.1016/j.diabet.2012.04.002

17. Volpato S, Leveille SG, Blaum C, Fried LP, Guralnik JM. Risk factors for falls in older disabled women with diabetes: the women's health and aging study. J Gerontol A Biol Sci Med Sci. 2005; 60:1539–45. doi: 10.1093/gerona/60.12.1539

18. Wingard DL. The sex differential in morbidity, mortality, and lifestyle. Annu Rev Public Health. 1984; 5:433–58. doi: 10.1146/annurev.pu.05.050184.002245

19. Wannamethee SG, Papacosta O, Lawlor DA, Whincup PH, Lowe GD, Ebrahim S, Sattar N. Do women exhibit greater differences in established and novel risk factors between diabetes and non-diabetes than men? The British Regional Heart Study and British Women's Heart Health Study. Diabetologia. 2012; 55:80–87. doi: 10.1007/s00125-011-2284-4

20. Watts G. Why the exclusion of older people from clinical research must stop. BMJ. 2012; 344:e3445. doi: 10.1136/bmj.e3445

21. Cahn A, Raz I, Kleinman Y, Balicer R, Hoshen M, Lieberman N, Brenig N, Del Prato S, Cefalu WT. Clinical assessment of individualized glycemic goals in patients with type 2 diabetes: formulation of an algorithm based on a survey among leading worldwide diabetologists. Diabetes Care. 2015; 38:2293–300. doi: 10.2337/dc15-0187

22. Crandall J, Schade D, Ma Y, Fujimoto WY, Barrett-Connor E, Fowler S, Dagogo-Jack S, Andres R, and Diabetes Prevention Program Research Group. The influence of age on the effects of lifestyle modification and metformin in prevention of diabetes. J Gerontol A Biol Sci Med Sci. 2006; 61:1075–81. doi: 10.1093/gerona/61.10.1075

23. Fried LP, Tangen CM, Walston J, Newman AB, Hirsch C, Gottdiener J, Seeman T, Tracy R, Kop WJ, Burke G, McBurnie MA, and Cardiovascular Health Study Collaborative Research Group. Frailty in older adults: evidence for a phenotype. J Gerontol A Biol Sci Med Sci. 2001; 56:M146–56. doi: 10.1093/gerona/56.3.M146

Research Perspective

The stress polarity pathway: AMPK 'GIV'-es protection against metabolic insults

Pradipta Ghosh[1]

[1]Departments of Medicine and Cellular and Molecular Medicine, University of California at San Diego, La Jolla, CA 92093, USA

Correspondence to: Pradipta Ghosh; **email:** prghosh@ucsd.edu doi:10.18632/aging.101179
Keywords: LKB1, AMP-kinase, epithelial tight junctions, gut barrier, metabolic syndrome, heterotrimeric G proteins, energetic stress
Received: January 15, 2017 **Accepted:** February 9, 2017 **Published:** February 15, 2017

ABSTRACT

Loss of cell polarity impairs organ development and function; it can also serve as one of the first triggers for oncogenesis. In 2006-2007 two groups simultaneously reported the existence of a special pathway for maintaining epithelial polarity in the face of environmental stressors. In this pathway, AMPK, a key sensor of metabolic stress stabilizes tight junctions, preserves cell polarity, and thereby, maintains epithelial barrier functions. Accumulating evidence since has shown that pharmacologic activation of AMPK by Metformin protects the epithelial barrier against multiple environmental and pathological stressful states and suppresses tumorigenesis. How AMPK protects the epithelium remained unknown until recently Aznar et al. identified GIV/Girdin as a novel effector of AMPK at the cell-cell junctions; phosphorylation of GIV at a single site by AMPK appears to be both necessary and sufficient for strengthening tight junctions and preserving cell polarity and epithelial barrier function in the face of energetic stress. Here we review the fundamentals of this specialized signaling pathway that buttresses cell-cell junctions against stress-induced collapse and discuss its pathophysiologic relevance in the context of a variety of diseases, including cancers, diabetes, aging, and the growing list of beneficial effects of the AMPK-activator, Metformin.

Epithelial cells usually display a polarized organization such that, localization of membrane proteins and positioning of organelles differ between the apical and basolateral sides of the cell [1]. Cell polarity is fundamental for both the architecture and function of epithelial tissues; its loss triggers organ dysfunction, neoplastic transformation and cancer progression, all via dysregulation of cell growth and division [2]. Epithelial polarization is established and maintained by a set of evolutionarily conserved signaling pathways, whose integration in space and time dictates overall epithelial morphogenesis [3]; together they collaborate to assemble, stabilize and turnover the cell-cell junctions, e.g. CDC42 and PAR proteins, such as the PAR3-PAR6-aPKC complex [4], and pathways that regulate membrane exocytosis and lipid modifications [4, 5].

The stress-polarity pathway, a special force that resists junctional collapse during energetic stress

Besides the pathways mentioned above, regulation of polarity requires an additional signaling component which is triggered exclusively under conditions of energetic stress. Three studies [6-8] published in 2006-07 simultaneously reported a surprising role of AMP-activated protein kinase (AMPK) in the maintenance of epithelial cell polarity and barrier functions (Figure 1). Discovered in 1984 [9-12], and named subsequently in 1988 [13], AMPK is unique in that it is a metabolic sensor protein which is activated exclusively during energetic stress. It is because of its ability to couple energy sensing to cell polarity, activation of AMPK was critical for protecting cell junctions against stress-induced collapse. Using polarized epithelial [Madin Darby Canine Kidney (MDCK)] cells it was

demonstrated that AMPK is activated during calcium (Ca^{2+})-induced tight junction (TJ) assembly [6, 7]. The catalytic activity of AMPK is critical because either depletion of the AMPK catalytic α-subunit or expression of a kinase-dead mutant of AMPK inhibits TJ assembly as indicated by a loss of transepithelial electrical resistance (TEER); the latter is a measure of paracellular ion flow which depends on TJ stability. Pharmacological activation of AMPK with 5-aminoimidizole-4-carboxamide riboside (AICAR) partially protects TJs despite Ca^{2+} depletion [6, 7]. These findings closely followed another major revelation that the tumor suppressor LKB1 (Liver Kinase B1; also known as Serine/Threonine Kinase 11 - STK11) is a direct activator of AMPK [14-17], and that defects in cell polarity precede the development of tumors (pancreatic ductal adenocarcinoma) in genetically modified mice with tissue-specific deletion of LKB1 [18]. Together, these discoveries established the first links between energetic stress, cell polarity and oncogenesis. Since then, multiple studies (summarized in Figure 1) have reported the protective role of AMPK in maintaining cell-cell junctions across a variety of cell types in diverse tissues [airway and lungs [19, 20], heart [21], the blood-brain barrier [22, 23], kidney [24], intestine [25-29], liver [30]] while mounting a pathologic response to a variety of stressors, from bacterial invasion [31] to ischemia [24].

Although there is a wide consensus on the role of the LKB1-AMPK axis, and in particular AMPK's role in reinforcing TJs and preserving cell polarity during adverse environmental changes, how this kinase actually accomplishes this task, apparently in a Ca^{2+}-independent manner [32], remained largely unknown until recently. One study suggested that muscle myosin

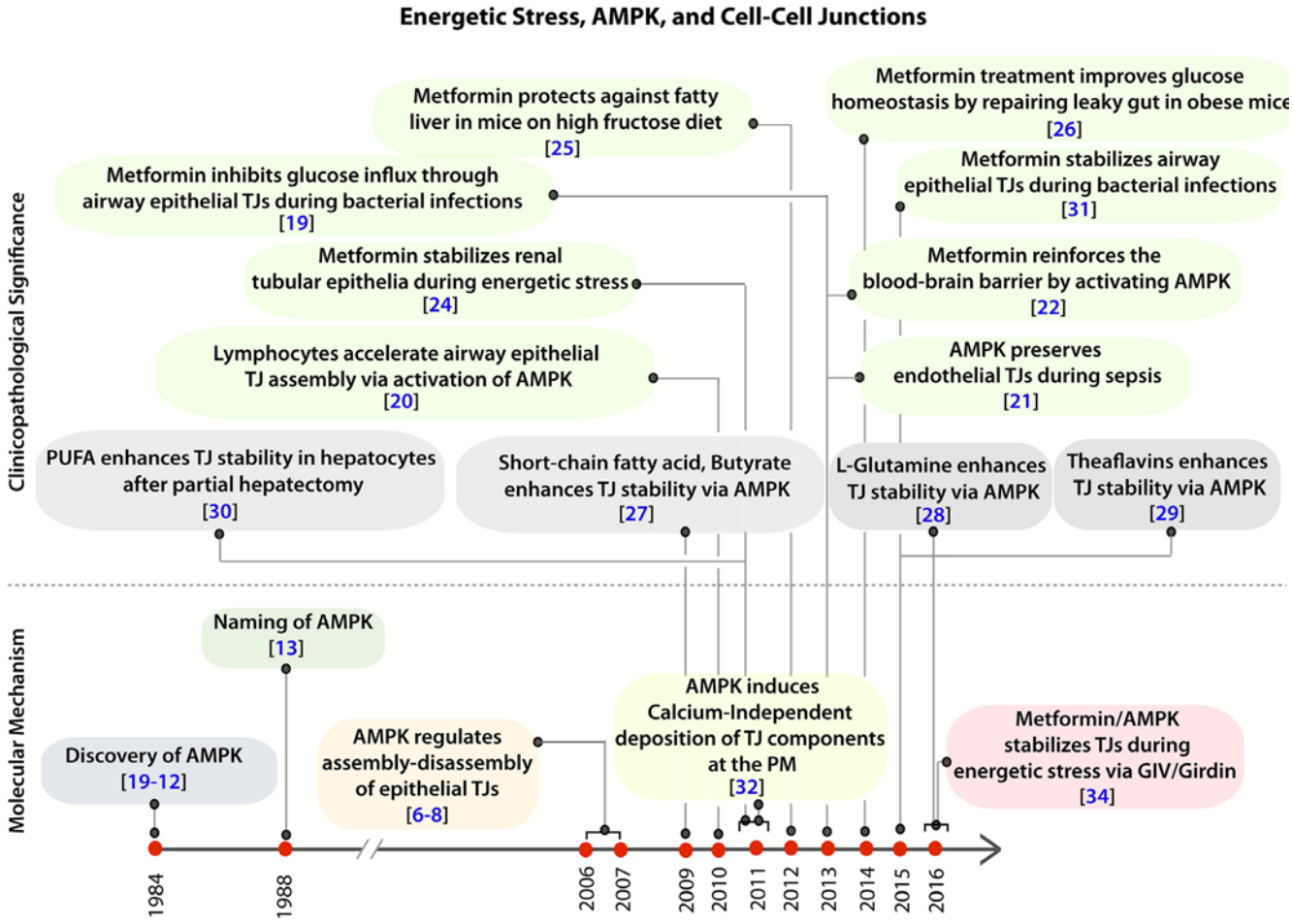

Figure 1. Clinical and pathologic significance of the protective role of AMPK in the epithelium during stress. Schematic showing the time line of publications on the topic of AMPK and cell-cell junctions, as determined by a PubMed search in 2016, and their relationship to the recently published work by Aznar et al. [34]. *Top*: Clinical and pathological significance of pharmacologic activation of AMPK, either by the widely prescribed anti-diabetic drug, Metformin (green) or by other nutritional / dietary supplements (grey) in the regulation of tight junction stability and function. *Bottom*: Time line of publications unraveling the role of AMPK in the regulation of epithelial tight junctions and in the establishment of cell polarity.

regulatory light chain (MRLC) may be the effector of AMPK during energetic stress in the fly [8], but those findings have since come into question [33] because the phosphosites on MRLC do not conform to the optimal AMPK substrate motif found in all other established *in vivo* AMPK substrates. Thus, even though it had been a decade since the first studies revealed AMPK's ability to preserve the epithelial architecture and function in the setting of energetic stress, effectors of AMPK that orchestrate these functions had not been identified.

The polarity scaffold, GIV, is a novel substrate and effector of AMPK within the stress polarity pathway

A recent study [34] demonstrated that GIV (G-alpha interacting vesicle associated protein, a.k.a. Girdin), a multimodular polarity scaffold protein is a novel substrate of AMPK, and defined the molecular mechanisms by which the AMPK-GIV signaling axis protects the epithelium by stabilizing TJs and preserving cell polarity when challenged with energetic stress. GIV, a guanine nucleotide exchange factor (GEF) for trimeric G proteins, had previously been shown to serve as a polarity scaffold protein that regulates epithelial cell polarity and morphogenesis [35-37]. GIV's role at cell-cell junctions has been attributed to its ability to assemble various functional complexes with its C-terminus, e.g., (i) binding the Par3/Par6/aPKC polarity complex [36, 38]; (ii) binding and modulating the endocytic trafficking of E-cadherin [39]; (iii) linking cadherin-catenin complexes to the actin cytoskeleton [37]; and finally, (iv) binding and activating G protein, Gαi via its GEF motif and maintaining epithelial polarity through the Par polarity complex [36]. Each of these functional associations of GIV earned it the title of 'polarity scaffold protein' and have been implicated in the generation of cell polarity.

By demonstrating that GIV is a direct target and an effector of the energy sensing kinase AMPK, Aznar et al., [34] defined the stress polarity pathway at a greater resolution, nearly a decade after the discovery of the pathway. They showed that energetic stress triggers localized activation of AMPK at the tricellular TJs, which mark the most vulnerable cell-cell contacts in sheets of polarized cells. Activation of AMPK triggers

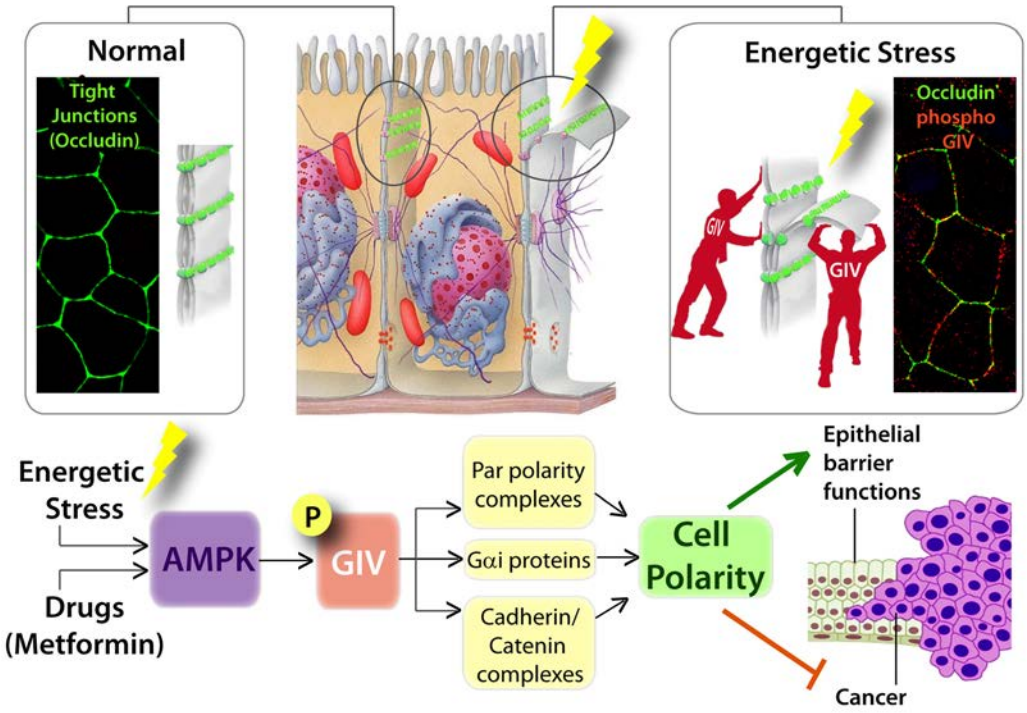

Figure 2. Graphical abstract summarizing how AMP-activated protein kinase fortifies epithelial tight junctions during energetic stress via its effector GIV/Girdin. Schematic showing the pertinent findings reported in by Aznar et al. [34]. *Top (from left to right)*: In normal physiologic states, sheets of polarized epithelial cells maintain barrier integrity by assembling tight junctions TJs; stained here with the TJ-marker and integral membrane protein, Occludin in green. Exposure to energetic stress triggers the activation of AMPK, a sensor of cellular energy stores, which in turn phosphorylates GIV at Ser245. Phospho-GIV [stained red] localizes to the TJs [marked with occluding] and serves to stabilize TJs and resist stress-induced collapse. *Bottom*: Schematic summarizing how the AMPK-GIV signaling axis preserves TJ integrity via multiple interacting partners of the polarity scaffold, GIV, and how this stress-polarity pathway enhances barrier functions and inhibits neoplastic transformation.

phosphorylation at a single site within GIV, i.e., Ser(S)245. When phosphorylated by AMPK, pS245-GIV preferentially localizes to the bicellular and tricellular TJs. Such localization is seen exclusively during TJ turnover, i.e., localization is seen both during TJ assembly as cells come in contact to form a monolayer and during TJ-disassembly as monolayers collapse in response to energetic stress or Ca^{2+}-depletion. Their findings also led to the conclusion that phosphorylation on GIV S245 is a key determinant of normal epithelial morphogenesis-- phosphorylation favors polarized normal cysts, whereas absence of phosphorylation favors branching tubules and multi-lumen structures that are associated with loss of cell polarity. Finally, they showed that pS245-GIV, which is generated only when the AMPK-GIV axis is intact, is both necessary and sufficient to fortify TJs, avoid junctional collapse and preserve cell polarity in the face of energetic stress, all in a Ca^{2+}-independent manner. They further concluded that a significant part of the junction-stabilizing effects of AMPK agonists AICAR and Metformin during energetic stress [6, 7] are mediated by AMPK via its downstream effector, pS245-GIV. In demonstrating these, the authors revealed an elusive link between the stress-sensing components and the cell polarity pathways, and shed light onto how epithelial monolayers are protected despite being constantly bombarded by energetic stressors by fortifying cell-cell junctions against stress-induced collapse.

Mechanistically, they showed that pS245-GIV localizes to the TJ-associated microtubule tracks; 3D reconstruction of deconvolved confocal images revealed that pS245-GIV colocalized with and followed the bundles of polymerized microtubule tracks at the cell-cell borders, raising the possibility that the phosphoevent may impact GIV's ability to bind α- and/or β-tubulin heterodimers. Such localization appears to be facilitated by a direct interaction between the N-terminus of GIV [exclusively when phosphorylated at S245] and the short (~100 aa) C-terminus of α-tubulin; the latter is known to project as helices from polymerized MT tracks [40, 41]. Once localized to the TJs, GIV may subsequently impact cell polarity and junctional integrity by assembling various aforementioned functional complexes with its C-terminus. Because AMPK regulates acetylation of the C-terminus of α-Tubulin during energetic stress [42] and because it is capable of stimulating microtubule polymerization at the cell periphery via phosphorylation of the microtubule plus-end protein, CLIP-170 [43], it is possible that either or both of these phenomena contribute to restricting the distribution of pS245-GIV exclusively at or near the junction-associated microtubule tracks.

It is also noteworthy that GIV's C-terminus (which binds Par complexes, G protein, and cadherin-catenin complexes), its N-terminally located AMPK substrate site, and α-tubulin-binding domain are highly conserved across all mammals and in birds; however, GIV lacks a consensus AMPK site in drosophila, and its C-terminus is poorly conserved in fish. These observations are consistent with others' observation that the LKB1/AMPK stress polarity pathway is not evolutionarily conserved; it is not required for the maintenance of polarity during energetic stress in either flies [44, 45] or fish [46, 47] [no evidence exists in amphibians, reptiles, or birds], instead, the pathway is evolutionarily young, raising the possibility that it may have co-evolved with GIV to meet the metabolic demands of endotherms (birds and mammals).

Pathophysiologic implications of the AMPK-GIV stress signaling pathway

Barrier (dys)function: Although the stress polarity pathway was originally demonstrated in polarized epithelial cells, studies using the AMPK activator, Metformin have demonstrated that AMPK fortifies cell-cell junctions in both epithelial [19, 24, 25, 31] and in endothelial cells such as those lining the lung alveoli [48], blood vessels [21] and the blood-brain barrier [22, 23, 49, 50] in the setting of stressors such as ischemia or sepsis (see Figure 1). Because GIV is ubiquitously expressed junctional scaffold, in both epithelial [36] and endothelial cells [39], it is possible that the stress-triggered mechanisms outlined by Aznar et al., [34] enable the barrier-protective role of AMPK at TJs observed in a diverse organs and tissues, both epithelial and endothelial linings, when challenged with chemical, bacterial and metabolic stressors (Figure 1).

Among the different body cavity linings (barriers), the mucosal barrier where the stress polarity pathway may be of greatest relevance is the intestinal mucosa. This barrier represents a huge mucosal surface, which separates billions of bacteria from the largest immune system of the body. On the one hand, the TJs of an intact intestinal barrier protect us against potential barrier disruptors, e.g., hypoperfusion of the gut, microorganisms and toxins, over-dosed nutrients [high fat], drugs, and other elements of lifestyle. On the other hand, this barrier must be open to absorb essential fluids and nutrients. Over the years, the beneficial [protective] effect of multiple nutritional components, dietary supplements, and pharmacologic agents, including the widely-prescribed AMPK-activator, Metformin on intestinal permeability in health and disease has been investigated; all studies converge on AMPK activation as a common pre-requisite for rendering such protection (see Figure 1). These studies raise the possibility that

the AMPK-GIV stress polarity pathway defined by Aznar et al., may affect a variety of diseases that are associated with increased intestinal permeability (reviewed in [51]) such as critical illness, inflammatory bowel diseases [52, 53], celiac disease, food allergy, irritable bowel syndrome [54, 55], Alzheimer's [56], Parkinson's [57], multiple sclerosis [58-60], autism [61, 62], chronic heart failure [63-65], aging (expanded below) and obesity and metabolic diseases (expanded below). All these diseases are characterized by systemic inflammation due to chronic endotoxemia that might be triggered by the translocation of endotoxins from the gut lumen into the host circulation.

Cancers: Previous work has shown that polarity defects precede the onset of tumorigenesis when the LKB1-AMPK pathway is inhibited (demonstrated in mice lacking the tumor suppressor and AMPK activating kinase, LKB1; [18]). These findings had fueled speculation that polarity defects may be one of the major mechanisms for tumor initiation when the energy sensing pathway is dysregulated [66]. Aznar et al., [34] showed that the AMPK-GIV stress-polarity pathway inhibits oncogenic transformation and growth, and that disruption of this pathway (accomplished via mutations identified during genomic sequencing of colorectal cancers) helps tumor cells escape such inhibition and gain proliferative advantage during 3D growth (Figure 2). Because LKB1 is a master kinase that can activate all 13 members of the AMPK kinase family [67], and given the overlapping substrate specificity of AMPK and its related kinases (reviewed in [33]), it seems likely that AMPK-related family members, such as MARK/Par1, may phosphorylate S245 on GIV under specific conditions and in certain cancers. For example, in the case of gastric cancers, where elevated GIV expression carries poor prognosis [68], junctional/ polarity defects are often observed. In this cancer, the carcinopathogen *H. pylori* drives cell transformation by delivering its virulence factor CagA (cytotoxin-associated gene A) into gastric epithelial cells through a bacterial type IV secretion system [69]. Upon entering the epithelial cells, CagA specifically binds and inhibits MARK/Par1 polarity kinase, triggering junctional and polarity defects [70]. It is tempting to speculate that MARK/Par1 may phosphorylate GIV at S245, and that inhibition of MARK/Par1 by CagA could deregulate the MARK-GIV signaling axis, thereby heralding neo-plastic transformation. Future studies are planned to investigate if such is the case.

Obesity, metabolic syndrome and type II diabetes: Accumulating evidence shows that gut barrier dysfunction can influence whole-body metabolism [71, 72] by affecting the energy balance [71], gut permeability [73, 74], metabolic endotoxemia [75] and inflammation [72, 73, 75, 76] that are associated with obesity and the spectrum of disorders associated with metabolic syndrome [25, 77, 78]. Numerous studies using the AMPK-activator, Metformin, squarely implicate the AMPK-dependent stress polarity pathway as a major therapeutic target in these metabolic disorders [79-81]. Metformin administration enhances gut barrier integrity, attenuates endotoxemia and enhances insulin signaling in high-fat fed mice, which accounts for the beneficial effects of metformin on glucose metabolism, enhanced metabolic insulin response, and reduced oxidative stress in liver and muscle of the mice [79]. Clinical trials using a delayed release formulation of Metformin (Metformin DR, which is designed to target the lower bowel and limit absorption into the blood) have shown that metformin works largely in the colon; despite the reduced levels of absorption of Metformin DR, this formulation was effective in lowering blood glucose [81]. Metformin treatment directly impacts the colonic mucosa and the gut microbiome [26]; the number of goblet cells and mucin production increases, senescence is reduced, and *Akkermansia muciniphila*, which is a mucin-degrading bacterium that resides in the mucus layer becomes abundant. Others have demonstrated that the presence of this bacterium directly correlates with gut barrier integrity [80, 82] and inversely correlates with body weight and visceral adiposity in rodents and humans [80]. These studies have challenged the conventional thinking and the importance of the gut barrier as the primary defect in metabolic diseases has gained traction [83-85]. These studies also highlight the effectiveness of activation of AMPK as a therapeutic strategy to reinforce the gut barrier and correct metabolic disorders.

Aging: Aging is characterized by the functional decline of individual organ systems of an organism, and progressively increases the probability of death. Among the various organ systems that decline during aging, dysfunction of the intestinal barrier has been correlated with increasing age in a variety of species. For example, dysfunction of the intestinal barrier predicts impending death in individual flies regardless of the chronological age [86]. Much like humans, these flies show an age-related increase in immunity-related gene expression (e.g., IL6) accompanies such dysregulation of barrier [86]. Evidence also shows that intestinal barrier dysfunction during aging is conserved in worms (*C. elegans*) and fish (*D. rerio*) [87, 88], and in mammals (rats [89] and baboons; [90]), thus raising the possibility that it may also be the case in humans. However, studies in humans have shown that intestinal permeability is not increased simply due to aging, but increases in the setting of coexisting stressors such as low-grade inflammation and/or type II diabetes [91].

As for the mechanism of increased permeability, colonic biopsies from aging baboons showed that increased permeability is associated with age-associated remodeling of epithelial TJs (decreased zonula occluden-1, occludin, and junctional adhesion molecule-A tight junction protein expression and increased claudin-2 expression; the latter promotes the formation of pores that allow the paracellular movement of cations and small molecules and increases permeability) [90]. In fact, several important physio- logical processes that are dependent on TJ integrity and cell polarity are altered during aging, involving both epithelial and endothelial cells (reviewed in [92]). It is possible that the observed anti-ageing properties of Metformin (via multiple widely pleiotropic effects reviewed in [93]), as in the case of obesity and diabetes, may begin by preserving the gut barrier function, thereby reducing age-related inflammation and metabolic derangements. If so, Metformin is expected to act via the AMPK-GIV stress polarity pathway to resist aging related increase in gut permeability. Ongoing clinical trials approved by the FDA (such as Targeting Ageing with Metformin; TAME) are likely to provide the best opportunity to investigate these possibilities.

Mechanism of action of the wonder drug, metformin: For almost a century, ever since the biosynthesis of the xenobiotic metformin by Emil Werner and James Bell in 1922, scientists have been revisiting the mechanism of action of this first-line treatment for type II diabetes. Metformin (Glucophage) is now the most widely prescribed type II diabetes drug in the world; it reduces blood glucose by activating the LKB1-AMPK pathway [94] and inhibiting hepatic gluconeogenesis (reviewed in [33]). Besides its ability to lower blood glucose, Metformin also exerts two other effects in an AMPK-dependent manner: (i) it stabilizes cell-cell junctions and protects barrier functions of both epithelial and endothelial monolayers in the setting of a variety of pathologic stressors; and (ii) it suppresses the growth of a variety of tumor cells and embryonic stem cells in culture and tumor xenografts in mice [reviewed in [33]]. By demonstrating that phosphorylation of GIV by AMPK is required for Metformin to exert both these effects efficiently, Aznar et al., [34] implicated the AMPK-GIV signaling axis as an important mechanism of action of Metformin. It is noteworthy that although multiple retrospective clinical trials have generally concluded that prolonged use of Metformin reduces the incidence of cancer, others have reported conflicting results, and several prospective clinical trials are underway to identify which target populations may specifically benefit from this drug (reviewed in [95, 96]). Given the widespread long-term use of metformin as a prescription drug and its potential utility both in chemoprevention as well as chemotherapy, further studies are warranted to investigate if the GIV-expression status in tumors (e.g., its expression as a spliced isoform lacking the C-terminus [97] or mutants that prevent phosphorylation by AMPK [34], or its overexpression as full length [98]) may help identify which patients may benefit from the tumor suppressive actions of the Metformin.

In conclusion, just when investigations on the phenomenon of stress polarity pathway had hit a cold trail, findings reported by Aznar et al. have reopened the topic by netting a strong set of clues (GIV) and have raised many more important questions. Also remains unknown how the interplay between the newly discovered AMPK→GIV signaling axis with multiple other inputs and outputs within the AMPK energy-sensing pathway (reviewed in [99, 100]), with the plethora of interactions within the expanding AMPK interactome [101], with newly emerging substrates within new pathways, e.g., neucleosome modeling [102], the glycolytic pathway [103], mitochondrial dynamics [104], junctional scaffolds, like cingulin [105], regulators of microtubule dynamics, like CLIP 170 [43]. Future studies are warranted to seek answers to these questions so that the pathophysiologic implications of this pathway and its potential as therapeutic target in a plethora of chronic diseases can be fully realized.

CONFLICTS OF INTEREST

The author has no conflict of interests to declare.

FUNDING

This work was funded by NIH (R01CA160911, R01CA100768 and DK099226) to P.G.

REFERENCES

1. Kaplan NA, Liu X, Tolwinski NS. Epithelial polarity: interactions between junctions and apical-basal machinery. Genetics. 2009; 183:897–904. doi: 10.1534/genetics.109.108878

2. Martin-Belmonte F, Perez-Moreno M. Epithelial cell polarity, stem cells and cancer. Nat Rev Cancer. 2011; 12:23–38.

3. St Johnston D, Sanson B. Epithelial polarity and morphogenesis. Curr Opin Cell Biol. 2011; 23:540–46. doi: 10.1016/j.ceb.2011.07.005

4. Wodarz A, Näthke I. Cell polarity in development and cancer. Nat Cell Biol. 2007; 9:1016–24. doi: 10.1038/ncb433

5. St Johnston D, Ahringer J. Cell polarity in eggs and epithelia: parallels and diversity. Cell. 2010; 141:757–74. doi: 10.1016/j.cell.2010.05.011

6. Zheng B, Cantley LC. Regulation of epithelial tight junction assembly and disassembly by AMP-activated protein kinase. Proc Natl Acad Sci USA. 2007; 104:819–22. doi: 10.1073/pnas.0610157104

7. Zhang L, Li J, Young LH, Caplan MJ. AMP-activated protein kinase regulates the assembly of epithelial tight junctions. Proc Natl Acad Sci USA. 2006; 103:17272–77. doi: 10.1073/pnas.0608531103

8. Lee JH, Koh H, Kim M, Kim Y, Lee SY, Karess RE, Lee SH, Shong M, Kim JM, Kim J, Chung J. Energy-dependent regulation of cell structure by AMP-activated protein kinase. Nature. 2007; 447:1017–20. doi: 10.1038/nature05828

9. Easom RA, Zammit VA. Diurnal changes in the fraction of 3-hydroxy-3-methylglutaryl-CoA reductase in the active form in rat liver microsomal fractions. Biochem J. 1984; 220:739–45. doi: 10.1042/bj2200739

10. Easom RA, Zammit VA. A cold-clamping technique for the rapid sampling of rat liver for studies on enzymes in separate cell fractions. Suitability for the study of enzymes regulated by reversible phosphorylation-dephosphorylation. Biochem J. 1984; 220:733–38. doi: 10.1042/bj2200733

11. Harwood HJ Jr, Brandt KG, Rodwell VW. Allosteric activation of rat liver cytosolic 3-hydroxy-3-methylglutaryl coenzyme A reductase kinase by nucleoside diphosphates. J Biol Chem. 1984; 259:2810–15.

12. Ferrer A, Caelles C, Massot N, Hegardt FG. Activation of rat liver cytosolic 3-hydroxy-3-methylglutaryl coenzyme A reductase kinase by adenosine 5 - monophosphate. Biochem Biophys Res Commun. 1985; 132:497–504. doi: 10.1016/0006-291X(85)91161-1

13. Munday MR, Campbell DG, Carling D, Hardie DG. Identification by amino acid sequencing of three major regulatory phosphorylation sites on rat acetyl-CoA carboxylase. Eur J Biochem. 1988; 175:331–38. doi: 10.1111/j.1432-1033.1988.tb14201.x

14. Hong SP, Leiper FC, Woods A, Carling D, Carlson M. Activation of yeast Snf1 and mammalian AMP-activated protein kinase by upstream kinases. Proc Natl Acad Sci USA. 2003; 100:8839–43. doi: 10.1073/pnas.1533136100

15. Hawley SA, Boudeau J, Reid JL, Mustard KJ, Udd L, Mäkelä TP, Alessi DR, Hardie DG. Complexes between the LKB1 tumor suppressor, STRAD alpha/beta and MO25 alpha/beta are upstream kinases in the AMP-activated protein kinase cascade. J Biol. 2003; 2:28. doi: 10.1186/1475-4924-2-28

16. Woods A, Johnstone SR, Dickerson K, Leiper FC, Fryer LG, Neumann D, Schlattner U, Wallimann T, Carlson M, Carling D. LKB1 is the upstream kinase in the AMP-activated protein kinase cascade. Curr Biol. 2003; 13:2004–08. doi: 10.1016/j.cub.2003.10.031

17. Shaw RJ, Kosmatka M, Bardeesy N, Hurley RL, Witters LA, DePinho RA, Cantley LC. The tumor suppressor LKB1 kinase directly activates AMP-activated kinase and regulates apoptosis in response to energy stress. Proc Natl Acad Sci USA. 2004; 101:3329–35. doi: 10.1073/pnas.0308061100

18. Hezel AF, Gurumurthy S, Granot Z, Swisa A, Chu GC, Bailey G, Dor Y, Bardeesy N, Depinho RA. Pancreatic LKB1 deletion leads to acinar polarity defects and cystic neoplasms. Mol Cell Biol. 2008; 28:2414–25. doi: 10.1128/MCB.01621-07

19. Garnett JP, Baker EH, Naik S, Lindsay JA, Knight GM, Gill S, Tregoning JS, Baines DL. Metformin reduces airway glucose permeability and hyperglycaemia-induced Staphylococcus aureus load independently of effects on blood glucose. Thorax. 2013; 68:835–45. doi: 10.1136/thoraxjnl-2012-203178

20. Tang XX, Chen H, Yu S, Zhang L, Caplan MJ, Chan HC. Lymphocytes accelerate epithelial tight junction assembly: role of AMP-activated protein kinase (AMPK). PLoS One. 2010; 5:e12343. doi: 10.1371/journal.pone.0012343

21. Castanares-Zapatero D, Bouleti C, Sommereyns C, Gerber B, Lecut C, Mathivet T, Horckmans M, Communi D, Foretz M, Vanoverschelde JL, Germain S, Bertrand L, Laterre PF, et al. Connection between cardiac vascular permeability, myocardial edema, and inflammation during sepsis: role of the α1AMP-activated protein kinase isoform. Crit Care Med. 2013; 41:e411–22. doi: 10.1097/CCM.0b013e31829866dc

22. Takata F, Dohgu S, Matsumoto J, Machida T, Kaneshima S, Matsuo M, Sakaguchi S, Takeshige Y, Yamauchi A, Kataoka Y. Metformin induces up-regulation of blood-brain barrier functions by activating AMP-activated protein kinase in rat brain microvascular endothelial cells. Biochem Biophys Res Commun. 2013; 433:586–90. doi: 10.1016/j.bbrc.2013.03.036

23. Liu Y, Tang G, Li Y, Wang Y, Chen X, Gu X, Zhang Z, Wang Y, Yang GY. Metformin attenuates blood-brain barrier disruption in mice following middle cerebral artery occlusion. J Neuroinflammation. 2014; 11:177. doi: 10.1186/s12974-014-0177-4

24. Seo-Mayer PW, Thulin G, Zhang L, Alves DS, Ardito T, Kashgarian M, Caplan MJ. Preactivation of AMPK by metformin may ameliorate the epithelial cell damage caused by renal ischemia. Am J Physiol Renal Physiol. 2011; 301:F1346–57. doi: 10.1152/ajprenal.00420.2010

25. Spruss A, Kanuri G, Stahl C, Bischoff SC, Bergheim I. Metformin protects against the development of fructose-induced steatosis in mice: role of the intestinal barrier function. Lab Invest. 2012; 92:1020–32. doi: 10.1038/labinvest.2012.75

26. Shin NR, Lee JC, Lee HY, Kim MS, Whon TW, Lee MS, Bae JW. An increase in the Akkermansia spp. population induced by metformin treatment improves glucose homeostasis in diet-induced obese mice. Gut. 2014; 63:727–35. doi: 10.1136/gutjnl-2012-303839

27. Peng L, Li ZR, Green RS, Holzman IR, Lin J. Butyrate enhances the intestinal barrier by facilitating tight junction assembly via activation of AMP-activated protein kinase in Caco-2 cell monolayers. J Nutr. 2009; 139:1619–25. doi: 10.3945/jn.109.104638

28. Wang B, Wu Z, Ji Y, Sun K, Dai Z, Wu G. L-Glutamine Enhances Tight Junction Integrity by Activating CaMK Kinase 2-AMP-Activated Protein Kinase Signaling in Intestinal Porcine Epithelial Cells. J Nutr. 2016; 146:501–08. doi: 10.3945/jn.115.224857

29. Park HY, Kunitake Y, Hirasaki N, Tanaka M, Matsui T. Theaflavins enhance intestinal barrier of Caco-2 Cell monolayers through the expression of AMP-activated protein kinase-mediated Occludin, Claudin-1, and ZO-1. Biosci Biotechnol Biochem. 2015; 79:130–37. doi: 10.1080/09168451.2014.951027

30. Yan XP, Wang S, Yang Y, Qiu YD. Effects of n-3 polyunsaturated fatty acids on rat livers after partial hepatectomy via LKB1-AMPK signaling pathway. Transplant Proc. 2011; 43:3604–12. doi: 10.1016/j.transproceed.2011.10.045

31. Patkee WR, Carr G, Baker EH, Baines DL, Garnett JP. Metformin prevents the effects of Pseudomonas aeruginosa on airway epithelial tight junctions and restricts hyperglycaemia-induced bacterial growth. J Cell Mol Med. 2016; 20:758–64. doi: 10.1111/jcmm.12784

32. Zhang L, Jouret F, Rinehart J, Sfakianos J, Mellman I, Lifton RP, Young LH, Caplan MJ. AMP-activated protein kinase (AMPK) activation and glycogen synthase kinase-3β (GSK-3β) inhibition induce Ca2+-independent deposition of tight junction components at the plasma membrane. J Biol Chem. 2011; 286:16879–90. doi: 10.1074/jbc.M110.186932

33. Shackelford DB, Shaw RJ. The LKB1-AMPK pathway: metabolism and growth control in tumour suppression. Nat Rev Cancer. 2009; 9:563–75. doi: 10.1038/nrc2676

34. Aznar N, Patel A, Rohena CC, Dunkel Y, Joosen LP, Taupin V, Kufareva I, Farquhar MG, Ghosh P. AMP-activated protein kinase fortifies epithelial tight junctions during energetic stress via its effector GIV/Girdin. eLife. 2016; 5:5. doi: 10.7554/eLife.20795

35. Bhandari D, Lopez-Sanchez I, To A, Lo IC, Aznar N, Leyme A, Gupta V, Niesman I, Maddox AL, Garcia-Marcos M, Farquhar MG, Ghosh P. Cyclin-dependent kinase 5 activates guanine nucleotide exchange factor GIV/Girdin to orchestrate migration-proliferation dichotomy. Proc Natl Acad Sci USA. 2015; 112:E4874–83. doi: 10.1073/pnas.1514157112

36. Sasaki K, Kakuwa T, Akimoto K, Koga H, Ohno S. Regulation of epithelial cell polarity by PAR-3 depends on Girdin transcription and Girdin-Gαi3 signaling. J Cell Sci. 2015; 128:2244–58. doi: 10.1242/jcs.160879

37. Houssin E, Tepass U, Laprise P. Girdin-mediated interactions between cadherin and the actin cytoskeleton are required for epithelial morphogenesis in Drosophila. Development. 2015; 142:1777–84. doi: 10.1242/dev.122002

38. Ohara K, Enomoto A, Kato T, Hashimoto T, Isotani-Sakakibara M, Asai N, Ishida-Takagishi M, Weng L, Nakayama M, Watanabe T, Kato K, Kaibuchi K, Murakumo Y, et al. Involvement of Girdin in the determination of cell polarity during cell migration. PLoS One. 2012; 7:e36681. doi: 10.1371/journal.pone.0036681

39. Ichimiya H, Maeda K, Enomoto A, Weng L, Takahashi M, Murohara T. Girdin/GIV regulates transendothelial permeability by controlling VE-cadherin trafficking through the small GTPase, R-Ras. Biochem Biophys Res Commun. 2015; 461:260–67. doi: 10.1016/j.bbrc.2015.04.012

40. Nogales E, Wolf SG, Downing KH. Structure of the alpha beta tubulin dimer by electron crystallography. Nature. 1998; 391:199–203. doi: 10.1038/34465

41. Nogales E, Whittaker M, Milligan RA, Downing KH. High-resolution model of the microtubule. Cell. 1999; 96:79–88. doi: 10.1016/S0092-8674(00)80961-7

42. Herms A, Bosch M, Reddy BJ, Schieber NL, Fajardo A, Rupérez C, Fernández-Vidal A, Ferguson C, Rentero C, Tebar F, Enrich C, Parton RG, Gross SP, Pol A. AMPK activation promotes lipid droplet dispersion on detyrosinated microtubules to increase mitochondrial fatty acid oxidation. Nat Commun. 2015; 6:7176.

doi: 10.1038/ncomms8176

43. Nakano A, Kato H, Watanabe T, Min KD, Yamazaki S, Asano Y, Seguchi O, Higo S, Shintani Y, Asanuma H, Asakura M, Minamino T, Kaibuchi K, et al. AMPK controls the speed of microtubule polymerization and directional cell migration through CLIP-170 phosphorylation. Nat Cell Biol. 2010; 12:583–90. doi: 10.1038/ncb2060

44. Mirouse V, Swick LL, Kazgan N, Johnston DS, Brenman JE. LKB1 and AMPK maintain epithelial cell polarity under energetic stress. J Cell Biol. 2013; 203:373. doi: 10.1083/jcb.20070205310112013r

45. Haack T, Bergstralh DT, St Johnston D. Damage to the Drosophila follicle cell epithelium produces "false clones" with apparent polarity phenotypes. Biol Open. 2013; 2:1313–20. doi: 10.1242/bio.20134671

46. van der Velden YU, Haramis AP. Insights from model organisms on the functions of the tumor suppressor protein LKB1: zebrafish chips in. Aging (Albany NY). 2011; 3:363–67. doi: 10.18632/aging.100319

47. van der Velden YU, Wang L, Zevenhoven J, van Rooijen E, van Lohuizen M, Giles RH, Clevers H, Haramis AP. The serine-threonine kinase LKB1 is essential for survival under energetic stress in zebrafish. Proc Natl Acad Sci USA. 2011; 108:4358–63. doi: 10.1073/pnas.1010210108

48. Jian MY, Alexeyev MF, Wolkowicz PE, Zmijewski JW, Creighton JR. Metformin-stimulated AMPK-α1 promotes microvascular repair in acute lung injury. Am J Physiol Lung Cell Mol Physiol. 2013; 305:L844–55. doi: 10.1152/ajplung.00173.2013

49. Farbood Y, Sarkaki A, Khalaj L, Khodagholi F, Badavi M, Ashabi G. Targeting Adenosine Monophosphate-Activated Protein Kinase by Metformin Adjusts Post-Ischemic Hyperemia and Extracellular Neuronal Discharge in Transient Global Cerebral Ischemia. Microcirculation. 2015; 22:534–41. doi: 10.1111/micc.12224

50. Zhao B, Wang X, Zheng J, Wang H, Liu J. Effects of metformin treatment on glioma-induced brain edema. Am J Transl Res. 2016; 8:3351–63.

51. Bischoff SC, Barbara G, Buurman W, Ockhuizen T, Schulzke JD, Serino M, Tilg H, Watson A, Wells JM. Intestinal permeability--a new target for disease prevention and therapy. BMC Gastroenterol. 2014; 14:189. doi: 10.1186/s12876-014-0189-7

52. Lee SY, Lee SH, Yang EJ, Kim EK, Kim JK, Shin DY, Cho ML. Metformin Ameliorates Inflammatory Bowel Disease by Suppression of the STAT3 Signaling Pathway and Regulation of the between Th17/Treg Balance. PLoS One. 2015; 10:e0135858. doi: 10.1371/journal.pone.0135858

53. Xue Y, Zhang H, Sun X, Zhu MJ. Metformin Improves Ileal Epithelial Barrier Function in Interleukin-10 Deficient Mice. PLoS One. 2016; 11:e0168670. doi: 10.1371/journal.pone.0168670

54. Barbara G. Mucosal barrier defects in irritable bowel syndrome. Who left the door open? Am J Gastroenterol. 2006; 101:1295–98. doi: 10.1111/j.1572-0241.2006.00667.x

55. Camilleri M, Gorman H. Intestinal permeability and irritable bowel syndrome. Neurogastroenterol Motil. 2007; 19:545–52. doi: 10.1111/j.1365-2982.2007.00925.x

56. Alam MZ, Alam Q, Kamal MA, Abuzenadah AM, Haque A. A possible link of gut microbiota alteration in type 2 diabetes and Alzheimer's disease pathogenicity: an update. CNS Neurol Disord Drug Targets. 2014; 13:383–90. doi: 10.2174/18715273113126660151

57. Clairembault T, Leclair-Visonneau L, Coron E, Bourreille A, Le Dily S, Vavasseur F, Heymann MF, Neunlist M, Derkinderen P. Structural alterations of the intestinal epithelial barrier in Parkinson's disease. Acta Neuropathol Commun. 2015; 3:12. doi: 10.1186/s40478-015-0196-0

58. Buscarinu MC, Cerasoli B, Annibali V, Policano C, Lionetto L, Capi M, Mechelli R, Romano S, Fornasiero A, Mattei G, Piras E, Angelini DF, Battisitni L, et al. Altered intestinal permeability in patients with relapsing-remitting multiple sclerosis: A pilot study. Mult Scler. 20161352458516652498.

59. Nouri M, Bredberg A, Weström B, Lavasani S. Intestinal barrier dysfunction develops at the onset of experimental autoimmune encephalomyelitis, and can be induced by adoptive transfer of auto-reactive T cells. PLoS One. 2014; 9:e106335. doi: 10.1371/journal.pone.0106335

60. Yacyshyn B, Meddings J, Sadowski D, Bowen-Yacyshyn MB. Multiple sclerosis patients have peripheral blood CD45RO+ B cells and increased intestinal permeability. Dig Dis Sci. 1996; 41:2493–98. doi: 10.1007/BF02100148

61. Samsam M, Ahangari R, Naser SA. Pathophysiology of autism spectrum disorders: revisiting gastrointestinal involvement and immune imbalance. World J Gastroenterol. 2014; 20:9942–51. doi: 10.3748/wjg.v20.i29.9942

62. van De Sande MM, van Buul VJ, Brouns FJ. Autism and nutrition: the role of the gut-brain axis. Nutr Res

Rev. 2014; 27:199–214. doi: 10.1017/S0954422414000110

63. Sandek A, Bjarnason I, Volk HD, Crane R, Meddings JB, Niebauer J, Kalra PR, Buhner S, Herrmann R, Springer J, Doehner W, von Haehling S, Anker SD, Rauchhaus M. Studies on bacterial endotoxin and intestinal absorption function in patients with chronic heart failure. Int J Cardiol. 2012; 157:80–85. doi: 10.1016/j.ijcard.2010.12.016

64. Sandek A, Rauchhaus M, Anker SD, von Haehling S. The emerging role of the gut in chronic heart failure. Curr Opin Clin Nutr Metab Care. 2008; 11:632–39. doi: 10.1097/MCO.0b013e32830a4c6e

65. Sandek A, Bauditz J, Swidsinski A, Buhner S, Weber-Eibel J, von Haehling S, Schroedl W, Karhausen T, Doehner W, Rauchhaus M, Poole-Wilson P, Volk HD, Lochs H, Anker SD. Altered intestinal function in patients with chronic heart failure. J Am Coll Cardiol. 2007; 50:1561–69. doi: 10.1016/j.jacc.2007.07.016

66. Hezel AF, Bardeesy N. LKB1; linking cell structure and tumor suppression. Oncogene. 2008; 27:6908–19. doi: 10.1038/onc.2008.342

67. Lizcano JM, Göransson O, Toth R, Deak M, Morrice NA, Boudeau J, Hawley SA, Udd L, Mäkelä TP, Hardie DG, Alessi DR. LKB1 is a master kinase that activates 13 kinases of the AMPK subfamily, including MARK/PAR-1. EMBO J. 2004; 23:833–43. doi: 10.1038/sj.emboj.7600110

68. Wang C, Lin J, Li L, Wang Y. Expression and clinical significance of girdin in gastric cancer. Mol Clin Oncol. 2014; 2:425–28.

69. Hatakeyama M. Helicobacter pylori CagA and gastric cancer: a paradigm for hit-and-run carcinogenesis. Cell Host Microbe. 2014; 15:306–16. doi: 10.1016/j.chom.2014.02.008

70. Hatakeyama M. Linking epithelial polarity and carcinogenesis by multitasking Helicobacter pylori virulence factor CagA. Oncogene. 2008; 27:7047–54. doi: 10.1038/onc.2008.353

71. Turnbaugh PJ, Ley RE, Mahowald MA, Magrini V, Mardis ER, Gordon JI. An obesity-associated gut microbiome with increased capacity for energy harvest. Nature. 2006; 444:1027–31. doi: 10.1038/nature05414

72. Cani PD, Osto M, Geurts L, Everard A. Involvement of gut microbiota in the development of low-grade inflammation and type 2 diabetes associated with obesity. Gut Microbes. 2012; 3:279–88. doi: 10.4161/gmic.19625

73. Cani PD, Possemiers S, Van de Wiele T, Guiot Y, Everard A, Rottier O, Geurts L, Naslain D, Neyrinck A, Lambert DM, Muccioli GG, Delzenne NM. Changes in gut microbiota control inflammation in obese mice through a mechanism involving GLP-2-driven improvement of gut permeability. Gut. 2009; 58:1091–103. doi: 10.1136/gut.2008.165886

74. Muccioli GG, Naslain D, Bäckhed F, Reigstad CS, Lambert DM, Delzenne NM, Cani PD. The endocannabinoid system links gut microbiota to adipogenesis. Mol Syst Biol. 2010; 6:392. doi: 10.1038/msb.2010.46

75. Cani PD, Amar J, Iglesias MA, Poggi M, Knauf C, Bastelica D, Neyrinck AM, Fava F, Tuohy KM, Chabo C, Waget A, Delmée E, Cousin B, et al. Metabolic endotoxemia initiates obesity and insulin resistance. Diabetes. 2007; 56:1761–72. doi: 10.2337/db06-1491

76. Cani PD, Delzenne NM, Amar J, Burcelin R. Role of gut microflora in the development of obesity and insulin resistance following high-fat diet feeding. Pathol Biol (Paris). 2008; 56:305–09. doi: 10.1016/j.patbio.2007.09.008

77. Escobedo G, López-Ortiz E, Torres-Castro I. Gut microbiota as a key player in triggering obesity, systemic inflammation and insulin resistance. Rev Invest Clin. 2014; 66:450–59.

78. Gummesson A, Carlsson LM, Storlien LH, Bäckhed F, Lundin P, Löfgren L, Stenlöf K, Lam YY, Fagerberg B, Carlsson B. Intestinal permeability is associated with visceral adiposity in healthy women. Obesity (Silver Spring). 2011; 19:2280–82. doi: 10.1038/oby.2011.251

79. Zhou ZY, Ren LW, Zhan P, Yang HY, Chai DD, Yu ZW. Metformin exerts glucose-lowering action in high-fat fed mice via attenuating endotoxemia and enhancing insulin signaling. Acta Pharmacol Sin. 2016; 37:1063–75. doi: 10.1038/aps.2016.21

80. Everard A, Belzer C, Geurts L, Ouwerkerk JP, Druart C, Bindels LB, Guiot Y, Derrien M, Muccioli GG, Delzenne NM, de Vos WM, Cani PD. Cross-talk between Akkermansia muciniphila and intestinal epithelium controls diet-induced obesity. Proc Natl Acad Sci USA. 2013; 110:9066–71. doi: 10.1073/pnas.1219451110

81. Buse JB, DeFronzo RA, Rosenstock J, Kim T, Burns C, Skare S, Baron A, Fineman M. The Primary Glucose-Lowering Effect of Metformin Resides in the Gut, Not the Circulation: Results From Short-term Pharmacokinetic and 12-Week Dose-Ranging Studies. Diabetes Care. 2016; 39:198–205.

82. Li J, Lin S, Vanhoutte PM, Woo CW, Xu A. Akkermansia Muciniphila Protects Against Atherosclerosis by Preventing Metabolic Endotoxemia-Induced Inflammation in Apoe-/- Mice. Circulation. 2016; 133:2434–46.

doi: 10.1161/CIRCULATIONAHA.115.019645

83. Wu T, Horowitz M, Rayner CK. New insights into the anti-diabetic actions of metformin: from the liver to the gut. Expert Rev Gastroenterol Hepatol. 2016; 1–10.

84. Bauer PV, Duca FA. Targeting the gastrointestinal tract to treat type 2 diabetes. J Endocrinol. 2016; 230:R95–113. doi: 10.1530/JOE-16-0056

85. McCreight LJ, Bailey CJ, Pearson ER. Metformin and the gastrointestinal tract. Diabetologia. 2016; 59:426–35. doi: 10.1007/s00125-015-3844-9

86. Rera M, Clark RI, Walker DW. Intestinal barrier dysfunction links metabolic and inflammatory markers of aging to death in Drosophila. Proc Natl Acad Sci USA. 2012; 109:21528–33. doi: 10.1073/pnas.1215849110

87. Dambroise E, Monnier L, Ruisheng L, Aguilaniu H, Joly JS, Tricoire H, Rera M. Two phases of aging separated by the Smurf transition as a public path to death. Sci Rep. 2016; 6:23523. doi: 10.1038/srep23523

88. Tricoire H, Rera M. A New, Discontinuous 2 Phases of Aging Model: lessons from Drosophila melanogaster. PLoS One. 2015; 10:e0141920. doi: 10.1371/journal.pone.0141920

89. Katz D, Hollander D, Said HM, Dadufalza V. Aging-associated increase in intestinal permeability to polyethylene glycol 900. Dig Dis Sci. 1987; 32:285–88. doi: 10.1007/BF01297055

90. Tran L, Greenwood-Van Meerveld B. Age-associated remodeling of the intestinal epithelial barrier. J Gerontol A Biol Sci Med Sci. 2013; 68:1045–56. doi: 10.1093/gerona/glt106

91. Valentini L, Ramminger S, Haas V, Postrach E, Werich M, Fischer A, Koller M, Swidsinski A, Bereswill S, Lochs H, Schulzke JD. Small intestinal permeability in older adults. Physiol Rep. 2014; 2:e00281. doi: 10.14814/phy2.281

92. Soares H, Marinho HS, Real C, Antunes F. Cellular polarity in aging: role of redox regulation and nutrition. Genes Nutr. 2014; 9:371. doi: 10.1007/s12263-013-0371-5

93. Barzilai N, Crandall JP, Kritchevsky SB, Espeland MA. Metformin as a Tool to Target Aging. Cell Metab. 2016; 23:1060–65. doi: 10.1016/j.cmet.2016.05.011

94. Shaw RJ, Lamia KA, Vasquez D, Koo SH, Bardeesy N, Depinho RA, Montminy M, Cantley LC. The kinase LKB1 mediates glucose homeostasis in liver and therapeutic effects of metformin. Science. 2005; 310:1642–46. doi: 10.1126/science.1120781

95. Pryor R, Cabreiro F. Repurposing metformin: an old drug with new tricks in its binding pockets. Biochem J. 2015; 471:307–22. doi: 10.1042/BJ20150497

96. Kourelis TV, Siegel RD. Metformin and cancer: new applications for an old drug. Med Oncol. 2012; 29:1314–27. doi: 10.1007/s12032-011-9846-7

97. Ghosh P, Beas AO, Bornheimer SJ, Garcia-Marcos M, Forry EP, Johannson C, Ear J, Jung BH, Cabrera B, Carethers JM, Farquhar MG. A Galphai-GIV molecular complex binds epidermal growth factor receptor and determines whether cells migrate or proliferate. Mol Biol Cell. 2010; 21:2338–54. doi: 10.1091/mbc.E10-01-0028

98. Ghosh P, Tie J, Muranyi A, Singh S, Brunhoeber P, Leith K, Bowermaster R, Liao Z, Zhu Y, LaFleur B, Tran B, Desai J, Jones I, et al. Girdin (GIV) Expression as a Prognostic Marker of Recurrence in Mismatch Repair-Proficient Stage II Colon Cancer. Clin Cancer Res. 2016; 22:3488–98. doi: 10.1158/1078-0432.CCR-15-2290

99. Ross FA, MacKintosh C, Hardie DG. AMP-activated protein kinase: a cellular energy sensor that comes in 12 flavours. FEBS J. 2016; 283:2987–3001. doi: 10.1111/febs.13698

100. Hardie DG, Schaffer BE, Brunet A. AMPK: An Energy-Sensing Pathway with Multiple Inputs and Outputs. Trends Cell Biol. 2016; 26:190–201. doi: 10.1016/j.tcb.2015.10.013

101. Moon S, Han D, Kim Y, Jin J, Ho WK, Kim Y. Interactome analysis of AMP-activated protein kinase (AMPK)-α1 and -β1 in INS-1 pancreatic beta-cells by affinity purification-mass spectrometry. Sci Rep. 2014; 4:4376. doi: 10.1038/srep04376

102. Marin TL, Gongol B, Zhang F, Martin M, Johnson DA, Xiao H, Wang Y, Subramaniam S, Chien S, Shyy JY. AMPK promotes mitochondrial biogenesis and function by phosphorylating the epigenetic factors DNMT1, RBBP7, and HAT1. Sci Signal. 2017; 10:eaaf7478. doi: 10.1126/scisignal.aaf7478

103. Cantelmo AR, Conradi LC, Brajic A, Goveia J, Kalucka J, Pircher A, Chaturvedi P, Hol J, Thienpont B, Teuwen LA, Schoors S, Boeckx B, Vriens J, et al. Inhibition of the Glycolytic Activator PFKFB3 in Endothelium Induces Tumor Vessel Normalization, Impairs Metastasis, and Improves Chemotherapy. Cancer Cell. 2016; 30:968–85. doi: 10.1016/j.ccell.2016.10.006

104. Ducommun S, Deak M, Sumpton D, Ford RJ, Núñez Galindo A, Kussmann M, Viollet B, Steinberg GR, Foretz M, Dayon L, Morrice NA, Sakamoto K. Motif affinity and mass spectrometry proteomic approach for the discovery of cellular AMPK targets: identification of mitochondrial fission factor as a

new AMPK substrate. Cell Signal. 2015; 27:978–88.
doi: 10.1016/j.cellsig.2015.02.008

105. Yano T, Matsui T, Tamura A, Uji M, Tsukita S. The association of microtubules with tight junctions is promoted by cingulin phosphorylation by AMPK. J Cell Biol. 2013; 203:605–14.
doi: 10.1083/jcb.201304194

Research Paper

Rapamycin treatment benefits glucose metabolism in mouse models of type 2 diabetes

Peter C. Reifsnyder[1], Kevin Flurkey[1], Austen Te[1], David E. Harrison[1]

[1]The Jackson Laboratory, Bar Harbor, ME 04609, USA

Correspondence to: David E. Harrison; **email:** David.Harrison@jax.org
doi:10.18632/aging.101117
Keywords: rapamycin, type 2 diabetes, strain survey, insulin sensitivity, pancreatic insulin content
Received: August 24, 2016 **Accepted:** November 16, 2016 **Published:** November 30, 2016

ABSTRACT

Numerous studies suggest that rapamycin treatment promotes insulin resistance, implying that rapamycin could have negative effects on patients with, or at risk for, type 2 diabetes (T2D). New evidence, however, indicates that rapamycin treatment produces some *benefits* to energy metabolism, even in the context of T2D. Here, we survey 5 mouse models of T2D (KK, KK-Ay, NONcNZO10, BKS-*db/db*, TALLYHO) to quantify effects of rapamycin on well-recognized markers of glucose homeostasis within a wide range of T2D environments. Interestingly, dietary rapamycin treatment did not exacerbate impaired glucose or insulin tolerance, or elevate circulating lipids as T2D progressed. In fact, rapamycin *increased* insulin sensitivity and reduced weight gain in 3 models, and decreased hyperinsulinemia in 2 models. A key covariate of this genetically-based, differential response was pancreatic insulin content (PIC): Models with low PIC exhibited more beneficial effects than models with high PIC. However, a minimal PIC threshold may exist, below which hypoinsulinemic hyperglycemia develops, as it did in TALLYHO. Our results, along with other studies, indicate that beneficial or detrimental metabolic effects of rapamycin treatment, in a diabetic or pre-diabetic context, are driven by the interaction of rapamycin with the individual model's pancreatic physiology.

INTRODUCTION

Rapamycin increases lifespan in mice and several other organisms [1-8], presumably via inhibition of mTORC (mechanistic Target Of Rapamycin Complex). mTORC activation is associated with the response to nutrients, and it is involved in the regulation of insulin and glucose homeostasis [9-13]. Both glucose and insulin can hyperactivate mTOR, creating a negative feedback loop via S6 kinase to degrade insulin receptor substrate 1/2, impairing insulin signaling, and leading to insulin resistance [14]. Rapamycin can reduce glucose-stimulated insulin secretion and pancreatic islet cell proliferation in mice and in cell lines [reviewed in 9, 10]. Studies of humans taking rapamycin after tissue transplant or as an anti-cancer agent have shown that glucose metabolism is unaffected in most patients; however, a minority (~3–22%) can develop hyperglycemia, with rates depending on dose of rapamycin, patient population, and individual study [9]. Because rapamycin may alter glucose homeostasis, researchers have evaluated effects of rapamycin on glucose clearance, insulin sensitivity, and adiposity in mice [10-22]. Studies principally used C57BL6 or heterogeneous stocks, but a few have tested models of type 2 diabetes (T2D), such as KK/Hl [15], NONcNZO10 [21], and BKS-*db/db* [17, 18]. In normoglycemic strains, rapamycin treatment delays glucose clearance but reduces weight gain and adiposity (particularly when mice are fed a high fat diet). However, rapamycin inconsistently affects insulin sensitivity and serum insulin values. Effects of rapamycin on glucose clearance in already glucose intolerant strains have not been reported, but increased insulin sensitivity has been shown in the insulin resistant BKS-*db/db* mouse [17]. Rapamycin treatment also reduces weight gain in strains that are models of T2D [17, 18, 21]. Furthermore, effects can change over time. In a non-diabetic heterogeneous mouse model, negative effects on glucose clearance and insulin sensitivity faded with treatment duration [13]. It is difficult to compare these studies because of the differences among the methods of rapamycin treatment

(intraperitoneal injections or encapsulated in diet), fat content of diets, lengths of treatment, and phenotypic evaluations. Therefore, the present study analyzes the effects of rapamycin across a broad range of diabesity models using a consistent protocol to delineate both common and idiosyncratic responses to the compound. The 5 models selected represent distinct type 2 diabetic etiologies (Table 1), with differing severities of obesity, hyperglycemia, and hyperinsulinemia [23-28].

RESULTS

We analyzed effects of rapamycin treatment on 10 T2D phenotypes in 5 models of diabetic mice that represent distinct etiologies. Encapsulated rapamycin was administered through the diet (rapa-treatment), which replicates the alimentary mode of administration used for humans. We evaluated responses, as T2D initially progressed, through 2–6 weeks of rapa-treatment that

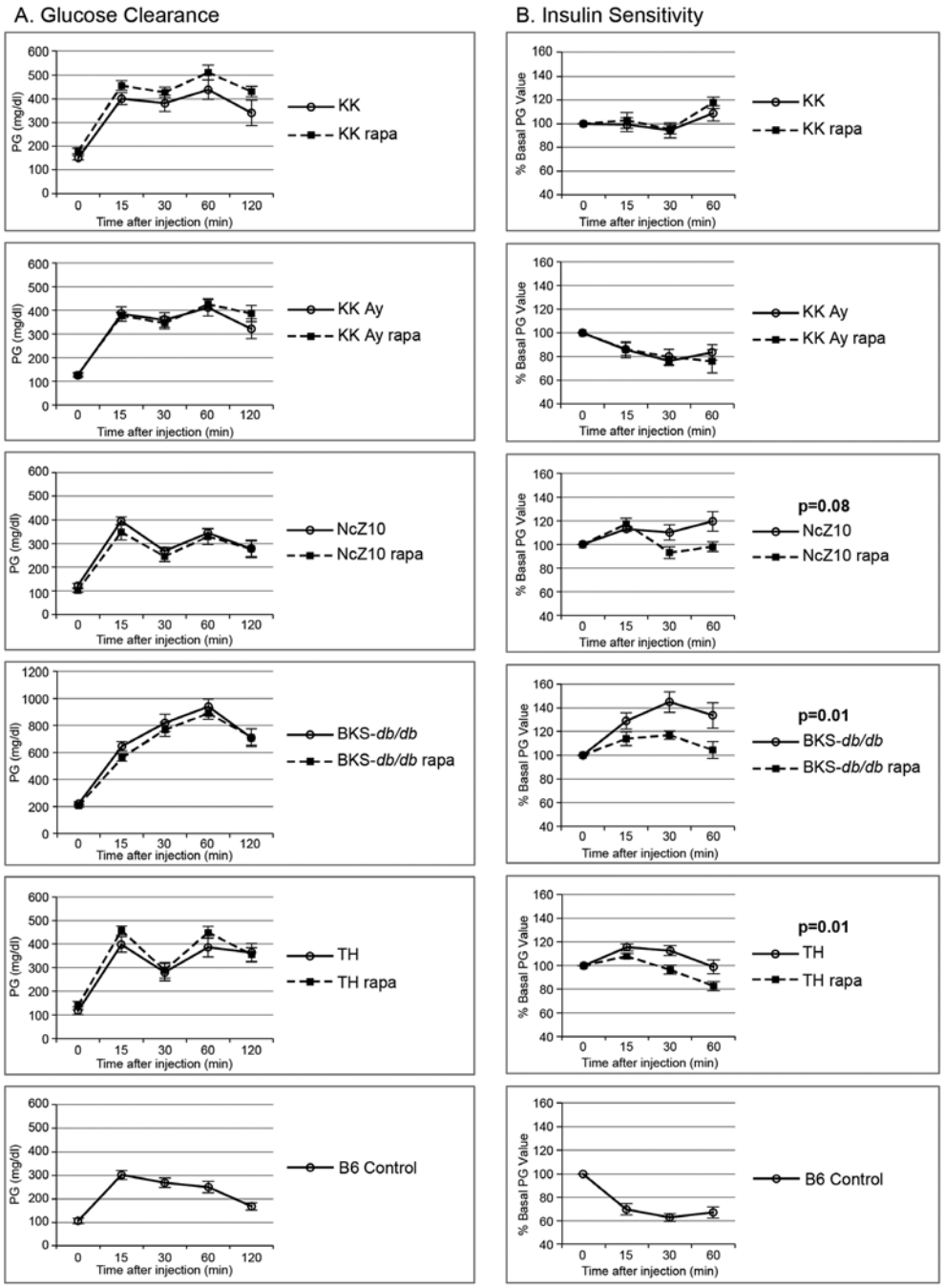

Figure 1. Effect of rapamycin on glucose clearance and insulin sensitivity in 5 diabesity models. (**A**) Rapamycin does not exacerbate glucose intolerance in 5 glucose intolerant strains. (**B**) Rapamycin improves insulin sensitivity in the insulin-resistant NcZ10, BKS-*db/db*, and TH strains. Two or three B6 controls were tested with each strain (cumulative data shown, n = 13–16) to serve as positive controls for the glucose and insulin injections, as quality controls, and for reference values. P values are given for repeated measures MANOVA (n = 5–6 per strain/treatment group except for NcZ10, n = 11).

began at 8–11 weeks of age. Rapa-treatment did not exacerbate the expression of 5 T2D phenotypes (insulin resistance, glucose intolerance, circulating lipids [triglycerides, cholesterol, non-esterified fatty acids]) in any of these diabesity models (Figure 1 and Table 2).

Rapa-treatment elevated hyperglycemia in only one of the 5 models (TH, Table 2). In fact, rapa-treatment produced some benefits. Weight gain was diminished and insulin sensitivity was improved in 3 models (BKS-db/db, NcZ10, TH), and hyperinsulinemia was reduced

Table 1. Characteristics of the 5 T2D mouse models used in the study.

Diabetes strain	Pancreatic insulin content	Hyper-phagia	Obesity	Hyper-insulinemia	Hyper-glycemia	Glucose intolerance	Insulin resistance
KK	High	Yes	Moderate	Severe, by 8 wk	Mild, by 10 wk	Yes	Yes
KK-Ay	High	Yes	Moderate	Very Severe, by 8 wk	Severe, by 16 wk	Yes	Yes
NcZ10	Intermediate	No	Moderate	Mild, by 12–20 wk	Moderate, by 12–20 wk	Yes	Yes
BKS-*db/db*	Low	Yes	Morbid	Severe, by 4–8 wk	Severe, by 4–8 wk	Yes	Yes
TH	Low	No	Moderate	Moderate, by 10–14 wk	Moderate, by 10–14 wk	Yes	Yes

Data references [23-28].

Table 2. Rapamycin treatment effects on markers of metabolism in 5 T2D strains.

Strain	Group (n)	Glucose clearance (GTT) 3 wk*	Insulin sensitivity (ITT) 2 wk*	Glucose (mg/dl)			Insulin (ng/ml)		TG (mg/dl) fed 6 wk	Cholesterol (mg/dl) fed 6 wk	NEFA (mEq/L) fed 6 wk	Pan-creatic insulin content (ng/mg) 6 wk
				Overnight fasting 3 wk	Fed 2 wk (Glu-2)	Fed 6 wk (Glu-6)	Overnight fasting 3 wk	Fed 6 wk (Ins-6)				
KK	Untreated (6)	Glucose intolerant	Insulin resistant	151 ± 9	190 ± 25	210 ± 14	1.11 ± 0.16	13.9 ± 2.8	388 ± 43	180 ± 2	4.66 ± .24	175 ± 50
	Rapa (6)	No change	No change	176 ± 11	197 ± 23	250 ± 25	3.67 ± 1.56	23.9 ± 9.4	385 ± 96	171 ± 9	4.01 ± .45	167 ± 34
KK-Ay	Untreated (6)	Glucose intolerant	Insulin responsive**	126 ± 9	350 ± 47	519 ± 64	1.27 ± 0.12	168.7 ± 34.6	938 ± 129	162 ± 8	5.92 ± .33	161 ± 43
	Rapa (6)	No change	No change	129 ± 5	373 ± 24	418 ± 64	0.83 ± 0.10 **p = .02**	54.6 ± 9.3 **p = .01**	691 ± 140	185 ± 8 **p = .06**	5.44 ± .33	73 ± 8 **p = .06**
NcZ10	Untreated (11)	Glucose intolerant	Insulin resistant	120 ± 11	177 ± 14	218 ± 21	0.45 ± 0.10	1.80 ± .51	286 ± 18	129 ± 5	3.66 ± .11	63 ± 5
	Rapa (11)	No change	Increased sensitivity	102 ± 9	173 ± 10	258 ± 20	0.26 ± 0.03 **p = .10**	1.23 ± .18	249 ± 15	127 ± 5	3.34 ± .10 **p = .06**	43 ± 4 **p = .004**
BKS-*db/db*	Untreated (5–6)	Glucose Intolerant	Insulin resistant	220 ± 11	321 ± 20	638 ± 47	1.81 ± 0.38	7.86 ± 1.15	117 ± 11	207 ± 9	1.92 ± .15	25 ± 4
	Rapa (6)	No change	Increased sensitivity	207 ± 11	375 ± 17 **p = .07**	707 ± 29	1.86 ± 0.23	5.96 ± 1.03	98 ± 7	201 ± 7	1.55 ± .10 **p = .06**	16 ± 2 **p = .08**
TH	Untreated (6)	Glucose intolerant	Insulin resistant	118 ± 15	222 ± 33	365 ± 60	1.79 ± 0.25	4.17 ± 0.84	259 ± 33	226 ± 8	2.97 ± .14	26 ± 6
	Rapa (6)	No change	Increased sensitivity	140 ± 16	278 ± 18	502 ± 16 **p = .05**	1.20 ± 0.25	1.21 ± 0.34 **p = .009**	272 ± 22	247 ± 12	3.31 ± .10 **p = .08**	11 ± 2 **p = .03**

p-values from 1-way ANOVA

*weeks of treatment. See Figure 1 for graphs.

**See Discussion for commentary regarding this result.

in 2 models (TH, KK-Ay) (Figure 2, Figure 1B, and Tables 2 & 3). However, rapa-treatment did have a potential negative effect: Pancreatic insulin content (PIC) was diminished in 4 models (significant [$p < 0.05$] in NcZ10 and TH, suggestive [$p = 0.05$ to 0.1] in BKS-*db/db*, KK-Ay, Table 2). Results are summarized in Table 4 and Figure 3. Given the expectation that rapamycin would exacerbate disease phenotypes in diabetic models, our results are both surprising and novel.

DISCUSSION

Specific model-based differences in T2D phenotypes following rapa-treatment

KK and KK-Ay

The two KK models that we studied have very high PIC and supraphysiological circulating insulin levels, which distinguishes them from the other 3 models studied.

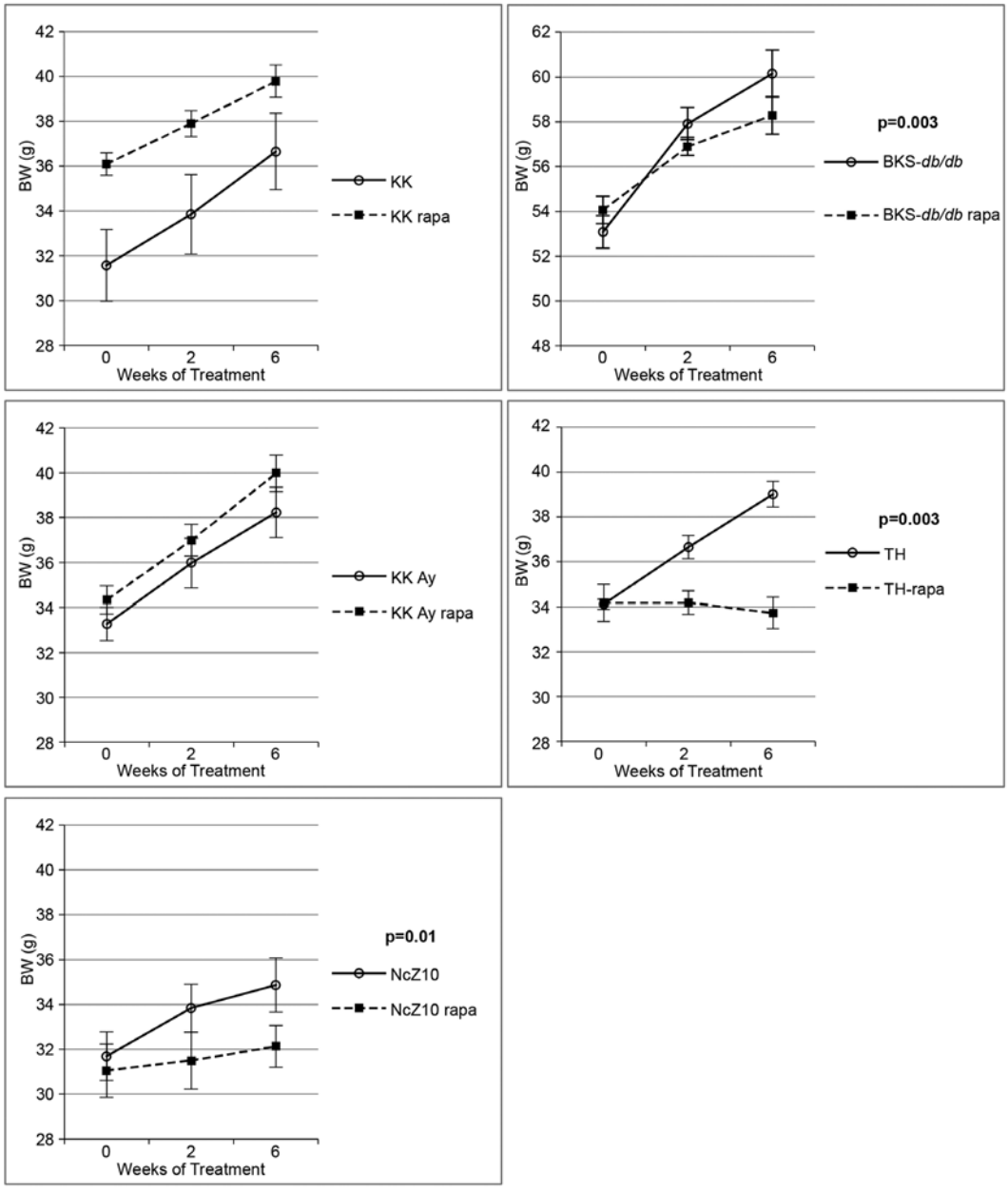

Figure 2. Effect of rapamycin on body weight gain in 5 diabesity models. Rapamycin significantly reduces body weight gain in NcZ10, BKS-*db/db*, and TH strains, but not in KK-Ay or KK strains. P values are given for repeated measures MANOVA (n = 5–6 per strain/treatment group, except n = 11 for both NcZ10 groups). Note that the Y-axis scale for BKS-*db/db* is over a different 14-g span than the other 4 strains.

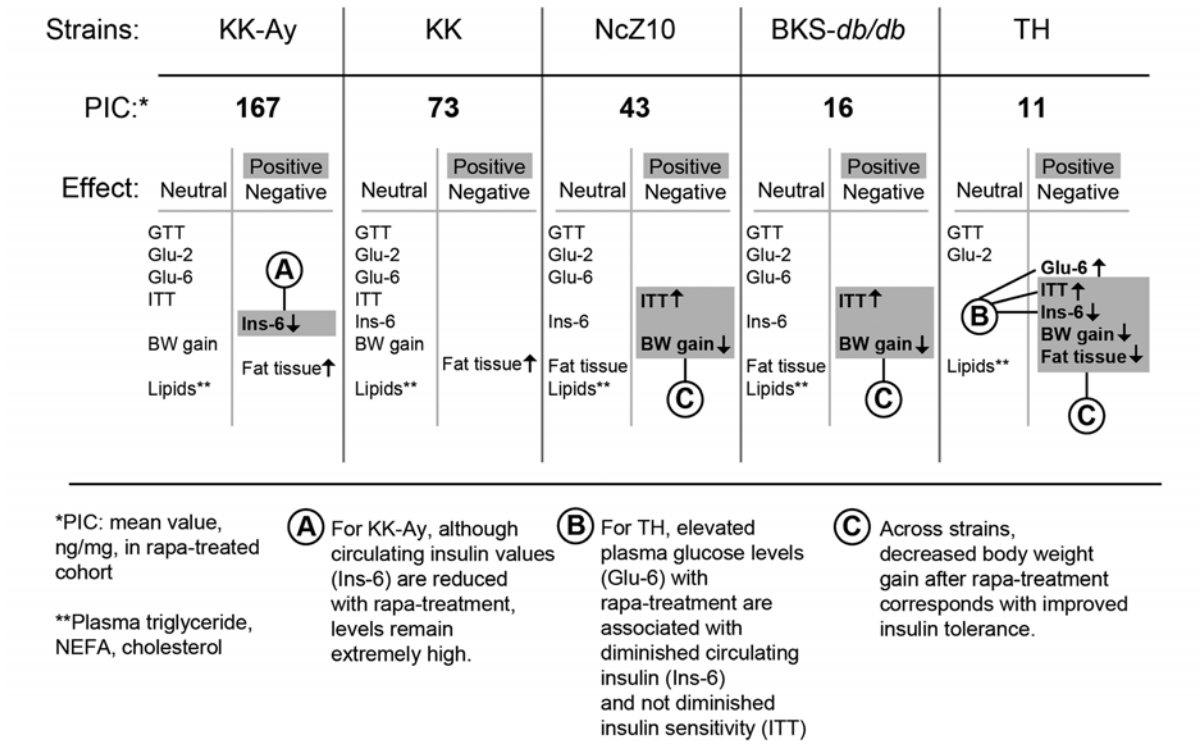

Figure 3. Phenotypic response pattern to rapamycin treatment scales inversely with PIC. The balance of positive and negative responses to rapamycin may be shaped by strain differences that control the pancreatic insulin content (PIC) response to rapamycin. The progress of diabetes within the first 6 weeks of treatment is relatively unaffected in strains that retain a relatively high PIC. With intermediate PIC levels, benefits appear that are associated with diminished gain in body weight, including diminished insulin resistance. At the lowest PIC level, glycemic management is impaired and hypoinsulinemic hyperglycemia emerges. *PIC: pancreatic insulin content (ng/mg) after rapa-treatment. **Lipids: plasma triglycerides, NEFA, cholesterol. Terms: GTT = glucose tolerance test; Glu-2 = non-fasting plasma glucose after 2 weeks of treatment; Glu-6 = non-fasting plasma glucose after 6 weeks of treatment; ITT = insulin tolerance test; Ins-6 = non-fasting plasma insulin after 6 weeks of treatment; BW = body weight.

Rapa-treatment had no effect on insulin resistance in KK and KK-Ay, whereas it diminished insulin resistance in the other 3 models. It is possible that rapa-treatment generally diminishes insulin resistance in diabetic mice, but that sustained, excessive circulating insulin, characteristic of the two KK models, overwhelms this effect. The rapamycin-induced increased adipose tissue weight in the two KK models also contrasted with the response of the other 3 models. The overall 30–40% increase in adipose tissue weight in the KK strains, despite the absence of an increase in food intake or in body weight, suggests that rapa-treatment induced a shift in nutrient partitioning in these models, potentially by *increasing* adipose tissue sensitivity to insulin.

These results stand in contrast to those observed in a previous study of rapa-treatment in high-fat fed KK/HlJ mice [15], a different KK substrain than that used in our study. In both rapa-treated and control KK/HlJ mice [15], mean values of circulating insulin were in the normal range, and, while the authors did not report the glycemic status of their KK/HlJ mice, they did report that their mice maintained a normal glucose clearance after challenge. Results in the KK/HlJ mice studied by Chang et al. [15] may be more typical of our results for NcZ10 and TH than our results for KK and KK-Ay. Like the NcZ10 and TH mice, the KK/HlJ mice studied by Chang et al. had more normal levels of insulin and responded to rapa-treatment with diminished weight gain and lower fat pad weights. Presumably, the high fat-fed KK/HlJ mice model a physiologic state of T2D that provides an environment in which rapa-treatment can have beneficial effects. It may be that the differences between the 2 studies in the responses to rapa-treatment are consequent to an interaction of rapamycin with the dissimilar physiological states established by the large pre-existing differences in insulin levels. Of course, substrain variation or differences in study design and husbandry may be involved.

Table 3. Rapamycin treatment effects on adiposity in 5 T2D strains.

Strain	Treatment (n)	% Fat pad weight of body weight		
		Epididymal	Retroperitoneal	Inguinal
KK	Untreated (6)	1.75 ± 0.09	0.70 ± 0.05	0.77 ± 0.08
	Rapa (5)	2.18 ± 0.05 **p = .003**	1.25 ± 0.07 **p = .0001**	0.78 ± 0.06
KK-Ay	Untreated (6)	1.36 ± 0.09	0.74 ± 0.07	1.01 ± 0.06
	Rapa (6)	2.47 ± 0.08 **p < .0001**	1.34 ± 0.05 **p < .0001**	0.92 ± 0.09
NcZ10	Untreated (11)	2.25 ± 0.08	0.51 ± 0.04	1.07 ± 0.06
	Rapa (11)	2.03 ± 0.11	0.52 ± 0.04	0.91 ± 0.06 **p = .09**
BKS-*db/db*	Untreated (6)	2.43 ± 0.07	1.42 ± 0.06	3.59 ± 0.14
	Rapa (6)	2.62 ± 0.07 **p = .08**	1.26 ± 0.11	3.62 ± 0.05
TH	Untreated (6)	2.24 ± 0.12	0.49 ± 0.04	1.38 ± 0.08
	Rapa (6)	2.17 ± 0.18	0.35 ± 0.05 **p = .04**	1.05 ± 0.11 **p = .04**

p-values from 1-way ANOVA.

Table 4. Summary of effects of rapamycin treatment on T2D-related phenotypes in 5 T2D mouse models.

	Glucose/insulin metabolism					Body composition		Circulating lipids		
Diabetic strains	PG elevated	Glucose clearance delayed	Insulin sensitivity increased	Plasma insulin reduced	Pancreatic insulin content reduced	Weight gain reduced	Fat pad weights altered	Serum TG altered	Serum cholesterol altered	Serum NEFA altered
KK	NO	NO	NO	NO	NO	NO	yes↓	NO	NO	NO
KK-Ay	NO	NO	NO	yes	NO*	NO	yes↓	NO	NO*	NO
NcZ10	NO	NO	yes	NO	yes	yes	yes+	NO	NO	NO*
BKS-*db/db*	NO	NO	yes	NO	NO*	yes	NO	NO	NO	NO*
TH	yes	NO	yes	yes	yes	yes	yes+	NO	NO	NO*

yes = significant difference ($p < .05$) between rapa-treated and untreated mice within each strain.
*Suggestive difference, $p = .06–.09$.

An unusual characteristic of the KK-Ay strain is that their insulin resistance is not fully reflected by the insulin tolerance test. Insulin resistance is observed in KK mice for adipocyte lipogenesis and suppression of hepatic gluconeogenesis [23, 28]. In contrast, when we evaluated insulin responsiveness using a standard *in vivo* insulin tolerance test, we observed modest insulin responsiveness. We are confident that the circumstances of our test procedure, glucose assay, and insulin preparation were not a cause of this seemingly anomalous insulin responsiveness, as the quality control group (C57BL/6J males) tested at the same time

exhibited a normal response to insulin, consistent with the other runs of the insulin tolerance test (ITT) in the study. Furthermore, our observation is consistent with previous reports of modest responsiveness to an insulin tolerance test in KK-Ay mice [29, 30]. The co-existence of even modest insulin sensitivity with the extreme hyperinsulinemia in the same mice is surprising, and it suggests that the yellow obese mutation on the KK genetic background may provide a unique model for elucidation of the mechanisms by which insulin regulates energy metabolism.

TALLYHO

PIC in rapa-treated TH mice was significantly reduced to the lowest levels of the 5 models studied. This correlated with a significant decrease in plasma insulin levels and concomitant exacerbation of hyperglycemia, despite the *increased* insulin sensitivity in rapa-treated TH mice. Rapa-treatment also diminished weight gain and adipose tissue weight. This phenotypic pattern in TH — beneficial responses combined with a detrimental response — may be a consequence of the very low PIC levels produced by rapa-treatment specifically in TH mice. Such extremely low PIC levels may cross a threshold for pancreatic maintenance of circulating insulin, resulting in the elevation of circulating glucose. The diminished bodyweight gain and lower fat pad weights in the rapa-treated TH mice may also have resulted from the lower circulating insulin.

BKS-db/db

Rapa-treatment tended to diminish PIC in BKS-*db/db* mice to a level similar to, but not quite as low as, that in rapa-treated TH mice. In BKS-*db/db* mice, however, the effect was suggestive but not significant ($p = 0.08$). While the difference between the models is subtle, it may be critical. In TH mice, plasma glucose levels were significantly increased as plasma insulin decreased, while in BKS-*db/db* mice, both plasma insulin and glucose were unaffected and remained elevated, despite increased insulin sensitivity. This suggests that, as T2D initially progressed in rapa-treated BKS-*db/db* mice, a hypoinsulinemic PIC-threshold had not yet been reached. However, over time, some detrimental effect of rapa-treatment emerges in this model, as lifelong rapa-treatment in BKS-*db/db* mice has been shown to shorten their lifespan [31]. In untreated BKS-*db/db* mice circulating insulin progressively declines over time [32], and we have confirmed that plasma insulin values decrease at the same rate in both untreated and rapa-treated BKS-*db/db* mice with age (unpublished). Given the tendency toward diminished PIC in rapa-treated BKS-*db/db* mice after 6 weeks, we speculate that rapa-induced PIC depletion accelerates the inherent model-driven islet malfunction to further advance the progression to hypoinsulinemia.

Weight gain in the BKS-*db/db* mice was reduced with rapa-treatment, an effect also seen in previous studies [17, 18, 29]. The effect is subtle at 6 weeks of treatment, at which time fat pad weights were unaffected in our study. A longer treatment-duration, such as the 6-month treatment used by Deepa et al. [17], may be needed to observe effects directly on adipose tissue.

NcZ10

PIC in NcZ10 mice is intermediate between that of the two KK models and the TH and BKS-*db/db* models. Rapa-treatment significantly reduced PIC in NcZ10 mice. Insulin resistance, weight gain, and adipose tissue weight were diminished, as in the TH model; but, in contrast, circulating insulin levels were not diminished and plasma glucose was not elevated. Apparently, the diminished PIC value after rapa-treatment in this model remains sufficient to sustain the pre-treatment relationship of circulating insulin to plasma glucose.

A comparison of our present, 6-week study to a previous, 14-week, rapa-treatment study of NcZ10 males from our laboratory [21] suggests the importance of treatment duration on some outcomes. Diminished weight gain was observable by 6 weeks of treatment in both studies, and suppression of weight gain continued with further rapa-treatment [21]. Although, in both studies, plasma glucose was unaffected at 6 weeks of rapa-treatment, continued treatment elevated plasma glucose [21]. This further elevation of hyperglycemia in the rapa-treated mice was associated with diminished circulating insulin, suggesting that a hypoinsulinemic-associated hyperglycemia can develop over time with rapa-treatment. Similarly, plasma cholesterol (but not plasma triglycerides or non-esterified fatty acids) also was elevated by 14 weeks of treatment in the previous study, but not at 6 weeks of treatment in the present study. These observations suggest that specific effects of rapa-treatment on glucose and lipid metabolism may appear only with long-term treatment.

CONCLUSION

Rapamycin has extraordinary potential as a treatment for a wide range of chronic diseases. It is already being prescribed to suppress tissue rejection or graft vs. host reactions in patients with tissue and bone marrow transplants. It also is being investigated for treatment of specific cancers and autoimmune diseases [9]. Furthermore, rapamycin is the first drug found to reliably increase maximum lifespan in a mammalian

model [1, 2], suggesting that numerous age-related diseases may respond to rapamycin treatment [33]. But an important concern regarding rapamycin treatment is the elevation of circulating glucose observed in some patients. Initial conjecture that this elevation is due to rapamycin-driven insulin resistance [reviewed in 10, 11, 14] is presently tempered by a growing body of evidence that, depending upon the mouse model, rapamycin can have no effect on insulin resistance [12, 13] or can actually promote insulin sensitivity [17, 34]. The foremost finding of our study is that 6 weeks of rapa-treatment does not promote further insulin resistance, glucose intolerance or hyperlipidemia in the diabetic physiologic context represented by multiple T2D mouse models. On the contrary, a number of beneficial effects appeared among some of the T2D strains; the most common were diminished gain in body weight and improved insulin sensitivity.

The potential beneficial effects of rapa-treatment contrast with a potential detrimental effect on PIC. Genetic differences in the regulation of PIC and its response to rapamycin may be key in determining whether a beneficial phenotypic response profile is produced (Figure 3). In diabetic strains with high PIC, rapa-treatment may produce minimal beneficial effects, primarily due to sustained supraphysiologic levels of circulating insulin. In diabetic strains with intermediate or low PIC, rapa-treatment may diminish weight gain and adiposity. The reduced expression of such pathogenic physiological phenotypes with rapamycin treatment could contribute to the associated protection from numerous pathologic sequalae of T2D, including retinopathy, [34], nephropathy [21] and cardiomyopathy [18]. Such observations are consistent with the idea that elevations of circulating insulin levels in diabetic states may play a greater role in the development of T2D-associated lesions than currently appreciated [35].

In mice at risk for or expressing T2D, however, the pre-existing diabetogenic ß-cell stress interacts with an additional stress associated with initial rapamycin treatment (reviewed in 36) to potentially exacerbate T2D-driven ß-cell impairment. Thus, the potential for rapamycin-facilitated pathogenesis may be determined by the balance between the pre-existing T2D susceptibility and the rate of adjustment to rapamycin-driven ß-cell stress. If ß-cell impairment reaches a critical threshold, indicated by extreme PIC depletion, a terminal hypoinsulimic crisis can result. This model is consonant with an emerging emphasis on the role of pancreatic ß-cell physiology in shaping the risk for, and progression of, T2D [37].

We propose that the effect of long-term rapa-treatment on survival in individuals at risk for, or expressing, T2D is determined by the balance of beneficial effects on insulin responsiveness, body composition, and T2D-associated diseases against the detrimental effect on PIC itself. Future research should emphasize investigation of means to ameliorate detrimental effects of rapamycin on PIC while maintaining the positive effects on other tissues. Resolution of this challenge could provide a major advance in the treatment of complex degenerative diseases.

METHODS

Animals

The study comprised males of 5 classic "diabesity" models of mice, all obtained from the Jackson Laboratory at 7–10 weeks of age. The models were: BKS.Cg-*Dock7*^{m} +/+ *Lepr*^{db}/J (BKS-*db/db*), KK.Cg-*a/a*/J (KK; normal, wild-type nonagouti), KK.Cg-*A*^{y}/J (KK-Ay; agouti yellow), NONcNZO10/LtJ (NcZ10), and TALLYHO/JngJ (TH). At 8–11 weeks of age, the mice were separated into 2 groups of 6, weighed, and put onto diet (5LA0, 11% fat, Purina) with or without encapsulated rapamycin (14 PPM, [1]). All mice were fed *ad lib* and given acidified water. Mice were housed in double pen boxes (3 mice per side) with pine shaving bedding. The mouse room was maintained at ~25°C and 40–50% humidity. The specific pathogen free health status of the room can be viewed at (http: //myjax.jax.org/lahs/healthreports/RAF/d1.0814.pdf). Two separate cohorts of the NcZ10 strain (5 or 6 mice per treatment group) were studied 3 months apart. The second cohort weighed 3.5 g more than the first cohort at the beginning of treatment, but body weights between the two cohorts, within each treatment group, did not differ at the end of the experiment. The 2 cohorts did not differ for any phenotypic response to rapamycin. All other groups were studied in single cohorts.

Protocols

After 2 weeks on diets ± rapamycin, an insulin tolerance test (ITT) was performed. Food was removed from the mice at 7:00 a.m. At ~10:00–10:30, mice were weighed and bled from the tail (~2 µl from a nick in the tail tip), glucose was measured (OneTouch Ultra, Lifescan), and mice were then injected i.p. with 1.0 U/kg insulin (Humulin, Eli Lilly) in PBS. Glucose was measured additionally at 15, 30, and 60 minutes post injection. After 3 weeks of treatment, a glucose tolerance test (GTT) was performed. At ~5:00 p.m. on the day before the test, the mice were moved to clean cages and food was removed for overnight fasting. At ~10:00–10:30 a.m. the following morning, the mice were weighed, bled for glucose measurement, and injected with 1 g/kg

glucose from a 10% glucose solution in PBS. Glucose was then measured at 15, 30, 60, and 120 minutes. For the 0- and 15-minute time points, the mice were bled by retro-orbital sinus to collect enough blood to measure plasma insulin by ELISA (Meso Scale Discovery). For the remaining time points, blood was collected from the tail tip. For each day that we performed a GTT or an ITT, 2–3 age-matched B6/J males on 4% fat irradiated diet (5LG6, Purina) were included in the testing as positive controls, quality controls, and for reference values. The mean values for each GTT and ITT of the quality control groups, expressed as the percent change from the initial value, were comparable across all runs ($n = 5$ for the GTT; $n = 6$ for the ITT; $p = 0.12$ for the difference among runs for both the GTT and ITT [repeated measures MANOVA]). After 4–5 weeks on diets, food consumption over periods of 3–7 days was measured: the grain in the hopper was weighed before and after the allotted time; after the allotted time, the bedding was sifted and the weight of the wasted food was subtracted from the weight of the food removed from the hopper. Rapamycin did not decrease food intake for any strain. Mice were sacrificed after 6 weeks on the diets. The mice were weighed and bled for sera by retro-orbital sinus immediately before sacrifice by cervical dislocation. Pancreas and a portion of the liver from each mouse were frozen in liquid nitrogen and stored at −80°C. Epididymal, retroperitoneal, and inguinal fat pads were weighed and frozen in liquid nitrogen and stored at −80°C. Pancreatic Insulin Content (PIC) was determined by extracting the insulin from the weighed pancreas by homogenization in acid/ethanol (1.5% HCl, 70% EtOH); insulin concentration was determined by ELISA (Meso Scale Discovery, Gaithersburg, MD, USA). Aliquots of acid/ethanol samples were neutralized in an equal volume of 1M Tris (pH 7.5) before further dilution (50 fold) in "Diluent 100" provided in the ELISA kit. Sera from sacrifice were measured for glucose, triglycerides, total cholesterol, and non-esterified free fatty acids using the UniCel DxC 600 Synchron clinical system (Beckman Coulter, Inc., Brea, CA, USA), and for insulin by ELISA (MSD).

Statistical analysis

ANOVA (JMP, SAS Institute, Inc., Cary, NC, USA) was used for within-strain comparisons for effect of treatment. Repeated measures MANOVA (JMP) was used to determine within-strain effects of treatment on ITT, GTT and body weight gain.

ACKNOWLEDGEMENTS

The authors wish to thank Clinton M. Astle for help procuring the diets; Vicki Ingalls, Nelson Durgin, Leonor Robidoux, and Jennifer Davidson for excellent care and maintenance of the mice; Joanne Currer for her help editing the manuscript; Dr. Edward H. Leiter for reviewing the manuscript. All procedures were approved by the Animal Care and Use Committee of the Jackson Laboratory (Animal Use Summary #99084) to comply with the guidelines of the United States of America Federal Government.

CONFLICTS OF INTEREST

The authors have no conflict of interests to declare.

FUNDING

This work was supported by the National Institutes of Health (AG022308 to DEH) and by support to the Jackson Laboratory Summer Student Program (Barbara H. Sanford Endowed Scholarship Fund). The authors report no conflicts of interest.

REFERENCES

1. Harrison DE, Strong R, Sharp ZD, Nelson JF, Astle CM, Flurkey K, Nadon NL, Wilkinson JE, Frenkel K, Carter CS, Pahor M, Javors MA, Fernandez E, Miller RA. Rapamycin fed late in life extends lifespan in genetically heterogeneous mice. Nature. 2009; 460:392–95. doi: 10.1038/nature08221

2. Miller RA, Harrison DE, Astle CM, Baur JA, Boyd AR, de Cabo R, Fernandez E, Flurkey K, Javors MA, Nelson JF, Orihuela CJ, Pletcher S, Sharp ZD, et al. Rapamycin, but not resveratrol or simvastatin, extends life span of genetically heterogeneous mice. J Gerontol A Biol Sci Med Sci. 2011; 66:191–201. doi: 10.1093/gerona/glq178

3. Wilkinson JE, Burmeister L, Brooks SV, Chan CC, Friedline S, Harrison DE, Hejtmancik JF, Nadon N, Strong R, Wood LK, Woodward MA, Miller RA. Rapamycin slows aging in mice. Aging Cell. 2012; 11:675–82. doi: 10.1111/j.1474-9726.2012.00832.x

4. Kaeberlein M, Powers RW 3rd, Steffen KK, Westman EA, Hu D, Dang N, Kerr EO, Kirkland KT, Fields S, Kennedy BK. Regulation of yeast replicative life span by TOR and Sch9 in response to nutrients. Science. 2005; 310:1193–96. doi: 10.1126/science.1115535

5. Powers RW 3rd, Kaeberlein M, Caldwell SD, Kennedy BK, Fields S. Extension of chronological life span in yeast by decreased TOR pathway signaling. Genes Dev. 2006; 20:174–84. doi: 10.1101/gad.1381406

6. Jia K, Chen D, Riddle DL. The TOR pathway interacts with the insulin signaling pathway to regulate *C. elegans* larval development, metabolism and life

span. Development. 2004; 131:3897–906. doi: 10.1242/dev.01255

7. Kapahi P, Zid BM, Harper T, Koslover D, Sapin V, Benzer S. Regulation of lifespan in *Drosophila* by modulation of genes in the TOR signaling pathway. Curr Biol. 2004; 14:885–90. doi: 10.1016/j.cub.2004.03.059

8. Vellai T, Takacs-Vellai K, Zhang Y, Kovacs AL, Orosz L, Müller F. Genetics: influence of TOR kinase on lifespan in *C. elegans.* Nature. 2003; 426:620. doi: 10.1038/426620a

9. Barlow AD, Nicholson ML, Herbert TP. Evidence for rapamycin toxicity in pancreatic β-cells and a review of the underlying molecular mechanisms. Diabetes. 2013; 62:2674–82. doi: 10.2337/db13-0106

10. Blagosklonny MV. Once again on rapamycin-induced insulin resistance and longevity: despite of or owing to. Aging (Albany NY). 2012; 4:350–58. doi: 10.18632/aging.100461

11. Lamming DW, Ye L, Katajisto P, Goncalves MD, Saitoh M, Stevens DM, Davis JG, Salmon AB, Richardson A, Ahima RS, Guertin DA, Sabatini DM, Baur JA. Rapamycin-induced insulin resistance is mediated by mTORC2 loss and uncoupled from longevity. Science. 2012; 335:1638–43. doi: 10.1126/science.1215135

12. Lamming DW, Ye L, Astle CM, Baur JA, Sabatini DM, Harrison DE. Young and old genetically heterogeneous HET3 mice on a rapamycin diet are glucose intolerant but insulin sensitive. Aging Cell. 2013; 12:712–18. doi: 10.1111/acel.12097

13. Fang Y, Westbrook R, Hill C, Boparai RK, Arum O, Spong A, Wang F, Javors MA, Chen J, Sun LY, Bartke A. Duration of rapamycin treatment has differential effects on metabolism in mice. Cell Metab. 2013; 17:456–62. doi: 10.1016/j.cmet.2013.02.008

14. Blagosklonny MV. TOR-centric view on insulin resistance and diabetic complications: perspective for endocrinologists and gerontologists. Cell Death Dis. 2013; 4:e964. doi: 10.1038/cddis.2013.506

15. Chang GR, Wu YY, Chiu YS, Chen WY, Liao JW, Hsu HM, Chao TH, Hung SW, Mao FC. Long-term administration of rapamycin reduces adiposity, but impairs glucose tolerance in high-fat diet-fed KK/HlJ mice. Basic Clin Pharmacol Toxicol. 2009; 105:188–98. doi: 10.1111/j.1742-7843.2009.00427.x

16. Chang GR, Chiu YS, Wu YY, Chen WY, Liao JW, Chao TH, Mao FC. Rapamycin protects against high fat diet-induced obesity in C57BL/6J mice. J Pharmacol Sci. 2009; 109:496–503. doi: 10.1254/jphs.08215FP

17. Deepa SS, Walsh ME, Hamilton RT, Pulliam D, Shi Y, Hill S, Li Y, Van Remmen H. Rapamycin modulates markers of mitochondrial biogenesis and fatty acid oxidation in the adipose tissue of db/db mice. J Biochem Pharmacol Res. 2013; 1:114–23.

18. Das A, Durrant D, Koka S, Salloum FN, Xi L, Kukreja RC. Mammalian target of rapamycin (mTOR) inhibition with rapamycin improves cardiac function in type 2 diabetic mice: potential role of attenuated oxidative stress and altered contractile protein expression. J Biol Chem. 2014; 289:4145–60. doi: 10.1074/jbc.M113.521062

19. Liu Y, Diaz V, Fernandez E, Strong R, Ye L, Baur JA, Lamming DW, Richardson A, Salmon AB. Rapamycin-induced metabolic defects are reversible in both lean and obese mice. Aging (Albany NY). 2014; 6:742–54. doi: 10.18632/aging.100688

20. Makki K, Taront S, Molendi-Coste O, Bouchaert E, Neve B, Eury E, Lobbens S, Labalette M, Duez H, Staels B, Dombrowicz D, Froguel P, Wolowczuk I. Beneficial metabolic effects of rapamycin are associated with enhanced regulatory cells in diet-induced obese mice. PLoS One. 2014; 9:e92684. doi: 10.1371/journal.pone.0092684

21. Reifsnyder PC, Doty R, Harrison DE. Rapamycin ameliorates nephropathy despite elevating hyperglycemia in a polygenic mouse model of type 2 diabetes, NONcNZO10/LtJ. PLoS One. 2014; 9:e114324. doi: 10.1371/journal.pone.0114324

22. Leontieva OV, Paszkiewicz GM, Blagosklonny MV. Weekly administration of rapamycin improves survival and biomarkers in obese male mice on high-fat diet. Aging Cell. 2014; 13:616–22. doi: 10.1111/acel.12211

23. Iwatsuka H, Shino A, Suzuoki Z. General survey of diabetic features of yellow KK mice. Endocrinol Jpn. 1970; 17:23–35. doi: 10.1507/endocrj1954.17.23

24. Bray GA, York DA. Genetically transmitted obesity in rodents. Physiol Rev. 1971; 51:598–646.

25. Leiter EH, Reifsnyder PC. Differential levels of diabetogenic stress in two new mouse models of obesity and type 2 diabetes. Diabetes. 2004 (Suppl 1); 53:S4–11. doi: 10.2337/diabetes.53.2007.S4

26. Hummel KP, Coleman DL, Lane PW. The influence of genetic background on expression of mutations at the diabetes locus in the mouse. I. C57BL-KsJ and C57BL-6J strains. Biochem Genet. 1972; 7:1–13. doi: 10.1007/BF00487005

27. Kim JH, Sen S, Avery CS, Simpson E, Chandler P, Nishina PM, Churchill GA, Naggert JK. Genetic analysis of a new mouse model for non-insulin-dependent diabetes. Genomics. 2001; 74:273–86. doi: 10.1006/geno.2001.6569

28. Wu C, Okar DA, Newgard CB, Lange AJ. Increasing fructose 2,6-bisphosphate overcomes hepatic insulin resistance of type 2 diabetes. Am J Physiol Endocrinol Metab. 2002; 282:E38–45.

29. Yin J, Zuberi A, Gao Z, Liu D, Liu Z, Ye J. Shilianhua extract inhibits GSK-3beta and promotes glucose metabolism. Am J Physiol Endocrinol Metab. 2009; 296:E1275–80. doi: 10.1152/ajpendo.00092.2009

30. Chen LN, Lyu J, Yang XF, Ji WJ, Yuan BX, Chen MX, Ma X, Wang B. Liraglutide ameliorates glycometabolism and insulin resistance through the upregulation of GLUT4 in diabetic KKAy mice. Int J Mol Med. 2013; 32:892–900.

31. Sataranatarajan K, Ikeno Y, Bokov A, Feliers D, Yalamanchili H, Lee HJ, Mariappan MM, Tabatabai-Mir H, Diaz V, Prasad S, Javors MA, Ghosh Choudhury G, Hubbard GB, et al. Rapamycin increases mortality in *db/db* mice, a mouse model of type 2 diabetes. J Gerontol A Biol Sci Med Sci. 2016; 71:850–57. doi: 10.1093/gerona/glv170

32. Coleman DL, Leiter EH, Schwizer RW. Therapeutic effects of dehydroepiandrosterone (DHEA) in diabetic mice. Diabetes. 1982; 31:830–33. doi: 10.2337/diab.31.9.830

33. Wilkinson JE, Burmeister L, Brooks SV, Chan CC, Friedline S, Harrison DE, Hejtmancik JF, Nadon N, Strong R, Wood LK, Woodward MA, Miller RA. Rapamycin slows aging in mice. Aging Cell. 2012; 11:675–82. doi: 10.1111/j.1474-9726.2012.00832.x

34. Leontieva OV, Demidenko ZN, Blagosklonny MV. Rapamycin reverses insulin resistance (IR) in high-glucose medium without causing IR in normoglycemic medium. Cell Death Dis. 2014; 5:e1214. doi: 10.1038/cddis.2014.178

35. Forbes JM, Cooper ME. Mechanisms of diabetic complications. Physiol Rev. 2013; 93:137–88. doi: 10.1152/physrev.00045.2011

36. Leibowitz G, Cerasi E, Ketzinel-Gilad M. The role of mTOR in the adaptation and failure of beta-cells in type 2 diabetes. Diabetes Obes Metab. 2008 (Suppl 4); 10:157–69.
doi: 10.1111/j.1463-1326.2008.00952.x

37. Schwartz SS, Epstein S, Corkey BE, Grant SF, Gavin JR 3rd, Aguilar RB. The time is right for a new classification system for diabetes: rationale and implications of the ß-cell-centric classification schema. Diabetes Care. 2016; 39:179–86. doi: 10.2337/dc15-1585

Research Paper

Biological and biophysics aspects of metformin-induced effects: cortex mitochondrial dysfunction and promotion of toxic amyloid pre-fibrillar aggregates

Pasquale Picone[1], Silvia Vilasi[2], Fabio Librizzi[2], Marco Contardi[2,4], Domenico Nuzzo[1], Luca Caruana[1], Sara Baldassano[3], Antonella Amato[3], Flavia Mulè[3], Pier Luigi San Biagio[2], Daniela Giacomazza[2], and Marta Di Carlo[1]

[1]Istituto di Biomedicina e Immunologia Molecolare, CNR, Palermo, Italy
[2]Istituto di Biofisica, CNR, Palermo, Italy
[3]Departimento di Scienze e Tecnologie Biologiche, Chimiche e Farmaceutiche, University of Palermo, Palermo, Italy
[4]Current address: Italian Institute of Technology, Genova, Italy

Correspondence to: Daniela Giacomazza; Marta Di Carlo; **email:** daniela.giacomazza@cnr.it; marta.dicarlo@ibim.cnr.it
Key words: Alzheimer's disease, metformin, mitochondrial dysfunction, cell degeneration, mitochondrial pores, β-amyloid aggregation
Received: June 28, 2016 **Accepted:** July 15, 2016 **Published:** July 28, 2016 doi:10.18632/aging.101004

ABSTRACT

The onset of Alzheimer disease (AD) is influenced by several risk factors comprising diabetes. Within this context, antidiabetic drugs, including metformin, are investigated for their effect on AD. We report that in the C57B6/J mice, metformin is delivered to the brain where activates AMP-activated kinase (AMPK), its molecular target. This drug affects the levels of β-secretase (BACE1) and β-amyloid precursor protein (APP), promoting processing and aggregation of β-amyloid (Aβ), mainly in the cortex region. Moreover, metformin induces mitochondrial dysfunction and cell death by affecting the level and conformation of Translocase of the Outer Membrane 40 (TOM40), voltage-dependent anion-selective channels 1 (VDAC1) and hexokinase I (HKI), proteins involved in mitochondrial transport of molecules, including Aβ. By using biophysical techniques we found that metformin is able to directly interact with Aβ influencing its aggregation kinetics and features. These findings indicate that metformin induces different adverse effects, leading to an overall increase of the risk of AD onset.

INTRODUCTION

According to Rotterdam Study, individuals with metabolic pathologies such as Type2 diabetes (T2DM) or Obesity have almost a two-fold greatest risk of developing Alzheimer's disease (AD) [1]. AD is the most common cause of dementia in the elderly and it is associated with a progressive impairment of cognitive function, orientation, and difficulties with problem-solving or language. Thus, in patients with AD, gradually, over the time, more parts of the brain are damaged developing progressive symptoms, leading to death. Thirty-five millions of persons in the world are now considered to be affected by AD and this number is expected to double in the next few decades [2]. Even if the etiological defects in AD are not well known, prevalent ideas implicate build-up of soluble β-amyloid (Aβ) oligomers or insoluble plaques or neurofibrillary tangles [3,4]. Aβ is a 39–43 amino acid peptide formed from the cleavage of amyloid precursor protein (APP), a transmembrane glycoprotein. Neurofibrillary tangles are, instead, produced by hyperphosphorylation of Tau, a protein associated with microtubules in neurons [5]. Aging is the primary risk factor for the development of AD and many other pathological conditions occurring in older people, including T2DM. Change in cognitive function and increase of neurodegeneration markers were found both in patients with T2DM and/or obesity [6] and in insulin-resistant obese mice [7], suggesting the existence of a common molecular mechanism. Some

studies have identified in insulin resistance condition the link among the pathophysiology of metabolic disorders and the brain alteration [8–10]. Insulin has a significant role in modulation of synaptic plasticity and learning memory and a high number of Insulin Receptor (IR) are present in brain [9,11]. Modification in the insulin concentration and IR number have been reported in AD cell model [12] and AD brain, leading to the result that AD can be considered as a brain diabetes or "Type 3 Diabetes" [13]. On the basis of this association between metabolic disorders and impaired cognition it should be relevant to investigate whether a potential risk or benefit could occur by using antidiabetic treatments on brain health [14,15].

Evidences on the association between antidiabetic medication and the risk of AD are conflicting and not well documented [16]. One of the few classes of therapeutics, efficient in lowering glucose production are the biguanides, which include molecules as phenformin (2-N-phenethylcarbamimidoyl guanidine) and metformin (1,2-dimethylbiguanide hydrochloride). In particular, the last is the most frequently prescribed drug for T2DM or other metabolic diseases. On the basis of its physicochemical structure and properties, metformin is a small amphoteric molecule (129 Da) with pKa values of 2.8 and 11.5. These characteristics are associated to high water solubility and low lipid solubility. Studies both in vitro and in vivo, indicate that metformin increases the production of Aβ [17], suggesting that its long-term administration may promote AD onset. On the contrary, a neuropathological study has reported that people treated both with insulin and oral antidiabetic drugs had developed a significantly lower amyloid plaque density [18]. A recent population-based case-control study examined the relationship between T2DM and administration of different antidiabetic drugs and risk of AD development. The authors conclude that long-term users of metformin may have a somewhat higher risk of AD onset and development [19]. However, poor information is available about the molecular mechanism activated by metformin. Some reports indicate that it is able to stimulate AMP activated protein kinase (AMPK), an enzyme activated when cellular energy levels are altered [20]. Recently, in vitro and ex vivo studies have demonstrated that metformin favors APP and presenilin increase and induces Aβ production and aggregation [21]. Furthermore, metformin acts as a pro-oxidant molecule inducing oxidative stress and mitochondrial dysfunction that, in turn, activates Nf-κB, a transcription factor involved in regulation of APP and presenilin gene expression. Lastly, these molecular mechanisms are counteracted by insulin co-administration [21].

Functional and structural mitochondrial defects contribute to the pathogenesis of aged-related diseases. Metformin affects mitochondria by inducing depolarization of the mitochondrial phospholipidic membrane [21,22] and inhibiting the mitochondrial complex I of the respiratory chain [23,24]. Moreover, the use of metformin changes the expression of several proteins involved in metabolic processes, the regulation of apoptosis and the structural preservation of brain mitochondria [25]. Impairing of exchange of molecule between cytoplasm and mitochondria is one of the cause of mitochondrial dysfunction. The Translocase of the Outer Membrane (TOM) complex, of which TOM40 is the key subunit, is the main gateway for the import of most mitochondrial proteins synthesized in the cytoplasm. The complex is relevant also for mitochondrial biogenesis and its damage triggers mitochondrial dysfunction [26]. Furthermore, opening and closure of the mitochondrial permeability transition (MPT) pore, in which voltage-dependent anion-selective channels 1 (VDAC1), also known as mitochondrial porin, is one of the main proteins, is impaired in patients with neurodegenerative diseases [27]. Moreover, VADC1 interacts with hexokinase I (HKI) and this binding protects against cell death [28]. Thus, the correct mitochondrial transport of ions, metabolites and molecules affects cell survival and death mechanisms.

From a molecular point of view, the overproduction and aberrant self-assembly of the amyloid β peptide (Aβ) into fibrillar aggregates constitute the first step of the so-called amyloid cascade hypothesis, thought to trigger AD [29]. These extremely toxic oligomers [30,31] have high hydrophobicity, are small [32] and constitute a heterogeneous group characterized by several highly dynamic different assemblies with multiple conformational states. Although the mechanism of cytotoxicity is not yet fully understood, it has been ascertained that amyloid oligomers are the most toxic species [30,31]; in fact, they directly interact with and affect cell plasma membranes by forming pores and consequently disrupting several cellular processes. Amyloid fibrils have also been recently demonstrated to modify the membrane integrity. In fact, they interacting with lipid bilayers are destabilized and disassembled in the pre-fibrillar toxic forms, inducing cell dysfunction, although to a lesser extent [31,33–35].

From a molecular point of view, the self-assembly of Aβ peptides in well-ordered fibrils constituting the senile plaques found in AD brains, is a complex process composed by several steps. It is characterized by multiple transitional aggregation species as initial seeds, soluble small oligomers, protofibrils and insoluble

amyloid fibrils, with a β-sheet conformation. The kinetics of amyloid formation is best described by a sigmoid curve and can be schematically described in three stages [36,37]:

1) the slow lag nucleation phase, in which monomers gradually undergo a secondary structure conformational change from random coil to β-sheet and associate to form oligomeric nuclei/protofibrils;
2) the fast exponential elongation phase, in which the soluble species are progressively arranged at the ends of preformed β-sheet rich structures in a thermo-dynamically favorable process.
The initial oligomeric nuclei rapidly grow by further addition of monomers forming larger fibrils;
3) the saturation phase, in which the fibrils are completely formed and associate each other giving rise to stable mature fibers.

In this study we assessed the molecular effects of metformin in specific brain area of mice. Difference in Aβ deposits, expression of AD markers and proteins involved in mitochondrial dysfunction were found between cortex and hippocampus regions of quite young mice. Furthermore, the direct interaction between metformin and Aβ aggregate formation was determined by in vitro biophysical study.

RESULTS

Metformin is a fluorescent molecule able to reach the brain

Absorption or fluorescence phenomena of ultraviolet or visible lights by a molecule depend on electron transitions between molecular orbital energy levels. Due to the presence of two double conjugated bonds the possibility of fluorescence phenomenon in metformin has been investigated. The emission spectrum obtained by fluorescence measurements indicates that metformin, once excited at 395 or 488 nm, has the emission peaks at 475 and 520 nm, respectively (data not shown). This property allows analyzing the presence of metformin into the brain of mice after its dispersion in drinking water. Metformin was administered to C57B6/J mice and after seven days the mice were sacrificed and the brains analyzed by using an imaging instrument. A strong signal was detected in the treated mice whereas no signal was found in the control, thus indicating that metformin has reached the brain (Fig. 1a,b). The delivery of metformin to the brain was confirmed by the increased levels of phosphorylated AMP-activated kinase (AMPK), one of the main molecular target of metformin (Fig. 1c,d). Thus, metformin crosses the blood brain barrier (BBB) and has an impact on the brain biochemical pathways.

Chronic metformin treatment stimulates APP processing mainly in brain cortex region

To ascertain the possibility that metformin is a risk factor for AD onset, especially in long term administration, C57B6/J mice were treated with metformin for seven days or three months. After these treatments proteins extracted from cortex and hippocampus, two-brain area mainly damaged in AD, were submitted to Western blot. Changes in the levels of BACE1, an enzyme required for APP processing to produce Aβ, its pathogenic cleavage product, and the same APP were measured. Activation of AMPK was evaluated for confirming the biochemical activity of metformin in the brain (Fig. 2). An increase of the levels of BACE1 and APP expression was detected in the cortex after seven days of treatment (Fig. 2a). In contrast, an increase of BACE1, and a decrease of APP were found after chronic treatment in the cortex, suggesting that an enhanced processing may be occurred (Fig. 2c). Furthermore, after both treatments, no significant differences in BACE1 and APP expression in the hippocampus were detected (Fig. 2b, d). To validate the hypothesis that the decreased presence of APP in the cortex was a consequence of the β-secretase increased activity, a quantitative real-time PCR (qRT-PCR) experiment was performed. No significant change was observed in APP transcript, strongly signifying that the produced protein was quickly processed (Fig. 2e).

Metformin induces accumulation of Aβ aggregates mainly in brain cortex region

Since the obtained results after three months of treatment suggested an augmented processing of APP mainly in the cortex, we explored the possibility that an increase of Aβ production could have enhanced its aggregation and deposition in the extracellular area. By immunofluorescence analysis, using coronary brain sections, in which cerebral cortex and hippocampus were visible, and anti-APP antibody we observed a diffuse staining around the nuclei of the control and a punctate staining around the cells of treated cortex, suggesting presence of aggregates due to increased processing (Fig. 3a). However, this result was confirmed by staining with Thioflavin T (Fig. 3b), a dye used to reveal the presence of β-sheet protein aggregates because of the increase of its fluorescence emission intensity upon binding to the linear array of β-strand aggregates [38,39]. In particular, we observed aggregates with a dimension ranging below 1 μm mainly in the cortex (Fig. 3b). In contrast, no significant immunoreactivity, or presence of Aβ aggregates, was detectable in hippocampus (Fig. 3a, b).

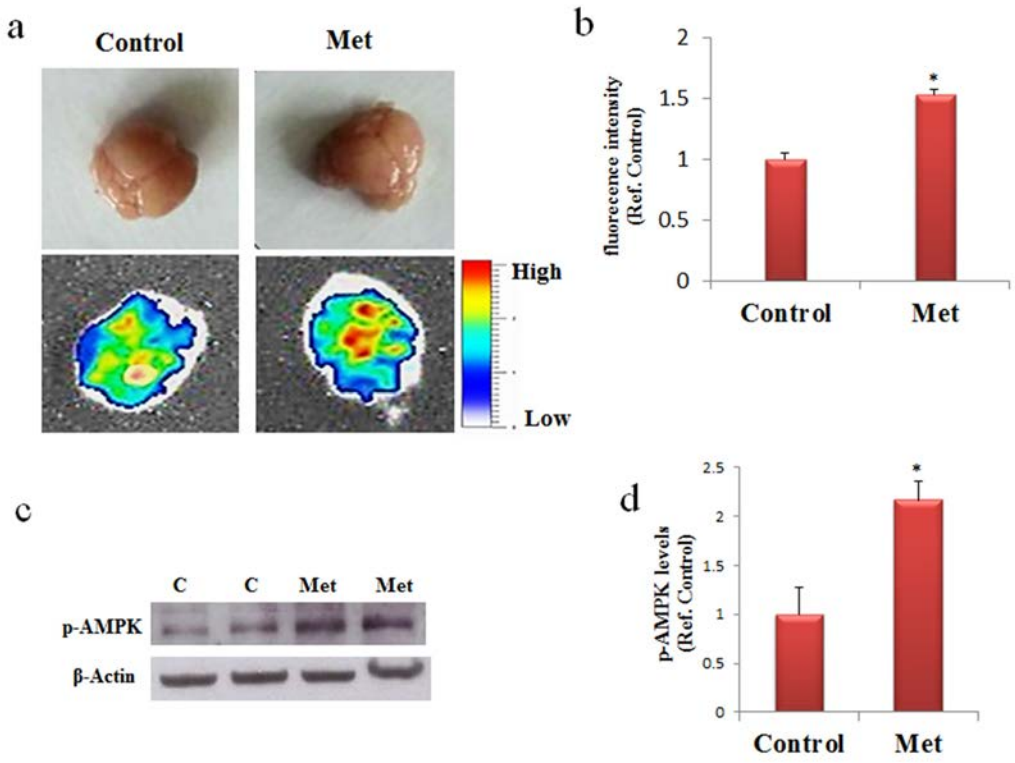

Figure 1. Metformin reaches the brain and activate AMPK. **(a)** and **(b)** Mice were untreated or treated with metformin for seven days and the fluorescence in the brain was quantified by bioimaging. Fluorescence values are referred to the control. **(c)** Western blot of proteins extracted from brains of metformin untreated (C) or treated mice (Met) and incubated with phospho-AMPK (p-AMPK) and β-Actin (loading control) antibodies. **(d)** Quantification of immunoreactivity using densitometric analysis. Representative images from 2 animals for condition are shown. n=5 per group.

Metformin induces mitochondrial dysfunction by impairing MPT pores and membrane channels

Specific mitochondrial proteins involved in distinctive structures regulate cross talk and transport of proteins and metabolites between cytoplasm and mitochondria. We addressed the question if metformin treatment might contribute to the alteration of the components of mitochondrial machinery. After three months of treatment changes in levels of expression were analyzed for some proteins involved in mitochondrial transport of different molecules and markers of mitochondrial dysfunction such as TOM40, VDAC1 and HKI. Western blot of proteins extracted from both cortex and hippocampus of mice treated with metformin and controls were incubated with antibodies against TOM40, VDAC1 and HKI. In agreement with previous data, Western blot analysis showed changes in the levels of expression of the analyzed proteins only in the cortex region. An increase of TOM40 was detected indicating an impairing of MPT pores (Fig. 4a). Further, an increase of total VDAC1 levels were observed in cortex where, in particular, we found together with VDAC1 monomers some dimers and trimers, suggesting that a fraction of the VDAC1 in the membrane is organized in oligomers (Fig. 4c). Moreover, the lower band, indicated by the red arrow in Figure 4C, represents a monomeric species whose electrophoretic mobility is modified by the intramolecular crosslinking of the VDAC1 N-terminal domain. A decrease of HKI amount was also detected suggesting that probably a detachment from VDAC1 was occurred (Fig. 4e). TOM40, VDAC1 and HKI levels were not significantly affected in the hippocampus brain area (Fig. 4b, d, f).

Metformin induces neuronal apoptosis

To assess whether, after chronic metformin treatment, apoptotic cell death occurred in vivo, presence of fragmented DNA was examined in cortex and hippocampus brain sections by the terminal deoxynucleotidyl

transferase-mediated, dUTP, nick end labeling (TUNEL) method. TUNEL-positive cells in brain sections of metformin treated mice were markedly higher in cortical region than in hippocampal region or control (Fig. 5a, b).

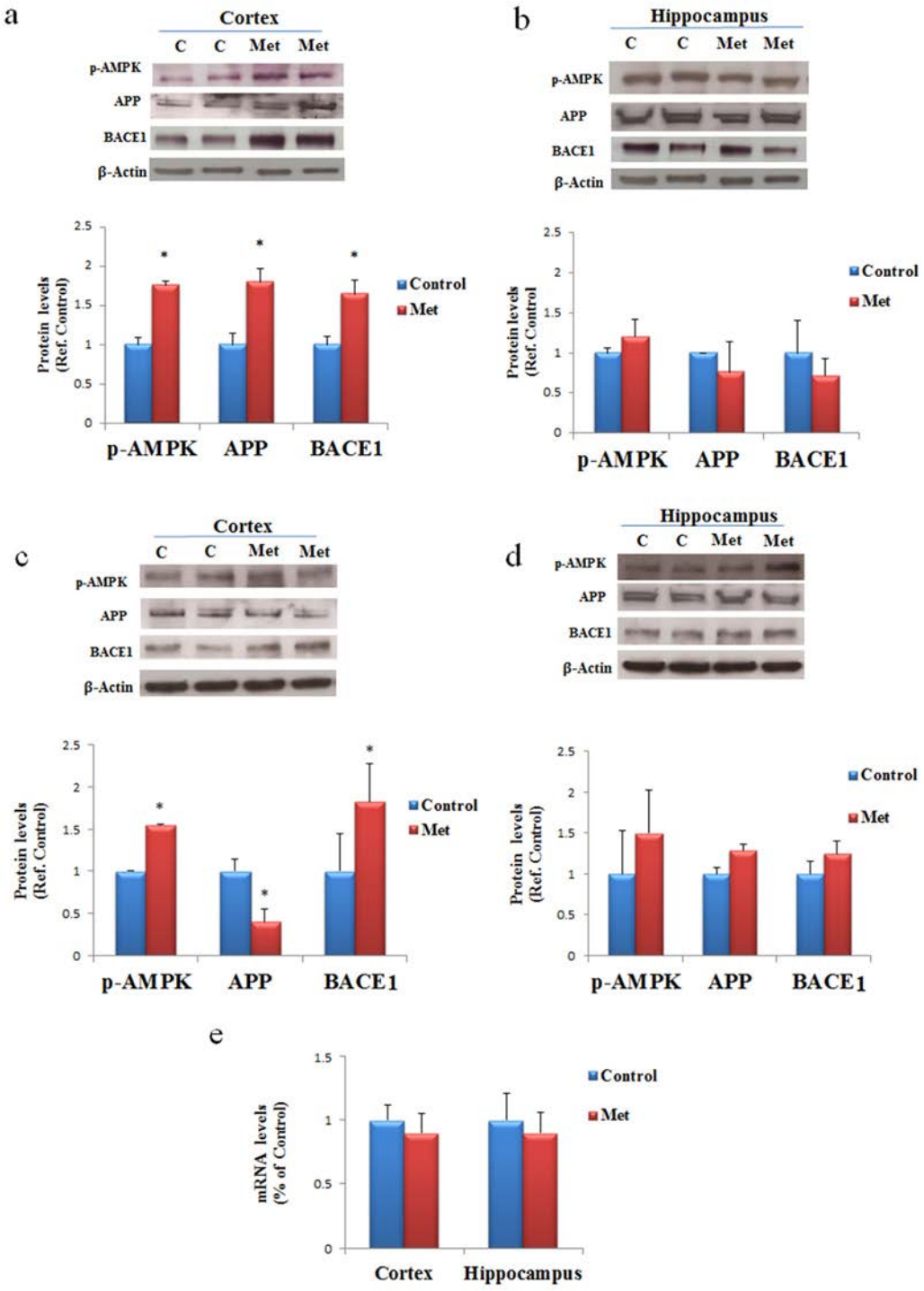

Figure 2. AD biomarkers are differently activated by metformin treatment in brain regions. Western blot of protein extracted from brain lysates of mice cortex **(a)** and hippocampus **(b)** after seven days of metformin treatment and incubated with anti-phospho-AMPK (p-AMPK), APP, BACE and β-Actin (loading control) antibodies. Western blot of protein extracted from brain lysates of mice cortex **(c)** and hippocampus **(d)** after chronic metformin treatment and incubated with anti-phospho-AMPK (p-AMPK), APP, BACE1 and β-Actin (loading control) antibodies. Quantification of immunoreactivity was performed using densitometric analysis. **(e)** Effect of chronic metformin treatment on APP transcript levels determined by quantitative real-time PCR in cortex and hippocampus regions. n=5 per group.

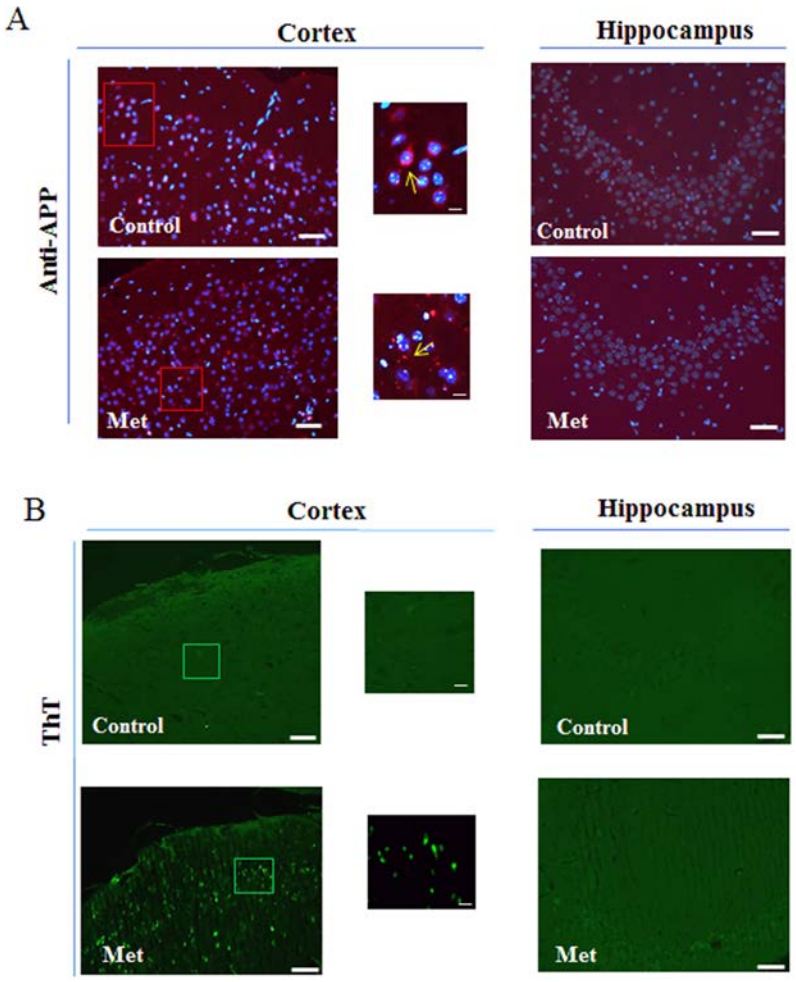

Figure 3. Metformin induces accumulation of Aβ aggregates. (a) Immunofluorescence of cerebral cortex and hippocampus sections of metformin treated mice stained using anti-APP. Nuclei were stained with Hoechst 33258 and merged images with anti-APP staining are shown. **(b)** ThT staining of Aβ aggregates on coronary sections. High magnification of the squared areas is shown. Yellow arrows in the zoomed images indicate diffuse or punctate anti-APP staining. 20X original magnification. Scale bars = 50 μm and 5 μm in the zoomed images. n=5 per group.

Metformin directly interacts with Aβ peptide influencing its aggregation kinetics in vitro

In order to assess whether metformin is also able to directly interact with Aβ peptide influencing its aggregation process we performed the fibrillogenesis kinetics by ThT assay. Figure 6 shows the time course of the ThT signal during the fibrillation kinetics of 50 μM Aβ incubated at 37°C in the absence and in the presence of 2mM metformin. The kinetics followed the typical nucleation-polymerization process, described by the sigmoidal profile [36]. In the presence of metformin, the lag phase increased and the amount of final fibrils is reduced in comparison with control. Metformin addition seemed to reduce the effective Aβ concentration leading to initial nuclei, thus interfering with lag-phase.

This result was confirmed by circular dichroism (CD) experiments. CD spectra are sensitive to the secondary structure variation accompanying amyloid cross-β-structure formation during fibrillogenesis. In the initial phase of the aggregation process, the Aβ CD spectrum presents a single minimum that, typical of a random coil structure, is around 200 nm. The minimum shifts towards higher wavelength during amyloid formation. Our results have shown that the presence of 2 mM of

metformin delayed the β-sheet structure formation of a 50 μM Aβ1-40 solution. In fact, while the control sample reached the end point of the aggregation reaction (Fig. 7a) after 0.5 h, no significant changes were observed in the presence of the drug in the same time interval indicating that the peptide retained its disordered structure (Fig. 7b), in fully agreement with the fluorescence data. Always in accordance with ThT assay, after 2 h both the samples completed their conversion.

The reduced amount of Aβ1-40 fibrils detected by ThT assay in the presence of metformin was confirmed by AFM measurements. In Figure 8a-d the morphology of the aggregates formed at the end of the kinetics in the absence and in the presence of metformin are reported. Amyloid fibrils result reduced in number and length when metformin is added in solution. Moreover, prefibrillar oligomeric aggregates are observed at the end of the kinetics of the peptide incubated with the drug.

The characterization of the action of metformin on the aggregation process of Aβ1-40 peptide was followed by Dynamic Light Scattering (DLS) experiments. Although not specifically focused on chemico-physical features characterizing amyloid formation, like conversion to cross-β-structure, the addition of DLS to other biophysical techniques provides important quantitative information on the hydrodynamic size variation occurring during an aggregation process. In this sense, it represents a suitable technique to monitor the influence of an exogenous molecule on the protein assembly, and, therefore, it is often used for testing drugs for therapeutic purposes. Moreover, light scattering technique does not need the use of extrinsic probes, whose evaluation of their potential influence on the process under study requires high carefulness [40]. Figures 8e and f show the hydrodynamic diameter DH distribution functions of a sample of Aβ1-40 peptide undergone to the amyloid formation protocol (37°C and 200 rpm under stirring) with and without metformin,

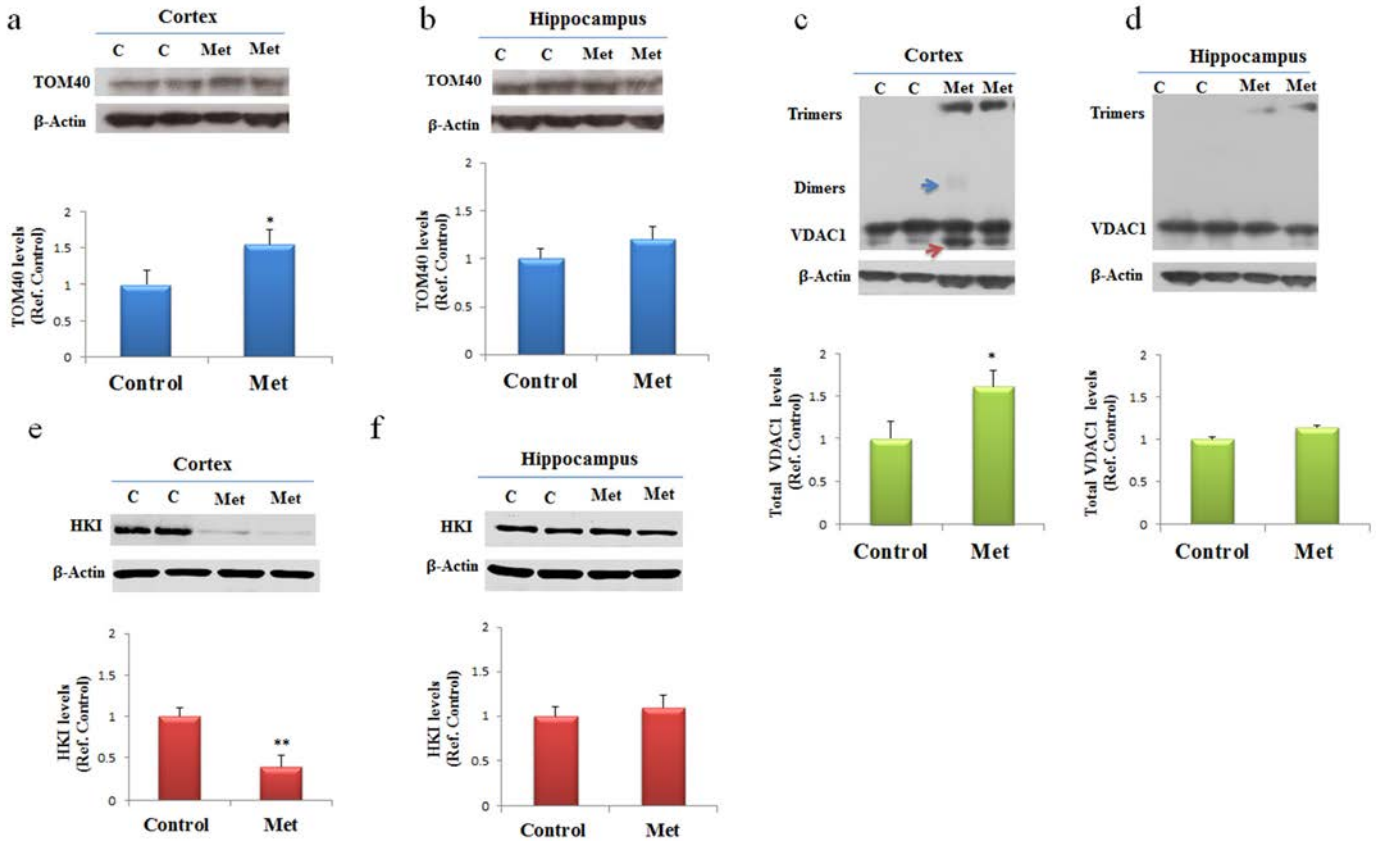

Figure 4. Metformin after chronic administration, changes TOM40 expression levels and induces VDAC1 oligomerization, and affects Hexokinase I (HKI) in the cortex region. We stern blot of protein extracted from brain lysates of mice cortex **(a, c, e)** and hippocampus **(b, d, f)** after chronic metformin treatment and incubated with anti- TOM40, VDAC1, Hexokinase I (HKI), and β-Actin (loading control) antibodies. Quantitative analysis of total VDAC1, HKI and TOM40 levels relative to β-actin was performed using densitometric analysis. The blue arrow indicates a VDAC1 dimers and the red arrow indicates VDAC1 monomers with modified electrophoretic mobility. n=5 per group.

respectively after 0.5 h from the beginning of the process and at the end of the experiment observation (2 h). The increase in ThT assay (Fig. 6) and variation in CD spectra (Fig. 7) reveal that, at that time, in the absence of metformin a significant amyloid cross-β-structure has already formed. Correspondently, two size distributions are revealed by DLS analysis: one centered at around 300 nm and the other one corresponding to larger species of the order of microns. At the same time, in the presence of metformin this higher size species is not formed and only the appearance of species at around 300 nm occurs.

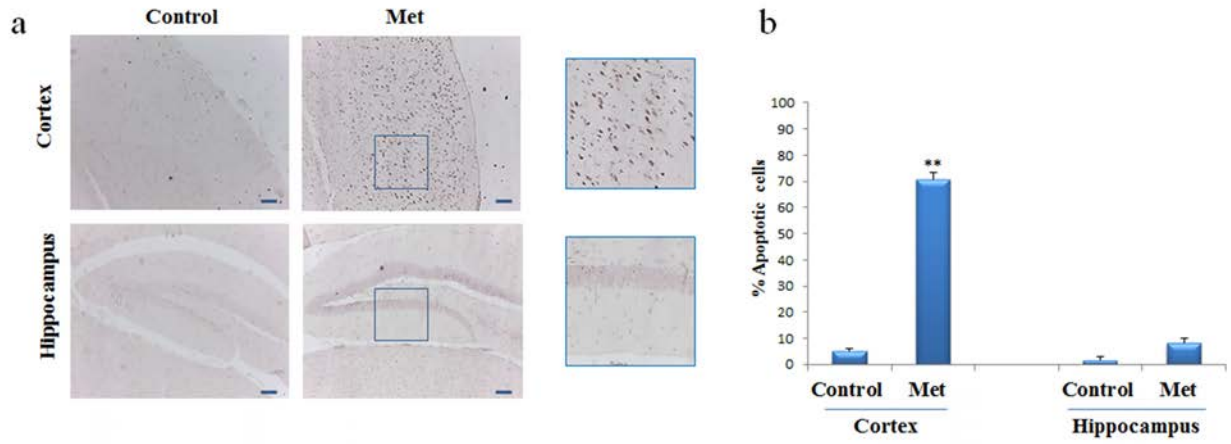

Figure 5. Metformin induces apoptosis mainly in neurons of cortex region. TUNEL assay was performed on the paraffin sections of cortex and hippocampus obtained from mice untreated or treated with metformin to detect apoptotic nuclei (brown). **(a)** Representative cortex and hippocampus brain sections stained with TUNEL in control and metformin treated mice. High magnification of the squared areas is shown. **(b)** The histogram indicates the percentage of positive cells both in cortex and hippocampus regions normalized to the control. 10X original magnification. Scale bars = 100 μm. n=5 per group.

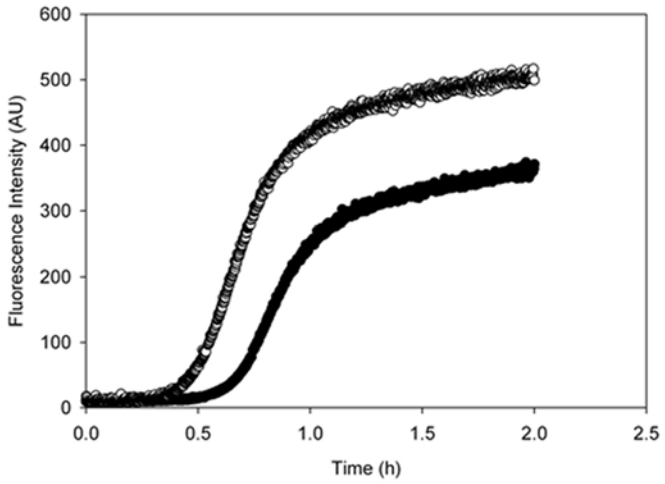

Figure 6. Metformin increases the lag-phase duration and reduces the final amount of amyloid fibrils. Aggregation kinetics of 50 μM $A\beta_{1-40}$ was followed in the absence (empty circles) and in the presence (black circles) of 2mM metformin by ThT assay. The dye concentration was 12μM.

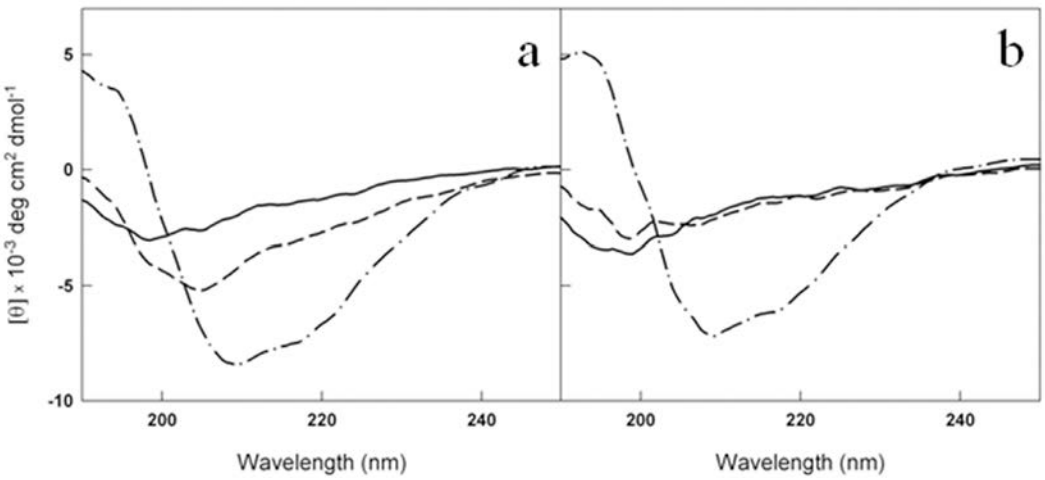

Figure 7. Metformin delays the conversion of $A\beta_{1-40}$ from disordered coil to β-sheet structure. Far-UV CD spectra of 50 μM $A\beta_{1-40}$ at t0 (solid lines), t=0.5 h (dashed lines) and t=2h (dot dashed lines) at 37 °C in the absence **(a)** and in the presence **(b)** of 2mM metformin. The signals from the buffer and metformin in buffer have been subtracted from the spectra in **(a)** and **(b)**, respectively.

The size distribution for samples collected at the end of aggregation kinetics reveals for the Aβ1-40 sample grown in the absence of metformin, a marked shift towards higher values in comparison to the initial time, probably corresponding to mature fibril formation. In contrast, only a little increase in the average hydrodynamic diameter (from 300 to 600 nm) in the correspondent sample incubated with the drug is detectable. The overall results from biophysical techniques converge in indicating that the metformin delays amyloid aggregation of Aβ1-40 peptide, reduces the amount of mature fibrils formed and, more important, stabilizes prefibrillar oligomeric species.

DISCUSSION

We analyzed both biological and biophysical aspects to understand the molecular mechanisms induced by metformin and leading to neurodegeneration in mouse brain. Fluorescence measurements of ex vivo mouse brain performed by using the intrinsic fluorescence signal of the metformin gave us the direct confirmation that the drug had reached the central organ by crossing the BBB. For mouse treatment, an experimental dose, deduced by those utilized in other works, which uses the same C57B6/J strain, was employed [17,21]. In particular, Chen et al. administrating 2mg/ml, and using liquid chromatography-mass spectrometry, measured that metformin reaches a concentration of about 2 μM and 1 μM in the plasma and in the brain, respectively, well below the 10–40 μM achieved in human plasma [20]. Moreover, since the drug is eliminated via renal secretion in few hours, the mice were treated for three months to determine the incidence of long-term administration on the risk of AD developing. Activation of AMPK was considered as a marker of metformin-induced biochemical answer in brain, even if we cannot exclude that the response to metformin could not be limited only to its activation, but mediated by additional mechanisms depending directly or not by AMPK. Furthermore, these data are supported by the finding that metformin uptake in the brain can be mediated by the organic cation transporter 3 (OCT3), a member of the SLC22A family, which in turn modulates the pharmacologic action of metformin on AMPK [41]. After metformin chronic treatment BACE1 and APP, the enzyme-substrate required for Aβ production, are differently modulated, mainly in the cortex where an enhanced APP processing was assumed. This result coincides with the discovery that metformin increases Aβ generation in cultured neurons due to induction of BACE expression [17]. Modulation of BACE transcription has been reported to depend on the pathway involving activated AMPK, being antagonized by the AMPK inhibitor compound C [17]. It has been postulated that metformin modulates BACE1 and APP transcription activating a signal including AMPK and leading to increase Aβ production [17]. More recently it has been demonstrated that metformin induces up-regulation of APP and PSN1 through a mechanism involving oxidative stress, mitochondrial dysfunction and Nf-κB activation [21]. Further support to these

findings was given by immunofluorescence analysis in the mouse brain regions that are vulnerable in AD pathogenesis. The inspection showed a large number of Aβ aggregates in the cerebral cortex, whereas no significant Aβ deposits were detected in the hippocampus. In particular, in the cortex we found a quite different distribution of APP in control and metformin treated mice, confirming that an increased processing leading to Aβ oligomerization or aggregate formation were occurred.

However, this result was in agreement with the evolution of the temporal-spatial accumulation of Aβ described in AD [42]. In line with these results, increase of typical AD biomarkers and Aβ aggregates in the cortex area and no in the hippocampus, denotes that we have focalized a molecular moment comparable to an early neurodegenerative stage. However, we can hypothesize that the different effects of metformin in cortex and hippocampus areas could be due to a diverse metformin distribution or accumulation. In fact, analysis

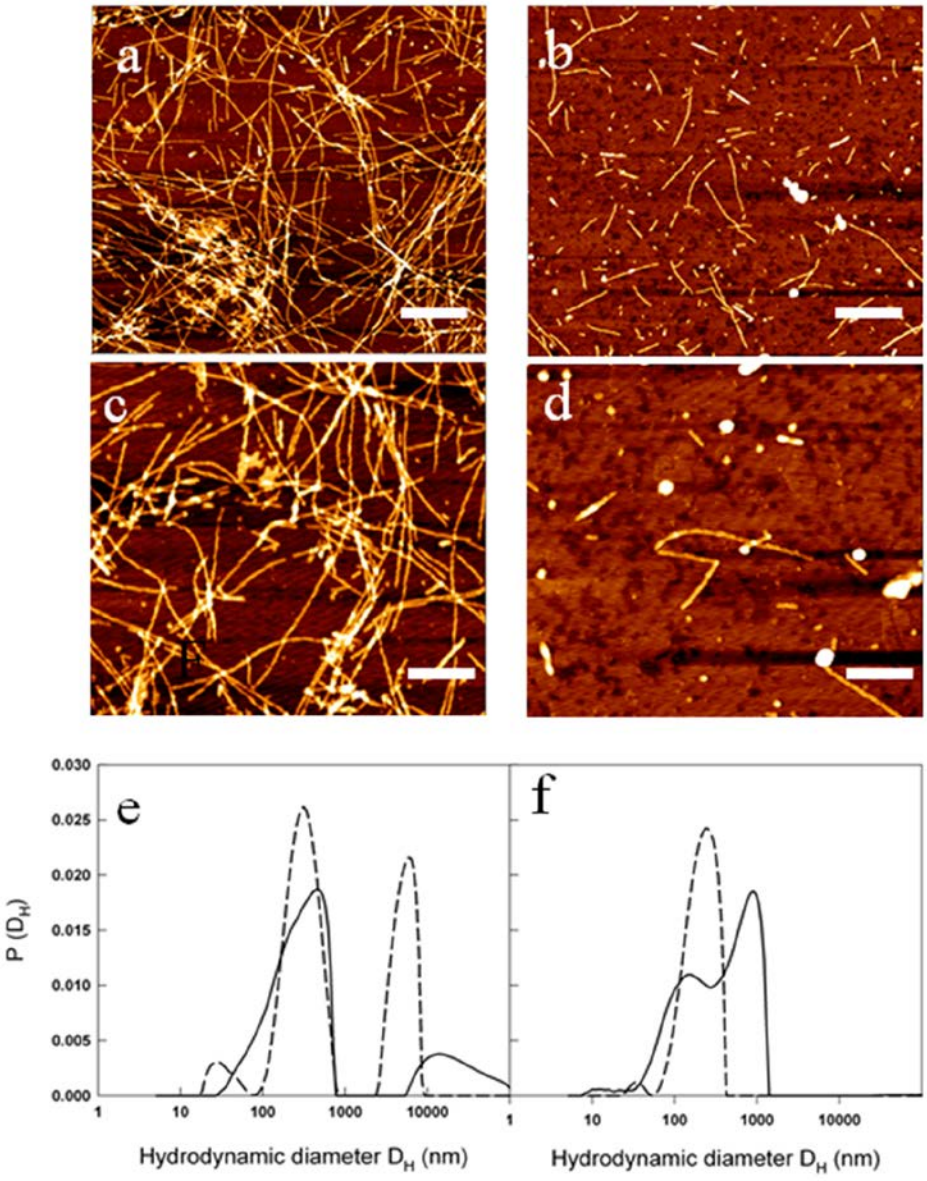

Figure 8. Metformin effects on fibril size and growth. (a-d) AFM images acquired for: 50 μM $A\beta_{1-40}$ at the end of the kinetics at 37 °C and 200 rpm at two different magnifications: scale bar = 1μm and Z-range = 8.9 nm **(a)**; scale bar = 500 nm; Z-range = 8.3 nm **(b).** The samples were compared with 50 μM $A\beta_{1-40}$ + 2 mM metformin at the end of the kinetics at 37 °C and 200 rpm at two different magnifications: scale bar = 1μm and Z-range = 7.0 nm **(c)**; scale bar = 500 nm; Z-range = 8.3 nm **(d)**. Particle size distribution from DLS of 50 μM $A\beta_{1-40}$ incubated at 37 °C and 200 rpm in the absence **(e)** and in the presence **(f)** of 2mM metformin after 0.5 h (dashed lines) and 2 hrs (solid lines) from the beginning of amyloid aggregation process.

of seven rat brain regions, by HPLC method, has demonstrated that metformin concentrations varied in the different brain regions and, both after acute and chronic administration, it was higher in the cortex than in the hippocampus [43].

Our findings suggest that increased APP and Aβ production, due to metformin exposition, could impair mitochondrial function in brain neurons acting in multiple ways on different targets. Metformin treatment changes the levels of expression of TOM40, VDAC1 and HKI, proteins involved in mitochondrial import and export of molecules and metabolites, in cortex region where Aβ aggregates are mainly present. Studies on human brain biopsies have demonstrated that TOM40 pore mediates the internalization of Aβ and APP [44]. Depending on the size of the molecules, the whole APP can block TOM40 channel and the small Aβ can be imported in the inner membrane where affects the respiratory chain. Moreover, influx of Aβ via the TOM40 pore increases Reactive Oxygen Species (ROS) within the organelle, leading to mitochondrial dysfunction and structural and functional damage of neurons [45]. In addition, ROS triggers events that include the increase of Aβ production thus nourishing a vicious circle by which Aβ self-feed its own production [21]. Thus, increased TOM40 could favor transport of Aβ into the mitochondria and their impairing. In their physiological state, the dimensions of the VDAC1 pores are sufficient to selectively allow the passage of small molecules. During cell death processes, in which the release of folded proteins like cytochrome C is required, the formation of larger channels is necessary [46]. In line with this study we found VDAC1 in monomeric, with different electrophoretic mobility, dimeric and oligomeric configurations. VDAC1 is a β-barrel protein with a flexible N-Terminal domain that can be located within the pore by intramolecular crosslinking (Cys-Lys) or exposed to the cytosolic face that could associate with the N-Terminal region of another VDAC1 molecule leading to oligomerization [47]. Moreover, using different stimuli it has been demonstrated that the lower monomeric band appears only when apoptosis is induced [48], indicating that a neurodegenerative process has been locally produced. Furthermore, VDAC1 N-terminus has been found mediate the interaction of VDAC1 with anti-apototic proteins such as HKI [47], and VDAC1 oligomerization is considered relevant for interactions with proteins involved in apoptosis [46]. In the cortex region, where metformin-induced Aβ aggregates are accumulated, and apoptotic neurons were observed, a decrease in the amount of monomers and an increase of intramolecular crosslinked products with a concomitant increase in oligomers formation were found. Furthermore, decrease of HKI suggests that its binding to VDAC1 was displaced and the increased concentration of free VDAC1 molecules has promoted VDAC1 oligo-merization. This is in line with the observation that Aβ mediated neurodegeneration involves detachment of HKI from VDAC1 that oligomerizes and promotes cytochrome C release, events leading to apoptosis [28]. Thus, the increased presence of Aβ, due to metformin treatment, could compete with the binding of HKI and/or other anti-apoptotic proteins with VDAC1 and be the apoptotic stimulus for enhancing VDAC1 oligomerization to produce enlarged pores capable to change permeability and mediate cytochrome C release, in critical brain region. In support of this observation direct interaction of Aβ and phosphorylated tau with VDAC1 has been demonstrated [27,28]. Aβ interaction is able to block mitochondrial pores and interfere with the transport of ATP, ADP and other metabolites between mitochondria and cytoplasm, leading to mitochondrial dysfunction and neurodegeneration [27]. Thus, the observed related increase of VDAC1, Aβ and apoptotic cells, due to metformin administration, mainly in the cortex, could be an initial neurodegenerative event that could be spread to other brain regions as the disease progresses. However, this concept need of additional experimental supports. Lastly, being mitochondrial dysfunction considered an early pathophysiological event in AD, TOM40 and VDAC1 may be proposed as potential timeline biomarkers for this pathology [49]. Consistent with data is the change in expression levels of TOM40 and VDAC1 mainly in cerebral cortex, in a very local specific manner. However, our observations suggest a strong association between metformin-induced Aβ accumulation and mitochondrial dysfunction via impaired TOM40 and VDAC1 expression that is cause of mitochondrial stress and, in turn, source of increased Aβ production. Because many of these factors can be either a cause or a consequence of the others, it is difficult to establish a clear sequence of events. Finally, we cannot exclude that the effect of metformin seen in brain of mice after three months of exposition could be exacerbated by the damage induced by the physiological aging. However, the potentiality of this drug to produce side effects could be counteracted, as suggested in other studies, by its use in combination with insulin [17,18,21].

Very interestingly, by biophysical methods, our study also demonstrates that metformin is able to directly interact with Aβ amyloid species involved in AD influencing their aggregation kinetics and features. Indeed, in the presence of metformin the typical sigmoidal profile of the fibrillogenesis shows an increased lag-phase and final reduction of amyloid fibrils, stabilizing the prefibrillar oligomeric species.

The direct influence on lag-phase reveals that metformin is able to influence the nucleation step of the process by the formation of a drug-Aβ complex [50]. The molecule could exert a stabilizing effect on the on-pathway seeding species involved in β-sheet formation and monomer amyloid assembly.

From DLS and AFM, the presence of metformin sizably reduces the formation of large amyloid fibers, favoring the formation of smaller aggregates. Furthermore, these aggregates have dimensions comparable to that observed in mouse brains even if we cannot exclude that in vivo the size of the aggregates could be influenced by other entrapped extracellular components [3].

These results could provide the hypothesis on a different route by which, together with the others above described, metformin could be negatively correlated to AD pathogenesis. Indeed, in the wide structural polymorphism of Aβ oligomers, the accredited assumption is that, rather than mature fibrils, the species more involved in pathogenesis of AD are prefibrillar oligomeric species that form at the beginning of the process [51,52]. These species expose larger hydrophobic surfaces to the solvent and, therefore, could directly interact with cell membranes influencing calcium homeostasis and ROS production. It cannot be excluded, therefore, that the smaller species stabilized by metformin in vitro are those with higher cytotoxic potentiality, whereas mature fibrils, considered harmless, are much reduced in length and number. In this respect, also by a direct action on the product of APP cleavage, i.e. Aβ peptide, the use of metformin could contribute to toxicity associated to AD.

The high prevalence of AD and T2DM in the elderly population suggests that concomitant pharmacotherapy could be desirable. Our findings indicate that metformin, the drug usually administered for T2DM, is able to reach the brain in C57B6/J mice, where it activates neurodegenerative pathways, including mitochondrial dysfunction and apoptosis, mainly in the brain cortex. Furthermore, metformin is able to directly interacts in vitro with Aβ, modifying its aggregation profile, reducing the amount of mature fibrils and stabilizing toxic prefibrillar oligomeric species. A summary of the proposed mechanism is shown in figure 9. Thus, metformin induces different adverse effects, possibly leading to an overall increase of the risk of AD onset.

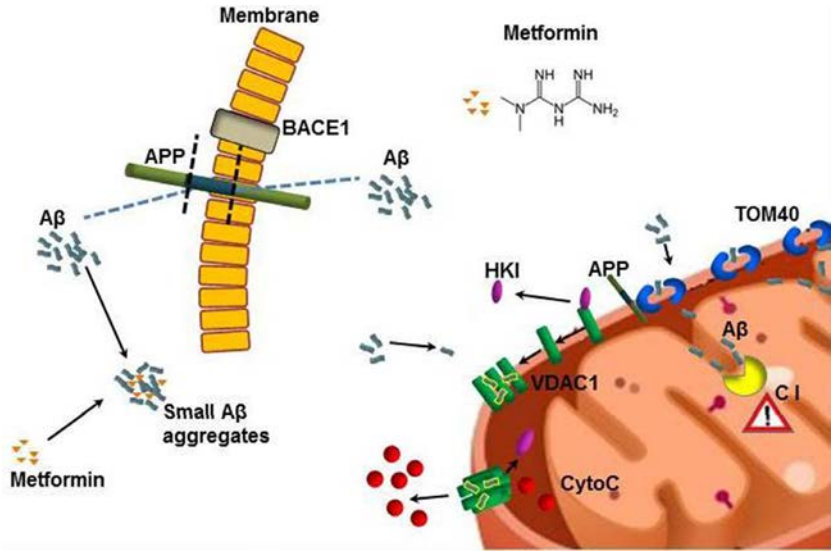

Figure 9. Model describing how metformin induces Aβ aggregates formation and mitochondrial dysfunction. Metformin increases BACE1 production that stimulates APP processing and Aβ production at cell membrane level. Metformin stabilizes small Aβ aggregates that could be internalized. TOM40 pore mediates the mitochondrial internalization of Aβ and APP. The whole APP can block TOM40 channel and the small Aβ can be imported in the inner membrane where affects the Complex I (C I) of the respiratory chain. Small Aβ aggregates displace the binding of HKI with mitochondrial VDAC1 leading to its oligomerization and the formation of large pores that are capable to change permeability and mediate the cytochrome C release. All these coexistent events lead to mitochondrial dysfunction and neuronal apoptosis.

MATERIALS AND METHODS

Mice

The experimental procedures employed in the present study were in accordance with the Italian D.L. no. 116 of 27 January 1992 and subsequent variations and the recommendations of the European Economic Community (86/609/ECC). The studies were approved by Ministero della Sanità (Rome, Italy). Male C57BL/6J (B6) mice, purchased from Harlan Laboratories (San Pietro al Natisone Udine, Italy) at 4 weeks of age, were housed under standard conditions of light (12h light: 12h darkness cycle) and temperature (22–24°C), with free access to water and food. After acclimatization (1 week), the animals were divided in two groups (n=10 per group), control and metformin treated. Mice were provided food and received metformin in drinking water (2 mg/mL) for 7 days or three months. After this treatment, animals were sacrificed by cervical dislocation and the brain of age-matched animals were immediately exported and processed for subsequent analysis, as previously described [7]. When necessary, hippocampus and cortex were separated. Biodistribution of metformin in ex vivo brain was detected by using Biospace Lab Imaging Instrument.

Total protein extraction and western blotting

Brain of mice were homogenized in RIPA buffer (20 mM Tris, pH 7.4, 150 mM NaCl, 1 mM Na3VO4, 10 mM NaF, 1mM EDTA, 1 mM EGTA, 0.2 mM phenyl-methylsulfonyl fluoride, 1% Triton, 0.1%SDS, and 0.5% deoxycholate) with protease inhibitors (Amersham) and phosphatase inhibitor cocktail II and III (SIGMA). To remove insoluble material, tissue lysates were sonicated and centrifuged (14,000 rpm, at 4°C, for 30 min). Proteins (50 µg) were resolved by 10% SDS-PAGE gel and transferred onto nitrocellulose filters for Western blotting using anti-APP (1:1000), anti-BACE1 (1:1000) anti-phospho-AMPK (1:1000), anti-TOM40 (1:1000), anti-VDAC1 (1:1000), and anti-HKI (1:1000) purchased from Santa Cruz, anti-β-actin (1:5000) purchased from Sigma. Secondary antibodies conjugated to horseradish peroxidase (1:2000) purchased from Cell Signaling were detected using the NOVEX® ECL HRP chemiluminescence kit (Cat. n° WP20005, Invitrogen) according to the manufacturer's instructions. In some instances, antibodies were stripped from blots with Restore Western Blot Stripping Buffer (Thermo Scientific) for 10 minutes at room temperature, for antibody reprobing. Band intensities were analyzed with a gel documentation system (BioRad), expression was normalized with β-actin expression. The protein levels were expressed as densitometry and percentage of controls.

Immunofluorescence

For immunofluorescence the brains (n=5 per group) were embedded in paraffin as previously described [7] and coronally sectioned (5µm) using a microtome. Brain sections including the cerebral cortex and the hippocampus were mounted on slides and deparaffinized in xylene solution. Then, the slides were hydrated in a series of graded ethanol (96%, 85%, 70%, 50%) for 5 minutes each. After washing in water and PBS the slides were incubated with 3% BSA/PBS for 1 h. Next, the sections were incubated with anti-APP (1:50) (Santa Cruz) at 4 °C overnight. After washing in PBS, the samples were incubated with anti-rabbit Cy3-conjugate secondary antibody (1:500; SIGMA). For nuclear staining, the sections were incubated with Hoechst 33258 (5µg/ml) for 20 minutes. After washing in PBS the slides were mounted with cover slips and images were visualized by using a Leica DM5000 upright microscope (Leica Microsystems, Heidelberg, Germany) at 20X magnification.

Thioflavin T staining

For Thioflavin-T (ThT) staining the brain sections including the cerebral cortex and the hippocampus were mounted on slides The slides were deparaffinized in xylene solution and hydrated in a series of graded ethanol (96%, 85%, 70%, 50%) for 5 minutes each. After washing in water, the sections were incubated in filtered 1% aqueous ThT solution for 8 minutes at room temperature. The slides were then dehydrated in ethanol 80% and 95%, for 5 minutes each. After washing in water the slides were mounted with cover slips and the images were visualized by using a Leica DM5000 upright microscope (Leica Microsystems, Heidelberg, Germany) at 20x magnification.

TUNEL assay

Terminal deoxynucleotidyl Transferase Biotin-dUTP Nick End Labeling (TUNEL)-positive apoptotic nuclei were detected in brain paraffin sections using an in situ cell death detection kit (Promega) according to manufacturer's instructions. The number of apoptotic cells was counted in randomly selected fields to calculate the ratio of apoptotic cell per brain area.

Quantitative real-time PCR

Total RNA was extracted using RNEasy Mini Kit (Qiagen). Two ng of RNA was used to synthesize the

first strand cDNA using RT First-Strand kit (Qiagen). Synthesized cDNAs were amplified using RT2 SYBR Green/ROX qPCR Mastermix (Qiagen) and StepOne Real-Time instrument (Applied Biosystem). Gene expression validation was performed using RT2 qPCR Primer Assay for human APP, Presenilin1, β-actin (SABiosciences). Gene expression was normalized to β-actin.

Statistical analysis

All experiments were repeated at least three times and each experiment was performed in triplicate. The results are presented as mean + SD. A one-way ANOVA was performed, followed by Dunnet's post hoc test for analysis of significance. Results with a p-value <0.05 were considered statistically significant, *P < 0.05, **P<0.02.

Sample preparation for biophysics experiments

The synthetic peptide $A\beta_{1-40}$ (Anaspec) was pretreated according to the procedure of Fezoui et al. [53] for improving the reliability of experiments at neutral pH. Stock aliquots (200 μg each) were stored at -80 °C. Metformin was purchased from Sigma Aldrich. $A\beta_{1-40}$ samples were prepared by dissolving the lyophilized peptide in 50 mM phosphate buffer, pH 7.4, at a concentration of about 70 μM. The solution was filtered through 0.22 μm and 20 nm filters into a fluorescence quartz cuvette containing a small magnetic stirring bar. $A\beta_{1-40}$ concentration was determined by tyrosine absorption at 276 nm using an extinction coefficient of 1390 cm^{-1M-1}. The sample was then diluted to the working concentration of 50 μ M by adding the appropriate amount of buffer, concentrated solution of ThT (1mM), and concentrated solution of metformin (20 mM) when required.

Final samples containing Aβ and metformin were obtained by appropriate aseptically mixing of the protein solutions and placed in closed cuvettes in a cold room at 4 °C, before incubation at higher temperatures. The aggregation kinetics were followed at controlled temperature (37 °C) and under controlled stirring (200 rpm) for 24 hours.

ThT spectrofluorometric measurements

ThT fluo-rescence emission was monitored by using a JASCO FP-6500 spectrometer. The excitation and emission wavelengths were 450 and 485 nm, respectively, with 3 nm slit width. ThT concentration was 12 μM. The sample was placed at 37 °C in the thermostated cell compartment (10 mm). When required, a magnetic stirrer at 200 rpm (mod. 300, Rank Brothers Ltd., Cambridge) was used.

Control fluorimetric experiments between Thioflavin T and metformin with the purpose of excluding undesired pitfalls due to potential interaction between the dye and the molecule [54] have been performed under the same conditions of aggregation kinetics (37 °C, under stirring).

Circular dichroism spectroscopy

CD measurements were acquired by using a JASCO J-815 CD Spectrometer. Particularly, during the aggregation kinetics, withdrawals of samples at appropriate time were observed. Spectra were recorded at 20 °C using a quartz cell with 0.2 mm path length. Each spectrum measurement was obtained by averaging over eight scans and subtracting the blank solvent contribution.

The aggregation of Aβ peptide in the presence or absence of metformin was investigated by Dynamic Light Scattering. The samples were placed into a dust-free quartz cell without further filtering and kept at 37°C in the thermostatic cell compartment of a Brookhaven Instruments BI200-SM goniometer. The temperature was controlled within 0.1 °C using a thermostatic recirculating bath. The light scattered intensity and its autocorrelation function were measured at θ = 90° by using a Brookhaven BI-9000 correlator and a 50 mW He–Ne laser tuned at a wavelength λ = 632.8 nm. Due to their Brownian motion, particles moving in solution give rise to fluctuations in the intensity of the scattered light [55, 56]. The autocorrelator measures the homodyne intensity–intensity correlation function that, for a Gaussian distribution of the intensity profile of the scattered light, is related to the electric field correlation function:

$$g^{(2)}(q,t) = [A + Bg^{(1)}(q,t)]^2 \qquad (1)$$

where *A* and *B* are the experimental baseline and the optical constant, respectively. For polydisperse particles, $g^{(1)}(q,t)$ is given by:

$$g^{(1)}(q,t) = \int_0^\infty G(\Gamma)\exp(-\Gamma t)d\Gamma \qquad (2)$$

Here, $G(\Gamma)$ is the normalized number distribution function for the decay constant $\Gamma = q^2 D_T$, where $q=(4\pi n/\lambda)\sin(\theta/2)$ is the scattering vector defining the spatial resolution with n and D_T being the solvent refractive index and the translational diffusion coefficient, respectively. The hydrodynamic diameter

D_H is calculated from D_T through the Stokes–Einstein relationship:

$$D_T = \frac{k_B T}{3\pi\eta D_H} \quad (3)$$

where k_B is the Boltzmann constant, T is the absolute temperature, and η is the solvent viscosity. Intensity-weighted distribution functions P_I of the z-average hydrodynamic diameter D_H were obtained by the analysis of the intensity autocorrelation functions were analyzed by means of a CONTIN-like smoothing-constrained regularization method [57].

Atomic Force Microscopy (AFM)

AFM measurements were performed by using a Nanowizard III (JPK Instruments, Germany) mounted on an Axio Observer D1 (Carl Zeiss, Germany) or on an Eclips Ti (Nikon, Japan) inverted optical microscope. Aliquots of protein solutions were deposited onto freshly cleaved mica surfaces (Agar Scientific, Assing, Italy) and incubated for up to 20 min before rinsing with deionized water and drying under a low pressure nitrogen flow. Imaging of the protein was carried out in intermittent contact mode in air by using NCHR silicon cantilever (Nanoworld, Switzerland) with nominal spring constant ranging from 21 to 78 N/m and typical resonance frequency ranging from 250 to 390 kHz.

ACKNOWLEDGEMENTS

The authors wish to thank Alessia Provenzano and Fulvio Ferrante for their useful technical support.

FUNDING

This research was partially supported by the grant from the Department of Productive Activities of the Sicilian Region (PO FESR 2007/2013) “Piattaforma Regionale di Ricerca Traslazionale per la Salute” (B65E12000570008) and by the Italian grant FIRB “Future in Research” RBFR12SIPT MIND: “Multisciplinary Investigations for the Development of Neuroprotective Drugs”.

CONFLICTS OF INTEREST

The authors declare no conflicts of interest.

REFERENCES

1. Ott A, Stolk RP, van Harskamp F, Pols HA, Hofman A, Breteler MM. Diabetes mellitus and the risk of dementia: the Rotterdam Study. Neurology. 1999; 53:1937–42.

2. Alzheimer’s Association. Alzheimer’s disease facts and figures Alzheimer’s & Dementia. 2015; 11:1-83 .

3. Selkoe DJ. The cell biology of β-amyloid precursor protein and presenilin in Alzheimer’s disease. Trends Cell Biol. 1998; 8:447–53.

4. Walsh DM, Klyubin I, Fadeeva JV, Cullen WK, Anwyl R, Wolfe MS, Rowan MJ, Selkoe DJ. Naturally secreted oligomers of amyloid beta protein potently inhibit hippocampal long-term potentiation in vivo. Nature. 2002; 416:535–39.

5. Weingarten MD, Lockwood AH, Hwo SY, Kirschner MW. A protein factor essential for microtubule assembly. Proc Natl Acad Sci USA. 1975; 72:1858–62.

6. Hildreth KL, Van Pelt RE, Schwartz RS. Obesity, insulin resistance, and Alzheimer’s disease. Obesity (Silver Spring). 2012; 20:1549–57.

7. Nuzzo D, Picone P, Baldassano S, Caruana L, Messina E, Marino Gammazza A, Cappello F, Mulè F, Di Carlo M. Insulin resistance as common molecular denominator linking obesity to Alzheimer’s disease. Curr Alzheimer Res. 2015; 12:723–35.

8. Watson GS, Craft S. The role of insulin resistance in the pathogenesis of Alzheimer’s disease: implications for treatment. CNS Drugs. 2003; 17:27–45.

9. Watson GS, Craft S. Modulation of memory by insulin and glucose: neuropsychological observations in Alzheimer’s disease. Eur J Pharmacol. 2004; 490:97–113.

10. De Felice FG. Alzheimer’s disease and insulin resistance: translating basic science into clinical applications. J Clin Invest. 2013; 123:531–39.

11. Ghasemi R, Haeri A, Dargahi L, Mohamed Z, Ahmadiani A. Insulin in the brain: sources, localization and functions. Mol Neurobiol. 2013; 47:145–71.

12. Picone P, Giacomazza D, Vetri V, Carrotta R, Militello V, San Biagio PL, Di Carlo M. Insulin-activated Akt rescues Aβ oxidative stress-induced cell death by orchestrating molecular trafficking. Aging Cell. 2011; 10:832–43.

13. Steen E, Terry BM, Rivera EJ, Cannon JL, Neely TR, Tavares R, Xu XJ, Wands JR, de la Monte SM. Impaired insulin and insulin-like growth factor expression and signaling mechanisms in Alzheimer’s disease--is this type 3 diabetes? J Alzheimers Dis. 2005; 7:63–80.

14. Di Carlo M, Picone P, Carrotta R, Giacomazza D, San Biagio PL. Insulin promotes survival of amyloid-beta oligomers neuroblastoma damaged cells via caspase 9 inhibition and Hsp70 upregulation. J Biomed Biotechnol. 2010; 2010:147835.

15. Picone P, Ditta LA, Sabatino MA, Militello V, San Biagio PL, Di Giacinto ML, Cristaldi L, Nuzzo D, Dispenza C, Giacomazza D, Di Carlo M. Ionizing radiation-engineered nanogels as insulin nanocarriers for the development of a new strategy for the treatment of Alzheimer’s disease. Biomaterials. 2016; 80:179–94.

16. Wang J, Gallagher D, DeVito LM, Cancino GI, Tsui D, He L, Keller GM, Frankland PW, Kaplan DR, Miller FD. Metformin activates an atypical PKC-CBP pathway to promote neurogenesis and enhance spatial memory formation. Cell Stem Cell. 2012; 11:23–35.

17. Chen Y, Zhou K, Wang R, Liu Y, Kwak YD, Ma T, Thompson RC, Zhao Y, Smith L, Gasparini L, Luo Z, Xu H, Liao FF. Antidiabetic drug metformin (GlucophageR) increases biogenesis of Alzheimer's amyloid peptides via up-regulating BACE1 transcription. Proc Natl Acad Sci USA. 2009; 106:3907–12.

18. Beeri MS, Schmeidler J, Silverman JM, Gandy S, Wysocki M, Hannigan CM, Purohit DP, Lesser G, Grossman HT, Haroutunian V. Insulin in combination with other diabetes medication is associated with less Alzheimer neuropathology. Neurology. 2008; 71:750–57.

19. Imfeld P, Bodmer M, Jick SS, Meier CR. Metformin, other antidiabetic drugs, and risk of Alzheimer's disease: a population-based case-control study. J Am Geriatr Soc. 2012; 60:916–21.

20. Zhou G, Myers R, Li Y, Chen Y, Shen X, Fenyk-Melody J, Wu M, Ventre J, Doebber T, Fujii N, Musi N, Hirshman MF, Goodyear LJ, Moller DE. Role of AMP-activated protein kinase in mechanism of metformin action. J Clin Invest. 2001; 108:1167–74.

21. Picone P, Nuzzo D, Caruana L, Messina E, Barera A, Vasto S, Di Carlo M. Metformin increases APP expression and processing via oxidative stress, mitochondrial dysfunction and NF–κB activation: use of insulin to attenuate metformin's effect. Biochim Biophys Acta. 2015; 1853:1046-1059.

22. Schäfer G, Rieger E. Interaction of biguanides with mitochondrial and synthetic membranes. Effects on ion conductance of mitochondrial membranes and electrical properties of phospholipid bilayers. Eur J Biochem. 1974; 46:613–23.

23. Detaille D, Guigas B, Leverve X, Wiernsperger N, Devos P. Obligatory role of membrane events in the regulatory effect of metformin on the respiratory chain function. Biochem Pharmacol. 2002; 63:1259–72.

24. Carvalho C, Correia S, Santos MS, Seiça R, Oliveira CR, Moreira PI. Metformin promotes isolated rat liver mitochondria impairment. Mol Cell Biochem. 2008; 308:75–83.

25. Suski M, Olszanecki R, Chmura Ł, Stachowicz A, Madej J, Okoń K, Adamek D, Korbut R. Influence of metformin on mitochondrial subproteome in the brain of apoE knockout mice. Eur J Pharmacol. 2016; 772:99–107.

26. Gottschalk WK, Lutz MW, He YT, Saunders AM, Burns DK, Roses AD, Chiba-Falek O. The broad impact of TOM40 on neurodegenerative diseases in aging. J Parkinsons Dis Alzheimers Dis. 2014; 1:1–25.

27. Manczak M, Reddy PH. Abnormal interaction of VDAC1 with amyloid beta and phosphorylated tau causes mitochondrial dysfunction in Alzheimer's disease. Hum Mol Genet. 2012; 21:5131–46.

28. Smilansky A, Dangoor L, Nakdimon I, Ben-Hail D, Mizrachi D, Shoshan-Barmatz V. The voltage-dependent anion channel 1 mediates amyloid β toxicity and represents a potential target for Alzheimer disease therapy. J Biol Chem. 2015; 290:30670–83.

29. Karran E, Mercken M, De Strooper B. The amyloid cascade hypothesis for Alzheimer's disease: an appraisal for the development of therapeutics. Nat Rev Drug Discov. 2011; 10:698–712.

30. Carrotta R, Di Carlo M, Manno M, Montana G, Picone P, Romancino D, San Biagio PL. Toxicity of recombinant beta-amyloid prefibrillar oligomers on the morphogenesis of the sea urchin Paracentrotus lividus. FASEB J. 2006; 20:1916–17.

31. Picone P, Carrotta R, Montana G, Nobile MR, San Biagio PL, Di Carlo M. Abeta oligomers and fibrillar aggregates induce different apoptotic pathways in LAN5 neuroblastoma cell cultures. Biophys J. 2009; 96:4200–11.

32. Mannini B, Mulvihill E, Sgromo C, Cascella R, Khodarahmi R, Ramazzotti M, Dobson CM, Cecchi C, Chiti F. Toxicity of protein oligomers is rationalized by a function combining size and surface hydrophobicity. ACS Chem Biol. 2014; 9:2309–17.

33. Novitskaya V, Bocharova OV, Bronstein I, Baskakov IV. Amyloid fibrils of mammalian prion protein are highly toxic to cultured cells and primary neurons. J Biol Chem. 2006; 281:13828–36.

34. Bucciantini M, Nosi D, Forzan M, Russo E, Calamai M, Pieri L, Formigli L, Quercioli F, Soria S, Pavone F, Savistchenko J, Melki R, Stefani M. Toxic effects of amyloid fibrils on cell membranes: the importance of ganglioside GM1. FASEB J. 2012; 26:818–31.

35. Bucciantini M, Rigacci S, Stefani M. Amyloid aggregation: role of biological membranes and the aggregate–membrane system. J Phys Chem Lett. 2014; 5:517–27.

36. Lomakin A, Teplow DB, Kirschner DA, Benedek GB. Kinetic theory of fibrillogenesis of amyloid beta-protein. Proc Natl Acad Sci USA. 1997; 94:7942–47.

37. Lee CC, Nayak A, Sethuraman A, Belfort G, McRae GJ. A three-stage kinetic model of amyloid fibrillation. Biophys J. 2007; 92:3448–58.

38. LeVine H 3rd. Thioflavine T interaction with synthetic Alzheimer's disease beta-amyloid peptides: detection of amyloid aggregation in solution. Protein Sci. 1993; 2:404–10.

39. Naiki H, Higuchi K, Hosokawa M, Takeda T. Fluorometric determination of amyloid fibrils in vitro using the fluorescent dye, thioflavin T1. Anal Biochem. 1989; 177:244–49.

40. Coelho-Cerqueira E, Pinheiro AS, Follmer C. Pitfalls associated with the use of Thioflavin-T to monitor anti-fibrillogenic activity. Bioorg Med Chem Lett. 2014; 24:3194–98.

41. Chen L, Pawlikowski B, Schlessinger A, More SS, Stryke D, Johns SJ, Portman MA, Chen E, Ferrin TE, Sali A, Giacomini KM. Role of organic cation transporter 3 (SLC22A3) and its missense variants in the pharmacologic action of metformin. Pharmacogenet Genomics. 2010; 20:687–99.

42. Khan UA, Liu L, Provenzano FA, Berman DE, Profaci CP, Sloan R, Mayeux R, Duff KE, Small SA. Molecular drivers and cortical spread of lateral entorhinal cortex dysfunction in preclinical Alzheimer's disease. Nat Neurosci. 2014; 17:304–11.

43. Łabuzek K, Suchy D, Gabryel B, Bielecka A, Liber S, Okopień B. Quantification of metformin by the HPLC method in brain regions, cerebrospinal fluid and plasma of rats treated with lipopolysaccharide. Pharmacol Rep. 2010; 62:956–65.

44. Hansson Petersen CA, Alikhani N, Behbahani H, Wiehager B, Pavlov PF, Alafuzoff I, Leinonen V, Ito A, Winblad B, Glaser E, Ankarcrona M. The amyloid β-peptide is imported into mitochondria via the TOM import machinery and localized to mitochondrial cristae. Proc Natl Acad Sci USA. 2008; 105:13145–50.

45. Reddy PH. Amyloid beta, mitochondrial structural and functional dynamics in Alzheimer's disease. Exp Neurol. 2009; 218:286–92.

46. Zalk R, Israelson A, Garty ES, Azoulay-Zohar H, Shoshan-Barmatz V. Oligomeric states of the voltage-dependent anion channel and cytochrome c release from mitochondria. Biochem J. 2005; 386:73–83.

47. Geula S, Ben-Hail D, Shoshan-Barmatz V. Structure-based analysis of VDAC1: n-terminus location, translocation, channel gating and association with anti-apoptotic proteins. Biochem J. 2012; 444:475–85.

48. Keinan N, Tyomkin D, Shoshan-Barmatz V. Oligomerization of the mitochondrial protein voltage-dependent anion channel is coupled to the induction of apoptosis. Mol Cell Biol. 2010; 30:5698–709.

49. Reddy PH. Is the mitochondrial outer membrane protein VDAC1 therapeutic target for Alzheimer's disease?. Biochim Biophys Acta. 2013; 1832:67–75.

50. Bartolini M, Bertucci C, Bolognesi ML, Cavalli A, Melchiorre C, Andrisano V. Insight into the kinetic of amyloid beta (1-42) peptide self-aggregation: elucidation of inhibitors' mechanism of action. ChemBioChem. 2007; 8:2152–61.

51. Hata S, Saito Y, Suzuki T. Alzheimer's Disease as a Membrane-Associated Enzymopathy of ß-Amyloid Precursor Protein (APP) Secretases In: Lipids and cellular membranes in amyloid diseases, R Jelinek editor. 2011. New York: John Wiley.

52. Canale C, Seghezza S, Vilasi S, Carrotta R, Bulone D, Diaspro A, San Biagio PL, Dante S. Different effects of Alzheimer's peptide Aβ(1-40) oligomers and fibrils on supported lipid membranes. Biophys Chem. 2013; 182:23–29.

53. Fezoui Y, Hartley DM, Harper JD, Khurana R, Walsh DM, Condron MM, Selkoe DJ, Lansbury PT Jr, Fink AL, Teplow DB. An improved method of preparing the amyloid beta-protein for fibrillogenesis and neurotoxicity experiments. Amyloid. 2000; 7:166–78.

54. Hudson SA, Ecroyd H, Kee TW, Carver JA. The thioflavin T fluorescence assay for amyloid fibril detection can be biased by the presence of exogenous compounds. FEBS J. 2009; 276:5960–72.

55. Pusey PN. Introduction to scattering experiments In: Netrons, X-ray and light: scattering method applied to soft condensed matter, Th Zemb, P Lindner, editors. Amsterdam: Elsevier; 2002; 3-22.

56. Berne BJ, Pecora R. Dynamic Light Scattering. New York: John Wiley; 1976.

57. Stepanek P. The method and some applications In: Dynamic ligth scattering, W Brown editor. Oxford, UK: Clarendon Press; 1993.

Research Paper

Fat-specific Dicer deficiency accelerates aging and mitigates several effects of dietary restriction in mice

Felipe C. G. Reis[1], Jéssica L. O. Branquinho[1], Bruna B. Brandão[1], Beatriz A. Guerra[1], Ismael D. Silva[2], Andrea Frontini[3], Thomas Thomou[4], Loris Sartini[5], Saverio Cinti[5], C. Ronald Kahn[4], William T. Festuccia[6], Alicia J.Kowaltowski[7], and Marcelo A. Mori[1,8]

[1]*Department of Biophysics, Escola Paulista de Medicina, Universidade Federal de São Paulo, São Paulo, Brazil*
[2]*Department of Gynecology, Escola Paulista de Medicina, Universidade Federal de São Paulo, São Paulo, Brazil*
[3]*Department of Public Health, Experimental and Forensic Medicine, University of Pavia, Pavia, Italy*
[4]*Section on Integrative Physiology and Metabolism, Joslin Diabetes Center, Harvard Medical School, Boston, MA 02215, USA*
[5]*Department of Clinical and Experimental Medicine, Università Politecnica delle Marche, Ancona, Italy*
[6]*Departament of Physiology, Instituto de Ciências Biomédicas, Universidade de São Paulo, São Paulo, Brazil*
[7]*Department of Biochemistry, Instituto de Química, Universidade de São Paulo, São Paulo, Brazil*
[8]*Department of Biochemistry and Tissue Biology, Instituto de Biologia, Universidade Estadual de Campinas, Campinas, Brazil*

Key words: *dicer, adipose tissue, aging, dietary restriction, insulin resistance*
Received: *02/22/16; Accepted: 05/15/16; Published: 05/28/16*
Correspondence to: *Marcelo A. Mori, PhD;* ***E-mail:*** *morima@unicamp.br* doi:10.18632/aging.100970

Abstract: Aging increases the risk of type 2 diabetes, and this can be prevented by dietary restriction (DR). We have previously shown that DR inhibits the downregulation of miRNAs and their processing enzymes - mainly Dicer - that occurs with aging in mouse white adipose tissue (WAT). Here we used fat-specific Dicer knockout mice (AdicerKO) to understand the contributions of adipose tissue Dicer to the metabolic effects of aging and DR. Metabolomic data uncovered a clear distinction between the serum metabolite profiles of Lox control and AdicerKO mice, with a notable elevation of branched-chain amino acids (BCAA) in AdicerKO. These profiles were associated with reduced oxidative metabolism and increased lactate in WAT of AdicerKO mice and were accompanied by structural and functional changes in mitochondria, particularly under DR. AdicerKO mice displayed increased mTORC1 activation in WAT and skeletal muscle, where Dicer expression is not affected. This was accompanied by accelerated age-associated insulin resistance and premature mortality. Moreover, DR-induced insulin sensitivity was abrogated in AdicerKO mice. This was reverted by rapamycin injection, demonstrating that insulin resistance in AdicerKO mice is caused by mTORC1 hyperactivation. Our study evidences a DR-modulated role for WAT Dicer in controlling metabolism and insulin resistance.

INTRODUCTION

Aging is an important risk factor for chronic diseases such as type 2 diabetes (T2D) [1]. Dietary restriction (DR) increases lifespan and delays the onset of T2D in mammals, including humans [2, 3]. This is thought to be a consequence of increased insulin sensitivity and improved glucose disposal, although the mechanisms underlying these effects of DR have not yet been elucidated in detail. Among the proposed mechanisms, DR has been shown to ameliorate oxidative imbalance [4] and inflammation [5, 6] in a variety of tissues, including the white adipose tissue (WAT), contributing therefore to enhance local and whole body insulin signaling [7-9].

WAT plays a major role in glycemic control and in nutrient homeostasis, serving as the main site for calorie storage during the fed state and as the source of circulating free fatty acids during the fasting state [10]. WAT is also a major endocrine organ [11] and the primary site of branched-chain amino acid (BCAA, *e.g.* valine, leucine, and isoleucine) oxidation [12]. Indeed, impaired BCAA metabolism in adipose tissue and BCAA accumulation in the blood stream have been associated with T2D [13].

Dicer is a type III endoribonuclease that processes pre-miRNAs into mature miRNAs and exerts a variety of other functions related to double-stranded RNA processing and degradation [14]. We have previously reported that DR prevents the age-associated downregulation of Dicer in murine WAT, reversing a global decline in miRNAs that occurs with aging [15]. Dicer expression in adipose tissue is also downregulated in response to obesity and lipodystrophy in mice and humans [16-18], and is affected by aging and DR in *C. elegans* in a manner that resembles the phenomenon observed in mouse adipose tissue [15]. Worms overexpressing Dicer in the intestine - the analog of mammalian adipose tissue - are stress resistant, while whole body Dicer loss-of-function mutations render worms short-lived [15]. Fat-specific Dicer knockout (AdicerKO) mice are insulin resistant and hyperglycemic when subjected to high fat diet [16], suggesting that downregulation of Dicer in adipose tissue contributes to aging and age-associated T2D. Here we tested this hypothesis and asked if DR provides beneficial metabolic outcomes through the upregulation of Dicer in WAT. We found that Dicer is required for proper nutrient utilization by the adipose tissue particularly in catabolic states. Moreover, Dicer loss-of-function in adipocytes directly impacts on the accumulation of circulating metabolites that play a role in controlling whole body insulin action. Consequently, DR is unable to improve insulin sensitivity in AdicerKO mice. Finally, these mice exhibit age-dependent insulin resistance and premature mortality, suggesting a critical role of adipose tissue Dicer in the onset of age-related metabolic diseases.

RESULTS

Altered serum metabolite profiles in AdicerKO mice

Twelve-week old AdicerKO and Lox mice were maintained on DR or *ad libitum* (AL) regimens and euthanized when fasting at the end of the protocol. As expected, mice on DR lost weight and visceral adiposity, and this was independent of the genotype (Supplementary Fig. 1A and B). AdicerKO mice had larger brown adipose tissue mass and smaller epididymal mal WAT depots when fed AL, as previously described [16], and these differences persisted under the DR condition (Supplementary Fig. 1B). Surprisingly, DR promoted more subcutaneous inguinal WAT (henceforth referred to simply as WAT) loss in AdicerKO than in the Lox mice (Supplementary Fig. 1B).

To test if the absence of Dicer in adipocytes could lead to systemic metabolic changes in AL or DR mice, we performed serum metabolomics. Partial least squares discriminant analysis (PLS-DA) (Supplementary Fig. 2A) and hierarchical clustering analysis (Supplementary Fig. 2B) revealed a distinct pattern between the groups, in particular between DR and AL, but also between AdicerKO and Lox mice. Pathway analysis demonstrated that metabolites related to fatty acid oxidation, BCAA degradation and biosynthesis, pantothenate and CoA biosynthesis, aromatic amino acid biosynthesis, and glycerophospholipid metabolism were the most overrepresented among the differentially expressed serum constituents when comparing all conditions (Supplementary Table 1). Dicer knockout in adipocytes did not completely abrogate the effects of DR on the levels of specific serum metabolites; however it did increase the circulating levels of BCAA and other essential amino acids both under AL (Supplementary Table 2) and DR conditions (Fig. 1A and B). Short-chain acylcarnitines (SCAC) (Supplementary Fig. 2C and D) and glycerol-phospholipids (Supplementary Fig. 2B) were also higher in the serum of AdicerKO mice under these conditions.

Metabolic rewiring in the adipose tissue of AdicerKO mice

The changes in circulating BCAA and SCAC levels in AdicerKO mice prompted us to investigate potential differences in the expression of genes related to amino acid and fatty acid metabolism in WAT - a major site for BCAA and fatty acid oxidation [12, 19]. Genes encoding branched-chain aminotransferases (*Bcat1* - cytoplasmic and *Bcat2* -mitochondrial) – the first step in the BCAA degradation pathway - were lower by 52 to 89% in AdicerKO WAT, especially the mitochondrial isoform *Bcat2*, which was also induced by DR in both genotypes (Fig. 1C). Branched-chain alpha-ketoacid dehydrogenase mRNA (*Bckdha*) was not changed (Fig. 1C). We also measured the mRNA expression of enzymes involved in the catabolism of other amino acids, *e.g.* L-amino acid oxidase 1 (*Lao1*), tyrosine aminotransferase (*Tat*), and glutamic-oxaloacetic transaminases (*Got1* – cytoplasmic and *Got2* – mitochondrial) (Fig. 1D). We observed no

changes except for *Got1*, which was dramatically increased by 7.5- and 86.3-fold with DR in Lox and AdicerKO mice, respectively. Acetyl-CoA carboxylase beta mRNA (*Acacb*) expression was markedly reduced in the WAT of AdicerKO mice under both AL and DR conditions, despite minor or no consistent changes in mRNA expression of carnitine palmitoyltransferase Ia (*Cpt1a*) and Ib (*Cpt1β*) or short chain fatty acid acyl-coenzyme A dehydrogenase (*Acads*) (Fig. 1E). The mRNA encoding for long chain fatty acid acyl-coenzyme A dehydrogenase (*Acadl*) was lower in the WAT of AdicerKO mice only during DR (Fig. 1E). Taken together with elevated serum SCAC levels in AdicerKO mice (Supplementary Fig. 2C and D) with no changes in palmitoylcarnitine (Supplementary Fig. 2E) or carnitine (Supplementary Fig. 2F), these results suggest reduced BCAA catabolism and altered fatty acid oxidation. In agreement with this hypothesis, two of the major transcription factors involved in the regulation of genes of the mitochondrial β-oxidation, *i.e.* PGC-1α and PPAR-α, had their mRNAs dramatically decreased in WAT of AdicerKO mice in both AL and DR regimens (*Ppargc1a* and *Ppara* - Fig. 1E).

Surprisingly, isolated WAT or skeletal muscle of AdicerKO mice were able to efficiently oxidize valine (Supplementary Fig. 3A-H) or palmitate (Supplementary Fig. 3I-L) into CO_2, or direct their carbons to ward lipid synthesis (Supplementary Fig. 3M-R), independently of the diet, when these substrates were offered in excess as an exogenous energy source. These data suggest that oxidative capacity of AdicerKO WAT and muscle is not compromised. Indeed, the capacity to reduce cytochrome c was preserved in the WAT of AdicerKO mice when NADH was offered as a substrate to promote electron transport starting at complex I (Fig. 2A). However, electron transport was less efficient in AdicerKO WAT when succinate was used to feed complex II directly (Fig. 2B). These results indicate that electron transport function is impaired at the level of complex II in AdicerKO WAT. Consistently, AdicerKO adipocytes displayed lower respiratory rates in the presence of succinate (Fig. 2C), indicating that fat cells in which Dicer was knocked out engage less in oxidative metabolism.

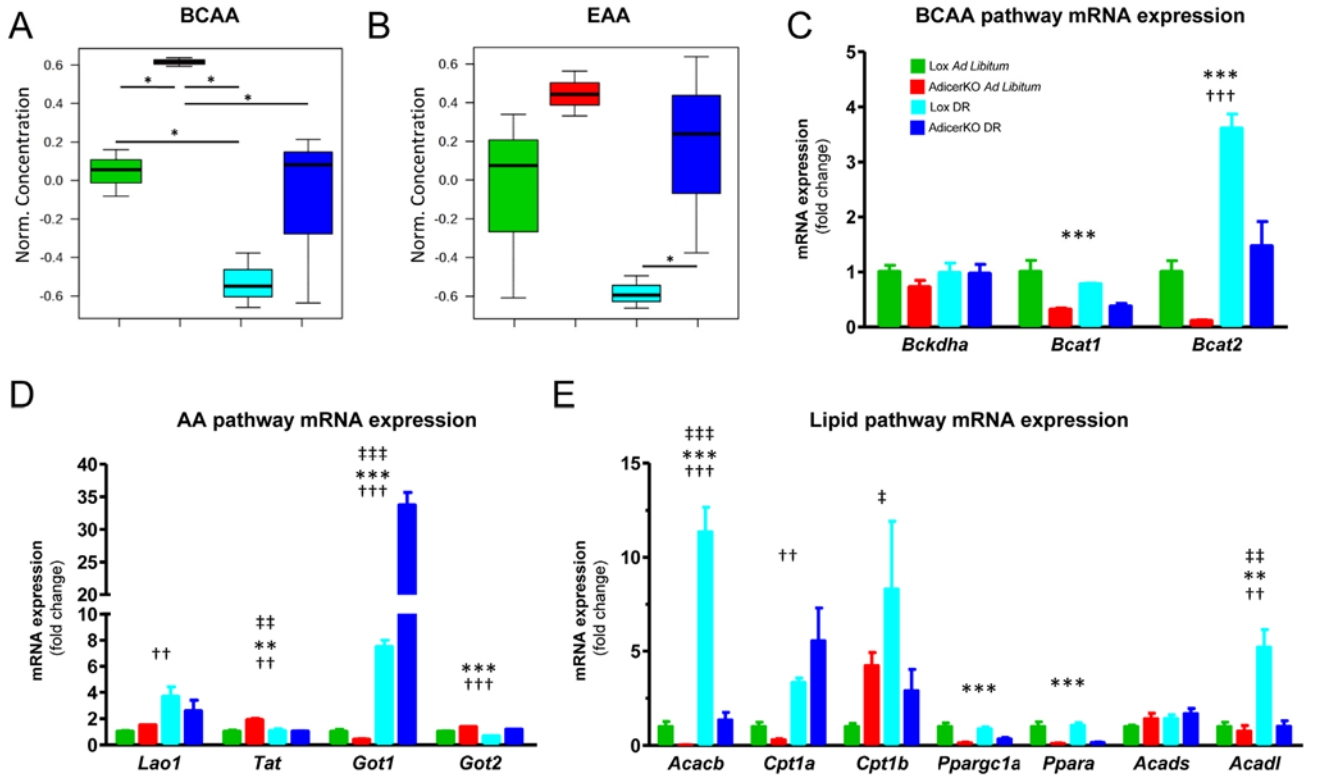

Figure 1. Metabolic changes in fat-specific Dicer knockout mice (AdicerKO). Twelve-week old mice were subjected to *ad libitum* (AL) or dietary restriction (DR) regimens for three months. Mice were euthanized at the end of the protocol after overnight fasting and serum (**A**) branched-chain amino acid (BCAA) or (**B**) essential amino acid (EAA) levels were assessed (N=3 per condition). Values of individual amino acids were summed, normalized by the average of the Lox AL group, Log2 transformed and Pareto scaled. Data are mean ± SE. * P < 0.05. (**C**-**E**) Gene expression in inguinal white adipose tissue (N=5-7 per condition). Mean ± SEM. ** P < 0.01, *** P < 0.001 for genotype effect; †† P < 0.01, ††† P < 0.001 for diet effect; ‡‡ P < 0.01, ‡‡‡ P < 0.001 for diet-genotype interaction.

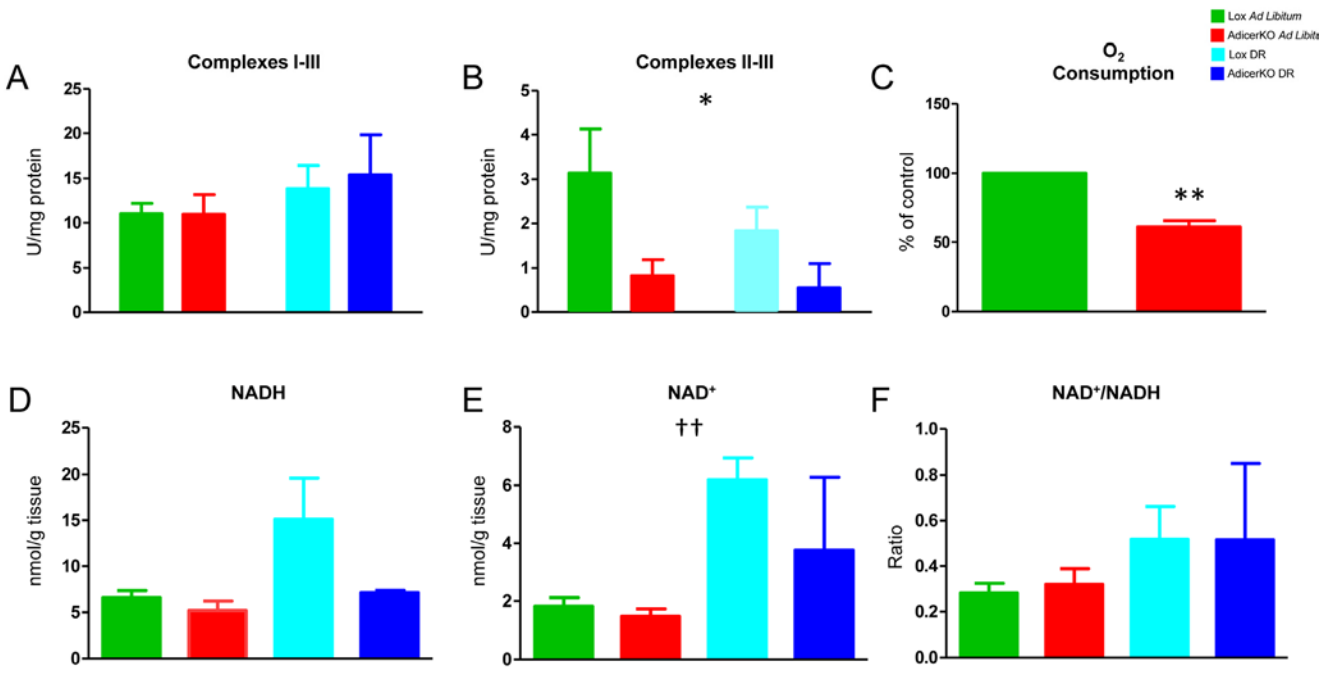

Figure 2. Respiration in white adipose tissue of AdicerKO mice. Twelve-week old mice were subjected to *ad libitum* (AL) or dietary restriction (DR) regimens for one month. Inguinal white adipose tissue (WAT) was isolated and cytochrome c reduction was measured when NADH (**A**) or succinate (**B**) was used as substrate to assess ETC complex I-III or II-III activity, respectively (N=3-5 per condition). (**C**) Adipocytes were isolated and succinate-induced oxygen consumption was measured (N=4 pools of at least 2 animals per condition). (**D**) NADH, (**E**) NAD^+ and (**F**) NAD^+/NADH ratio were determined in whole WAT (representative of two independent experiments with N=2-6 per condition in each experiment). Values are mean ± SEM. * $P < 0.05$, ** $P < 0.01$ for genotype effect; †† $P < 0.01$ for diet effect.

Decreased respiration in the WAT of AdicerKO mice could be caused by low substrate availability. The levels of NADH – the major substrate for the electron transport chain (ETC) – did not differ in WAT of Lox vs. AdicerKO mice, but trended upwards more dramatically in Lox compared to AdicerKO mice with DR, although these differences did not reach statistical significance (Fig. 2D). NAD^+ levels were similarly increased with DR independently of the genotype (Fig. 2E) and no differences were observed in the NAD^+/NADH ratios (Fig. 2F). ATP levels were similar between the groups (Fig. 3A), while lactate levels were 3.3-fold higher in AdicerKO mice subjected to DR when compared to the Lox controls on the same regimen (Fig. 3B), indicating a counterintuitive shift towards anaerobic metabolism in AdicerKO mice during a state of negative energy balance.

Reduced mitochondrial biogenesis in AdicerKO WAT under DR

We next hypothesized that reduced oxidative metabolism could be linked to a reduction in mitochondrial mass and/or number in the WAT of AdicerKO mice. Mitochondrial DNA (mtDNA), a marker of mitochondrial mass, was reduced in the WAT of AdicerKO mice fed AL when compared to the Lox controls, and increased by a similar level in both genotypes upon DR (Fig. 3C). Citrate synthase level - a second mitochondrial mass marker - was not different when comparing Lox and AdicerKO mice under the AL regimen; however it increased significantly in response to DR in Lox but not in AdicerKO WAT (Fig. 3D). Similar patterns were observed when we measured the expression of nuclear- and mitochondria-encoded genes of the ETC (Fig. 3E), as well as the mitochondrial transcription factor *Tfam* (Fig. 3F).

Consistent with a causal role of Dicer in promoting WAT mitochondrial biogenesis in response to DR, and reinforcing the importance of this protein in the early events of the dietary intervention, both Dicer protein levels and the mitochondrial complex I marker *Ndufs8* were upregulated by as early as 3.5-days of DR (Supplementary Fig. 4 A-C). Dicer expression was further increased with time and reached maximum

upregulation within 10.5-days of DR (Supplementary Fig. 4B). In addition, to test if it was the ablation of Dicer in adipocytes or the consequent age-dependent lipodystrophic phenotype of AdicerKO mice that blocked the effect of DR over mitochondrial biogenesis in WAT, we studied the effect of the regimen in young mice, before the onset of lipodystrophy [16]. Consistent with a direct role of Dicer in mitochondrial biogenesis, DR induced the expression of ETC genes in WAT of 8-week old Lox mice, but not in aged matched AdicerKO mice (Supplementary Fig. 4D). These data demonstrate that DR promotes a robust induction of mitochondrial biogenesis in WAT that is blocked by adipocyte-specific Dicer loss-of-function.

In agreement with the molecular data, electron microscopies of the WAT revealed less abundant mitochondria in the WAT of AL-fed AdicerKO mice (Fig. 4A). On the other hand, while DR induced accumulation of healthy-looking mitochondria in the adipocytes of Lox mice, it resulted in fewer mitochondria with highly irregular shapes and aberrant cristae in AdicerKO mice, hallmarks of a dysfunctional organelle (Fig. 4A and B).

Structural changes in the WAT of AdicerKO mice upon DR

To assess if the differences in substrate utilization and mitochondrial mass were associated with morphological changes in the WAT of AdicerKO mice, we performed histological analyses. Adipocytes of AdicerKO mice tended to be larger and more unilocular than those of Lox mice on the AL diet (Fig. 4C and Supplementary 5A and B), but these differences did not reach statistical significance. Under DR, adipocytes of Lox became multilocular, while the tissue of AdicerKO appeared fibrotic and filled with cell infiltrate in some areas (Fig. 4C). Consistently, markers of inflammation were increased in the WAT of AdicerKO mice upon DR, in contrast with the effect of DR on Lox mice, which decreased inflammation markers (Fig. 4D).

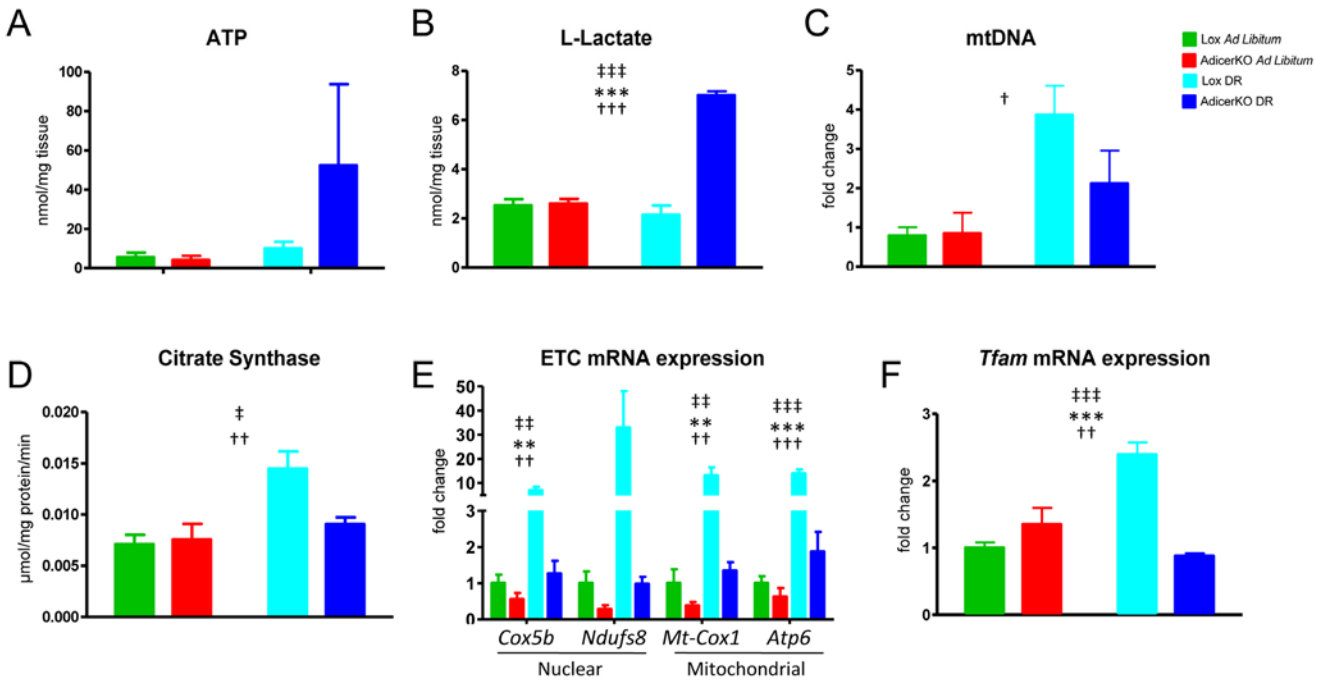

Figure 3. Mitochondrial function and biogenesis in adipose tissue of AdicerKO mice. Twelve-week old mice were subjected to *ad libitum* (AL) or dietary restriction (DR) regimens for one (**A,B,D**) or three (**C,E,F**) months. WAT was isolated and (**A**) ATP and (**B**) L-lactate levels were measured in protein-free extracts (N=3-4 per condition); (**C**) mitochondrial DNA (mtDNA) (normalized by nuclear DNA) was assessed by qPCR (N=3 per condition); (**D**) Citrate Synthase activity was determined in protein extracts (N=4-5 per condition); and (E-F) gene expression was quantitated by RT-qPCR (N=4 per condition). Mean ± SEM. ** P< 0.01, *** P < 0.001 for genotype effect; † P < 0.05, †† P < 0.01, ††† P < 0.001 for diet effect; ‡ P < 0.05, ‡‡ P < 0.01, ‡‡‡ P < 0.001 for diet-genotype interaction.

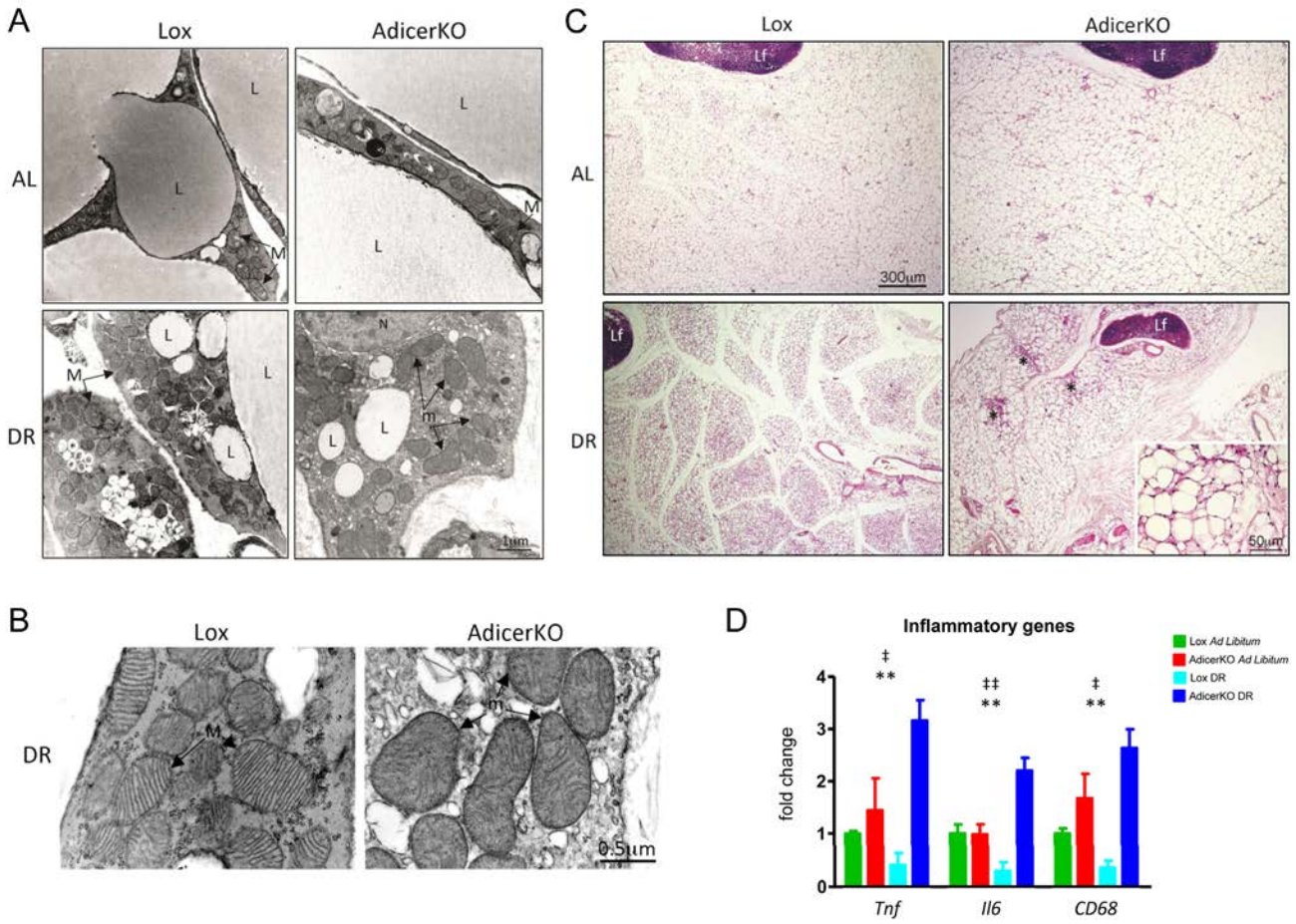

Figure 4. Morphology of white adipose tissue of AdicerKO mice. Twelve-week old mice were subjected to *ad libitum* (AL) or dietary restriction (DR) regimens for one (**A**-**C**) or three (**D**) months. Inguinal white adipose tissue (WAT) was isolated and analyzed at the (A,B) ultrastructure level (electron microscopy) or at the (C) histological level (H&E) (N=4-5 animals per condition). L, lipid droplet. M, healthy mitochondrium. m, damaged hypertrophic mitochondrium. Lf, lymph node. N, nucleus. *, fibrosis. (D) Inflammation markers were assessed by RT-qPCR (N=3-4 per condition). Mean ± SEM. ** P < 0.01 for genotype effect; ‡ P < 0.05, ‡‡ P < 0.01 for diet-genotype interaction.

Surprisingly, protein carbonylation (Supplementary Fig. 5C) and glutathione levels (Supplementary Fig. 5D) - markers of oxidative damage - were not changed or minimally affected among the groups.

Insulin resistance in AdicerKO mice

Mitochondrial dysfunction in the adipose tissue and increased inflammation are often associated with insulin resistance [20, 21]. Indeed, AdicerKO mice are insulin resistant, in particular at the level of the adipose tissue [[16] and Fig. 5]. Strikingly, AdicerKO mice remained insulin resistant even under the DR regimen (Fig. 5A), despite showing improved glucose tolerance (Supplementary Fig. 6A) when compared to mice on the AL condition. Whole body insulin resistance in Adicer KO mice was associated with reduced insulin signaling in WAT as measured by Akt and Erk1/2 phosphorylation (Fig. 5B). Interestingly, deletion of Dicer in adipocytes led to downregulation of total Akt levels and selective inhibition of insulin-induced p42 (Erk2) phosphorylation (Fig. 5B). Akt is phosphorylated at Ser473 by the insulin-dependent, rapamycin-insensitive mTORC2 complex [22]. On the other hand, mTORC2 is inhibited by chronic stimulation of the mTORC1 complex, which is in turn activated by BCAA [23]. We thus estimated basal mTORC1 activity by assessing the phosphorylation of the ribosomal protein S6. S6 phosphorylation was markedly increased in WAT of AdicerKO mice, both under the AL and DR regimens (Fig. 5C), indicating hyperactivation of mTORC1. Since we found increased levels of

circulating BCAA in AdicerKO mice, we asked whether other non-adipose tissues also showed elevated mTORC1 activity. Indeed, S6 phosphorylation was increased in skeletal muscle of AdicerKO mice under both regimens, despite no changes in Akt or Erk phosphorylation (Fig. 5D). On the other hand, phosphorylation of Erk was reduced in liver of AdicerKO mice with no changes in Akt (Supplementary Fig. 6B).

If hyperactivation of mTORC1 in insulin-sensitive tissues was the cause of insulin resistance in AdicerKO mice, one would expect this phenotype to be reversed by selective inhibition of mTORC1, as previously shown [24]. In agreement with this notion, acute rapamycin injection not only markedly improved insulin sensitivity in AdicerKO mice on the AL diet, but also completely reversed insulin resistance of these mice under the DR regimen (Fig. 5E and F). These results demonstrate that increased mTORC1 activation - possibly due to elevated levels of circulating BCAA - leads to whole body insulin resistance in AdicerKO mice.

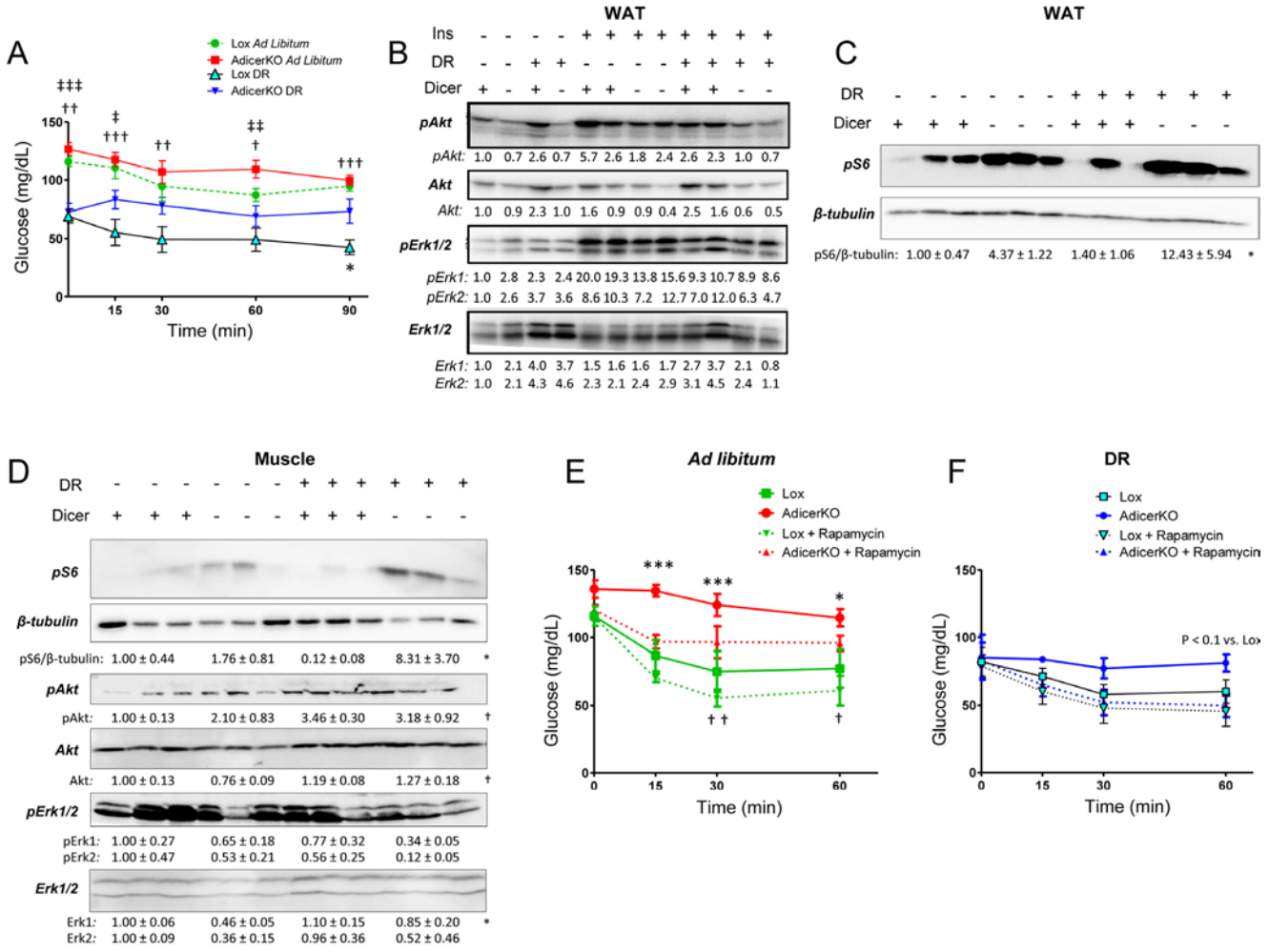

Figure 5. Insulin resistance and mTORC1 hyperactivation in AdicerKO mice. Twelve-week old mice were subjected to *ad libitum* (AL) or dietary restriction (DR) regimens for one (**A,B**) or three (**C**-**F**) months. (**A**) Insulin tolerance test (N=5-7 per condition). * P < 0.05 Lox DR vs. AdicerKO DR; † P < 0.05, †† P < 0.01, ††† P < 0.001 Lox AL vs. Lox DR; ‡ P < 0.05, ‡‡ P < 0.01, ‡‡‡ P < 0.001 AdicerKO AL vs. AdicerKO DR. (**B**-**D**) Western blots of tissue extracts when (**B**) insulin was injected in the inferior vena cava and WAT was collected 5 minutes after, or (**C,D**) at basal, random fed state. WAT, inguinal white adipose tissue. Muscle, gastrocnemius. +, the presence of the protein or intervention. -, the absence of the protein or intervention. pS6, phospho-S6. pAkt, phospho-Akt. pErk1/2, phospho-Erk1/2. Numbers are quantitation of blots (fold expression in comparison to control group) ± SEM. * P < 0.05 for genotype effect; † P < 0.05 for diet effect. (**E,F**) Mice subjected to AL (**E**) or DR (**F**) diets were treated with Rapamycin for 2h prior to an insulin tolerance test (N=3-5 per condition). Mean ± SEM. * P < 0.05, *** P < 0.001 Lox vs. AdicerKO; † P < 0.05, †† P < 0.01 Lox + Rapamycin vs. AdicerKO + Rapamycin.

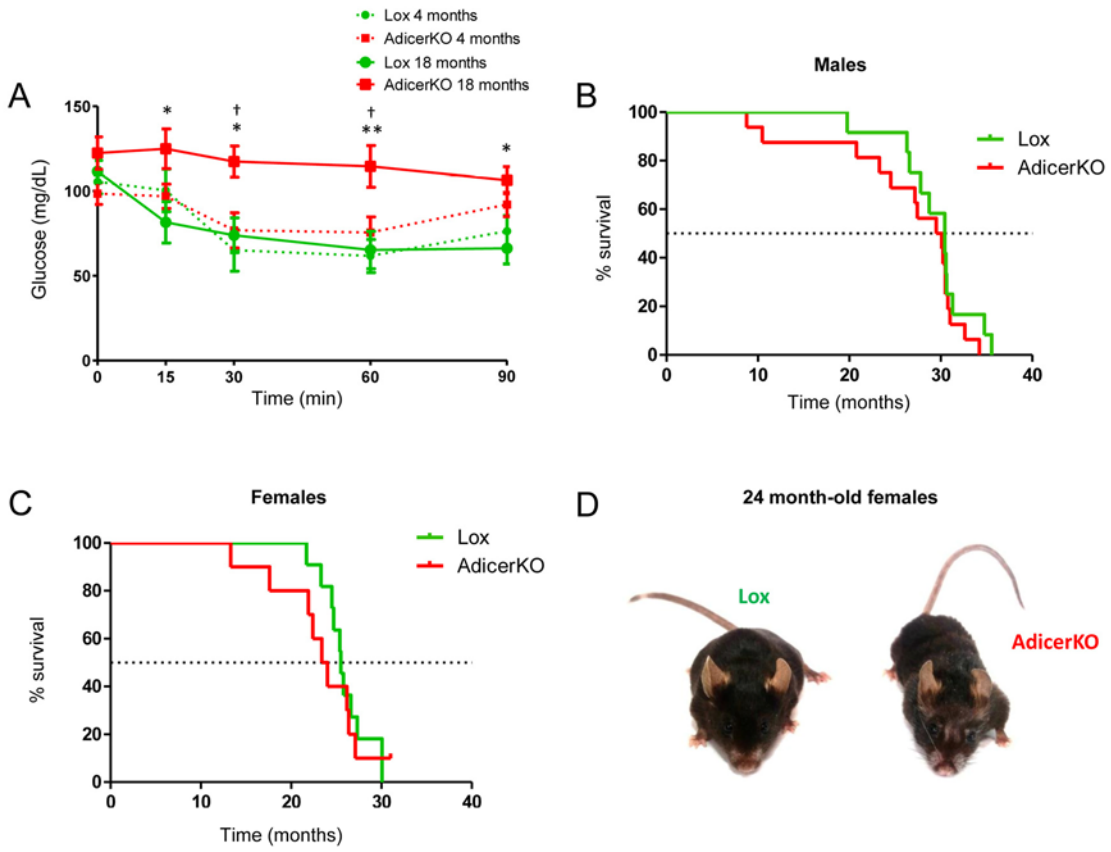

Figure 6. Increased risk of mortality and premature age-related complications in AdicerKO mice. (**A**) Insulin tolerance test in young (4-month old) or old (18-month old) male AdicerKO and Lox mice (N=6-7 per condition). Mean ± SEM. * P < 0.05, ** P < 0.01 Lox 18 months vs. AdicerKO 18 months; † P < 0.05 AdicerKO 18 months vs. AdicerKO 4 months. (**B**,**C**) Kaplan-Meier curves of (**B**) male (N=12-16 per genotype) and (**C**) female (N=10-11 per genotype) Lox and AdicerKO mice. (**D**) Representative pictures of 24-month old females. Mice were fed *ad libitum* during these experiments.

AdicerKO mice exhibit age-associated insulin resistance and increased premature mortality risk

Next, to test whether insulin resistance in AdicerKO mice was associated with aging, we performed insulin tolerance tests in young (4 month-old) and old (18-month-old) mice that had AL access to chow during their entire lifespan. Insulin resistance was minimal in young AdicerKO mice, while in old animals it was markedly different (Fig. 6A). We also determined the life expectancy of these mice. Median survival was not different between Lox and AdicerKO mice [Males: Lox vs. AdicerKO = 30.4 vs. 29.8 months, P = 0.3601 (Fig. 6B); Females: Lox vs. AdicerKO = 25.5 vs. 23.7 months, P = 0.5579 (Fig. 6C)], but Gompertz modeling [25] revealed that the initial mortality rate (vulnerability) was significantly higher in AdicerKO mice with no difference in age-dependent mortality (aging rate). Furthermore, female AdicerKO mice exhibited more frequent signs of senescence (such as hair loss or graying) at their median lifespan (24 months of age) than did Lox mice (Fig. 6D). Hence, AdicerKO mice are more prone to early death and trend toward premature aging, but the animals that survive to the last quartile of their lifespan seem to be as sensitive to age-dependent mortality as Lox controls.

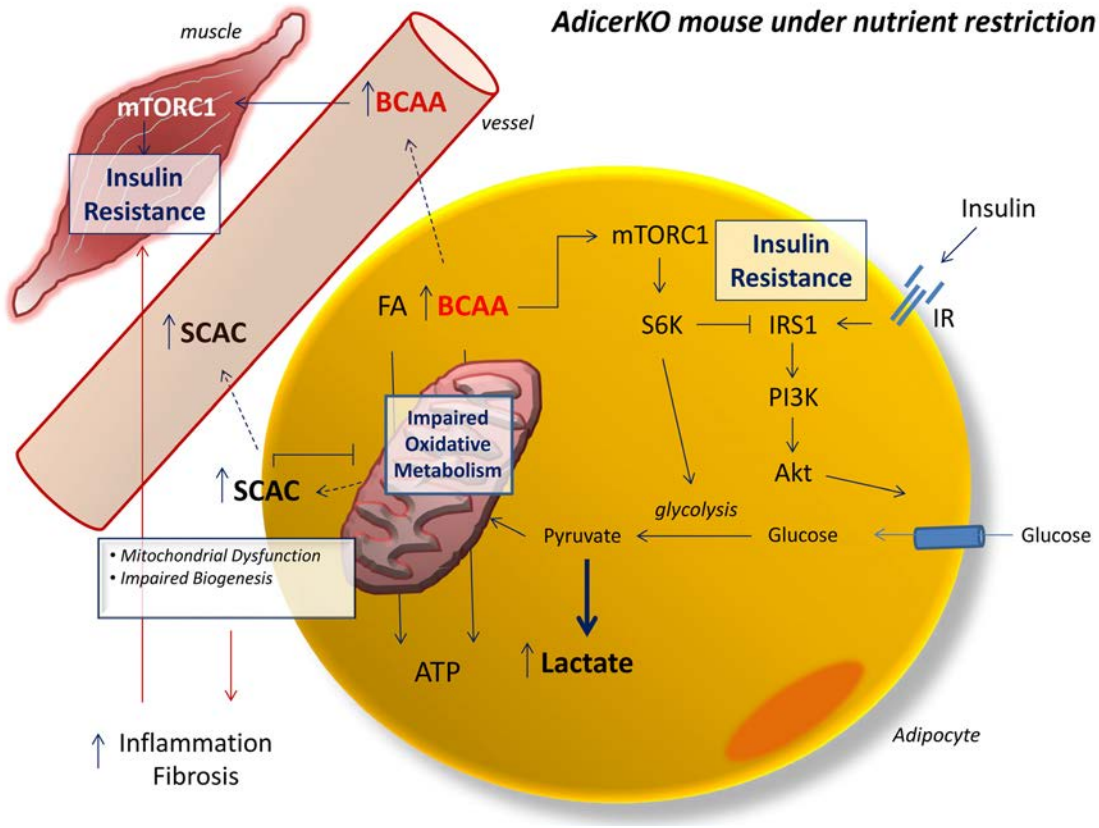

Figure 7. Metabolic dysfunction in AdicerKO mice under nutrient restriction. Schematic model of the metabolic consequences of fat-specific Dicer knockout in mice under nutrient restriction. FA, fatty acid. BCAA, branched-chain amino acid. SCAC, short-chain acylcarnitines. IR, insulin receptor. Solid arrows, activation. Dashed arrows, transport. T-bars, inhibition.

DISCUSSION

The regulation of Dicer expression in the adipose tissue and its consequent impact on global miRNA levels have been proposed to represent an evolutionarily conserved feature of aging and a mechanism through which DR delays the aging process [15, 18]. Here we used mice lacking Dicer in adipocytes (AdicerKO) to directly test these hypotheses. Metabolomic analyses reveal marked changes in the levels of BCAA and SCAC in the blood stream of fasted, middle-aged AdicerKO in comparison to Lox mice, both under the DR and AL regimens. These changes are in agreement with the low oxidative profile of AdicerKO adipocytes. Under short-term DR, the adipose tissue of Lox mice activates a program of mitochondrial biogenesis and oxidative metabolism, whereas the fat tissue of AdicerKO mice shifts its metabolism towards anaerobic glycolysis while abrogating mitochondrial biogenesis. In turn, this leads to tissue dysfunction and inflammation, which contributes to insulin resistance [18, 20, 21, 26] (Fig. 7).

Insulin resistance in AdicerKO mice is partially or entirely explained by hyperactivation of mTORC1, depending on the dietary regimen. mTORC1 is activated by BCAA [23], which are elevated in the serum of AdicerKO mice. When activated, mTORC1 leads to phosphorylation of S6 kinase, which in turn phosphorylates IRS1 in a serine residue, therefore inhibiting it and impairing insulin signaling [27, 28]. S6 kinase knockout mice are long-lived and display characteristics that resemble the effects of DR, such as protection from age-dependent insulin resistance [29]. Conversely, high levels of circulating BCAA in obesity and chronic mTORC1 activation have been previously linked to T2D and aging in humans and animal models [13, 30-34]. Another facet of BCAA-induced insulin resistance is related to increased BCAA catabolism in the muscle, which leads to incomplete fatty acid oxidation, gives rise to SCAC that allosterically inhibit citrate synthase, results in mitochondrial stress and impairs insulin action [13]. Hyperactivation of mTORC1 also shifts metabolism towards glycolysis and

de novo lipid biosynthesis [35], which in sum are phenotypes observed in the AdicerKO mouse under DR. Adipose tissue is a major site for BCAA oxidation and this process is impaired during T2D [12, 13, 19, 30]. Dicer expression is decreased in the adipose tissue of mouse models and humans with increased risk for T2D, such as during obesity, aging and lipodystrophy [15, 16, 18], while increased upon DR [15]. Based on this scenario, we conclude that higher levels of Dicer in adipose tissue are necessary to sustain a proper response to fluctuations in energy demands by conferring adequate substrate utilization and promoting oxidative metabolism. When nutrients are particularly limiting, reduced levels of Dicer negatively impact on adipose tissue oxidative metabolism, raising the blood levels of BCAA and SCAC, contributing to mTORC1 activation and resulting in whole body insulin resistance (Fig. 7). Consistent with this notion, AdicerKO mice do not benefit from some of the classic metabolic outcomes of DR, such as increased insulin sensitivity and decreased inflammation, and have accelerated age-dependent insulin resistance and premature mortality.

Dicer knockout in adipocytes leads to partial lipodystrophy in middle-aged mice as manifested by decreased intra-abdominal fat accumulation and hypertrophy and "whitening" of the interscapular brown fat depot [16]. Since the subcutaneous inguinal fat pad is not grossly affected in size or morphology in chow diet fed, young adult AdicerKO mice [[16] and this study], and given that the impact of aging and DR on Dicer expression is more clearly manifested in this tissue [15], we decided to focus our efforts on this depot. By doing so we wanted to minimize developmental changes in adipose tissue composition and essentially look for changes that occurred in response to DR or aging. Indeed, some of the observations made in 3-month old AdicerKO mice subjected to DR were confirmed in younger mice, prior to the onset of lipodystrophy. These experiments corroborate the notion that Dicer expression in adipocytes is required for a proper response to DR, and not that lipodystrophy mitigates the effect of the diet. In agreement, short term (3.5 days), moderate (10%) DR is able to upregulate Dicer in adipose tissue of wild type mice while also upregulating genes of the mitochondrial ETC, prior to changes in body weight.

The differences in the expression of mitochondrial and β-oxidation-related genes in the adipose tissue of AdicerKO versus Lox mice are particularly evident under DR. Likewise, lactate levels are increased in the fat tissue of AdicerKO mice only in response to this dietary regimen, pointing towards a shift to anaerobic glycolysis during a state of chronic catabolism. Intriguingly, there is a concomitant increase in triglyceride synthesis from valine in the adipose tissue of AdicerKO mice on DR, which suggests diversion of carbons to lipid anabolism. Increases in anaerobic glycolysis and in the flux through anabolic pathways under nutrient limiting states also occur in many cancer cells and are often referred to as the Warburg effect [36]. Interestingly, as in Dicer knockout adipocytes, many of these cancer cells have decreased Dicer levels [37] and reduced oxidative activity [36]. Thus, our data suggest that Dicer knockout adipocytes exhibit a Warburg-like behavior when put on nutrient restriction, somewhat resembling the behavior of cancer cells. This could be linked to the activation of senescence and inflammation pathways that are hallmarks in the adipose tissue of AdicerKO mice and in Dicer knockout preadipocytes (this study and [15]).

The question that remains is why Dicer knockout adipocytes actively divert to non-oxidative metabolism when subjected to nutrient restriction despite having adequate mitochondrial capacity and plenty of substrates. One possible explanation is that under DR, Dicer upregulation in wild type adipocytes leads to the increase of miRNAs that suppress glycolytic genes to favor oxidative metabolism, a phenomenon that would not occur in AdicerKO mice. Dicer levels may be rate-limiting for these miRNAs or their effects may become more evident in a situation when catabolic flux is promoted. Indeed, when lactate or mitochondrial gene expression is assessed in various cell culture models of Dicer knockout preadipocytes, no differences are observed when comparing these cells to the wild type (unpublished data). These cells are cultured and differentiated into adipocytes in an atmosphere of 20% oxygen and in high glucose, high growth factor medium, which is distant from the pseudo-hypoxic, highly oxidative and growth limiting conditions of DR *in vivo*. Moreover, the cells are not exposed to the changes in circulating factors that occur during DR or in response to fat-specific Dicer knockout. Hence, more studies are required to determine the exact mechanism through which Dicer controls adipocyte metabolism during catabolic states.

We and others have shown that Dicer is pivotal in stress responses, metabolic diseases and aging [15, 38, 39]. miRNAs are involved in specific aspects of these mechanisms [39-43], but they are differently expressed, play different roles in distinct cell types and conditions and are unlikely to individually explain the plethora of phenotypes that are characteristic of aging or T2D [44]. Furthermore, while miRNAs are likely to participate as downstream molecular players involved in the phenotypes of AdicerKO mice, Dicer also binds to and

directly controls the levels of a wide range of RNAs in the cell, including other non-coding RNAs such as tRNAs or even mitochondrial-encoded mRNAs [14]. Therefore, we propose a scenario where during metabolic stress, Dicer becomes rate-limiting for the biosynthesis of certain RNAs while promoting the degradation of others. These downstream RNAs may vary depending on the cell type, condition or degree of cell differentiation. Dicer upregulation will then favor these processes to promote context-specific adaptation to stress and increase cell robustness [45]. When this occurs in adipocytes, context-specific adaptation to metabolic stress leads to proper substrate utilization and results in efficient nutrient mobilization to metabolic tissues that depend largely on the adipose tissue in situations of calorie deprivation, such as the skeletal muscle. This confers more efficient usage of the scarcely available energy and also contributes to organismal metabolic plasticity, which in turn protects from premature metabolic diseases and eventually death. It also prevents the accumulation of circulating metabolites (such as BCAA) that act as signaling molecules to activate pathways that are positively involved in growth and energy storage while negatively involved in longevity (such as the mTOR pathway) (Fig. 7).

In conclusion, we now provide direct evidence that adipose tissue Dicer is necessary for proper nutrient utilization by adipocytes and essential for the beneficial effects of DR, such as improved whole-body insulin sensitivity. We also demonstrate that adipocyte-specific Dicer knockout is sufficient to accelerate the appearance of insulin resistance in mice, while leading to premature mortality. Our study and the evolutionary conserved association between Dicer regulation, metabolic diseases and aging set the stage for new interventions to prolong healthspan in humans.

MATERIALS AND METHODS

Animals. Fat-specific Dicer knockout mice (AdicerKO) and their littermate controls (Lox) were obtained from the Centro de Desenvolvimento de Modelos Experimentais para Medicina e Biologia (CEDEME) of the Universidade Federal de São Paulo. Males were used in all cases unless stated otherwise. Mice were maintained on a 12-hr light-dark cycle with *ad libitum* access to tap water and chow diet. Dietary restriction was performed according to the protocol of the National Institute on Aging [15, 46]. Food intake and body weight was assessed weekly. Mice were euthanized at the indicated time-points during random feeding unless indicated otherwise. After euthanasia, tissues were collected, weighed and immediately used or frozen in dry ice and stored at -80^{o}C. Protocols for animal use were approved by the IACUC of the Universidade Federal de São Paulo (CEP-0218/11, CEP-0237/12 and CEUA4603261015) and were in accordance with NIH guidelines.

Metabolomics. Serum metabolites were measured by mass spectrometry (BIOCRATES Life Sciences). The results were analyzed using MetaboAnalyst (www.metaboanalyst.ca) [47]. Values were normalized by the pooled average value from the Lox AL group, Log2 transformed, and Pareto scaled (mean-centered and divided by the square root of standard deviation of each variable).

Western blotting and qPCR. These methods were performed as described previously [15, 16]. For mitochondrial DNA quantitation, total DNA was extracted using DNeasy Blood & Tissue kit (Qiagen) and subjected to qPCR using primers targeting mitochondrial or nuclear DNA. Antibodies were: Dicer (Ab13502) from Abcam and phosphor-S6 (5364), Akt (9272), phosphor-Akt (9271), Erk (9102), phospho-Erk (9101), and β-tubulin (2146) from Cell Signaling. The primer sequences will be made available upon request.

Mitochondrial enzymatic activity. Inguinal white adipose tissue was disrupted in 0.1 M potassium phosphate buffer with 5 mM EDTA using a Dounce homogenizer. The homogenate was centrifuged at 10,000 x g for 10 min at 4 ˚C to remove the fat, and the supernatant was used for protein quantification (BCA kit, Pierce) and determination of citrate synthase and electron transport activities. Citrate synthase was determined as previously described [48] using 3-10 µg of total homogenate. Activity of complexes II-III or I-III was assayed as described in [49], using 80-150 µg of total homogenate and succinate or NADH as substrates, respectively. The rate of cytochrome c reduction that was insensitive to antimycin A was subtracted from all measurements.

Substrate oxidation. Valine oxidation into CO_2 or α-ketoisovaleric acid (αKIV) was measured according to [12] with slight modifications. Palmitate oxidation and incorporation into lipids was measured as described previously [50]. Briefly, tissues were minced, weighed and placed into glass tubes (approximately 10 mg per tube) containing 0.5 ml of Krebs-Ringer bicarbonate buffer [in mM: 118 NaCl, 4.8 KCl, 1.25 $CaCl_2$, 1.2 KH_2PO_4, 1.2 $MgSO_4$, 25 $NaHCO_3$, 10 HEPES (pH 7.4)]. For valine assays, the buffer was supplemented with 5 mM glucose and 1 mM valine containing 0.2 µCi [U-^{14}C] valine per tube. For palmitate assays, the buffer was supplemented with 100 µM palmitate containing

0.2 μCi [U-^{14}C] palmitate per tube. For adipose tissue samples, the buffer was also supplemented with 2% (w/v) BSA (fatty acid free). For muscle samples, the buffer was supplemented with 0.2% (w/v) BSA. A dry piece of Whatman paper was placed inside the tube around its upper part, with no direct contact with the buffer, in order to absorb the CO_2 produced. The tubes were sealed with parafilm and tissue explants were incubated with shaking at 37 °C. After 1h, the reaction was terminated with the injection of 200 μL of 6N sulfuric acid into the reaction mixture and 200 μL of phenyletilamine:methanol (1:1) onto the Whatman paper. After 20 min the paper was collected. In the valine assays, the paper was replaced and the tubes were resealed. Hydrogen peroxide (200 μL, 30% w/v) was injected into the reaction mixture and 200 μL of phenyletilamine:methanol (1:1) onto the paper for collecting the CO_2 generated by the decarboxylation of αKIV. Explants were removed and destined to lipid extraction with 1 mL of chloroform:methanol (2:1). ^{14}C radioactivity was assessed in the papers or lipid extracts and normalized by tissue weight.

Oxygen consumption. Oxygen consumption was performed in isolated adipocytes using the Oroboros O2k oxygraph. Adipocytes from the inguinal fat depots were isolated and respiratory rate was measured as previously described [51, 52]. Adipocytes from 3-5 mice per group were pooled in KRP buffer (130 mM NaCl, 4.7 mM KCl, 1.24 mM $MgSO_4$, 2.5 mM $CaCl_2$, 10 mM HEPES, 2.5 mM NaH_2PO_4, 5 mM D-glucose, 2% BSA). Respiration was measured in KRP devoid of BSA. 1 mM succinate and 0.5 μg/ml antimycin A were added sequentially. Respiration before addition of succinate was subtracted from all rates. Succinate-dependent respiration was obtained by subtracting antimycin A-insensitive respiratory rate. Values were normalized by the number of cells and expressed as percentage of Lox.

Biochemical analyses. For lactate and ATP assays, tissues were homogenized in 4% trichloroacetic acid and subjected to two rounds of centrifugations for 5 min at 13,000 g and 4 ˚C. The supernatant had the pH adjusted to 7.0 and was used for lactate quantitation as described in [53] or ATP measurement using an ATP Bioluminescent Assay Kit from Sigma-Aldrich. NAD^+ and NADH were measured using the NAD/NADH Assay Kit from Bioassays. Values were normalized by tissue weight. For glutathione determination, tissue homogenates (diluted in 0.1 M potassium phosphate buffer/5 mM EDTA) were de-proteinized by addition of 0.6% sulfosalycilic acid/0.1% Triton X-100 and centrifugation for 10 min at 8,000 x g and 4 ˚C. The supernatant was used for glutathione determination as described in [54]. Glutathione levels were normalized by the protein content in the pre de-proteinized aliquot, as measured by the BCA kit (Pierce).

Protein carbonylation. One volume of protein extract (maximum protein concentration of 4 mg/mL) was mixed with one volume of 24% SDS and one volume of 40 mM 2,4-dinitrophenylhydrazine solution. The mixture was incubated for 30 min at room temperature in the dark. A neutralizing solution containing 2 M Tris, 30% Glycerol and 19% mercaptoethanol was titrated into the mixture until it became orange. The neutralized mixture was then subjected to western blotting using equal amounts of protein and an antibody targeting dinitrophenyl (D9656) from Sigma-Aldrich.

Microscopy. Microscopy analyses were performed as previously described [55]. Briefly, mice were anesthetized and transcardiacally perfused for 5-8 min with 2% glutaraldehyde in 0.1 M phosphate buffer (pH 7.4). After perfusion, WAT was isolated and kept in 0.1% glutaraldehyde/0.1 M phosphate buffer (pH 7.4). Thin sections were obtained with an MT-X ultratome (RMC). Slices were separated for histological analyses and stained with hematoxylin and eosin (H&E). For transmission electron microscopy, slices were stained with lead citrate and examined with a CM10 transmission electron microscope (Philips). Morphometric evaluation of adipocytes was performed blindly using image analysis software (Lucia IMAGE Software, Laboratory Imaging). H&E images were used for determination of mean adipocyte size and adipocyte type.

Insulin sensitivity and glucose tolerance. Glucose and insulin tolerance tests were performed one week prior to the euthanasia and followed the protocols described elsewhere [16]. Briefly, mice were injected intraperitoneally with glucose (1 g/kg body weight) after overnight fasting or insulin (0.75U/kg body weight; Humalog, Eli Lilly) after 2h fasting. Blood samples were collected at the indicated time-points through a small cut at the tail tip of the mouse and glucose levels were measured using a glucometer (Accu-Chek, Roche). When indicated, rapamycin (LC laboratories) was given i.p. (5 mg/kg body weight in 0.2% methylcellulose) 2h prior to the insulin injection. To assess insulin signaling, mice were fasted overnight, anesthetized and injected with a bolus of insulin (10 U) into the inferior vena cava. After 5 min, mice were euthanized and WAT was collected. Phosphorylation of Akt and Erk was determined by western blotting.

Life expectancy. Kaplan-Meier curves were determined for *ad libitum*, chow diet fed male and female mice.

Median lifespan was assessed using GraphPrism and Gompertz modeling using JMP.

Statistical analysis. Results are expressed as the mean ± standard error of the mean (SEM) unless indicated otherwise. We used Student t test to compare two independent groups and ANOVA to compare more than two groups. Two-way ANOVA was used when data had more than one categorical independent variable. We used the MetaboAnalyst package of statistical tools to analyze and test the metabolomic data. Statistical significance was consider when $P < 0.05$.

ACKNOWLEDGEMENTS

We thank Emanuel B. Cabral, Ivan H. Cordeiro, Grazielle C. R. da Silva and Mariana C. dos Santos, of the Federal University of Sao Paulo, for technical support.

Author Contributions

M.A.M., F.C.G.R., A.J.K., B.B.B., B.A.G., I.D.S., A.F. and W.T.F. provided study concept or design. F.C.G.R., J.L.O.B., B.B.B, B.A.G., T.T., A.F., L.S. and W.T.F. acquired data. M.A.M., F.C.G.R., J.L.O.B., B.B.B., B.A.G., I.D.S., A.F., L.S., S.C., W.T.F., and A.J.K. provided analysis and interpretation of data. M.A.M. and F.C.G.R. drafted the manuscript. All authors critically revised the manuscript for important intellectual content. M.A.M., T.T., I.D.S., A.F., S.C., C.R.K., W.T.F, and A.J.K. provided material support. M.A.M., A.F., S.C., C.R.K., W.T.F, and A.J.K. supervised the study.

Funding

This study was supported by grants of FAPESP (2010/52557-0, 2015/01316-7, and 2011/24109-6), CNPq and CAPES.

Conflict of interest statement

The authors declare no conflict of interest.

REFERENCES

1. Lopez-Otin C, Blasco MA, Partridge L, Serrano M and Kroemer G. The hallmarks of aging. Cell. 2013; 153:1194-1217.

2. Fontana L and Partridge L. Promoting health and longevity through diet: from model organisms to humans. Cell. 2015; 161:106-18.

3. Barzilai N, Huffman DM, Muzumdar RH and Bartke A. The critical role of metabolic pathways in aging. Diabetes. 2012; 61:1315-22.

4. Martin-Montalvo A and de Cabo R. Mitochondrial metabolic reprogramming induced by calorie restriction. Antioxidants & redox signaling. 2013; 19:310-20.

5. Robertson LT and Mitchell JR. Benefits of short-term dietary restriction in mammals. Experimental gerontology. 2013; 48:1043-48.

6. Fontana L. Neuroendocrine factors in the regulation of inflammation: excessive adiposity and calorie restriction. Experimental gerontology. 2009; 44:41-5.

7. Speakman JR and Mitchell SE. Caloric restriction. Molecular aspects of medicine. 2011; 32:159-221.

8. Soare A, Weiss EP and Pozzilli P. Benefits of caloric restriction for cardiometabolic health, including type 2 diabetes mellitus risk. Diabetes/metabolism research and reviews. 2014; Suppl 1:41-7.

9. Barzilai N, Banerjee S, Hawkins M, Chen W and Rossetti L. Caloric restriction reverses hepatic insulin resistance in aging rats by decreasing visceral fat. The Journal of clinical investigation. 1998; 101:1353-61.

10. Sun K, Kusminski CM and Scherer PE. Adipose tissue remodeling and obesity. The Journal of clinical investigation. 2011; 121:2094-2101.

11. Waki H and Tontonoz P. Endocrine functions of adipose tissue. Annu Rev Pathol. 2007; 2:31-56.

12. Herman MA, She P, Peroni OD, Lynch CJ and Kahn BB. Adipose tissue branched chain amino acid (BCAA) metabolism modulates circulating BCAA levels. The Journal of biological chemistry. 2010; 285:11348-56.

13. Newgard CB. Interplay between lipids and branched-chain amino acids in development of insulin resistance. Cell metabolism. 2012; 15:606-14.

14. Rybak-Wolf A, Jens M, Murakawa Y, Herzog M, Landthaler M and Rajewsky N. A variety of dicer substrates in human and C. elegans. Cell. 2014; 159:1153-67.

15. Mori MA, Raghavan P, Thomou T, Boucher J, Robida-Stubbs S, Macotela Y, Russell SJ, Kirkland JL, Blackwell TK and Kahn CR. Role of MicroRNA Processing in Adipose Tissue in Stress Defense and Longevity. Cell metabolism. 2012; 16:336-47.

16. Mori MA, Thomou T, Boucher J, Lee KY, Lallukka S, Kim JK, Torriani M, Yki-Jarvinen H, Grinspoon SK, Cypess AM and Kahn CR. Altered miRNA processing disrupts brown/white adipocyte determination and associates with lipodystrophy. The Journal of clinical investigation. 2014; 124:3339-51.

17. Torriani M, Srinivasa S, Fitch KV, Thomou T, Wong K, Petrow E, Kahn CR, Cypess AM and Grinspoon SK. Dysfunctional subcutaneous fat with reduced Dicer and brown adipose tissue gene expression in HIV-infected patients. The Journal of clinical endocrinology and metabolism. 2016; 101:1225-34.

18. Oliverio M, Schmidt E, Mauer J, Baitzel C, Hansmeier N, Khani S, Konieczka S, Pradas-Juni M, Brodesser S, Van TM, Bartsch D, Bronneke HS, Heine M, et al. Dicer1-miR-328-Bace1 signalling controls brown adipose tissue differentiation and function. Nature cell biology. 2016; 18:328-36.

19. Green CR, Wallace M, Divakaruni AS, Phillips SA, Murphy AN, Ciaraldi TP and Metallo CM. Branched-chain amino acid catabolism fuels adipocyte differentiation and lipogenesis. Nature chemical biology. 2016; 12:15-21.

20. Vernochet C, Damilano F, Mourier A, Bezy O, Mori MA, Smyth G, Rosenzweig A, Larsson NG and Kahn CR. Adipose tissue mitochondrial dysfunction triggers a lipodystrophic syndrome

with insulin resistance, hepatosteatosis, and cardiovascular complications. Faseb J. 2014; 28:4408-19.

21. Mori MA, Liu M, Bezy O, Almind K, Shapiro H, Kasif S and Kahn CR. A systems biology approach identifies inflammatory abnormalities between mouse strains prior to development of metabolic disease. Diabetes. 2010; 59:2960-71.

22. Zhang Z, Zhang G, Xu X, Su W and Yu B. mTOR-rictor is the Ser473 kinase for AKT1 in mouse one-cell stage embryos. Molecular and cellular biochemistry. 2012; 361:249-57.

23. Bar-Peled L and Sabatini DM. Regulation of mTORC1 by amino acids. Trends in cell biology. 2014; 24:400-06.

24. Leontieva OV, Demidenko ZN and Blagosklonny MV. Rapamycin reverses insulin resistance (IR) in high-glucose medium without causing IR in normoglycemic medium. Cell death & disease. 2014; 5:e1214.

25. Simons MJ, Koch W and Verhulst S. Dietary restriction of rodents decreases aging rate without affecting initial mortality rate -- a meta-analysis. Aging cell. 2013; 12:410-14.

26. Osborn O and Olefsky JM. The cellular and signaling networks linking the immune system and metabolism in disease. Nature medicine. 2012; 18:363-74.

27. Patti ME, Brambilla E, Luzi L, Landaker EJ and Kahn CR. Bidirectional modulation of insulin action by amino acids. The Journal of clinical investigation. 1998; 101:1519-1529.

28. Um SH, D'Alessio D and Thomas G. Nutrient overload, insulin resistance, and ribosomal protein S6 kinase 1, S6K1. Cell metabolism. 2006; 3:393-402.

29. Selman C, Tullet JM, Wieser D, Irvine E, Lingard SJ, Choudhury AI, Claret M, Al-Qassab H, Carmignac D, Ramadani F, Woods A, Robinson IC, Schuster E, et al. Ribosomal protein S6 kinase 1 signaling regulates mammalian life span. Science (New York, NY. 2009; 326:140-44.

30. Newgard CB, An J, Bain JR, Muehlbauer MJ, Stevens RD, Lien LF, Haqq AM, Shah SH, Arlotto M, Slentz CA, Rochon J, Gallup D, Ilkayeva O, et al. A branched-chain amino acid-related metabolic signature that differentiates obese and lean humans and contributes to insulin resistance. Cell metabolism. 2009; 9:311-26.

31. Boulet MM, Chevrier G, Grenier-Larouche T, Pelletier M, Nadeau M, Scarpa J, Prehn C, Marette A, Adamski J and Tchernof A. Alterations of plasma metabolite profiles related to adipose tissue distribution and cardiometabolic risk. American journal of physiology. 2015; 309:736-46.

32. Giesbertz P, Padberg I, Rein D, Ecker J, Hofle AS, Spanier B and Daniel H. Metabolite profiling in plasma and tissues of ob/ob and db/db mice identifies novel markers of obesity and type 2 diabetes. Diabetologia. 2015; 58:2133-43.

33. Catalan V, Gomez-Ambrosi J, Rodriguez A, Ramirez B, Andrada P, Rotellar F, Valenti V, Moncada R, Marti P, Silva C, Salvador J and Fruhbeck G. Expression of S6K1 in human visceral adipose tissue is upregulated in obesity and related to insulin resistance and inflammation. Acta diabetologica. 2015; 52:257-66.

34. Sengupta S, Peterson TR, Laplante M, Oh S and Sabatini DM. mTORC1 controls fasting-induced ketogenesis and its modulation by ageing. Nature. 2010; 468:1100-04.

35. Duvel K, Yecies JL, Menon S, Raman P, Lipovsky AI, Souza AL, Triantafellow E, Ma Q, Gorski R, Cleaver S, Vander Heiden MG, MacKeigan JP, Finan PM, et al. Activation of a metabolic gene regulatory network downstream of mTOR complex 1. Molecular cell. 2010; 39:171-83.

36. Senyilmaz D and Teleman AA. Chicken or the egg: Warburg effect and mitochondrial dysfunction. F1000 prime reports. 2015; 7:41.

37. Lu J, Getz G, Miska EA, Alvarez-Saavedra E, Lamb J, Peck D, Sweet-Cordero A, Ebert BL, Mak RH, Ferrando AA, Downing JR, Jacks T, Horvitz HR, et al. MicroRNA expression profiles classify human cancers. Nature. 2005; 435:834-38.

38. Castel SE, Ren J, Bhattacharjee S, Chang AY, Sanchez M, Valbuena A, Antequera F and Martienssen RA. Dicer promotes transcription termination at sites of replication stress to maintain genome stability. Cell. 2014; 159:572-83.

39. Emde A and Hornstein E. miRNAs at the interface of cellular stress and disease. The EMBO journal. 2014; 33:1428-37.

40. Kim HJ, Cho H, Alexander R, Patterson HC, Gu M, Lo KA, Xu D, Goh VJ, Nguyen LN, Chai X, Huang CX, Kovalik JP, Ghosh S, et al. MicroRNAs are required for the feature maintenance and differentiation of brown adipocytes. Diabetes. 2014; 63:4045-4056.

41. Price NL, Ramirez CM and Fernandez-Hernando C. Relevance of microRNA in metabolic diseases. Critical reviews in clinical laboratory sciences. 2014; 51:305-20.

42. Jung HJ and Suh Y. MicroRNA in Aging: From Discovery to Biology. Current genomics. 2012; 13:548-57.

43. Dumortier O, Hinault C and Van Obberghen E. MicroRNAs and metabolism crosstalk in energy homeostasis. Cell metabolism. 2013; 18:312-24.

44. Arner P and Kulyte A. MicroRNA regulatory networks in human adipose tissue and obesity. Nat Rev Endocrinol. 2015; 11:276-88.

45. Leung AK and Sharp PA. MicroRNA functions in stress responses. Molecular cell. 2010; 40:205-15.

46. Turturro A, Witt WW, Lewis S, Hass BS, Lipman RD and Hart RW. Growth curves and survival characteristics of the animals used in the Biomarkers of Aging Program. J Gerontol A Biol Sci Med Sci. 1999; 54:492-501.

47. Xia J, Sinelnikov IV, Han B and Wishart DS. MetaboAnalyst 3.0--making metabolomics more meaningful. Nucleic acids research. 2015; 43:251-57.

48. Cerqueira FM, Cunha FM, Laurindo FR and Kowaltowski AJ. Calorie restriction increases cerebral mitochondrial respiratory capacity in a NO*-mediated mechanism: impact on neuronal survival. Free radical biology & medicine. 2012; 52:1236-41.

49. Spinazzi M, Casarin A, Pertegato V, Salviati L and Angelini C. Assessment of mitochondrial respiratory chain enzymatic activities on tissues and cultured cells. Nature protocols. 2012; 7:1235-46.

50. DiGirolamo M. Measurements of glucose conversion to its metabolites. Methods in molecular biology (Clifton, NJ. 2001; 155:181-92.

51. Cannon B and Nedergaard J. Studies of thermogenesis and mitochondrial function in adipose tissues. Methods in molecular biology (Clifton, NJ). 2008; 456:109-21.

52. Wang T, Si Y, Shirihai OS, Si H, Schultz V, Corkey RF, Hu L, Deeney JT, Guo W and Corkey BE. Respiration in adipocytes is inhibited by reactive oxygen species. Obesity (Silver Spring). 2010; 18:1493-1502.

53. Engels RC, and Jones, J.B. Causes and elimination of erratic blanc in enzymatic metabolic assays involving the use of NAD in alkaline hydrazine buffers: Improved conditions for assay of L-glutamate, L-lactate and other metabolites. Analytical Biochemistry. 1978; 88:475- 84.

54. Rahman I, Kode A and Biswas SK. Assay for quantitative determination of glutathione and glutathione disulfide levels using enzymatic recycling method. Nature protocols. 2006; 1:3159-65.

55. Giordano A, Murano I, Mondini E, Perugini J, Smorlesi A, Severi I, Barazzoni R, Scherer PE and Cinti S. Obese adipocytes show ultrastructural features of stressed cells and die of pyroptosis. Journal of lipid research. 2013;54:2423-36.

SUPPLEMENTARY DATA

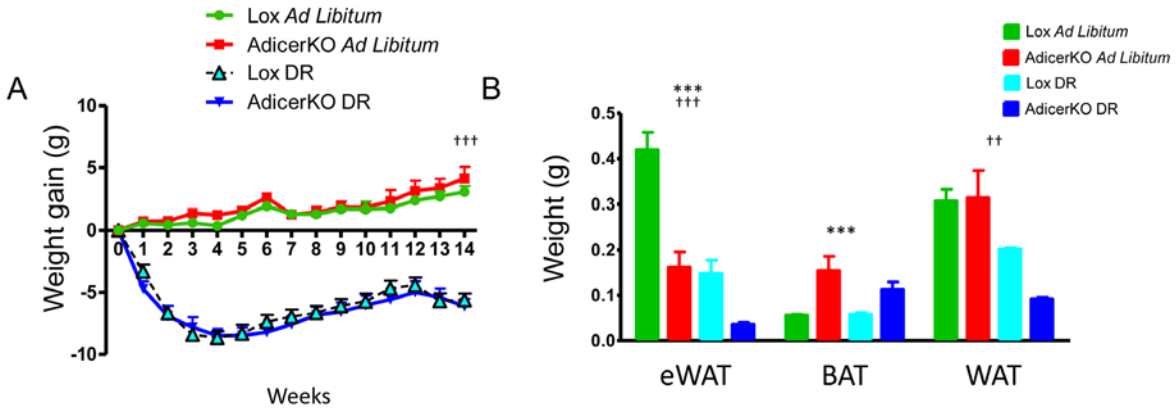

Supplementary Figure 1. Body weight and fat mass of AdicerKO mice. Twelve-week old mice were subjected to *ad libitum* (AL) or dietary restriction (DR) regimens for three months. (**A**) Body weight. (**B**) Fat mass (N=4-8 per condition). Mean ± SEM. *** P < 0.001 for genotype effect. †† P < 0.01, ††† P < 0.001 for diet effect. WAT, inguinal white adipose tissue. eWAT, epididymal white adipose tissue. BAT, interscapular brown adipose tissue.

Supplementary Table 1. Pathway analysis of serum metabolomics data comparing all conditions. Differentially expressed pathways when all conditions were compared (Lox AL, AdicerKO AL, Lox DR and AdicerKO DR).

Pathway Name	*Total*	*Hits*	*p*	*FDR*
Fatty acid metabolism	***39***	***1***	***0.012752***	***0.12663***
Valine, leucine and isoleucine biosynthesis	***11***	***3***	***0.017801***	***0.12663***
Valine, leucine and isoleucine degradation	***38***	***3***	***0.017801***	***0.12663***
Pantothenate and CoA biosynthesis	***15***	***1***	***0.025044***	***0.12663***
Glycerophospholipid metabolism	***30***	***2***	***0.026662***	***0.12663***
Phenylalanine, tyrosine and tryptophan biosynthesis	***4***	***2***	***0.033377***	***0.12663***
Phenylalanine metabolism	***11***	***2***	***0.033377***	***0.12663***
Aminoacyl-tRNA biosynthesis	***69***	***17***	***0.04653***	***0.12663***
Selenoamino acid metabolism	***15***	***1***	***0.047154***	***0.12663***
Taurine and hypotaurine metabolism	*8*	*1*	*0.053879*	*0.12663*
Primary bile acid biosynthesis	*46*	*1*	*0.053879*	*0.12663*
Tyrosine metabolism	*44*	*1*	*0.056882*	*0.12663*
Ubiquinone and other terpenoid-quinone biosynthesis	*3*	*1*	*0.056882*	*0.12663*
Arachidonic acid metabolism	*36*	*1*	*0.058074*	*0.12663*
Linoleic acid metabolism	*6*	*1*	*0.058074*	*0.12663*
alpha-Linolenic acid metabolism	*9*	*1*	*0.058074*	*0.12663*
Histidine metabolism	*15*	*4*	*0.059795*	*0.12663*

Arginine and proline metabolism	*44*	*9*	*0.18956*	*0.37912*
Cysteine and methionine metabolism	*27*	*2*	*0.21403*	*0.40408*
Glycine, serine and threonine metabolism	*31*	*2*	*0.22678*	*0.40408*
Alanine, aspartate and glutamate metabolism	*24*	*5*	*0.2624*	*0.40408*
Lysine biosynthesis	*4*	*1*	*0.27126*	*0.40408*
Biotin metabolism	*5*	*1*	*0.27126*	*0.40408*
Tryptophan metabolism	*40*	*3*	*0.27569*	*0.40408*
Methane metabolism	*9*	*1*	*0.30306*	*0.40408*
Cyanoamino acid metabolism	*6*	*1*	*0.30306*	*0.40408*
Sphingolipid metabolism	*21*	*1*	*0.30306*	*0.40408*
beta-Alanine metabolism	*17*	*3*	*0.37459*	*0.47022*
Lysine degradation	*23*	*2*	*0.37879*	*0.47022*
Glutathione metabolism	*26*	*4*	*0.39554*	*0.47464*
Nitrogen metabolism	*9*	*3*	*0.5897*	*0.68481*
Butanoate metabolism	*22*	*1*	*0.63277*	*0.6903*
Porphyrin and chlorophyll metabolism	*27*	*1*	*0.63277*	*0.6903*
D-Glutamine and D-glutamate metabolism	*5*	*2*	*0.84868*	*0.89236*
Purine metabolism	*68*	*1*	*0.89236*	*0.89236*
Pyrimidine metabolism	*41*	*1*	*0.89236*	*0.89236*

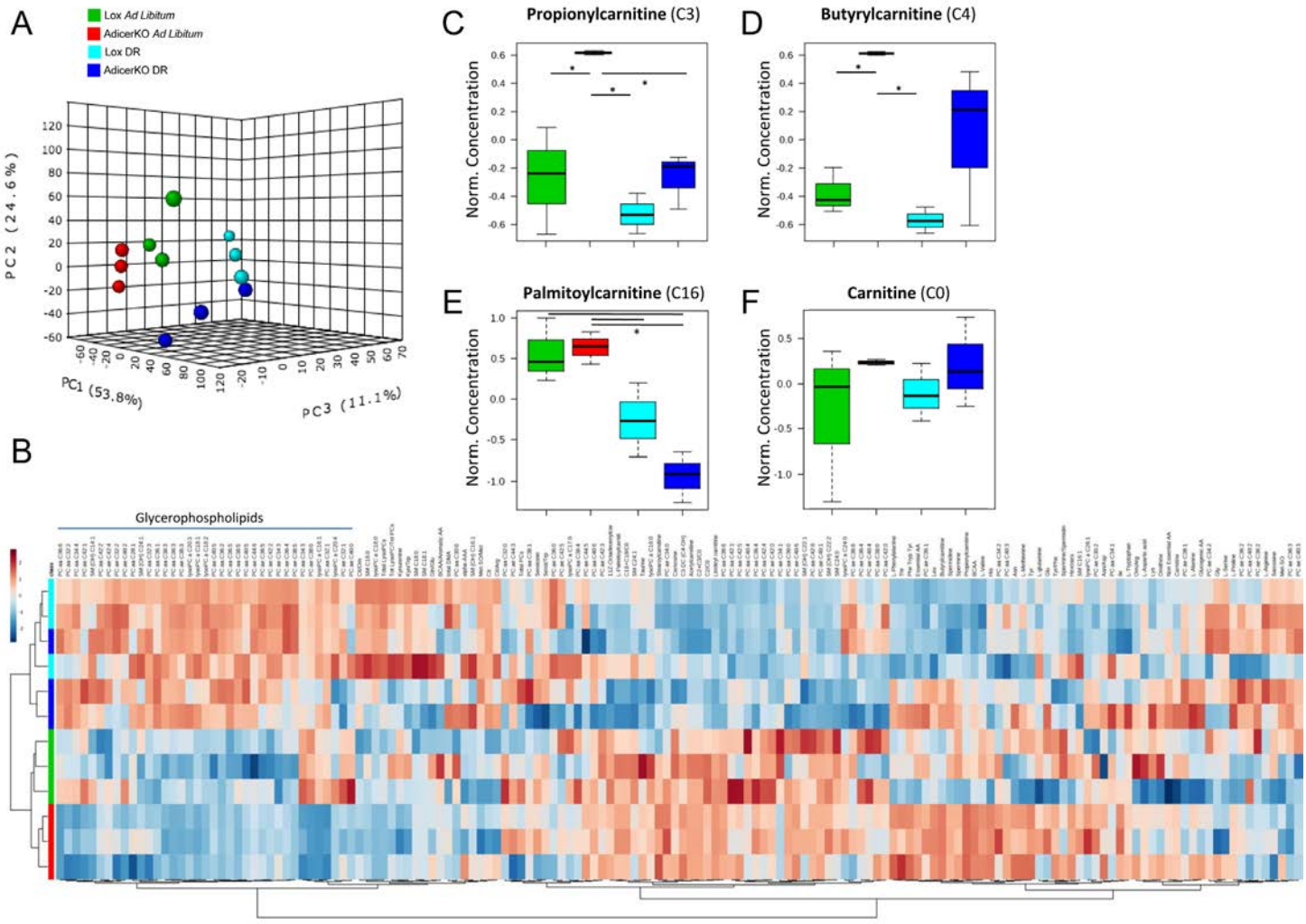

Supplementary Figure 2. Serum metabolite changes in AdicerKO mice. Twelve-week old mice were subjected to *ad libitum* (AL) or dietary restriction (DR) regimens for three months. Mice were euthanized at the end of the protocol after overnight fasting and metabolomics was conducted in the serum samples. Values were normalized by the average of the Lox AL group, Log2 transformed and Pareto scaled. Data was subjected to (**A**) Partial Least Squares Discriminant Analysis (PLS-DA) and (**B**) Hierarchical Clustering Analysis. (C-F) Selected metabolites. N=3 per condition. Data are mean ± SE. * $P < 0.05$.

Supplementary Table 2. Pathway analysis of serum metabolomics data in AdicerKO mice.
Differentially expressed pathways when Lox *ad libitum* and AdicerKO *ad libitum* were compared.

Pathway Name	*Total*	*Hits*	*p*	*FDR*
Valine, leucine and isoleucine biosynthesis	***11***	***3***	***2.20E-04***	***0.0039647***
Valine, leucine and isoleucine degradation	***38***	***3***	***2.20E-04***	***0.0039647***
Phenylalanine, tyrosine and tryptophan biosynthesis	*4*	*2*	*0.058927*	*0.44812*
Phenylalanine metabolism	*11*	*2*	*0.058927*	*0.44812*
Selenoamino acid metabolism	*15*	*1*	*0.078201*	*0.44812*
Aminoacyl-tRNA biosynthesis	*69*	*17*	*0.0869*	*0.44812*
Tyrosine metabolism	*44*	*1*	*0.099581*	*0.44812*
Ubiquinone and other terpenoid-quinone biosynthesis	*3*	*1*	*0.099581*	*0.44812*
Pantothenate and CoA biosynthesis	*15*	*1*	*0.11684*	*0.46735*
Alanine, aspartate and glutamate metabolism	*24*	*5*	*0.21123*	*0.7081*
Tryptophan metabolism	*40*	*3*	*0.21636*	*0.7081*
Cysteine and methionine metabolism	*27*	*2*	*0.25371*	*0.73455*
Arachidonic acid metabolism	*36*	*1*	*0.30606*	*0.73455*
Linoleic acid metabolism	*6*	*1*	*0.30606*	*0.73455*
alpha-Linolenic acid metabolism	*9*	*1*	*0.30606*	*0.73455*
Glycerophospholipid metabolism	*30*	*2*	*0.37639*	*0.77163*
Histidine metabolism	*15*	*4*	*0.38953*	*0.77163*
Nitrogen metabolism	*9*	*3*	*0.41275*	*0.77163*
beta-Alanine metabolism	*17*	*3*	*0.41291*	*0.77163*
Arginine and proline metabolism	*44*	*9*	*0.48213*	*0.77163*
Lysine degradation	*23*	*2*	*0.49067*	*0.77163*
Glutathione metabolism	*26*	*4*	*0.50355*	*0.77163*
Purine metabolism	*68*	*1*	*0.53907*	*0.77163*
Pyrimidine metabolism	*41*	*1*	*0.53907*	*0.77163*
Butanoate metabolism	*22*	*1*	*0.57659*	*0.77163*
Porphyrin and chlorophyll metabolism	*27*	*1*	*0.57659*	*0.77163*
D-Glutamine and D-glutamate metabolism	*5*	*2*	*0.57872*	*0.77163*
Methane metabolism	*9*	*1*	*0.66013*	*0.79215*
Cyanoamino acid metabolism	*6*	*1*	*0.66013*	*0.79215*
Sphingolipid metabolism	*21*	*1*	*0.66013*	*0.79215*
Glycine, serine and threonine metabolism	*31*	*2*	*0.69424*	*0.80621*
Fatty acid metabolism	*39*	*1*	*0.76257*	*0.85789*
Taurine and hypotaurine metabolism	*8*	*1*	*0.89892*	*0.92402*
Primary bile acid biosynthesis	*46*	*1*	*0.89892*	*0.92402*
Lysine biosynthesis	*4*	*1*	*0.92402*	*0.92402*
Biotin metabolism	*5*	*1*	*0.92402*	*0.92402*

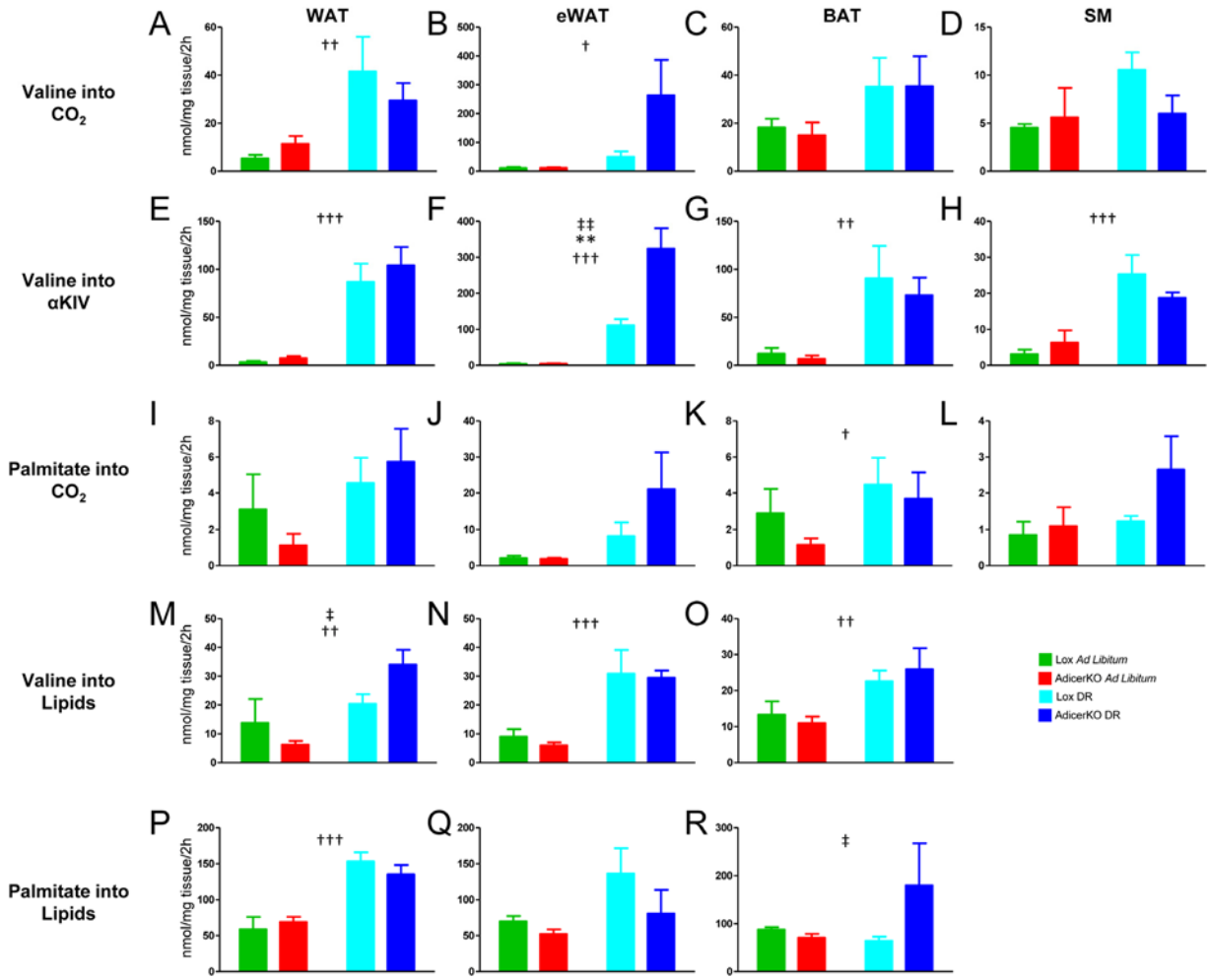

Supplementary Figure 3. Substrate oxidation and lipid synthesis in WAT of AdicerKO mice. Twelve-week old mice were subjected to ad libitum (AL) or dietary restriction (DR) regimens for one month. At the end of the protocol, tissues were isolated, minced and explants were used to assess (**A**-**D**) complete oxidation of valine, (**E**-**H**) oxidation of valine into α-ketoisovaleric acid (αKIV), (**I**-**L**) complete oxidation of palmitate, (**M**-**O**) lipid synthesis from valine, and (**P**-**R**) lipid synthesis from palmitate. WAT, inguinal white adipose tissue. eWAT, epididymal white adipose tissue. BAT, interscapular brown adipose tissue. SM, gastrocnemius skeletal muscle. N=3-5 per condition. Mean ± SEM. ** P < 0.01 for genotype effect; † P < 0.05, †† P < 0.01, ††† P < 0.001 for diet effect; ‡ P < 0.05, ‡‡ P < 0.01 for diet-genotype interaction.

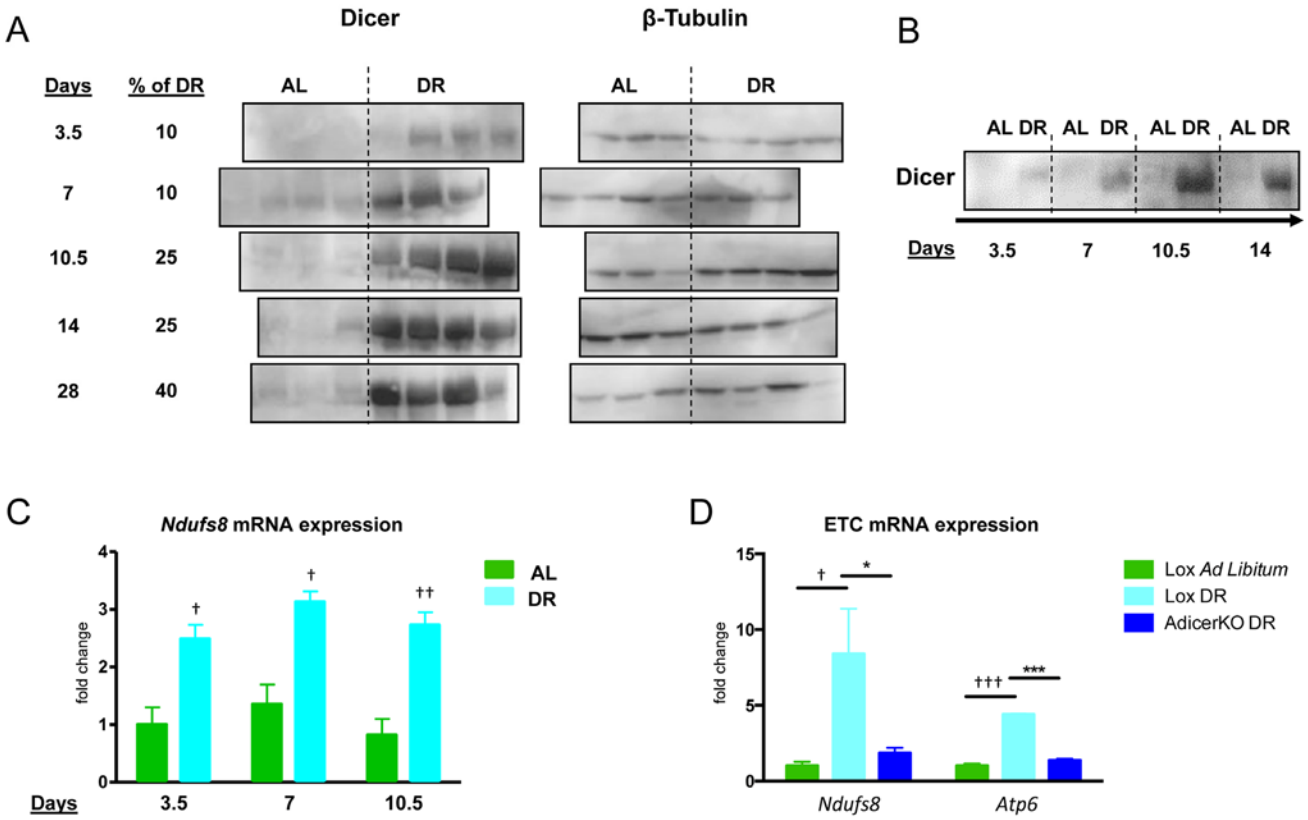

Supplementary Figure 4. Kinetics of Dicer and mitochondrial gene expression in WAT upon DR. Twelve-week old C57BL/6 mice were subjected to *ad libitum* (AL) or dietary restriction (DR) regimens for up to one month. Mice were euthanized at different time-points and WAT was collected. (**A**) Western blotting for Dicer and β-tubulin. (**B**) Representative blot. (**C,D**) Gene expression of components of the Electron Transport Chain (ETC) was assessed by RT-qPCR (N=3-5 per condition). Mean ± SEM. * $P < 0.05$, *** $P < 0.05$ for genotype effect; † $P < 0.05$, †† $P < 0.01$, ††† $P < 0.001$ for diet effect.

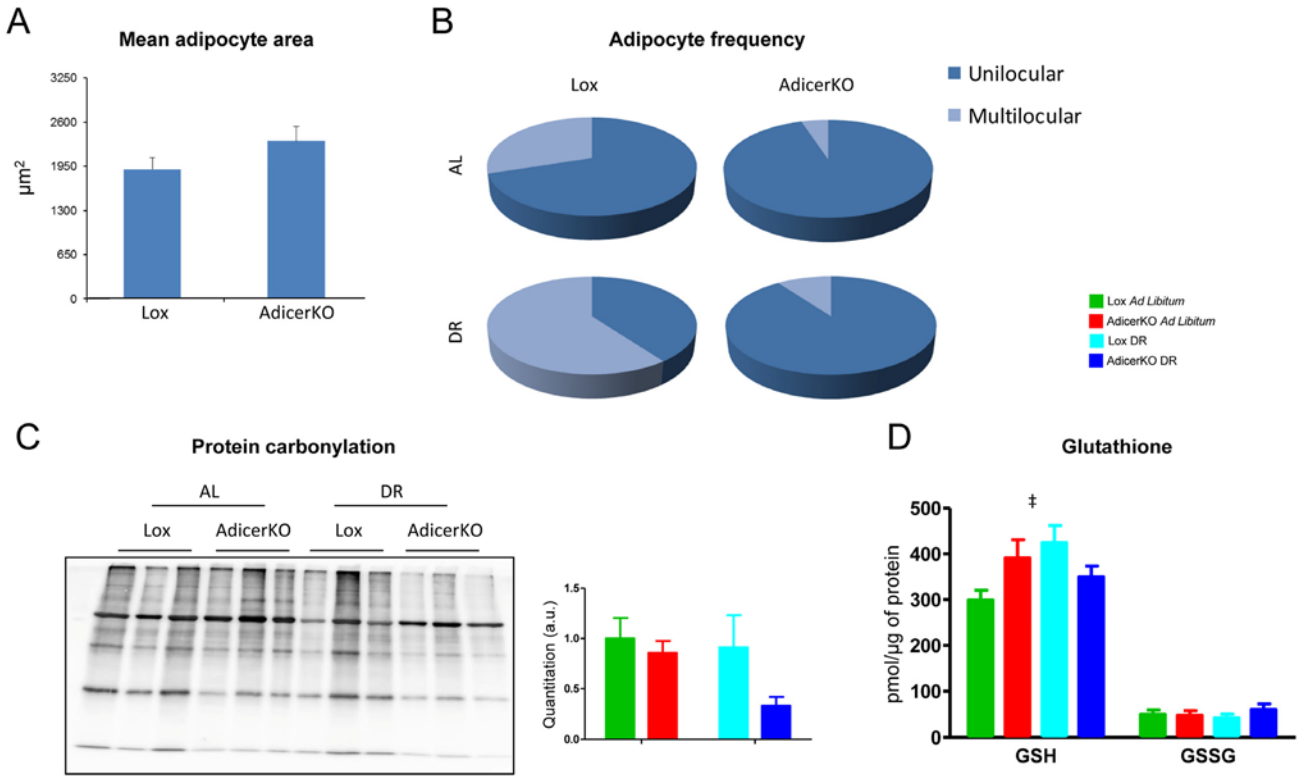

Supplementary Figure 5. Adipocyte size and redox balance of WAT of AdicerKO mice. Twelve-week old mice were subjected to *ad libitum* (AL) or dietary restriction (DR) regimens for one month and WAT was isolated. (**A,B**) Tissue was processed for H&E staining and (**A**) mean adipocyte size and (**B**) adipocyte type were blindly assessed using microscopic images (N=4-5 animals per condition, one image per animal collected always in the same anatomical location, *i.e.* around the inguinal lymph node). (**C**) Overall protein carbonylation was assessed by immunoblot and quantitated (right panel) using image densitometry. (**D**) Reduced (GSH) and oxidized (GSSG) glutathione levels were measured in tissue extracts (N=3-5 animals per condition). Mean ± SEM. ‡ P < 0.05 for diet-genotype interaction.

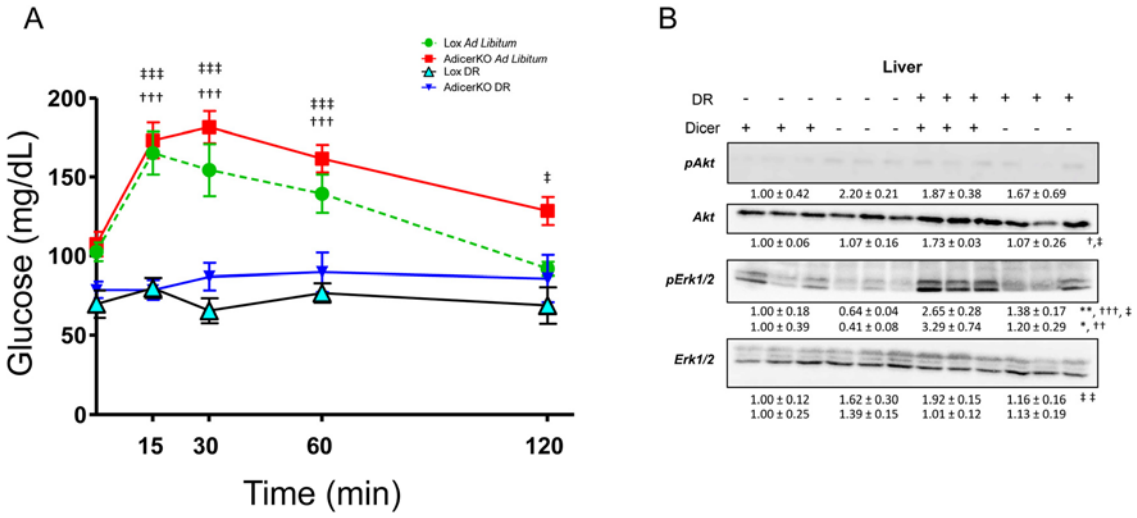

Supplementary Figure 6. Glucose tolerance test and liver insulin signaling in AdicerKO mice. Twelve-week old mice were subjected to *ad libitum* (AL) or dietary restriction (DR) regimens for three (**A**) or one (**B**) month. (**A**) Glucose tolerance test was performed one week prior to the end of the protocol (N=5-7 per condition). Mean ± SEM. ††† P < 0.001 Lox AL vs. Lox DR; ‡ P < 0.05, ‡‡‡ P < 0.001 AdicerKO AL vs. AdicerKO DR. (**B**) Western blots of liver extracts pAkt, phospho-Akt. pErk1/2, phospho-Erk1/2. Numbers are quantitation of blots (fold expression in comparison to control group) ± SEM. * P < 0.05, ** P < 0.01 for genotype effect; †† P < 0.01, ††† P < 0.001 for diet effect; ‡ P < 0.05, ‡‡ P < 0.01 for diet-genotype interaction.

Research Paper

Metabolic consequences of long-term rapamycin exposure on common marmoset monkeys (*Callithrix jacchus*)

Corinna Ross[1,2], Adam Salmon[2,3], Randy Strong[2], Elizabeth Fernandez[2,3], Marty Javors[2,3], Arlan Richardson[4], and Suzette Tardif[2,5]

[1] *Department of Arts & Sciences, Texas A&M University San Antonio, San Antonio, TX 78224, USA;*
[2] *Barshop Institute for Longevity & Aging Studies, University of Texas Health Science Center San Antonio, San Antonio, TX 78224, USA;*
[3] *Geriatric Research, Education & Clinical Center, South Texas Veteran's Health Care System, San Antonio, TX 78224, USA;*
[4] *University of Oklahoma Health Sciences Center and the Oklahoma City VA Medical Center, Oklahoma City, OK 73104, USA;*
[5] *Southwest National Primate Research Center, Texas Biomedical Research Institute, San Antonio, TX 78224, USA.*

Key words: *nonhuman primate, antiaging, longevity, healthspan, animal models, sirolimus*
Received: *08/04/15; Accepted: 11/02/15; Published: 11/13/15*
Correspondence to: *Corinna Ross, PhD;* ***E-mail:*** *cnross@tamusa.tamus.edu* doi:10.18632/aging.100843

Abstract **Rapamycin has been shown to extend lifespan in rodent models, but the effects on metabolic health and function have been widely debated in both clinical and translational trials. Prior to rapamycin being used as a treatment to extend both lifespan and healthspan in the human population, it is vital to assess the side effects of the treatment on metabolic pathways in animal model systems, including a closely related non-human primate model. In this study, we found that long-term treatment of marmoset monkeys with orally-administered encapsulated rapamycin resulted in no overall effects on body weight and only a small decrease in fat mass over the first few months of treatment. Rapamycin treated subjects showed no overall changes in daily activity counts, blood lipids, or significant changes in glucose metabolism including oral glucose tolerance. Adipose tissue displayed no differences in gene expression of metabolic markers following treatment, while liver tissue exhibited suppressed G6Pase activity with increased PCK and GPI activity. Overall, the marmosets revealed only minor metabolic consequences of chronic treatment with rapamycin and this adds to the growing body of literature that suggests that chronic and/or intermittent rapamycin treatment results in improved health span and metabolic functioning. The marmosets offer an interesting alternative animal model for future intervention testing and translational modeling.**

INTRODUCTION

Rapamycin has been found by multiple laboratories to extend mouse lifespan even when mice began receiving rapamycin relatively late in life at 20 months of age, or roughly the equivalent of 55 human years [1]. In addition, rapamycin has been shown to delay the onset of several age-related diseases, including Alzheimer's disease, cardiovascular disease, and cancer in mouse models of these pathologies [2-5]. These findings have led to significant interest in the potential effects of rapamycin as an anti-aging intervention in humans particularly because rapamycin is already approved for use in cancer therapy and as an adjunct immuno-suppressive agent for transplant patients.

However, clinical administration of rapamycin has the potential for several side-effects include hyperlipidemia and hyperglycemia [6], raising concerns as to the potential negative impacts of rapamycin exposure in aged human populations that may have a high underlying prevalence of obesity- and age-induced insulin resistance and hyperlipidemia. However, results from clinical populations suggests that some side effects, such as hypertriglyceridemia, may improve over time and that others may be dose-dependent [6]. The nature of the human data accumulated thus far paints a far from complete picture of why and how rapamycin might affect metabolism and lipid trafficking. Moreover, these clinical studies have focused on patients with pre-existing conditions and have largely utilized combination therapies with other immunosupressants or steroids that can cause metabolic dysfunctions of their own [7]. There have, however, been no long-term studies of the effects of monothereapy with rapamycin or its analogs in populations of otherwise healthy humans. Thus, it is not clear whether the previously reported metabolic risks of rapamycin and its analogs are due to this drug directly or to other confounding factors.

In rodent models, monotherapy with rapamycin has largely, though not equivocally, been associated with impairment of glucose metabolism as measured in glucose tolerance tests. A notable exception is a study by Fang et al. suggesting that chronic treatment with rapamycin has a biphasic effect on glucose metabolism with short-term rapamycin treatment being detrimental to glucose metabolism whereas long-term (20 wk) treatment with rapamycin may promote an insulin-sensitive state in mice with a transition state in between [8]. Further examination has revealed that long term treatment of rapamycin leads to a metabolic switch resulting in enhanced insulin signaling and better triglyceride processing [9]. These rodent studies have largely been performed in animals maintained on a relatively standardized rodent chow, though there is evidence that rapamycin has similar effects on both lifespan and metabolic function in mice fed diets high in caloric content due to increased levels of sugar and/or fat [10,11]. Mice given intermittent treatment of rapamycin and placed on a high fat diet have no gross changes in metabolic markers, and rapa appears to prevent weight gain [12]. Combining the intervention therapies of rapamycin and resveratrol treatment in mice was found to prevent insulin resistance in mice being fed a high fat diet and suggests that combination therapy may be beneficial in a high fat environment [13]. Human glucose metabolism is regulated by a complex interaction of genetics and environment (including diet) that cannot be fully recapitulated in laboratory rodents [14]. Even the timing of or causes of eating/overeating differ between rodent models and humans, further complicating this issue [15, 16]. At the molecular level, there are significant discrepancies between rodents and humans in alterations of gene regulation in metabolic dysfunction suggesting there is little overlap between the two models [17]. Lastly, many of the complications of metabolic dysfunction including nephropathy, neuropathy, and cardiac dysfunction cannot be successfully replicated in single genetic mouse models of metabolic dysfunction or in high fat-fed rodents [18]. Thus, a significant question remains whether the choice of diet (as well as sex of animals or background genetics) could potentially complicate the potential for translation [19-21]. An approach to address whether the effects (and potential side-effects like metabolic dysfunction) of rapamycin in otherwise healthy rodents may also be relevant to humans is to perform such experiments in other species that are predicted to have similar phenotypic metabolic regulation as humans. In other words, studies of rapamycin's effects in a species more closely related to humans can inform as to the generalizability of the rodent findings and issues likely to impede the general use of rapamycin as an anti-aging treatment in humans.

The common marmoset (*Callithrix jacchus*) is a small monkey with a relatively short lifespan. Both its small size and associated shorter lifespan make this species a valuable nonhuman primate model for the study of aging and chronic disease [22, 23]. Captive marmosets display many similarities to humans in terms of obesity and its sequelae. Spontaneous obesity has been described in multiple captive marmoset colonies that are socially housed and fed a relatively low fat, high fiber diet [22, 24-28]. Obesity in marmosets, defined in a fashion similar to that used in humans, is statistically associated with increased risk to metabolic dysfunction and cardiovascular disease [16]. In addition to displaying evidence of insulin resistance, marmosets at extremely high weights (over 500 grams) show higher age-specific mortality rates as adults when compared to animals of average weight [22]. From 2010-2011, we conducted a year-long study of daily dosing of a group of common marmosets with rapamycin. We previously reported that we were able to maintain circulating blood levels of rapamycin at 5.2 ng/mL by giving the animals a dose of eudragit encapsulated rapamycin in yogurt of 1mg/kg/day. Subjects demonstrated a decrease in mTORC1 after two weeks of treatment. There was no evidence of clinical anemia, mouth ulcers, lung fibrotic changes, significant changes in wound healing, or increased mortality [29]. This report describes a set of metabolic outcomes from this study.

RESULTS

Body composition

Rapamycin treated subjects displayed a significant loss of body fat mass at two months post-dosing while control subjects displayed a statistically insignificant change in body fat mass, as illustrated in Fig. 1A (treatment x time interaction, $p < 0.0097$; difference in month 0 and month 2 mean for rapamycin treated subjects, $p < 0.05$, Sidak's multiple comparison test).

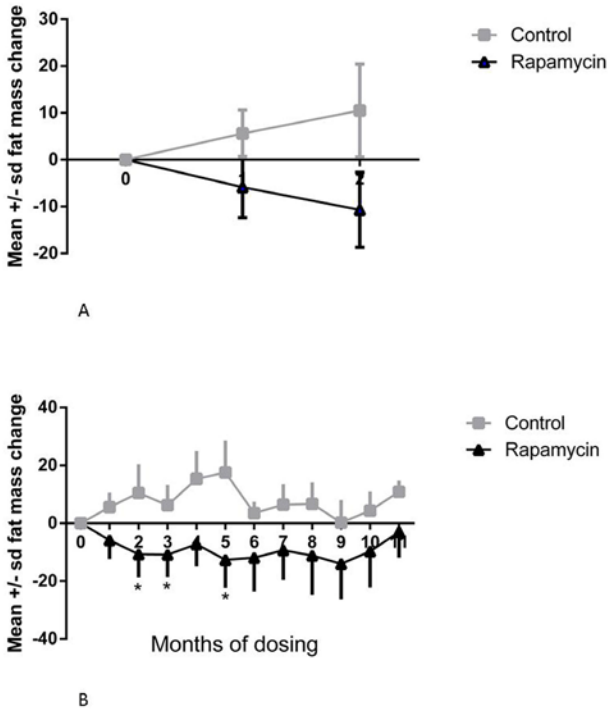

Figure 1. Change in fat mass. (**A**) Change in fat mass at 1 and 2 months, post-dosing, from pre-dosing (month 0) measurement. Squares = control subjects; triangles = rapamycin subjects (mean ± SD); treatment x time interaction, $p < 0.0097$; difference in month 0 and month 2 mean for rapamycin treated subjects, $p < 0.05$, Sidak's multiple comparison test. (**B**) Change in fat mass from pre-dosing measurement for months 1-11 for rapamycin subjects. * treatment effect, F=5.385, p=0.018, Dunnett's multiple comparison test significant, $p < 0.05$, for month 0 versus months 2, 3, and 5.

The rapamycin treated subjects had significantly reduced body fat mass in months 2, 3 and 5, after which their mean fat mass did not differ from the pre-dosing mean (treatment effect, F=5.385, p=0.018, Dunnett's multiple comparison test significant, $p < 0.05$, for month 0 versus months 2, 3, and 5), resulting in no difference between control and rapamycin treated subjects at the end of the study as illustrated in Fig. 1B. There were no significant differences between controls and rapamycin treated subjects and no effects of rapamycin treated subjects over time on body lean mass.

Food intake and activity levels

There were no significant differences between controls and rapamycin treated subjects in food intake at two months post-dosing. In rapamycin-treated marmosets, there was a significant increase in food intake at month 5, over the pre-dosing food intake (treatment effect, F=8.353, p=0.001, Dunnett's multiple comparison test significant, $p < 0.05$, for month 0 versus month 5), as illustrated in Fig. 2.

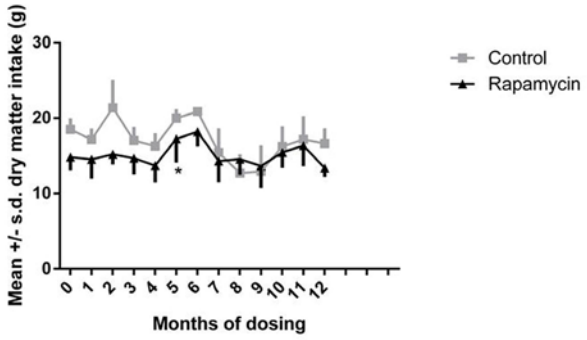

Figure 2. Food intake. Daily dry matter intake for months 0-12, month 0 is a pre-dosing measurement. Squares = control subjects; triangles = rapamycin subjects (mean ± SD). * treatment effect, F=8.353, p=0.001, Dunnett's multiple comparison test significant, $p < 0.05$, for month 0 versus month 5.

In both control and rapamycin-treated subjects activity scored as accelerometer counts per hour declined significantly after the second month of dosing, as illustrated in Fig. 3, then remained stable over the remainder of the study. There were no significant differences between controls and rapamycin treated subjects. Because both groups were affected, these data suggest that this decline was a result of habituation to wearing the harness holding the accelerometer.

Lipid and glucose metabolic measures

There were no significant differences between controls and rapamycin-treated subjects in pre- versus post-dosing mean circulating triglyceride concentrations.

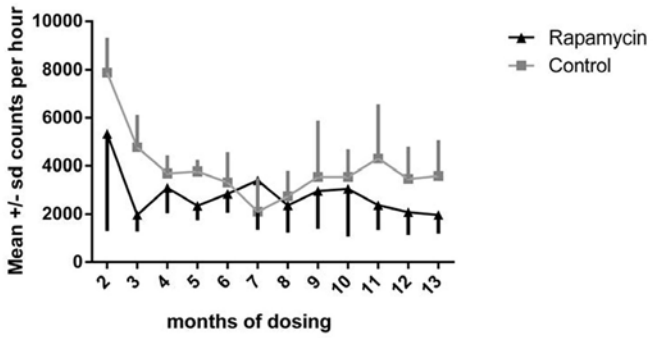

Fiure 3. Daily activity. Accelerometer counts per hour for months 2-13 of dosing. Squares = control subjects; triangles= rapamycin subjects (mean ± SD).

There was, however considerable inter-individual variation in both baseline triglyceride concentration and in change over time, as illustrated in Fig. 4. Two of the rapamycin treated subjects that were borderline hypertriglyceridemic (476 and 402 mg/dl, with > 400 mg/dl defined as hypertriglyceridemic, [24] before dosing, displayed dramatic increases in circulating triglyceride concentration at month 2 (702 and 1,359 mg/dl); however, their triglyceride concentrations then varied considerably over the next 7 months. There was no consistent hypertriglyceridemia caused by rapamycin among subjects who began with normal circulating triglyceride concentrations There were two subjects (one control and one rapamycin treated) that displayed severe hypertriglycerimedia before dosing (603 and 1,611 mg/dl respectively). They both remained hypertriglyceridemic through the study.

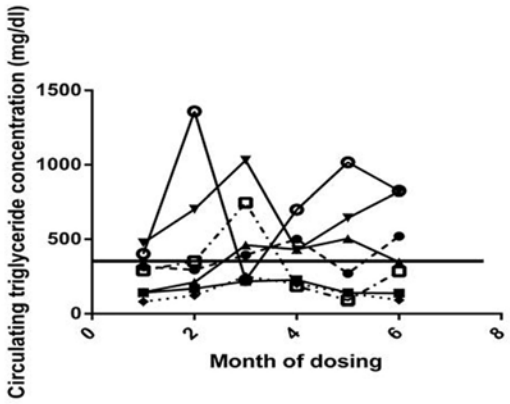

Figure 4. Circulating triglyceride. Circulating triglyceride concentrations for each rapamycin subject for months 0-6, month 0 is a pre-dosing measurement. The solid horizontal line represents the previously established cut-off point for normal triglyceride concentrations in this species.

Three measures of glucose metabolic function were assessed: fasting blood glucose, QuickI index, and AUC. There were no significant changes in fasting glucose concentrations as illustrated in Fig. 5A. The QuickI index, calculated as 1/[log(fasting insulin) + log(fasting glucose)], is the typical measure reported in nonhuman primate studies to provide an estimate of insulin sensitivity, with higher values indicating more insulin sensitivity. The area under the curve (AUC) for the glucose tolerance tests represents the relative glucose excursion caused by a consistent dose of glucose and is a measure of the efficiency with which the entire system can remove glucose from the circulation. As illustrated in Fig. 5D, the mean QuickI index for the control group was higher than that for the rapamycin treated group prior to treatment ($F=5.396$, $p = 0.0453$, Sidak's multiple comparison test, $p < 0.05$ for month 0 control vs rapamycin treated), suggesting that the animals that became the control group were, on average, more insulin sensitive than those in the group randomly selected to be treated with rapamycin. However, the rapamycin-treated group displayed a reduced QuickI measurement even prior to treatment that was not altered during these first two months of dosing as indicated by the lack of a significant interaction effect. We also found that QuickI did not differ among rapamycin-treated animals through 8 months of rapamycin treatment as illustrated in Fig. 5C. There were no differences between control and rapamycin treated subjects and no interaction effect on the glucose AUC. There were also no significant differences in post-dosing average glucose AUC in the rapamycin treated subjects through 8 months of dosing, as illustrated in Fig. 5B. Together, these data suggest limited to no impairment of glucose metabolism in healthy marmosets treated with daily administration of rapamycin at doses sufficient to reduce mTOR signaling.

Assessment of molecular effects

The long-term administration of rapamycin in rodents has been associated with hyperglycemia caused in part by increased gluconeogenesis [27-29]. In the liver of rapamycin treated animals, we found significant upregulation of the expression of phosphoenolpyruvate carboxykinase (PCK1), indicative of altered gluconeogenic capacity. Surprisingly, we found that glucose 6 phosphatase expression in rapamycin treated animals was significantly reduced (Fig. 6). Rapamycin did not alter the expression of other markers of gluconeogenesis. The lack of a consistent alteration in the expression of gluconeogenic effectors may explain why rapamycin-treated marmosets showed no significant change in fasting blood glucose levels.

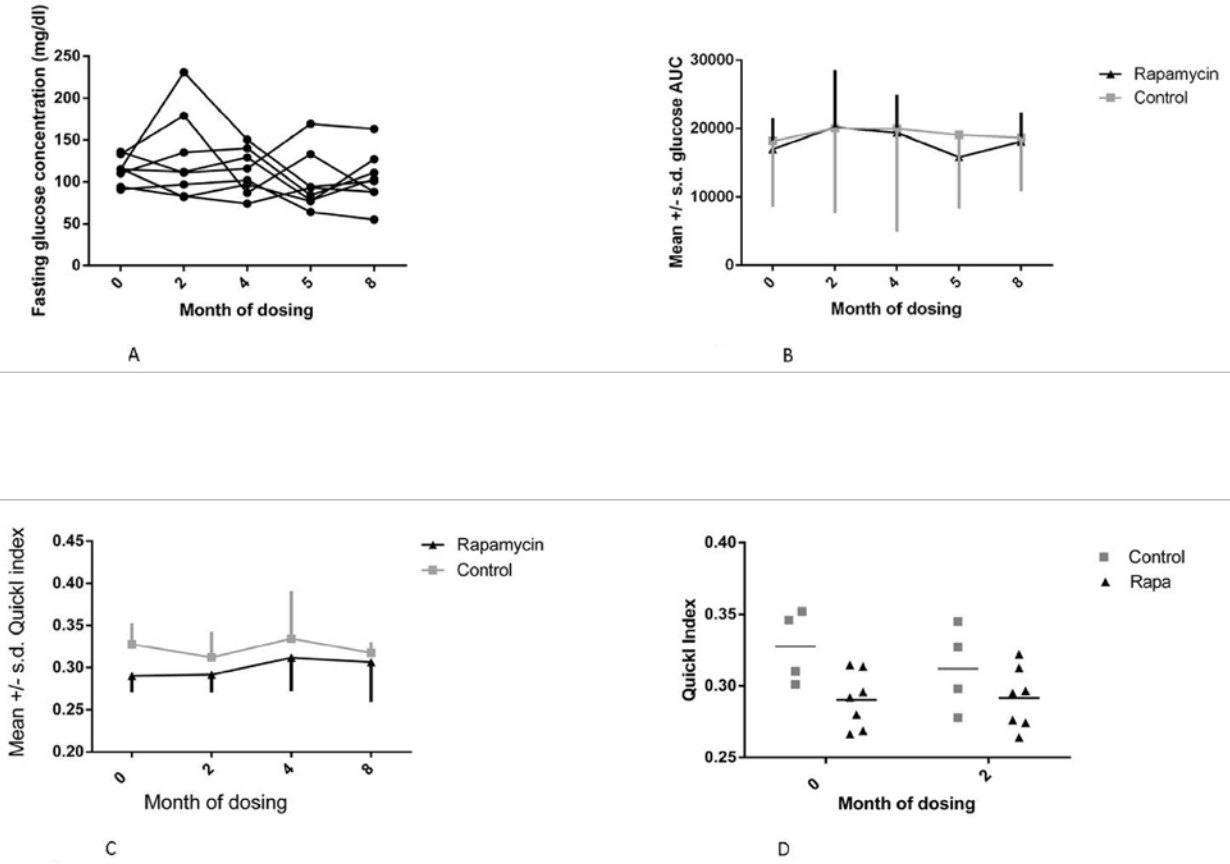

Figure 5. Metabolic measures. (**A**) Fasting glucose concentration for months 0-8 for rapamycin subjects, month 0 is a pre-dosing measurement. (**B**) Glucose area under the curve (AUC) for months 0-8 for rapamycin subjects. (C) Quickl index for rapamycin subjects for months 0-8. (**D**) Quickl index - 1/[log(fasting insulin) + log(fasting glucose)] for months 0 and 2 of dosing, *(F=5.396, p = 0.0453, Sidak's multiple comparison test, p < 0.05 for month 0 control vs rapamycin treated). For all panels squares = control subjects; triangles = rapamycin subjects (mean ± SD).

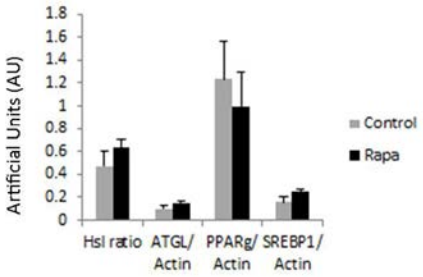

Figure 6A

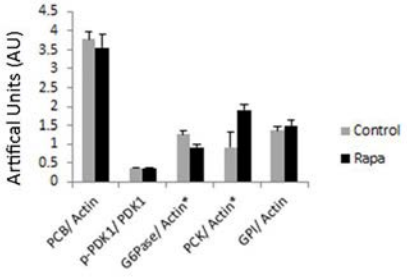

Because rapamycin modulated fat content of marmosets in the early periods of treatment, we assessed the potential modulation of effectors of lipolysis/lipogenesis in adipose. In visceral adipose samples, we found no significant effects on the phosphorylation or expression of any of these markers, suggesting little effect of rapamycin. However, at the time of sacrifice, rapamycin-treated marmosets were not significantly leaner than control animals. Due to limitations of the design of this study, we could not determine whether these effectors were altered by rapamycin at earlier time points when fat mass was reduced by treatment (Fig. 1B).

Figure 6. Immunoblot results. Immunoblot results for the following: adipose triglyceride lipase (ATGL), pyruvate carboxylase (PCB), glucose-6-phosphatase α (G6Pase), glucose-6-phosphate isomerase (GPI), peroxisome proliferator-activated receptor γ (PPARγ), phospho-pyruvate dehydrogenase kinase (p-PDK1), pyruvate dehydrogenase kinase (PDK1), phosphoenol-pyruvate carboxykinase 1 (PCK1), sterol regulatory element-binding protein 1 (SREBP1) corrected by actin. A. Adipose tissue collected at sacrifice following 14 months of rapamycin (black) or control dosing (grey) (mean ± SE) B. Liver tissue collected at sacrifice following 14 months of rapamycin (black) or control dosing (grey) (mean ± SE) *indicates significance p<0.05.

DISCUSSION

Prior to assessing the effectiveness of rapamycin as an anti-aging treatment in humans, it is first necessary to elucidate the potential effects on long term health outcomes. In particular, there has been a great deal of controversy and inconsistent results in the clinical studies of rapamycin, which have highlighted the potential increased risk for metabolic defects such as hyperlipidemia and hyperglycemia that are consistent with increasing risk of cardiovascular disease and type 2 diabetes [30]. However, the effects of this drug on relatively healthy humans are largely unknown. A recent short term study (6 weeks) of elderly patients given doses of a rapamycin analog found few side effects significant from placebo control subjects and reported a significant increase in serological response to flu vaccination, however, this study did not examine any markers of metabolic health in these subjects during treatment [31]. In order to assess potential consequences of long term rapamycin treatment on primate metabolic health we tested the effects of rapamycin on a group of healthy, aged, non-human primates, the common marmoset. We previously reported the ability to reliably and routinely dose socially housed marmoset monkeys with yogurt mixtures containing eudragit encapsulated rapamycin [29]. Dosing with 0.4 mg/day resulted in average blood rapamycin levels of 5.2 ng/mL, which is well within the range found in studies of other model species, and humans [1-5]. Further, we previously reported evidence of suppressed phospho-rpS6 in PBMC samples of rapamycin subjects suggesting down-regulation in mTORC1. In this study we reported several markers that suggest that chronic oral dosing with eudragit-encapsulated rapamycin has little impact on the metabolic status of marmosets.

Many have proposed that rapamycin is a mimic of calorie restriction which is the gold-standard for anti-aging intervention resulting in both extended life span and health span in many rodent models. Rapamycin has been shown to suppress mTOR activity, potentially decrease weight and fat mass, and extend healthspan and life span in a similar manner as calorie restriction [1-4]. In marmosets we demonstrated no overall change in body weight while being treated with rapamycin, but the marmosets did have significant loss of body fat. However, the loss of body fat stabilized at approximately five months of treatment and this time point was associated with an increase in food intake of rapamycin subjects. While we are unable to elucidate the underlying mechanisms for the sudden shift in dietary intake at 5 months of dosing, it is interesting to consider the possibility that the rapamycin-dosed animals altered caloric intake in response to the fat mass loss [32].

One of the major reported risks of rapamycin administration clinically is the development of new-onset type 2 diabetes as shown in clinical studies of kidney transplant patients treated with rapamycin analogs [33, 34]. However, the interpretation of these data is complicated by several factors including the impaired health status of the subjects and the use of combination therapies using additional drugs that are known to cause metabolic impairment on their own. Recent clinical studies of kidney transplant patients suggest that Tacrolimus rather than Sirolimus may be the leading cause of new onset diabetes within 10 weeks of treatment, however all research suggests that continued examination of monotherapies are needed to elucidate the side effects of each immunosuppressant [35, 36]. In rodents, the chronic administration of rapamycin as a mono-therapy has often been shown to impair glucose metabolism. For example, both inbred and genetically heterogeneous mouse strains develop glucose intolerance with oral administration of encapsulated rapamycin [11, 37, 38]. In inbred C57BL/6 mice, but not genetically heterogeneous mice, rapamycin is also associated with the development of insulin resistance. Interestingly, these effects of rapamycin on metabolism are dependent on both dose of rapamycin and sex of subjects [38] and do not appear to be permanent alterations as the metabolic defects can be reversed by ending rapamycin treatment [11]. Similarly, rapamycin treatment to normoglycemic, pre-diabetic *P. obesus* treated with rapamycin display heightened hyperglycemia and increased insulin resistance in part by reducing pancreatic β-cell function. In this rodent model it was suggested that rapamycin exacerbated the pre-existing diabetic symptoms and metabolic disorder in high risk animals [39]. Alternatively the effect of rapamycin is thought to mimic the metabolic changes associated with starvation diabetes or Type 0 diabetes [40, 41, 42]; which is often thought to be a positive, adaptive form of metabolic changes associated with enhanced metabolic efficiency and decreased risk of true diabetes. Evidence of enhanced insulin signaling following long term rapa [9], and intermittent rapa [11], as well as little evidence for detrimental mitochondrial function following rapamycin [42], supports the hypothesis that rapamycin may in fact be inducing changes similar to starvation diabetes [13, 40-42]. Interestingly, in our current study we found no evidence that rapamycin negatively impairs glucose metabolism in marmosets. One possible interpretation of these findings could be that rapamycin treatment might negatively and significantly affect only subjects that are predisposed to metabolic disease. This also

might explain some of the slight differences in rapamycin's effect on glucose metabolic dysfunction in C57BL/6 but not genetically mixed mice. Another possible explanation could be the length of treatment utilized here. Recent studies have suggested a bi-phasic effect of rapamycin on glucose metabolism, with long-term administration of rapamycin to mice associated with increased, rather than reduced insulin sensitivity [8, 9, 44]. However, others have shown rapamycin in eudragit-encapsulated form (as we used in this study) does not show this bi-phasic effect, but rather continuously impairs glucose metabolism in mice [11,37]. In part, the metabolic impairments of rapamycin are thought to be due to inhibition of mTORC2 rather than mTORC1 [45]; while we previously showed that this rapamycin dose was sufficient to inhibit mTORC1 [29], it may not be sufficient to inhibit mTORC2 signaling in the marmoset and thus minimize the presumed metabolic defects of rapamycin treatment.

The increased risk of hyperglycemia with rapamycin treatment has been attributed to increased hepatic gluconeogenesis in rodent studies. In both mice and rats, rapamycin treatment significantly increases hepatic glucose production following injection with pyruvate and increases the expression of the gluconeogenic effectors like PCK1 and G6Pase [45, 46]. In this study, we also confirmed that a significant increase in PCK1 with rapamycin treatment, but paradoxically, found a significant decrease in G6Pase. While the rise in PCK1 would be consistent with increased gluconeogenesis, the decrease in G6Pase might be interpreted as inhibiting this process. It is not clear why rapamycin treatment has this contrasting effect in marmosets, but this might explain why marmosets did not display hyperglycemia with this treatment.

In addition to its well-known roles in cell survival and growth, recent studies have linked the mTOR signaling pathway with the regulation of lipid metabolism [47]. However, the direct effects of rapamycin on lipid metabolism have often been contradictory in published reports. For example, rapamycin has been reported to both improve and impair fatty acid oxidation in skeletal muscle cell lines [44, 48]. Reports regarding rapamycin's effects on lipid utilization in vivo in rodents are similarly inconsistent; rapamycin has been reported to decrease, increase or not effect fat accumulation among several different studies [1, 11, 37, 38, 49, 50]. Here, we found that rapamycin significantly reduced fat mass in marmosets at early time points in our treatment regime. However, after approximately 5 months of treatment, fat mass no longer differed between rapamycin-treated and control marmosets and we found no evidence for differences in lipolysis or lipogenesis in adipose tissue collected at the end of this study. Interestingly, this change coincided with a significant increase in food consumption among the rapamycin-treated marmosets. This alteration could represent a compensatory effect for the long-term inhibition of mTOR signaling. Further temporal studies regarding the effect of rapamycin in this model will be necessary to address this possibility.

Treatment with rapamycin as an intervention in the aging process for humans offers many possibilities but some studies have reported deleterious side effects that raise concern regarding the efficacy of this treatment. This study represents the first to examine the metabolic consequences of rapamycin dosing in healthy non-human primates. We have reported here evidence that long term rapamycin treatment at a dose that has been used in previous studies and reduces mTOR signaling in marmosets [29] does not result in notable negative side-effects on metabolic function in healthy marmosets. We believe that marmosets offer a unique non-human primate model that will allow detailed evaluation of the effect of potential anti-aging treatments on primate metabolic function, dietary intake, and activity patterning.

MATERIALS AND METHODS

Subjects. The subjects for this study were common marmosets (*Callithrix jacchus*) housed at the Southwest National Primate Research Center. Basic husbandry and housing for this colony have been described previously [51]. Thirteen subjects between the ages of 7.1 and 9.1 years were housed as female-vasectomized male pairs. Four pairs received daily oral dosing of 1.0 mg/kg/day (0.40 mg/day) rapamycin in a yogurt vehicle via syringe for 14 months as described [29]. Two pairs (5 subjects, one male died mid-way through the study and was replaced with another male) received daily doses of empty eudragit capsules in yogurt as control. Throughout the long term dosing regimen several markers of metabolic health were assessed.

Body composition: Marmoset lean and fat mass was assessed monthly via quantitative magnetic resonance (QMR) imaging using an Echo MRI unit [26]. Unsedated animals were placed in a plastic tube which was then inserted into the magnetic chamber with scans taking less than 2 minutes on average for each animal. Animals were weighed biweekly throughout the project by placing a scale within the cage and rewarding the animal's for maintaining position on the scale.

Caloric intake. Subjects participated in a 2 day food intake trial once per month for the length of the trial [28]. For these trials the subjects were separated from each other within the cage and fed their daily base diet consisting of two feed types from Harlan Teklad and Purina. Samples of each diet were taken from each prepared batch, frozen and stored until analysis. Diet fed to the subjects was weighed prior to feeding. After 24 hours all remaining food was removed and weighed, and fresh food was weighed and fed. After 48 hours all remaining food was removed and weighed and the subjects were returned to normal housing and feeding schedule. Samples were dried and dry weight consumption and caloric consumption was calculated and averaged over the 48 hour period.

Activity. Daily activity patterns were assessed with the Mini actiwatch (CamNtech) which were placed in a marmoset pouch (Lomar) on a ferret harness (Petco). Subjects were gradually habituated to the ferret harnesses over the course of three weeks, increasing time in the harness incrementally throughout training until 24 hours in the harness had been achieved. The miniwatches are data loggers that batch data in 15 second epochs. For these trials animals were separated from each other within the cage and placed in harnesses with the actiwatch in the pouch secured across the back of the animal. Animals remained in the harness for 48 hours of data collection during which normal husbandry and feeding continued. At the end of the trial the animals were captured in transfer boxes and the harnesses were removed. Data was downloaded from the device. The activity counts from the first 15 minutes and last 15 minutes of the collection were removed from analysis as these represented handling and cage manipulation.

Blood chemistry. Each month animals were fasted overnight and 2 ml of blood were drawn to assess circulating triglyceride concentrations, fasting glucose and insulin concentrations. Fasting glucose was determined immediately following the blood collection via glucometer. Blood was collected into serum separator tubes, spun and frozen in -80°C until further analysis. Triglyceride concentrations were assessed at the SNPRC clinical pathology lab. Samples were shipped to Wisconsin for analysis of insulin concentrations as described [52].

Glucose challenge. Animals were fasted overnight prior to an oral glucose tolerance test [24], and placed in a restraint device used for blood collection to which they had previously been habituated. An EDTA coated needle and syringe were used to collect 0.5 ml of blood from the femoral vein for the baseline bleed. The animals were then dosed orally with a 40% dextrose solution receiving a calculated glucose dose equal to 0.5% of their current body weight. Subjects remained in the restraint for a 15 and 30 minute post dose blood sample drawn from the tail vein via an EDTA coated butterfly needle. Subjects were removed from the restraint device following the 30 minute sample and placed in a transport box until the 60 minute sample, and this was repeated for the 120 minute sample. The 15, 60 and 120 minute samples were glucometer reads only. For the 30 minute sample 0.5 ml of blood was collected for further analysis. Following the 120 minute bleed the animals were returned to their home cage and fed. The 0 and 30 minute samples were spun and frozen until shipment to Wisconsin for insulin assay analysis.

Immunoblots. Total protein extracts were isolated from liver and visceral fat tissue that had been snapped frozen in liquid nitrogen after sacrifice and stored at -80°C until use. Protein extracts were homogenized in RIPA buffer with additional protease and phosphatase inhibitors (Thermo Scientific, Rockford, IL, USA), centrifuged at 14,000g at 4°C for 15 minutes, and then stored at -80°C until needed. Equal amounts of protein samples were separated electrophoretically by SDS-PAGE and then transferred to polyvinylidene difluoride membrane (Millipore, Billerica, MA, USA). Primary antibodies and their sources used in this study: adipose triglyceride lipase (ATGL), pyruvate carboxylase (PCB), glucose-6-phosphatase α (G6Pase), glucose-6-phosphate isomerase (GPI), and actin from Santa Cruz (Santa Cruz CA), peroxisome proliferator-activated receptor γ (PPARγ), phospho-pyruvate dehydrogenase kinase (p-PDK1), pyruvate dehydrogenase kinase (PDK1), phosphoenolpyruvate carboxykinase 1 (PCK1) from Cell Signaling (Beverly MA), sterol regulatory element-binding protein 1 (SREBP1) from Abcam (Cambridge MA) and deptor from Millipore with all alkaline phosphatase-conjugated secondary antibodies (anti-rabbit and anti-mouse) from Santa Cruz. Protein bands on immunoblots were detected using ECL reagent and analyzed using ImageJ.

Analyses. Variables of interest included body mass, fat mass, fat-free mass, 24 hour total actimeter counts, 24 hour caloric intake, triglyceride concentration, fasting glucose concentration, fasting insulin concentration, and glucose AUC following an oral glucose challenge. For each variable, the change in pre- Rapa dose value to post- Rapa dose value, measured following (one month) of dosing was compared for control subjects versus rapamycin-treated subjects in a two-way, repeated measures ANOVA. An additional repeated measures ANOVA was used to compare values within each rapamycin-treated subject over time for the entire

dosing period. Comparisons of tissue protein activity were done using MANOVA with Bonferroni corrections. Analyses were conducted using GraphPad/ Prism and SPSS 13.0.

ACKNOWLEDGEMENTS

The efforts of Joselyn Artavia, Talia Melber, and Jenny Spross for animal training, dosing and data collection are gratefully acknowledged. The technical assistance of Drs. Kathleen Brasky and Michael Owston at the Southwest National Primate Research Center is also gratefully acknowledged.

Funding

This research was financially supported by the Barshop Institute for Longevity and Aging Studies, the Glenn Foundation, the San Antonio Nathan Shock Center of Excellence in the Basic Biology of Aging and the Southwest National Primate Research Center (P51-OD-13986).

Conflict of interest statement

The authors have no conflict of interests to declare.

REFERENCES

1. Harrison DE, Strong R, Sharp ZD, Nelson JF, Astle CM, Flurkey K, Nadon NL, Wilkinson JE, Frenkel K, Carter CS, Pahor M, Javors MA, Fernandez E, Miller. Rapamycin fed late in life extends lifespan in genetically heterogeneous mice. Nature. 2009; 460:392-395.

2. Wilkinson JE, Burmeister L, Brooks SV, Chan CC, Friedline S, Harrison DE, Hejtmancik JF, Nadon N, Strong R, Wood LK, Woodward MA, Miller RA. Rapamycin slows aging in mice. Aging Cell. 2012; 11:675–682.

3. Zhang Y, Bokov A, Gelfond J, Soto V, Ikeno Y, Hubbard G, Diaz V, Sloane L, Maslin K, Treaster S, Réndon S, van Remmen H, Ward W, et al. Rapamycin extends life and health in C57Bl/6 mice. The Journals of Gerontology. Series A, Biological sciences and medical sciences. 2013; 69A:119–130.

4. Fok WC, Chen Y, Bokov A, Zhang **Y**, Salmon AB, Diaz V, Javors M, Wood WH 3rd, Zhang **Y**, Becker KG, Pérez VI, Richardson A. Mice fed rapamycin have an increase in lifespan associated with major changes in the liver transcriptome. PLoS One. 2014; 9:e83988.

5. Halloran J, Hussong SA, Burbank R, Podlutskaya N, Fischer KE, Sloane LB, Austad SN, Strong R, Richardson A, Hart MJ, Galvan V. Chronic inhibition of mammalian target of rapamycin by rapamycin modulates cognitive and non-cognitive components of behavior throughout lifespan in mice. Neuroscience. 2012; 223:102-113.

6. Stallone G, Infante B, Grandaliano G, Gesualdo L. Management of side effects of sirolimus therapy. Transplantation. 2009; 87:S23–S26.

7. Montalbano M, Neff GW, Yamashiki N, Meyer D, Bettiol M, Slapak-Green G, Ruiz P, Manten E, Safdar K, O'Brien C, Tzakis AG. A retrospective review of liver transplant patients treated with sirolimus from a single center: an analysis of sirolimus-related complications. Transplantation. 200;78:264–268.

8. Fang Y, Westbrook R, Hill C, Boparai RK, Arum O, Spong A, Wang F, Javors MA, Chen J, Sun LY, Bartke A. Duration of rapamycin treatment has differential effects on metabolism in mice. Cell Metabolism. 2013; 17:456-462.

9. Fang Y, Bartke A. Prolonged rapamycin treatment led to beneficial metabolic switch. Aging. 2013;5:328-329.

10. Leontieva OV, Paszkiewicz GM, Blagosklonny MV. Weekly administration of rapamycin improves survival and biomarkers in obese male mice on high-fat diet. Aging Cell. 2014; 13:616-622

11. Liu Y, Diaz V, Fernandez E, Strong R, Ye L, Baur JA, Lamming DW, Richardson A, Salmon AB. Rapamycin-induced metabolic defects are reversible in both lean and obese mice. Aging (Albany NY). 2014; 6:742-754.

12. Leontieva OV, Pasckiewicz GM, Blagosklonny MV. Comparison of rapamycin schedules in mice on high-fat diet. Cell Cycle. 2014; 13:3350-3356.

13. Leontieva OV, Paszkiewicz G, Demidenko ZN, Blagosklonny MV. Resveratrol potentiates rapamycin to prevent hperinsulinemia and obesity in male mice on high fat diet. Cell Death and Disease. 2013; 4:e472.

14. Grarup N, Andersen G. Gene–environment interactions in the pathogenesis of type 2 diabetes and metabolism. Current Opinion in Clinical Nutrition & Metabolic Care. 2007; 10:420-426.

15. Halford JC, Boyland EJ, Blundell JE, Kirkham TC, Harrold JA. Pharmacological management of appetite expression in obesity. Nature Reviews Endocrinology. 2010; 6:255-269.

16. Jensen T, Kiersgaard M, Sørensen D, Mikkelsen L. Fasting of mice: a review. Laboratory Animals. 2013; 47:225-240.

17. Li S, Zhang HY, Hu CC, Lawrence F, Gallagher KE, Surapaneni A, Estrem ST, Calley JN, Varga G, Dow ER, Chen Y. Assessment of diet-induced obese rats as an obesity model by comparative functional genomics. Obesity. 2008;16:811-818.

18. Lai M, Chandrasekera PC, Barnard ND. You are what you eat, or are you? The challenges of translating high-fat-fed rodents to human obesity and diabetes. Nutrition & Diabetes. 2014; 4:e135.

19. Ikemoto S, Takahashi M, Tsunoda N, Maruyama K, Itakura H, Ezaki O. High-fat diet-induced hyperglycemia and obesity in mice: differential effects of dietary oils. Metabolism. 1996; 45:1539-1546.

20. Gallou-Kabani C, Vigé A, Gross MS, Rabès JP, Boileau C, Larue-Achagiotis C, Tomé D, Jais JP, Junien C. C57BL/6J and A/J mice fed a high-fat diet delineate components of metabolic syndrome. Obesity. 2007; 15:1996-2005.

21. Warden CH, Fisler JS. Comparisons of diets used in animal models of high-fat feeding. Cell Metabolism. 2008;7:277.

22. Tardif SD, Mansfield K, Ratnam R, Ross CN, Ziegler TE. The marmoset as a model of aging and age related disease. Institute for Laboratory Animal Research Journal. 2011; 52:54–65.

23. Ross CN, Davis K, Dobek G, Tardif SD. Aging phenotypes of common marmosets (*Callithrix jacchus*). Journal of Aging Research. 2012; 2012:567143.

24. Tardif SD, Power ML, Ross CN, Rutherford JN, Layne-Colon DG, Paulik MA. Characterization of obese phenotypes in a small

nonhuman primate, the common marmoset (*Callithrix jacchus*). Obesity. 2009; 17:1499-1505.

25. Wachtman LM, Kramer JA, Miller AD, Hachey AM, Curran EH, Mansfield KG. Differential contribution of dietary fat and monosaccharide to metabolic syndrome in the common marmoset (*Callithrix jacchus*). Obesity. 2011; 19:1145-1156.

26. Power ML, Ross CN, Schulkin J, Tardif SD. The development of obesity begins at an early age in captive common marmosets (*Callithrix jacchus*). American Journal of Primatology. 2012; 74:261–269.

27. Power ML, Ross CN, Schulkin J, Ziegler TE, Tardif SD. Metabolic consequences of the early onset of obesity in common marmoset monkeys. Obesity. 2013; 21:E592–E598.

28. Ross CN, Power ML, Artavia J, Tardif SD. Relation of food intake behaviors and obesity development in young common marmoset monkeys. Obesity. 2013; 21:1891-1899.

29. Tardif SD, Ross CN, Bergman P, Fernandez E, Javors M, Salmon A, Spross J, Strong R, Richardson A. Testing efficacy of administration of the antiaging drug rapamycin in a nonhuman primate, the common marmoset. Journals of Gerontology: Biological Sciences. 2015; 70:577-587.

30. Verges B, Walter T, Cariou B. Effects of anti-cancer targeted therapies on lipid and glucose metabolism. European Journal of Endocrinology. 2014; 170:R43-55.

31. Mannick JB, Giudice G, Lattanzi M, Valiante NM, Praestgaard J, Huang B, Lonetto MA, Maexker HT, Kovarik J, Carson S, Glass DJ, Kickstein LB. mTOR inhibition improves immune function in the elderly. Science Translational Medicine. 2014, 268:268ra179.

32. Morton GJ, Cummings DE, Baskin DG, Barsh GS, Schwartz MW. Central nervous system control of food intake and body weight. Nature. 2006; 443:289-295.

33. Teutonico A, Schena PF, Di Paolo S. Glucose metabolism in renal transplant recipients: effect of calcineurin inhibitor withdrawal and conversion to sirolimus. Journal of the American Society of Nephrology. 2005; 16:3128-3135.

34. Johnston O, Rose CL, Webster AC, Gill JS. Sirolimus is associated with new-onset diabetes in kidney transplant recipients. Journal of the American Society of Nephrology. 2008;197:1411-1418.

35. Yates CJ, Fourlanos S, Hjelmesaeth J, Colman PG, Cohney SJ. New-onset diabetes after kidney transplantation-changes and challenges. American Journal of Transplantation. 2012; 12:820-828.

36. Pavlakis M, Goldfarb-Rumyantzev AS. Diabetes after transplantation and sirolimus: what's the connection? Journal of the American Society of Nephrology. 2008; 19:1255-1256.

37. Lamming DW, Ye L, Astle CM, Baur JA, Sabatini DM, Harrison DE. Young and old genetically heterogeneous HET3 mice on a rapamycin diet are glucose intolerant but insulin sensitive. Aging Cell. 2013; 12:712-718.

38. Miller RA, Harrison DE, Astle CM, Fernandez E, Flurkey K, Han M, Javors MA, Li X, Nadon NL, Nelson JF, Pletcher S, Salmon AB, Sharp ZD, Van Roekel S, Winkleman L, Strong R. Rapamycin-mediated lifespan increase in mice is dose and sex dependent and metabolically distinct from dietary restriction. Aging Cell. 2014; 13:468-477.

39. Fraenkel M, Ketzinel-Gilad M, Ariav Y, Pappo O, Karaca M, Castel J, Berthault MF, Magnan C, Cerasi E, Kaiser N, Leibowitz G. mTOR inhibition by rapamycin prevents cell adaptation to hyperglycemia and exacerbates the metabolic state in Type 2 diabetes. Diabetes. 2008; 57:945-957.

40. Blagosklonny MV. Rapamycin-induced glucose intolerance: hunger or starvation diabetes. Cell Cycle. 2011; 10:4217-4224.

41. Blagosklonny MV. Once again on rapamycin-induced insulin resistance and longevity: despite of or owing to. Aging. 2012; 4: 350-358.

42. Blagosklonny MV. TOR-centric view on insulin resistance and diabetic complications: perspecitve for endocrinologists and gerontologists. Cell Death and Disase. 2013; 4: e964.

43. Ye L, Widlund AL, Sims CA, Lamming DW, Guan Y, Davis JG, Sabatini DM, Harrison DE, Vang O, Baur JA. Rapamycin doses sufficient to extend lifespan do not compromise muscle mitochondrial content or endurance. Aging. 2013; 5:539-550.

44. Ye L, Varamini B, Lamming DW, Sabatini DM, Baur JA. Rapamycin has a biphasic effect on insulin sensitivity in C2C12 myotubes due to sequential disruption of mTORC1 and mTORC2. Frontiers in Genetics. 2012; 3:177.

45. Lamming DW, Ye L, Katajisto P, Goncalves MD, Saitoh M, Stevens DM, Davis JG, Salmon AB, Richardson A, Ahima RS, Guertin DA, Sabatini DM, Baur JA. Rapamycin-induced insulin resistance is mediated by mTORC2 loss and uncoupled from longevity. Science. 2012; 335:1638-1643.

46. Festuccia WT, Blanchard PG, Belchior T, Chimin P, Paschoal VA, Magdalon J, Hirabara SM, Simões D, St-Pierre P, Carpinelli A, Marette A, Deshaies Y. PPARγ activation attenuates glucose intolerance induced by mTOR inhibition with rapamycin in rats. American Journal of Physiology-Endocrinology and Metabolism. 2014; 306:E1046-E1054.

47. Lamming DW, Sabatini DM. A central role for mTOR in lipid homeostasis. Cell Metabolism. 2013; 18:465-469.

48. Sipula IJ, Brown NF, Perdomo G. Rapamycin-mediated inhibition of mammalian target of rapamycin in skeletal muscle cells reduces glucose utilization and increases fatty acid oxidation. Metabolism. 2006; 55:1637-1644.

49. Yu Z, Wang R, Fok WC, Coles A, Salmon AB, Perez VI. Rapamycin and dietary restriction induce metabolically distinctive changes in mouse liver. The Journals of Gerontology. Series A, Biological sciences and medical sciences. 2015; 70:410-420.

50. Houde VP, Brule S, Festuccia WT, Blanchard PG, Bellmann K, Deshaies Y, Marette A. Chronic Rapamycin treatment causes glucose intolerance and hyperlipidemia by upregulating hepatic gluconeogenesis and impairing lipid deposition in adipose tissue. Diabetes. 2010; 59:1338-1348.

51. Layne DG, Power RA. Husbandry, handling, and nutrition for marmosets. Comparative Medicine. 2003; 53:351–359.

52. Ziegler TE, Colman RJ, Tardif SD, Sosa ME, Wegner FH, Wittwer DJ, Shrestha H. Development of metabolic function biomarkers in the common marmoset, *Callithrix jacchus*. American Journal of Primatology. 2013; 75:500-508.

Research Paper

Rapamycin-induced metabolic defects are reversible in both lean and obese mice

Yuhong Liu[1], Vivian Diaz[1], Elizabeth Fernandez[1,2,3], Randy Strong[1,2,3], Lan Ye[4], Joseph A. Baur[4], Dudley W. Lamming[5], Arlan Richardson[6], and Adam B. Salmon[1,2,7]

[1] The Sam and Ann Barshop Institute for Longevity and Aging Studies, The University of Texas Health Science Center at San Antonio, San Antonio TX 78245, USA;
[2] The Geriatric Research Education and Clinical Center, South Texas Veterans Health Care System, San Antonio, TX 78229, USA;
[3] Departments of Pharmacology, The University of Texas Health Science Center at San Antonio, San Antonio TX 78245, USA;
[4] Institute for Diabetes, Obesity, and Metabolism and Department of Physiology, Perelman School of Medicine, University of Pennsylvania, Philadelphia PA 19104, USA;
[5] Department of Medicine, University of Wisconsin School of Medicine and Public Health, Madison WI 53726, USA;
[6] Reynolds Oklahoma Center on Aging, University of Oklahoma Health Sciences Center and Oklahoma City VA Medical Center, Oklahoma OK 73104, USA;
[7] Departments of Molecular Medicine, The University of Texas Health Science Center at San Antonio, San Antonio TX 78245, USA

Key words: *rapamycin, glucose, insulin, obesity, mTOR*
Received: *6/16/14; Accepted: 8/31/14; Published: 9/02/14*
Correspondence to: *Adam Salmon, PhD;* ***E-mail:*** *salmona@uthscsa.edu* doi:10.18632/aging.100688

Abstract: The inhibition of mTOR (mechanistic target of rapamycin) by the macrolide rapamycin has many beneficial effects in mice, including extension of lifespan and reduction or prevention of several age-related diseases. At the same time, chronic rapamycin treatment causes impairments in glucose metabolism including hyperglycemia, glucose intolerance and insulin resistance. It is unknown whether these metabolic effects of rapamycin are permanent or whether they can be alleviated. Here, we confirmed that rapamycin causes glucose intolerance and insulin resistance in both inbred and genetically heterogeneous mice fed either low fat or high fat diets, suggesting that these effects of rapamycin are independent of genetic background. Importantly, we also found that these effects were almost completely lost within a few weeks of cessation of treatment, showing that chronic rapamycin treatment does not induce permanent impairment of glucose metabolism. Somewhat surprisingly, chronic rapamycin also promoted increased accumulation of adipose tissue in high fat fed mice. However, this effect too was lost when rapamycin treatment was ended suggesting that this effect of rapamycin is also not permanent. The reversible nature of rapamycin's alterations of metabolic function suggests that these potentially detrimental side-effects might be managed through alternative dosing strategies or concurrent treatment

INTRODUCTION

The mTOR (mechanistic target of rapamycin) signaling pathway serves as a central regulator of cell metabolism in response to nutrient and growth factor stimuli. The serine/threonine protein kinase mTOR acts as a catalytic core unit of both mTORC1 and mTORC2. Each mTORC complex likely plays discrete roles in metabolic function: mTORC1 integrates nutrient, growth factor and cellular energy status to regulate cell

proliferation, growth and metabolism, whereas mTORC2 acts upon several downstream kinases including the Akt/PKB to regulate cell metabolism and survival [reviewed in [1]]. Due to its role in regulating cellular metabolism, aberrant mTOR signaling may be fundamental to the development of metabolic disease and dysfunction. For example, chronic activation of mTORC1 signaling in obesity is thought to play a significant role in the development of insulin resistance in muscle, adipose and liver tissue [2-4].

As the name implies, mTOR signaling is targeted by the bacterial macrolide rapamycin which interacts with the binding protein FKBP12 to inhibit some, but not all, mTOR functions [5]. While rapamycin is thought to primarily inhibit mTORC1 signaling through a direct mechanism, recent studies suggest chronic rapamycin treatment also down-regulates mTORC2 activity [6, 7]. Rapamycin and its analogues are approved for treatment of some forms of cancer and as immunosuppressants following organ transplantation. Rapamycin is also the first pharmacological agent capable of extending lifespan in both male and female mice according to the rigorous criteria established by the NIA's Intervention Testing Program [8-11]. Chronic rapamycin treatment has been shown to slow the progression of some, but not all, of the physiological declines associated with mouse aging [12-14]. Surprisingly, chronic rapamycin also promotes metabolic changes generally thought to be unfavorable, including glucose intolerance, insulin resistance and dyslipidemia, in several different rodent models [6, 15-20]. There is some evidence that the degree of metabolic dysfunction caused by rapamycin may be dependent on genetic background, length and means of administration of treatment and diet [6, 17, 18]. This is also a consideration in the clinical administration of rapamycin as the incidence of insulin resistance and new onset diabetes was shown to be significantly elevated in kidney transplant patients receiving rapamycin therapy [21, 22].

These potentially detrimental effects glucose regulation (glucose intolerance, insulin resistance, etc.) are concerns that currently may preclude the use of rapamycin and its analogues to treat and prevent age-related diseases. An important question heretofore unaddressed is whether chronic rapamycin treatment induces permanent alterations to metabolic function *in vivo*. In this study, we tested whether cessation of chronic rapamycin treatment could reverse its impairment of glucose metabolism in mice. In addition, we tested whether feeding mice a high fat diet, which also impairs glucose regulation, would exacerbate the impairment caused by rapamycin. Our results suggest that the metabolic effects of chronic rapamycin treatment are not permanent but rather dependent on its continued presence and activity suggesting that these adverse effects may be reduced or prevented through alternative treatment plans.

RESULTS

Chronic oral delivery of encapsulated rapamycin impairs glucose metabolism

Chronic rapamycin treatment has been shown to impair several measurements of glucose metabolism including increased circulating levels of glucose and insulin and impaired glucose and insulin tolerance [6, 17, 18, 23, 24]. At least some of these effects seem to be dependent on genetic strain of the model system, means of administration and length of treatment [6, 17, 18, 23, 24]. Here, we found that chronic treatment with enteric rapamycin (eRAPA) significantly impairs glucose intolerance and promotes insulin resistance in C57BL/6 mice when given in combination with either a low fat or a high fat diet (Figure 1). The same group of mice were tested longitudinally, first after 2 months and then after 4 months of eRAPA treatment. Both high fat diet and eRAPA impaired glucose and insulin tolerance at each time points, but we found no significant interaction effect suggesting that eRAPA promoted metabolic dysfunction equally in both low fat and high fat diets (Figure 1B, D). Moreover, time on diet had no significant effect on either markers suggesting that the effects of eRAPA occur quickly but do not become progressively worse at least in the time frame at which we studied. Fasting blood glucose levels were unaffected by eRAPA at both time points on both diets, though high fat diet did significantly increase these levels (Figure 2A). We also measured glucose-stimulated insulin secretion to determine if this might explain the impaired glucose tolerance. While high fat diet significantly increased blood insulin levels in both fasted and glucose-stimulated mice, these levels were unaffected by treatment with eRAPA on both diets (Figure 2B).

There is some evidence that the effects of rapamycin on insulin sensitivity differs among genetic strains of mice. For example, while inbred mice like C57BL/6 tend to become insulin resistant with rapamycin treatment, mice with heterogeneous genetic background have shown variable effects in terms of insulin sensitivity [6, 17, 18]. Here, we found that genetically heterogeneous UT-HET3 mice respond in a similar manner as C57BL/6 mice to chronic eRAPA in both diet formulations we used. In UT-HET3 mice, eRAPA impaired glucose tolerance and caused insulin resistance in combination with both low fat and high fat diets but

did not affect fasting glucose or insulin levels (Figure 4). The degree of glucose intolerance caused by eRAPA in UT-HET3 mice was similar to that of C57BL/6 while insulin resistance was milder in the genetically heterogeneous mice. Together, these data suggest the negative effects on glucose metabolism caused by eRAPA on glucose metabolism is largely independent of genetic background.

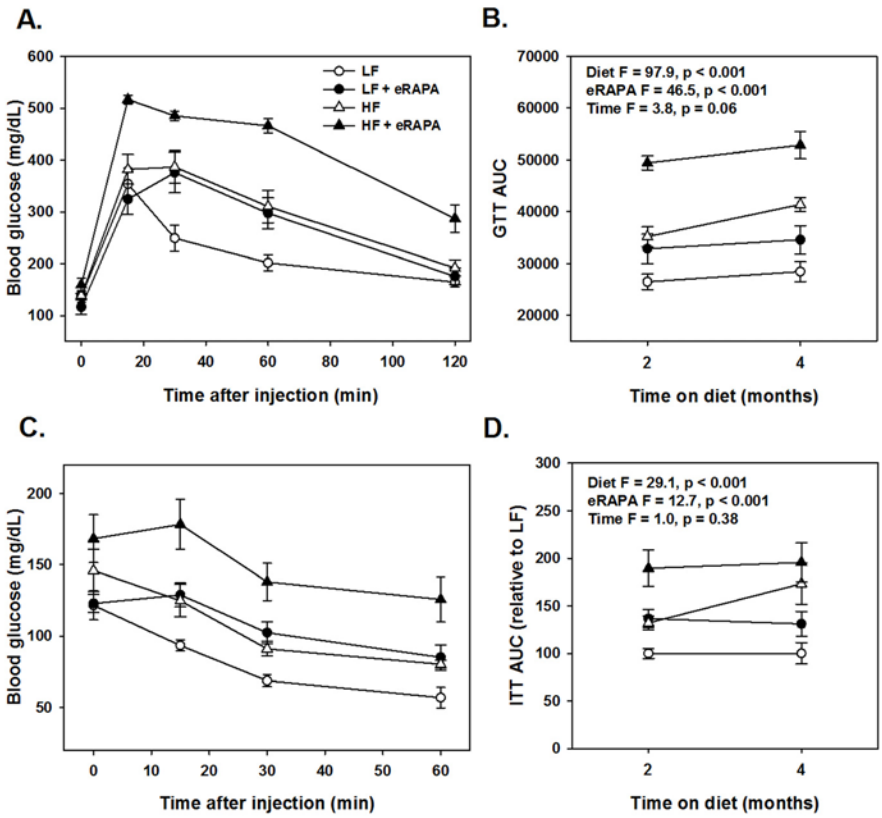

Figure 1. (**A**) Glucose tolerance tests for C57BL/6 males fed indicated diets for 2 months. (**B**) Area under curve (AUC) calculations for glucose tolerance tests following 2 or 4 months feeding indicated diets. (**C**) Insulin tolerance tests for C57BL/6 males fed indicated diets for 2 months. (**D**) AUC for insulin tolerance tests for insulin tolerance tests following 2 or 4 months feeding indicated diets. For all, symbols represent average (± SEM) values for n=6 mice at indicated time point for mice fed low fat (circle) or high fat (triangle) diets with (solid) or without (open) encapsulated rapamycin (eRAPA). F and p values are given for 3 way ANOVA testing indicated variables.

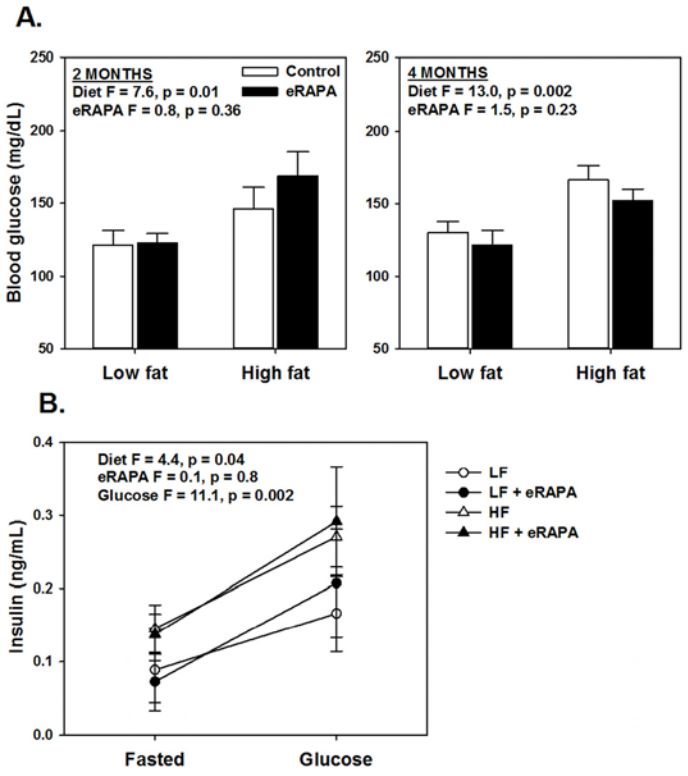

Figure 2. (**A**) Fasting blood glucose levels after feeding indicated diets for 2 and 4 months. (**B**) Fasting and glucose stimulated insulin levels in whole blood. For all, symbols represent average (± SEM) values for n=6 mice treated with (solid) or without (open) encapsulated rapamycin (eRAPA) for the indicated diet. F and p values are given for either 2 way (**A**) or 3 way (**B**) ANOVA testing indicated variables.

We found evidence that chronic eRAPA treatment significantly down-regulated both mTORC1 and mTORC2 signaling to a greater extent in high fat-fed mice compared to low fat fed mice (Figure 4). We assessed mTOR signaling in skeletal muscle and adipose tissue collected from UT-HET3 mice treated with eRAPA for 3 months. Both tissues showed significant reduction of phosphorylation of S6 in eRAPA - treated mice, indicative of inhibition of mTORC1 signaling. Chronic eRAPA treatment also inhibited mTORC2 signaling as measured by phosphorylation of Akt at Ser473; however, we only found this reduction of Akt phosphorylation in e-RAPA treated mice fed high fat diets. The interaction of mTOR with either raptor (mTORC1) or rictor (mTORC2) was reduced by eRAPA treatment with, again, a stronger inhibition in high fat-fed mice.

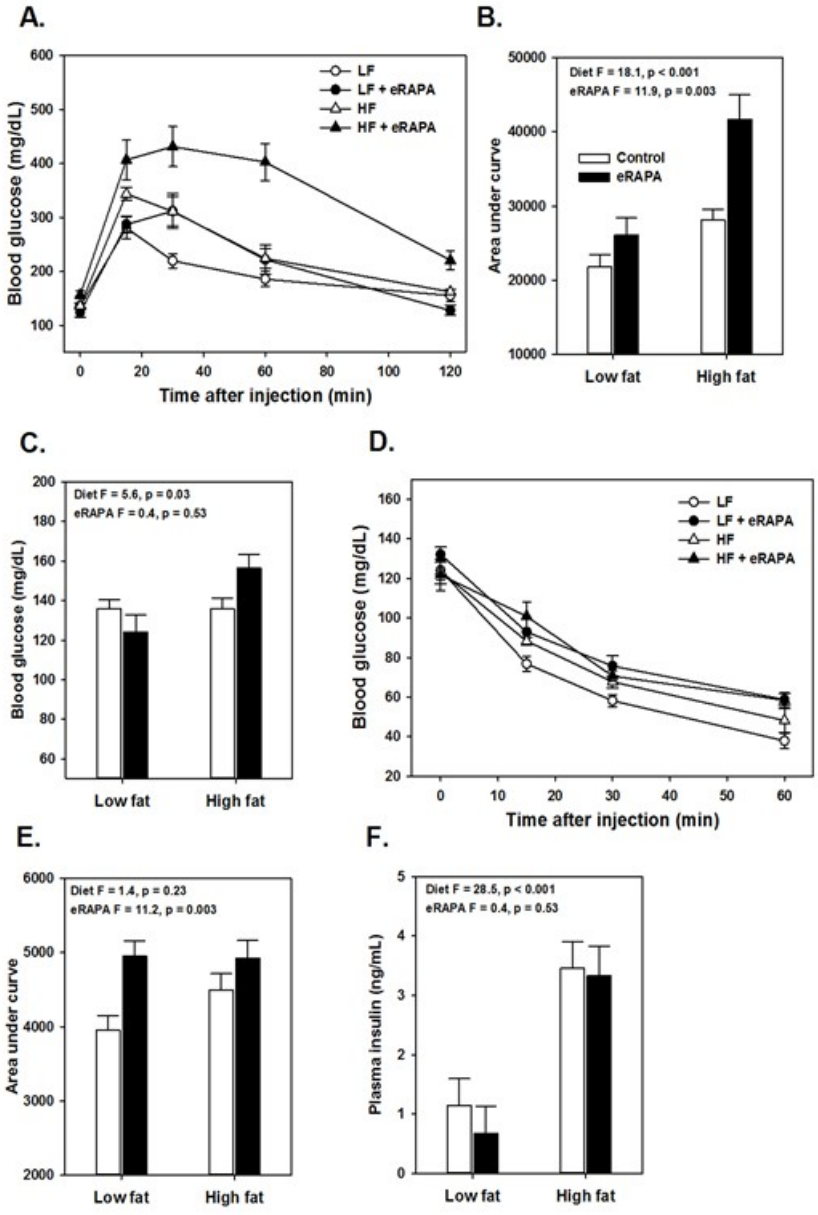

Figure 3. (**A**) Glucose tolerance tests for UT-HET3 males fed indicated diets for 3 months. (**B**) Area under curve (AUC) calculations for glucose tolerance tests shown in A. (**C**) Fasting blood glucose levels for mice in A. (**D**) Insulin tolerance tests for UT-HET3 males fed indicated diets for 3 months. (**E**) AUC for insulin tolerance tests for insulin tolerance tests. (**F**) Fasted plasma insulin levels. For all, symbols represent average (± SEM) values for n=6-10 mice at indicated time point for mice fed low fat (circle) or high fat (triangle) diets with (solid) or without (open) encapsulated rapamycin (eRAPA). F and p values are given for 2 way ANOVA testing indicated variables.

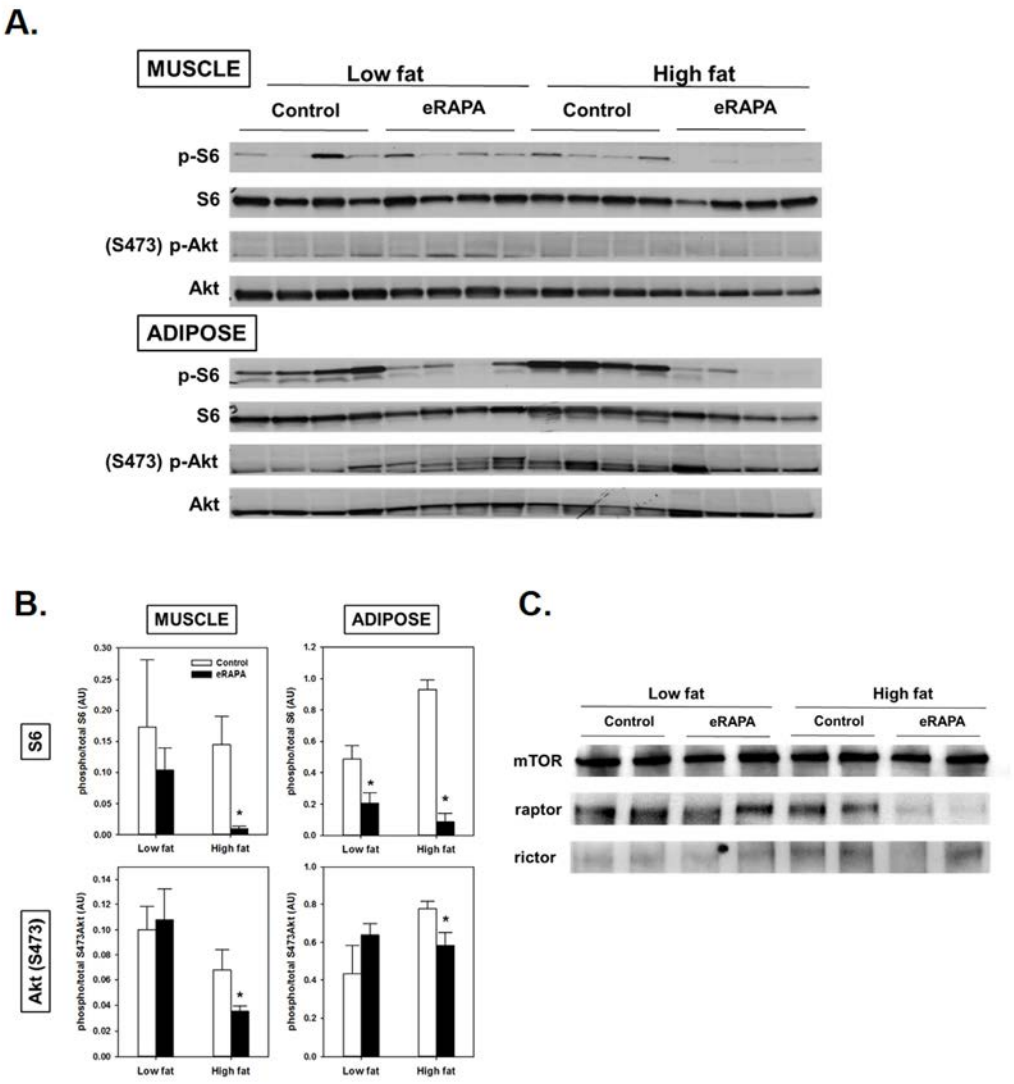

Figure 4. (**A**) Representative blots of p-S6, total S6, pAkt (Ser473) and total Akt in skeletal muscle and adipose of mice fed low fat or high fat diets with or without encapsulated rapamycin (eRAPA). (**B**) Quantification of relative phosphorylation of S6 or Akt (Ser473) of blots in A. Bars represent average (± SEM) values for n=4 mice treated with (solid) or without (open) eRAPA. Asterisks indicate significant difference between control and eRAPA group. (**C**) Representative blot of immunoprecipitation of mTOR from skeletal muscle protein homogenates and probed for the indicated proteins.

Metabolism is normalized by ending rapamycin administration

An important question heretofore unaddressed is whether chronic eRAPA treatment induces permanent changes *in vivo* to physiological processes altered by rapamycin. We addressed this question by shifting C57BL/6 mice that had been treated with eRAPA for 4 months to their equivalent diets without eRAPA (i.e, mice fed high fat diet with eRAPA were now fed high fat diet without eRAPA, etc.). While treated with eRAPA, both diet ($F = 56.3$, $p<0.001$) and eRAPA ($F = 19.7$, $p<0.001$) caused significant reduction in glucose tolerance in these mice (Figure 5A). Within 2 weeks of cessation of eRAPA treatment, glucose tolerance values were "normalized" to that of mice that had never been treated with eRAPA (Figure 5A). At this point, prior eRAPA treatment had no significant effect on glucose tolerance ($F = 2.6$, $p = 0.13$) while high fat diet still significantly impaired glucose tolerance ($F = 66.2$, $p<0.001$). Similarly, insulin sensitivity in these mice was relatively "normalized" within 2 weeks of cessation of eRAPA (Figure 5B). These data suggest that the impairment of glucose metabolism by eRAPA *in vivo* is reversible and can be mitigated by cessation of treatment.

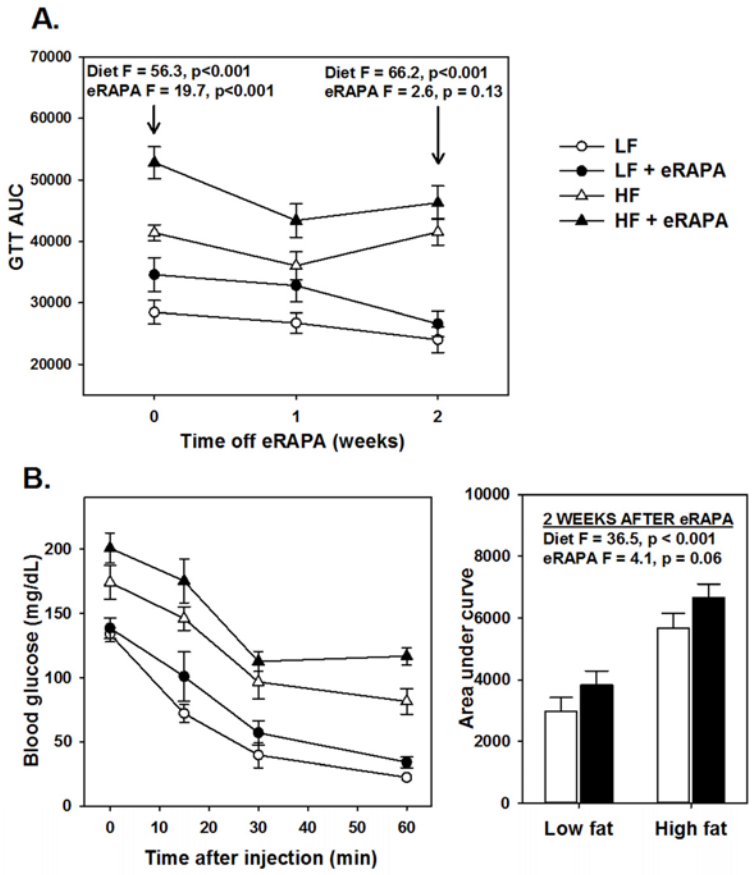

Figure 5. (**A**) Area under curve (AUC) calculations for glucose tolerance tests following 0, 1 and 2 weeks after cessation of encapsulated rapamycin (eRAPA) treatment. (**B**) Insulin tolerance tests (left) and AUC calculations (right) in mice 2 weeks after cessation of eRAPA treatment. For both, symbols represent average (± SEM) values for n=6 mice treated with (solid) or without (open) eRAPA for the indicated diet. F and p values are given for either 2 way ANOVA testing indicated variables.

Chronic administration of encapsulated rapamycin promotes adiposity

Under our experimental paradigm, eRAPA when treated in combination with low fat diet had no effect on body mass, fat mass or fat-free mass (Figures 6 and 7). Contrary to reports suggesting that rapamycin treatment reduces body mass and adiposity [16, 19, 20, 25], we found that eRAPA treatment actually promoted increased adiposity in high fat fed mice. In high fat-fed C57BL/6 mice, both body mass and fat mass were significantly increased with continuous eRAPA treatment (Figure 6). Fat-free mass, likely consisting largely of muscle and bone, was unchanged with eRAPA treatment. We also found a similar increase in fat mass in high fat-fed UT-HET3 mice treated with eRAPA (Figure 7). Surprisingly, the differences in body mass and fat mass caused by eRAPA treatment were not permanent in C57BL/6 mice. Within only a few weeks of removing eRAPA from the diet, body weight and fat mass declined in high fat-fed mice previously treated with eRAPA such that there was no significant difference between this group and the high fat-fed "control" group of mice (Figure 6, arrow represents time of diet switch).

These data suggest that the obesogenic effect of eRAPA in combination with high fat or high caloric intake may be through pathways of fat mobilization. In vitro, inhibition of mTOR blocks adipogenesis and stimulates

lipolysis [26-28]. In adipose tissue, we found that chronic eRAPA in combination with low fat diet reduces the phosphorylation of hormone sensitive lipase (HSL), the rate limiting step in lipolysis (Figure 8). In high fat-fed mice, there was almost no measurable phosphorylation of HSL in both control and eRAPA treated mice. These data suggest that lipolysis then is inhibited in vivo by chronic eRAPA treatment in mice fed the low fat fed mice. However, we also saw that adipose triglyceride lipase (ATGL), was elevated by eRAPA in both low fat and high fat diets suggesting increased breakdown of adipose resources (Figure 8). ATGL catalyzes the initial step in triacylglyceride hydrolysis, whereas HSL may have more specificity to the diacylglyceride form. These data then suggests a potentially complex effect of chronic eRAPA treatment that contributes to the adipose gain of these mice when also exposed to a high fat diet.

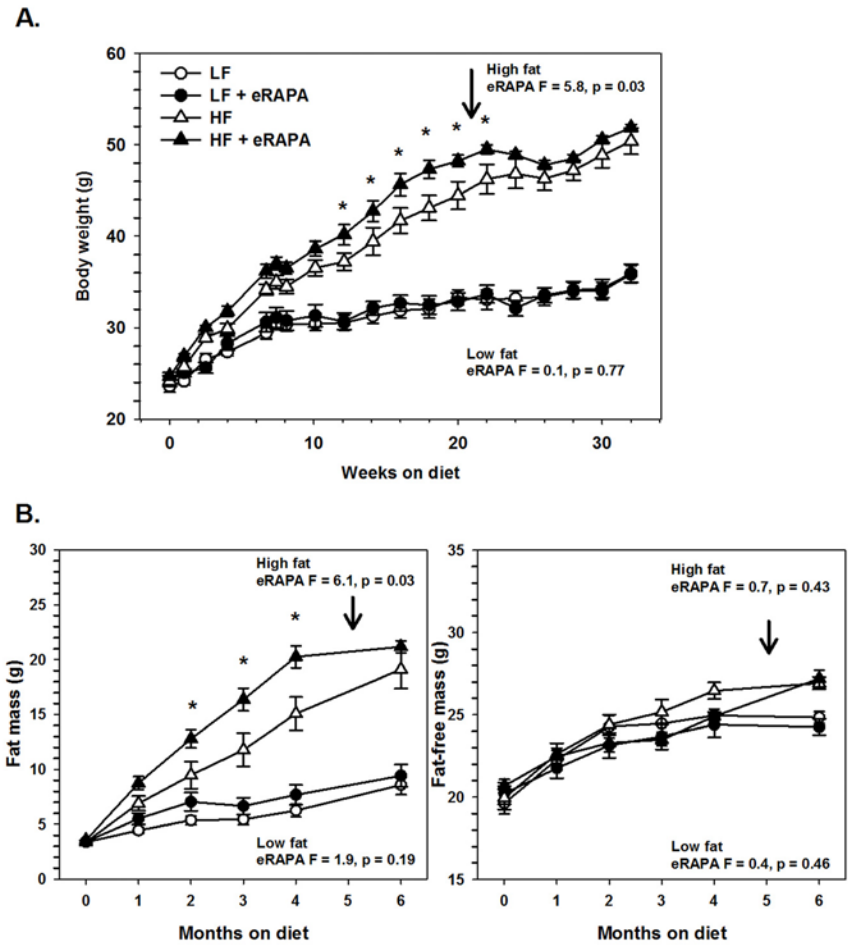

Figure 6. (**A**) Body weight of C57BL/6 males fed low fat (circles) or high fat (triangles) diets either with (solid) or without (open) encapsulated rapamycin (eRAPA). (**B**) Total fat content (left) and fat-free content (right) of mice in A. For all, symbols represent average (± SEM) values for n=6 mice. Downward arrow indicates time point of cessation of eRAPA treatment. F and p values given for repeated measures ANOVA testing the effect of eRAPA for the indicated diet. Asterisks indicate significant difference at time point between eRAPA and control for given diet from post-hoc analysis of ANOVA.

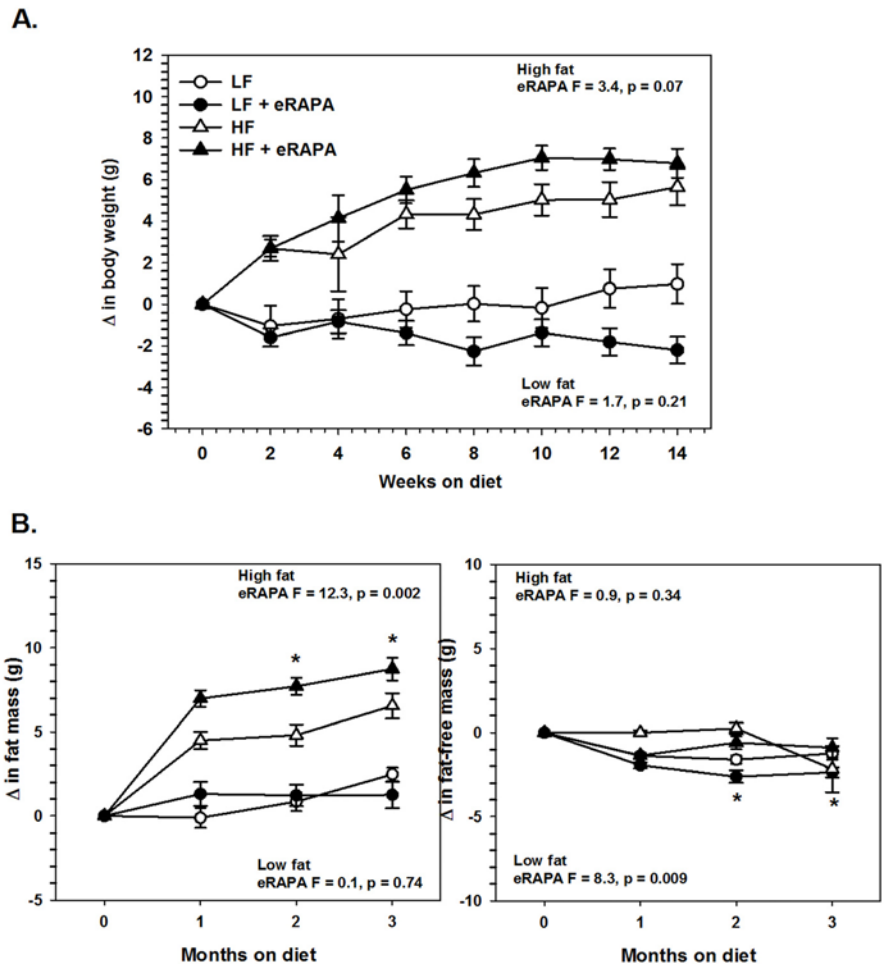

Figure 7. (**A**) Body weight of UT-HET3 males fed low fat (circles) or high fat (triangles) diets either with (solid) or without (open) encapsulated rapamycin (eRAPA). (**B**) Total fat content (left) and fat-free content (right) of mice in A. For all, symbols represent average (± SEM) values for n=6-10 mice. F and p values given for repeated measures ANOVA testing the effect of eRAPA for the indicated diet. Asterisks indicate significant difference at time point between eRAPA and control for given diet from post-hoc analysis of ANOVA.

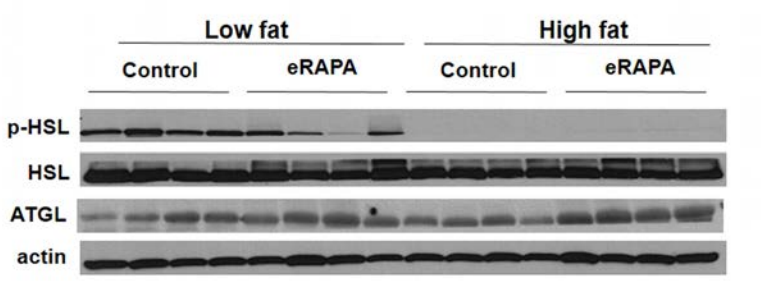

Figure 8. Representative western blot of p-HSL, HSL, and ATGL in adipose tissue from mice fed indicated diets.

DISCUSSION

One important side-effect of long-term rapamycin treatment in both rodents and humans is the potential for significant impairment of the normal regulation of glucose metabolism [6, 15-22]. Despite the potential of rapamycin both clinically and as an anti-aging therapeutic, the risk of new onset type 2 diabetes or other metabolic diseases is a significant obstacle for chronic use of rapamycin in humans. Our results confirm that chronic delivery of encapsulated rapamycin (eRAPA) does cause insulin resistance and glucose intolerance in both inbred and genetically heterogeneous strains of mice. Further, mice these effects are exacerbated in mice fed a high fat diet, supporting the notion that rapamycin treatment may drive the onset of type 2 diabetes. However, the key finding of this study is that the impairment of glucose metabolism by eRAPA in both low fat (lean) and high fat-fed (obese) mice are completely reversed by ending eRAPA treatment. This suggests that the administration of rapamycin through this paradigm does not induce permanent changes to the gluco-regulatory system. These data raise the possibility that metabolic defects caused by long-term rapamycin use could be mitigated transient withdrawal from the treatment, or by concurrent or alternative therapies. Festuccia et al. recently showed that rosiglitazone reduces hyperglycemia, glucose intolerance and insulin resistance caused by short-term treatment of rapamycin in rats [29]. It remains to be seen whether preventing metabolic dysfunction by treatments like this will further potentiate the beneficial effects of rapamycin in cancer treatment and prevention or longevity extension. There has been some suggestion that rapamycin-mediated modulation of different markers of glucose metabolism may differ depending on the time course of treatment, though this may be dependent on the model used and method of treatment. For example, Ye et al. showed that rapamycin treatment of C2C12 muscle cell lines had a biphasic effect on insulin response in that short-term treatment with rapamycin caused insulin sensitivity whereas long-term treatment caused insulin resistance [30]. This insulin resistance was associated with rapamycin-mediated inhibition of mTORC2 signaling. Similar to our work here, Lamming et al also showed that a chronic, 2 week treatment of rapamycin in C57BL/6 mice caused glucose intolerance and insulin resistance that was, at least in part, mediated by down-regulation of mTORC2 signaling [6]. Houde et al. also found that 15 days of rapamycin treatment caused similar metabolic impairments in Sprague-Dawley rats [19]. Likewise, data from Fang et al. suggest that chronic treatment with rapamycin in a mixed genetic background results in sustained glucose intolerance, but found that insulin sensitivity as assessed by an insulin tolerance test was dependent upon the length of treatment, with mice treated for 20 weeks actually showing increased insulin sensitivity (albeit glucose intolerance) relative to control mice [18]. In contrast, Lamming et al. found that both short (3 week) and long (3 month) term treatment of female UM-HET3 mice with diet-delivered eRAPA caused glucose intolerance but neither treatment, nor treatment for over a year resulted in dramatic changes in insulin sensitivity [17]. It is a challenge to integrate the results from all of these studies due to difference in the genetic backgrounds of the models used, diets used and whether rapamycin was administered by injection or in an encapsulated form in the diet. Our data show no evidence of any metabolic switch with long term oral eRAPA treatment (similar to Lamming et al. [17]) suggesting that this may not occur with chronic oral delivery of encapsulated rapamycin. Also similar to Lamming et al., we found that eRAPA did not dramatically affect insulin levels suggesting that encapsulated rapamycin may not impair pancreatic function at least in the time-frame of these studies [18, 31, 32]. It remains to be determined whether this means of administration is essential for the reversibility of rapamycin's effects on glucose metabolism.

We found it surprising that chronic eRAPA treatment tended to promote increased adiposity in both high fat fed C57BL/6 and genetically heterogeneous UT-HET3 mice. Chronic activation of mTORC1 by obesity and metabolic stress appears to play a primary role in the development of insulin resistance and type 2 diabetes [3, 4, 33]. Inhibition of mTOR by rapamycin impairs adipocyte differentiation in cell culture [34]. Reduced mTORC1 signaling either in adipose tissue (by adipose-specific Raptor deletion) or through genetic ablation of the mTORC1 effector S6K1 prevents high fat diet-induced metabolic dysfunction [3, 4, 35]. Furthermore, some, though not all, studies have suggested that rapamycin treatment may be sufficient to reduce adiposity both in high fat fed, obese animals and in normal fed, lean animals [8, 16, 20, 23, 25, 36, 37]. On the other hand, inhibition of mTORC2 has been shown to negatively affect glucose regulation; deletion of Rictor in adipose tissue leads to weight gain and insulin resistance [38, 39], deletion of Rictor in liver leads to impaired glucose tolerance and increased gluconeogenesis [6], and ubiquitous deletion of Rictor leads to hyperglycemia and hepatic insulin resistance [6]. Our data do suggest that rapamycin treatment is associated with reduced mTORC2 in high fat-, but not low fat-, fed mice suggesting a plausible mechanism for the increased adiposity in this group of mice. It seems also likely too that the development of insulin resistance in adipose tissue could contribute to the expansion of this

tissue. It is also interesting to note that removal of eRAPA, and presumably the concurrent return of mTORC2 signaling and relative insulin sensitivity, completely reverses this phenotype.

The beneficial effects of rapamycin on lifespan, cancer and other diseases have largely been performed in models utilizing standard dietary conditions, i.e., normal, low fat rodent chow consisting of largely vegetable matter. In general, our results suggest that the physiological and cellular effects of chronic rapamycin are relatively similar even on diets containing differently levels of fat, and in fact may be actually exacerbated in conjunction with high fat diet. While more formal diet studies will be necessary, it seems likely that rapamycin may be effective under a variety of different conditions. In support of this, a recent study showed that the lifespan of C57BL/6 mice can be extended by rapamycin even when mice are fed a high fat diet [37]. However, the gluco-regulatory dysfunction experienced by mice treated with rapamycin while on a high fat diet highlights a potential concern with regard to the therapeutic use of rapamycin in humans, in which the dietary intake is much more varied in both content and composition.

The reversible nature of rapamycin's effects in this study also raises an important question about whether chronic treatment is required to reap the beneficial effects of rapamycin on longevity, cancer, etc.. It has been shown that rapamycin treatment extends longevity in mice to a similar degree whether it is started relatively early or late in life [8, 9]. Similarly, rapamycin impairs glucose metabolism in both young and old mice [17]. While these studies suggest that this compound may work equally well across ages, it is still not clear if short-term rapamycin treatments within a particular window(s) of time may cause persistent effects later in life. There is evidence that some physiological effects of dietary restriction, the most well-studied method to extend lifespan, are retained after this treatment is ended. For example, dietary restricted mice that are subsequently switched to an ad libitum diet retain significantly improved markers of glucose metabolism for months after this dietary modulation [40, 41]. In contrast though, the switch from dietary restricted to ad libitum feeding has also been shown to rapidly increase oxidative damage and alter the transcriptome to that of mice fed ad libitum their entire life [42, 43].

It has been suggested that the negative side effects of rapamycin treatment, including impaired glucose metabolism, will limit the use of rapamycin for the treatment of age-related diseases [44]. To our knowledge, the work presented here is the first to show that the metabolic defects caused by rapamycin are reversible after ending the treatment and suggests the possibility that the side effects of rapamycin could be minimized by short-term treatment with rapamycin. There is evidence that intermittent, rather than chronic, treatment with rapamycin is sufficient to extend lifespan in some mouse models [37, 45, 46]. Moreover, short-term or even single treatments with rapamycin have been shown to delay incidence or reduce prevalence in different mouse models of disease [46-48]. It will be of interest in the future to determine whether similar short-term treatments with rapamycin, or even treatment only at a few given points of life is also sufficient to extend lifespan and reduce disease burden in normally healthy mice without also causing potentially detrimental effects such as metabolic dysfunction.

METHODS

Animals. Male C57BL/6J mice were purchased from Jackson Labs (Bar Harbor ME) at 2 months of age and were randomly assigned to cages in our animal facility at a density of 3 mice/cage. Genetically heterogeneous UT-HET3 mice were generated at UTHSCSA using a cross previously described [8, 9]. Male UT-HET3 mice were used at approximately 10-12 months of age and housed at a density of 3-4 mice/cage. For both groups of mice, cages were randomly assigned to one of four different defined diets based on commercially available formulations. Both low fat (10% kCal from fat, D12450B, Purina/Test Diet, St. Louis MO) and high fat diets (45% kCal from fat, D12451, Purina/Test Diet) were prepared containing either encapsulated (enteric-released) rapamycin (eRAPA) or the eudragit vehicle (control) at concentrations of 14 ppm (mg of drug per kg of diet). eRAPA was provided through the San Antonio Nathan Shock Center of Excellence in the Basic Biology of Aging and details on preparation of eRAPA have previously been described in detail [8, 9]. Diets were provided *ad libitum*, mice were checked daily and food consumption and body weight were monitored bi-weekly. Body composition of non-anesthetized mice was analyzed by Quantitative Magnetic Resonance imaging (QMRi) using an EchoMRI 3-in-1 composition analyzer (Echo Medical Systems, Houston TX). For diet shift experiments, mice fed eRAPA-containing diet were given eudragit-containing control diet of the equivalent dietary fat concentration at the indicated time point.

Glucose metabolism. Glucose and insulin tolerance tests were performed 2 and 4 months (C57BL/6) or 3 months (UT-HET3) after beginning dietary treatment. For glucose tolerance tests, mice were fasted 6 hours

(09:00-15:00) prior to each test and then injected intraperitoneally (IP) with glucose (1.5 g kg^{-1}) in saline. For insulin tolerance tests, mice were fasted 6 hours (09:00-15:00) prior to each test and then injected IP with insulin (1 U kg^{-1}) in saline. Blood glucose levels were measured at indicated time points from tail vein bleeding by hand-held glucometer (LifeScan, Milpitas CA). Area under curve (AUC) was calculated for each animal using the Trapezoid method. For glucose-stimulated insulin secretion, mice were fasted 6 hours (09:00-15:00) prior to each test and then injected intraperitoneally with glucose (1.5 g kg^{-1}) in saline. Whole blood was collected in EDTA-containing tubes from the tail vein prior to and 15 minutes after injection with glucose as previously described [6, 17]. Insulin levels in whole blood and plasma were measured using Crystal Chem ultra-sensitive mouse insulin ELISA (Downer's Grove IL).

Immunoblots. Total protein extracts were isolated from skeletal muscle (gastrocnemius) and visceral adipose (epigonadal) that was collected from mice, snap-frozen in liquid nitrogen, and stored at -80º C until use. Mice were fasted overnight and sacrificed 10 minutes after IP injection of insulin (1 U kg^{-1}). Protein extracts were made in RIPA buffer with added protease and phosphatase inhibitors (Thermo Scientific, Rockford IL), centrifuged at 13,000 g and 4º C for 15 min, then stored at -80ºC until use. Total protein content was measured by the Pierce BCA assay (Bio-Rad, Hercules CA). Proteins were separated by SDS-PAGE and transferred to PVDF membrane for immunoblotting. Phospho-S6, S6, Phospho-Akt (ser473), Akt, mTOR, raptor, rictor, phospho-HSL, HSL and ATGL antibodies were from Cell Signaling (Beverly MA). Actin antibody was from Sigma (St. Louis MO). For immuno-precipitation, muscle samples were lysed in cold 0.3% CHAPS lysis buffer [40 mM Hepes (pH 7.5), 120 mM NaCl, 1 mM EDTA, 0.3% CHAPS, 10 mM pyrophosphate, 10 mM β-glycerophosphate, 50 mM NaF, 0.5 mM orthovanadate, and protease inhibitors], then centrifuged 16,000 rpm for 15 min at 4°C. Protein A agarose beads were added to the supernatant and incubated with rotation for 1 h, centrifuged and mTOR antibodies were added to the cleared lysates. After overnight rotation at 4°C, protein A agarose beads were added incubated at 4°C for an additional hour. Immunoprecipitated complexes were washed in 0.3% CHAPS lysis buffer three times, boiled in SDS-sample buffer, separated by SDS-PAGE, and analyzed by immunoblotting. Protein bands were visualized by ECL and densitometry analyzed using Image J.

Statistical analysis. For glucose tolerance, insulin tolerance, and plasma glucose and insulin measurements, the effect of both diet (low fat vs. high fat) and rapamycin (control vs. eRAPA) were analyzed using two way ANOVA. Longitudinal studies in C57BL/6 mice were analyzed by three way ANOVA to determine effect of diet, rapamycin and time (2 mo. treatment vs. 4 mo. treatment). Glucose stimulated insulin secretion was assessed using three way ANOVA to determine effect of diet, rapamycin and glucose injection. Body weight, fat mass and fat-free mass were analyzed by repeated measures two-way ANOVA. Post-hoc multiple comparison tests were performed using the Holm-Sidak method. Immunoblots were analyzed by t-test comparing the effect of rapamycin within each diet treatment group.

ACKNOWLEDGEMENTS

This work was funded in part through the San Antonio Nathan Shock Center of Excellence in the Basic Biology of Aging funded by the NIA (1P30-AG-13319) and by a National Institutional of Health RC2 Grand Opportunity grant (AG036613). Animal studies were performed in the Healthspan and Functional Assessment Core of the San Antonio Shock Center. A.B.S. is funded in part by the American Federation for Aging Research and the Geriatric Research Education and Clinical Center of the South Texas Veterans Healthcare System. D.W.L is supported in part by a K99/R00 Pathway to Independence Award from the NIH/NIA (AG-041765). A.R. is supported in part by a grant from the Biomedical Laboratory Research & Development Service of the Veteran's Affairs Office of Research and Development (1I01BX000547).

Conflict of interest statement

A.R. (share-holder) and R.S. (uncompensated member of the scientific advisory board) have relationships with Rapamycin Holdings, Inc.

REFERENCES

1. Laplante M and Sabatini David M. mTOR Signaling in Growth Control and Disease. Cell. 2012; 149:274-293.

2. Khamzina L, Veilleux A, Bergeron S and Marette A. Increased Activation of the Mammalian Target of Rapamycin Pathway in Liver and Skeletal Muscle of Obese Rats: Possible Involvement in Obesity-Linked Insulin Resistance. Endocrinology. 2005; 146:1473-1481.

3. Um SH, D'Alessio D and Thomas G. Nutrient overload, insulin resistance, and ribosomal protein S6 kinase 1, S6K1. Cell Metab. 2006; 3:393-402.

4. Um SH, Frigerio F, Watanabe M, Picard F, Joaquin M, Sticker M, Fumagalli S, Allegrini PR, Kozma SC, Auwerx J and Thomas G. Absence of S6K1 protects against age- and diet-induced obesity while enhancing insulin sensitivity. Nature. 2004;431:200-205.

5. Sabatini DM, Erdjument-Bromage H, Lui M, Tempst P and Snyder SH. RAFT1: A mammalian protein that binds to FKBP12 in a rapamycin-dependent fashion and is homologous to yeast TORs. Cell. 1994; 78:35-43.

6. Lamming DW, Ye L, Katajisto P, Goncalves MD, Saitoh M, Stevens DM, Davis JG, Salmon AB, Richardson A, Ahima RS, Guertin DA, Sabatini DM and Baur JA. Rapamycin-Induced Insulin Resistance Is Mediated by mTORC2 Loss and Uncoupled from Longevity. Science. 2012; 335:1638-1643.

7. Sarbassov DD, Ali SM, Sengupta S, Sheen J-H, Hsu PP, Bagley AF, Markhard AL and Sabatini DM. Prolonged Rapamycin Treatment Inhibits mTORC2 Assembly and Akt/PKB. Molecular Cell. 2006; 22:159-168.

8. Harrison DE, Strong R, Sharp ZD, Nelson JF, Astle CM, Flurkey K, Nadon NL, Wilkinson JE, Frenkel K, Carter CS, Pahor M, Javors MA, Fernandez E, et al. Rapamycin fed late in life extends lifespan in genetically heterogeneous mice. Nature. 2009; 460:392-395.

9. Miller RA, Harrison DE, Astle CM, Baur JA, Boyd AR, de Cabo R, Fernandez E, Flurkey K, Javors MA, Nelson JF, Orihuela CJ, Pletcher S, Sharp ZD, et al. Rapamycin, But Not Resveratrol or Simvastatin, Extends Life Span of Genetically Heterogeneous Mice. The Journals of Gerontology Series A: Biological Sciences and Medical Sciences. 2011; 66A:191-201.

10. Fok WC, Chen Y, Bokov A, Zhang Y, Salmon AB, Diaz V, Javors M, Wood WH, 3rd, Zhang Y, Becker KG, Pérez VI and Richardson A. Mice Fed Rapamycin Have an Increase in Lifespan Associated with Major Changes in the Liver Transcriptome. PLoS ONE. 2014; 9:e83988.

11. Zhang Y, Bokov A, Gelfond J, Soto V, Ikeno Y, Hubbard G, Diaz V, Sloane L, Maslin K, Treaster S, Réndon S, van Remmen H, Ward W, et al. Rapamycin Extends Life and Health in C57BL/6 Mice. The Journals of Gerontology Series A: Biological Sciences and Medical Sciences. 2014; 69A:119-130.

12. Wilkinson JE, Burmeister L, Brooks SV, Chan C-C, Friedline S, Harrison DE, Hejtmancik JF, Nadon N, Strong R, Wood LK, Woodward MA and Miller RA. Rapamycin slows aging in mice. Aging Cell. 2012; 11:675-682.

13. Flynn JM, O'Leary MN, Zambataro CA, Academia EC, Presley MP, Garrett BJ, Zykovich A, Mooney SD, Strong R, Rosen CJ, Kapahi P, Nelson MD, Kennedy BK, et al. Late-life rapamycin treatment reverses age-related heart dysfunction. Aging Cell. 2013; 12:851-862.

14. Neff F, Flores-Dominguez D, Ryan DP, Horsch M, Schr, xF, der S, Adler T, Afonso LC, Aguilar-Pimentel JA, Becker L, Garrett L, Hans W, et al. Rapamycin extends murine lifespan but has limited effects on aging. The Journal of Clinical Investigation. 2013; 123:3272-3291.

15. Cunningham JT, Rodgers JT, Arlow DH, Vazquez F, Mootha VK and Puigserver P. mTOR controls mitochondrial oxidative function through a YY1-PGC-1alpha transcriptional complex. Nature. 2007; 450:736-740.

16. Chang G-R, Wu Y-Y, Chiu Y-S, Chen W-Y, Liao J-W, Hsu H-M, Chao T-H, Hung S-W and Mao FC. Long-term Administration of Rapamycin Reduces Adiposity, but Impairs Glucose Tolerance in High-Fat Diet-fed KK/HlJ Mice. Basic & Clinical Pharmacology & Toxicology. 2009; 105:188-198.

17. Lamming DW, Ye L, Astle CM, Baur JA, Sabatini DM and Harrison DE. Young and old genetically heterogeneous HET3 mice on a rapamycin diet are glucose intolerant but insulin sensitive. Aging Cell. 2013; 12:712-718.

18. Fang Y, Westbrook R, Hill C, Boparai Ravneet K, Arum O, Spong A, Wang F, Javors Martin A, Chen J, Sun Liou Y and Bartke A. Duration of Rapamycin Treatment Has Differential Effects on Metabolism in Mice. Cell Metabolism. 2013; 17:456-462.

19. Houde VP, Brûlé S, Festuccia WT, Blanchard P-G, Bellmann K, Deshaies Y and Marette A. Chronic Rapamycin Treatment Causes Glucose Intolerance and Hyperlipidemia by Upregulating Hepatic Gluconeogenesis and Impairing Lipid Deposition in Adipose Tissue. Diabetes. 2010; 59:1338-1348.

20. Deblon N, Bourgoin L, Veyrat-Durebex C, Peyrou M, Vinciguerra M, Caillon A, Maeder C, Fournier M, Montet X, Rohner-Jeanrenaud F and Foti M. Chronic mTOR inhibition by rapamycin induces muscle insulin resistance despite weight loss in rats. British Journal of Pharmacology. 2012; 165:2325-2340.

21. Teutonico A, Schena PF and Di Paolo S. Glucose Metabolism in Renal Transplant Recipients: Effect of Calcineurin Inhibitor Withdrawal and Conversion to Sirolimus. Journal of the American Society of Nephrology. 2005; 16:3128-3135.

22. Johnston O, Rose CL, Webster AC and Gill JS. Sirolimus Is Associated with New-Onset Diabetes in Kidney Transplant Recipients. Journal of the American Society of Nephrology. 2008; 19:1411-1418.

23. Miller RA, Harrison DE, Astle CM, Fernandez E, Flurkey K, Han M, Javors MA, Li X, Nadon NL, Nelson JF, Pletcher S, Salmon AB, Sharp ZD, et al. Rapamycin-mediated lifespan increase in mice is dose and sex dependent and metabolically distinct from dietary restriction. Aging Cell. 2014; 13:468-477.

24. Fok WC, Zhang Y, Salmon AB, Bhattacharya A, Gunda R, Jones D, Ward W, Fisher K, Richardson A and Pérez VI. Short-Term Treatment With Rapamycin and Dietary Restriction Have Overlapping and Distinctive Effects in Young Mice. The Journals of Gerontology Series A: Biological Sciences and Medical Sciences. 2013; 68:108-116.

25. Chang G-R, Chiu Y-S, Wu Y-Y, Chen W-Y, Liao J-W, Chao T-H and Mao FC. Rapamycin Protects Against High Fat Diet-Induced Obesity in C57BL/6J Mice. Journal of Pharmacological Sciences. 2009; 109:496-503.

26. Pereira MJ, Palming J, Rizell M, Aureliano M, Carvalho E, Svensson MK and Eriksson JW. The immunosuppressive agents rapamycin, cyclosporin A and tacrolimus increase lipolysis, inhibit lipid storage and alter expression of genes involved in lipid metabolism in human adipose tissue. Molecular and Cellular Endocrinology. 2013; 365:260-269.

27. Soliman G, Acosta-Jaquez H and Fingar D. mTORC1 Inhibition via Rapamycin Promotes Triacylglycerol Lipolysis and Release of Free Fatty Acids in 3T3-L1 Adipocytes. Lipids. 2010; 45:1089-1100.

28. Chakrabarti P, English T, Shi J, Smas CM and Kandror KV. Mammalian target of rapamycin complex 1 suppresses lipolysis, stimulates lipogenesis, and promotes fat storage. Diabetes. 2010; 59:775-781.

29. Festuccia WT, Blanchard P-G, Belchior T, Chimin P, Paschoal VA, Magdalon J, Hirabara SM, Simões D, St-Pierre P, Carpinelli AR, Marette A and Deshaies Y. PPARγ activation attenuates glucose intolerance induced by mTOR inhibition with rapamycin in rats. 2014; 306:E1046-1054.

30. Ye L, Varamini B, Lamming DW, Sabatini DM and Baur JA. Rapamycin has a biphasic effect on insulin sensitivity in C2C12 myotubes due to sequential disruption of mTORC1 and mTORC2. Frontiers in genetics. 2012; 3:177.

31. Yang S-B, Lee H, Young D, Tien A-C, Rowson-Baldwin A, Shu Y, Jan Y and Jan L. Rapamycin induces glucose intolerance in mice by reducing islet mass, insulin content, and insulin sensitivity. J Mol Med. 2012; 90:575-585.

32. Fraenkel M, Ketzinel-Gilad M, Ariav Y, Pappo O, Karaca M, Castel J, Berthault MF, Magnan C, Cerasi E, Kaiser N and Leibowitz G. mTOR inhibition by rapamycin prevents beta-cell adaptation to hyperglycemia and exacerbates the metabolic state in type 2 diabetes. Diabetes. 2008; 57:945-957.

33. Cota D, Proulx K, Smith KA, Kozma SC, Thomas G, Woods SC and Seeley RJ. Hypothalamic mTOR signaling regulates food intake. Science. 2006; 312:927-930.

34. Bell A, Grunder L and Sorisky A. Rapamycin Inhibits Human Adipocyte Differentiation in Primary Culture. Obesity Research. 2000; 8:249-254.

35. Polak P, Cybulski N, Feige JN, Auwerx J, Rüegg MA and Hall MN. Adipose-Specific Knockout of raptor Results in Lean Mice with Enhanced Mitochondrial Respiration. Cell metabolism. 2008; 8:399-410.

36. Leontieva OV, Paszkiewicz G, Demidenko ZN and Blagosklonny MV. Resveratrol potentiates rapamycin to prevent hyperinsulinemia and obesity in male mice on high fat diet. Cell death & disease. 2013; 4:e472.

37. Leontieva OV, Paszkiewicz GM and Blagosklonny MV. Weekly administration of rapamycin improves survival and biomarkers in obese male mice on high-fat diet. Aging Cell. 2014; 13:616-622.

38. Cybulski N, Polak P, Auwerx J, Rüegg MA and Hall MN. mTOR complex 2 in adipose tissue negatively controls whole-body growth. Proceedings of the National Academy of Sciences. 2009; 106:9902-9907.

39. Kumar A, Lawrence JC, Jung DY, Ko HJ, Keller SR, Kim JK, Magnuson MA and Harris TE. Fat Cell–Specific Ablation of Rictor in Mice Impairs Insulin-Regulated Fat Cell and Whole-Body Glucose and Lipid Metabolism. Diabetes. 2010; 59:1397-1406.

40. Cameron K, Miwa S, Walker C and von Zglinicki T. Male mice retain a metabolic memory of improved glucose tolerance induced during adult onset, short-term dietary restriction. Longevity & Healthspan. 2012; 1:3.

41. Selman C and Hempenstall S. Evidence of a metabolic memory to early-life dietary restriction in male C57BL/6 mice. Longevity & Healthspan. 2012; 1:2.

42. Dhahbi JM, Kim H-J, Mote PL, Beaver RJ and Spindler SR. Temporal linkage between the phenotypic and genomic responses to caloric restriction. Proceedings of the National Academy of Sciences of the United States of America. 2004; 101:5524-5529.

43. Forster MJ, Sohal BH and Sohal RS. Reversible Effects of Long-Term Caloric Restriction on Protein Oxidative Damage. The Journals of Gerontology Series A: Biological Sciences and Medical Sciences. 2000; 55:B522-B529.

44. Lamming DW, Ye L, Sabatini DM and Baur JA. Rapalogs and mTOR inhibitors as anti-aging therapeutics. J Clin Invest. 2013; 123:980-989.

45. Chen C, Liu Y, Liu Y and Zheng P. mTOR Regulation and Therapeutic Rejuvenation of Aging Hematopoietic Stem Cells. Sci Signal. 2009; 2:ra75.

46. Anisimov VN, Zabezhinski MA, Popovich IG, Piskunova TS, Semenchenko AV, Tyndyk ML, Yurova MN, Antoch MP and Blagosklonny MV. Rapamycin extends maximal lifespan in cancer-prone mice. The American journal of pathology. 2010; 176:2092-2097.

47. Johnson SC, Yanos ME, Kayser EB, Quintana A, Sangesland M, Castanza A, Uhde L, Hui J, Wall VZ, Gagnidze A, Oh K, Wasko BM, Ramos FJ, et al. mTOR inhibition alleviates mitochondrial disease in a mouse model of Leigh syndrome. Science. 2013; 342:1524-1528.

48. Comas M, Toshkov I, Kuropatwinski KK, Chernova OB, Polinsky A, Blagosklonny MV, Gudkov AV and Antoch MP. New nanoformulation of rapamycin Rapatar extends lifespan in homozygous p53-/- mice by delaying carcinogenesis. Aging. 2012; 4:715-722.

Research Paper

Centenarians as super-controls to assess the biological relevance of genetic risk factors for common age-related diseases: A proof of principle on type 2 diabetes

Paolo Garagnani[1,2,3 *], Cristina Giuliani[4 *], Chiara Pirazzini[1,2], Fabiola Olivieri[5,6], Maria Giulia Bacalini[1,2], Rita Ostan[1,2], Daniela Mari[7], Giuseppe Passarino[8], Daniela Monti[9], Anna Rita Bonfigli[10], Massimo Boemi[10], Antonio Ceriello[11,12], Stefano Genovese[13], Federica Sevini[1,2], Donata Luiselli[4], Paolo Tieri[14], Miriam Capri[1,2], Stefano Salvioli[1,2], Jan Vijg[15,17], Yousin Suh[15,16,17,18], Massimo Delledonne[19,20], Roberto Testa[21], and Claudio Franceschi[1]

[1] DIMES - Department of Experimental, Diagnostic and Specialty Medicine, University of Bologna, Bologna, 40126 Italy
[2] C.I.G. Interdepartmental Center "L. Galvani", University of Bologna, Bologna, Italy
[3] CRBA - Applied Biomedical Research Center, S. Orsola-Malpighi Polyclinic, Bologna, 40138 Italy
[4] Department of Biological, Geological and Environmental Sciences, Laboratory of Molecular Anthropology & Centre for Genome Biology, University of Bologna, Bologna 40126, Italy
[5] Department of Clinical and Molecular Sciences, Università Politecnica delle Marche, Ancona, Italy
[6] Center of Clinical Pathology and Innovative Therapy, Italian National Research Center on Aging INRCA-IRCCS, Ancona, Italy
[7] Geriatric Unit IRCCS Ca' Granda Foundation Maggiore Policlinico Hospital and Department of Clinical Sciences and Community Health, University of Milano, Italy
[8] Department of Cell Biology, University of Calabria, Rende, Italy
[9] Department of Experimental and Clinical Biomedical Sciences, University of Florence, Florence, Italy
[10] Metabolic Diseases and Diabetology Unit, IRCCS-INRCA, Ancona, Italy
[11] Institut d'Investigacions Biomèdiques August Pi i Sunyer (IDIBAPS), Barcelona, Spain
[12] Centro de Investigación Biomédica en Red de Diabetes y Enfermedades Metabólicas Asociadas (CIBERDEM), Barcelona, Spain
[13] Department of Cardiovascular and Metabolic Diseases, IRCCS Gruppo Multimedica Sesto San Giovanni (MI), Italy
[14] IAC-CNR Istituto per le Applicazioni del Calcolo, Consiglio Nazionale delle Ricerche, Rome, Italy
[15] Department of Genetics, Albert Einstein College of Medicine, Bronx, NY 10461, USA
[16] Department of Medicine, Albert Einstein College of Medicine, Bronx, NY 10461, USA
[17] Institute for Aging Research, Diabetes Research and Training Center, Albert Einstein College of Medicine, Bronx, NY 10461, USA
[18] Institute of Aging Research, Guangdong Medical College, Dongguan 523808, China
[19] Personal Genomics SRL, Strada le Grazie 15, 37133 Verona – Italy
[20] Functional Genomics Center, Dept. of Biotechnologies, University of Verona, Strada le Grazie 15, 37133 Verona - Italy
[21] Experimental Models in Clinical Pathology, IRCCS-INRCA, Ancona, Italy
** equally contributed*

Key words: *Type 2 diabetes, TCF7L2, centenarians, extreme phenotypes, age-related diseases*
Received: *5/17/13; Accepted: 5/31/13; Published: 5/31/13*
Correspondence to: *Paolo Garagnani, PhD;* ***E-mail:*** *paolo.garagnani2@unibo.it* doi:10.18632/aging.100562

Abstract: Genetic association studies of age-related, chronic human diseases often suffer from a lack of power to detect modest effects. Here we propose an alternative approach of including healthy centenarians as a more homogeneous and extreme control group. As a proof of principle we focused on type 2 diabetes (T2D) and assessed allelic/genotypic associations of 31 SNPs associated with T2D, diabetes complications and metabolic diseases and SNPs of genes relevant for telomere stability and age-related diseases. We hypothesized that the frequencies of risk variants are inversely correlated with decreasing health and longevity. We performed association analyses comparing diabetic patients and non-diabetic controls followed by association analyses with extreme phenotypic groups (T2D patients with complications and centenarians). Results drew attention to rs7903146 (TCF7L2 gene) that showed a constant increase in the frequencies of risk genotype (TT) from centenarians to diabetic patients who developed macro-complications and the strongest genotypic association was detected when diabetic patients were compared to centenarians (p_value = $9.066*10^{-7}$). We conclude that robust and biologically relevant associations can be obtained when extreme phenotypes, even with a small sample size, are compared.

INTRODUCTION

In the last ten years the scientific community has devoted a consistent effort to identify the genetic basis of the most common age-related diseases, as they represent one of the most important public health and socio-economical burden all over the world and particularly in Western Countries. This challenge was mainly faced up by genome wide association studies (GWASs) based on microarray technology that allows the simultaneous analyses of hundred thousands of single nucleotide polymorphisms (SNPs), within the framework of the "common variant common disease" theory [1]. So far, more than 1,000 published GWASs reported significant associations of ~4,000 SNPs for more than 200 traits/diseases [2]. GWASs of age-related, chronic human diseases often suffer from a lack of power to detect modest effects, which can to some extent explain why the identified genetic effects comprise only a small fraction of the estimated trait heritability. These limitations can be overcome simply by ever increasing sample size in order to achieve the necessary statistical power to detect variants with small effects, which is not always feasible. Moreover, in most cases the biological role/relevance of the genetic variants emerged from GWASs is still unclear. In past, several strategies were proposed to increase detection power without affecting the cohort size, such as the use of genetically isolated populations characterized by a reduced genetic diversity that facilitate the discovery of relevant loci for complex diseases [3,4]. To date this approach has not been successful to boost the discovery of relevant associations with complex traits [5]. Thus, there is an urgent need for an effective strategy to obtain biological insights from the genetic knowledge derived from GWASs that can be translated into clinical benefits.

The aim of this study was to test the hypothesis that GWASs sensitivity can be boosted by including extreme phenotypic groups. As a proof of principle study, we considered one of the major age-related diseases, *i.e.* type 2 diabetes (T2D). We applied a candidate gene approach to assess associations of a limited set of SNPs (31) in or nearby genes relevant for T2D, diabetes complications, metabolic diseases, telomere stability and age-related diseases. The extreme phenotypic groups we focused on are as follows: i) *CENTENARIANS* who reached the extreme limit of human life, escaping or largely postponing the major age-related diseases, including T2D, and who can be considered a paradigm of healthy aging [6]. In particular, a major characteristic of centenarians is their extraordinarily well preserved glucose metabolism. Aging is frequently associated with impaired glucose metabolism related to a raise in insulin resistance (IR), not fully compensated by a sufficient β-cell function. Such age-related metabolic changes are key risk factors for T2D and are associated with a variety of intermediate phenotypes (hypertension, atherosclerosis, obesity) strongly affecting morbidity, disability and mortality among elderly. In a pioneering study, Paolisso et al. [7], using an oral glucose tolerance test and euglycemic glucose clamp, showed that centenarians had a 2-h plasma glucose concentration that was lower than that of aged subjects but not different from adults, and an insulin-mediated glucose uptake higher than that reported for aged subjects but not different from that found in adults. In a subsequent study, involving a large cohort of individuals (age range: 28-111 years) carefully selected for health status, we showed that the age-related trajectories of IR and β-cell function increase with age (the increase of β-cell function is necessary to compensate for the raise in IR). However, beyond 85–90 years of age, people with a lower degree

of IR and with a lower β-cell function emerge, indicating that in very old people lower IR does not require a compensatory increment in β-cell function, thus allowing to preserve endocrine pancreas secretion and to prevent the development of T2D [8]. On the whole, these results point towards IR and β-cell function as phenotypes under strong selective forces during aging, supporting the hypothesis that effective peripheral glucose disposal is pivotal in determining longevity. These observations are confirmed by studies from our and other groups showing that centenarians offspring and nonagenarian siblings have a better health status than subjects of the same cohort, without the parental extreme longevity [9], and a reduced risk of diabetes and an enhanced insulin sensitivity [10–14]. ii) *PATIENTS WITH T2D PLUS ONE OR MORE COMPLICATIONS*. The T2D patients included in the present study have been fully characterized from a phenotypical (clinical, biochemical, pharmacological, among others) point of view, and have been extensively studied regarding a variety of genetic [15–18] and non-genetic factors. In particular, we showed that T2D patients undergo accelerated aging [19] and that *IL-10* polymorphisms [20], telomere length in peripheral blood cells [21] and mitochondrial DNA variants [22] are able to distinguish between patients with and without complications. Thus, the presence of one or more micro- and macro-vascular complications not only represents the most severe and extreme phenotype of T2D, of relevance from a clinical and therapeutic point of view, but also has a biological counterpart which is still largely unknown. In this study, T2D patients have been compared with age-, gender- and geography-matched control group.

Here we considered a limited set of SNPs belonging to four classes of genetic variants: i) SNPs previously found associated with T2D by GWASs; ii) variants of genes involved in vascular pathology potentially involved in the development of T2D complications; iii) SNPs previously associated with metabolic diseases, including T2D; and iv) SNPs of genes relevant for telomere stability and involved in age-related diseases, including T2D complications.

RESULTS

In this study we analyzed the following cohorts described in depth in Methods: the whole cohort of diabetic patients (D), diabetic patients with complications (D+Co), diabetic patients who developed micro-vascular complications (D+microCo), diabetic patients who developed macro-vascular complications (D+macroCo), non diabetic controls matched for age, gender and geographical origin with diabetic patients (CTR) and centenarians (100+). These samples were tested for 31 SNPs, 22 of which passed the quality check. Results from association analyses are reported in Supplemental Materials (S1, S2, S3, S4). The most significant results involve *TCF7L2* and *ADIPOQ* gene variants, which are reported in Table 1 and summarized in Figure 1. The comparisons that have been performed to test the effectiveness of our approach are reported in the following five sections.

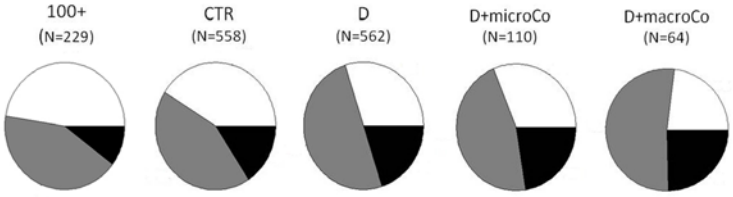

rs 7903146 – TCF7L2					
	Genotypes frequencies (%)				
CC	47.5	41.1	30.0	29	23.4
TC	42.1	43.0	50.0	50	53.1
TT	10.4	15.8	20.0	21	23.4
	Allele frequencies (%)				
C	31.7	62.6	55	54.3	51.8
T	68.3	37.4	45	45.7	48.2

Figure 1. *TCF7L2* rs7903146 genotypic and allelic frequencies among the different groups analyzed. *TCF7L2* rs7903146 genotypic and allelic frequencies were reported according to the decreasing of health/longevity and the increasing of T2D severity (from left to right).

Table 1. Allelic and genotypic association analyses. Samples considered were diabetic patients (N=562), non diabetic controls (N=558), diabetic individuals with complications (N=241), centenarians (N=229), diabetic patients with macro-vascular complications (N=64) and diabetic patients with micro-vascular complications (N=110).

	Cohorts	Gene	SNP (ID)	Allele/ Genotype	Frequency (%)		p_value	OR (95% CI)	Model
					1	2			
Allelic Association	D (1) vs 100+ (2)	*ADIPOQ*	rs266729	G	24.6	31.6	$5.89*10^{-3}$	0.71 (0.55-0.91)	/
	D (1) vs CTR (2)	*TCF7L2*	rs7903146	T	45	37	$3.1*10^{-4}$	1.37 (1.16-1.63)	/
	D+Co (1) vs CTR (2)	*TCF7L2*	rs7903146	T	46.1	37	$1.66*10^{-3}$	1.43 (1.14-1.79)	/
	D (1) vs 100+ (2)	*TCF7L2*	rs7903146	T	44.8	31.4	$1.34*10^{-6}$	1.77 (1.40-2.24)	/
	D+Co (1) vs 100+ (2)	TCF7L2	rs7903146	T	45	31.4	$1.06*10^{-6}$	1.78 (1.41-2.25)	/
	D+macroCo (1) vs 100+ (2)	TCF7L2	rs7903146	T	50	31.4	$1.13*10^{-4}$	2.177 (1.46-3.24)	/
	D+microCo (1) vs 100+ (2)	*TCF7L2*	rs7903146	T	46	31.4	$2.64*10^{-4}$	1.85 (1.33-2.57)	/
Genotypic association	D (1) vs 100+ (2)	*ADIPOQ*	rs266729	G/C	36.6	50.7	$4.19*10^{-4}$	0.56 (0.41-0.77)	Over dominant
	D (1) vs CTR (2)	*TCF7L2*	rs7903146	TC/TT	58.9	70.0	$1.41*10^{-4}$	1.63 (1.26-2.09)	Dominant
	D+Co (1) vs CTR (2)	*TCF7L2*	rs7903146	TC/TT	58.8	71.9	$5.96*10^{-4}$	1.79 (1.28-2.52)	Dominant
	D (1) vs 100+ (2)	*TCF7L2*	rs7903146	CC TC TT	30 50 20	47.5 42.1 10.4	$9.07*10^{-7}$	1.78 (1.41-2.26)	Log-additive
	D+Co (1) vs 100+ (2)	*TCF7L2*	rs7903146	CC TC TT	28.1 51.1 20.8	47.5 42.1 10.4	$5.47*10^{-6}$	1.89 (1.43-2.50)	Log-additive
	D+macroCo (1) vs 100+ (2)	*TCF7L2*	rs7903146	CC TC TT	23.4 53.1 23.4	47.5 42.1 10.4	$1.54*10^{-4}$	2.18 (1.45 -3.29)	Log-additive
	D+microCo (1) vs 100+ (2)	*TCF7L2*	rs7903146	CC TC TT	29.1 50.0 20.9	47.5 42.1 10.4	$3.30*10^{-4}$	1.84 (1.31 -2.58)	Log-additive

All diabetic patients (D) *vs* non diabetic controls (CTR) (classical approach of genetic association studies)

Allelic and genotypic association analyses were performed on all diabetic patients *vs* the classical control group. Only *TCF7L2* rs7903146 T-allele was associated with T2D with an odds ratio (OR) of 1.372 per risk allele (95% CI 1.155-1.629) (Table 1). Genotypic association of the *TCF7L2* rs7903146 was significantly detected (p_value = $1.415*10^{-4}$, OR = 1.63 (95% CI 1.26-2.09)) under a dominant model (Table 1).

All diabetic patients (D) *vs* centenarians (100+)

Allelic and genotypic association analyses were performed on all diabetic patients *vs* centenarians. Two nominal significant differences in the allelic frequencies of diabetic patients and centenarians were observed in the *ADIPOQ* rs266729 (OR = 0.706 (95% CI 0.551 - 0.905), p_value = $5.89*10^{-3}$) and in *TCF7L2* rs7903146. In this comparison the *TCF7L2* rs7903146 was highly associated with T2D with an OR = 1.775 per risk allele (95% CI 1.404-2.243, p_value = $1.35*10^{-6}$) (Table 1). *TCF7L2* association was supported by genotypic association analysis. Indeed, significant differences in genotypic frequencies for rs7903146 were reported (OR = 1.78 (95% CI 1.41-2.26), p_value = $9.066*10^{-7}$) (Table 1). Genotypic association was found also for rs266729 in *ADIPOQ* gene (p_value = $4.19*10^{-4}$).

Diabetic patients with complications (D+Co) *vs* non diabetic controls (CTR)

Allelic and genotypic association analyses were performed on diabetic patients with at least one complication *vs* non diabetic controls. Only *TCF7L2* rs7903146 showed an allelic association with T2D susceptibility with an OR = 1.434 (95% CI 1.145-1.795, p_value = $1.66*10^{-3}$). No allelic associations were detected for the other SNPs genotyped (Supplementary Table 2). Genotypic association was observed for the same SNP with an OR = 1.79 (95% CI 1.28-2.52, p_value = $5.96*10^{-4}$) (Table 1).

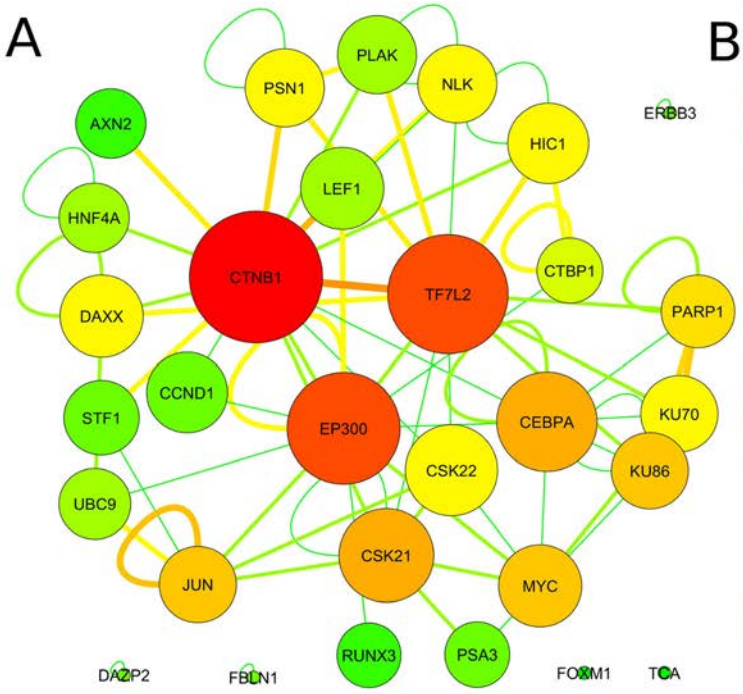

B

ID	Description	Betweenness Centrality
CTNB1	Catenin beta-1	0,40266851
EP300	Histone acetyltransferase p300	0,24471762
TF7L2	Transcription factor 7-like 2	0,22068380
CSK21	Casein kinase II subunit alpha	0,06825972
MYC	Myc proto-oncogene protein	0,06162008
CEBPA	CCAAT/enhancer-binding protein alpha	0,05398838
JUN	Transcription factor AP-1	0,02933057
HIC1	Hypermethylated in cancer 1 protein	0,02041063
CSK22	Casein kinase II subunit alpha'	0,02025247
DAXX	Death domain-associated protein 6	0,01678744
UBC9	SUMO-conjugating enzyme UBC9	0,00712560
KU86	ATP-dependent DNA helicase 2 subunit 2	0,00545491
KU70	ATP-dependent DNA helicase 2 subunit 1	0,00545491
LEF1	Lymphoid enhancer-binding factor 1	0,00467995
STF1	Steroidogenic factor 1	0,00465839
CTBP1	C-terminal-binding protein 1	0,00395531
NLK	Serine/threonine kinase NLK	0,00314010
PARP1	Poly [ADP-ribose] polymerase 1	0,00072464
AXN2	Axin-2	0,00000000
CCND1	G1/S-specific cyclin-D1	0,00000000
DAZP2	DAZ-associated protein 2	0,00000000
ERBB3	Receptor tyrosine-protein kinase erbB-3	0,00000000
FBLN1	Fibulin-1	0,00000000
FOXM1	Forkhead box protein M1	0,00000000
HNF4A	Hepatocyte nuclear factor 4-alpha	0,00000000
PLAK	Junction plakoglobin	0,00000000
PSN1	Presenilin-1	0,00000000
PSA3	Proteasome subunit alpha type-3	0,00000000
RUNX3	Runt-related transcription factor 3	0,00000000
TCA	T-cell receptor alpha chain C region	0,00000000

Figure 2. Tcf7l2 interactome. Graph of the Tcf7l2 interactome (**A**) and list of its elements (**B**). The most central elements in terms of betweenness centrality and node degree [85,89] are *Ctnb1*, *Tfc7l2* (as expected) and *Ep300.* Non-connected nodes: *TCF7L2* gene-listed gene interactions only, and no PPIs, are reported. (**A**) Node color code: from red to green, from highest to lowest values of betweeness centrality; interaction link color code: from red to green, from higher to lower number of experimental evidences. (**B**) Direct physical interactors are in blue, other types of interaction, such as colocalization and physical association are in black.

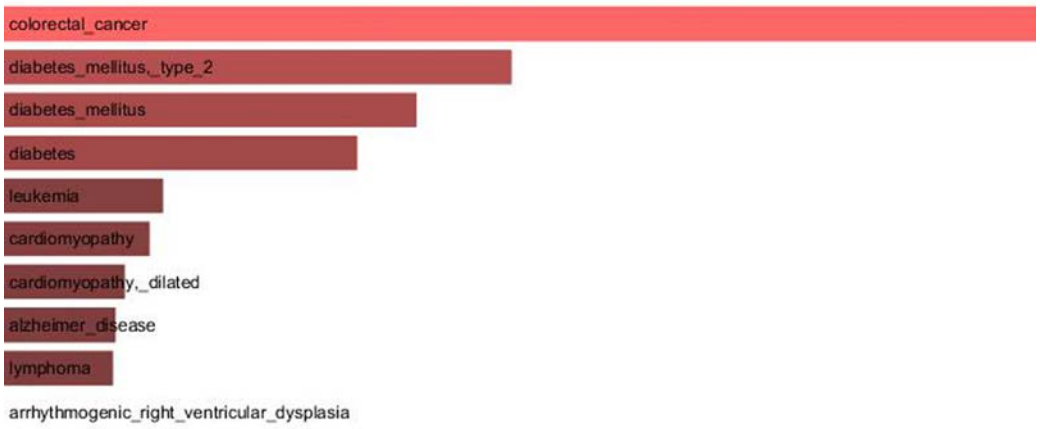

Figure 3. Major OMIM diseases linked to the Tcf7l2 interactome. OMIM enrichment analysis of the Tcf7l2 interactome was performed using the Enrichr web service (http://amp.pharm.mssm.edu/Enrichr/) and the first ten OMIM diseases significantly linked to the interactome ("Enrichr combined score") are reported.

D+Co *vs* 100+, D+macroCo *vs* 100+, and D+microCo *vs* 100+ (comparison between extreme phenotypes)

Genotypic association analyses were performed on diabetic patients with at least one complication *vs* centenarians as a non-diabetes control group. When we compared D+Co *vs* 100+, D+macroCo *vs* 100+ and D+microCo *vs* 100+, the *TCF7L2* rs7903146 resulted associated with T2D complicated patients with an OR = 1.89 (95% CI 1.43-2.50, p_value = $5.473*10^{-6}$), 2.18 (95% CI 1.45 -3.29, p value = $1.538*10^{-4}$) and 1.84 (95% CI 1.31 - 2.58, p_value = $2.68*10^{-4}$), respectively (Table 1). In Figure 1 allele and genotype frequencies for rs7903146 were reported for each group considered.

TCF7L2 interactome analysis

Since our results confirmed a core role of *TCF7L2* in T2D pathogenesis, consistent with its implicated role in T2D [23,24], an interactome analysis was performed. Tcf7l2 is a 619 AA-long transcription factor that participates in the Wnt signaling pathway and modulates *MYC* expression by binding to its promoter in a sequence-specific manner. The most central elements of the Tcf7l2 interactome are Ctbn1 (ranking 1st) and Ep300, and, on a second order of importance, Csk21, Myc and Cebpa (Figure 2A). Among the whole Tcf7l2 interactome (including co-localization and physical association) with 30 elements (Figure 2), there is evidence of direct physical interactions (experimentally validated protein-protein interaction) of Tcf7l2 (Figure 2B, red line) with 12 other proteins (Figure 2B, blue lines). Listing OMIM enrichment analysis of the Tcf7l2 interactome was performed and the first ten OMIM diseases significantly connected to the interactome are reported in Figure 3.

DISCUSSION

In the last few years GWASs provided a great amount of data regarding genetic risk factors for major age-related diseases. Most variants identified so far confer relatively small increments in risk, and explain only a small proportion of the estimated trait heritability. Increasing sample size has been suggested as an answer to the missing heritability to increase sensitivity to detect variants with smaller effects. As an alternative for dramatically increasing cohort size, we tested a strategy that involves extreme phenotypes replicating a limited set of SNPs emerged and validated in GWASs. Individuals that are at the extreme ends of a trait distribution have been proposed for identifying variants that are rare but not private and that have modest to high effect sizes.

We hypothesized that the frequencies of GWASs risk variants are inversely correlated with increasing health and longevity, and extreme phenotypic differences between cases and controls would allow detection of the genetic variants with the most relevant biological and clinical value at relatively small sample size. For an extreme-trait approach, accurate phenotyping will be of vital importance. Central to our approach is the "control" group. The proper "normal" controls, especially in relation to common age-related diseases, are difficult to define, especially when large numbers of

"healthy" subjects are collected from different regions, characterized by peculiar lifestyle habits, population genetics, among others. To circumvent these difficulties, we propose to use centenarians as an additional, more informative and defined control group for studies on the genetic determinants of age-related diseases, and particularly to establish the biological and clinical relevance of the genetic variants emerged in GWASs. Indeed, this group can be considered as a "super-control", as most centenarians achieved their remarkable age avoiding or largely postponing major age-related diseases, and thus, at variance with much younger controls, we can be sure that they never developed such diseases. We reasoned that if a given genetic variant emerged from GWASs and considered a statistically significant but "weak" risk factor for the disease of interest, is present at similar frequency in centenarians and in patients, its biological relevance is reasonably negligible. On the contrary, if a given genetic variant considered a risk factor for an age-associated disease has a frequency much higher in patients than in centenarians, we can reasonably argue that this variant is a strong candidate to play a consistent biological role in the pathogenesis of the disease. We also assumed that centenarians, as the best model of healthy aging in humans [6], are a control group less blurred and undefined than the usually employed "age-matched controls". Moreover, in order to properly take into account the above-mentioned largely neglected clinical heterogeneity/severity of age-related diseases in studies on their genetic determinants, we focused on T2D and more specifically on two main groups of patients, *i.e*. those who did not develop complications and can enjoy a relatively long and acceptable quality of life, and those who developed one or more (micro– and macro-vascular) complications with a poorer quality of life. Accordingly, this approach allowed us to compare *extreme phenotypes, i.e.* centenarians on one side and T2D patients with severe complications on the other, thus maximizing possible genetic differences among patients and controls.

Using this methodological approach on a total of 1,349 individuals we tested 31 SNPs in or nearby 16 different genes that were previously strongly associated with T2D and metabolic diseases and that could be considered good candidate to play a role in T2D complications, on the basis of other large genetic studies.

Our results indicate that most of the SNPs analyzed were not significantly associated with T2D, even when extreme groups of cases and controls were used. This somewhat unexpected result could be due to a lack of biological relevance in spite of their previously strong association signal in GWASs. Indeed, a major drawback of GWASs is the observation of many significant association signals from loci of weak effect. Therefore, we have to consider the possibility that such SNPs, despite having reached statistical significance in large GWASs, could have a weak biological relevance. Indeed, the presence of risk alleles at the same frequency in T2D patients with or without complications and in centenarians suggests that *per se* they do not represent a strong biological risk, being compatible with exceptional longevity, and that they likely necessitate to interact (epistatic effects) with (many) other risk alleles and/or specific environmental conditions to give a certain phenotype. Further studies, possibly in more than one population, are needed to test this possibility.

The two SNPs that reached statistical significance in our study were *ADIPOQ* rs266729 and *TCF7L2* rs7903146, the last one being the strongest. *ADIPOQ* encodes for adiponectin, the most abundant adipokine in human plasma. Low adiponectin levels are associated to IR and T2D [26–28] and the chromosome locus 3q27, where *ADIPOQ* is located, is linked to metabolic syndrome and T2D [29]. Several studies have investigated the association between *ADIPOQ* polymorphisms and T2D, but their results are controversial, probably due to differences in the size and in the composition of the analyzed cohorts [30] . To this regard it is interesting to note that the statistical significance of *ADIPOQ* rs266729, a polymorphism associated to decreased adiponectin levels, emerged only when T2D patients were compared with centenarians. Regarding *TCF7L2* rs7903146, localized in an intronic region of the gene, the most interesting findings were that the risk allele T and the genotype TT showed an increasing statistical significance, from modest genotypic association with the disease when all T2D patients (D) were compared with the age-matched controls (CTR) (OR=1.63; 95% CI 1.26-2.09) to intermediate values (OR=1.79; 95% CI 1.28-2.52) when T2D patients with complications (D+Co) were compared with CTR. These OR values perfectly overlap OR previously described in literature [31] in GWASs that analyzed thousands of samples. Finally, the OR and p_values showed the most significant results when centenarians were compared with T2D patients, and a further increase in OR was observed when centenarians and patients with complications, the extreme phenotypes, were compared (D *vs* 100+*:* OR=1.78 (95% CI 1.41-2.26), p_value=$9.066*10^{-7}$; D+Co *vs* 100+*:* OR=1.89 (95% CI 1.43-2.50), p_value=$5.473*10^{-6}$). It is important to note that the reverse is true for the C allele and the CC genotype. Notably, centenarians show not only the lowest frequency of T allele and TT genotype, but also

the highest frequency of C allele and CC genotype, which emerges as a robust protective longevity variant. These data also suggest that *TCF7L2* rs7903146 is a robust genetic risk variant and indicate that further analyses based on the use of centenarians as super-controls, possibly at genome wide level, are worthwhile to pursue in T2D study, and likely in other age-related diseases. TT genotype frequency was found to be higher not only in diabetic patients but also in patients with macro-vascular complications (Figure 1), reaching a frequency of 23.4%. These results demonstrate an important role of rs7903146 not only in T2D susceptibility but also in susceptibility to develop macro-vascular complications. Different studies investigated the relationship between macro-vascular complications, cardiovascular diseases and diabetes but the molecular mechanisms are still unknown [32–35]. The *TCF7L2* polymorphism rs7903146 was one of the first to be related to diabetes [36] and subsequently its association has been confirmed in several studies, placing it among the most reproducible markers of T2D [37–40]. Recent studies have shown that this SNP leads to conformational changes in chromatin structure according to the allele type. In particular the risk allele (T) induces an open conformation of the chromatin, resulting in an increased transcriptional activity and *TCF7L2* mRNA levels [39,41,42]. It has been demonstrated that the increase of expression of *TCF7L2* leads to a progressive reduction of glucose tolerance *in vivo* [43] .

In order to gain information about the biological relevance of *TCF7L2* gene, we performed an interactome analysis, which identified a complex network of interactions with Ctnb1 and Ep300 as the central elements. Ctnb1 is a Beta-catenin (adherens junction protein), critical for the establishment and maintenance of epithelial layers, and a key downstream component of the canonical Wnt signaling pathway. Ep300 is a histone acetyltransferase and regulates transcription via chromatin remodeling. Chromatin remodeling and epigenetic mechanisms seem to play a fundamental role in susceptibility to diabetes and related complications [44–47] even if mechanisms are not completely understood and further studies should be designed to clarify them. The *in silico* analysis suggests that Tcf7l2 interactome is involved in a variety of age-related pathologies, such as Alzheimer's disease, cardiovascular diseases and colorectal cancer [48–52], all sharing vascular alterations, as a further support to the biological relevance of this gene and to the emerging idea that the same gene can play a major role in apparently different diseases [53].

On the whole, our data on *TCF7L2* rs7903146 indicate that the frequency of T2D risk genotypes decreases according to the severity of the disease phenotype, supporting the assumption that centenarians represent a powerful and informative control group in association studies on T2D, a pathology characterized by significant clinical heterogeneity. Different authors have emphasized the problem of phenotypical heterogeneity of cohorts, which can seriously affect the ability to detect genetic associations [54]. Our data suggest that the use of relatively small numbers of cases and controls with extreme phenotypes (thus reducing sample heterogeneity) in genetic association studies of age-related diseases can be successful in detecting significant associations as suggested by other authors [55] .

METHODS

Samples. A total of 1,349 individuals from Northern/Central Italy, including 562 T2D patients (D) (mean age: 65.76 ± 8.11) and 558 unrelated age-, gender- and geographically-matched controls (CTR) (mean age: 58.11 ± 12.40), and 229 centenarians (100+) (mean age: 105.0 ± 2.9) have been considered in this study. D and CTR subjects were collected by the Diabetology Unit, INRCA (National Institute on Health and Science on Aging) in Ancona (Italy). T2D diagnosis was made according to the American Diabetes Association Criteria (http://www.diabetes.org/). All patients were fully characterized from a clinical point of view and a large number of biochemical/endocronological parameters were measured. To avoid population stratification effects, only patients and controls with at least two generations of maternal ancestry from the Marche region (Central Italy) were included in this study. CTR subjects were carefully assessed and fully characterized according to the same protocol used for T2D patients, and a detailed clinical history was recorded in order to exclude the presence of T2D and of any other overt illness. Within the group of diabetic patients, N = 241 were affected by complications (D+Co), and in particular N = 110 had only micro-vascular (D+microCo) and N = 64 had only macro-vascular complications (D+macroCo). The main phenotypical and clinical characteristics of D and CTR are summarized in Table 2.

The presence/absence of microvascular and macrovascular diabetic complications was assessed according to the following criteria: i) *microvascular*: diabetic retinopathy by fundoscopy through dilated pupils and/or fluorescence angiography; incipient nephropathy, defined by an excessive urinary albumin excretion (>30 mg/24 h) and a normal creatinine clearance; renal failure, detected as an estimated glomerular filtration rate > 60 mL/min per 1.73 m2;

Table 2. Diabetic patients and non diabetic controls collected by the Diabetology Unit in Ancona: samples description

		All samples		Males		Females	
	Variables	Diabetic Patients (N=562)	Controls (N=558)	Diabetic Patients (N=305)	Controls (N=214)	Diabetic Patients (N=257)	Controls (N=344)
Traits	Age ± STD	65.76± 8.11	58.11 ± 12.40	64.93 ± 8.42	58.35 ± 11.88	66.75 ± 7.64	57.96 ±12.73
	Sex (M/F)	306/258	213/345	…	…	…	…
	BMI ± STD	28.76 ±4.62	27.14 ± 4.46	28.24 ± 4.15	27.29±3.51	29.40 ± 5.07	27.04 ±5.00
Complications	Retinopathy (%)	27.22 %	…	27.21 %	…	27.24 %	…
	Somatic Neuropathy (%)	17.79 %	…	21.64 %	…	13.23 %	…
	Renal failure (%)	3.56 %	…	4.92 %	…	1.94 %	…
	Nephropathy (%)	12.81 %	…	16.06 %	…	8.95 %	…
	Ischemic heart disease (%)	17.08 %	…	20.33 %	…	13.23 %	…
	Acute myocardial infarction (%)	9.07 %	…	13.11 %	…	4.28 %	…
	Ictus (%)	6.76 %	…	6.88 %	…	6.61%	…

neuropathy established by electromyography; ii) *macrovascular*: ictus by clinical history; ischemic heart disease and acute myocardial infarction by clinical history and by resting electrocardiogram; peripheral vascular disease by clinical history and, for lower limbs, by ankle-brachial index. Hypertension was defined as a systolic blood pressure >140 mmHg and/or a diastolic blood pressure >90 mmHg. The values were measured while the subjects were sitting and confirmed at least three times. Overnight fasting venous blood samples from all subjects were collected from 8:00 to 9:00 a.m. Blood concentrations for HDL cholesterol, triglycerides, HbA1c, fasting insulin, fibrinogen, high-sensitivity C reactive protein (hsCRP), creatinine, urea nitrogen, and white blood cells count were measured by standard procedures.

All centenarians were born in Italy between the 1900 and 1908. Trained physicians and nursing staff collected demographic and lifestyle data, anthropometric measurements, functional, cognitive and health status, clinical anamnesis, and details on drug use, as previously described [9].

SNPs selection. A total of 31 SNPs mapping within and nearby 16 different genes (Table S5) were genotyped in the 1,349 individuals included in the study. The SNPs were selected according to the following criteria: *i) SNPs reported to be risk* factor for T2D [56–62] such as Transcription factor 7-like 2 (*TCF7L2*), Insulin-like growth factor 2 mRNA-binding proteins (*IGF2BP*), Potassium inwardly-rectifying channel, subfamily J, member 11 (*KCNJ11*), Potassium voltage-gated channel KQT-like sub-family, member 1 (*KCNQ1*); *ii) SNPs of candidate genes for the development of T2D complications*, such as Catalase (*CAT*), erythropoietin (*EPO*) [61] , hypoxia-inducible factor 1 α subunit (*HIF1A*) [63] and *DDAH1*. Interestingly, significant association of *CAT* and *SOD* polymorphisms with T2D were recently reported [64] . Genetic variations in the *DDAH1* and *DDAH2* genes are significantly associated with serum Asymmetric DiMethylArginine (ADMA) levels in T2D patients [65]. Moreover, it was reported that *DDAH* gene polymorphisms play a central role in determining ADMA in diabetic renal impairment [66]. *iii) SNPs of genes reported to be involved in metabolic diseases, including T2D,* such as *ADIPOQ* and *IRS1*

encoding for adiponectin and insulin receptor substrate 1 respectively, and *FTO*, a major gene for obesity susceptibility [62–65]. Adiponectin is an adipocyte-produced protein involved in regulating glucose, lipid and energy metabolism, and *ADIPOQ* polymorphisms were previously associated with T2D in Caucasian and non-Caucasian populations [59,71,72]. *IRS1* polymorphisms have been associated with risk of T2D and adiposity in GWASs. Recently, it was reported that *IRS1* rs2943641 interacts with carbohydrate and fat intakes in incident T2D in a sex-specific manner [73] ; *iv) SNPs of genes relevant for aging and age-related diseases*, such as *hTERT* and *TERC*, involved in telomere stability/attrition and in T2D complications [21,74,75] .

SNPs genotyping. DNA was extracted from whole blood (QIAmp 96 DNA Blood kit, QIAGEN). Genotyping analysis was performed by using SEQUENOM MassArray iPLEX technology, following the manufacturer's instructions and as previously described [76,77]. Genotype calls were analyzed by using SEQUENOM Typer 4.0 software and the individual spectrograms were checked in order to evaluate the presence of calling errors.

SNP analysis and quality control. Four SNPs (rs16889462, rs4880, rs8047395 and rs10434) that did not satisfy the Hardy-Weinberg equilibrium (HWE) in the control group and five SNPs (rs669173, rs2853669, rs3025021, rs13266634 and rs7901695) that showed 25% missing call rates were excluded from the analysis (Table S5). Diabetic patients were also analyzed after stratifications for the type of complications (micro and macro-vascular).

Only SNPs with call rates higher than 95%, without significant deviation from HWE in controls and with minor allele frequency (MAF) exceeding 5% were retained for the association analysis. Genotypic analysis was performed using R 2.15.2 and SNPassoc package (http://www.r-project.org/) [78] that implements binary logistic regression methods under five different genetic models. Allelic association analyses were performed using PLINK 1.07, an open-source whole genome association analysis toolset (http://pngu.mgh.harvard.edu/purcell/plink/) [71].

Interactome analysis. Protein-protein interaction (PPI) data have been retrieved from the Agile Protein Interactions Database APID [80] accessed through the dedicated plugin APID2NET [81] and from the metadatabase InnateDB [82] and then integrated to form the Tcf7l2 interactome (i.e. the set of molecular interactions related to Tcf7l2) and analyzed with the network analysis platform Cytoscape [83, 84]. Topological measures such as betweenness centrality and node degree are used to rank the importance of the interactome elements [85,86]. The betweenness centrality of a node reflects the amount of control that this node exerts over the interactions of other nodes in the network. This measure favors nodes that join communities (dense subnetworks), rather than nodes that lie inside a community [87,88]. OMIM diseases overrepresentation analyses and ranking have been performed using Enrichr (http://amp.pharm.mssm.edu/Enrichr/).

ACKNOWLEDGEMENTS

We thank Vilma Mantovani and Elena Marasco for their technical support during experimental procedure of genotyping at CRBA (Applied Biomedical Research Center, S. Orsola-Malpighi Polyclinic, Bologna, Italy). We also thank and mention the European Union's Seventh Framework Programme (grant agreement no. 259679, "IDEAL" and grand agreement no. 600803, "MISSION T2D") and the Italian Ministry of University and Research (Project PRIN 2006 to DM and Project PRIN 2009 to CF).

Conflict of Interest Statement

The authors declare no conflicts of interest.

REFERENCES

1. Bodmer W, Bonilla C. Common and rare variants in multifactorial susceptibility to common diseases. Nature Genetics. 2008; 40:695–701.

2. Tazearslan C, Cho M, Suh Y. Discovery of functional gene variants associated with human longevity: opportunities and challenges. J. Gerontol. A Biol. Sci. Med. Sci. 2012; 67:376–383.

3. Heutink P, Oostra BA. Gene finding in genetically isolated populations. Hum. Mol. Genet. 2002; 11:2507–2515.

4. Garagnani P, Laayouni H, González-Neira A, Sikora M, Luiselli D, Bertranpetit J, et al. Isolated populations as treasure troves in genetic epidemiology: the case of the Basques. Eur. J. Hum. Genet. 2009; 17:1490–1494.

5. Lowe JK, Maller JB, Pe'er I, Neale BM, Salit J, Kenny EE, et al. Genome-wide association studies in an isolated founder population from the Pacific Island of Kosrae. PLoS Genet. 2009; 5:e1000365.

6. Franceschi C, Bonafè M. Centenarians as a model for healthy aging. Biochem. Soc. Trans. 2003; 31:457–461.

7. Paolisso G, Gambardella A, Ammendola S, D'Amore A, Balbi V, Varricchio M, et al. Glucose tolerance and insulin action in healty centenarians. Am. J. Physiol. 1996; 270:E890–894.

8. Paolisso G, Barbieri M, Rizzo MR, Carella C, Rotondi M, Bonafè M, et al. Low insulin resistance and preserved beta-cell function contribute to human longevity but are not associated with TH-INS genes. Exp. Gerontol. 2001; 37:149–156.

9. Vitale G, Brugts MP, Ogliari G, Castaldi D, Fatti LM, Varewijck AJ, et al. Low circulating IGF-I bioactivity is associated with human longevity: findings in centenarians' offspring. Aging (Albany NY). 2012; 4:580–589.

10. Evert J, Lawler E, Bogan H, Perls T. Morbidity profiles of centenarians: survivors, delayers, and escapers. J. Gerontol. A Biol. Sci. Med. Sci. 2003; 58232–52837.

11. Atzmon G, Schechter C, Greiner W, Davidson D, Rennert G, Barzilai N. Clinical phenotype of families with longevity. J Am Geriatr Soc. 2004; 52:274–277.

12. Westendorp RGJ, van Heemst D, Rozing MP, Frölich M, Mooijaart SP, Blauw G-J, et al. Nonagenarian siblings and their offspring display lower risk of mortality and morbidity than sporadic nonagenarians: The Leiden Longevity Study. J Am Geriatr Soc. 2009; 57:1634–1637.

13. Wijsman CA, Rozing MP, Streefland TCM, le Cessie S, Mooijaart SP, Slagboom PE, et al. Familial longevity is marked by enhanced insulin sensitivity. Aging Cell. 2011; 10:114–121.

14. Kowall B, Peters A, Thorand B, Rathmann W, Meisinger C. Associations between longevity of parents and glucose regulation in their offspring: the KORA S4/F4 Study. Diabetologia. 2013; 56:268-274.

15. Testa R, Olivieri F, Bonfigli AR, Sirolla C, Boemi M, Marchegiani F, et al. Interleukin-6-174 G > C polymorphism affects the association between IL-6 plasma levels and insulin resistance in type 2 diabetic patients. Diabetes Res. Clin. Pract. 2006; 71:299–305.

16. Cormio A, Milella F, Marra M, Pala M, Lezza AMS, Bonfigli AR, et al. Variations at the H-strand replication origins of mitochondrial DNA and mitochondrial DNA content in the blood of type 2 diabetes patients. Biochim. Biophys. Acta. 2009; 1787: 547–552.

17. Bonfigli AR, Sirolla C, Testa R, Cucchi M, Spazzafumo L, Salvioli S, et al. The p53 codon 72 (Arg72Pro) polymorphism is associated with the degree of insulin resistance in type 2 diabetic subjects: a cross-sectional study. Acta Diabetol. 2012; in press.

18. Marra M, Marchegiani F, Ceriello A, Sirolla C, Boemi M, Franceschi C, et al. Chronic renal impairment and DDAH2-1151 A/C polymorphism determine ADMA levels in type 2 diabetic subjects. Nephrol. Dial. Transplant. 2013; 28:964-971.

19. Spazzafumo L, Olivieri F, Abbatecola AM, Castellani G, Monti D, Lisa R, et al. Remodelling of biological parameters during human ageing: evidence for complex regulation in longevity and in type 2 diabetes. Age (Dordr). 2013; 35:419-429.

20. Forte GI, Pilato G, Vaccarino L, Sanacore M, Candore G, Romano GC, et al. Risk profiles in type 2 diabetes (metabolic syndrome): integration of IL-10 polymorphisms and laboratory parameters to identify vascular damages related complications. Curr. Pharm. 2010; 16:898–903.

21. Testa R, Olivieri F, Sirolla C, Spazzafumo L, Rippo MR, Marra M, et al. Leukocyte telomere length is associated with complications of type 2 diabetes mellitus. Diabet. Med. 2011; 28:1388–1394.

22. Achilli A, Olivieri A, Pala M, Hooshiar Kashani B, Carossa V, Perego UA, et al. Mitochondrial DNA backgrounds might modulate diabetes complications rather than T2DM as a whole. PLoS ONE. 2011; 6:e21029.

23. Grant SFA, Thorleifsson G, Reynisdottir I, Benediktsson R, Manolescu A, Sainz J, et al. Variant of transcription factor 7-like 2 (TCF7L2) gene confers risk of type 2 diabetes. Nat. Genet. 2006; 38:320–323.

24. Zhao J, Schug J, Li M, Kaestner KH, Grant SFA. Disease-associated loci are significantly over-represented among genes bound by transcription factor 7-like 2 (TCF7L2) in vivo. Diabetologia. 2010; 53:2340–2346.

25. Franceschi C, Bonafè M. Centenarians as a model for healthy aging. Biochem. Soc. Trans. 2003; 31:457–461.

26. Hotta K, Funahashi T, Arita Y, Takahashi M, Matsuda M, Okamoto Y, et al. Plasma concentrations of a novel, adipose-specific protein, adiponectin, in type 2 diabetic patients. Arterioscler. Thromb. Vasc. Biol. 2000; 20:1595–1599.

27. Daimon M, Oizumi T, Saitoh T, Kameda W, Hirata A, Yamaguchi H, et al. Decreased serum levels of adiponectin are a risk factor for the progression to type 2 diabetes in the Japanese Population: the Funagata study. Diabetes Care. 2003; 26:2015–2020.

28. Lindsay RS, Funahashi T, Hanson RL, Matsuzawa Y, Tanaka S, Tataranni PA, et al. Adiponectin and development of type 2 diabetes in the Pima Indian population. Lancet. 2002; 360:57–58.

29. Vionnet N, Hani EH, Dupont S, Gallina S, Francke S, Dotte S, et al. Genomewide search for type 2 diabetes-susceptibility genes in French whites: evidence for a novel susceptibility locus for early-onset diabetes on chromosome 3q27-qter and independent replication of a type 2-diabetes locus on chromosome 1q21-q24. Am. J. Hum. Genet. 2000; 67:1470–1480.

30. Han LY, Wu QH, Jiao ML, Hao YH, Liang LB, Gao LJ, et al. Associations between single-nucleotide polymorphisms (+45T>G, +276G>T, -11377C>G, -11391G>A) of adiponectin gene and type 2 diabetes mellitus: a systematic review and meta-analysis. Diabetologia. 2011; 54:2303–2314.

31. Scott RA, Lagou V, Welch RP, Wheeler E, Montasser ME, Luan J, et al. Large-scale association analyses identify new loci influencing glycemic traits and provide insight into the underlying biological pathways. Nat. Genet. 2012; 44:991–1005.

32. Mohlke KL, Boehnke M, Abecasis GR. Metabolic and cardiovascular traits: an abundance of recently identified common genetic variants. Hum. Mol. Genet. 2008; 17:R102–108.

33. Sousa AG, Selvatici L, Krieger JE, Pereira AC. Association between genetics of diabetes, coronary artery disease, and macrovascular complications: exploring a common ground hypothesis. Rev Diabet Stud. 2011; 8:230–244.

34. Ciccacci C, Di Fusco D, Cacciotti L, Morganti R, D'Amato C, Novelli G, et al. TCF7L2 gene polymorphisms and type 2 diabetes: association with diabetic retinopathy and cardiovascular autonomic neuropathy. Acta Diabetol. 2012; in press.

35. Muendlein A, Saely CH, Geller-Rhomberg S, Sonderegger G, Rein P, Winder T, et al. Single nucleotide polymorphisms of TCF7L2 are linked to diabetic coronary atherosclerosis. PLoS ONE. 2011; 6:e17978.

36. Reynisdottir I, Thorleifsson G, Benediktsson R, Sigurdsson G, Emilsson V, Einarsdottir AS, et al. Localization of a susceptibility gene for type 2 diabetes to chromosome 5q34-q35.2. Am. J. Hum. Genet. 2003; 73:323–335.

37. Mayans S, Lackovic K, Lindgren P, Ruikka K, Agren A, Eliasson M, et al. TCF7L2 polymorphisms are associated with type 2 diabetes in northern Sweden. Eur. J. Hum. Genet. 2007; 15:342–346.

38. Sladek R, Rocheleau G, Rung J, Dina C, Shen L, Serre D, et al. A genome-wide association study identifies novel risk loci for type 2 diabetes. Nature. 2007; 445:881–885.

39. Stitzel ML, Sethupathy P, Pearson DS, Chines PS, Song L, Erdos MR, et al. Global epigenomic analysis of primary human pancreatic islets provides insights into type 2 diabetes susceptibility loci. Cell Metab. 2010; 12:443–455.

40. Van Vliet-Ostaptchouk JV, Shiri-Sverdlov R, Zhernakova A, Strengman E, van Haeften TW, Hofker MH, et al. Association of variants of transcription factor 7-like 2 (TCF7L2) with susceptibility to type 2 diabetes in the Dutch Breda cohort. Diabetologia. 2007; 50:59–62.

41. Lyssenko V, Lupi R, Marchetti P, Del Guerra S, Orho-Melander M, Almgren P, et al. Mechanisms by which common variants in the TCF7L2 gene increase risk of type 2 diabetes. J. Clin. Invest. 2007; 117:2155–2163.

42. Gaulton KJ, Nammo T, Pasquali L, Simon JM, Giresi PG, Fogarty MP, et al. A map of open chromatin in human pancreatic islets. Nat. Genet. 2010; 42:255–259.

43. Ip W, Chiang Y-TA, Jin T. The involvement of the wnt signaling pathway and TCF7L2 in diabetes mellitus: The current understanding, dispute, and perspective. Cell Biosci. 2012; 2:28.

44. Ling C, Groop L. Epigenetics: a molecular link between environmental factors and type 2 diabetes. Diabetes. 2009; 58:2718–2725.

45. Pinney SE, Simmons RA. Epigenetic mechanisms in the development of type 2 diabetes. Trends Endocrinol. Metab. 2010; 21:223–229.

46. Pons D, de Vries FR, van den Elsen PJ, Heijmans BT, Quax PHA, Jukema JW. Epigenetic histone acetylation modifiers in vascular remodelling: new targets for therapy in cardiovascular disease. Eur. Heart J. 2009; 30:266–277.

47. Villeneuve LM, Natarajan R. The role of epigenetics in the pathology of diabetic complications. Am. J. Physiol. Renal Physiol. 2010; 299:F14–25.

48. Pimentel-Coelho PM, Rivest S. The early contribution of cerebrovascular factors to the pathogenesis of Alzheimer's disease. Eur. J. Neurosci. 2012; 35:1917–1937.

49. Camici PG. Coronary microvascular dysfunction in patients with cardiomyopathies. Circ Heart Fail. settembre 2008; 1:150–152.

50. Sainz J, Rudolph A, Hoffmeister M, Frank B, Brenner H, Chang-Claude J, et al. Effect of type 2 diabetes predisposing genetic variants on colorectal cancer risk. J. Clin. Endocrinol. Metab. 2012; 97:E845–851.

51. Sun J, Wang D, Jin T. Insulin alters the expression of components of the Wnt signaling pathway including TCF-4 in the intestinal cells. Biochim. Biophys. Acta. 2010; 1800:344–351.

52. Jin T. Why diabetes patients are more prone to the development of colon cancer? Med. Hypotheses. 2008; 71:241–244.

53. Vidal M, Cusick ME, Barabási A-L. Interactome networks and human disease. Cell. 2011; 144:986–998.

54. Moonesinghe R, Khoury MJ, Liu T, Ioannidis JPA. Required sample size and nonreplicability thresholds for heterogeneous genetic associations. Proc. Natl. Acad. Sci. U.S.A. 2008; 105:617–622.

55. Perry JRB, Voight BF, Yengo L, Amin N, Dupuis J, Ganser M, et al. Stratifying type 2 diabetes cases by BMI identifies genetic risk variants in LAMA1 and enrichment for risk variants in lean compared to obese cases. PLoS Genet. 2012; 8:e1002741.

56. Qi L, Cornelis MC, Kraft P, Stanya KJ, Linda Kao WH, Pankow JS, et al. Genetic variants at 2q24 are associated with susceptibility to type 2 diabetes. Hum. Mol. Genet. 2010; 19:2706–2715.

57. Tsai F-J, Yang C-F, Chen C-C, Chuang L-M, Lu C-H, Chang C-T, et al. A genome-wide association study identifies susceptibility variants for type 2 diabetes in Han Chinese. PLoS Genet. 2010; 6:e1000847.

58. Yamauchi T, Hara K, Maeda S, Yasuda K, Takahashi A, Horikoshi M, et al. A genome-wide association study in the Japanese population identifies susceptibility loci for type 2 diabetes at UBE2E2 and C2CD4A-C2CD4B. Nat. Genet. 2010; 42:864–868.

59. Mtiraoui N, Ezzidi I, Turki A, Chaieb A, Mahjoub T, Almawi WY. Single-nucleotide polymorphisms and haplotypes in the adiponectin gene contribute to the genetic risk for type 2 diabetes in Tunisian Arabs. Diabetes Res. Clin. Pract. 2012; 97:290–297.

60. Dupuis J, Langenberg C, Prokopenko I, Saxena R, Soranzo N, Jackson AU, et al. New genetic loci implicated in fasting glucose homeostasis and their impact on type 2 diabetes risk. Nat. Genet. 2010; 42:105–116.

61. Williams WW, Salem RM, McKnight AJ, Sandholm N, Forsblom C, Taylor A, et al. Association testing of previously reported variants in a large case-control meta-analysis of diabetic nephropathy. Diabetes. 2012; 61:2187–2194.

62. Voight BF, Scott LJ, Steinthorsdottir V, Morris AP, Dina C, Welch RP, et al. Twelve type 2 diabetes susceptibility loci identified through large-scale association analysis. Nat. Genet. 2010; 42:579–589.

63. Gu HF, Zheng X, Abu Seman N, Gu T, Botusan IR, Sunkari VG, et al. Impact of the Hypoxia-Inducible Factor-1 α (HIF-1α) Pro582Ser Polymorphism on Diabetes Nephropathy. Diabetes Care. 2013; 36:415-421.

64. Ghattas MH, Abo-Elmatty DM. Association of polymorphic markers of the catalase and superoxide dismutase genes with type 2 diabetes mellitus. DNA Cell Biol. 2012; 31:1598–1603.

65. Abhary S, Burdon KP, Kuot A, Javadiyan S, Whiting MJ, Kasmeridis N, et al. Sequence variation in DDAH1 and DDAH2 genes is strongly and additively associated with serum ADMA concentrations in individuals with type 2 diabetes. PLoS ONE. 2010; 5:e9462.

66. Marra M, Marchegiani F, Ceriello A, Sirolla C, Boemi M, Franceschi C, et al. Chronic renal impairment and DDAH2-1151 A/C polymorphism determine ADMA levels in type 2 diabetic subjects. Nephrol. Dial. Transplant. 2013; 28:964-971.

67. Frayling TM, Timpson NJ, Weedon MN, Zeggini E, Freathy RM, Lindgren CM, et al. A common variant in the FTO gene is associated with body mass index and predisposes to childhood and adult obesity. Science. 2007; 316:889–894.

68. Sällman Almén M, Rask-Andersen M, Jacobsson JA, Ameur A, Kalnina I, Moschonis G, et al. Determination of the obesity-associated gene variants within the entire FTO gene by ultra-deep targeted sequencing in obese and lean children. Int J Obes (Lond). 2013; 37:424-314.

69. Jacobsson JA, Schiöth HB, Fredriksson R. The impact of intronic single nucleotide polymorphisms and ethnic diversity for studies on the obesity gene FTO. Obes Rev. 2012; 13:1096–1109.

70. Dina C, Meyre D, Gallina S, Durand E, Körner A, Jacobson P, et al. Variation in FTO contributes to childhood obesity and severe adult obesity. Nat. Genet. 2007; 39:724–726.

71. Han LY, Wu QH, Jiao ML, Hao YH, Liang LB, Gao LJ, et al. Associations between single-nucleotide polymorphisms (+45T>G, +276G>T, -11377C>G, -11391G>A) of adiponectin gene and type 2 diabetes mellitus: a systematic review and meta-analysis. Diabetologia. 2011; 54:2303–2314.

72. Hivert M-F, Manning AK, McAteer JB, Florez JC, Dupuis J, Fox CS, et al. Common variants in the adiponectin gene (ADIPOQ) associated with plasma adiponectin levels, type 2 diabetes, and diabetes-related quantitative traits: the Framingham Offspring Study. Diabetes. 2008; 57:3353–3359.

73. Ericson U, Rukh G, Stojkovic I, Sonestedt E, Gullberg B, Wirfält E, et al. Sex-specific interactions between the IRS1 polymorphism and intakes of carbohydrates and fat on incident type 2 diabetes. Am. J. Clin. Nutr. 2013; 97:208-216.

74. Olivieri F, Lazzarini R, Recchioni R, Marcheselli F, Rippo MR, Di Nuzzo S, et al. MiR-146a as marker of senescence-associated pro-inflammatory status in cells involved in vascular remodelling. Age (Dordr). 2012; in press.

75. Olivieri F, Lorenzi M, Antonicelli R, Testa R, Sirolla C, Cardelli M, et al. Leukocyte telomere shortening in elderly Type2DM patients with previous myocardial infarction. Atherosclerosis. 2009; 206:588–593.

76. Hasan SK, Buttari F, Ottone T, Voso MT, Hohaus S, Marasco E, et al. Risk of acute promyelocytic leukemia in multiple sclerosis: coding variants of DNA repair genes. Neurology. 22 marzo 2011; 76:1059–1065.

77. Mantovani V, Garagnani P, Selva P, Rossi C, Ferrari S, Cenci M, et al. Simple method for haplotyping the poly(TG) repeat in individuals carrying the IVS8 5T allele in the CFTR gene. Clin. Chem. 2007;53:531–533.

78. González JR, Armengol L, Solé X, Guinó E, Mercader JM, Estivill X, et al. SNPassoc: an R package to perform whole genome association studies. Bioinformatics. 2007; 23:644–645.

79. Purcell S, Neale B, Todd-Brown K, Thomas L, Ferreira MAR, Bender D, et al. PLINK: a tool set for whole-genome association and population-based linkage analyses. Am. J. Hum. Genet. 2007; 81:559–575.

80. Prieto C, De Las Rivas J. APID: Agile Protein Interaction DataAnalyzer. Nucleic Acids Res. 2006; 34:W298–302.

81. Hernandez-Toro J, Prieto C, De las Rivas J. APID2NET: unified interactome graphic analyzer. Bioinformatics. 2007; 23:2495–2497.

82. Lynn DJ, Winsor GL, Chan C, Richard N, Laird MR, Barsky A, et al. InnateDB: facilitating systems-level analyses of the mammalian innate immune response. Mol. Syst. Biol. 2008; 4:218.

83. Killcoyne S, Carter GW, Smith J, Boyle J. Cytoscape: a community-based framework for network modeling. Methods Mol. Biol. 2009; 563:219–239.

84. Smoot ME, Ono K, Ruscheinski J, Wang P-L, Ideker T. Cytoscape 2.8: new features for data integration and network visualization. Bioinformatics. 2011; 27:431–432.

85. Platzer A, Perco P, Lukas A, Mayer B. Characterization of protein-interaction networks in tumors. BMC Bioinformatics. 2007; 8:224.

86. Barabási A-L, Oltvai ZN. Network biology: understanding the cell's functional organization. Nat. Rev. Genet. 2004; 5:101–113.

87. Yoon J, Blumer A, Lee K. An algorithm for modularity analysis of directed and weighted biological networks based on edge-betweenness centrality. Bioinformatics. 2006; 22:3106–3108.

88. Assenov Y, Ramírez F, Schelhorn S-E, Lengauer T, Albrecht M. Computing topological parameters of biological networks. Bioinformatics. 2008; 24:282–284.

89. Potapov AP, Voss N, Sasse N, Wingender E. Topology of mammalian transcription networks. Genome Inform. 2005; 16:270–278.

SUPPLEMENTAL DATA

Supplemental Tables of this manuscript are found in full version at www.impactaging.com/papers/v5/n5/full/100562.html.

Research paper

The Tellurium compound, AS101, increases SIRT1 level and activity and prevents type 2 diabetes

Meital Halperin-Sheinfeld, Asaf Gertler, Eitan Okun, Benjamin Sredni*, and Haim Y. Cohen*

The Mina and Everard Goodman Faculty of Life Sciences, Bar-Ilan University, Ramat-Gan 52900, Israel

** These authors corresponded equally to this work*

Key words: *AS101, SIRT1, T2D*

Abbreviations: *T2D - Type 2 diabetes, IGF-1 - Insulin like growth factor 1, STZ – Streptozotocin, PPAR γ - Peroxisome Proliferator Activated Receptor γ*

Received: *6/13/12; Accepted: 6/28/12; Published: 6/30/12* doi:10.18632/aging.100468

Correspondence to: *Haim Y. Cohen, PhD, Benjamin Sredni PhD;* ***E-mail:*** *Haim_cohen@mail.biu.ac.il; srednib@mail.biu.ac.il*

Abstract: The histone deacetylase, SIRT1, plays a major role in glucose regulation and lipid metabolism. Ammonium Trichloro (dioxoethylene-o,o') Tellurate, AS101, is a potent in vitro and in vivo immunomodulator, with several potential therapeutic applications. AS101 administration resulted in upregulation of SIRT1 protein expression and activity. These effects were associated with decreased levels of serum insulin like growth factor-1 (IGF-1) and of insulin. The properties of AS101 prompted us to investigate its potential therapeutic role in rats with type 2 diabetes (T2D). T2D was induced by a high fat diet combined with a low dose of Streptozotocin (STZ). Treatment with AS101 before manifestation of hyperglycemia, resulted in increased insulin sensitivity, and decreased blood glucose levels, and prevented symptoms of diabetes including defective glucose clearance, fatty liver, and abnormal distribution of insulin-producing beta cells in the pancreas. Treatment after disease emergence resulted in partial restoration of normal glucose homeostasis. Diabetic rats showed a reduction in liver SIRT1 levels. In both treatment regimens the reduction in SIRT1 levels in the liver were blocked by AS101 consumption. Together, these findings demonstrate the therapeutic potential of AS101 for treating T2D, and for reversing impaired fat and glucose metabolism.

INTRODUCTION

The incidence of Type 2 diabetes (T2D) depends on complex interaction of genetic and environmental factors [1-3]. T2D is characterized by chronic irregular lipid and carbohydrate metabolism followed by insulin resistance in target tissues [1] and increasing to epidemic proportions [4]. Insulin lowers blood glucose levels by facilitating glucose uptake, mainly into skeletal muscle and fat tissue, and by inhibiting endogenous glucose production in the liver. However, insulin resistance occurs when a normal dose of insulin is incapable of eliciting these metabolic responses [5]. In this progressive disease, susceptible individuals develop impaired peripheral tissue responses to insulin and compensatory hyperinsulinemia. In many patients, β-cells fail to secrete sufficient amounts of insulin to compensate for insulin resistance, and they therefore fail to maintain normal glucose levels, marking the on-set of diabetes. In a significant portion of Type 2 diabetic patients, the disease progresses to a complete loss of β-cell insulin secretion [6], thus necessitating exogenous administration of insulin, in addition to other medications, to achieve adequate glycemic control [7, 8]. It has been proposed that persistent insulin resistance accelerates β-cell failure. Therefore, earlier intervention to correct insulin resistance and/or to protect β-cells may prevent negative development and progression of the disease [9, 10].

A recent series of studies in several organisms revealed multiple important functions of the sirtuin family of proteins in energy metabolism [11]. Sirtuins are highly conserved NAD+ dependent deacetylases [12, 13]. The mammalian sirtuins, SIRT1-SIRT7, are implicated in a number of cellular and physiological functions including gene silencing, stress resistance, apoptosis, mitochondrial function, energy homeostasis, and

extension of lifespan. Anti-diabetic drugs inhibit obesity-linked phosphorylation of PPARgamma by Cdk5 [14, 15]. SIRT1 also promotes cell survival and inhibits apoptotic cell death by deacetylating the p53 [16], Ku70 [17], and fork-head transcription factors [18-20]. Therefore, SIRT1 is considered a key regulator of cell survival under various stressful conditions [21, 22]. Among its multiple reported targets, SIRT1 deacetylates and thereby activates PGC1α [23], an essential cofactor in mitochondrial biogenesis, regulating metabolic rate. Other studies have shown that SIRT1 represses Peroxisome Proliferator-Activated Receptor γ (PPARγ) function, increasing lipolysis in white adipose tissue [24]. SIRT1 was also shown to act as a regulator of insulin secretion in pancreatic β-cells by repressing uncoupling protein 2 [25] and its levels were inversely correlated with insulin and insulin like growth factor IGF-1 [26]. Another novel function of SIRT1 overexpression is the protection of pancreatic β-cells from cytokine toxicity [27].

An organotellurium compound previously developed in our laboratory, Ammonium Trichloro (dioxoethylene-o,o') Tellurate, AS101, is a potent *in vitro* and *in vivo* immunomodulator [28-30]. This non-toxic compound has been shown to have beneficial effects in diverse preclinical and clinical studies. Accumulated research suggests that much of the biological activity of organotellurium compounds is directly related to their specific chemical interactions with endogenous thiols [31]. Such tellurium thiol compounds may be important for the manifestation of the biological function or for transportation of the tellurium species to its target location. In a previous study, we clarified several mechanistic aspects of this chemistry and discussed its relationship to the biological activity of AS101 [32]. AS101 exhibits diverse biological effects; some of its activities have been primarily attributed to the direct inhibition of the anti-inflammatory cytokine, IL-10 [33]. Other features of AS101, including regulation of growth factors levels [34] and immunomodulatory activity in different systems [35], give the compound its therapeutic activity.

In this study, the role of AS101 on SIRT1 activity and T2D progression was examined. T2D was generated by the STZ+HFD rat model which imitates the disease development in humans. The HFD disrupts metabolism and causes insulin resistance, which results from a chronic disruption in carbohydrate and lipid metabolism, and plays a major role in the progression and pathogenesis of T2D. Therefore, HFD sensitizes pancreatic β cells to low doses of STZ [36].

Here, we characterized the ability of AS101 to enhance the expression and activity of the SIRT1 protein. Those effects may protect cells from physiological injury caused by the metabolic syndrome in a rat model of T2D induced by high fat diet (HFD) and low dose of streptozotocin (STZ).

Thus, activation of SIRT1 by AS101 may signify a promising strategy for prevention and treatment of metabolic syndrome.

RESULTS

AS101 affects SIRT1 expression and activity

The effect of the telluric compound AS101 on SIRT1 protein expression was first examined in an *in vitro* assay using cell lines. AS101 induced SIRT1 expression in a dose dependent manner in three different cell lines, HEK293, HL-60 and Rin-5f (Figure 1a-c). Similar to other therapeutic compounds, AS101 also exhibits an optimal range, beyond which the effective activity is reduced. The effect of AS101 on SIRT1 protein levels was next examined in healthy rats treated with AS101 or PBS for 14 days. AS101 treated rats showed a large increase in SIRT1 protein levels in the liver (Figure 1d) and kidney extracts of rats treated with AS101 (Supplementary 1a). In order to determine the minimal AS101 treatment time that results in SIRT1 induction, SIRT1 levels were measured at different times after AS101 injection. Significant induction of SIRT1 expression was already seen after 5 days of AS101 treatment (Figure 1e). These results show that AS101 treatment significantly induces SIRT1 protein expression *in vitro* and in *vivo*.

To determine if the increase in SIRT1 levels upon AS101 treatment is reflected in an increase in SIRT1 enzymatic activity, several approaches were taken. First, the direct activity of AS101 on recombinant SIRT1 was examined *in vitro*. SIRT1 activity was measured by a deacetylation assay using fluorogenic acetylated peptide, representing human p53, which is a known SIRT1 substrate [37]. A significant increase in SIRT1 activity was observed ($p<0.05$) (Figure 2a). Next, the acetylation levels of two known SIRT1 substrates, p53 and PGC1α [38], were tested *in vivo*, in tissue samples from rats treated with AS101 or PBS. Tissue extracts from rats treated with 0.25 and 0.5 mg/kg AS101 for 14 days, exhibited significantly reduced levels of acetylation relative to extract from PBS treated control animals (Figure 2b-c). This decrease may partially reflect the higher expression of SIRT1 protein in AS101 treated animals. Therefore, together with the *in vitro* examination, we suggest that SIRT1 activity was increased and AS101 treatment is

capable of enhancing SIRT1 expression and deacetylation activity.

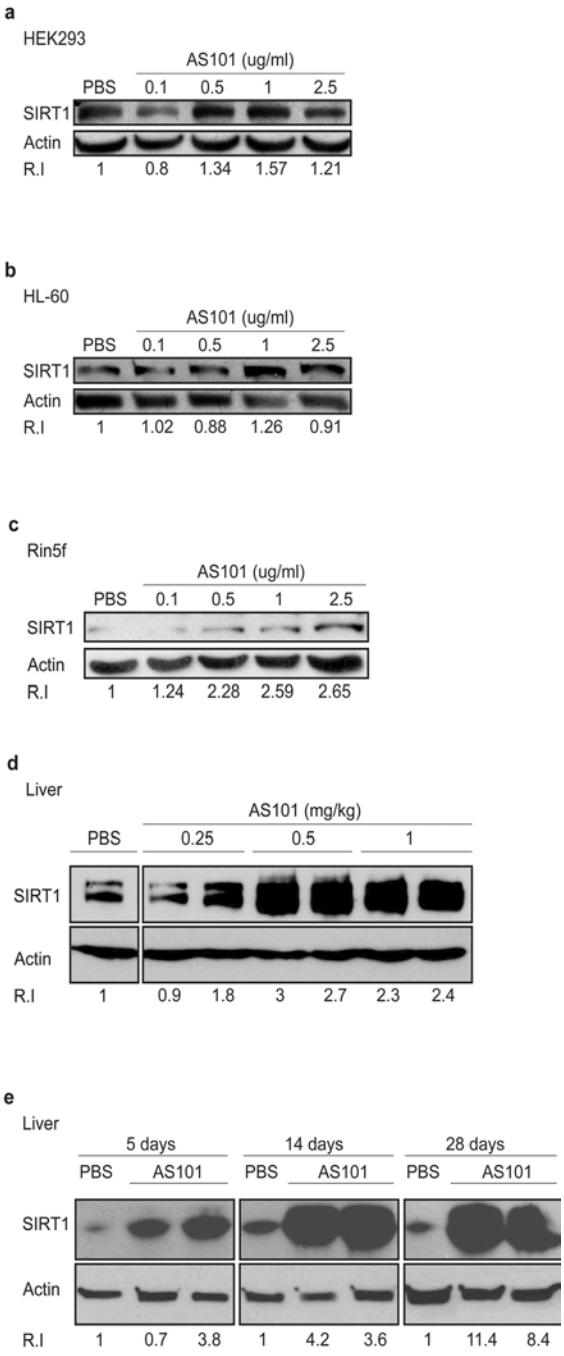

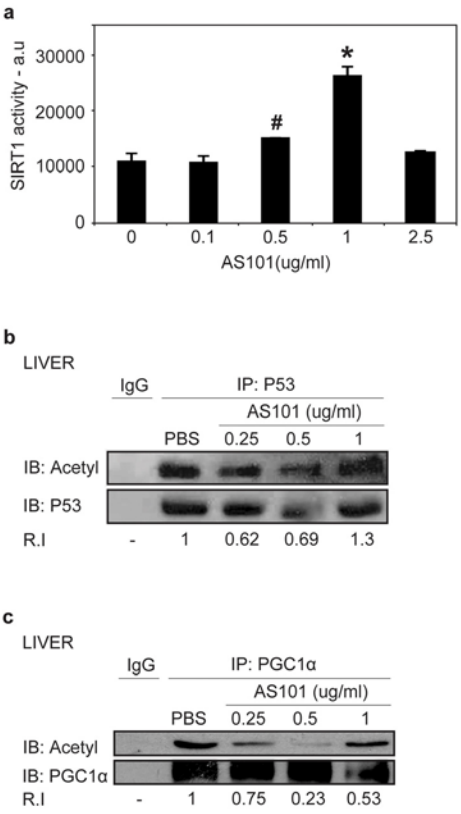

Figure 2. AS101 increases SIRT1 protein activity *in vitro* and *in vivo*. (**A**) AS101 induces activity of recombinant SIRT1. To determine in vitro SIRT1 activity, recombinant SIRT1 was incubated with AS101 at different concentration (0.1-2.5 μg/ml) or with PBS for 1 hour. Activity was examined based on SIRT1 de-acetylation of a fluorogenic acetylated peptide substrate. Results shown are average ±SEM of three independent experiments (#p=0.05,*p<0.05 versus PBS). (**B**-**C**) AS101 treatment reduces the acetylation levels of SIRT1 substrates. In vivo SIRT1 activity was measured by de-acetylation of its substrates PGC1α (**B**), and p53 (**C**) in rat liver extracts from treated for 14 days with AS101 or PBS at different concentrations. To detect acetylation levels, immuno-precipitated PGC1α and p53 were immunoblotted with antibodies against themselves and against pan acetyl antibodies. IgG was used as a control for the immunoprecipitation. Results shown are representative of the experiments from three independent replicates that gave similar results.

Figure 1. AS101 increases SIRT1 levels *in vitro* and in *vivo*. (**A**-**C**) AS101 increases SIRT1 expression in several cell lines. For in vitro studies, AS101 and PBS were added to cultures of HEK293 (**A**), HL-60 (**B**) and Rin-5f (**C**) cells at a concentration of 0.1-2.5μg/ml, for 48 hours. Each experiment was done in three independent replicates and representative blots are shown. (D-E) AS101 increases SIRT1 expression in healthy rat livers. For the in vivo assay, healthy rats were injected daily i.p with AS101 or PBS at different concentrations for 14 days (0.25-1mg/kg AS101(**D**)) and for different periods of time (0.5 mg/kg) (**E**)). (n=4 for each group.) SIRT1 levels in protein extracts from cell lines or rat liver, were measured by western blot analysis with anti- SIRT1 antibodies; actin was used as a loading control.

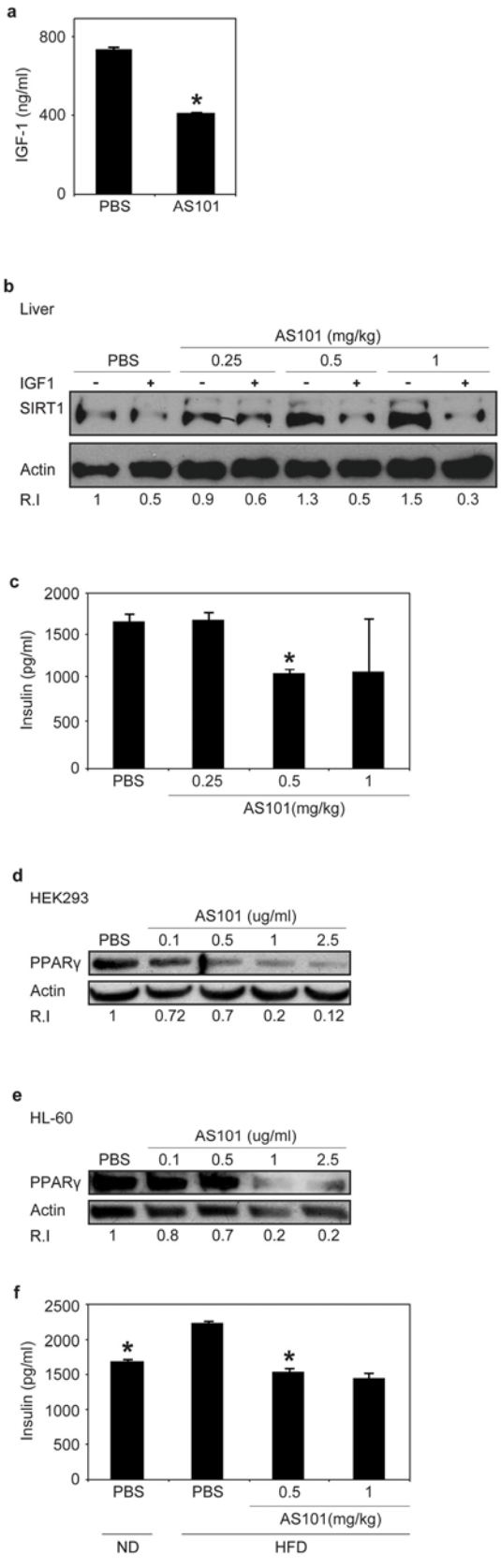

Figure 3. AS101 treatment increases SIRT1 expression through a possible mechanism of serum IGF-1 reduction. (A) Sera from AS101 treated rats contained significantly reduced IGF-1 levels. AS101 (0.5mg/kg) or PBS was injected daily i.p into healthy rats for 14 days and IGF-1 levels were measured by ELISA (*p<0.01 versus PBS). Error bars represent the ±SEM of all animals (AS101 n=5, PBS n-4). (**B**) SIRT1 expression increased in HEK293 cells incubated with AS101-treated rat serum. Supplementing with rIGF-1 back to normal levels (500 ng/ml) restored SIRT1 levels as in control mice. Cell extracts, were used for western blot analysis with anti- SIRT1 antibodies; Actin was used as a loading control. (C) Sera from AS101 treated rats contained significantly reduced insulin levels. AS101 (0.25-1mg/kg) and PBS were injected daily i.p to healthy rats for 14 days. Serum insulin levels were measured by ELISA kit after 4 hours starvation (*p<0.001 versus PBS) (n=3 in each group). (**D**-**E**) AS101 decreases PPARγ levels in tissue culture in vitro. AS101 and PBS were added to tissue cultures of HEK293 (D) and HL-60 (**E**) cells at the indicated concentrations for 48 hours. Western blots were probed with PPARγ antibody; actin was used as a loading control. (**F**) AS101 maintains normal insulin levels in HFD fed rats. AS101 (0.5-1mg/kg) and PBS was injected daily i.p into HFD/ND rats for 14 days. Serum insulin was measured by ELISA after 4 hours of fasting (*p<0.001 versus HFD+PBS, n=3 in each group). Error bars represent the SEM. Results shown in **B**, **D** and **E** are representative of three independent replicates that gave similar results (using different batches of rat sera).

The mechanism for the increase in SIRT1 expression in response to AS101

Previous studies indicated an inverse relationship between serum levels of insulin-like growth factor 1 (IGF-1) and SIRT1 expression in rats fed a calorie restricted (CR) diet [26], in an unknown mechanism. To explore the mechanism underlying the increase in SIRT1 expression, the effect of AS101 on IGF-1 levels were tested. Treatment with AS101 resulted in a significant reduction of serum IGF-1, compared to PBS control treatment ($p<0.001$) (Figure 3a). These findings show that AS101 treatment mimics the influence of CR on IGF-1 and SIRT1 levels.

To investigate whether IGF-1 or another mediator is responsible for the effect of AS101 on SIRT1 protein expression, a cell culture model was used. Human embryonic kidney (HEK) 293T cells were cultured in the presence of serum from AS101 or PBS treated rats. SIRT1 expression was significantly higher in HEK293 cells grown in the presence of AS101 treated rat serum compared to cells grown in serum from PBS treated rats (Figure 3b). Supplementing cells grown in AS101 sera with recombinant IGF-1 to a concentration equal to the IGF-1 concentration in the normal rat sera resulted in reduced SIRT1 protein expression (Figure 3b). These results suggest that AS101 increases SIRT1 protein expression, at least in part, by reducing IGF-1 levels.

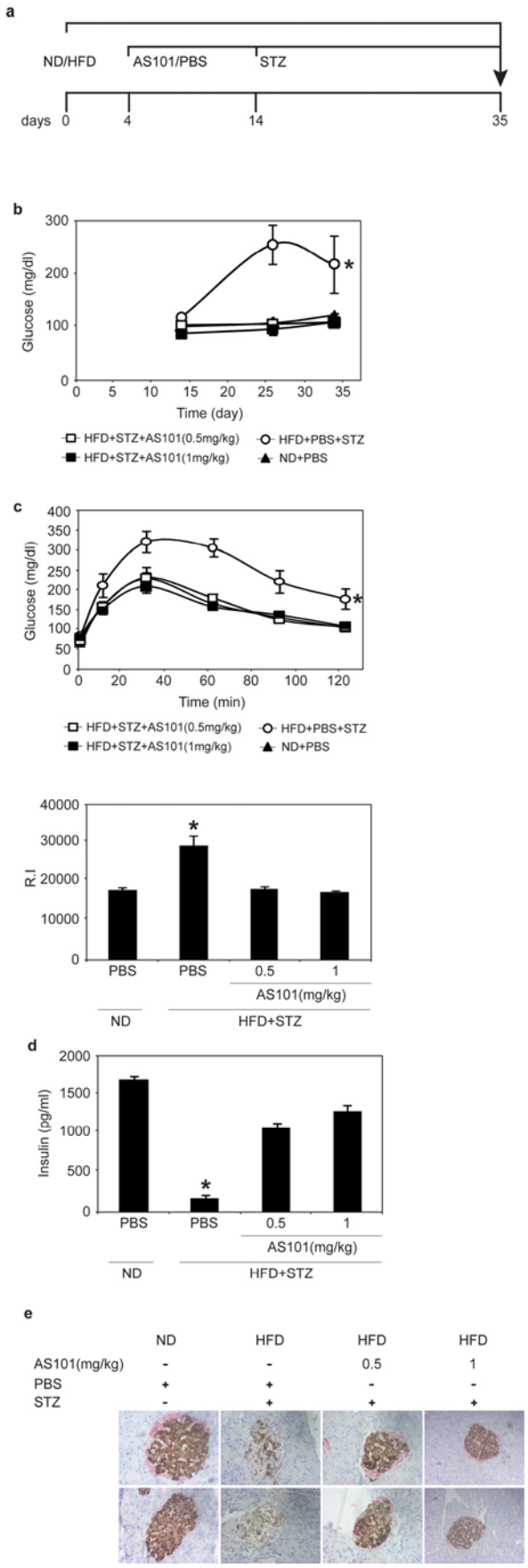

Figure 4. AS101 reverses HFD+STZ induced T2D. (A) Course of experiment. (B) AS101 treatment prevents glucose increase in HFD+STZ induced T2D rat model. (*p<0.01 all groups vs. HFD+PBS group, n=6 in each group). (C) AS101 treatment maintains glucose tolerance. On day 17 (following the onset of diabetes) rats were fasted for 12 hours before i.p injection of 2mg/kg glucose. (*p<0.001 versus HFD+PBS+STZ, n=6 in each group). The histogram represents the incremental area under the glucose curve. (D) AS101 treatment maintains proper insulin levels in the serum of rats after 4 hours starvation (*p<0.001 all groups versus HFD+PBS+STZ, n=6 for each group). (E) AS101 preserves insulin production in the pancreas. Immuno-histological staining for insulin (brown) and glucagon (red) of the rat pancreas. Pictures represent two out of the six animals in each group. Error bars represent the ±SEM.

The effect of AS101 on SIRT1 metabolic pathways

Similar to IGF-1 levels, previous studies have described an inverse correlation between serum levels of SIRT1 and insulin, which is a possible mechanisms through which SIRT1 regulates metabolic pathways [26]. Insulin levels were therefore examined in the rat sera after daily treatment with AS101 (0.25-1mg/kg) or PBS for 14 days. At a dose of 0.5 mg/kg AS101, treated rats showed 35% lower insulin levels versus the PBS treated rat sera ($p<0.001$) (Figure 3c). Picard et al., have shown that SIRT1 activation, promotes lipolysis and a reduction in fat accretion, due to repression of PPARγ. [24]. In order to examine if AS101 affects additional SIRT1 dependent metabolic pathways, the level of Peroxisome Proliferator Activated Receptor Gamma (PPARγ) was tested. Incubation of HEK293 and HL-60 cell lines with AS101 (0.1-2.5µg/ml) resulted in a dose dependent reduction in PPARγ protein expression relative to the control cells (Figure 3d-e). Incubation with AS101 reduced PPARγ expression in parallel to increased SIRT1 expression. The effects of AS101 on several important metabolic factors, led us to investigate the effects of AS101 on insulin resistance.

AS101 prevents development of insulin resistance *in vivo*

Treatment with AS101 reduced insulin levels and induced SIRT1 expression and activity, leading us to examine whether AS101 treatment can also mimic the reported inhibition of increased insulin levels in SIRT1 overexpressing or activated rodents fed with a high fat diet (HFD) [39, 40].

Normal rats were fed with HFD with AS101 or PBS for 14 days. In comparison to control rats fed with HFD and treated with PBS, serum insulin levels were significantly lower by 30% and 35% in rats treated with

AS101 at concentrations of 0.5 and 1 mg/kg respectively (Figure 3f). Moreover, AS101 treatment also prevented development of insulin resistance (data not shown). Thus, AS101 affects SIRT1 related metabolic pathways by changing the insulin levels.

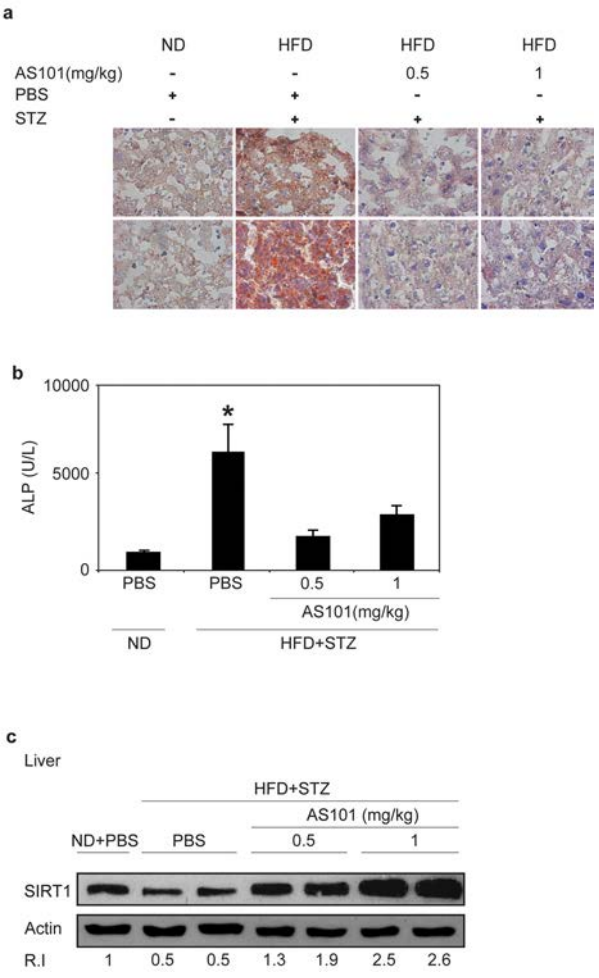

Figure 5. AS101 treatment protects rats from HFD+STZ induced hepatosteatosis. (**A**) Oil red staining of lipid droplets in frozen liver sections. Pictures represent two out of the six animals in each group. (**B**) AS101 treatment reduces serum ALP levels. (*p<0.05 decrease vs. diabetic group, n=6 in each group). (**C**) SIRT1 expression in the liver. Liver extracts were used for western blot analysis with anti- SIRT1 antibodies; actin was used as a loading control.

AS101 treatment prevents T2D in the HFD+STZ rat model

Next, we tested the ability of AS101 to prevent T2D in a rat model. Diabetes was induced by a combination of HFD and a single low dose Streptozotocin (STZ) injection, which is toxic to insulin-producing beta cells [36]. The rats were fed a high fat diet (HFD) for the whole experiment period, and two weeks into the experiment the rats were injected with an intraperitoneal injection of a low dose of STZ (35 mg/kg) (see figure 4a for experimental design). The effect of AS101 was first examined when administered before the onset of hyperglycemia. This experiment included four groups: Control group of normal diet (ND) fed rats injected with PBS (ND + PBS) (group 1), Diabetic groups of HFD fed rats with single dose STZ divided to treatment injected with PBS as control (HFD + STZ + PBS) (group 2), AS101 treatment in two concentrations 0.5 mg/kg (group 3) or 1 mg/kg (group 4) (HFD + STZ + 0.5 mg/kg AS101 and HFD + STZ + 1 mg/kg AS101 respectively). AS101 treatment started four days after the beginning of the HFD and was injected daily for 14 days and then continued every other day. As seen in Figure 4b, pretreatment with AS101 prevented the increase in blood glucose ($P<0.01$), and preserved optimal glucose tolerance (Figure 4c) and insulin levels ($p<0.001$) (Figure 4d). In addition, immunostaining of insulin and glucagon indicated that treatment with AS101 preserved normal insulin production by the pancreatic β cells and maintained the islets structure [41] (Figure 4e). Finally, AS101 treatment reduced serum triglycerides to a normal level (data not shown). Thus, AS101 treatment prevents hyperglycemia associated with T2D and some of the symptoms of the disease in the HFD+STZ rat model.

Chronic HFD causes an accumulation of lipids in the liver leading to fatty liver disease [42] and SIRT1 was recently shown as a potential therapeutic target for treatment fatty liver disease [43, 44]. Therefore, frozen liver sections were stained with Oil Red to follow the effect of AS101 on hepatic accumulation of lipids. AS101 (0.5 and 1 mg/kg) treatment protected rats from HFD+STZ induced hepatosteatosis and retained healthy tissue (Figure 5a). In agreement with these findings, Alkaline Phosphatase (ALP), a marker of liver damage, was examined. ALP levels increased seven fold in the serum of HFD + STZ diabetic rats; these increases were blocked in AS101 treated rats and ALP levels remained similar to the ALP levels of normal rats ($p<0.05$) (Figure 5b). Further, in agreement with Peng et al, [45] the baseline levels of SIRT1 were decreased in the liver of mice treated with HFD and STZ (Figure 5c), in contrast, treatment with AS101 restored to normal or elevated the levels of SIRT1 protein in comparison to the diabetic rats (Figure 5c). These findings show that AS101 treatment started before the manifestation of hyperglycemia in the HFD+STZ T2D model prevented onset of symptoms.

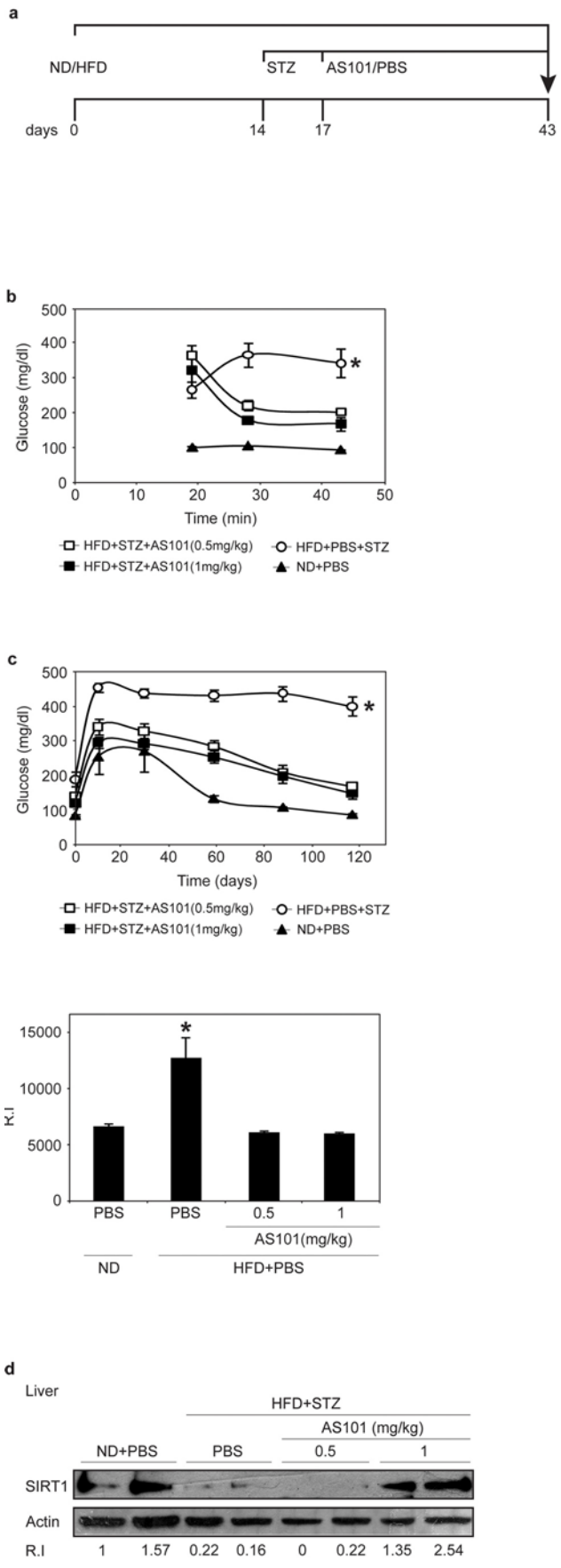

Figure 6. AS101 treatment after disease induction results in partial beneficial effects in the HFD+STZ T2D rat model. (**A**) Course of experiment. (**B**) AS101 reduced glucose levels in HFD+STZ T2D rat model. Glucose levels were measured in peripheral blood at different times (*p<0.05 all groups vs. HFD+PBS group, n=6 in each HFD group, n=3 in ND group). (**C**) AS101 treatment restores proper glucose tolerance. Rats fasted for 12 hours before i.p injection of 2mg/kg glucose. (*p<0.01 versus HFD+PBS+STZ, n=6 in each group). The histogram represents the incremental area under the glucose curve. (**D**) AS101 (1 mg/kg) treated rats show higher SIRT1 protein levels in liver extract prepared at the end of the experiment. Western blot analysis was done with anti- SIRT1 antibodies; actin was used as a loading control. Error bars represent the±SEM.

Treatment of T2D with AS101 in the HFD+STZ rat model

The effect of treatment with AS101 after the onset of disease (glucose >250 mg/dL) was also tested. Here, AS101/PBS treatments were given after 17 days of HFD and 3 days after a single low dose of STZ (Figure 6a). AS101 treatment of diabetic rats resulted in significant beneficial effects. As shown in Figure 6b, after only 3 days of AS101 treatment, blood glucose levels were significantly reduced ($p<0.05$). Glucose tolerance test (GTT) assay, demonstrated that AS101 significantly ($p<0.01$) improved the glucose clearance in HFD+STZ treated rats to a level similar to that of the PBS treated rats under regular diet (Figure 6c).

Finally, these beneficial effects were accompanied by increases in SIRT1 protein expression in rats treated with 1 mg/kg AS101 (Figure 6d).

Taken together, these results suggest the use of AS101 as a novel pharmacological means to regulate metabolic disorders by increasing SIRT1 levels and activity, and interfering with T2D development and progression.

DISCUSSION

This study demonstrates that AS101 can decrease the pathological symptoms and block the development of T2D disease in rat model. We also showed that AS101 enhances SIRT1 expression and activity. Furthermore, AS101 exhibited the most significant improvements of T2D when treatment was given at the onset of diabetes induction, whereas treatment after the onset of the disease resulted in partial restoration of normal glucose metabolism. We further demonstrated an association between the ability of AS101 to increase SIRT1 protein levels and the beneficial effects on glucose metabolism [46-49].

In some animal models of T2D, SIRT1 protein levels decrease [50-52], suggesting a role for SIRT1 in regulating T2D. In support to this notion, mice overexpressing SIRT1 are protected from the metabolic damage of HFD, including the development of T2D, via induction of antioxidants and stimulation of PGC1alpha [39]. Thus, this unique affect of AS101 on SIRT1 protein *in vivo* and *in vitro* may lead to a new therapeutic approach [49]. The gradual progression of T2D in patients [53] suggests the possibility of therapeutic intervention at several stages of the disease process. For example, by regulating metabolic disorders via increasing SIRT1 levels to inhibit disease progression. The results described in this study, signify the clinical value of AS101 in treating T2D. Moreover, whereas most SIRT1 activating agents described to-date affect only protein activity, this study shows that AS101, a non toxic compound, increases both SIRT1 protein expression and activity. Thus, the therapeutic potential of AS101 against T2D is at least similar to those achieved by other SIRT1 activators.

We suggest that SIRT1 is responsible to the protective effect of AS101 in the current rat model of T2D. Similar findings were observed in transgenic mice over-expressing SIRT1 that were protected against obesity dependent impaired glucose tolerance [39]. Importantly, other features of AS101 may also mediate the beneficial activities of the compound. AS101 may influence the metabolic syndrome through interference in insulin pathways. In addition, anti inflammatory and anti apoptotic properties [32, 35, 54] of the compound may potentially enable it to preserve β cells.

The insulin signal cascades, which include PKB/Akt through PI3K and mTOR, stimulate S6K1, resulting in a negative feedback, which may cause insulin resistance [55, 56]. AS101 was shown to inhibit PKB/Akt in a model of multiple myeloma [57]. This inhibition may be mediated through reduction in the levels of growth factors [34], analogous to the reduction of insulin or IGF-1, as was shown here.

In addition, AS101 has an anti apoptotic effect due to its selective inhibition of cysteine protease proteins, notably caspases 1, 3, and 9 *in vitro* and *in vivo* [31-33, 54, 58]. Caspase1 inhibition provides the compound with anti inflammatory properties by repressing specific inflammation cytokines including IL1-β, IL-18 and TNFα. [59]. IL1-β and TNFα induce IRS-2 phosphorylation, which leads to insulin resistance, followed by the apoptotic death of β cells [60, 61]; the inhibition of cytokines by AS101 may contribute to β cell preservation. In this study, AS101 treatment indeed preserved β cells as shown by immunohistochemical staining (Figure 4e). In addition to the inhibition of inflammatory cytokines, AS101 can positively affect β cell production via its known immunomodulator function, which reduces IL-10, and thereby enhances GDNF production [32, 35, 62]. GDNF increases β cell production and prevents their apoptosis in an STZ model [63].

Numerous studies have been performed to identify a compound that promotes SIRT1 protein activity only [64-66]. In comparison to previously published SIRT1 activators, AS101 have several unique properties. First, AS101 enhance the expression and activity of the SIRT1 whereas the other activators enhanced SIRT1 activity only. Second, no side effects were found for AS101 while other SIRT1 activators results in significant side effects when supplemented in high concentrations [67-69].

Here, we suggest that AS101, a non toxic compound currently in clinical trials for other indications [70, 71], may be effective as a treatment for T2D by enhancing SIRT1 protein expression and activity.

Understanding the mechanisms and actions of AS101 in T2D, including the elucidation of the role of SIRT1 upregulation as well as additional properties of AS101 that might evoke beneficial effects, may contribute to the development of new pharmacological means to control this devastating disease.

MATERIALS AND METHODS

Cell cultures and experimental treatment. HEK293 cells were maintained in DMEM (Biological Industries, Beit Haemek, Israel) containing 10% FBS (Biological Industries, Beit Haemek Israel) and 1% Pen/strep (100U/ml) (Biological Industries, Beit Haemek, Israel). HL-60 and Rin5f were maintained in RPMI (Biological Industries, Beit Haemek Israel) containing 10% FBS and 1% Pen/strep (100U/ml) at 370C in a 5% CO2 humidified atmosphere. In some of the experiments, FBS was replaced with serum from AS101/PBS treated rats; in those experiments the cells were plated with commercial serum, and serum replaced after the cells adhered. After serum replacement, cells were incubated for 48 hours, and were then lysed with a lysis buffer (1M Tris (pH=7.4), 1.5M NaCl, 1% Triton-X, 10% Glycerol, 50mM EDTA (pH=8), 0.1M Sodium vanadate, 0.1M PMSF, 0.1% protease inhibitor cocktail (Calbiochem, San Diego, CA, USA)).

PGC1α and p53 acetylation assays. PGC1α and p53 lysine acetylation was analyzed by immunoprecipitation followed by western blot using an antibody specific for

acetyl lysine (Cell signaling, Danvers, MA, USA). Liver extracts of AS101 or PBS treated rats after 14 days of treatment were immunoprecipitated using anti-PGC1α and anti-p53 antibodies. The immuno-precipitated complex was divided into equal aliquots and further immunoblotted with antibodies against the acetylated residue, stripped and reblotted against the substrate. IgG of irrelevant specificity was used as a control for the immunoprecipitation.

Immunoblotting. Samples were boiled for 5 minutes, electrophoresed on 8% SDS-PAGE, transferred to nitrocellulose, and immunoblotted with specific Abs (SIRT1, p53, PGC1-α, and PPARγ, Santa Cruz (Heidelberg, Germany); actin, HRP (Sigma Aldrich, St. Louis, MO, USA). Blots were developed using horseradish peroxidase-conjugated secondary Ab's and the ECL detection system (Thermo scientific Pierce protein research protein products, Rockford, IL, USA). Animal Experiments. Male Sprague Dawley rats (160-180 gr) were purchased from Harlan Laboratories (Jerusalem, Israel). Animal experiments were performed in accordance with approved institutional protocols and all experiments were approved by the Institutional Animal Care and Use Committee.

T2D model in rats. The rats were allocated into two dietary regimens by feeding them either a normal diet (ND, n=6 animals) or high fat diet (HFD, n=18) (60% fat) ad libitum, respectively, for a period of 1 month. After 2 weeks of dietary manipulation, the HFD fed rats were injected intraperitoneally (i.p) with a low dose of STZ, Calbiochem (San Diego, CA, USA) (35 mg/kg). The rats were maintained on their respective diets until the end of the study. AS101 (0.5 or 1 mg/kg) or PBS were injected i.p daily for 14 days, and then every 2 days. The T2D model last for 34 days, and treatment with AS101 or PBS started from the fourth day of the high fat diet (Figure 4a) or for 43 days with AS101 or PBS starting on day 17 (Figure 6a).

Blood glucose level, GTT. After 12 hr fast, rats received an i.p injection of 2 g/kg glucose, Sigma Aldrich (St. Louis, MO, USA). Blood glucose concentrations were measured via tail bleed at the indicated times before and after the injections. All glucose measurements were performed using a glucometer, Free Style Freedom (Alameda, CA, USA).

Protein level/activity. SIRT1 activity levels were determined using recombinant SIRT1 (b; SIRT1 was incubated with AS101 or PBS at different concentrations for 1 hour. Activity was measured using the SIRT1 Fluorometric Activity Assay/Drug Discovery Kit Biomol (Exter, United Kingdom). IGF-1 levels were determined in the serum of AS101/PBS treated rats using Active IGF-1 Kit, DSL (Webster, Texas, USA). Insulin levels were determined in treated rat serum using a rat/mouse insulin ELISA kit, Millipore (Billerica, MA, USA).

Metabolic measurements. ALP was determined at the Veterinary Institute service in Beit Dagan, Israel.

Oil Red O staining. Frozen liver was sectioned serially at 4μm thickness with a cytostat, placed on slides, and dried for 15 min at 37°C. Sections were then fixed for 10 min in neutral buffered 10% formalin. To detect neutral lipid accumulation, sections were stained with Red Oil 'O' for 10 min, counterstained with hematoxylin for 2 min, and coverslipped with a water-based mounting medium.

Insulin and glucagon staining. Pancreatic paraffin sections were prepared and stained with Picture – double staining kit- insulin and glucagons, Zymed Laboratories, Inc. (San Francisco, CA, USA).

Statistical Analysis. For repeated experiments, data are presented as means +/-S.E.M. Statistical analysis was performed using a two tailed unpaired Student's t-test. $P<0.05$ or 0.01 (as specified) was considered to be statistically significant. For several time course experiments, ANOVA statistical analysis was performed.

ACKNOWLEDGEMENTS

This work was partly supported by Mr. Edmundo Safdié of Sao Paulo, Brazil, by The Dr. Tovi Comet-Walerstein Cancer Research Chair and by The Dave and Florence Muskovitz Chair in Cancer Research for B.S. and grants from the Israeli Academy of Sciences, Binational US-Israel Science Foundation, Israel Cancer Association, Koret Foundation, the Israel Cancer Research Fund, I-Core, the Israel Health Ministry and the ERC: European Research Council for H.Y.C. This study is part of MHS Ph.D's thesis.

CONFLICT OF INTERESTS STATEMENT

The authors of this manuscript have no conflict of interest to declare.

REFERENCES

1. Zierath JR, He L, Guma A, Odegoard Wahlstrom E, Klip A and Wallberg-Henriksson H. Insulin action on glucose transport and plasma membrane GLUT4 content in skeletal muscle from patients with NIDDM. Diabetologia. 1996;39:1180-1189.

2. Doria A, Patti ME and Kahn CR. The emerging genetic architecture of type 2 diabetes. Cell Metab. 2008; 8:186-200.

3. Kahn CR, Vicent D and Doria A. Genetics of non-insulin-dependent (type-II) diabetes mellitus. Annu Rev Med. 1996; 47:509-531.

4. Zimmet P, Alberti KG and Shaw J. Global and societal implications of the diabetes epidemic. Nature. 2001; 414:782-787.

5. Saltiel AR. New perspectives into the molecular pathogenesis and treatment of type 2 diabetes. Cell. 2001; 104:517-529.

6. Chang-Chen KJ, Mullur R and Bernal-Mizrachi E. Beta-cell failure as a complication of diabetes. Rev Endocr Metab Disord. 2008; 9:329-343.

7. Scheen AJ and Lefebvre PJ. Insulin action in man. Diabetes Metab. 1996; 22:105-110.

8. Das SK and Chakrabarti R. Non-insulin dependent diabetes mellitus: present therapies and new drug targets. Mini Rev Med Chem. 2005; 5:1019-1034.

9. Buchanan TA, Xiang AH, Peters RK, Kjos SL, Marroquin A, Goico J, Ochoa C, Tan S, Berkowitz K, Hodis HN and Azen SP. Preservation of pancreatic beta-cell function and prevention of type 2 diabetes by pharmacological treatment of insulin resistance in high-risk hispanic women. Diabetes. 2002; 51:2796-2803.

10. Prentki M and Nolan CJ. Islet beta cell failure in type 2 diabetes. J Clin Invest. 2006; 116:1802-1812.

11. Blander G and Guarente L. The Sir2 family of protein deacetylases. Annu Rev Biochem. 2004; 73:417-435.

12. Vaquero A, Scher M, Lee D, Erdjument-Bromage H, Tempst P and Reinberg D. Human SirT1 interacts with histone H1 and promotes formation of facultative heterochromatin. Mol Cell. 2004; 16:93-105.

13. Frye RA. Phylogenetic classification of prokaryotic and eukaryotic Sir2-like proteins. Biochem Biophys Res Commun. 2000; 273:793-798.

14. Afshar G and Murnane JP. Characterization of a human gene with sequence homology to Saccharomyces cerevisiae SIR2. Gene. 1999; 234(1):161-168.

15. Haigis MC and Guarente LP. Mammalian sirtuins--emerging roles in physiology, aging, and calorie restriction. Genes Dev. 2006; 20:2913-2921.

16. Langley E, Pearson M, Faretta M, Bauer UM, Frye RA, Minucci S, Pelicci PG and Kouzarides T. Human SIR2 deacetylates p53 and antagonizes PML/p53-induced cellular senescence. EMBO J. 2002; 21:2383-2396.

17. Cohen HY, Lavu S, Bitterman KJ, Hekking B, Imahiyerobo TA, Miller C, Frye R, Ploegh H, Kessler BM and Sinclair DA. Acetylation of the C terminus of Ku70 by CBP and PCAF controls Bax-mediated apoptosis. Mol Cell. 2004; 13:627-638.

18. Qiao L and Shao J. SIRT1 regulates adiponectin gene expression through Foxo1-C/enhancer-binding protein alpha transcriptional complex. J Biol Chem. 2006; 281:39915-39924.

19. Aoyama H, Daitoku H and Fukamizu A. Nutrient control of phosphorylation and translocation of Foxo1 in C57BL/6 and db/db mice. Int J Mol Med. 2006; 18:433-439.

20. Dowell P, Otto TC, Adi S and Lane MD. Convergence of peroxisome proliferator-activated receptor gamma and Foxo1 signaling pathways. J Biol Chem. 2003; 278:45485-45491.

21. Chong ZZ and Maiese K. Enhanced tolerance against early and late apoptotic oxidative stress in mammalian neurons through nicotinamidase and sirtuin mediated pathways. Curr Neurovasc Res. 2008; 5:159-170.

22. Brunet A, Sweeney LB, Sturgill JF, Chua KF, Greer PL, Lin Y, Tran H, Ross SE, Mostoslavsky R, Cohen HY, Hu LS, Cheng HL, Jedrychowski MP, et al. Stress-dependent regulation of FOXO transcription factors by the SIRT1 deacetylase. Science. 2004; 303:2011-2015.

23. Rodgers JT, Lerin C, Gerhart-Hines Z and Puigserver P. Metabolic adaptations through the PGC-1 alpha and SIRT1 pathways. FEBS Lett. 2008; 582:46-53.

24. Picard F, Kurtev M, Chung N, Topark-Ngarm A, Senawong T, Machado De Oliveira R, Leid M, McBurney MW and Guarente L. Sirt1 promotes fat mobilization in white adipocytes by repressing PPAR-gamma. Nature. 2004; 429:771-776.

25. Bordone L, Motta MC, Picard F, Robinson A, Jhala US, Apfeld J, McDonagh T, Lemieux M, McBurney M, Szilvasi A, Easlon EJ, Lin SJ and Guarente L. Sirt1 regulates insulin secretion by repressing UCP2 in pancreatic beta cells. PLoS Biol. 2006; 4:e31.

26. Cohen HY, Miller C, Bitterman KJ, Wall NR, Hekking B, Kessler B, Howitz KT, Gorospe M, de Cabo R and Sinclair DA. Calorie restriction promotes mammalian cell survival by inducing the SIRT1 deacetylase. Science. 2004; 305:390-392.

27. Lee JH, Song MY, Song EK, Kim EK, Moon WS, Han MK, Park JW, Kwon KB and Park BH. Overexpression of SIRT1 protects pancreatic beta-cells against cytokine toxicity by suppressing the nuclear factor-kappaB signaling pathway. Diabetes. 2009; 58:344-351.

28. Sredni B, Caspi RR, Klein A, Kalechman Y, Danziger Y, Ben Ya'akov M, Tamari T, Shalit F and Albeck M. A new immunomodulating compound (AS-101) with potential therapeutic application. Nature. 1987; 330:173-176.

29. Sredni B, Xu RH, Albeck M, Gafter U, Gal R, Shani A, Tichler T, Shapira J, Bruderman I, Catane R, Kaufman B, Whisnant JK, Mettinger KL, et al. The protective role of the immunomodulator AS101 against chemotherapy-induced alopecia studies on human and animal models. Int J Cancer. 1996; 65:97-103.

30. Sredni B, Weil M, Khomenok G, Lebenthal I, Teitz S, Mardor Y, Ram Z, Orenstein A, Kershenovich A, Michowiz S, Cohen YI, Rappaport ZH, Freidkin I, et al. Ammonium trichloro-(dioxoethylene-o,o')tellurate (AS101) sensitizes tumors to chemotherapy by inhibiting the tumor interleukin 10 autocrine loop. Cancer Res. 2004; 64:1843-1852.

31. Albeck A, Weitman H, Sredni B and Albeck M. Tellurium Compounds: Selective Inhibition of Cysteine Proteases and Model Reaction with Thiols. Inorg chem. 1998; 37(8):1704-1712.

32. Sredni B, Geffen-Aricha R, Duan W, Albeck M, Shalit F, Lander HM, Kinor N, Sagi O, Albeck A, Yosef S, Brodsky M, Sredni-Kenigsbuch D, Sonino T, et al. Multifunctional tellurium molecule protects and restores dopaminergic neurons in Parkinson's disease models. FASEB J. 2007; 21:1870-1883.

33. Strassmann G, Kambayashi T, Jacob CO and Sredni D. The immunomodulator AS-101 inhibits IL-10 release and augments TNF alpha and IL-1 alpha release by mouse and human mononuclear phagocytes. Cell Immunol. 1997; 176:180-185.

34. Hayun M, Saida H, Albeck M, Peled A, Haran-Ghera N and Sredni B. Induction therapy in a multiple myeloma mouse model using a combination of AS101 and melphalan, and the activity of AS101 in a tumor microenvironment model. Exp Hematol. 2009; 37:593-603.

35. Kalechman Y, Sredni B, Weinstein T, Freidkin I, Tobar A, Albeck M and Gafter U. Production of the novel mesangial autocrine growth factors GDNF and IL-10 is regulated by the immunomodulator AS101. J Am Soc Nephrol. 2003; 14:620-630.

36. Srinivasan K, Viswanad B, Asrat L, Kaul CL and Ramarao P. Combination of high-fat diet-fed and low-dose streptozotocin-treated rat: a model for type 2 diabetes and pharmacological screening. Pharmacol Res. 2005; 52:313-320.

37. Smith J. Human Sir2 and the 'silencing' of p53 activity. Trends Cell Biol. 2002; 12:404-406.

38. Rodgers JT, Lerin C, Haas W, Gygi SP, Spiegelman BM and Puigserver P. Nutrient control of glucose homeostasis through a complex of PGC-1alpha and SIRT1. Nature. 2005; 434:113-118.

39. Pfluger PT, Herranz D, Velasco-Miguel S, Serrano M and Tschop MH. Sirt1 protects against high-fat diet-induced metabolic damage. Proc Natl Acad Sci U S A. 2008; 105:9793-9798.

40. Minor R, Baur J, Gomes A, Ward T, Csiszar A, Mercken E, Abdelmohsen K, Shin Y, Canto C, Scheibye-Knudsen M, Krawczyk M, Irusta P, Martín-Montalvo A, et al. SRT1720 improves survival and healthspan of obese mice. scientific reports. 2011; 1.

41. Hopcroft DW, Mason DR and Scott RS. Structure-function relationships in pancreatic islets: support for intraislet modulation of insulin secretion. Endocrinology. 1985; 117:2073-2080.

42. Marchesini G, Bugianesi E, Forlani G, Cerrelli F, Lenzi M, Manini R, Natale S, Vanni E, Villanova N, Melchionda N and Rizzetto M. Nonalcoholic fatty liver, steatohepatitis, and the metabolic syndrome. Hepatology. 2003; 37:917-923.

43. Colak Y, Ozturk O, Senates E, Tuncer I, Yorulmaz E, Adali G, Doganay L and Enc FY. SIRT1 as a potential therapeutic target for treatment of nonalcoholic fatty liver disease. Med Sci Monit. 2011; 17:HY5-9.

44. Escande C, Chini CC, Nin V, Dykhouse KM, Novak CM, Levine J, van Deursen J, Gores GJ, Chen J, Lou Z and Chini EN. Deleted in breast cancer-1 regulates SIRT1 activity and contributes to high-fat diet-induced liver steatosis in mice. J Clin Invest. 2010; 120:545-558.

45. Peng Y, Rideout D, Rakita S, Lee J and Murr M. Diet-induced obesity associated with steatosis, oxidative stress, and inflammation in liver. Surg Obes Relat Dis. 2011.

46. Sun C, Zhang F, Ge X, Yan T, Chen X, Shi X and Zhai Q. SIRT1 improves insulin sensitivity under insulin-resistant conditions by repressing PTP1B. Cell Metab. 2007; 6:307-319.

47. Deng XQ, Chen LL and Li NX. The expression of SIRT1 in nonalcoholic fatty liver disease induced by high-fat diet in rats. Liver Int. 2007; 27:708-715.

48. Lagouge M, Argmann C, Gerhart-Hines Z, Meziane H, Lerin C, Daussin F, Messadeq N, Milne J, Lambert P, Elliott P, Geny B, Laakso M, Puigserver P, et al. Resveratrol improves mitochondrial function and protects against metabolic disease by activating SIRT1 and PGC-1alpha. Cell. 2006; 127:1109-1122.

49. Banks AS, Kon N, Knight C, Matsumoto M, Gutierrez-Juarez R, Rossetti L, Gu W and Accili D. SirT1 gain of function increases energy efficiency and prevents diabetes in mice. Cell Metab. 2008; 8:333-341.

50. Deng X, Cheng J, Zhang Y, Li N and Chen L. Effects of caloric restriction on SIRT1 expression and apoptosis of islet beta cells in type 2 diabetic rats. Acta Diabetol. 2010; 47:177-185.

51. de Kreutzenberg SV, Ceolotto G, Papparella I, Bortoluzzi A, Semplicini A, Dalla Man C, Cobelli C, Fadini GP and Avogaro A. Downregulation of the longevity-associated protein sirtuin 1 in insulin resistance and metabolic syndrome: potential biochemical mechanisms. Diabetes. 2010; 59:1006-1015.

52. Song R, Xu W, Chen Y, Li Z, Zeng Y and Fu Y. The expression of Sirtuins 1 and 4 in peripheral blood leukocytes from patients with type 2 diabetes. Eur J Histochem. 2011; 55:e10.

53. Sesti G. Pathophysiology of insulin resistance. Best Pract Res Clin Endocrinol Metab. 2006; 20:665-679.

54. Brodsky M, Hirsh S, Albeck M and Sredni B. Resolution of inflammation-related apoptotic processes by the synthetic tellurium compound, AS101 following liver injury. J Hepatol. 2009; 51:491-503.

55. Um SH, Frigerio F, Watanabe M, Picard F, Joaquin M, Sticker M, Fumagalli S, Allegrini PR, Kozma SC, Auwerx J and Thomas G. Absence of S6K1 protects against age- and diet-induced obesity while enhancing insulin sensitivity. Nature. 2004; 431:200-205.

56. Um SH, D'Alessio D and Thomas G. Nutrient overload, insulin resistance, and ribosomal protein S6 kinase 1, S6K1. Cell Metab. 2006; 3:393-402.

57. Hayun M, Naor Y, Weil M, Albeck M, Peled A, Don J, Haran-Ghera N and Sredni B. The immunomodulator AS101 induces growth arrest and apoptosis in multiple myeloma: association with the Akt/survivin pathway. Biochem Pharmacol. 2006; 72:1423-1431.

58. Okun E, Arumugam TV, Tang SC, Gleichmann M, Albeck M, Sredni B and Mattson MP. The organotellurium compound ammonium trichloro(dioxoethylene-0,0') tellurate enhances neuronal survival and improves functional outcome in an ischemic stroke model in mice. J Neurochem. 2007; 102:1232-1241.

59. Brodsky M, Yosef S, Galit R, Albeck M, Longo DL, Albeck A and Sredni B. The synthetic tellurium compound, AS101, is a novel inhibitor of IL-1beta converting enzyme. J Interferon Cytokine Res. 2007; 27:453-462.

60. Jager J, Gremeaux T, Cormont M, Le Marchand-Brustel Y and Tanti JF. Interleukin-1beta-induced insulin resistance in adipocytes through down-regulation of insulin receptor substrate-1 expression. Endocrinology. 2007; 148:241-251.

61. Nieto-Vazquez I, Fernandez-Veledo S, Kramer DK, Vila-Bedmar R, Garcia-Guerra L and Lorenzo M. Insulin resistance associated to obesity: the link TNF-alpha. Arch Physiol Biochem. 2008; 114:183-194.

62. Okun E, Saida H, Albeck M, Sredni B and Avtalion RR. Upregulation of carp GDNF mRNA by the immunomodulator AS101. Dev Comp Immunol. 2006; 30:441-446.

63. Mwangi S, Anitha M, Mallikarjun C, Ding X, Hara M, Parsadanian A, Larsen CP, Thule P, Sitaraman SV, Anania F and Srinivasan S. Glial cell line-derived neurotrophic factor increases beta-cell mass and improves glucose tolerance. Gastroenterology. 2008; 134:727-737.

64. Kaeberlein M, McDonagh T, Heltweg B, Hixon J, Westman EA, Caldwell SD, Napper A, Curtis R, DiStefano PS, Fields S, Bedalov A and Kennedy BK. Substrate-specific activation of sirtuins by resveratrol. J Biol Chem. 2005; 280:17038-17045.

65. Borra MT, Smith BC and Denu JM. Mechanism of human SIRT1 activation by resveratrol. J Biol Chem. 2005; 280:17187-17195.

66. Chen KH, Cheng ML, Jing YH, Chiu DT, Shiao MS and Chen JK. Resveratrol ameliorates metabolic disorders and muscle wasting in streptozotocin-induced diabetic rats. Am J Physiol Endocrinol Metab. 2011.

67. Espin JC, Garcia-Conesa MT and Tomas-Barberan FA. Nutraceuticals: facts and fiction. Phytochemistry. 2007; 68:2986-3008.

68. Vang O, Ahmad N, Baile CA, Baur JA, Brown K, Csiszar A, Das DK, Delmas D, Gottfried C, Lin HY, Ma QY, Mukhopadhyay P, Nalini N, et al. What is new for an old molecule? Systematic review and recommendations on the use of resveratrol. PLoS One. 2011; 6:e19881.

69. Engineer MS BT, Newman RA, Siddick ZH. Pharmacology of AS101 after multiple doses of dogs. Proc Am Assoc Cancer Res. 1989; 30:584.

70. Sredni B, Tichler T, Shani A, Catane R, Kaufman B, Strassmann G, Albeck M and Kalechman Y. Predominance of TH1 response in tumor-bearing mice and cancer patients treated with AS101. J Natl Cancer Inst. 1996; 88:1276-1284.

71. Sredni B, Albeck M, Tichler T, Shani A, Shapira J, Bruderman I, Catane R, Kaufman B and Kalechman Y. Bone marrow-sparing and prevention of alopecia by AS101 in non-small-cell lung cancer patients treated with carboplatin and etoposide. J Clin Oncol. 1995; 13:2342-2353.

SUPPLEMENTARY FIGURE

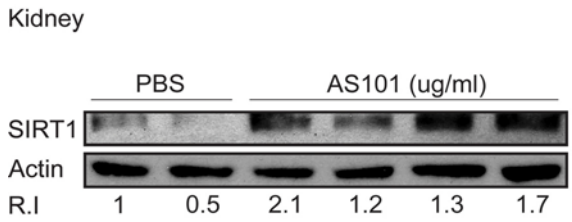

Supplementary Figure 1. AS101 increases SIRT1 levels in rats kidneys. AS101 increases SIRT1 expression in healthy rat kidneys. For *in vivo* assay, healthy rats were injected daily i.p with AS101 (0.5 mg/kg) or PBS for 14 days. (n=4 for each group.) kidney extracts, were used for western blot analysis with anti-SIRT1 antibodies; actin was used as a loading control.

Research Paper

Once again on rapamycin-induced insulin resistance and longevity: despite of or owing to

Mikhail V. Blagosklonny

Department of Cell Stress Biology, Roswell Park Cancer Institute, Buffalo, NY, USA

Key words: *aging, diabetes, retinopathy, nephropathy, diseases, anti-aging drugs, growth hormone*
Received: *5/20/12; Accepted: 5/30/12; Published: 5/31/12* doi:10.18632/aging.100461
Correspondence to: *Mikhail V. Blagosklonny, MD/PhD;* ***E-mail:*** *blagosklonny@oncotarget.com*

Abstract: Calorie restriction (CR), which deactivates the nutrient-sensing mTOR pathway, slows down aging and prevents age-related diseases such as type II diabetes. Compared with CR, rapamycin more efficiently inhibits mTOR. Noteworthy, severe CR and starvation cause a reversible condition known as "starvation diabetes." As was already discussed, chronic administration of rapamycin can cause a similar condition in some animal models. A recent paper published in Science reported that chronic treatment with rapamycin causes a diabetes-like condition in mice by indirectly inhibiting mTOR complex 2. Here I introduce the notion of benevolent diabetes and discuss whether starvation-like effects of chronic high dose treatment with rapamycin are an obstacle for its use as an anti-aging drug.

Starvation diabetes-like condition with low mTOR activity

If you read the Abstract, you might wonder whether rapamycin extends lifespan despite or because of "starvation-like diabetes". As described by Lamming et al [1, 2] extending several previous observations [3-6], chronic administration of high doses of rapamycin causes insulin resistance in mice. Yet, at similar doses, rapamycin prolongs life span in mice [7, 8]. Moreover, in several studies, rapamycin prevented complications of diabetes such as nephropathy [9-14]. Also, theoretical considerations indicate rapamycin for retinopathy [15], which was recently confirmed in an animal model [16]. Rapamycin prevents atherosclerosis in rodents [17-20] and coronary re-stenosis in humans [21, 22]. In contrast, diabetes promotes nephropathy, retinopathy, atherosclerosis and coronary disease. How could this be reconciled? mTOR is a part of a nutrient-sensing pathway [23-27]. Nutrients and insulin activate mTOR. Rapamycin, which inhibits mTOR, is a "starvation-mimetic", making the organism "think" that food is in a short supply. The most starvation-sensitive organ is the brain. The brain consumes only glucose and ketones. Therefore, to feed the brain during starvation, the liver produces glucose from amino acids (gluconeogenesis) and ketones from fatty acids (ketogenesis). Since insulin blocks both processes, the liver needs to become resistant to insulin. Also secretion of insulin by beta-cells is decreased. And adipocytes release fatty acids (lipolysis) to fuel ketogenesis by the liver. Thus, there are five noticeable metabolic alterations of starvation: gluconeogenesis, ketogenesis, insulin resistance, low insulin levels and increased lipolysis. This metabolic switch is known as starvation diabetes, a reversible condition, described 160 years ago (see for references [28]). Starvation diabetes could be explained by deactivation of mTOR, which otherwise is activated by nutrients. In theory, rapamycin can cause similar symptoms in the presence of nutrients.

Type II diabetes: insulin-resistance due to active mTOR

Starvation-diabetes is not a true type II diabetes. Type II diabetes is a consequence of insulin-resistance in part due to excessive nutrients and obesity. Even brief overfeeding may induce insulin resistance [29]. Nutrients and insulin activate mTOR. In turn, over-activated mTOR causes insulin resistance [30-42]. This feedback loop is shown in figure 1A. mTOR activates S6 kinase (S6K), which causes degradation of insulin-

receptor substrates (IRS), thus impairing insulin signaling. Also, mTOR causes insulin resistance by an additional feedback mechanism [43, 44].

In high fat-fed obese rats, the mTOR pathway is activated in the liver and muscle, leading to insulin resistance [35]. In mice, sustained activation (by high fat feeding) of mTOR is associated with hepatic insulin resistance [45]. Chronic increase of insulin levels (hyperinsulinemia) causes insulin resistance, preventable by rapamycin [46]. In some animal models, removal of visceral fat prevents insulin resistance [47-49]. In humans, infusion of amino acids activate mTOR/S6K1, causing insulin resistance [38, 40]. In healthy men, rapamycin prevented activation of mTOR and insulin resistance caused by amino acid mixture [50]. Insulin stimulates glucose uptake and also activates mTOR. By a feedback loop, mTORC1 promotes insulin-resistance, decreasing glucose uptake by the cell. And most detrimentally, mTOR is involved in diabetic complications and age-related diseases [24-27, 51, 52-54].

The two opposite conditions?

Type II diabetes and starvation diabetes seem to be the two opposite conditions: the first is associated with activation of nutrient-sensing pathways, whereas the second is associated with deactivation of nutrient sensing pathways such as mTOR. Type II diabetes is dangerous by its complications such as retinopathy, neuropathy and accelerated atherosclerosis and cancer. Long-term effects of prolonged "starvation diabetes" is not known of course: it could not last for a long time, otherwise an animal (or human) would die from starvation. Or would not? An outstanding study by Fontana et al provides some answers [55]. Among individuals who had been practicing sever CR for an average of 7 years, 40% of CR individuals exhibited "diabetic-like" glucose intolerance, despite low levels of fasting glucose, insulin and inflammatory cytokines as well as excellent other metabolic profiles. In comparison with the rest CR individuals, they had lower BMI, leptin, circulating IGF-I, testosterone, and high levels of adiponectin, which are key adoptations to CR in rodents, suggesting severe CR [55]. The authors speculated that the "insulin resistance" in this severe CR group might have the effect of slowing aging, also based on the finding that a number of insulin-resistant strains of mice are long-lived [55]. The same conclusion could be reached from the mTOR perspective (Appendix 1).

"The paradox of the insu-lin/IGF-1 signaling pathway in longevity" was first discussed by Nir Barzilai and co-workers, who precisely noticed that insulin-resistance, which is so detrimental in obese and aging mammals, can be associated with genetic manipulations that extend life span in model organisms [56]. Later Barzilai et al suggested that insulin-resistance might serve as an adaptive mechanism in some tissues by preventing excess uptake of nutrients by cells [57]. This very interesting idea implies that insulin resistance is partially beneficial and partially hazardous in the same condition such as type II diabetes. But still insulin resistance in type II diabetes is overall harmful (leading to retinopathy and other complications), whereas insulin resistance during severe CR is benevolent. These are clearly different conditions. In fact, they are the opposite conditions. So insulin resistance may be harmful or beneficial depending on the underlying condition.

The model of TOR-driven hyper-functional aging almost automatically solves paradoxes of aging, including the insulin paradox (see paradox 7 and figure 4 in "Paradoxes of aging" [58]). From the TOR perspective, insulin resistance is beneficial or harmful when it is associated with ether low or high TOR activity, respectively (Appendix, Fig. 1 and 3). And this should not be surprising. Consider insulin resistance as a symptom. The assessment of symptoms depends on the underlying cause. For example, weight loss due to calorie restriction is good, whereas weight loss in terminal cancer is bad. Positive Tuberculosis Skin (PPD) Test due to vaccination indicates protection from tuberculosis, whereas positive test due to tuberculosis is a symptom of tuberculosis. Similarly, hyperlipidemia in obesity is bad, whereas hyperlipidemia due to rapamycin-induced lipolysis is good (see figure 2 in reference [53]). The list of examples is endless. Similarly, insulin resistance, associated with TOR overactivation, is bad (Fig. 1 B-C). But either insulin sensitivity (Fig. 2) or insulin resistance (Fig. 3), associated with inactive TOR, is good.

Type zero or benevolent diabetes

There are two types of diabetes, which at advanced stages may become similar. Insulin resistance may develop in type I diabetes (due to high glucose), whereas insulin insufficiency in type II diabetes (due to loss of beta-cells). Both types of diabetes lead to complications. In comparison, starvation diabetes [28] is only superficially resembles either type of diabetes. Also, diabetes-like symptoms may occur in rapamycin-treated mice and animals with genetically inhibited insulin/IGFI signaling (Fig. 3). To encompass all these

cases, I suggest the term type 0 (zero) or benevolent diabetes. It is possible that some patients with diabetes have inactivating mutations in the insulin/IGFI pathway and thus "suffer" from benevolent diabetes. Furthermore, the condition can be imitated by chronic administration of rapamycin at least in some strains of mice. Both calorie restriction and rapamycin extend life span in mice. Rapamycin prevents retinopathy and nephropathy. Also CR prevents type II diabetes and other diseases [59], [60], [61], [62]. One can suggest that type 0 diabetes should prevent type 2 diabetes. Should type 0 diabetes be treated? Perhaps CR-associated type 0 diabetes should not. What about rapamycin-associated diabetes? Definitely, it should not be treated with insulin. It was discussed that in theory the most rational combinations with rapamycin are mild calorie and fat restriction, physical exercise and metformin [52]. Metformin may in theory counteract rapamycin-induced gluconeogenesis in the liver. And this rational drug combination may be also considered as treatment of type 0 diabetes.

Inconsistencies in the literature on rapamycin-induced insulin resistance

As demonstrated by Lamming et al, chronic administration of rapamycin caused insulin-resistance due to deactivation of mTORC2 and Akt [1]. This is consistent with previous data that IRS signaling and AKT activation was impaired in patients treated with rapamycin [63]. However, there are some inconsistencies. In another clinical study, rapamycin therapy in contrast caused activation of Akt [64]. Second, whereas Lamming et al found that rapamycin increased insulin levels after feeding [1], other studies reported that rapamycin in contrast inhibited insulin secretion [3], 4, 65]. Furthermore, inhibition of beta-cell adaptation and insulin production by rapamycin was considered as the main mechanism of rapamycin-induced diabetes in mice [6, 66-69]. On the other hand, selective inactivation of mTORC2 in the liver can cause hyperinsulinemia [70].

Finally, diabetic-like symptoms were not observed in numerous studies in mice. And rapamycin-induced diabetes is rare in human patients, even though most of them are prone to diabetes for other reasons.

Diabetes in patients receiving rapamycin

In renal transplant patients, who are prone to diabetes (due to several reasons), chronic administration of rapamycin modestly increases incidence of diabetes [71, 72]. Although the increase is statistically significant, it took many years to detect it. For many years it was thought that, unlike other agents used in these patients, rapamycin either do not increase the incidence of diabetes or increases it in combinations with tacrolimus [73-79]. In the study involving 20124 recipients of kidney transplant sirolimus (rapamycin) was independently associated with new onset diabetes [72]. And although it statistically significantly increases the incidence of diabetes in renal transplant patient, we do not know whether this is true diabetes, which is dangerous by its complications, or starvation-like diabetes, that prevents the complications of true diabetes . Will chronic high doses of rapamycin cause or prevent diabetes in humans without organ transplantation? More investigations are needed.

Intermittent administration of rapamycin

Is glucose intolerance a part of therapeutic effects of starvation-like drugs such as rapamycin? And may such condition be not only benign but also prevent true diabetes and its complications? Although these questions are very intriguing, the answers are not immediately crucial. Simply, the most rational anti-aging schedule is an intermittent (rather than chronic) administration of rapamycin [53, 80]. First, this will eliminate potential side effects. Second, intermittent administration of rapamycin may in theory rejuvenate stem and wound-healing cells and (in contrast to chronic treatment) improve wound healing [80]. And intermittent administration of rapamycin extended life span in mice [81-86]. Also, brief treatment with rapamycin does not affect mTORC2 [87].

Rapalogs (rapamycin and its analogs such evirolimus and temsirolimus) inhibit only one target (mTORC1). That was considered as a disadvantage of rapalogs for cancer therapy. Inhibitors of both mTORC1 and mTORC2 are under development [88, 89]. But if inhibition of mTORC2 is not needed for the longevity effect, then mTORC1 selectivity is an advantage for anti-aging therapy. Rapalogs (rapamycin and its analogs) are selective inhibitors of TORC1 and inhibitors of mTORC1 will have the same side effects as rapalogs. Yet, these (non-rapalog) inhibitors of the TOR kinase also have off-target effects and side effects. Therefore, rapamycin will remain the least toxic anti-aging drug in the near future [90].

ACKNOWLEDGMENTS

I thank Nir Barzilai (Albert Einstein College of Medicine, Bronx NY) and Luigi Fontana (Washington University, St. Louis, MO) and helpful and expiring discussion and critical reading of the manuscript.

Appendix 1: Paradoxes of diabetes

Previously I discussed that the mTOR-centered model can solve so called insulin paradox [58], which was exploited by Tom Kirkwood to undermine the notion that aging is genetically regulated: "it seems paradoxical that reduced insulin/ IGF-1 signaling extends life span but insulin resistance leads to type II diabetes. The real paradox is why, in mammals, low insulin levels are associated with good health, but low insulin responsiveness with bad health" [91]. In other words, (a) low insulin signaling are associated with good health and longevity and (b) insulin resistance is associated with poor health. In both cases (A and B), the insulin signaling is decreased. So why? From the mTOR point of view, the cases are opposites. In case A (Fig. 2), low insulin signaling is insufficient to activate mTOR (and this is good). In case B (Fig. 1 B-C), insulin signaling is low because of the active mTOR (this is bad), which blocks insulin signaling. In case B, active mTOR is a cause of insulin resistance and low insulin signaling (Fig. 1 B-C). In case A, low insulin signaling keeps mTOR inactive (Fig. 2).

Noteworthy, dwarf (GH-/-) (Fig. 2) and Klotho (Fig. 3) mice have an extended longevity. But Klotho induces IGF-1 and insulin resistance, whereas dwarf mice with reduced IGF-1 and insulin levels have enhanced insulin sensitivity. Bartke et al suggested that signaling downstream from IGF-1 and insulin receptors is reduced in both Klotho and dwarf mice [92, 93]. This is in agreement with the mTOR-centric model [58], given that the mTOR pathway is downstream from insulin/IGF receptors.

The same mTOR-centered point of view is applicable to the diabetes paradox. When diabetes is caused by high mTOR activity, then it is associated with complications, diseases and shortened life span (Fig. 1). This is type 2 diabetes. But when diabetic-like condition is caused by either starvation or rapamycin, then it might be benevolent (Fig. 3).

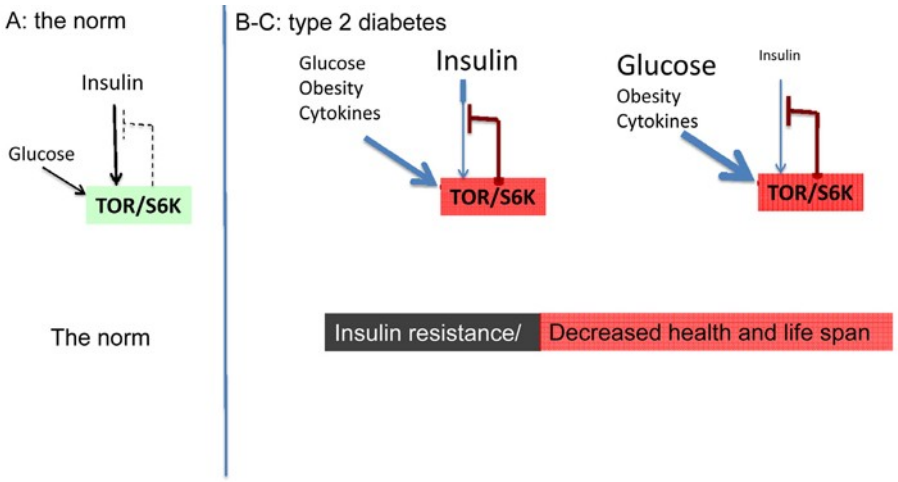

Figure 1. The norm and type 2 diabetes (simplified schema).
(A) The norm. Insulin and nutrients such as glucose stimulate mTOR, which blocks insulin signaling (feedback loop).
(**B-C**) **High mTOR/S6K activity: insulin resistance plus decreased lifespan.**
(B) Overactivated by nutrients, cytokins, insulin and other hormones, mTOR blocks insulin signaling causing insulinresistance. Nutrients overstimulate beta-cells and insulin is increased.
(C) In type II diabetes, beta-cells eventually fail and levels of insulin may be decreased.

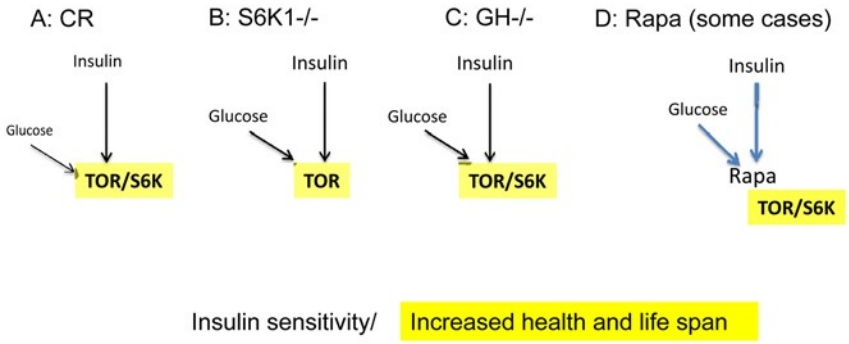

Figure 2. Low mTOR/S6K activity: insulin sensitivity plus longevity.
(A) Calorie restriction. Deactivation of the nutrient-sensing mTOR pathway results in insulin sensitivity.
(B) Knockout of S6K1 in mice abolishes feedback block of insulin signaling, resulting in insulin sensitivity [94].
(C) Decreased levels of growth hormone (GH). In mice, absence of GH or GH receptor leads to a remarkable extension of longevity [95]. GH receptor deficiency is associated with a reduction in pro-aging signaling, cancer, and diabetes in humans [96]. Growth hormone signaling accelerates aging in mammals [97]. Remarkably, growth stimulation promotes cellular aging, when cells cannot proliferate [98, 99]. Thus, the growth promoting pathways such as mTOR are involved in both organismal and cellular aging.
(D) Acute treatment with rapamycin. Deactivation of the nutrient-sensing mTOR pathway abolishes a feedback block of insulin signaling, resulting in insulin sensitivity [50].

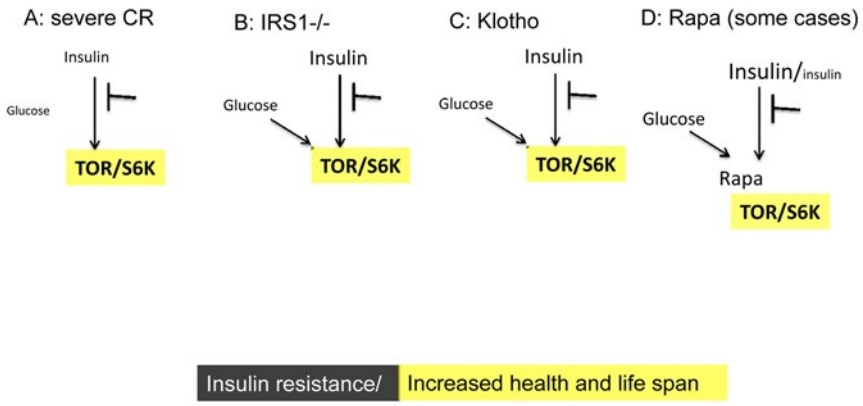

Figure 3. Low TOR/S6K activity: insulin resistance plus longevity (type 0 diabetes).
(A) Severe CR and starvation. Insulin resistance and symptoms of diabetes are observed during starvation [28] and prolong severe CR [55]. Furthermore, CR may reduce rather than enhance insulin effects in the insulin-sensitive dwarf mice[100].
(B) IRS1 knockout. Insulin receptor substrate 1 null mice live longer despite insulin resistance [101].
(C) Klotho mice. Overexpression of Klotho in mice extends life span. Klotho protein represses intracellular signals of insulin and insulin-like growth factor 1 (IGF1), [102]. Also, Klotho interferes with insulin/IGF-like signaling to improve longevity in *Caenorhabditis elegans* [103].
(D) Chronic treatment with high doses of rapamycin causes insulin resistance and glucose intolerance. This condition can be associated with normal/increased and decreased levels of insulin. Noteworthy, rapamycin induces Klotho [64].

CONFLICT OF INTERESTS STATEMENT

The author of this manuscript has no conflict of interest to declare.

REFERENCES

1. Lamming DW, Ye L, Katajisto P, Goncalves MD, Saitoh M, Stevens DM, Davis JG, Salmon AB, Richardson A, Ahima RS, Guertin DA, Sabatini DM, Baur JA. Rapamycin-induced insulin resistance is mediated by mTORC2 loss and uncoupled from longevity. Science. 2012; 335: 1638-1643.

2. Hughes KJ, Kennedy BK. Cell biology. Rapamycin paradox resolved. Science. 2012; 335: 1578-1579.

3. Fraenkel M, Ketzinel-Gilad M, Ariav Y, Pappo O, Karaca M, Castel J, Berthault MF, Magnan C, Cerasi E, Kaiser N, Leibowitz G. mTOR inhibition by rapamycin prevents beta-cell adaptation to hyperglycemia and exacerbates the metabolic state in type 2 diabetes. Diabetes. 2008; 57: 945-957.

4. Chang GR, Wu YY, Chiu YS, Chen WY, Liao JW, Hsu HM, Chao TH, Hung SW, Mao FC. Long-term administration of rapamycin reduces adiposity, but impairs glucose tolerance in high-fat diet-fed KK/HlJ mice. Basic Clin Pharmacol Toxicol. 2009; 105: 188-198.

5. Houde VP, Brule S, Festuccia WT, Blanchard PG, Bellmann K, Deshaies Y, Marette A. Chronic rapamycin treatment causes glucose intolerance and hyperlipidemia by upregulating hepatic gluconeogenesis and impairing lipid deposition in adipose tissue. Diabetes. 2010; 59: 1338-1348.

6. Yang SB, Lee HY, Young DM, Tien AC, Rowson-Baldwin A, Shu YY, Jan YN, Jan LY. Rapamycin induces glucose intolerance in mice by reducing islet mass, insulin content, and insulin sensitivity. J Mol Med (Berl). 2011.

7. Harrison DE, Strong R, Sharp ZD, Nelson JF, Astle CM, Flurkey K, Nadon NL, Wilkinson JE, Frenkel K, Carter CS, Pahor M, Javors MA, Fernandezr E, Miller RA. Rapamycin fed late in life extends lifespan in genetically heterogenous mice. Nature. 2009; 460: 392-396.

8. Miller RA, Harrison DE, Astle CM, Baur JA, Boyd AR, de Cabo R, Fernandez E, Flurkey K, Javors MA, Nelson JF, Orihuela CJ, Pletcher S, Sharp ZD, Sinclair D, Starnes JW, Wilkinson JE et al . Rapamycin, But Not Resveratrol or Simvastatin, Extends Life Span of Genetically Heterogeneous Mice. J Gerontol A Biol Sci Med Sci. 2011; 66: 191-201.

9. Lloberas N, Cruzado JM, Franquesa M, Herrero-Fresneda I, Torras J, Alperovich G, Rama I, Vidal A, Grinyo JM. Mammalian target of rapamycin pathway blockade slows progression of diabetic kidney disease in rats. J Am Soc Nephrol. 2006; 17: 1395-1404.

10. Sakaguchi M, Isono M, Isshiki K, Sugimoto T, Koya D, Kashiwagi A. Inhibition of mTOR signaling with rapamycin attenuates renal hypertrophy in the early diabetic mice. Biochem Biophys Res Commun. 2006; 340: 296-301.

11. Wittmann S, Daniel C, Stief A, Vogelbacher R, Amann K, Hugo C. Long-term treatment of sirolimus but not cyclosporine ameliorates diabetic nephropathy in the rat. Transplantation. 2009; 87: 1290-1299.

12. Flaquer M, Lloberas N, Franquesa M, Torras J, Vidal A, Rosa JL, Herrero-Fresneda I, Grinyo JM, Cruzado JM. The combination of sirolimus and rosiglitazone produces a renoprotective effect on diabetic kidney disease in rats. Life Sci. 2010; 87: 147-153.

13. Cruzado JM, Poveda R, Ibernon M, Diaz M, Fulladosa X, Carrera M, Torras J, Bestard O, Navarro I, Ballarin J, Romero R, Grinyo JM. Low-dose sirolimus combined with angiotensin-converting enzyme inhibitor and statin stabilizes renal function and reduces glomerular proliferation in poor prognosis IgA nephropathy. Nephrol Dial Transplant. 2011; 26: 3596-3602.

14. Lu MK, Gong XG, Guan KL. mTOR in podocyte function: is rapamycin good for diabetic nephropathy? Cell Cycle. 2011; 10: 3415-3416.

15. Demidenko ZN, Blagosklonny MV. The purpose of the HIF-1/PHD feedback loop: to limit mTOR-induced HIF-1alpha. Cell Cycle. 2011; 10: 1557-1562.

16. Kolosova NG, Muraleva NA, Zhdankina AA, Stefanova NA, Fursova AZ, Blagosklonny MV. Prevention of age-related macular degeneration (AMD)-like retinopathy by rapamycin in rats. Am J Pathol. 2012; in press

17. Pakala R, Stabile E, Jang GJ, Clavijo L, Waksman R. Rapamycin attenuates atherosclerotic plaque progression in apolipoprotein E knockout mice: inhibitory effect on monocyte chemotaxis. J Cardiovasc Pharmacol. 2005; 46: 481-486.

18. Mueller MA, Beutner F, Teupser D, Ceglarek U, Thiery J. Prevention of atherosclerosis by the mTOR inhibitor everolimus in LDLR-/- mice despite severe hypercholesterolemia. Atherosclerosis. 2008; 198: 39-48.

19. Chen WQ, Zhong L, Zhang L, Ji XP, Zhang M, Zhao YX, Zhang C, Zhang Y. Oral rapamycin attenuates inflammation and enhances stability of atherosclerotic plaques in rabbits independent of serum lipid levels. Br J Pharmacol. 2009; 156: 941-951.

20. Zhao L, Ding T, Cyrus T, Cheng Y, Tian H, Ma M, Falotico R, Pratico D. Low-dose oral sirolimus reduces atherogenesis, vascular inflammation and modulates plaque composition in mice lacking the LDL receptor. Br J Pharmacol. 2009; 156: 774-785.

21. Keogh A, Richardson M, Ruygrok P, Spratt P, Galbraith A, O'Driscoll G, Macdonald P, Esmore D, Muller D, Faddy S. Sirolimus in de novo heart transplant recipients reduces acute rejection and prevents coronary artery disease at 2 years: a randomized clinical trial. Circulation. 2004; 110: 2694-2700.

22. Rodriguez AE, Granada JF, Rodriguez-Alemparte M, Vigo CF, Delgado J, Fernandez-Pereira C, Pocovi A, Rodriguez-Granillo AM, Schulz D, Raizner AE, Palacios I, O'neill W, Kaluza GL, Stone G, Investigators OI. Oral Rapamycin After Coronary Bare-Metal Stent Implantation to Prevent Restenosis The Prospective, Randomized Oral Rapamycin in Argentina (ORAR II) Study. J Am Coll Cardiol. 2006; 47: 1522-1529.

23. Sarbassov dos D, Ali SM, Sabatini DM. Growing roles for the mTOR pathway. Curr Opin Cell Biol. 2005; 17: 596-603.

24. Wullschleger S, Loewith R, Hall MN. TOR signaling in growth and metabolism. Cell. 2006; 124: 471-484.

25. Blagosklonny MV, Hall MN. Growth and aging: a common molecular mechanism. Aging (Albany NY). 2009; 1: 357-362.

26. Loewith R, Hall MN. Target of rapamycin (TOR) in nutrient signaling and growth control. Genetics. 2011; 189: 1177-1201.

27. Zoncu R, Efeyan A, Sabatini DM. mTOR: from growth signal integration to cancer, diabetes and ageing. Nat Rev Mol Cell Biol. 2011; 12: 21-35.

28. Blagosklonny MV. Rapamycin-induced glucose intolerance: Hunger or starvation diabetes. Cell Cycle. 2011; 10: 4217 -4224.

29. Wang J, Obici S, Morgan K, Barzilai N, Feng Z, Rossetti L. Overfeeding rapidly induces leptin and insulin resistance. Diabetes. 2001; 50: 2786-2791.

30. Haruta T, Uno T, Kawahara J, Takano A, Egawa K, Sharma PM, Olefsky JM, Kobayashi M. A rapamycin-sensitive pathway down-regulates insulin signaling via phosphorylation and proteasomal degradation of insulin receptor substrate-1. Mol Endocrinol. 2000; 14: 783-794.

31. Ozes ON, Akca H, Mayo LD, Gustin JA, Maehama T, Dixon JE, Donner DB. A phosphatidylinositol 3-kinase/Akt/mTOR pathway mediates and PTEN antagonizes tumor necrosis factor inhibition of insulin signaling through insulin receptor substrate-1. Proc Natl Acad Sci U S A. 2001; 98: 4640-4645.

32. Um SH, Frigerio F, Watanabe M, Picard F, Joaquin M, Sticker M, Fumagalli S, Allegrini PR, Kozma SC, Auwerx J, Thomas G. Absence of S6K1 protects against age- and diet-induced obesity while enhancing insulin sensitivity. Nature. 2004; 431: 200-205.

33. Shah OJ, Wang Z, Hunter T. Inappropriate activation of the TSC/Rheb/mTOR/S6K cassette induces IRS1/2 depletion, insulin resistance, and cell survival deficiencies. Curr Biol. 2004; 14: 1650-1656.

34. Tzatsos A, Kandror KV. Nutrients suppress phosphatidylinositol 3-kinase/Akt signaling via raptor-dependent mTOR-mediated insulin receptor substrate 1 phosphorylation. Mol Cell Biol. 2006; 26: 63-76.

35. Khamzina L, Veilleux A, Bergeron S, Marette A. Increased activation of the mammalian target of rapamycin pathway in liver and skeletal muscle of obese rats: possible involvement in obesity-linked insulin resistance. Endocrinology. 2005; 146: 1473-1481.

36. Manning BD, Logsdon MN, Lipovsky A, Abbott D, Kwiatkowski DJ, Cantley LC. Feedback inhibition of Akt signaling limits the growth of tumors lacking Tsc2. Genes Dev. 2005; 19: 1773-1778.

37. Harrington LS, Findlay GM, Lamb RF. Restraining PI3K: mTOR signalling goes back to the membrane. Trends Biochem Sci. 2005; 30: 35-42.

38. Tremblay F, BržlŽ, S., Hee, Um. S., Li, Y., Masuda, K., Roden, M., Sun, X.J., Krebs, M., Polakiewicz, R.D., Thomas, G., Marette, A. Identification of IRS-1 Ser-1101 as a target of S6K1 in nutrient- and obesity-induced insulin resistance. Proc Natl Acad Sci U S A. 2007; 104: 14056-14061.

39. Tremblay F, Marette A. Amino acid and insulin signaling via the mTOR/p70 S6 kinase pathway. A negative feedback mechanism leading to insulin resistance in skeletal muscle cells. J Biol Chem. 2001; 276: 38052-38060.

40. Tremblay F, Krebs M, Dombrowski L, Brehm A, Bernroider E, Roth E, Nowotny P, WaldhŠusl W, Marette A, Roden M. Overactivation of S6 kinase 1 as a cause of human insulin resistance during increased amino acid availability. Diabetes. 2005; 54: 2674-2684.

41. Mordier S, Iynedjian PB. Activation of mammalian target of rapamycin complex 1 and insulin resistance induced by palmitate in hepatocytes. Biochem Biophys Res Commun. 2007; 362: 206-211.

42. Saha AK, Xu XJ, Balon TW, Brandon A, Kraegen EW, Ruderman NB. Insulin resistance due to nutrient excess: is it a consequence of AMPK downregulation? Cell Cycle. 2011; 10: 3447-3451.

43. Hsu PP, Kang SA, Rameseder J, Zhang Y, Ottina KA, Lim D, Peterson TR, Choi Y, Gray NS, Yaffe MB, Marto JA, Sabatini DM. The mTOR-regulated phosphoproteome reveals a mechanism of mTORC1-mediated inhibition of growth factor signaling. Science. 2011; 332: 1317-1322.

44. Yu Y, Yoon SO, Poulogiannis G, Yang Q, Ma XM, Villen J, Kubica N, Hoffman GR, Cantley LC, Gygi SP, Blenis J. Phosphoproteomic analysis identifies Grb10 as an mTORC1 substrate that negatively regulates insulin signaling. Science. 2011; 332: 1322-1326.

45. Korsheninnikova E, van der Zon GC, Voshol PJ, Janssen GM, Havekes LM, Grefhorst A, Kuipers F, Reijngoud DJ, Romijn JA, Ouwens DM, Maassen JA. Sustained activation of the mammalian target of rapamycin nutrient sensing pathway is associated with hepatic insulin resistance, but not with steatosis, in mice. Diabetologia. 2006; 49: 3049-3057.

46. Ueno M, Carvalheira JB, Tambascia RC, Bezerra RM, Amaral ME, Carneiro EM, Folli F, Franchini KG, Saad MJ. Regulation of insulin signalling by hyperinsulinaemia: role of IRS-1/2 serine phosphorylation and the mTOR/p70 S6K pathway. Diabetologia. 2005; 48: 506-518.

47. Barzilai N, She L, Liu BQ, Vuguin P, Cohen P, Wang J, Rossetti L. Surgical removal of visceral fat reverses hepatic insulin resistance. Diabetes. 1999; 48: 94-98.

48. Gabriely I, Ma XH, Yang XM, Atzmon G, Rajala MW, Berg AH, Scherer P, Rossetti L, Barzilai N. Removal of visceral fat prevents insulin resistance and glucose intolerance of aging: an adipokine-mediated process? Diabetes. 2002; 51: 2951-2958.

49. Muzumdar R, Allison DB, Huffman DM, Ma X, Atzmon G, Einstein FH, Fishman S, Poduval AD, McVei T, Keith SW, Barzilai N. Visceral adipose tissue modulates mammalian longevity. Aging Cell. 2008; 7: 438-440.

50. Krebs M, Brunmair B, Brehm A, Artwohl M, Szendroedi J, Nowotny P, Roth E, FŸrnsinn C, Promintzer M, Anderwald C, Bischof M, Roden M. The Mammalian target of rapamycin pathway regulates nutrient-sensitive glucose uptake in man. Diabetes. 2007; 56: 1600-1607.

51. Blagosklonny MV. Aging and immortality: quasi-programmed senescence and its pharmacologic inhibition. Cell Cycle. 2006; 5: 2087-2102.

52. Blagosklonny MV. An anti-aging drug today: from senescence-promoting genes to anti-aging pill. Drug Disc Today. 2007; 12: 218-224.

53. Blagosklonny MV. Validation of anti-aging drugs by treating age-related diseases. Aging (Albany NY). 2009; 1: 281-288.

54. Blagosklonny MV. mTOR-driven aging: speeding car without brakes. Cell Cycle. 2009; 8: 4055-4059.

55. Fontana L, Klein S, Holloszy JO. Effects of long-term calorie restriction and endurance exercise on glucose tolerance, insulin action, and adipokine production. Age (Dordr). 2010; 32: 97-108.

56. Rincon M, Muzumdar R, Atzmon G, Barzilai N. The paradox of the insulin/IGF-1 signaling pathway in longevity. Mech Ageing Dev. 2004; 125: 397-403.

57. Barzilai N, Huffman DM, Muzumdar RH, Bartke A. The critical role of metabolic pathways in aging. Diabetes. 2012; 61: 1315-1322.

58. Blagosklonny MV. Paradoxes of aging. Cell Cycle. 2007; 6: 2997-3003.

59. Weiss EP, Racette SB, Villareal DT, Fontana L, Steger-May K, Schechtman KB, Klein S, Holloszy JO, Group. WUSoMC. Improvements in glucose tolerance and insulin action induced by

increasing energy expenditure or decreasing energy intake: a randomized controlled trial. Am J Clin Nutr. 2006; 84: 1033-1042.

60. Fontana L. The scientific basis of caloric restriction leading to longer life. Curr Opin Gastroenterol. 2009; 25:144-150.

61. Fontana L, Partridge L, Longo VD. Extending healthy life span--from yeast to humans. Science. 2010; 328: 321-326.

62. Blagosklonny MV. Calorie restriction: Decelerating mTOR-driven aging from cells to organisms (including humans). Cell Cycle. 2010; 9: 683-688.

63. Di Paolo S, Teutonico A, Leogrande D, Capobianco C, Schena PF. Chronic inhibition of mammalian target of rapamycin signaling downregulates insulin receptor substrates 1 and 2 and AKT activation: A crossroad between cancer and diabetes? J Am Soc Nephrol. 2006; 17: 2236-2244.

64. Tataranni T, Biondi G, Cariello M, Mangino M, Colucci G, Rutigliano M, Ditonno P, Schena FP, Gesualdo L, Grandaliano G. Rapamycin-Induced Hypophosphatemia and Insulin Resistance Are Associated With mTORC2 Activation and Klotho Expression. Am J Transplant. 2011; 11: 1656-1664.

65. Velazquez-Garcia S, Valle S, Rosa TC, Takane KK, Demirci C, Alvarez-Perez JC, Mellado-Gil JM, Ernst S, Scott DK, Vasavada RC, Alonso LC, Garcia-Ocana A. Activation of protein kinase C-zeta in pancreatic beta-cells in vivo improves glucose tolerance and induces beta-cell expansion via mTOR activation. Diabetes. 2011; 60: 2546-2559.

66. Rachdi L, Balcazar N, Osorio-Duque F, Elghazi L, Weiss A, Gould A, Chang-Chen KJ, Gambello MJ, Bernal-Mizrachi E. Disruption of Tsc2 in pancreatic beta cells induces beta cell mass expansion and improved glucose tolerance in a TORC1-dependent manner. Proc Natl Acad Sci U S A. 2008; 105: 9250-9255.

67. Leibowitz G, Cerasi E, Ketzinel-Gilad M. The role of mTOR in the adaptation and failure of beta-cells in type 2 diabetes. Diabetes Obes Metab. 2008; 10 Suppl 4: 157-169.

68. Xie J, Herbert TP. The role of mammalian target of rapamycin (mTOR) in the regulation of pancreatic beta-cell mass: implications in the development of type-2 diabetes. Cell Mol Life Sci. 2011.

69. Blandino-Rosano M, Chen AY, Scheys JO, Alejandro EU, Gould AP, Taranukha T, Elghazi L, Cras-Meneur C, Bernal-Mizrachi E. mTORC1 signaling and regulation of pancreatic beta-cell mass. Cell Cycle. 2012; 11.

70. Hagiwara A, Cornu M, Cybulski N, Polak P, Betz C, Trapani F, Terracciano L, Heim MH, Ruegg MA, Hall MN. Hepatic mTORC2 Activates Glycolysis and Lipogenesis through Akt, Glucokinase, and SREBP1c. Cell Metab. 2012; 15: 725-738.

71. Teutonico A, Schena PF, Di Paolo S. Glucose metabolism in renal transplant recipients: effect of calcineurin inhibitor withdrawal and conversion to sirolimus. J Am Soc Nephrol. 2005; 16: 3128-3135.

72. Johnston O, Rose CL, Webster AC, Gill JS. Sirolimus is associated with new-onset diabetes in kidney transplant recipients. J Am Soc Nephrol. 2008; 19: 1411-1418.

73. Schwarz C, Oberbauer R. The future role of target of rapamycin inhibitors in renal transplantation. Curr Opin Urol. 2002; 12: 109-113.

74. Legendre C, Campistol JM, Squifflet JP, Burke JT. Cardiovascular risk factors of sirolimus compared with cyclosporine: early experience from two randomized trials in renal transplantation. Transplant Proc. 2003; 35: 151S-153S.

75. Gonwa T, Mendez R, Yang HC, Weinstein S, Jensik S, Steinberg S. Randomized trial of tacrolimus in combination with sirolimus or mycophenolate mofetil in kidney transplantation: results at 6 months. Transplantation. 2003; 75:1213-1220.

76. Romagnoli J, Citterio F, Violi P, Nanni G, Castagneto M. Posttransplant diabetes mellitus after kidney transplantation with different immunosuppressive agents. Transplant Proc. 2004; 36: 690-691.

77. Sulanc E, Lane JT, Puumala SE, Groggel GC, Wrenshall LE, Stevens RB. New-onset diabetes after kidney transplantation: an application of 2003 International Guidelines. Transplantation. 2005; 80: 945-952.

78. Araki M, Flechner SM, Ismail HR, Flechner LM, Zhou L, Derweesh IH, Goldfarb D, Modlin C, Novick AC, Faiman C. Posttransplant diabetes mellitus in kidney transplant recipients receiving calcineurin or mTOR inhibitor drugs. Transplantation. 2006; 81: 335-341.

79. Pavlakis M, Goldfarb-Rumyantzev AS. Diabetes after transplantation and sirolimus: what's the connection? J Am Soc Nephrol. 2008; 19: 1255-1256.

80. Blagosklonny MV. Aging, stem cells, and mammalian target of rapamycin: a prospect of pharmacologic rejuvenation of aging stem cells. Rejuvenation Res. 2008; 11: 801-808.

81. Anisimov VN, Zabezhinski MA, Popovich IG, Piskunova TS, Semenchenko AV, Tyndyk ML, Yurova MN, Antoch MP, Blagosklonny MV. Rapamycin extends maximal lifespan in cancer-prone mice. Am J Pathol. 2010; 176:2092-2097.

82. Anisimov VN, Zabezhinski MA, Popovich IG, Piskunova TS, Semenchenko AV, Tyndyk ML, Yurova MN, Rosenfeld SV, Blagosklonny MV. Rapamycin increases lifespan and inhibits spontaneous tumorigenesis in inbred female mice. Cell Cycle. 2011; 10: 4230-4236.

83. Khanna A, Kapahi P. Rapamycin: killing two birds with one stone. Aging (Albany NY). 3: 1043-1044.

84. Spong A, Bartke A. Rapamycin slows aging in mice. Cell Cycle. 11.

85. Longo VD, Fontana L. Intermittent supplementation with rapamycin as a dietary restriction mimetic. Aging (Albany NY). 2011; 3: 1039-1040.

86. Selman C, Partridge L. A double whammy for aging? Rapamycin extends lifespan and inhibits cancer in inbred female mice. Cell Cycle. 11: 17-18.

87. Jacinto E, Loewith R, Schmidt A, Lin S, Ruegg MA, Hall A, Hall MN. Mammalian TOR complex 2 controls the actin cytoskeleton and is rapamycin insensitive. Nat Cell Biol. 2004; 6:1122-1128.

88. Markman B, Dienstmann R, Tabernero J. Targeting the PI3K/Akt/mTOR pathway--beyond rapalogs. Oncotarget. 2010; 1: 530-543.

89. Benjamin D, Colombi M, Moroni C, Hall MN. Rapamycin passes the torch: a new generation of mTOR inhibitors. Nat Rev Drug Discov. 2011; 10: 868-880.

90. Blagosklonny MV. Increasing healthy lifespan by suppressing aging in our lifetime: Preliminary proposal. Cell Cycle. 2010; 9: 4788-4794.

91. Kirkwood TB. Understanding the odd science of aging. Cell. 2005; 120: 437-447.

92. Bartke A. Long-lived Klotho mice: new insights into the roles of IGF-1 and insulin in aging. Trends Endocrinol Metab. 2006; 17: 33-35.

93. Bartke A. Single-gene mutations and healthy ageing in mammals. Philos Trans R Soc Lond B Biol Sci. 2011; 366: 28-34.

94. Selman C, Tullet JM, Wieser D, Irvine E, Lingard SJ, Choudhury AI, Claret M, Al-Qassab H, Carmignac D, Ramadani F, Woods A, Robinson IC, Schuster E, Batterham RL, Kozma SC, Thomas G et al . Ribosomal protein S6 kinase 1 signaling regulates mammalian life span. Science. 2009; 326: 140-144.

95. Bartke A. Healthy Aging: Is Smaller Better? - A Mini-Review. Gerontology. 2012.

96. Guevara-Aguirre J, Balasubramanian P, Guevara-Aguirre M, Wei M, Madia F, Cheng CW, Hwang D, Martin-Montalvo A, Saavedra J, Ingles S, de Cabo R, Cohen P, Longo VD. Growth hormone receptor deficiency is associated with a major reduction in pro-aging signaling, cancer, and diabetes in humans. Sci Transl Med. 2011; 3: 70ra13.

97. Bartke A. Pleiotropic effects of growth hormone signaling in aging. Trends Endocrinol Metab. 2011; 22: 437-442.

98. Demidenko ZN, Blagosklonny MV. Growth stimulation leads to cellular senescence when the cell cycle is blocked. Cell Cycle. 2008; 7: 3355-3361.

99. Demidenko ZN, Zubova SG, Bukreeva EI, Pospelov VA, Pospelova TV, Blagosklonny MV. Rapamycin decelerates cellular senescence. Cell Cycle. 2009; 8: 1888-1895.

100. Wang Z, Al-Regaiey KA, Masternak MM, Bartke A. Adipocytokines and lipid levels in Ames dwarf and calorie-restricted mice. J Gerontol A Biol Sci Med Sci. 2006; 61: 323-331.

101. Selman C, Lingard S, Choudhury AI, Batterham RL, Claret M, Clements M, Ramadani F, Okkenhaug K, Schuster E, Blanc E, Piper MD, Al-Qassab H, Speakman JR, Carmignac D, Robinson IC, Thornton JM et al . Evidence for lifespan extension and delayed age-related biomarkers in insulin receptor substrate 1 null mice. Faseb J. 2008; 22: 807-818.

102. Kurosu H, Yamamoto M, Clark JD, Pastor JV, Nandi A, Gurnani P, McGuinness OP, Chikuda H, Yamaguchi M, Kawaguchi H, Shimomura I, Takayama Y, Herz J, Kahn CR, Rosenblatt KP, Kuro-o M. Suppression of aging in mice by the hormone Klotho. Science. 2005; 309: 1829-1833.

103. Chateau MT, Araiz C, Descamps S, Galas S. Klotho interferes with a novel FGF-signalling pathway and insulin/Igf-like signalling to improve longevity and stress resistance in Caenorhabditis elegans. Aging (Albany NY). 2010; 2: 567-581.

Research Perspective

Resveratrol-activated SIRT1 in liver and pancreatic ß-cells: a Janus head looking to the same direction of metabolic homeostasis

Laurène Vetterli and Pierre Maechler

Department of Cell Physiology and Metabolism, University of Geneva Medical Center, Geneva, Switzerland

Key words: *SIRT1, resveratrol, liver, pancreatic beta-cell, insulin secretion, glucose homeostasis*
Received: *3/31/11; Accepted: 4/4/11; Published: 4/6/11*
Corresponding author: *Pierre Maechler, PhD;* ***E-mail:*** *Pierre.Maechler@unige.ch* doi:10.18632/aging.100304

Abstract: Sirtuins are energy sensors which mediate effects of calorie restriction-induced lifespan extension. The mammalian sirtuin homolog SIRT1 is a protein deacetylase playing a central role in metabolic homeostasis. SIRT1 is one of the targets of resveratrol, a polyphenol that has been shown to increase lifespan and to protect animal models against high-calorie diet induced obesity and insulin resistance. The beneficial effects of resveratrol mediated by SIRT1 activation can be contributed by different organs. Among them, the liver and pancreatic ß-cells have been shown to be responsive to resveratrol in a SIRT1-dependent manner. Downstream of SIRT1, transcription factors being activated are tissue-specific, in turn inducing expression of metabolic genes in an apparent paradoxical way. In this review, we discuss specificities of SIRT1 effects in the liver versus pancreatic ß-cells, ultimately converging towards metabolic homeostasis at the organism level.

Effects of SIRT1 and its activation by resveratrol

SIRT1 is a member of the Sirtuins, a conserved family of NAD^+-dependent proteins found to be involved in aging processes. Over-expression of the yeast Sir2 increases lifespan in many organisms, whereas deletion or mutations of Sir2 lead to reduced lifespan [1-3]. Seven human homologs of Sir2 have been identified, named SIRT1 to SIRT7 [4, 5], which can function as deacetylase or as mono-ADP-ribosyltransferase. As sirtuins are dependent on the NAD^+/NADH ratio, they are sensitive to the cellular energy and redox state of the cell, conferring them a role as metabolic sensors. SIRT1 is mainly found in the nucleus, where it functions as a transcriptional repressor via histone deacetylation. Resveratrol, a natural polyphenol found for instance in red grapes and wine, is well recognized as a SIRT1 activator [6]. Accordingly, resveratrol is the subject of great interest since it was shown to exert beneficial effects on glucose and lipid metabolism, to improve exercise performance, and to extend lifespan in rodents [7, 8]. However, detailed mechanisms mediating resveratrol effects remain unclear since this molecule has various molecular targets; *e.g.* SIRT1, AMP-activated protein kinase (AMPK), or antioxidants properties. These targets might be activated differently regarding specific organs, rendering extrapolation of the mechanisms delineated in one tissue to the other hazardous. Therefore, the positive effects of resveratrol on glucose homeostasis reported in animal models deserves further investigations in order to understand the specific contribution of the different organs implicated in this response [7, 9, 10]. For instance, resveratrol effects might be explained by its action on the liver, but also contributed by effects on the pancreatic ß-cell. We will now discuss these two tissues in more details.

SIRT1 and resveratrol in pancreatic ß-cells

In pancreatic islets, functions and targets of SIRT1 are still poorly characterized, as very few studies have focused on ß-cells to date. Metabolic efficiency is crucial for ß-cell function as glucose metabolism is tightly coupled to the control of insulin secretion [11]. Originally, two papers have shown that SIRT1

positively regulates glucose-stimulated insulin secretion in pancreatic ß-cells [12, 13]. The SIRT1 activator resveratrol potentiates glucose-stimulated insulin secretion, both acutely and secondary to chronic treatment. Acutely, resveratrol effects are observed already at 1µM in INS-1E insulinoma cells (Figure 1A). Following a 24-hour exposure, the effects of resveratrol are maintained even after removal of the compound, as observed in INS-1E cells and human islets [14]. In islets obtained from a type 2 diabetic donor, resveratrol was reported to partially restore the secretory response to glucose [14]. Several alternative mechanisms may explain the chronic effects of resveratrol on insulin secreting cells.

Resveratrol can bind to the sulfonylurea receptors (SUR), the regulatory subunits of K_{ATP}-channels [15]. Closure of K_{ATP}-channels promotes elevation of cyto-solic Ca^{2+}, secondary to the opening of voltage-gated Ca^{2+} channels, thereby inducing insulin exocytosis. Resveratrol is structurally similar to DIDS (4,4'-dithiocyanatostilbene-2,2'-disulphonic acid), a synthetic K_{ATP}-channel activator. Moreover, resveratrol treatment has been shown to displace binding of the sulfonylurea glibenclamide from SUR channels [15]. Therefore, one might speculate that resveratrol effects would be similar to those of sulfonylureas. In order to test this option, we exposed INS-1E cells for 24 hours to sulfonylureas (glibenclamide and tolbutamide), DIDS, and resveratrol. Glucose-stimulated insulin secretion was then tested in the absence of the compounds following the 24-hour treatment. As shown in Figure1B, only resveratrol potentiated the secretory response, in accordance with previous data [14], showing that the chronic effects of this phenol are not mediated by SUR channels.

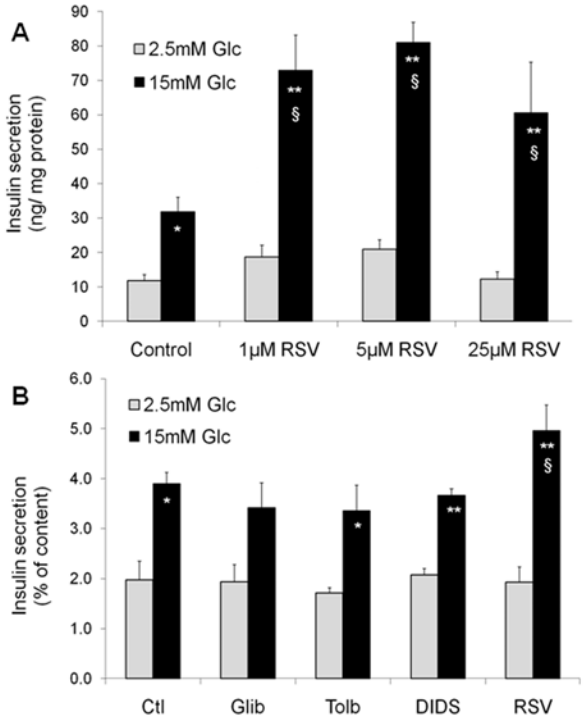

Figure 1. Acute and chronic effects of resveratrol (RSV) on glucose-stimulated insulin secretion in INS-1E ß-cells. Acute effects of RSV (**A**). Following a 2h pre-incubation period without glucose, INS-1E cells were stimulated for 30 min in KRBH with 2.5 or 15 mM glucose (Glc) in the absence (Control) or presence of 1, 5, and 25 µM of RSV. Values are means ± SE of 6 independent experiments. *p<0.05, **p<0.01 versus 2.5 mM Glc of the corresponding group; §p<0.05 versus Control group at 15 mM Glc. Chronic effect of sulfonylureas and RSV (**B**). INS-1E cells were cultured for 24h in the absence (Ctl) or the presence of 1 µM glibenclamide (Glib), 250 µM tolbutamide (Tolb), 5 µM DIDS, and 25 µM RSV. Next, cells were washed and pre-incubated without drugs and without glucose for 2h. Then, cells were incubated for 30 min in the absence of the tested compounds at 2.5 or 15 mM Glc. Values are means ± SE of 3 independent experiments. * p<0.05, **p<0.01 versus 2.5 mM Glc of the corresponding group; §p<0.05 versus Ctl group at 15 mM Glc.

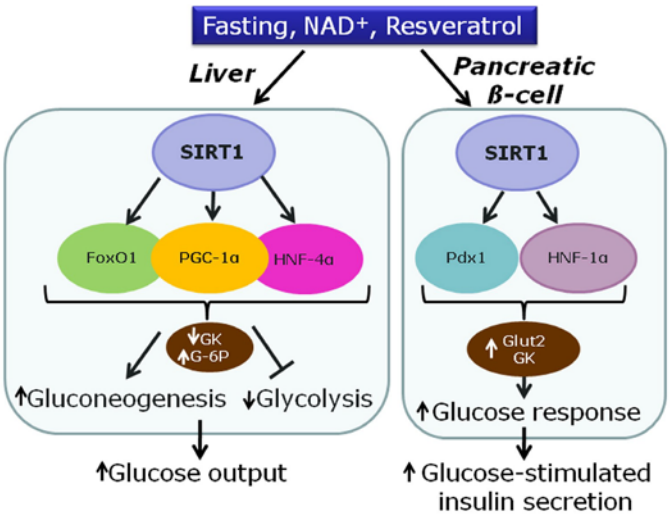

Figure 2. Proposed model for the effects of SIRT1 in the liver and the pancreatic ß-cell on transcription factors and metabolic enzymes (GK, glucokinase; G-6P, glucose-6-phosphatase; Glut-2, glucose transporter 2).

The effects of resveratrol on glucose-stimulated insulin secretion are associated with enhanced catabolic efficiency of the sugar. Indeed, chronic treatment of insulin-secreting cells with resveratrol results in elevated glycolytic flux, increased glucose oxidation and oxygen consumption, thereby producing more ATP upon glucose stimulation [14]. The increased metabolism-secretion coupling observed in resveratrol-treated cells is favoured by up-regulation of the glucose transporter Glut2 and the glycolysis-initiating enzyme glucokinase, permitting increased provision of substrates into the mitochondria. Elevated expression of Glut2 and glucokinase might be secondary to the reported up-regulation of Pdx1 and HNF-1α [14], as these transcription factors regulate Glut2 expression [16, 17]. Upstream of these regulations, we could show that the effects of resveratrol on ß-cells are fully mediated by SIRT1. Inhibition of SIRT1, either pharmacologically using the EX-527inhibitor or genetically through expression of a mutant form lacking deacetylase activity, reduces resveratrol effects on glucose-stimulated insulin secretion. Conversely, overexpression of SIRT1 in INS-1E cells further increases resveratrol effects on insulin secretion [14].

Collectively, data indicate a sequence of events in which resveratrol primarily activates SIRT1, inducing expression of key transcription factors for the ß-cell, such as Pdx-1 and HNF-1α (Figure 2). This in turn promotes expression of Glut2 and glucokinase, thereby increasing the secretory response to glucose [14]. Hence, resveratrol treatment might mimic starving conditions, rendering the ß-cell more sensitive for the awaited next rise in glucose levels.

Activation of AMPK by resveratrol and relationship to SIRT1

Resveratrol stimulates AMPK in HepG2 hepatoma [18] and INS-1E insulinoma [14] cell lines, as well as in various tissues [19-21]. Such AMPK pathway could account for some of the beneficial effects of resveratrol reported in mice fed a high-fat diet [7, 8]. Cross talk between AMPK and SIRT1 has been reported in different experimental systems [22, 23]. However, current information about the hierarchy governing the relationship between these two enzymes is at first sight contradictory, although discrepancies might reflect tissue specificities. Indeed, it was proposed that AMPK activation would be downstream of SIRT1 in hepato-

cytes [19], upstream in muscle cells [23, 24], and independent of SIRT1 in neurons [20]. In insulin secreting cells, we observed that resveratrol treatment increased AMPK phosphorylation [14]. However, although resveratrol activates both SIRT1 and AMPK, only SIRT1 activation accounts for the potentiating effects of resveratrol on metabolism-secretion coupling.

SIRT1 and resveratrol in hepatocytes

In the liver, SIRT1 is up-regulated after fasting or calorie restriction in rodents [25]. SIRT1 is also activated by resveratrol, inducing deacetylation of PGC-1α and thereby mitochondria biogenesis [7]. Overall, activation of hepatic SIRT1 increases gluconeogenic genes and represses glycolysis [26]. The gluconeogenic activity of hepatocyte nuclear factor 4α (HNF-4α) is increased by SIRT1-induced deacetylation of PGC-1α [26]. FoxO1, a member of the forkhead transcription factors, is also deacetylated by resveratrol, thereby promoting hepatic gluconeogenesis [27, 28]. In hepatocytes, activation of gluconeogenic gene expression by PGC-1α requires close cooperation with FoxO1 [29] and HNF-4α [30], regarding for instance glucose-6-phosphatase (Figure 2). In rats, administration of resveratrol results in FoxO1 deacetylation, accompanied by repression of glucokinase gene expression [27]. In isolated hepatocytes, it was shown that the repression of glucokinase induced by resveratrol is contributed by the interaction between FoxO1 and HNF-4α [27]. Taken as a whole, activation of SIRT1 by resveratrol in hepatocytes mimics starving conditions, reducing glucose usage and inducing glucose production (Figure 2).

SIRT1 mediates different effects in liver and pancreatic ß-cell

In most cells types, FoxO1 transcriptional activity is switched off by phosphorylation-mediated nuclear exclusion. However, when cells are subjected to stress, FoxO1 relocates to the nucleus where it is deacetylated by SIRT1 [31]. In ß-cells, FoxO1 is constitutively phosphorylated, and therefore cytoplasmic, presumably reflecting activation of insulin receptor signalling by endogenously produced insulin [32]. Induction of lipotoxicity by palmitate triggers accumulation of FoxO1 into the nucleus of insulin-secreting cells [33] and FoxO1 up-regulation impairs insulin secretion in ß-cells [34]. Therefore, under normal non-pathological conditions, FoxO1 is essentially cytoplasmic in ß-cells, regardless of glucose stimulation. Resveratrol treatment does not alter the cytoplasmic localization of FoxO1 in insulin-secreting cells [14]. In the liver, FoxO1 is phosphorylated upon insulin signalling, promoting nuclear exclusion [35]. Conversely, low-insulin fasting periods favour nuclear localization of FoxO1 in hepatocytes and induction of transcriptional activity through SIRT1-mediated deacetylation.

PGC-1α is another major target of SIRT1. In hepatocytes, PGC-1α induces gluconeogenic machinery and represses glucose consumption. In ß-cells, PGC-1α over-expression reduces glucose metabolism and the accompanying secretory response, suggesting a switch to lipid utilization [36]. In diabetic animal models, PGC-1α is up-regulated in islets [36] and in the liver [37], resulting in increased hepatic glucose production. Regarding hepatocyte nuclear factors, treatment of insulin secreting cells with resveratrol induces HNF-1α gene expression, while HNF-4α is not affected [14].

Overall, SIRT1 activation promotes up-regulation of glucokinase in ß-cells, while the same enzyme is down-regulated in hepatocytes. The apparent contradiction of such opposite effects indicates that the common master regulator SIRT1 signals starving state to different organs, thereby inducing specific metabolic responses.

Conclusion

The beneficial effects of resveratrol on the liver and pancreatic islets are dependent on SIRT1 activation, although SIRT1 targets are different according to each tissue (Figure 2). In the liver, resveratrol mostly acts on PGC-1α, FoxO1, HNF-4α, and AMPK. In the ß-cell the main identified targets are HNF-1α and Pdx1. To date, the precise mechanisms of SIRT1 activation are still poorly understood, in particular regarding pancreatic islets. Tissue specificity renders investigations more challenging but at the same time rather fascinating considering the whole metabolic control of energy homeostasis.

ACKNOWLEDGEMENTS

Current work in our laboratory is supported by the Swiss National Science Foundation and the State of Geneva. Authors are members of the Geneva Programme for Metabolic Disorders (GeMet).

CONFLICT OF INTERESTS STATEMENT

The authors have no conflict of interests to declare.

REFERENCES

1. Kaeberlein M, McVey M Guarente L. The SIR2/3/4 complex and SIR2 alone promote longevity in Saccharomyces cerevisiae by two different mechanisms. Genes Dev. 1999; 13: 2570-2580.

2. Tissenbaum HA Guarente L. Increased dosage of a sir-2 gene extends lifespan in Caenorhabditis elegans. Nature. 2001; 410: 227-230.

3. Rogina B Helfand SL. Sir2 mediates longevity in the fly through a pathway related to calorie restriction. Proc Natl Acad Sci U S A. 2004; 101: 15998-16003.

4. Frye RA. Characterization of five human cDNAs with homology to the yeast SIR2 gene: Sir2-like proteins (sirtuins) metabolize NAD and may have protein ADP-ribosyltransferase activity. Biochem Biophys Res Commun. 1999; 260: 273-279.

5. Frye RA. Phylogenetic classification of prokaryotic and eukaryotic Sir2-like proteins. Biochem Biophys Res Commun. 2000; 273: 793-798.

6. Howitz KT, Bitterman KJ, Cohen HY, Lamming DW, Lavu S, et al. Small molecule activators of sirtuins extend Saccharomyces cerevisiae lifespan. Nature. 2003; 425: 191-196.

7. Lagouge M, Argmann C, Gerhart-Hines Z, Meziane H, Lerin C, et al. Resveratrol improves mitochondrial function and protects against metabolic disease by activating SIRT1 and PGC-1alpha. Cell. 2006; 127: 1109-1122.

8. Baur JA, Pearson KJ, Price NL, Jamieson HA, Lerin C, et al. Resveratrol improves health and survival of mice on a high-calorie diet. Nature. 2006; 444: 337-342.

9. Su HC, Hung LM Chen JK. Resveratrol, a red wine antioxidant, possesses an insulin-like effect in streptozotocin-induced diabetic rats. Am J Physiol Endocrinol Metab. 2006; 290: E1339-1346.

10. Chi TC, Chen WP, Chi TL, Kuo TF, Lee SS, et al. Phosphatidylinositol-3-kinase is involved in the antihyperglycemic effect induced by resveratrol in streptozotocin-induced diabetic rats. Life Sci. 2007; 80: 1713-1720.

11. Maechler P, Li N, Casimir M, Vetterli L, Frigerio F, et al. Role of mitochondria in beta-cell function and dysfunction. Adv Exp Med Biol. 2010; 654: 193-216.

12. Moynihan KA, Grimm AA, Plueger MM, Bernal-Mizrachi E, Ford E, et al. Increased dosage of mammalian Sir2 in pancreatic beta cells enhances glucose-stimulated insulin secretion in mice. Cell Metab. 2005; 2: 105-117.

13. Bordone L, Motta MC, Picard F, Robinson A, Jhala US, et al. Sirt1 regulates insulin secretion by repressing UCP2 in pancreatic beta cells. PLoS Biol. 2006; 4: e31.

14. Vetterli L, Brun T, Giovannoni L, Bosco D Maechler P. Resveratrol Potentiates Glucose-stimulated Insulin Secretion in INS-1E {beta}-Cells and Human Islets through a SIRT1-dependent Mechanism. J Biol Chem. 2011; 286: 6049-6060.

15. Hambrock A, de Oliveira Franz CB, Hiller S, Grenz A, Ackermann S, et al. Resveratrol binds to the sulfonylurea receptor (SUR) and induces apoptosis in a SUR subtype-specific manner. J Biol Chem. 2007; 282: 3347-3356.

16. Boj SF, Parrizas M, Maestro MA Ferrer J. A transcription factor regulatory circuit in differentiated pancreatic cells. Proc Natl Acad Sci U S A. 2001; 98: 14481-14486.

17. Waeber G, Thompson N, Nicod P Bonny C. Transcriptional activation of the GLUT2 gene by the IPF-1/STF-1/IDX-1 homeobox factor. Mol Endocrinol. 1996; 10: 1327-1334.

18. Zang M, Xu S, Maitland-Toolan KA, Zuccollo A, Hou X, et al. Polyphenols stimulate AMP-activated protein kinase, lower lipids, and inhibit accelerated atherosclerosis in diabetic LDL receptor-deficient mice. Diabetes. 2006; 55: 2180-2191.

19. Hou X, Xu S, Maitland-Toolan KA, Sato K, Jiang B, et al. SIRT1 regulates hepatocyte lipid metabolism through activating AMP-activated protein kinase. J Biol Chem. 2008; 283: 20015-20026.

20. Dasgupta B Milbrandt J. Resveratrol stimulates AMP kinase activity in neurons. Proc Natl Acad Sci U S A. 2007; 104: 7217-7222.

21. Chan AY, Dolinsky VW, Soltys CL, Viollet B, Baksh S, et al. Resveratrol inhibits cardiac hypertrophy via AMP-activated protein kinase and Akt. J Biol Chem. 2008; 283: 24194-24201.

22. Canto C, Gerhart-Hines Z, Feige JN, Lagouge M, Noriega L, et al. AMPK regulates energy expenditure by modulating NAD+ metabolism and SIRT1 activity. Nature. 2009; 458: 1056-1060.

23. Canto C, Jiang LQ, Deshmukh AS, Mataki C, Coste A, et al. Interdependence of AMPK and SIRT1 for metabolic adaptation to fasting and exercise in skeletal muscle. Cell Metab. 2010; 11: 213-219.

24. Fulco M, Cen Y, Zhao P, Hoffman EP, McBurney MW, et al. Glucose restriction inhibits skeletal myoblast differentiation by activating SIRT1 through AMPK-mediated regulation of Nampt. Dev Cell. 2008; 14: 661-673.

25. Cohen HY, Miller C, Bitterman KJ, Wall NR, Hekking B, et al. Calorie restriction promotes mammalian cell survival by inducing the SIRT1 deacetylase. Science. 2004; 305: 390-392.

26. Rodgers JT, Lerin C, Haas W, Gygi SP, Spiegelman BM, et al. Nutrient control of glucose homeostasis through a complex of PGC-1alpha and SIRT1. Nature. 2005; 434: 113-118.

27. Ganjam GK, Dimova EY, Unterman TG Kietzmann T. FoxO1 and HNF-4 are involved in regulation of hepatic glucokinase gene expression by resveratrol. J Biol Chem. 2009; 284: 30783-30797.

28. Qiang L, Banks AS Accili D. Uncoupling of acetylation from phosphorylation regulates FoxO1 function independent of its subcellular localization. J Biol Chem. 2010; 285: 27396-27401.

29. Puigserver P, Rhee J, Donovan J, Walkey CJ, Yoon JC, et al. Insulin-regulated hepatic gluconeogenesis through FOXO1-PGC-1alpha interaction. Nature. 2003; 423: 550-555.

30. Rhee J, Inoue Y, Yoon JC, Puigserver P, Fan M, et al. Regulation of hepatic fasting response by PPARgamma coactivator-1alpha (PGC-1): requirement for hepatocyte nuclear factor 4alpha in gluconeogenesis. Proc Natl Acad Sci U S A. 2003; 100: 4012-4017.

31. Kitamura YI, Kitamura T, Kruse JP, Raum JC, Stein R, et al. FoxO1 protects against pancreatic beta cell failure through NeuroD and MafA induction. Cell Metab. 2005; 2: 153-163.

32. Harbeck MC, Louie DC, Howland J, Wolf BA Rothenberg PL. Expression of insulin receptor mRNA and insulin receptor substrate 1 in pancreatic islet beta-cells. Diabetes. 1996; 45: 711-717.

33. Hennige AM, Ranta F, Heinzelmann I, Dufer M, Michael D, et al. Overexpression of kinase-negative protein kinase Cdelta in pancreatic beta-cells protects mice from diet-induced glucose intolerance and beta-cell dysfunction. Diabetes. 2010; 59: 119-127.

34. Nakae J, Biggs WH, 3rd, Kitamura T, Cavenee WK, Wright CV, et al. Regulation of insulin action and pancreatic beta-cell function by mutated alleles of the gene encoding forkhead transcription factor Foxo1. Nat Genet. 2002; 32: 245-253.

35. Nakae J, Park BC Accili D. Insulin stimulates phosphorylation of the forkhead transcription factor FKHR on serine 253 through a Wortmannin-sensitive pathway. J Biol Chem. 1999; 274: 15982-15985.

36. Yoon JC, Xu G, Deeney JT, Yang SN, Rhee J, et al. Suppression of beta cell energy metabolism and insulin release by PGC-1alpha. Dev Cell. 2003; 5: 73-83.

37. Yoon JC, Puigserver P, Chen G, Donovan J, Wu Z, et al. Control of hepatic gluconeogenesis through the transcriptional coactivator PGC-1. Nature. 2001; 413: 131-138.

Research Paper

RasGrf1 deficiency delays dging in mice

Consuelo Borrás[1], Daniel Monleón[2], Raul López-Grueso[1], Juan Gambini[1], Leonardo Orlando[3], Federico V. Pallardó[1], Eugenio Santos[4], José Viña[1,*] and Jaime Font de Mora[3,*]

[1] *Department of Physiology, School of Medicine, University of Valencia, E46010, Valencia, Spain*
[2] *Fundación de Investigación del Hospital Clínico Universitario de Valencia / INCLIVA, E46010, Valencia*
[3] *Centro de Investigación Príncipe Felipe, 46012 Valencia, Spain*
[4] *Centro de Investigación del Cáncer (USAL-CSIC), University of Salamanca. Campus Miguel de Unamuno s/n. 37007, Salamanca, Spain*
**These authors contributed equally to this work*

Key words: *Longevity, Ras, metabolism, GEF, IGF-1, positron emission tomography*
Received: *2/18/11; Accepted: 03/12/11; Published: 3/14/11*
Corresponding author: *Jose Viña;* ***E-mail:*** *jose.vina@uv.es* doi:10.18632/aging.100279

Abstract: RasGRF1 is a Ras-guanine nucleotide exchange factor implicated in a variety of physiological processes including learning and memory and glucose homeostasis. To determine the role of RASGRF1 in aging, lifespan and metabolic parameters were analyzed in aged *RasGrf1*$^{-/-}$ mice. We observed that mice deficient for *RasGrf1*$^{-/-}$ display an increase in average and most importantly, in maximal lifespan (20% higher than controls). This was not due to the role of Ras in cancer because tumor-free survival was also enhanced in these animals. Aged *RasGrf1*$^{-/-}$ displayed better motor coordination than control mice. Protection against oxidative stress was similarly preserved in old *RasGrf1*$^{-/-}$. IGF-I levels were lower in *RasGrf1*$^{-/-}$ than in controls. Furthermore, SIRT1 expression was increased in *RasGrf1*$^{-/-}$ animals. Consistent with this, the blood metabolomic profiles of *RasGrf1*-deficient mice resembled those observed in calorie-restricted animals. In addition, cardiac glucose consumption as determined PET was not altered by aging in the mutant model, indicating that *RasGrf1*-deficienct mice display delayed aging. Our observations link Ras signaling to lifespan and suggest that *RasGrf1* is an evolutionary conserved gene which could be targeted for the development of therapies to delay age-related processes.

INTRODUCTION

RASGRF1 is a guanine nucleotide-releasing factor for RAS that is activated by calmodulin-mediated Ca^{2+} influx [1] as well as G-protein coupled receptors [2, 3]. RASGRF1 serves as an *in vivo* activator for H-RAS and members of the R-RAS and RAC subfamilies [4]. Guanine nucleotide-releasing factors interact with the inactive RAS bound to GDP and catalyze the exchange of GDP for GTP, thereby activating RAS. In contrast with other RAS-GTP exchange factors, RASGRF1 is expressed mainly in pancreatic β-cells where it regulates β-cell mass and in specific brain regions including the hippocampus and hypothalamus, thus linking RASGRF1-dependent RAS activation to glucose homeostasis and neuronal function [5, 6].

Previous reports have demonstrated that *RasGrf1*-defcient mice display defects in learning and memory, although the explanation for these impairments remains controversial [5, 7]. Similar to *RasGrf1* null mice generated in a different strain [8], our knockout mice display reduced body size. Additionally, we observed that *RasGrf1*-deficiency causes hypo-insulinemia due to a reduction in β-cell proliferation and β-cell mass [6]. However, perhaps owing to the fact that the size of these animals is reduced, insulin levels are sufficient to compensate under normal conditions and thus, diabetes does not develop in this model. Therefore, RASGRF1-mediated signaling is important in the regulation of β-cell proliferation and glucose homeostasis.

RAS has been shown conclusively to exert a role in aging in yeast. Mutations that decrease the activity of the RAS/Cyr1/PKA pathway extend longevity and increase stress resistance in yeast by activating transcription factors Msn2/Msn4 and the mitochondrial superoxide dismutase [9]. It has also been reported that *Ras* genes are a major homeostatic device in the regulation of the lifespan of *S. cerevisiae* [10]. The longevity-modulating function of IGF-I in *C. elegans* displays a signal bifurcation involving the *Ras* ortholog Let-60, consistent with a role for RAS signaling downstream of IGF-IR. Attenuated insulin/IGF-I signaling (IIS) is hypothesized to mediate some of the anti-aging effects of calorie restriction in mice [11]. Importantly, mice heterozygous for the IGF-IR live longer and are resistant to oxidative stress [12]. Moreover, calorie restriction has been suggested to down-regulate pathways including m-TOR, AKT and RAS [13].

Several studies with cultures of mammalian cells have suggested that RAS might be involved in aging and age-related processes such as apoptosis. Apoptosis in neurons, T cells, and human epithelial cells is mediated by the activation of RAS [14] [15, 16]. On the contrary, inhibition of RAS rescues PC12 cells from apoptosis [17]. Moreover, inhibition of RAS in these cells increases resistance to oxidative stress [18, 19].

However, few studies have addressed the potential role of RAS signaling in regulating lifespan in mammals [20]. Based on the previous data from our laboratory [6] as well as others [8], we hypothesized that *RasGrf1*-deficient mice could have increased longevity. We measured plasma IGF-I levels as it related to RAS and aging. We studied the expression of cytochrome c oxidase to determine whether oxidative stress is altered in *RasGrf1*-deficient mice. Finally, to test the idea that *RasGrf1* deficiency promotes beneficial metabolic changes, we compared the metabolomic profile of our *RasGrf1*-deficient mice with calorie restricted controls.

Our studies reveal that loss of *RasGrf1* (*RasGrf1*-KO) expands not only average but also maximal lifespan in mice. These mice display lower plasma levels of IGF-1, lower oxidative stress and a metabolic profile which resembles that observed in calorie-restricted wild-type animals. Thus, *RasGrf1* deficiency in mice promotes longevity consistent with the lifespan extension associated with loss of IGF-I signalling molecules from yeast to mammals.

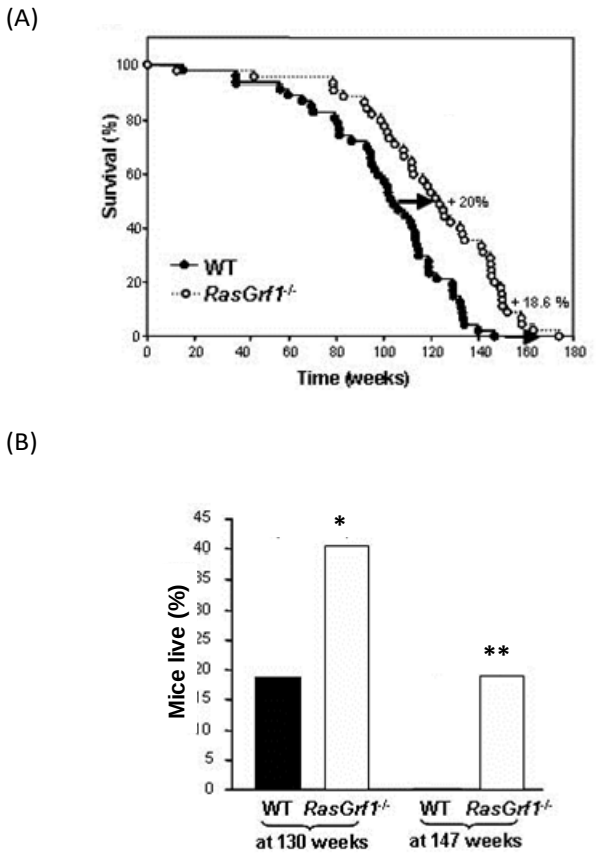

Figure 1. Delayed Ageing in *RasGrf1*$^{-/-}$ (**A**) Survival curve of *RasGrf1*$^{-/-}$ male mice and of WT of the same genetic background. WT n = 47; *RasGrf1*$^{-/-}$ n = 45. Report the Kaplan – Meyer representation of the two groups ($p<0.05$). (**B**) Percentage of mice alive after a hundred and thirty weeks (*$p<0.02$) and a hundred and forty-seven weeks (**$p<0.005$) of the two cohorts. Maximal lifespan in wild type was a hundred and forty-seven weeks. Thus 20% of all the *RasGrf1*$^{-/-}$ cohort survived longer than the maximal lifespan of the wild types.

RESULTS

Increased Average and Maximal Lifespan in *RasGrf1*$^{-/-}$ Mice

Survival curves revealed a marked increase (20%) in the average lifespan of *RasGrf1*$^{-/-}$ male mice (mean values WT: 100.5±4.2 weeks and *RasGrf1*$^{-/-}$: 120.7±4.7 weeks; median WT: 104 weeks; *RasGrf1*$^{-/-}$: 124 weeks) ($p= 6x10^{-5}$, Logrank test). The effects of *RasGrf1* deficiency were also evident on maximal lifespan; WT mice lived up to 146.7 weeks whereas *RasGrf1* mutants lived as long as 174 weeks (Figure 1A). This increase of 18.6%

to maximal lifespan supports a critical role for *RasGrf1* in longevity. In fact, 19,2% of *RasGrf1*$^{-/-}$ mice lived longer than the oldest WT (Figure 1B). The lifespan of our WT mice is within the range of variation reported for C57B1, 129 and hybrids [21-27].

One plausible explanation for these longevity promoting effects could be the role of RASGRF1 in RAS activation and hence, in cancer development. To test this possibility, we identified those animals that developed tumors and generated a tumor-free survival curve. Consistent with the curve generated for the total population, *RasGrf1*$^{-/-}$ without tumors displayed a 20% increase in average lifespan as compared with tumor-free control mice (mean values WT: 99±4.5 weeks and *RasGrf1*$^{-/-}$: 119±4.9; median WT: 102 weeks; *RasGrf1*$^{-/-}$: 121 weeks) (p= 0.0003, Logrank test) (Figure 1B). Thus, the role of RAS in cancer is not the reason for the longer longevity of *RasGrf1*$^{-/-}$ mice. No obvious pathological differences were observed at death between WT and *RasGrf1*$^{-/-}$ mice. The substantial increase in average and maximal lifespan suggests *RasGrf1* as a novel age-associated gene.

RasGrf1$^{-/-}$ Mice Show Better Motor Coordination than Controls

Maintaining good motor coordination in old age is important to ensure that living longer is accompanied by an adequate quality of life. Young *RasGrf1*$^{-/-}$ mice displayed superior motor coordination in the tightrope test as compared to WT controls (Figure 2A). Whereas motor coordination of WT mice declined significantly with age, old *RasGrf1*$^{-/-}$ maintained a level of motor coordination that was similar to young animals (Figure 2A). Thus, our analysis suggests that *RasGrf1*$^{-/-}$ mice not only live longer but they are less prone to frailty.

Expression of 16S rRNA is higher in *RasGrf1*$^{-/-}$ mice than in control mice

We examined the expression levels of 16S rRNA, which decreases significantly with age [28, 29] and oxidative stress [30]. 16S RNA levels were much higher in liver of *RasGrf1*$^{-/-}$ than WT of the same age (Figure 2B). This result is consistent with the increased lifespan observed in *RasGrf1*$^{-/-}$ mice.

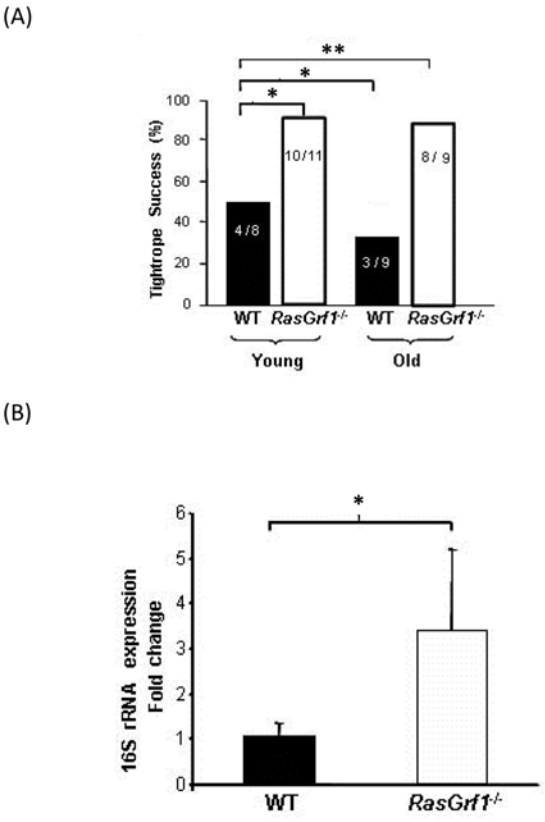

Figure 2. Increased Neuromuscular Coordination Coincided With Biomarkers of Aging in *RasGrf1*$^{-/-}$ Mice. (**A**) Neuromuscular coordination was quantified as the percentage of male mice that successfully passed the tightrope test. Numbers within the bars indicate animals that passed the test divided by the total number of animals which were subjected to the test. Young animals were 4-6 months old, and old animals were 20-22 months old. Significance is shown as *p<0.05; **p<0.01 vs. WT. (**B**) Liver extracts from male mice were used to assess 16S rRNA expression in 4-6 months old animals. Expression of 16S rRNA was significantly higher in *RasGrf1*$^{-/-}$ mice. WT n = 4; *RasGrf1*$^{-/-}$ = 3; *p=0.03.

RasGrf1$^{-/-}$ Mice Display Less Oxidative Stress

To analyze the contribution of the free radicals to the increased lifespan associated with *RasGrf1* deficiency, we assessed three of the critical parameters of oxidative stress: glutathione, protein oxidation, and malondialdehyde (MDA) which is a measurement of lipid peroxidation. Oxidative stress diminishes the levels of reduced-glutathione (GSH), the most abundant non-

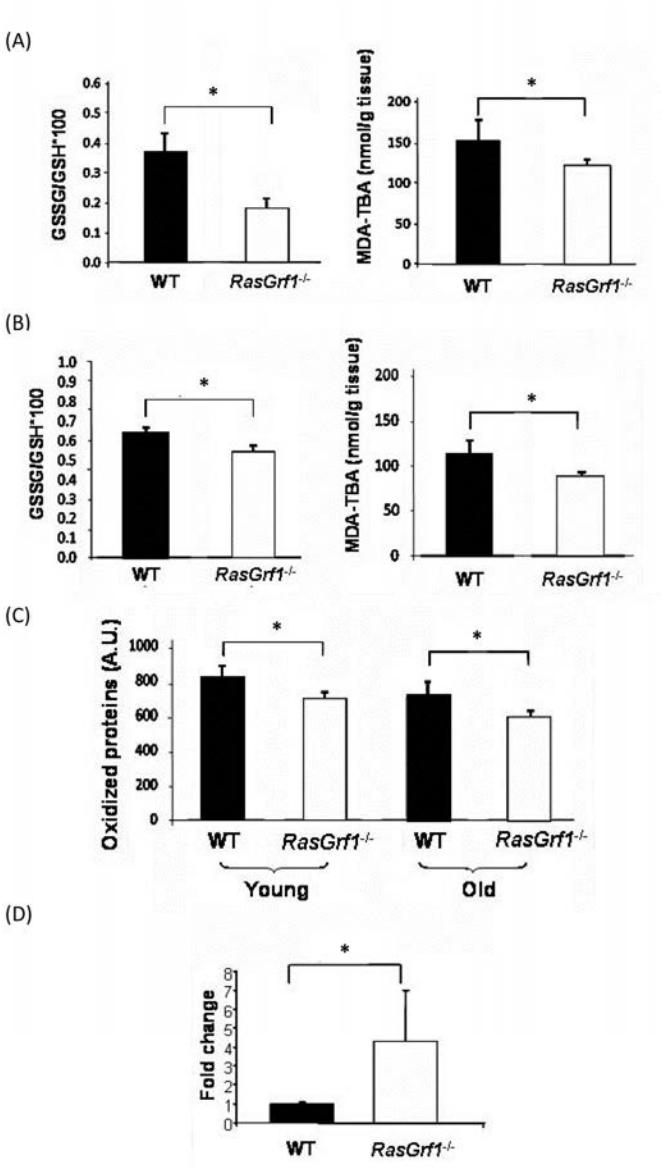

Figure 3. Decreased Oxidative Stress in *RasGrf1*$^{-/-}$ Mice. (A) Oxidative stress was measured in brain from 4-6 months old animals. Glutathione redox ratio was significantly higher in WT (n=7) than in *RasGrf1*$^{-/-}$ male mice (n=8). Malondialdehyde (MDA) levels were significantly lower in brain of *RasGrf1*$^{-/-}$ mice (n=8) than in that of WT (n=7). MDA was measured by the formation of the aduct malondialdehyde-thiobarbituric acid (MDA-TBA) (*p<0.05). (**B**) Oxidised glutathione and malondialdehyde levels were significantly lower in liver of *RasGrf1*$^{-/-}$ male mice. n for WT = 7 and for *RasGrf1*$^{-/-}$ = 8 (*p<0.05) (4-6 months old). (**C**) Oxidised proteins in young (4-6 months old) and old (20-22 months old) WT mice were significantly higher than in *RasGrf1*$^{-/-}$ male mice (*p<0.05). These were measured by western blot with antibodies directed against aldehydes in proteins. (**D**) Cytochrome c oxidase expression is significantly higher in *RasGrf1*$^{-/-}$ than in WT male mice of 4-6 months old (*p=0.037). Total RNA from selected tissues was isolated and used to quantify cytochrome c oxidase by real time RT-PCR.

protein antioxidant in cells, to form the disulphide bond-dimer (GSSG). The GSSG/GSH ratio was significantly lower in brain and liver of *RasGrf1*$^{-/-}$ mice as compared with controls (Figure 3A,B upper panels), indicating that *RasGrf1*$^{-/-}$mice are subjected to less oxidative stress. Additionally, lipid peroxide levels were significantly lower in *RasGrf1*$^{-/-}$ mice (Figure 3A,B lower panels). Since aging is characterized by the accumulation of oxidized proteins due to increased protein damage and/or decreased elimination, we evaluated this parameter in liver of young and old animals. The overall oxidized protein levels in liver of *RasGrf1*$^{-/-}$ were significantly lower than in age-matched WT mice (Figure 3C). These results support the idea that loss of *RasGrf1* protects against oxidative damage and hence, contributes to a younger phenotype. We next examined a possible molecular basis of these findings. Low levels of cytochrome c oxidase, the terminal enzyme in the mitochondrial electron transport chain, increase the production of reactive oxygen species (ROS) [31]. Interestingly, the expression levels of cytochrome c oxidase were significantly higher in liver of *RasGrf1*$^{-/-}$ mice (Figure 3D). Thus, disruption of the RAS signaling via deletion of *RasGrf1* up-regulates the expression of cytochrome c oxidase, providing at least one explanation for the lower oxidative stress in *RasGrf1*$^{-/-}$ mice.

Higher Glycogen Hepatic Content In *RasGrf1*$^{-/-}$ Mice

Aging is characterized by a diminished response to stress [32]. Maintenance of glycogen storage is important in the stress response [33]. We found that hepatic glycogen in WT mice was virtually absent after 24 hours of fasting whereas *RasGrf1*$^{-/-}$ mice maintained significant glycogen levels (Figure 4A). Our findings reveal a glycogen-sparing effect mediated by loss of a specific gene. Maintenance of relatively high levels of glycogen in fasting would be expected to convey a metabolic advantage in response to stress during aging.

Increased Expression of SIRT1 in *RasGrf1*$^{-/-}$ mice

Sirtuins have appear to play a role in determining longevity [34], but their importance in mammalian lifespan is not clear (Herranz & Serrano 2010). We observed that the levels of SIRT1 are increased in the liver and heart of *RasGrf1*$^{-/-}$ mice (Figure 4B). High sirtuin might explain the glycogen sparing effect that we have shown above (see discussion).

IGF-1 Levels Are Lower in *RasGrf1*$^{-/-}$ Mice

Long-lived animals display low IGF-1 levels [35-37]. We observed a significant decrease of IGF-1 in *RasGrf1*$^{-/-}$ mice when compared to controls (Figure 4C).

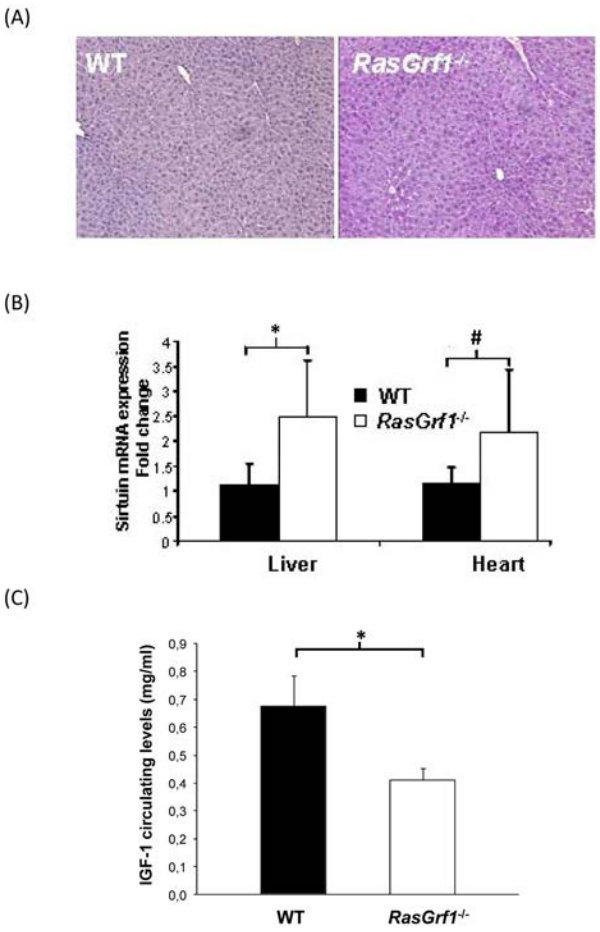

Figure 4. Metabolic Analysis of *RasGrf1*$^{-/-}$ Mice. (**A**) Liver of *RasGrf1*$^{-/-}$ male animals (4-6 months old) contains a significant amount of glycogen after 24 hours of fasting contrasting with the complete absence in WT animals (4-6 months old). PAS staining was quantified using color deconvolution with ImageJ software (Broken Symmetry Software). Values represent relative staining of three different sections (*p=0.01 determined by a paired T-test). (**B**) Sirtuin mRNA expression in liver and heart of *RasGrf1*$^{-/-}$ male mice is significantly higher than in WT mice (*p=0.033; #p=0.035). Wild-type n = 4, *RasGrf1*$^{-/-}$ n = 3 (4-6 months old). (**C**) IGF-I plasma levels was measured in 3-5 months old male mice by RIA revealing a 30% reduction in *RasGrf1*$^{-/-}$. Wild-type n = 10, *RasGrf1*$^{-/-}$ n = 9, *p<0.001.

Therefore, this could explain, at least in part, the increased longevity of *RasGrf1*$^{-/-}$ mice. Consistent with the low IGF-1 levels, somatic growth was also reduced in *RasGrf1*$^{-/-}$ mice (See Figure S3).

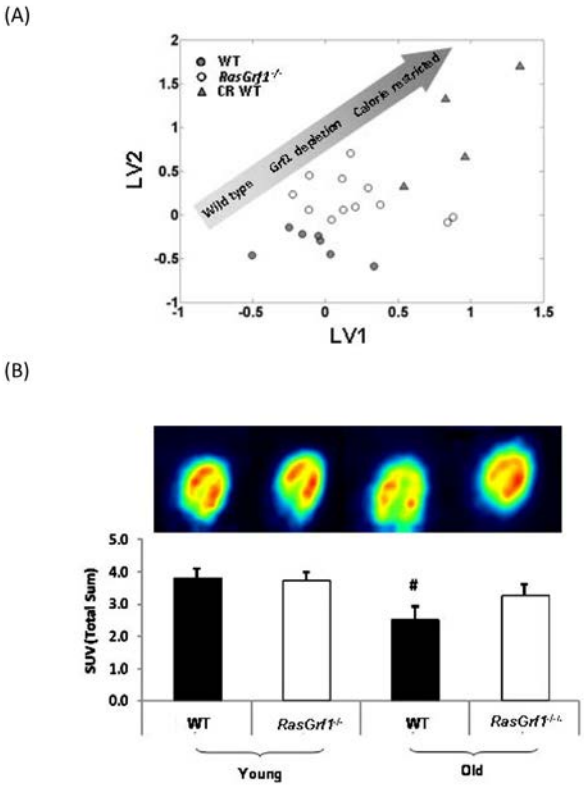

Figure 5. Analysis Of Metabolic Parameters in *RasGrf1* Deficient and Control Mice. (**A**) Metabolomic analysis reveals a metabolic shift of *RasGrf1*$^{-/-}$ fed male mice towards caloric restricted WT (4-6 months old). Multivariate analysis (PLS – DA) of NMR spectra of blood plasma showing global metabolic profiles of WT, *RasGrf1*$^{-/-}$, and calorie restricted WT mice. The graph represents the scores plot of the PLS-DA model for discrimination between WT and *RasGrf1*$^{-/-}$. The graph also shows the metabolic profile of WT animals on caloric restriction projected over the PLS-DA latent space. Each symbol represents an animal. (**B**) Glucose up-take *in vivo* by heart of WT and *RasGrf1*$^{-/-}$ male mice. Positron emission tomography (PET) analysis was used to estimate *in vivo* glucose uptake in young (4-6 months old) and old (20-22 months old) animals. The image is the result of a representative experiment. Histograms represent the means of glucose up-take measured in four animals in each group. Wild type n = 7, *RasGrf1*$^{-/-}$ n = 8; #p<0.01.

Metabolomics Reveal that the Metabolic Profile of *RasGrf1*$^{-/-}$ Mice Resembles Calorie Restricted Mice

To gain further insight into the mechanisms that promote increased average and maximal lifespan *RasGrf1*$^{-/-}$ mice, we performed metabolomic studies in which we compared *RasGrf1*$^{-/-}$ animals with WT animals, and calorie-restricted WT animals. Figure 5A presents the global metabolic profile of *RasGrf1*$^{-/-}$ and

WT animals as measured by NMR. The distribution of the three groups represented in the plot indicates that the metabolic profile exhibited by *RasGrf1*$^{-/-}$ animals is shifted towards that of the CR animals. The multivariate analysis reveals a set of metabolites with significant variations between WT and *RasGrf1*$^{-/-}$ mice (Figure S1). Most of these metabolic differences also occur in CR such as an increase in the levels of polyunsaturated fatty acids (PUFA; 14%, p=0.002), and decrease in glucose levels (10%, p=0.03) in *RasGrf1*$^{-/-}$.

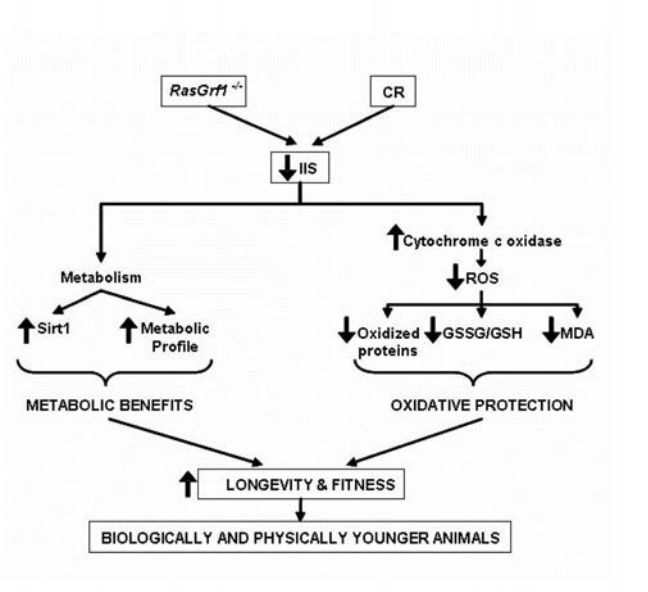

Figure 6. Schematic Representation of the Molecular and Physiological Characteristics of *RasGrf1*$^{-/-}$ Animals. *RasGrf1-/-* results in an increased longevity which is mediated by a lower insulin /IGF signaling (IIS) which eventually leads to metabolic benefits and in lower ROS production and subsequent oxidative protection. These two independent changes converge in a notable increase in longevity and fitness.

Glucose Uptake *In Vivo* Is Maintained in Aged *RasGrf1*$^{-/-}$ Mice But Not in Control Mice

We used positron emission tomography (PET) to analyze *in vivo* glucose uptake in young and old animals since reduced glucose uptake is associated with aging [38]. Glucose uptake by heart of control animals was significantly lowered with age. Surprisingly, this loss of glucose consumption did not occur with aging in *RasGrf1*$^{-/-}$ animals (Figure 5B). Thus, although the critical parameter of glucose incorporation in cardiac tissue declined considerably in aged WT controls, it was preserved in *RasGrf1*$^{-/-}$ animals.

DISCUSSION

Interest in genetic components that modulate longevity in mammals has grown in recent years [39, 40]. According to the National Institute on Aging (NIA), the genetically heterogeneous mouse model was deemed to be the most suitable for longevity studies [41], even if this increases the genetic variability of each mouse and decreases the power of attaining statistical significance [39]. We have recently reported that over-expressing two (p53/p16) [42] or three (p53/p16/telomerase) [43] genes results in significant increases in average lifespan but without increasing maximal lifespan. Here we report a significant increase in maximal lifespan by the deletion of *RasGrf1* in inbred mice with a heterogeneous background. Increasing maximal lifespan is important because it indicates a fundamental change in the aging process. Improvements in lifestyle conditions usually result in increases to average but not maximal lifespan [32]. Extrapolating to humans, curing all diseases would result in an increase of less than 20% in average lifespan without changing maximal lifespan [32].

Motor coordination is an important determinant of frailty, a major geriatric syndrome [44, 45]. Ladiges et al. have emphasized the importance of finding genetic modifications that improve patho-physiological functions associated with aging, such as motor coordination [39]. We have found that motor coordination is improved in the *RasGrf1* deficient mice (Figure 2A), thus indicating that these animals not only live longer but are less prone to frailty.

Based on genomic scanning with methylation sensitive enzymes, *RasGrf1* was postulated as a paternally imprinted gene in the mouse [46]. This was confirmed by the subsequent generation of *RasGrf1*-deficient mice; studies of heterozygous animals demonstrated that *RasGrf1* is an imprinted gene regulated by the male and modulates postnatal growth because it functions after, rather than before, birth [8]. The imprinted nature of *RasGrf1* was further validated by the characterization of two nonsense mutations that when paternally transmitted caused reduced body weight during postnatal development [47]. A more recent study with bi-maternal mice revealed that the sperm genome has a detrimental effect on longevity, most likely due to the repression of *RasGrf1* in this model [48]. In contrast to other imprinted genes that are implicated in fetal growth, *RasGrf1* regulates postnatal growth. RASGRF1 is expressed after birth in the hypothalamus of wild-type mice, but not in the pituitary, where it indirectly regulates the synthesis of growth hormone [8]. Many genes that modulate longevity directly or indirectly

target mitochondrial function. Mitochondria are inherited via the female parent. Similar to other paternally expressed genes, *RasGrf1* is involved in growth stimulation, whereas maternally expressed genes are responsible for growth suppression [8, 49]. Hence, our results describe a longevity-related gene which is solely determined by the male parent.

Circulating IGF-I levels and body size are important determinants of lifespan [37]. A previous publication reported reduced IGF-I circulating levels and adult body size in mice deficient for *RasGrf1*$^{-/-}$ [8]. However, this model was generated in pure 129 sv genetic background which is distinct from our own *RasGrf1*$^{-/-}$ mice which are genetically heterogeneous mice. Since genetic background can exert a profound effect in parameters such as metabolism and growth ratio, we measured IGF-I circulating levels in our own *RasGrf1*$^{-/-}$ model. In agreement with the other knockout model, circulating IGF-I was reduced by 39% in our *RasGrf1*$^{-/-}$ mice (Figure 4C). Hence, *RasGrf1*$^{-/-}$ mice display both low insulin and IGF-I levels that may significantly impact systemic IIS. In agreement with low IGF-1 levels, *RasGrf1*$^{-/-}$ mice display reduced body weight (See Figure S3). We previously reported that food intake, circulating leptin levels and leptin receptor expression in the hypothalamus are very similar between WT and *RasGrf1*$^{-/-}$ mice [6], suggesting that food intake is not the mechanism for the longer lifespan of *RasGrf1*$^{-/-}$ mice. Therefore, the increase in lifespan observed in *RasGrf1*$^{-/-}$ mice is most probably due to their lower insulin and IGF-1 levels.

Lower serum IGF-I and insulin levels are characteristic of animals subjected to caloric restriction and are associated with increased SIRT1 expression and reduced oxidative stress [50, 51]. In this paper we also show higher levels of SIRT1 expression (Figure 4B) and reduced oxidative stress (Figure 3) in *RasGrf1*$^{-/-}$ mice. Metabolomic results also indicate that *RasGrf1*$^{-/-}$ mice could resemble in some way calorie restricted mice, as it is shown in Figure 5. The positive effects of CR on lifespan extension may involve the down-regulation of pathways, including mTOR, AKT, and RAS [13]. Our results demonstrate a novel physiological function of the RAS modulator RASGRF1 in extending both median and maximum lifespan.

SIRT1 deacetylates PPARγ and its co-activator PGC1α, thereby promoting fat mobilization and increasing mitochondrial size and number [52-55]. Activation of SIRT1 stimulates hepatic energy expenditure by increasing the degradation of fatty acids [56]. Conversely, under fasting conditions (e.g. CR), glycolytic genes are repressed through a mechanism that involves PGC1α and SIRT1 [55]. Therefore, increased SIRT1 expression would be expected to enhance this repression and promote the accumulation of glucose reservoirs in the form of glycogen. Indeed, increased hepatic SIRT1 expression correlated with enhanced glycogen accumulation in the liver of fasted *RasGrf1*$^{-/-}$ mice (Figure 4A). Although glycogen storage is regulated through a plethora of conditions, the fact that *RasGrf1*$^{-/-}$ mice exhibit higher liver glycogen levels could also be consistent with increased SIRT1 levels mediated by FoxO1-dependent transcriptional activity [57]. In contrast, hepatic glycogen levels after a 24 hour fast were undetectable WT control mice.

Glucose uptake favors a metabolic phenotype that protects against age-associated susceptibility to ischemic injury [58]. Therefore, preservation of cardiac glucose uptake may represent yet another physiological advantage for the *RasGrf1*$^{-/-}$ extended lifespan. Decline in cardiac performance with age is prevented in *Drosophila* by disruption of insulin receptor signaling specifically in the heart [59]. Additionally, higher plasma concentrations of PUFA detected in *RasGrf1*$^{-/-}$ are also expected to have beneficial effects for cardiovascular disease and lifespan.

The increased longevity of *RasGrf1*$^{-/-}$ mice may be explained by the low IGF-1 levels [37]. The physiological explanation linking these low levels and *RasGrf1* deficiency at the cellular level is very difficult to obtain because *RasGrf1* is only expressed in hippo-campus, hypothalamic, β-pancreatic and mature adipocytes. Adipocytes do not synthesize IGF-I. Hypothalamic and β-pancreatic cell do but they cannot be obtained in sufficient amounts to perform cell- signaling studies. Cells usually used in these kinds of studies, like mouse embryonic fibroblasts do not express *RasGrf1*. The involvement of *Ras*, but not *RasGrf1*, in longevity has been extensively studied by Longo and coworkers [20, 60, 61]. These authors have shown in yeast, that RAS regulates stress resistance and longevity by activating transcription factors Msn2/Msn4 and the mitochondrial antioxidant enzyme superoxide dismutase (Sod2) [60]. We also observed less oxidative stress in the *RasGrf1* deficient mice, and we show that the mitochondrial antioxidant enzyme which is up-regulated is cytochrome c oxidase (Figure 3). Thus, the increased longevity and resistance to stress in *RasGrf1* deficient mice show that the negative influence of the RAS pathway may be conserved mechanism from yeast to mammals.

Moreover, based in a genome-wide association study, Sebastiani and co-workers found a set of 150 single nucleotide polymorphisms (SNPs) that can predict

exceptional longevity (EL) in humans [62]. This novel approach for predicting EL provided valuable information regarding genes that contribute to EL. *RasGrf1* was found to be one of such genes. We have demonstrated that deficiency in *RasGrf1* expands not only average but also maximal lifespan, thus revealing to be a longevity-conserved gene in rodents and humans. Recently, Kawahara and Kono found that bi-maternal mice (i.e. "mice without a father") exhibited increased longevity and this was attributed it to lack of *RasGrf1* [48].

In summary, our results demonstrate that *RasGrf1*$^{-/-}$ display less oxidative stress than control mice and also have lower insulin/IGF-1 circulating and higher sirtuin expression. Thus, the increase in maximal longevity in this model may be explained by the fact that two main theories of aging (the free radical and the IGF-I theories of aging) are at work in the *RasGrf1*$^{-/-}$ mice (Figure 6).

MATERIALS AND METHODS

Mice. Male wild-type (WT) and *RasGrf1*$^{-/-}$ mice were maintained in ventilated cages and survival function was estimated from lifespan data.

Handling, supervision and experimentation with mice was done in accordance to the Guidelines for Humane Endpoints for Animals Used in Biomedical Research. Mice were housed at the pathogen-free barrier area of the Prince Felipe Research Centre. Moribund criteria was established and approved by the Ethical Committee at the Prince Felipe Research Centre. These criteria were based on the suggested clinical endpoints for aging mice according to McGill University's Ethics Subcommittee (www.mcgill.ca/files/researchoffice/Aging-mice-6.doc). Briefly, animals were assigned a health score based on their general appearance, wounds, prolapses, size and location of tumors, etc., as described in Table S1. Depending of the score, animals were monitored daily when symptoms were minor. In more critical cases (loss of vital functions or a score over 18 points) animals were immediately euthanized.

RasGrf1$^{-/-}$ mice were originally generated in 1998 at NCI facilities in Frederick (MD). Transfections were done in RW-4 cells (derived from 129SvJ mouse strain) to obtain the gene deletion. Cells were injected into C57BL/6N blastocysts to generate chimera animals that were further backcrossed twice with C57Bl/6N mice to generate both, wild-type and *RasGrf1-/-* mice. No further backcrosses were done with C57Bl/6N.

From 1998 to present, the colony has been routinely propagated by homozygous matings [6]. However, animals for the longevity study were generated by crossing heterozygous animals in order to obtain sibling controls.

Diet provided was Harlan Teklad Global Maintenance 2014 (Harlan Italy). Animals used for the longevity curve were solely used for this study. Animals were allowed to die naturally except when their vital constants were compromised and were further euthanized.

Food intake. To measure food intake in mice, 5 male RasGrf1-/- mice and 5 age-matched (2 months old) wild-type mice were weight and kept in separate cages. Mice were provided with powder food (2014 Global Rodent Maintenance Powder, Harlan Teklad) and intake of the diet was measured by successive daily weighings of the food container to an accuracy of 0.01 g on a top-loading electronic balance (Sartorius). Food intake was not significative different between these mice [6]; wild-type 131±6 and *RasGrf1*$^{-/-}$ 141±7 mg/g body weight/day; p=0.4).

Tightrope test. The tightrope test is a widely used and extensively validated behavioural marker of ageing [63]. We performed the test with slight variations: mice were placed on a bar of circular section (60 cm long and 1.5 cm diameter) and the test was considered successful when a mouse did not fall during a period of 60 s in at least one out of five consecutive trials.

Quantitative real-time RT–PCR. Total RNA from tissues was extracted with Trizol (Life Technologies). Messenger RNA levels were measured by quantitative real-time polymerase chain reaction using the Tth DNA polymerase kit (Roche Diagnostics-Boehringer Mannheim), as described by the manufacturer. Real-time quantitation of mRNAs for 16S rRNA and situins relative to GAPDH mRNA was performed using the iCycler (Bio-Rad, Hercules, CA) with SYBR Green I detection. Target cDNAs were amplified in separate tubes: 10 min at 95°C, then 40 cycles of denaturation (95°C for 30 s) and annealing and extension (at 62°C for 1 min per cycle). The increase in fluorescence was measured during the extension step. The threshold cycle (Ct) was determined, and the relative gene expression was expressed as fold change = $2^{(-\Delta\Delta Ct)}$. Specific primers used were 16S rRNA, 5′-GACGAGAAGACCCTATGGAG-3′ and 5′-AGAAACCGACCTGGATTGC-3′; SIRT-1 5'-CCAGATCCTCAAGCCATG TT-3' and 5'-TTGCAGGAATCCAAAGGATC-3' and GAPDH, 5′-

CCTGGAGAAACC TGCCAA GTA TG-3′ and 5′-GGTCCTCAGTGTAGCCCAAGATG-3′. The error bars correspond to the relative error of the $2^{(-\Delta\Delta Ct)}$ values.

Measurement of oxidative stress parameters and IGF-I levels. Glutathione ratio (GSSG/GSH*100) was determined by high-performance liquid chromatography (HPLC) as described [64]. Lipid peroxidation was determined as accumulation of MDA, which was detected by HPLC as an MDA–thiobarbituric acid adduct [65]. Oxidative modification of total proteins was assessed by immunoblot detection of protein carbonyl groups using the 'OxyBlot' protein oxidation kit (Intergen) following the manufacturer's instructions. The procedure to quantify total protein carbonyls with the OxyBlot kit was densitometry of the oxyblot and of the Ponceau staining, followed by finding the ratio between the total density in the oxyblot and the total density in the Ponceau. Serum levels of IGF-I were measured using retro-orbital blood and the Mouse/Rat IGF-I kit from Diagnostic Systems Laboratories.

Determination of heart glucose consumption *in vivo*. Mice were deprived of food for 8–14 h before 18F-2-fluor-2-deoxiglucose (18F-FDG) injection. 18F-FDG (5.8–11.1 MBq) was injected intraperitoneally after anesthesia with isoflurane (1.5–2% in 100% oxygen, IsoFlo; Abbott Laboratories). PET was started 60 min after 18F-FDG injection as described in [66]. 18F-FDG was synthesized as previously described [67]. The administered dose (FDG activity) was indeed corrected for body weight. We acquired 20-min static images 60 min after injection of 18FFDG. The biodistribution of 18F-FDG by the heart was compared between all the studied groups. The PET images were obtained with the Albira small animal PET (ONCOVISION, GEM-Imaging). Regions of interest were manually drawn over the brain and heart with PMOD software. Tracer uptake by heart was quantified as SUV (Standardized Uptake Value, Total Sum).

Storage, preparation and ^{1}H NMR spectroscopic analysis of blood serum. Mice blood sera were stored at -80C and thawed before use. For NMR analysis, 20 µl of serum were mixed with 2 µl of D_2O (as a field lock). A total of 20 µL of the mixture of each sample was then transferred into a 1 mm high quality NMR capillary individually. All ^{1}H NMR spectra were acquired using a standard one-dimensional pulse sequence with water suppression (Bruker Avance 600 spectrometer operating at 600.13 MHz with a 1mm ^{1}H/^{13}C/^{15}N TXI probe). A total of 256 FIDs (free induction decay) were collected into 64k data points with a spectral width of 14 ppm and the recycle delay (RD) of 1 s. Water signal was saturated with a weak irradiation during the recycle delay. Before Fourier transformation, the free induction decay was multiplied by a 0.3 Hz exponential line broadening. Spectral chemical shift referencing on the Alanine CH_3 doublet signal at 1.475 ppm was performed in all spectra. Spectral regions between 0.5 and 4.5 ppm and between 5.5 and 9.5 ppm were binned in segments of 0.01 ppm width (6 Hz) for multivariate analysis. We normalized the binned data to total spectral area. We used available spectral databases and 2D NMR experiments to aid structural identification of relevant metabolites. All spectra were processed using MNova (MestreLab, Santiago de Compostela, Spain) and transferred to MATLAB® (MathWorks Inc, 2006) using in-house scripts for data analysis. Signals belonging to selected metabolites (Glucose, signal at 3.79 ppm and PUFA signal at 2.70 ppm) were integrated and quantified using semi-automated in-house MATLAB peak-fitting routines. These fitting routine were based on Levenburg-Marquard optimization procedures. The target function for the optimization included experimental spectra measured for standard solutions of selected metabolites with complex multiplet patterns and theoretically generated Lorentzian-shape signals for those metabolites with simpler spectral patterns. One-way-analysis of variance (ANOVA) was used for the determination of statistical significance between group means of the corresponding integrals.

Multivariate analysis of NMR spectra. We used PLS_Toolbox 5.0 (Eigenvector Research, WA, USA) for MATLAB® to build the PLS-DA models. PLS-DA is a classification technique that encompasses the properties of Partial Least Squares regression with the discrimination power of discriminant analysis [68]. The main advantage of PLS-DA models is that the main sources of variability in the data are modeled by the so-called latent variables (LVs), and consequently, in their associated scores and loadings, allowing the visualization and understanding of different patterns and relations in the data. Binned spectral regions for blood serum from normally fed WT and *RasGrf1*$^{-/-}$ mice were mean-centered for building a PLS-DA model. The PLS-DA model discriminating between WT and *RasGrf1*$^{-/-}$ was cross-validated by the leave-on-out method providing a cross-validation RMS of 0.3816 and a cross validation classification error of 0.0625. Q residual and Hotelling T^2 for 95% interval of confidence were 0.5047 and 14.28 respectively. Then, we project the spectra of blood serum from calorie restricted WT mice to this PLS-DA latent space for evaluating metabolic proximity between groups.

Glycogen content determination. Livers from 24 hours fasted animals were embedded in paraffin and 5µm

sections were stained for glycogen by standard periodic acid Schiff's (PAS) protocol.

ACKNOWLEDGEMENTS

This work was supported by grants SAF2008-00270; SAF2009-08334; BFU2007-65803/BFI from the Spanish Ministry of Education and Science (MEC); ISCIII2006-RED13-027 from the "Red Temática de investigación cooperativa en envejecimiento y fragilidad (RETICEF), and EU Funded COSTB35. D.M. is funded by the Ramon y Cajal Program of the MEC. This study has been co-fianaced by FEDER funds from the European Union. All authors state that there is no conflict of interests regarding this manuscript.

CONFLICT OF INTERESTS STATEMENT

The authors of this manuscript have no conflict of interests to declare.

REFERENCES

1. Farnsworth CL, Freshney NW, Rosen LB, Ghosh A, Greenberg ME and Feig LA. Calcium activation of Ras mediated by neuronal exchange factor Ras-GRF. Nature 1995; 376:524-527.

2. Mattingly RR and Macara IG. Phosphorylation-dependent activation of the Ras-GRF/CDC25Mm exchange factor by muscarinic receptors and G-protein beta gamma subunits. Nature 1996; 382:268-272.

3. Shou C, Wurmser A, Suen KL, Barbacid M, Feig LA and Ling K. Differential response of the Ras exchange factor, Ras-GRF to tyrosine kinase and G protein mediated signals. Oncogene 1995; 10:1887-1893.

4. Santos E and Fernandez-Medarde A. Rasgrf1. UCSD-Nature Molecule Pages 2009 Published online. doi:10.1038/mp.a002032.01.

5. Brambilla R, Gnesutta N, Minichiello L, White G, Roylance AJ, Herron CE, Ramsey M, Wolfer DP, Cestari V, Rossi-Arnaud C, Grant SG, Chapman PF, Lipp HP, Sturani E and Klein R. A role for the Ras signalling pathway in synaptic transmission and long-term memory. Nature 1997; 390:281-286.

6. Font de Mora J, Esteban LM, Burks DJ, Nunez A, Garces C, Garcia-Barrado MJ, Iglesias-Osma MC, Moratinos J, Ward JM and Santos E. Ras-GRF1 signaling is required for normal beta-cell development and glucose homeostasis. Embo J 2003; 22:3039-3049.

7. Giese KP, Friedman E, Telliez JB, Fedorov NB, Wines M, Feig LA and Silva AJ. Hippocampus-dependent learning and memory is impaired in mice lacking the Ras-guanine-nucleotide releasing factor 1 (Ras-GRF1). Neuropharmacology 2001; 41:791-800.

8. Itier JM, Tremp GL, Leonard JF, Multon MC, Ret G, Schweighoffer F, Tocque B, Bluet-Pajot MT, Cormier V and Dautry F. Imprinted gene in postnatal growth role. Nature 1998; 393:125-126.

9. Fabrizio P, Liou LL, Moy VN, Diaspro A, Valentine JS, Gralla EB and Longo VD. SOD2 functions downstream of Sch9 to extend longevity in yeast. Genetics 2003; 163:35-46.

10. De Benedictis G, Carrieri G, Garasto S, Rose G, Varcasia O, Bonafe M, Franceschi C and Jazwinski SM. Does a retrograde response in human aging and longevity exist? Exp Gerontol 2000; 35:795-801.

11. Fontana L, Partridge L and Longo VD. Extending healthy life span--from yeast to humans. Science 2010; 328:321-326.

12. Harrison DE, Strong R, Sharp ZD, Nelson JF, Astle CM, Flurkey K, Nadon NL, Wilkinson JE, Frenkel K, Carter CS, Pahor M, Javors MA, Fernandez E and Miller RA. Rapamycin fed late in life extends lifespan in genetically heterogeneous mice. Nature 2009; 460:392-395.

13. Wei M, Fabrizio P, Hu J, Ge H, Cheng C, Li L and Longo VD. Life span extension by calorie restriction depends on Rim15 and transcription factors downstream of Ras/PKA, Tor, and Sch9. PLoS Genet 2008; 4:e13.

14. Henkemeyer M, Rossi DJ, Holmyard DP, Puri MC, Mbamalu G, Harpal K, Shih TS, Jacks T and Pawson T. Vascular system defects and neuronal apoptosis in mice lacking ras GTPase-activating protein. Nature 1995; 377:695-701.

15. Gomez J, Martinez AC, Fernandez B, Garcia A and Rebollo A. Critical role of Ras in the proliferation and prevention of apoptosis mediated by IL-2. J Immunol 1996; 157:2272-2281.

16. Hall-Jackson CA, Jones T, Eccles NG, Dawson TP, Bond JA, Gescher A and Wynford-Thomas D. Induction of cell death by stimulation of protein kinase C in human epithelial cells expressing a mutant ras oncogene: a potential therapeutic target. Br J Cancer 1998; 78:641-651.

17. Ferrari G and Greene LA. Proliferative inhibition by dominant-negative Ras rescues naive and neuronally differentiated PC12 cells from apoptotic death. EMBO J 1994; 13:5922-5928.

18. Spear N, Estevez AG, Johnson GV, Bredesen DE, Thompson JA and Beckman JS. Enhancement of peroxynitrite-induced apoptosis in PC12 cells by fibroblast growth factor-1 and nerve growth factor requires p21Ras activation and is suppressed by Bcl-2. Arch Biochem Biophys 1998; 356:41-45.

19. Mills EM, Takeda K, Yu ZX, Ferrans V, Katagiri Y, Jiang H, Lavigne MC, Leto TL and Guroff G. Nerve growth factor treatment prevents the increase in superoxide produced by epidermal growth factor in PC12 cells. J Biol Chem 1998; 273: 22165-22168.

20. Wei M, Fabrizio P, Madia F, Hu J, Ge H, Li LM and Longo VD. Tor1/Sch9-regulated carbon source substitution is as effective as calorie restriction in life span extension. PLoS Genet 2009; 5: e1000467.

21. Bluher M, Kahn BB and Kahn CR. Extended longevity in mice lacking the insulin receptor in adipose tissue. Science 2003; 299: 572-574.

22. Coschigano KT, Holland AN, Riders ME, List EO, Flyvbjerg A and Kopchick JJ. Deletion, but not antagonism, of the mouse growth hormone receptor results in severely decreased body weights, insulin, and insulin-like growth factor I levels and increased life span. Endocrinology 2003; 144:3799-3810.

23. Festing MF and Blackmore DK. Life span of specified-pathogen-free (MRC category 4) mice and rats. Lab Anim 1971; 5:179-192.

24. Holzenberger M, Dupont J, Ducos B, Leneuve P, Geloen A, Even PC, Cervera P and Le Bouc Y. IGF-1 receptor regulates lifespan and resistance to oxidative stress in mice. Nature 2003; 421:182-187.

25. Rowlatt C, Chesterman FC and Sheriff MU. Lifespan, age changes and tumour incidence in an ageing C57BL mouse colony. Lab Anim 1976; 10:419-442.

26. Storer JB. Longevity and gross pathology at death in 22 inbred mouse strains. J Gerontol 1966; 21:404-409.

27. Yan L, Vatner DE, O'Connor JP, Ivessa A, Ge H, Chen W, Hirotani S, Ishikawa Y, Sadoshima J and Vatner SF. Type 5 adenylyl cyclase disruption increases longevity and protects against stress. Cell 2007; 130:247-258.

28. Borras C, Sastre J, Garcia-Sala D, Lloret A, Pallardo FV and Vina J. Mitochondria from females exhibit higher antioxidant gene expression and lower oxidative damage than males. Free Radic Biol Med 2003; 34:546-552.

29. Calleja M, Pena P, Ugalde C, Ferreiro C, Marco R and Garesse R. Mitochondrial DNA remains intact during Drosophila aging, but the levels of mitochondrial transcripts are significantly reduced. J Biol Chem 1993; 268:18891-18897.

30. Crawford DR, Wang Y, Schools GP, Kochheiser J and Davies KJ. Down-regulation of mammalian mitochondrial RNAs during oxidative stress. Free Radic Biol Med 1997; 22:551-559.

31. Kadenbach B, Ramzan R and Vogt S. Degenerative diseases, oxidative stress and cytochrome c oxidase function. Trends Mol Med 2009; 15:139-147.

32. Timiras PS. Physiological basis of aging and geriatrics. 2007: viii, 407

33. Longo VD and Fabrizio P. Regulation of longevity and stress resistance: a molecular strategy conserved from yeast to humans? Cell Mol Life Sci 2002; 59:903-908.

34. Guarente L. Sirtuins as potential targets for metabolic syndrome. Nature 2006; 444: 868-874.

35. Bartke A. Insulin and aging. Cell Cycle 2008; 7: p. 3338-3343.

36. Bartke A. New findings in gene knockout, mutant and transgenic mice. Exp Gerontol 2008; 43:11-14.

37. Bartke A. Impact of reduced insulin-like growth factor-1/insulin signaling on aging in mammals: novel findings. Aging Cell 2008; 7:285-290.

38. Borras C, Stvolinsky S, Lopez-Grueso R, Fedorova T, Gambini J, Boldyrev A and Vina J. Low in vivo brain glucose consumption and high oxidative stress in accelerated aging. FEBS Lett 2009; 583:2287-2293.

39. Ladiges W, Van Remmen H, Strong R, Ikeno Y, Treuting P, Rabinovitch P and Richardson A. Lifespan extension in genetically modified mice. Aging Cell 2009; 8:346-352.

40. Selman C, Tullet JM, Wieser D, Irvine E, Lingard SJ, Choudhury AI, Claret M, Al-Qassab H, Carmignac D, Ramadani F, Woods A, Robinson IC, Schuster E, Batterham RL, Kozma SC, Thomas G, Carling D, Okkenhaug K, Thornton JM, Partridge L, Gems D and Withers DJ. Ribosomal protein S6 kinase 1 signaling regulates mammalian life span. Science 2009; 326:140-144.

41. Nadon NL, Strong R, Miller RA, Nelson J, Javors M, Sharp ZD, Peralba JM and Harrison DE. Design of aging intervention studies: the NIA interventions testing program. Age (Dordr) 2008; 30:187-199.

42. Matheu A, Maraver A, Klatt P, Flores I, Garcia-Cao I, Borras C, Flores JM, Vina J, Blasco MA and Serrano M. Delayed ageing through damage protection by the Arf/p53 pathway. Nature 2007; 448:375-379.

43. Tomas-Loba A, Flores I, Fernandez-Marcos PJ, Cayuela ML, Maraver A, Tejera A, Borras C, Matheu A, Klatt P, Flores JM, Vina J, Serrano M and Blasco MA. Telomerase reverse transcriptase delays aging in cancer-resistant mice. Cell 2008; 135:609-622.

44. Gill TM, Gahbauer EA, Han L and Allore HG. Trajectories of disability in the last year of life. N Engl J Med 2010; 362:1173-1180.

45. Studenski S, Hayes RP, Leibowitz RQ, Bode R, Lavery L, Walston J, Duncan P and Perera S. Clinical Global Impression of Change in Physical Frailty: development of a measure based on clinical judgment. J Am Geriatr Soc 2004; 52:1560-1566.

46. Plass C, Shibata H, Kalcheva I, Mullins L, Kotelevtseva N, Mullins J, Kato R, Sasaki H, Hirotsune S, Okazaki Y, Held WA, Hayashizaki Y and Chapman VM. Identification of Grf1 on mouse chromosome 9 as an imprinted gene by RLGS-M. Nat Genet 1996; 14:106-109.

47. Clapcott SJ, Peters J, Orban PC, Brambilla R and Graham CF. Two ENU-induced mutations in Rasgrf1 and early mouse growth retardation. Mamm Genome 2003; 14:495-505.

48. Kawahara M and Kono T. Longevity in mice without a father. Hum Reprod 2010; 25:457-461.

49. Jaenisch R. DNA methylation and imprinting: why bother? Trends Genet 1997; 13:323-329.

50. Anderson RM, Barger JL, Edwards MG, Braun KH, O'Connor CE, Prolla TA and Weindruch R. Dynamic regulation of PGC-1alpha localization and turnover implicates mitochondrial adaptation in calorie restriction and the stress response. Aging Cell 2008; 7:101-111.

51. Longo VD. Linking sirtuins, IGF-I signaling, and starvation. Exp Gerontol 2009; 44:70-74.

52. Gerhart-Hines Z, Rodgers JT, Bare O, Lerin C, Kim SH, Mostoslavsky R, Alt FW, Wu Z and Puigserver P. Metabolic control of muscle mitochondrial function and fatty acid oxidation through SIRT1/PGC-1alpha. Embo J 2007; 26:1913-1923.

53. Lagouge M, Argmann C, Gerhart-Hines Z, Meziane H, Lerin C, Daussin F, Messadeq N, Milne J, Lambert P, Elliott P, Geny B, Laakso M, Puigserver P and Auwerx J. Resveratrol improves mitochondrial function and protects against metabolic disease by activating SIRT1 and PGC-1alpha. Cell 2006; 127: p. 1109-1122.

54. Picard F, Kurtev M, Chung N, Topark-Ngarm A, Senawong T, Machado De Oliveira R, Leid M, McBurney MW and Guarente L. Sirt1 promotes fat mobilization in white adipocytes by repressing PPAR-gamma. Nature 2004; 429:771-776.

55. Rodgers JT, Lerin C, Haas W, Gygi SP, Spiegelman BM and Puigserver P. Nutrient control of glucose homeostasis through a complex of PGC-1alpha and SIRT1. Nature 2005; 434:113-118.

56. Feige JN, Lagouge M, Canto C, Strehle A, Houten SM, Milne JC, Lambert PD, Mataki C, Elliott PJ and Auwerx J. Specific SIRT1 activation mimics low energy levels and protects against diet-induced metabolic disorders by enhancing fat oxidation. Cell Metab 2008; 8:347-358.

57. Nakae J, Cao Y, Daitoku H, Fukamizu A, Ogawa W, Yano Y and Hayashi Y. The LXXLL motif of murine forkhead transcription factor FoxO1 mediates Sirt1-dependent transcriptional activity. J Clin Invest 2006; 116:2473-2483.

58. Luptak I, Yan J, Cui L, Jain M, Liao R and Tian R. Long-term effects of increased glucose entry on mouse hearts during normal aging and ischemic stress. Circulation 2007; 116:901-909.
59. Wessells RJ, Fitzgerald E, Cypser JR, Tatar M and Bodmer R. Insulin regulation of heart function in aging fruit flies. Nat Genet 2004; 36:1275-1281.
60. Longo VD. The Ras and Sch9 pathways regulate stress resistance and longevity. Exp Gerontol 2003; 38: p. 807-811.
61. Longo VD. Ras: the other pro-aging pathway. Sci Aging Knowledge Environ 2004; 2004:pe36.
62. Sebastiani P, Solovieff N, Puca A, Hartley SW, Melista E, Andersen S, Dworkis DA, Wilk JB, Myers RH, Steinberg MH, Montano M, Baldwin CT and Perls TT. Genetic Signatures of Exceptional Longevity in Humans. Science 2010: in press
63. Ingram DK and Reynolds MA. Assessing the predictive validity of psychomotor tests as measures of biological age in mice. Exp Aging Res 1986; 12:155-162.
64. Asensi M, Sastre J, Pallardo FV, Estrela JM and Vina J. Determination of oxidized glutathione in blood: high-performance liquid chromatography. Methods Enzymol 1994; 234: 367-371.
65. Wong SH, Knight JA, Hopfer SM, Zaharia O, Leach CN, Jr. and Sunderman FW, Jr. Lipoperoxides in plasma as measured by liquid-chromatographic separation of malondialdehyde-thiobarbituric acid adduct. Clin Chem 1987; 33:214-220.
66. Fueger BJ, Czernin J, Hildebrandt I, Tran C, Halpern BS, Stout D, Phelps ME and Weber WA. Impact of animal handling on the results of 18F-FDG PET studies in mice. J Nucl Med 2006; 47: 999-1006.
67. Hamacher K, Coenen HH and Stocklin G. Efficient stereospecific synthesis of no-carrier-added 2-[18F]-fluoro-2-deoxy-D-glucose using aminopolyether supported nucleophilic substitution. J Nucl Med 1986; 27:235-238.
68. Trygg J, Holmes E and Lundstedt T. Chemometrics in metabonomics. J Proteome Res 2007; 6:469-479.

SUPPLEMENTARY MATERIAL

Table for data of Figure 1

Gender	Animal ID	*RasGrf1*	D.O.B.	D.O.D.	Weeks alive	
♂	705-2	KO	5/6/2007	8/1/2007	12.428571	
♂	302-2	KO	12/12/2005	10/23/2006	45	
♂	37-1	KO	1/28/2005	7/31/2006	78.428571	
♂	505-3(w)	KO	8/21/2006	2/23/2008	78.714286	
♂	92-1	KO	5/17/2005	12/18/2006	82.857143	
♂	173-1	KO	9/6/2005	6/11/2007	91.857143	
♂	274-1	KO	11/22/2005	9/1/2007	92.571429	
♂	5-5	KO	1/10/2005	11/5/2006	94.857143	
♂	427-2	KO	4/16/2006	3/6/2008	98.571429	
♂	504-2(w)	KO	8/21/2006	7/22/2008	100.14286	
♂	228-1	KO	10/18/2005	9/28/2007	101.42857	
♂	426-1	KO	4/16/2006	3/31/2008	102.14286	
♂	62-2	KO	2/21/2005	2/23/2007	104.57143	
♂	481-2(w)	KO	7/9/2006	8/5/2008	108.28571	
♂	611-2	KO	1/22/2007	2/19/2009	108.42857	
♂	699-1	KO	4/30/2007	6/20/2009	111.71429	
♂	389-2	KO	3/6/2006	4/27/2008	111.85714	
♂	610-1	KO	1/22/2007	3/19/2009	112.42857	
♂	625-1	KO	2/20/2007	5/15/2009	116.42857	
♂	303-3	KO	12/12/2005	3/20/2008	118.42857	
♂	701-3	KO	4/30/2007	8/15/2009	119.71429	
♂	480-1-(w)	KO	7/9/2006	11/7/2008	121.71429	
♂	190-2	KO	9/28/2005	2/10/2008	123.57143	
♂	182-1	KO	9/23/2005	2/15/2008	125	
♂	191-3	KO	9/28/2005	2/23/2008	125.42857	
♂	J9-1	KO	1/20/2005	7/6/2007	128.14286	
♂	64-1	KO	2/22/2005	9/7/2007	132.42857	
♂	231-1	KO	9/28/2005	4/17/2008	133.14286	
♂	48-1	KO	3/3/2005	9/27/2007	134	
♂	503-1(w)	KO	8/21/2006	5/5/2009	141.14286	
♂	230-1(w)	KO	9/28/2005	6/17/2008	141.85714	**TUMOR** Colon tumor
♂	479-1(b)	KO	7/9/2006	4/19/2009	145	
♂	40-1	KO	3/28/2005	1/8/2008	145.14286	
♂	251-1	KO	11/16/2005	8/30/2008	145.42857	**TUMOR** Chest wall tumor
♂	J3-3	KO	1/10/2005	10/26/2007	145.57143	**TUMOR** Fast growing tumor in the front right leg
♂	65-2	KO	2/22/2005	12/16/2007	146.71429	
♂	181-1	KO	9/19/2005	7/31/2008	149.42857	

♂	482-3(w)	KO	7/9/2006	5/23/2009	149.85714
♂	167-2	KO	8/28/2005	7/13/2008	150
♂	63-3	KO	2/21/2005	1/8/2008	150.14286
♂	140-3	KO	7/12/2005	6/11/2008	152.14286
♂	275-2	KO	11/22/2005	12/3/2008	158.14286
♂	J33-2(alb)	KO	1/27/2005	2/9/2008	158.28571
♂	43-4	KO	3/28/2005	5/13/2008	163.14286
♂	300-1 (w)	KO	12/12/2005	4/13/2009	174

SUPPLEMENTARY FIGURES

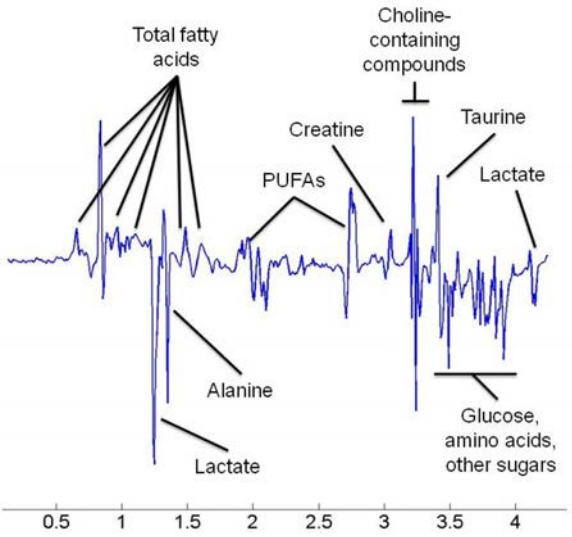

Figure S1. Loadings Plot for The First Latent Variable of The PLSDA Model for Discrimination Between *RasGrf1*$^{-/-}$ and WT male mice. The plot illustrates the contributions of most relevant metabolites (for assignments see Nicholson et al., 1995). Positive values over the baseline in this loading plot mean an increase in the level of the metabolite parallel to an increase in the value of the latent variable. For instance, WT mice in calorie restriction (gray triangles in figure 1c) have higher values of LV1 than WT with normal diet (gray circles in figure 1c). This means that WT mice in calorie restriction have higher levels of global fatty acids (positive value in this loadings plot) and lower levels of lactate (negative value in this loadings plot) than WT with normal diet.

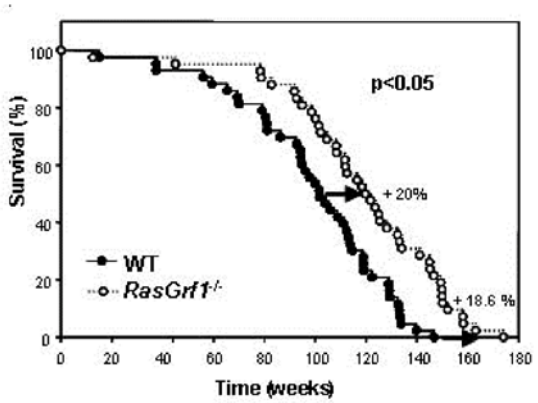

Figure S2. Survival curve without tumours. Survival curve of WT n=43 and *RasGrf1*$^{-/-}$ n=42 male mice, same group of animals as in Figure 1, but excluding those animals that presented tumours at the time of death ($p<0.05$).

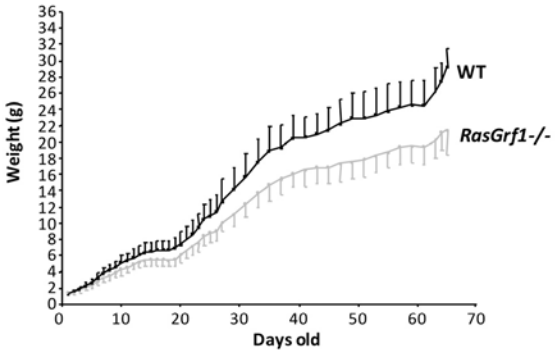

Figure S3. Body weight curves of WT and *RasGrf1*$^{-/-}$ male mice. Data are reported as mean weight ± SEM (n=24 for WT, n=19 for *RasGrf1*$^{-/-}$).

SUPPLEMENTARY TABLE

Table S1. Procedure 055: Monitor of Aging Mice
"Regulation of Longevity in RasGrf1 ko Mice"

Initial date of observation: Weight:

ID number of Cage/Animal:

Current weight								
			Date					
Parameters		Punctuation						
Body Weight Loss	None	0						
	5-10%	9						
	10-15%	12						
	>15%	18						
General Appearance	Normal	0						
	Loss of activity, lack of grooming	2						
	Poor hair condition	3						
	Dehydrated, inactivity, hunched posture (lordosis)	6						
	Moribund or cachexia	18						
	Derange vital functions*	18						
	Ascitis and/or abdominal distention	10						
Tumors Size	<7 mm	0						
	7-17mm	9						
	>18mm/abdominal distention (>10% weight)	12						
	Skin ulcer	18						
Wound Surface (S^2)	0-5% S^2 body	7						
	5-10% S^2 body	12						
	>10% S^2 body	18						
Tissue	Subcutaneous	3						
	Muscular	5						
	Mucosa	12						
Prolapses Localization	Penil	6						
	Rectal, vaginal- uterine	9						
	Ocular	18						
Mucosal	normal	0						
	congestive	9						
	necrosia	18						
FINAL PUNCTUATION								
SIGNATURE								

*__Vital functions:__ afflicting one of the 5 senses and physiological functions (food ingestion, urinate, defecate and motility)

0-7: daily monitoring

8-13: seek advice with veterinarians and plan for treatment (first aid, analgesics, etc.)

14-17: seek advice with veterinarians and plan for euthanasia

≥ 18: immediate euthanasia

Research Perspective

Reduced mitochondrial function in obesity-associated fatty liver: SIRT3 takes on the fat

Mahua Choudhury[1], Karen R. Jonscher[2], and Jacob E. Friedman[1,3]

Department of [1]Pediatrics, [2]Anesthesiology, and [3]Biochemistry and Molecular Genetics, University of Colorado School of Medicine, Aurora, CO 80045, USA

Key words: *aging, metabolism, obesity, SIRT3, mitochondria*
Received: *2/24/11; Accepted: 2/26/11; Published: 2/26/11* doi:10.18632/aging.100289
Corresponding author: *Jacob E. (Jed) Friedman, PhD;* ***Email:*** *jed.friedman@ucdenver.edu*

Abstract: Aging is associated with various metabolic disorders that may have their origin in the liver, including non-alcoholic fatty liver disease, obesity, type 2 diabetes mellitus, and atherosclerosis. Although well-characterized in models of caloric restriction, relatively little is known about the role of sirtuins an acetylation under conditions of caloric excess. Sirtuins are NAD (+)-dependent protein deacetylases that mediate adaptive responses to a variety of stresses, including calorie restriction and metabolic stress. Sirtuin 3 (SIRT3) is localized within the mitochondrial matrix, where it regulates acetylation levels of a diverse set of metabolic enzymes. When normal mice are fed a high fat diet they demonstrate reduced SIRT3 activity, impaired mitochondrial function, and hyperacetylation of a diverse set of proteins in their livers. Furthermore, SIRT3 knockout mice have signs of accelerated aging and cancer. Understanding SIRT3's biochemical function and regulation in the liver under conditions of caloric excess may potentially increase our understanding of the normal aging process and diseases associated with aging, such as diabetes, fatty liver disease, or cancer.

Aging is associated with various metabolic disorders that may have their origin in the liver, including obesity, type 2 diabetes mellitus, non-alcoholic fatty liver disease (NAFLD), and atherosclerosis [1,2]. These conditions are provoked by diverse factors, including reactive oxygen species, endoplasmic reticulum stress, hypoxia, lipotoxicity, and altered adipokine signaling [3-5]. In addition, saturated fatty acids, which are increased in obesity [5-8], have been implicated in the coordinate regulation of metabolism with inflammatory and immune responses in the liver [9-11].

The mitochondrial proteome also changes with disease state. Recently, mitochondrial dysfunction has been implicated in the pathology of chronic metabolic disease characterized by insulin resistance such as obesity, type 2 diabetes mellitus, and aging. Acetylation has emerged as an important mechanism for controlling metabolism of a broad array of metabolic fuels. Acetylation regulates many enzymes in key pathways including TCA cycle, gluconeogenesis, and beta oxidation in yeast and human liver [12,13]. This post-translational modification is governed, in part, by sirtuins, class III NAD+-dependent deacetylases (HDACs) that regulate lipid and glucose metabolism in liver during fasting and aging. SIRT3, a mitochondrial sirtuin, appears to be the primary mediator of mitochondrial acetylation, since no significant changes in acetylation status are detectable in mice lacking SIRT4 and SIRT5 [14].

Mice lacking SIRT3 show accelerated aging and liver phenotypes during fasting.

All sirtuins require NAD+ for their deacetylase activities, linking their functions as metabolic sensors. For example, increased Nampt-mediated NAD biosynthesis enhances SIRT1 activity in mouse fibroblasts [15]. Nampt also plays an important part in regulating cellular stress resistance through SIRT3 [16]. Under genotoxic stress, increased Nampt plays an important part in maintaining NAD levels in mitochondria and providing protection against cell death by suppressing translocation of apoptosis-inducing factor from mitochondria to the nucleus [16]. These protective effects of Nampt

require mitochondrial SIRT3 [16,17].

Previously it was shown that many mitochondrial proteins are hyperacetylated in SIRT3 knockout mice on a standard chow diet; however SIRT3-/- mice were only mildly distinguishable from WT littermates [14]. As they aged however, 13 month old SIRT3 knockout mice showed accelerated signs of aging in the heart, including cardiac hypertrophy and fibrosis [18]. In addition, SIRT3 knockout mice were also hypersensitive to cardiac stress induced by transverse aortic constriction (TAC), and to cancer [19]. Simultaneously, Someya et al. demonstrated that SIRT3 mediates protective effects of caloric restriction on age-related hearing loss by promoting the mitochondrial antioxidant system through regulation of isocitrate dehydrogenase 2 (Idh2) [20]. Qiu et al. illustrated that protective effects of caloric restriction (CR) on oxidative stress and damage are diminished in mice lacking SIRT3 [21]. SIRT3 reduces cellular ROS levels dependent on superoxide dismutase 2 (SOD2), a major mitochondrial antioxidant enzyme. Additionally, liver phenotypes appear to be mediated by SIRT3. Recent studies have demonstrated that during fasting, SIRT3-/- mice have diminished fatty acid oxidation, develop a fatty liver, have low levels of ATP production, and show a defect in thermogenesis and hypoglycemia during a cold test [22]. SIRT3 activates hepatic lipid catabolism via deacetylation of LCAD, a central enzyme in the fatty acid oxidation process. Similar phenotypes have been established in mice lacking the mitochondrial enzyme AceCS2—(it is also acetylated by SIRT3 [23]), which suggest that SIRT3 is an important adaptive signal during fasting. Hepatic SIRT3 protein expression increases during fasting [24], therefore both its protein levels and enzymatic activities are elevated during nutrient deprivation.

SIRT3 activity and NAD levels are suppressed in livers of obese animals.

Compared to caloric restriction, relatively little is known about the role of sirtuins and acetylation under conditions of caloric excess. Our recent study [25] adds to the understanding of SIRT3 metabolic function in the context of metabolic stress induced by high fat diet and obesity. We fed a chronic (up to 16 wk) high fat diet (HFD) to mice and demonstrated reduced SIRT3 activity in their livers, a 3-fold decrease in hepatic NAD+ levels, and increased mitochondrial protein oxidation. Using a targeted proteomics approach, we elucidated 193 proteins that were preferentially acetylated in mice on HFD compared to controls, including 11 proteins not previously identified in acetylation studies. HFD led to hyperacetylation of proteins involved in gluconeogenesis, mitochondrial oxidative metabolism, methionine metabolism, liver injury, and ER stress response. In contrast, neither SIRT1 nor histone acetyltransferase (HAT) activities were altered, implicating SIRT3 as a dominant factor contributing to the observed phenotype. Compared to wild-type mice, SIRT3-deficient animals demonstrated an even greater hyperacetylation of gluconeogenic and mitochondrial proteins under HFD conditions. In corroboration with increased acetylation, mice lacking SIRT3 demonstrated a disruption of mitochondrial oxidative phosphorylation complexes II, III, and V. This is the first study to identify acetylation patterns in liver proteins of HFD mice and suggests that SIRT3 and hyperacetylation may play an important role in the regulation of cellular and mitochondrial metabolism induced by high-fat feeding.

The study raises several important questions. Increased mitochondrial protein oxidation in the livers of HFD-fed mice is consistent with higher levels of production of mitochondrial ROS under stress conditions [26, 27], and suggests that hyperacetylation could play an important role in suppressing function of oxidative stress defense enzymes contributing to HFD-induced liver injury. In mice on HFD, reduced SIRT3 activity was highly correlated with reduced NAD+ levels as the animals became obese. However, the regulatory mechanisms for reduced NAD biosynthesis and distribution of NAD precursors affecting specific sirtuins remain undetermined. Likewise, could the biosynthesis of NAD intermediates and metabolites be effective therapeutic targets and/or reagents for mitochondrial disorders and other diseases? Obesity and fatty liver disease are characterized by the paradoxical accumulation of triglycerides in the insulin-resistant liver [28]. Strong evidence suggests that the maintenance of NAD+ concentration is required for normal mitochondrial fatty acid oxidation [28, 29]. It has been shown that pharmacological stimulation of mitochondrial NADH oxidation dramatically promotes beta-oxidation and ameliorates dyslipidemia, adiposity, and fatty liver in obese mice [28]. Nampt overexpression has been shown to maintain cellular NAD levels and thereby stimulates sirtuin activity, resulting in protection of cardiac myocytes from poly(ADP-ribose)polymerase (PARP)-induced cell death during heart failure [30]. Lastly, since diminished mitochondrial function may play a pivotal role in mechanisms regulating insulin resistance, non-alcoholic fatty liver disease, and other metabolic disorders, it remains to be seen whether specific molecular agonists for SIRT3 activity can reverse metabolic disorders such as obesity, type 2 diabetes mellitus and/or inflammatory complications of a high fat diet. If rescuing SIRT3

improves physiological response when challenged with dietary high fat feeding, it will add to the growing body of evidence suggesting that sirtuins might be potential pharmacological targets, not only for extending life span but also for treating metabolic syndrome.

To date, most studies on the biological functions of sirtuins have been conducted in cell culture and mouse models, with studies on possible correlations between human plasma. Therefore, more work needs to be done to elucidate the physiological relevance of sirtuins in normal individuals and in patients with metabolic and other diseases.

REFERENCES

1. Hummasti S, Hotamisligil GS. Endoplasmic reticulum stress and inflammation in obesity and diabetes. Circ Res.2010;107:579-591.
2. Gentile C, Pagliassotti M. The endoplasmic reticulum as a potential therapeutic target in nonalcoholic fatty liver disease. Curr Opin Investig Drugs. 2008;9:1084-1088.
3. Gregor M, Hotamisligil G. Adipocyte stress: The endoplasmic reticulum and metabolic disease. J Lipid Res. 2007;48:1905–1914.
4. Hotamisligil G. Endoplasmic reticulum stress and the inflammatory basis of metabolic disease. Cell. 2010;140:900-917.
5. Opie L, Walfish P. Plasma free fatty acid concentrations in obesity. N Engl J Med. 1963;268:757-760.
6. Lee Y, Wang M-Y, Kakuma T, Wang Z-W, Babcock E, McCorkle K, Higa M, Zhou Y-T, Unger RH. Liporegulation in diet-induced obesity. Journal of Biological Chemistry. 2001;276:5629-5635.
7. Wang Y-X, Lee C-H, Tiep S, Yu RT, Ham J, Kang H, Evans RM. Peroxisome-proliferator-activated receptor activates fat metabolism to prevent obesity. Cell. 2003;113:159-170.
8. Fessler M, Rudel L, Brown J. Toll-like receptor signaling links dietary fatty acids to the metabolic syndrome. Current Opinion in Lipidology. 2009;20:379-385
9. Olefsky JM, Glass CK. Macrophages, inflammation, and insulin resistance. Annual Review of Physiology. 2010;72:219-246.
10. Schaeffler A, Gross P, Buettner R, Bollheimer C, Buechler C, Neumeier M, Kopp A, Schoelmerich J, Falk W. Fatty acid-induced induction of toll-like receptor-4/nuclear factor-κb pathway in adipocytes links nutritional signalling with innate immunity. Immunology. 2009;126:233-245.
11. Shi H, Kokoeva MV, Inouye K, Tzameli I, Yin H, Flier JS. Tlr4 links innate immunity and fatty acid-induced insulin resistance. The Journal of Clinical Investigation. 2006;116:3015-3025.
12. Wang Q, Zhang Y, Yang C, Xiong H, Lin Y, Yao J, Li H, Xie L, Zhao W, Yao Y, Ning Z-B, Zeng R, Xiong Y, Guan K-L, Zhao S, Zhao G-P. Acetylation of metabolic enzymes coordinates carbon source utilization and metabolic flux. Science. 2010;327:1004-1007.
13. Zhao S, Xu W, Jiang W, Yu W, Lin Y, Zhang T, Yao J, Zhou L, Zeng Y, Li H, Li Y, Shi J, An W, Hancock SM, He F, Qin L, Chin J, Yang P, Chen X, Lei Q, Xiong Y, Guan K-L. Regulation of cellular metabolism by protein lysine acetylation. Science. 2010;327:1000-1004.
14. Lombard DB, Alt FW, Cheng H-L, Bunkenborg J, Streeper RS, Mostoslavsky R, Kim J, Yancopoulos G, Valenzuela D, Murphy A, Yang Y, Chen Y, Hirschey MD, Bronson RT, Haigis M, Guarente LP, Farese RV, Jr., Weissman S, Verdin E, Schwer B. Mammalian sir2 homolog sirt3 regulates global mitochondrial lysine acetylation. Mol. Cell. Biol. 2007;27:8807-8814.
15. Revollo JR, Grimm AA, Imai S-i. The nad biosynthesis pathway mediated by nicotinamide phosphoribosyltransferase regulates sir2 activity in mammalian cells. Journal of Biological Chemistry. 2004;279:50754-50763.
16. Garten A, Petzold S, Körner A, Imai S-i, Kiess W. Nampt: Linking nad biology, metabolism and cancer. Trends in Endocrinology & Metabolism. 2009;20:130-138.
17. Yang H, Yang T, Baur JA, Perez E, Matsui T, Carmona JJ, Lamming Dudley W, Souza-Pinto NC, Bohr VA, Rosenzweig A, de Cabo R, Sauve Anthony A, Sinclair DA. Nutrient-sensitive mitochondrial nad+ levels dictate cell survival. Cell. 2007;130:1095-1107.
18. Hafner A, Dai J, Gomes A, Xiao C, Palmeira C, Rosenzweig A, Sinclair D. Regulation of the mptp by sirt3-mediated deacetylation of cypd at lysine 166 suppresses age-related cardiac hypertrophy. Aging 2010; 2:914-923.
19. Kim H-S, Patel K, Muldoon-Jacobs K, Bisht KS, Aykin-Burns N, Pennington JD, van der Meer R, Nguyen P, Savage J, Owens KM, Vassilopoulos A, Ozden O, Park S-H, Singh KK, Abdulkadir SA, Spitz DR, Deng C-X, Gius D. Sirt3 is a mitochondria-localized tumor suppressor required for maintenance of mitochondrial integrity and metabolism during stress. Cancer Cell. 2010;17:41-52.
20. Someya S, Yu W, Hallows WC, Xu J, Vann JM, Leeuwenburgh C, Tanokura M, Denu JM, Prolla TA. Sirt3 mediates reduction of oxidative damage and prevention of age-related hearing loss under caloric restriction. Cell.2010;143:802-812.
21. Qiu X, Brown K, Hirschey MD, Verdin E, Chen D. Calorie restriction reduces oxidative stress by sirt3-mediated sod2 activation. Cell Metabolism. 2010;12:662-667.
22. Hirschey MD, Shimazu T, Goetzman E, Jing E, Schwer B, Lombard DB, Grueter CA, Harris C, Biddinger S, Ilkayeva OR, Stevens RD, Li Y, Saha AK, Ruderman NB, Bain JR, Newgard CB, Farese Jr RV, Alt FW, Kahn CR, Verdin E. Sirt3 regulates mitochondrial fatty-acid oxidation by reversible enzyme deacetylation. Nature. 2010;464:121-125.
23. Schwer B, Bunkenborg J, Verdin RO, Andersen JS, Verdin E. Reversible lysine acetylation controls the activity of the mitochondrial enzyme acetyl-coa synthetase 2. Proceedings of the National Academy of Sciences. 2006;103:10224-10229.
24. Verdin E, Hirschey MD, Finley LWS, Haigis MC. Sirtuin

regulation of mitochondria: Energy production, apoptosis, and signaling. Trends in Biochemical Sciences. 2010;35:669-675.

25. Kendrick AA, Choudhury M, Rahman SM, McCurdy CE, McCurdy CE, Friederich M, VanÂ Hove JLK, Watson PA, Birdsey N, Bao J, Gius D, Sack MN, Jing E, Kahn CR, Friedman JE, Jonscher KR. Fatty liver is associated with reduced sirt3 activity and mitochondrial protein hyperacetylation. Biochemical Journal.2010;433:505-514.

26. Sundaresan NR, Gupta M, Kim G, Rajamohan SB, Isbatan A, Gupta MP. Sirt3 blocks the cardiac hypertrophic response by augmenting foxo3a-dependent antioxidant defense mechanisms in mice. J Clin Invest. 2009;119:2758-2771.

27. Kim HS, Patel K, Muldoon-Jacobs K, Bisht KS, Aykin-Burns N, Pennington JD, van der Meer R, Nguyen P, Savage J, Owens KM, Vassilopoulos A, Ozden O, Park SH, Singh KK, Abdulkadir SA, Spitz DR, Deng CX, Gius D. Sirt3 is a mitochondria-localized tumor suppressor required for maintenance of mitochondrial integrity and metabolism during stress. Cancer Cell. 2010;17:41-52.

28. Jung Hwan Hwang, Dong Wook Kim, Eun Jin Jo, Yong Kyung Kim, Young Suk Jo, Ji Hoon Park, Sang Ku Yoo, Myung Kyu Park, Tae Hwan Kwak, Young Lim Kho, Jin Han, Hueng-Sik Choi, Sang-Hee Lee, Jin Man Kim, InKyu Lee, Taeyoon Kyung, Cholsoon Jang, Jongkyeong Chung, Gi Ryang Kweon, and Minho Shong Pharmacological Stimulation of NADH Oxidation Ameliorates Obesity and Related Phenotypes in Mice Diabetes. 2009; 58:965-974.

29. Puigserver P, Rhee J, Donovan J, Walkey CJ, Yoon JC, Oriente F, Kitamura Y, Altomonte J, Dong H, Accili D, Spiegelman BM. Insulin-regulated hepatic gluconeogenesis through foxo1-pgc-1alpha interaction. Nature. 2003;423:550-555.

30. Pillai JB, Isbatan A, Imai S-i, Gupta MP. Poly(adp-ribose) polymerase-1-dependent cardiac myocyte cell death during heart failure is mediated by nad+ depletion and reduced sir2-alpha deacetylase activity. Journal of Biological Chemistry. 2005;280:43121-43130.

Research Perspective

Controlling SIRT1 expression by microRNAs in health and metabolic disease

Jiyoung Lee and Jongsook Kim Kemper

Department of Molecular and Integrative Physiology, University of Illinois, Urbana-Champaign, IL 61801, USA

Key words: *FXR, SHP, miR-34a, p53, SIRT1, and metabolic syndrome*
Received: *07/30/10; accepted: 08/04/10; published on line: 08/05/10*
Corresponding author: *Jongsook Kim Kemper, PhD;* ***E-mail:*** *jongsook@uiuc.edu* doi:10.18632/aging.100184

Abstract: SIRT1 is a NAD$^+$-dependent deacetylase implicated in longevity and diverse physiological processes. SIRT1, as a key mediator of beneficial effects of caloric restriction, regulates lipid and glucose metabolism by deacetylating metabolic regulators, as well as histones, in response to nutritional deprivation. Here we discuss how SIRT1 levels are regulated by microRNAs (miRs) which are emerging as important metabolic regulators; the recently identified nuclear receptor FXR/SHP cascade pathway that controls the expression of miR-34a and its target SIRT1; and a FXR/SIRT1 positive feedback regulatory loop, which is deregulated in metabolic disease states. The FXR/miR-34a pathway and other miRs controlling SIRT1 may be useful therapeutic targets for age-related diseases, including metabolic disorders.

INTRODUCTION

Disruption in metabolic homeostasis and over accumulation of metabolites, cholesterol, bile acids, triglycerides (fat), or glucose, play causative roles in the development of metabolic disorders, such as, atherosclerosis and related heart disease, fatty liver, obesity, and diabetes. The NAD$^+$-dependent SIRT1 deacetylase plays a critical role in maintaining metabolic homeostasis which affects aging so that SIRT1 increases life spans in most organisms, including mammals [1-3]. Despite extensive studies on SIRT1 function and its beneficial metabolic effects, how the expression of SIRT1 is regulated under normal conditions and how SIRT1 levels are decreased in metabolic disease states remain unclear. In this review, we survey recent studies showing how SIRT1 expression is regulated at the post-transcriptional level, focusing on microRNAs (miRs) which have recently emerged as important cellular regulators [4-6]. We also review recent studies showing that the nuclear receptor FXR/SHP cascade pathway which controls expression of miR-34a and its target SIRT1 in normal conditions and is dysregulated in metabolic disease states.

SIRT1: a key regulator in cellular metabolism

Caloric restriction (CR) was shown to increase life span and promote survival in yeast, worms, flies, rodents and perhaps primates [1, 2]. SIRT1 mediates the beneficial metabolic effects of CR in an NAD$^+$-dependent manner by deacetylating and altering the activities of transcriptional factors which regulate metabolic genes [1, 2, 7]. SIRT1 deacetylates and activates transcriptional ability of metabolic regulators, such as PGC-1α, p53, Foxo 1, NF-κB, LXR, and FXR that are involved in lipid and glucose metabolism, inflammation, mitochondrial biogenesis, and energy balance [1, 2, 8-12]. In addition, SIRT1 was shown to be recruited to the promoter of metabolic target genes and suppress their transcription [13, 14]. It was reported that SIRT1 is associated with the promoter of PPARγ, a key adipogenic factor, and suppresses PPARγ transcription by recruiting the corepressors, NcoR1 and SMRT [14]. SIRT1 was reported to bind to the UCP 2 gene promoter and inhibit its transcription in pancreatic β-cells, resulting in increased ATP production and insulin secretion [13]. SIRT1 was also shown to improve insulin sensitivity by repressing transcription of protein

tyrosine phosphatase 1B, a major negative regulator of insulin action, via histone deacetylation [15]. Beneficial metabolic functions of SIRT1 have been demonstrated in studies using small molecule activators and transgenic mice that are null for SIRT1 or overexpress SIRT1 [16-20]. The natural compound resveratrol and the synthetic compound SRT1720 are activators of SIRT1 and have been shown to ameliorate insulin resistance, increase mitochondrial content, improve metabolic profiles, and increase survival in mice fed a high-fat diet [16-18]. Transgenic mice expressing SIRT1 were shown to be resistant to body weight gain and ameliorated insulin resistance and glucose intolerance in these mice compared to wild-type control mice [20]. Further, transgenic mice expressing moderate amounts of SIRT1 were also shown to protect livers from diet-induced metabolic damage [12, 21]. Consistent with these reports, in liver-specific SIRT1 null mice challenged with a high fat diet, fatty acid metabolism was altered and the development of fatty livers and inflammatory responses were promoted [19, 22]. Loss of function studies also showed that SIRT1 decreases endothelial activation in hypercholesterolemic ApoE-/- mice without affecting endothelium-dependent vasodilatation [23]. All these recent studies demonstrate that SIRT1 is a key regulator of cellular metabolism and mediates beneficial metabolic effects.

MicroRNAs: emerging metabolic regulators

MicroRNAs (miRNAs) are small (approximately 22 nt) non-coding RNAs that control gene expression [4-6]. MiRs are transcribed from DNA by RNA polymerase II as hairpin precursors which are further processed to mature forms [4-6]. MiRs bind to the 3'-untranslated region (UTR) of target mRNAs and inhibit their expression by causing mRNA cleavage or inhibition of translation. Approximately 30% of all human genes are thought to be regulated by miRs [5, 6] and indeed, miRs control gene expression in diverse biological processes including development, differentiation, cell proliferation, and apoptosis. Recent studies have demonstrated crucial roles of miRNAs in the regulation of cellular metabolism [24-32]. MiRs are involved in lipid and glucose metabolism in major metabolic tissues, such as, liver, pancreas, adipose, and muscle as summarized in Table 1. Mir-122 is the most abundant miR in the liver and plays important roles in a wide variety of liver functions ranging from cholesterol metabolism, liver cancer, stress responses, viral infection, to circadian regulation of hepatic genes [24, 28, 29]. MiR-33 has been shown to contribute to the regulation of cholesterol homeostasis by targeting the cholesterol transporter genes, ABCA1 and ABCG1 [25, 26]. Our group recently reported that miR-34a targets hepatic SIRT1 and, interestingly, expression of miR-34a was highly elevated and SIRT1 levels were decreased in fatty livers of diet-induced obese mice [30]. MiR-34a was also shown to suppress insulin secretion in pancreatic β-cells [33]. The roles of miR-375 in pancreatic islet functions, especially in insulin gene transcription, insulin secretion, and islet cell growth, are also well established [31, 32]. Mir-27 and miR-378 were reported to control adipocyte differentiation and lipid synthesis, respectively [34, 35]. MiR-223 was shown to regulate glucose uptake in cardiomyocytes and miR-696 to regulate mitochondria biogenesis and fatty acid oxidation in gastrocnemius muscle [36, 37]. In line with their critical functions, miRs are often underexpressed or overexpressed in disease states [4, 6, 24, 28, 30, 38-40]. Recent studies have shown that restoring miRs or downregulating miRs using antisense miR inhibitors, called antagomirs, has improved transcriptional and biological outcomes, demonstrating that miRs are promising therapeutic targets [4, 24, 38].

Down-regulation of SIRT1 by microRNAs

Consistent with its critical roles in diverse biological processes, the regulation of SIRT1 expression is fine tuned at multiple levels, including transcriptional, post-transcriptional, and post-translational levels. The general regulation of SIRT1 activity and expression has been thoroughly reviewed in excellent articles [1-3, 41] and, therefore, this review focuses on the regulation of SIRT1 expression by miRs (Table 2). MiR-34a was first identified as a posttranscriptional regulator of SIRT1 in the regulation of apoptosis under cellular genotoxic stress in human colon cancer HCT116 cells [42]. MiR-34a binds to the 3' UTR of SIRT1 mRNA in a partial complementary manner and represses its translation but does not affect mRNA degradation [30, 42]. Our group further reported that miR-34a targets hepatic SIRT1 in the regulation of cellular metabolism in human hepatoma HpeG2 cells and in mouse liver in vivo using adenoviral-mediated overexpression of miR-34a [30]. Remarkably, we observed that miR-34a levels are highly elevated and SIRT1 protein levels are substantially decreased in the fatty livers of both diet-induced obese mice and the leptin-deficient ob/ob mice [30]. These findings are in line with recent studies showing that miR-34a is the most elevated miR in livers exhibiting nonalcoholic steatohepatitis, a spectrum of nonalcoholic fatty liver diseases in humans [39]. Other miRs also target SIRT1. In response to nutritional availability, miR-132 was shown to downregulate SIRT1, resulting in activation of inflammatory pathways in adipose tissues [43]. MiR-199a was identified as a negative regulator of SIRT1 and HIF1a, a key mediator of hypoxia [44]. Low oxygen tension

results in acute downregulation of miR-199a in cardiac myocytes and in porcine heart and this reduction is required for upregulation of its targets, HIF-1a and SIRT1 in response to decreased oxygen [44]. Interestingly, a recent study showed that SIRT1 protein levels are much higher in mouse embryonic stem cells (ESCs) than in differentiated tissues and that miRNAs, miR-181a and b, miR-9, miR-204, miR-199b, and miR-135, post-transcriptionally down-regulate SIRT1 during mouse ESC differentiation and maintain low levels of SIRT1 expression in differentiated tissues [45].

Table 1. MicroRNAs regulating cellular metabolism in major metabolic tissues

MicroRNA	Direct targets [putative]	Functions in Metabolism (references)	Tissues (cultured cells)
miR-33	ABCA1, NPC1	Cholesterol homeostasis (25, 26)	Liver (HepG2)
miR-34a	SIRT1	Lipid metabolism, promotes fatty liver (30)	
miR-370	Cpt1a	Fatty acid and triglyceride biosynthesis (29)	
miR-122	CAT-1 ADAM17	Hepatic lipid metabolism (24, 29) Circadian gene expression (28)	
miR-34a	VAMP2	B-cell exocytosis (33)	Pancreatic Islets (MIN6, INS-1)
miR-124a	Foxa2	Intracellular signaling in pancreatic β-cell (27)	
miR-375	MTPN	Regulates catecholamine release Inhibits insulin secretion (31, 32)	
miR-27a	[PPARγ, C/EBPα]	Inhibits adipocyte formation, Down-regulated during adipogenic differentiation (34)	(Adipocytes, 3T3-L1, ST2)
miR-378/378*	[Ribosomal proteins]	Upregulates adipocyte differentiation and lipid synthesis (35)	
miR-223	Glut4	Glucose uptake and insulin resistance (36)	Muscle Gastrocnemius (Cardiomyocyte, C_2C_{12})
miR-696	[PGC1α]	Muscle metabolism, mitochondria biogenesis and fatty acid oxidation (37)	

Table 2. MicroRNAs targeting SIRT1

MicroRNA	Sequences of microRNAs	Size (nt)	Biological functions (references)
miR-34a	5'-uggcagugucuuagcuggguugu-3'	22	Hepatic lipid metabolism (30) Islet β-cell exocytosis (33) Cell apoptosis (42)
miR-132	5'-uaacagucuacagccauggucg-3'	22	Stress-induced chemokine production (43)
miR-199a	5'-cccaguguucagacuaccuguuc-3'	25	Hypoxia preconditioning (44)

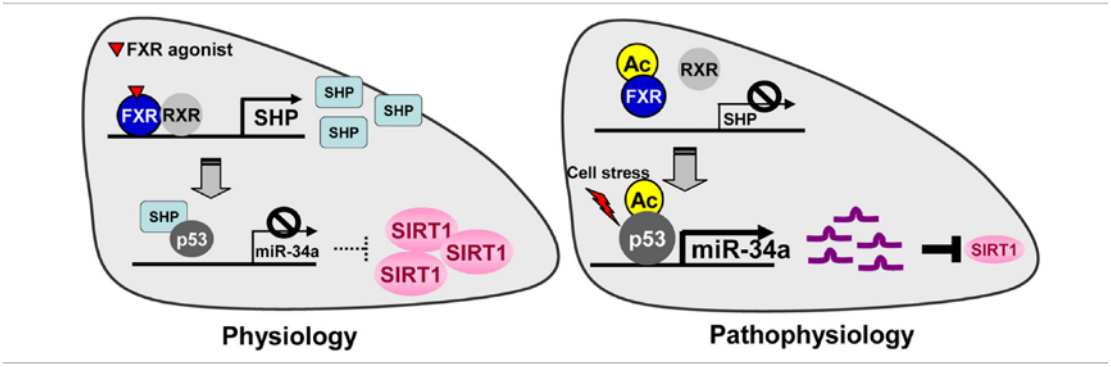

Figure 1. The FXR/SHP pathway controlling miR-34a and SIRT1 expression. Under normal conditions, activation of FXR signaling induces the metabolic repressor SHP in liver. SHP is then recruited to the miR-34a promoter and inhibits binding of the key activator p53 to the DNA, resulting in decreased miR-34a expression. Inhibition of miR-34a results in increased hepatic SIRT1 levels. In contrast, under pathophysiological conditions such as fatty livers of obese mice, the dysregulated FXR/SHP pathway due to highly elevated FXR acetylation no longer inhibits transcription of miR-34a. The dysregulated FXR/SHP pathway, along with acetylation of p53 due to cellular stress under metabolic disease states, result in elevated miR-34a expression, which contributes to decreased SIRT1 levels.

A novel FXR/SHP/miR-34a pathway controlling SIRT1 levels

The nuclear bile acid receptor, Farnesoid X Receptor (FXR), plays an important role in maintaining lipid and glucose levels by regulating expression of numerous metabolic genes mainly in the liver and intestine [46]. Consistent with its important metabolic functions, disruption of the FXR gene in transgenic mice was associated with metabolic diseases, including hypercholesterolemia, cholesterol gallstone disease, fatty liver, and type 2 diabetes [46-49]. Activation of FXR in diabetic obese mice improved metabolic outcomes by reducing serum glucose and lipid levels [50]. Although both FXR and SIRT1 have been shown to be critical for hepatic metabolism and activation of both proteins improves metabolic outcomes in diet-induced obese mice [17, 18, 46, 47, 50], it was unknown whether the expression and activity of these two proteins are coordinately regulated. In recent studies, we found that FXR positively regulates hepatic SIRT1 expression by inhibiting expression of miR-34a [30]. As shown in Figure 1, under normal conditions, miR-34a levels are down-regulated by a nuclear receptor cascade pathway involving FXR and orphan nuclear receptor and metabolic repressor, Small Heterodimer Partner (SHP) [51, 52]. Upon induction by activated FXR, SHP is recruited to the miR-34a promoter and suppresses its transcription by inhibiting the promoter occupancy of p53, the key activator of the miR-34a gene [53]. Subsequently, inhibition of miR-34a contributes to increased expression of SIRT1. This FXR/SHP pathway was also shown to play a crucial role in the regulation of hepatic bile acid synthesis by inhibiting the rate-limiting bile acid synthetic enzyme CYP7A1 [51, 52] and to suppress fatty liver formation by inhibiting the key lipogenic activator SREBP-1c [54]. Our group has identified molecular mechanisms by which SHP inhibits its target genes by coordinately recruiting chromatin modifying repressive cofactors, including HDACs, G9a metyltransferase, and Brm-containing Swi/Snf remodeling complex [55-57]. Consistent with these previous findings, we observed recruitment of HDACs to the miR-34a promoter in mouse liver after treatment with the synthetic FXR agonist, GW4064 (not shown). In contrast, in fatty livers of obese mice, the FXR/SHP pathway is dysregulated such that miR-34a levels are highly elevated, which contributes to reduced SIRT1 levels [30]. Interestingly, activation of FXR signaling in obese mice by daily treatment with GW4064 for 5 days or by hepatic expression of FXR using adenoviral delivery decreased miR-34a levels and restored SIRT1 levels [30]. Consistent with a critical role for FXR in positively controlling SIRT1 through the inhibition of miR-34a, miR-34a levels were indeed elevated and

SIRT1 protein levels are substantially decreased in FXR null mice [30]. Our findings suggest an intriguing link among FXR activation, decreased miR-34a levels, increased SIRT1 levels, and beneficial metabolic outcomes.

A positively interacting FXR/SIRT1 regulatory loop

In the FXR/SHP/miR-34a pathway, FXR positively regulates hepatic SIRT1 levels by inhibiting transcription of the miR-34a gene. These findings, along with previous studies showing the p53/miR-34a/SIRT1 feedback loop [42, 58], suggest intriguing regulatory loops controlling SIRT1 expression (Figure 2). In the short regulatory loop, SIRT1 positively auto-regulates its own expression by deacetylating p53 and histones at the miR-34a promoter, resulting in suppression of miR-34a [9, 30, 42, 53, 58]. In the long regulatory loop, SIRT1-mediated deacetylation of FXR increases FXR's transactivation ability by increasing binding of the FXR/RXR heterodimer to DNA resulting in induction of SHP and repression of miR-34a expression [11, 30]. We observed that FXR acetylation is dynamically controlled by p300 acetylase and SIRT1 deacetylase under normal conditions, and remarkably, FXR acetylation levels are highly elevated in fatty livers of obese mice [11]. Interestingly, treatment daily with the SIRT1 activator resveratrol for 1 week or adenoviral-mediated hepatic expression of SIRT1 substantially reduced FXR acetylation with beneficial metabolic effects [11]. These results are consistent with the idea that the transactivation activity of FXR is low in obese mice due to highly elevated FXR acetylation, which contributes to increased expression of miR-34a. Subsequently, elevated miR- 34a suppresses expression of SIRT1, which then further decreases FXR activity, resulting in a vicious FXR/miR-34a/SIRT1 regulatory loop in metabolic disease states. In addition to deacetylation of FXR, SIRT1 has been implicated as a positive regulator of the expression and activity of FXR. During fasting, PGC-1α was shown to increase expression of the FXR gene and function as a coactivator of FXR [59]. Since SIRT1 deacetylates and increases PGC-1α activity [8], SIRT1 should increase FXR expression and activity by enhancing PGC-1α activity. All these recent studies strongly suggest that the expression and activity of these two proteins are mutually and coordinately regulated.

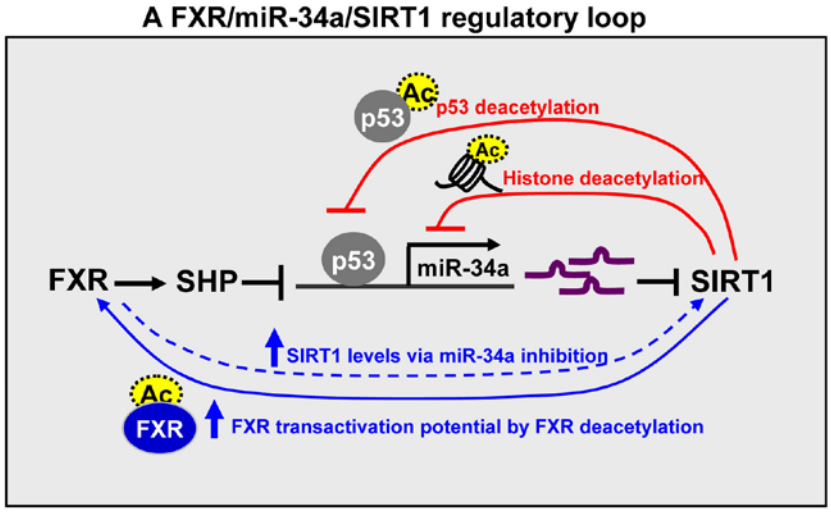

Figure 2. A FXR/SIRT1 positive-feedback regulatory loop. The expression and activity of FXR and SIRT1 are mutually and coordinately regulated. SIRT1 positively auto-regulates its own expression by inhibiting miR-34a via deacetylation (as indicated by dotted circles) of p53 and histones at the miR-34a promoter (short loop) and by increasing transactivation potential of FXR via deacetylating the FXR (long loop). SIRT1 also increases FXR expression and activity via deacetylation of PGC-1α. FXR in turn positively regulates hepatic SIRT1 expression by inhibiting miR-34a which targets SIRT1.

Concluding remarks

Because of SIRT1's anti-aging properties and its beneficial effects on a wide range of age-related disease [1-3, 21], it has been intensively studied. SIRT1 levels were reported to be decreased in liver, muscle, and adipose tissues of diet-induced obese mice in vivo as well as in cultured cell models of insulin resistance [15, 30, 60], but the underlying mechanisms remain unclear. The discovery of the FXR/miR-34a pathway controlling SIRT1 levels provides a partial explanation since elevated miR-34a levels in obese mice contribute to decreased SIRT1 levels [30]. Based on these findings, together with the development of effective inhibitors of miRs, the antagomirs [4, 24, 38], it will be interesting to see whether the reduction of elevated miR-34a in fatty livers of obesity improves transcriptional profiles of metabolic genes and metabolic outcomes. Also, it will be important to understand how the FXR/SIRT1 regulatory network is dysregulated in metabolic disease states which likely involves altered cellular kinase signaling pathways that post-transcriptionally affect SIRT1 and FXR levels and activities. Development of drugs that target the FXR/miR-34a pathway and other miRs controlling SIRT1 expression may lead to novel therapeutic options for treating age-related metabolic disease including fatty liver, obesity and type II diabetes.

CONFLICT OF INTERESTS STATEMENT

The authors of this manuscript have no conflict of interests to declare.

REFERENCES

1. Haigis MC, Sinclair DA. Mammalian sirtuins: biological insights and disease relevance. Annu Rev Pathol. 2010; 5: 253-295.

2. Donmez G, Guarente L. Aging and disease: connections to sirtuins. Aging Cell. 2010; 9: 285-290.

3. Brooks CL, Gu W. Anti-aging protein SIRT1: a role in cervical cancer? Aging. 2009; 1: 278-280.

4. Krutzfeldt J, Rajewsky N, Braich R, Rajeev KG, Tuschl T, Manoharan M, Stoffel M. Silencing of microRNAs in vivo with 'antagomirs'. Nature. 2005; 438: 685-689.

5. Neilson JR, Sharp PA. Small RNA regulators of gene expression. Cell. 2008; 134: 899-902.

6. Hobert O. Gene regulation by transcription factors and microRNAs. Science. 2008; 319: 1785-1786.

7. Canto C, Auwerx J. Caloric restriction, SIRT1 and longevity. Trends Endocrinol Metab. 2009; 20: 325-231.

8. Rodgers JT, Lerin C, Haas W, Gygi SP, Spiegelman BM, Puigserver P. Nutrient control of glucose homeostasis through a complex of PGC-1alpha and SIRT1. Nature. 2005; 434: 113-118.

9. Luo J, Nikolaev AY, Imai S, Chen D, Su F, Shiloh A, Guarente L, Gu W. Negative control of p53 by Sir2alpha promotes cell survival under stress. Cell. 2001; 107: 137-148.

10. Li X, Zhang S, Blander G, Tse JG, Krieger M, Guarente L. SIRT1 deacetylates and positively regulates the nuclear receptor LXR. Mol Cell. 2007; 28: 91-106.

11. Kemper JK, Xiao, Z., Ponugoti, B., Miao J., Fang, S., Kanamaluru, D., Tsang, S., Wu S., Chiang, C.M., and Veenstra, T.D. FXR acetylation is normally dynamically regulated by p300 and SIRT1 but constitutively elevated in metabolic disease states. Cell Metabolism. 2009; 10: 392-404.

12. Pfluger PT, Herranz D, Velasco-Miguel S, Serrano M, Tschop MH. Sirt1 protects against high-fat diet-induced metabolic damage. Proc Natl Acad Sci U S A. 2008; 105: 9793-9798.

13. Bordone L, Motta MC, Picard F, Robinson A, Jhala US, Apfeld J, McDonagh T, Lemieux M, McBurney M, Szilvasi A, Easlon EJ, Lin SJ, Guarente L. Sirt1 regulates insulin secretion by repressing UCP2 in pancreatic beta cells. PLoS Biol. 2006; 4: e31.

14. Picard F, Kurtev M, Chung N, Topark-Ngarm A, Senawong T, Machado De Oliveira R, Leid M, McBurney MW, Guarente L. Sirt1 promotes fat mobilization in white adipocytes by repressing PPAR-gamma. Nature. 2004; 429: 771-776.

15. Sun C, Zhang F, Ge X, Yan T, Chen X, Shi X, Zhai Q. SIRT1 improves insulin sensitivity under insulin-resistant conditions by repressing PTP1B. Cell Metab. 2007; 6: 307-319.

16. Feige JN, Lagouge M, Canto C, Strehle A, Houten SM, Milne JC, Lambert PD, Mataki C, Elliott PJ, Auwerx J. Specific SIRT1 activation mimics low energy levels and protects against diet-induced metabolic disorders by enhancing fat oxidation. Cell Metab. 2008; 8: 347-358.

17. Lagouge M, Argmann C, Gerhart-Hines Z, Meziane H, Lerin C, Daussin F, Messadeq N, Milne J, Lambert P, Elliott P, Geny B, Laakso M, Puigserver P, et al. Resveratrol improves mitochondrial function and protects against metabolic disease by activating SIRT1 and PGC-1alpha. Cell. 2006; 127: 1109-1122.

18. Baur JA, Pearson KJ, Price NL, Jamieson HA, Lerin C, Kalra A, Prabhu VV, Allard JS, Lopez-Lluch G, Lewis K, Pistell PJ, Poosala S, Becker KG, et al. Resveratrol improves health and survival of mice on a high-calorie diet. Nature. 2006; 444: 337-342.

19. Purushotham A, Schug TT, Xu Q, Surapureddi S, Guo X, Li X. Hepatocyte-specific deletion of SIRT1 alters fatty acid metabolism and results in hepatic steatosis and inflammation. Cell Metab. 2009; 9: 327-338.

20. Bordone L, Cohen D, Robinson A, Motta MC, van Veen E, Czopik A, Steele AD, Crowe H, Marmor S, Luo J, Gu W, Guarente L. SIRT1 transgenic mice show phenotypes resembling calorie restriction. Aging Cell. 2007; 6: 759-767.

21. Herranz D, Serrano M. Impact of Sirt1 on mammalian aging. Aging. 2: 315-316.

22. Purushotham A, Schug TT, Li X. SIRT1 performs a balancing act on the tight-rope toward longevity. Aging. 2009; 1: 669-673.

23. Stein S, Schafer N, Breitenstein A, Besler C, Winnik S, Lohmann C, Heinrich K, Brokopp CE, Handschin C, Landmesser U, Tanner FC, Luscher TF, Matter CM. SIRT1 reduces endothelial activation without affecting vascular function in ApoE-/- mice. Aging. 2010; 2: 353-360.

24. Esau C, Davis S, Murray SF, Yu XX, Pandey SK, Pear M, Watts L, Booten SL, Graham M, McKay R, Subramaniam A, Propp S, Lollo BA, et al. miR-122 regulation of lipid metabolism revealed by in vivo antisense targeting. Cell Metab. 2006; 3: 87-98.

25. Najafi-Shoushtari SH, Kristo F, Li Y, Shioda T, Cohen DE, Gerszten RE, Naar AM. MicroRNA-33 and the SREBP host genes cooperate to control cholesterol homeostasis. Science.2010; 328: 1566-1569.

26. Rayner KJ, Suarez Y, Davalos A, Parathath S, Fitzgerald ML, Tamehiro N, Fisher EA, Moore KJ, Fernandez-Hernando C. MiR-33 contributes to the regulation of cholesterol homeostasis. Science. 2010; 328: 1570-1573.

27. Baroukh N, Ravier MA, Loder MK, Hill EV, Bounacer A, Scharfmann R, Rutter GA, Van Obberghen E. MicroRNA-124a regulates Foxa2 expression and intracellular signaling in pancreatic beta-cell lines. J Biol Chem. 2007; 282: 19575-19588.

28. Gatfield D, Le Martelot G, Vejnar CE, Gerlach D, Schaad O, Fleury-Olela F, Ruskeepaa AL, Oresic M, Esau CC, Zdobnov EM, Schibler U. Integration of microRNA miR-122 in hepatic circadian gene expression. Genes Dev. 2009; 23: 1313-1326.

29. Iliopoulos D, Drosatos K, Hiyama Y, Goldberg IJ, Zannis VI. MicroRNA-370 controls the expression of MicroRNA-122 and Cpt1alpha and affects lipid metabolism. J Lipid Res. 2010; 51: 1513-1523.

30. Lee J, Padhye A, Sharma A, Song G, Miao J, Mo YY, Wang L, Kemper JK. A pathway involving farnesoid X receptor and small heterodimer partner positively regulates hepatic sirtuin 1 levels via microRNA-34a inhibition. J Biol Chem. 2010; 285: 12604-12611.

31. Poy MN, Eliasson L, Krutzfeldt J, Kuwajima S, Ma X, Macdonald PE, Pfeffer S, Tuschl T, Rajewsky N, Rorsman P, Stoffel M. A pancreatic islet-specific microRNA regulates insulin secretion. Nature. 2004; 432: 226-230.

32. Poy MN, Hausser J, Trajkovski M, Braun M, Collins S, Rorsman P, Zavolan M, Stoffel M. miR-375 maintains normal pancreatic alpha- and beta-cell mass. Proc Natl Acad Sci U S A. 2009; 106: 5813-5818.

33. Lovis P, Roggli E, Laybutt DR, Gattesco S, Yang JY, Widmann C, Abderrahmani A, Regazzi R. Alterations in microRNA expression contribute to fatty acid-induced pancreatic beta-cell dysfunction. Diabetes. 2008; 57: 2728-2736.

34. Lin Q, Gao Z, Alarcon RM, Ye J, Yun Z. A role of miR-27 in the regulation of adipogenesis. Febs J. 2009; 276: 2348-2358.

35. Gerin I, Bommer GT, McCoin CS, Sousa KM, Krishnan V, MacDougald OA. Roles for miRNA-378/378* in adipocyte gene expression and lipogenesis. Am J Physiol Endocrinol Metab. 2010; 299: E198-206.

36. Lu H, Buchan RJ, Cook SA. MicroRNA-223 regulates Glut4 expression and cardiomyocyte glucose metabolism. Cardiovasc Res. 2010; 86: 410-420.

37. Aoi W, Naito Y, Mizushima K, Takanami Y, Kawai Y, Ichikawa H, Yoshikawa T. The microRNA miR-696 regulates PGC-1{alpha} in mouse skeletal muscle in response to physical activity. Am J Physiol Endocrinol Metab. 2010; 298: E799-806.

38. Kota J, Chivukula RR, O'Donnell KA, Wentzel EA, Montgomery CL, Hwang HW, Chang TC, Vivekanandan P, Torbenson M, Clark KR, Mendell JR, Mendell JT. Therapeutic microRNA delivery suppresses tumorigenesis in a murine liver cancer model. Cell. 2009; 137: 1005-1017.

39. Cheung O, Puri P, Eicken C, Contos MJ, Mirshahi F, Maher JW, Kellum JM, Min H, Luketic VA, Sanyal AJ. Nonalcoholic steatohepatitis is associated with altered hepatic MicroRNA expression. Hepatology. 2008; 48: 1810-1820.

40. Nakanishi N, Nakagawa Y, Tokushige N, Aoki N, Matsuzaka T, Ishii K, Yahagi N, Kobayashi K, Yatoh S, Takahashi A, Suzuki H, Urayama O, Yamada N, et al. The up-regulation of microRNA-335 is associated with lipid metabolism in liver and white adipose tissue of genetically obese mice. Biochem Biophys Res Commun. 2009; 385: 492-496.

41. Kwon HS, Ott M. The ups and downs of SIRT1. Trends Biochem Sci. 2008; 33: 517-525.

42. Yamakuchi M, Ferlito M, Lowenstein CJ. miR-34a repression of SIRT1 regulates apoptosis. Proc Natl Acad Sci U S A. 2008; 105: 13421-13426.

43. Strum JC, Johnson JH, Ward J, Xie H, Feild J, Hester A, Alford A, Waters KM. MicroRNA 132 regulates nutritional stress-induced chemokine production through repression of SirT1. Mol Endocrinol. 2009; 23: 1876-1884.

44. Rane S, He M, Sayed D, Vashistha H, Malhotra A, Sadoshima J, Vatner DE, Vatner SF, Abdellatif M. Downregulation of miR-199a derepresses hypoxia-inducible factor-1alpha and Sirtuin 1 and recapitulates hypoxia preconditioning in cardiac myocytes. Circ Res. 2009; 104: 879-886.

45. Saunders LR, Sharma AD, Tawney J, Nakagawa M, Okita K, Yamanaka S, Willenbring H, Verdin E. miRNAs regulate SIRT1 expression during mouse embryonic stem cell differentiation and in adult mouse tissues. Aging. 2010; Jul, 415-432.

46. Cariou B, Staels B. FXR: a promising target for the metabolic syndrome? Trends Pharmacol Sci. 2007; 28: 236-243.

47. Sinal C, Tohkin M, Miyata M, Ward J, Lambert G, Gonzalez FJ. Targeted disruption of the nuclear receptor FXR/BAR impairs bile acid and lipid homeostasis. Cell. 2000; 102: 731-744.

48. Moschetta A, Bookout AL, Mangelsdorf DJ. Prevention of cholesterol gallstone disease by FXR agonists in a mouse model. Nat Med. 2004; 10: 1352-1358.

49. Ma K, Saha PK, Chan L, Moore DD. Farnesoid X receptor is essential for normal glucose homeostasis. J Clin Invest. 2006; 116: 1102-9.

50. Zhang Y, Lee FY, Barrera G, Lee H, Vales C, Gonzalez FJ, Willson TM, Edwards PA. Activation of the nuclear receptor FXR improves hyperglycemia and hyperlipidemia in diabetic mice. Proc Natl Acad Sci U S A. 2006; 103: 1006-1011.

51. Goodwin B, Jones SA, Price RR, Watson MA, McKee DD, Moore LB, Galardi C, Wilson JG, Lewis MC, Roth ME, Maloney PR, Wilson TM, Kliewer SA. A regulatory cascade of the nuclear receptors FXR, SHP-1, and LRH-1 represses bile acid biosynthesis. Molecular Cell. 2000; 6: 517-526.

52. Lu TT, Makishima M, Repa JJ, Schoonjans K, Kerr TA, Auwerx J, Mangelsdorf DJ. Molecular basis for feedback regulation of bile acid synthesis by nuclear receptors. Mol Cell. 2000; 6: 507-515.

53. Chang TC, Wentzel EA, Kent OA, Ramachandran K, Mullendore M, Lee KH, Feldmann G, Yamakuchi M, Ferlito M, Lowenstein CJ, Arking DE, Beer MA, Maitra A, et al. Transactivation of miR-34a by p53 broadly influences gene expression and promotes apoptosis. Mol Cell. 2007; 26: 745-752.

54. Watanabe M, Houten SM, Wang L, Moschetta A, Mangelsdorf DJ, Heyman RA, Moore DD, Auwerx J. Bile acids lower triglyceride levels via a pathway involving FXR, SHP, and

SREBP-1c. Journal of Clinical Investigation. 2004; 113: 1408-1418.

55. Fang S, Miao J, Xiang L, Ponugoti B, Treuter E, Kemper JK. Coordinated recruitment of histone methyltransferase G9a and other chromatin-modifying enzymes in SHP-mediated regulation of hepatic bile acid metabolism. Mol Cell Biol. 2007; 27: 1407-1424.

56. Kemper J, Kim H, Miao J, Bhalla S, Bae Y. Role of a mSin3A-Swi/Snf chromatin remodeling complex in the feedback repression of bile acid biosynthesis by SHP. Mol Cell Biol. 2004; 24: 7707-7719.

57. Miao J, Fang S, Lee J, Comstock C, Knudsen KE, Kemper JK. Functional specificities of Brm and Brg-1 Swi/Snf ATPases in the feedback regulation of hepatic bile acid biosynthesis. Mol Cell Biol. 2009; 29: 6170-6181.

58. Yamakuchi M, Lowenstein CJ. MiR-34, SIRT1 and p53: the feedback loop. Cell Cycle. 2009; 8: 712-715.

59. Zhang Y, Castellani LW, Sinal CJ, Gonzalez FJ, Edwards PA. Peroxisome proliferator-activated receptor-gamma coactivator 1alpha (PGC-1alpha) regulates triglyceride metabolism by activation of the nuclear receptor FXR. Genes Dev. 2004; 18: 157-169.

60. Coste A, Louet JF, Lagouge M, Lerin C, Antal MC, Meziane H, Schoonjans K, Puigserver P, O'Malley BW, Auwerx J. The genetic ablation of SRC-3 protects against obesity and improves insulin sensitivity by reducing the acetylation of PGC-1{alpha}. Proc Natl Acad Sci U S A. 2008; 105: 17187-17192.

Research Paper

Nutrient withdrawal rescues growth factor-deprived cells from mTOR-dependent damage

Emiliano Panieri[1]*, Gabriele Toietta[3]*, Marina Mele[1], Valentina Labate[1], Sofia Chiatamone Ranieri[1], Salvatore Fusco[1], Valentina Tesori[1], Annalisa Antonini[3], Giuseppe Maulucci[2], Marco De Spirito[2], Tommaso Galeotti[1], and Giovambattista Pani[1]

[1] Institute of General Pathology, Laboratory of Cell Signaling, Catholic University Medical School, Rome Italy
[2] Institute of Physics and Microscopy Core Facility, Catholic University Medical School, Rome Italy
[3] Vascular Pathology Laboratory, Istituto Dermopatico dell'Immacolata - IDI- IRCCS, Rome, Italy
** These authors contributed equally to this work*

Key words: *mTOR, nutrients, cell death, growth factor withdrawal, endothelial cells, ageing*
Abbreviations: *mTOR: mammalian Target of Rapamycin; 2,4 DNP: 2,4 Dinitrophenol; 2-DG: 2 deoxy glucose; 3-NPA: 3-Nitropropionic Acid; 4EBP1: Elongation Factor 4 Binding Protein; AMPK: AMP-activated protein kinase; BSA: Bovine Serum Albumin; DMEM: Dulbecco's Modified Eagle's Medium; ECL: Enhanced Chemiluminescence; ER: Endoplasmic Reticulum; FBS: Fetal Bovine Serum; H2-DCF-DA: Dihydro-dichlorofluorescein-diacetate; HEK-293-T; Human Embryonic Kidney 293- SV40 Large T Antigen; HRP: Horseradish Peroxidase; HUVEC: Human Umbilical Vein Endothelial Cells; IRS-1: Insulin Receptor Substrate-1; NAC: N-Acetyl-Cysteine NAF: Sodium Fluoride; NEAA: Non Essential Aminoacids; O-GlcNAc: O-linked N-acetyl Glucosamine; PI: Propidium Iodide; PKB: Protein Kinase B; ROS: Reactive Oxygen Species; rxYFP: redox Yellow Fluorescent Protein; S6K: S6 kinase; Sirt-1: Sirtuin 1; TBS-T: Tris Buffered Saline-Tween 20; TORC1 and TORC2: TOR Complex 1 and 2; TSC1/TSC2: Tuberous Sclerosis Complex 1/2; UPR: Unfolded Protein Response*
Received: *08/01/10; accepted: 08/22/10; published on line: 08/24/10*
Corresponding author: *Giovambattista Pani, MD/PhD;* ***E-mail:*** *gpani@rm.unicatt.it* doi:10.18632/aging.100183

Abstract: Deregulated nutrient signaling plays pivotal roles in body ageing and in diabetic complications; biochemical cascades linking energy dysmetabolism to cell damage and loss are still incompletely clarified, and novel molecular paradigms and pharmacological targets critically needed. We provide evidence that in the retrovirus-packaging cell line HEK293-T *Phoenix,* massive cell death in serum-free medium is remarkably prevented or attenuated by either glucose or aminoacid withdrawal, and by the glycolysis inhibitor 2-deoxy-glucose. A similar protection was also elicited by interference with mitochondrial function, clearly suggesting involvement of energy metabolism in increased cell survival. Oxidative stress did not account for nutrient toxicity on serum-starved cells. Instead, nutrient restriction was associated with reduced activity of the mTOR/S6 Kinase cascade. Moreover, pharmacological and genetic manipulation of the mTOR pathway modulated in an opposite fashion signaling to S6K/S6 and cell viability in nutrient-repleted medium. Additionally, stimulation of the AMP-activated Protein Kinase concomitantly inhibited mTOR signaling and cell death, while neither event was affected by overexpression of the NAD+ dependent deacetylase Sirt-1, another cellular sensor of nutrient scarcity. Finally, blockade of the mTOR cascade reduced hyperglycemic damage also in a more pathophysiologically relevant model, i.e. in human umbilical vein endothelial cells (HUVEC) exposed to hyperglycemia. Taken together these findings point to a key role of the mTOR/S6K cascade in cell damage by excess nutrients and scarcity of growth-factors, a condition shared by diabetes and other ageing-relatedpathologies.

INTRODUCTION

Mammalian cells sense availability of nutrients through a complex array of both paracrine/endocrine and cell-autonomous signaling cascades which regulate proliferation, differentiation and survival. Deregulated function of these cascades either due to nutrient excess or abnormal cell responses, play a central role in metabolic diseases such as diabetes and its complications [1,2], in body ageing [3] and cancer [4,5]. A better understanding of the molecular interactions underlying cellular consequences of exposure to energy substrates is therefore key to the understanding, the prevention and the therapy of severe and epidemiologically relevant human diseases.

The mTOR (mammalian Target of Rapamycin)/FRAP cascade serves a unique function in coordinating nutrient availability and energy metabolism with cell response to growth factors [6,7]. By phosphorylating and activating the S6 kinase or inhibiting the Elongation Factor 4 Binding Protein-1 (4EBP-1), mTOR stimulates the ribosomal translation of different classes of mRNAs, thereby promoting protein synthesis. It also acts directly on gene expression by phosphorylating transcription factors mainly involved in the orchestration of glucose and lipid metabolism [7]. Accordingly, mTOR activity is exquisitely sensitive to cell energy status, sensed through a complex circuitry involving the AMP-activated kinase, a serine threonine kinase activated by the reduction of intracellular ATP and the increase of AMP/ATP ratio [8]. Phosphorylation of the TSC1/TSC2 complex by AMPK and the consequent inactivation of the GTPase Rheb, an upstream activator of mTOR, profoundly inhibits mTOR signaling, thereby reducing protein synthesis and promoting cell survival under nutrient restriction [8]. mTOR is also directly regulated by aminoacids, through a distinct mechanism involving the GTPase Rag [9]. Finally, the mTOR cascade is crucial for signaling downstream of growth factor receptors including the insulin receptor. It is in fact, activated, in a TSC- and Rheb-dependent fashion, by growth factors through PI3 kinase and the serine-threonine kinase AkT/PKB [10]. Consequently, the mTOR cascade integrates nutritional and mitogenic/antiapoptotic cues ensuring that energy supply and protein synthesis are adequate to support cell growth (i.e. increase in cell size), proliferation, and accumulation of biomass.

Most of nutrient-related functions of mTOR are mediated by a multimolecular complex including mTOR itself and the scaffold protein Raptor (a complex indicated as TORC1) [11]. Nonetheless, additional mTOR signaling capacity directed towards AkT/PKB also involves a second, largely nutrient- and rapamycin-insensitive complex (TORC2) centered on Rictor as main scaffold component [12]. Thus, mTOR operates both upstream and downstream of PKB/AkT, revealing an intricate cross-talk with PKB-dependent survival and mitogenic signaling at the intersection between cell metabolism and regulation of normal tissue growth.

Hyperactivation of the mTOR/S6K axis has recently drawn significant attention as a key factor in the establishment of obesity and insulin resistance by nutrient overload [13]. S6K deficient mice display increased life span and resistance to age-related pathologies including loss of insulin sensitivity[14] Moreover, mTOR hyperactivation by excess nutrients negatively influences, both *in vivo* and *in vitro*, insulin and growth/trophic factor signaling, through the feed-back inhibition of upstream components such as the Insulin receptor Substrate 1 (IRS-1) [13, 15-17]. Finally, it has been demonstrated that mTOR activation leads to cell senescence in the context of block of the cell cycle [18], and, more in general, evidence exist that the mTOR cascade may play a central role in the signaling derangement that underlies tissue and body ageing [19].

Hence, converging lines of evidence indicate that mTOR and its downstream pathway, by transducing nutrient-triggered signals, may mediate cellular damage, through molecular mechanisms largely involving mTOR cross-talk with growth factor-triggered mitogenic and survival cascades.

Here we report a novel mechanism for cell survival regulation by nutrients. In particular, our findings reveal that unbalanced mTOR activity in the absence of adequate growth factor supply, may represent a general mechanism of cell death by excess nutrients. This may be relevant in the study of tissue hyperglycemic damage, in body senescence and cancer therapy, prospectively suggesting a possible pharmacological target for novel preventive and therapeutic strategies.

RESULTS

Nutrient restriction protects 293T *Phoenix* cells from death by serum deprivation

Most immortalized cell lines undergo mitotic catastrophe and cell death with morphological and biochemical features of apoptosis when deprived of fetal calf serum or growth factor supply [20]. Upon serum withdrawal, 293-T *Phoenix* cells, a retrovirus packaging line derived from E1A-transformed embryonic human kidney cells (HEK-293) carrying a

temperature sensitive T antigen, displayed severe and time-dependent loss of viability, as revealed by a Propidium Iodide uptake assay (Figure 1A). Nearly 100% of cells appeared dead by day 4 of culture (96 hours) (Figure 1A). Remarkably, removal from the culture medium of either Glucose or Aminoacid Supplement (Glutamine + DMEM Non Essential Aminoacids), the two main energy fuels for most cultured transformed cells [21], resulted in a drastic protection from cell death. Typically we detected a maximum of mortality of up to 30% at day 4 under glucose deprivation, and below 10%, comparable to average mortality in the presence of serum (Figure 1B), for aminoacid-starved cultures. Reduction of glucose from high (4.5 g/l) to low (1 g/l) concentration had no significant effect on cell viability, indicating that even physiological concentrations of glucose promote death of *Phoenix* cells in the absence of serum. Simultaneous removal of glucose and aminoacid supplement from the culture medium resulted in rapid (12 hours) loss of viability, in a fashion which could not be prevented by addition of Pyruvate, Dimethyl-Succinate or Free Fatty Acids (not shown); this confirms that glucose and glutamine account for most of the energy supply for these cells, at least in the tested experimental conditions.

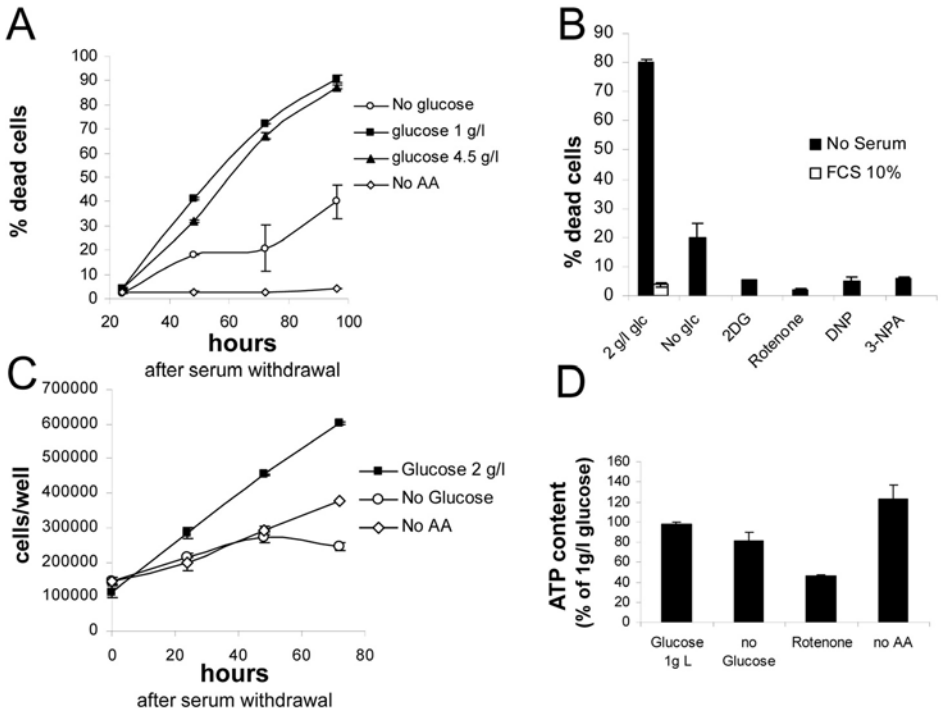

Figure 1. (**A**) Survival assay displaying progressive loss viability of nutrient-repleted *Phoenix* cells in serum free medium, and protection by either glucose or aminoacid deprivation. Values are Mean±SD of triplicate samples from one of several independent experiments. (**B**) Effect of metabolic inhibitors on cell death by serum deprivation in nutrient-rich medium. Death in the presence of serum was marginal, not affected by inhibitors and is therefore displayed only for the 2 g/l glucose sample. Extent of cell death in the absence of glucose is also reported. Values are Mean±SD of triplicate samples. Panel representative of several independent experiments with very similar results. (**C**) Growth curves for *Phoenix* cells grown in the absence of serum with or without nutrients. Numbers refer to live cells, based on morphological features and trypan blue exclusion. Values are Mean±SD of triplicate samples. Panel representative of two independent experiments. (**D**) Determination of ATP content in cells incubated for 24 hours in the indicated conditions. Values are % of the control (1 g/l glucose + aminoacids) sample. Chemiluminescence values were normalized for protein content of the different samples. Representative of two independent experiments.

Live cell count revealed that *Phoenix* cells continue proliferating robustly in the absence of serum, and are therefore, at least in part, self-sufficient for mitogenic stimulation. Cell proliferation and death appear to occur concomitantly (Figures 1A and 1C), and are likely to be mechanistically linked [22]. Proliferation also occurred, although to a lesser extent, in nutrient deprived cultures, yet associated with no or minimal cell loss (Figures 1A and 1C).

Beneficial effect of nutrient restriction on cell viability prompted us to evaluate the consequence of pharmacological interference with cellular metabolism. As expected, the glycolysis inhibitor 2-deoxyglucose fully rescued cells from death in the presence of glucose, to an even larger extent than glucose deprivation (Figure 1B). Similarly, significant protection was obtained by interference with mitochondrial respiration: in fact, both complex I inhibitor Rotenone and complex II inhibitor 3-Nitropropionic acid (NPA) drastically reduced death of serum-deprived cultures. Also the uncoupling agent 2,4-dinitrophenol(2,4-DNP), at non toxic concentration, had the same protective effect as mitochondrial inhibitors on cell survival in 2 g/l glucose (Figure 1B); noteworthy, both DNP and electron transport chain (ETC) blockers rapidly killed *Phoenix* cells in the absence of glucose (not shown), indicating that mitochondria are functional in this cell line and support energy demand when glycolysis is prevented.

In order to evaluate the impact of nutrient restriction on the energy balance of *Phoenix* cells, ATP content was measured 48 hours after cell transfer to the different culture media. As expected based on survival data, no drastic reductions in cellular ATP levels were observed upon nutrient withdrawal (Figure 1D). Glucose deprivation led to a modest (about 20%) decrease of cellular ATP, and aminoacid removal to no reduction at all, compared to standard growth medium (2 g/l glucose and aminoacid supplement). ATP reduction was more pronounced (about 50%) in cells treated with Rotenone (Figure 1D), indicating that mitochondria contribute significantly to ATP generation in this tumor cell line. Thus, survival of *Phoenix* cells in serum free medium is clearly subdued to a metabolic regulation by nutrient availability, that operates independently from severe changes in cellular energy levels.

Nutrient toxicity in serum-deprived Phoenix cells is not mediated by ROS

Cell death by serum withdrawal is associated with the formation of harmful reactive oxygen species (ROS) [20], and nutrients may generate ROS through their oxidation in mitochondria [23]. Since nutrient restriction or mitochondrial blockade rescued *Phoenix* cells from serum deprivation, we tested possibility that cell protection might be mediated by an attenuation of cellular oxidative stress. To this end, *Phoenix* cells were transiently transfected with a redox-sensitive variant of the yellow fluorescent protein (rxYFP) and the intracellular redox state evaluated by confocal microscopy and fluorescence ratiometric analysis, 24 hours after serum or serum and glucose deprivation. RxYFP consistently appeared more reduced (as indicated by higher values of the Ratiometric Index *R*) in glucose-fed than in glucose-starved cells, revealing significantly higher levels of ROS in the latter cell population (Figures 2A, a and b). This finding was further supported by evidence of higher content of reduced NAD(P)H in glucose-fed cultures, as determined by cell microfluorimetry (Figure 2A, c). No significant redox changes were observed in cells deprived of Glutamine and NEAA or exposed to the mTOR inhibitor Rapamycin. As expected, addition of FCS further reduced the intracellular environment in glucose-fed cells (Figure 2A, b).

Based on these findings, excess oxidative stress unlikely accounts for impaired cell viability by nutrients. In keeping with this conclusion, no major changes in cell viability were induced, in the presence or absence of glucose, by saturating concentration of the ROS scavenger and glutatione precursor N- acethyl-cysteine (NAC, 10 mM) (Figure 2B, a). Similarly, overexpression of the ROS scavengers Catalase (Figure 2B, a) and SOD2 (Figure 2C and 2D,
b) did not provide glucose-fed cells protection from death, nor affected cell viability in glucose free-medium. Notably, overexpression of Catalase effectively increased cell antioxidant capacity, as revealed by flow cytometry of cells loaded with the redox-sensitive dye Dichlorofluoresceine Diacetate (H2-DCF-DA) and exposed to a bolus of exogenous hydrogen peroxide (Figure 2B, b). Finally, overexpression of the class III deacetylase Sirt-1, a molecule linking, in model organisms and in mammalian cells, nutrient restriction to increased resistance to oxidative stress [24], did not rescue cells from glucose-induced death in serum-free medium (Figures 2C and 2D, a). Thus, collectively, these data suggest that generation of ROS and oxidative stress do not mediate the effects of glucose on cell viability in our experimental model. Additionally, failure of Sirtuin-1 to prevent or attenuate glucose-induced cell death indicates that this major nutrient sensor and regulator of cell survival is unlikely involved in the protective response of *Phoenix* cells to nutrient restriction.

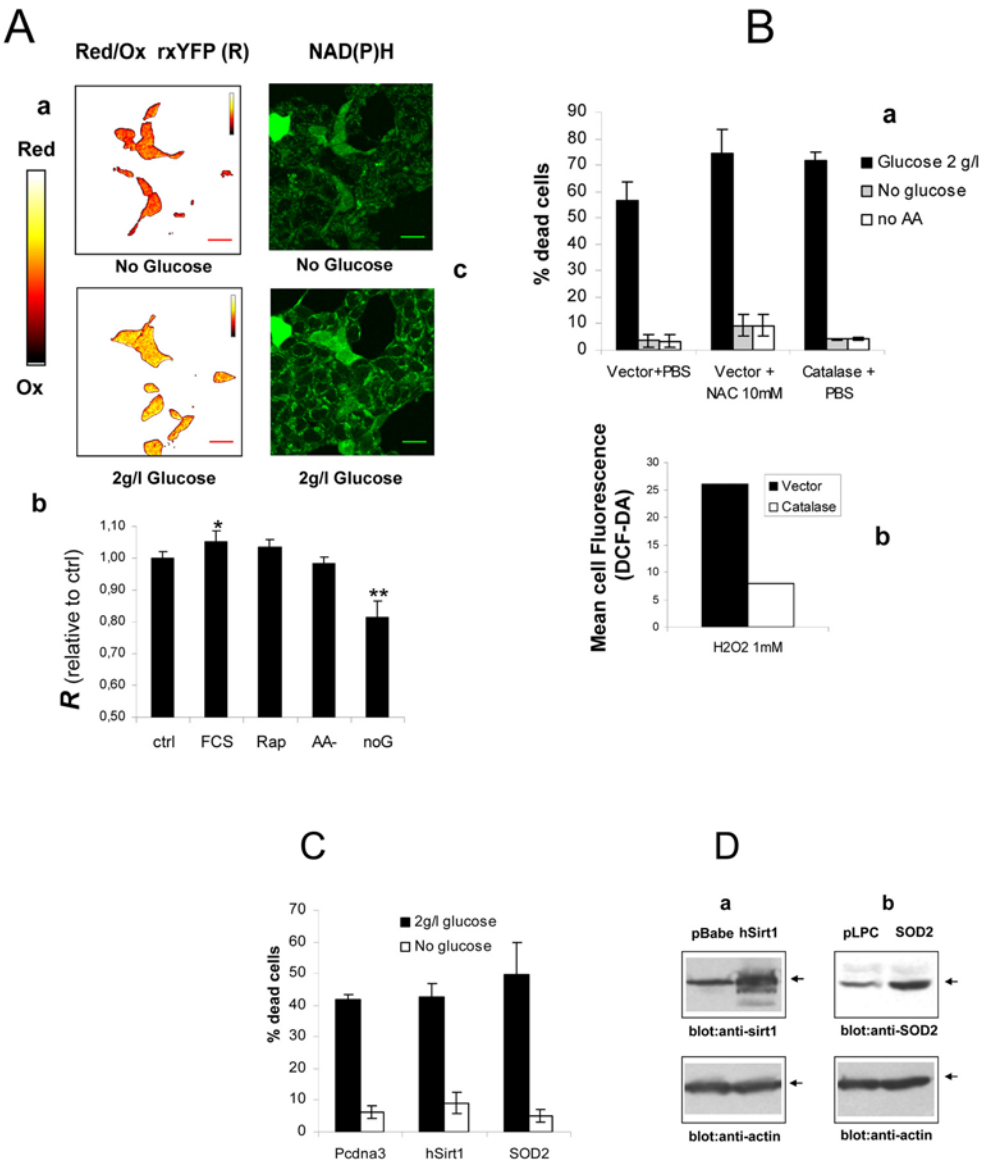

Figure 2. (**A**) ***a*** Intracellular redox state under nutrient restriction. ***a*** pseudocolor image (color bar on the left) of *Phoenix* cells expressing a redox-sensitive variant of the Yellow Fluorescent Protein (rxYFP) after 24 hours incubation in the absence of glucose (upper) and 30 minutes glucose re-feeding, in serum-free medium. Color shift from red to yellow indicates reduction of the fluorescent sensor. ***b*** Quantitation of mean R values over several regions of interest is reported. Data sets were compared by two-tailed t-test for independent samples. ***c*** Microfluorimetric analysis of reduced intracellular reduced NAD(P)H, based on cell green autofluorescence. Cells were excited in the two-photon mode at 366 nm and autofluorescence collected between 380 and 550 nm. Increase in cell brightness in the glucose-fed samples indicates accumulation of reduced pyridine nucleotides. (**B**) ***a*** Effect of antioxidants Catalase and N-Acetyl-Cysteine on cell viability in the presence and absence of glucose. Cells were transfected with a construct encoding human Catalase or the corresponding empty vector 48 hours before nutrient and serum starvation. Mock-transfected cells were also treated with 10 mM NAC as an alternative ROS scavenger. Values are mean±SD of triplicate wells. The experiment was repeated twice with identical results. ***b*** Cytofluorimetric analysis of cells loaded with the redox sensitive die H2-DCF-DA and exposed to a bolus (1 mM) of extracellular Hydrogen Peroxide. Decreased oxidation in the Catalase-transfected samples confirms elevated H2O2 degrading capacity in these cells. (**C**) Lack of effect of the longevity protein Sirt1 and the mitochondrial superoxide scavenger SOD2 on *Phoenix* cell viability in the presence of glucose and under glucose deprivation. Cell viability was scored at 72 hours after cell starvation. Representative of two comparable experiments. (**D**) Western blot analysis of Sirt1 (***a***) and SOD2 (***b***) expression in transfected cells. Transfection efficiency was normally around 50% based on expression of GFP.

Blockade of mTOR prevents nutrient-induced cell death

Since glucose and aminoacid withdrawal provided comparable protection to serum-starved *Phoenix* cells, in spite of having different effects on cell energy (Figure 1D) and redox balance (Figures 2A and B and data not shown), we reasoned that a common signaling mechanism might underlie the antiapoptotic action of the two starvation modes. The mTOR/S6K signaling cascade, which is modulated by both glucose and aminoacids and regulates cell proliferation and survival [6], was therefore evaluated as a potential candidate.

Even in the absence of exogenous growth factors, mTOR activity remained remarkably elevated in glucose-fed cells 24 hours after serum withdrawal, as revealed by the phosphorylation patterns of the major mTOR effectors S6 kinase and 4E-BP1, and of the downstream substrate S6 (Figure 3A, lane 1). Note that in this analysis phospho-site specific antibodies often recognize multiple bands, the uppermost, slowest-migrating one generally representing the most heavily phosphorylated form of the protein (see arrows) [25]. Based on this criterion, we observed a marked reduction of mTOR activity in glucose-starved, and to an even larger extent, in aminoacid-starved cells (Figure 3A, lanes 2 and 3). A drastic reduction in S6 kinase phosphorylation was also observed in glucose-fed cells treated with mitochondrial inhibitors or with the uncoupler 2,4-DNP, in keeping with the starvation-mimicking effects of these treatments on cell survival (Figures 3B and 1C). In glucose-starved cells we also observed a small increase in the phosphorylation of the AMP-activated protein kinase (AMPK-α) (Figure 3A), the putative negative regulator of mTOR in this experimental condition [8]. This modest, although detectable biochemical change, which reflects the small reduction in cellular ATP content reported in figure 1 D, likely accounts for reduced mTOR signaling (Figure 1B) [8] in *Phoenix* cells grown in the absence of glucose. Thus, collectively, these observations confirm that mTOR is responsive to glucose and aminoacids, and that its activity positively correlates with nutrient availability and extent of cell death in serum-deprived *Phoenix* cells.

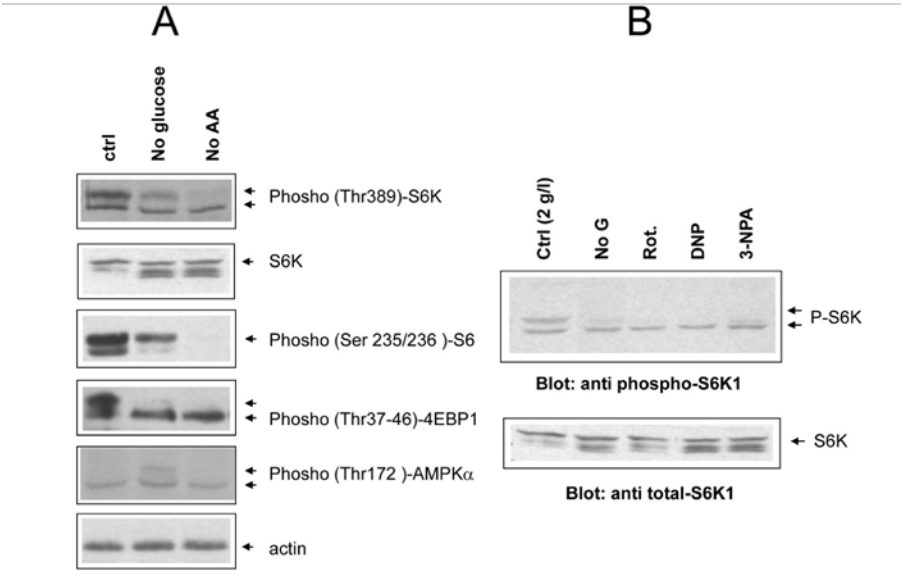

Figure 3. (**A**) Phospho-specific immunoblot analysis of mTOR/S6 kinase cascade activity under different cell feeding conditions. Cells were incubated for 24 hours in the indicated conditions (ctrl= 2g/l glucose + Aminoacids; noAA= glutamine and NEAA omitted). Where possible the same filter was cut into parallel strips and hybridized contemporarily with different antisera. When molecular weights of target proteins overlapped, filter were stripped and re-hybridized, or twin filters were prepared with the same protein lysates. Hyperphosphorylated protein species usually migrate slower and are indicated by separate arrows. Picture representative of several independent experiments. (**B**) Effect of metabolic inhibitors from figure 1B on S6 kinase phosphorylation. Upper arrows indicate the fully phosphorylated forms. Equal content of total S6 kinase in the different samples was verified by anti total S6K immunoblotting of the same protein lysates on a different nitrocellulose membrane. Picture representative of 2-3 three independent experiments.

In order to address the role of the mTOR/S6K cascade in nutrient-dependent death of *Phoenix* cells, we evaluated the effect of mTOR blockade on cell viability in standard and glucose-depleted medium. Rapamycin, a macrolide antibiotic widely used as an immunosuppressive drug, directly inhibits mTOR activity within the nutrient sensitive TORC1 complex, by complexing with the cellular protein FKBP12; another drug, 5-aminoimidazole-4-carboxamide ribonucleoside (AICAR), indirectly suppresses mTOR signaling through AMP kinase, by mimicking cell de-energization and accumulation of adenosine monophosphate (AMP) [26]. As expected, both drugs drastically decreased the phosphorylation of the mTOR substrate S6 kinase in cells grown in the presence of both glucose and aminoacids (Figure 4A). More importantly, both Rapamycin and AICAR dramatically reduced cell death in nutrient repleted medium (Figure 4B).

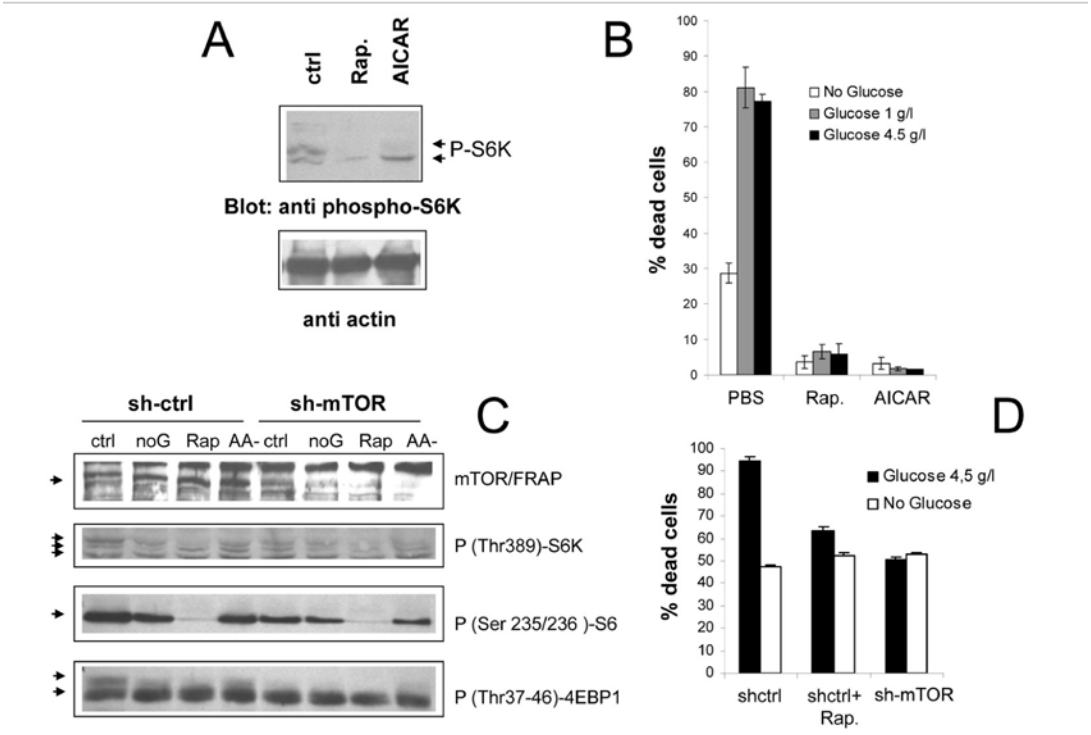

Figure 4. (**A**) Anti phospho S6K immunoblot analysis of *Phoenix* cells treated with the mTOR/FRAP inhibitor Rapamycin (200 nM) or the AMPK agonist AICAR (1 mM) for 24 hours in serum-free, nutrient rich medium. Ctrl=untreated cells. A lower strip of the same filter was hybridized with anti-actin antiserum, to confirm equal protein loading. (**B**) Effect of pharmacological inhibition of the mTOR pathway on cell survival to serum deprivation under different feeding conditions. Values are mean±SD of triplicate samples. Representative of several independent experiments. (**C**) Immunoblot analysis demonstrating effective downregulation of mTOR/FRAP by lentiviral transduction of a targeting (sh-mTOR) or non-targeting (sh-ctrl) short hairpin RNA, and effects on the downstream signaling cascade. Cells were analyzed 24 hours after serum starvation in the indicated media (ctrl=2 g/l glucose + Aminoacids; noG= no Glucose; Rap= Rapamycin 200nM; AA- = 2 g/l glucose without glutamine and NEAA). In the anti p-S6K and anti p-4EBP1 a selective loss of the slow migrating, hyperphosphorylated band by nutrient-repleted sh-mTOR samples can be appreciated. (**D**) Survival assay displaying reduced mortality of sh-mTOR transduced *Phoenix* cells in serum-free, nutrient repleted medium. Note that nutrient-independent loss of viability was unusually high in these experimental conditions. Values are mean±SD of triplicate samples. Panel representative of two experiments performed with cells from two independent infections.

In order to rule out potential non-specific effects of drug compounds, in a parallel series of experiments mTOR expression in *Phoenix* cells was genetically inactivated by shRNA technology. As displayed in figure 3C, lentiviral expression of a mTOR specific shRNA resulted in a substantial reduction of the mTOR expression level, and in a reduced phosphorylation of its downstream targets S6K, S6 and 4E-BP1, in nutrient-rich samples (Figure 4C, compare lanes 1 and 4 in each panel). In keeping with evidence of cell protection by Rapamycin and AICAR, mTOR inactivation allowed a higher percentage of cells (about 50%) to survive in nutrient repleted medium with respect to mock-infected cells, and nearly abolished protection by glucose withdrawal (Figure 4D). It should be noted, however, that here and in general in experiments involving genetic manipulation of *Phoenix* cells, mortality in the absence of nutrients was often higher than the usual (compare Figure 1A with 4D and S2,a), possibly due to cellular distress from the experimental procedure. Notwithstanding this limitation, survival data with mTOR-silenced cells confirm the observations made with chemical inhibitors, demonstrating that activation of the mTOR cascade is instrumental to nutrient-triggered cell death in the cell line under study, and that protection by nutrient restriction is conceivably mediated by the inhibition of this cascade.

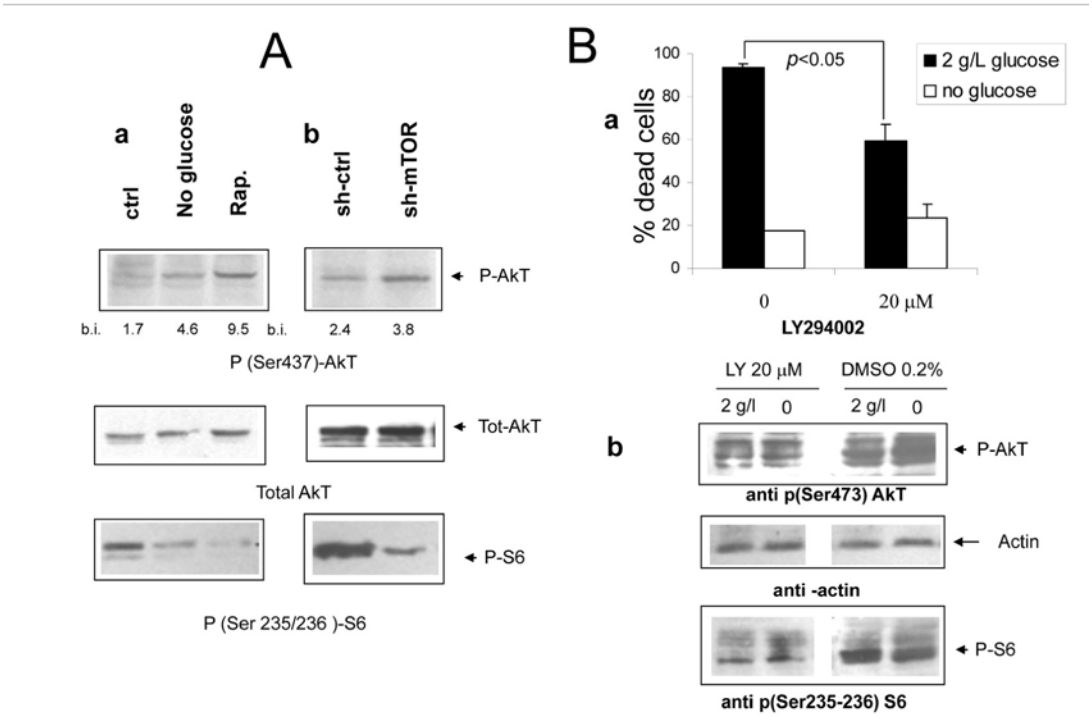

Figure 5. (**A**) ***a*** Immunoblot analysis revealing increased phosphorylation of AkT/PKB on serine 473 under nutrient deprivation (upper panel). The relevant band is indicated by the arrow. Band quantization values (band volume) in band intensity (b.i.) units are indicated. The same filter was stripped and re-hybridized with an anti total AkT antiserum to ensure equal protein expression and sample loading (central panel); a lower strip of the same filter was hybridized with an antiserum specific for phospho S6 (lower panel, band indicated by arrow). Picture representative of several independent experiments. **b** Protein lysates from mock and mTOR-silenced cells grown under serum free DMEM with glucose and aminoacids were treated as in A. Relevant bands are indicated by arrows. Densitometry of p-AkT bands is reported. (**B**) ***a*** Effect of the PI3 Kinase inhibitor compound LY294402 on *Phoenix* cell survival in serum-free medium. Cells were incubated for 72 hours with or without glucose as indicated. The inhibitor or vehicle alone (DMSO, 1:500 final dilution) were added at time 0. Values are Mean ±SD of triplicate wells. Representative of three independent experiments. Note that lower concentrations of LY294002 had no effect on cell survival in either medium. ***b*** Immunoblot analysis of protein lysates from cells treated as in a and incubated for 24 hours. Phospho-AkT (serine 473) and phospho-S6 (serine 235-236) were detected by specific antisera. Relevant bands (the middle one within the triplet for AkT) are indicated by arrows; equal protein loading was verified by reversible Ponceau S staining.

Akt is activated by mTOR inhibition but does not account for cell protection

While in most cancer-related models the mTOR cascade exerts antiapoptotic functions downstream of the PI3 kinase/AkT PKB signaling axis [27], few examples of cell protection by inhibition of mTOR/S6K have been reported [28-31]. It is also known that hyperactivation of the mTOR cascade can downregulate survival signaling by the AkT/PKB kinase [15, 16]. In search for a molecular mechanism linking nutrient-dependent mTOR signaling to massive cell death of serum-deprived *Phoenix* cells, we sought to evaluate the phosphorylation of AkT at serine 437, a biochemical correlate of AkT kinase activity. Consistent with previous reports, we found increased levels of AkT phosphorylation/activity in cells deprived of glucose or treated with Rapamycin, in a fashion which inversely correlated with the activation of the mTOR effector S6 kinase (Figure 5 A, a). mTOR-silenced cells also displayed increased phosphorylation of AkT in nutrient rich medium, although to a lower extent compared to control cells treated with Rapamycin (Figures 5A, a and b); moreover, transfection of rat mTOR cDNA in cells deprived of human mTOR rescued mTOR expression and activity (as assessed by phosphorylation of S6) and in parallel decreased the phosphorylation of AkT (Supplementary data, S1). Thus, taken together, these observations confirmed that, in serum-deprived *Phoenix* cells, nutrients downregulate AkT phosphorylation/activity through the mTOR cascade. This raises the possibility that increased AkT function might be responsible, at least in part, for the dramatic protection provided by restriction of glucose or aminoacid supply in this experimental model.

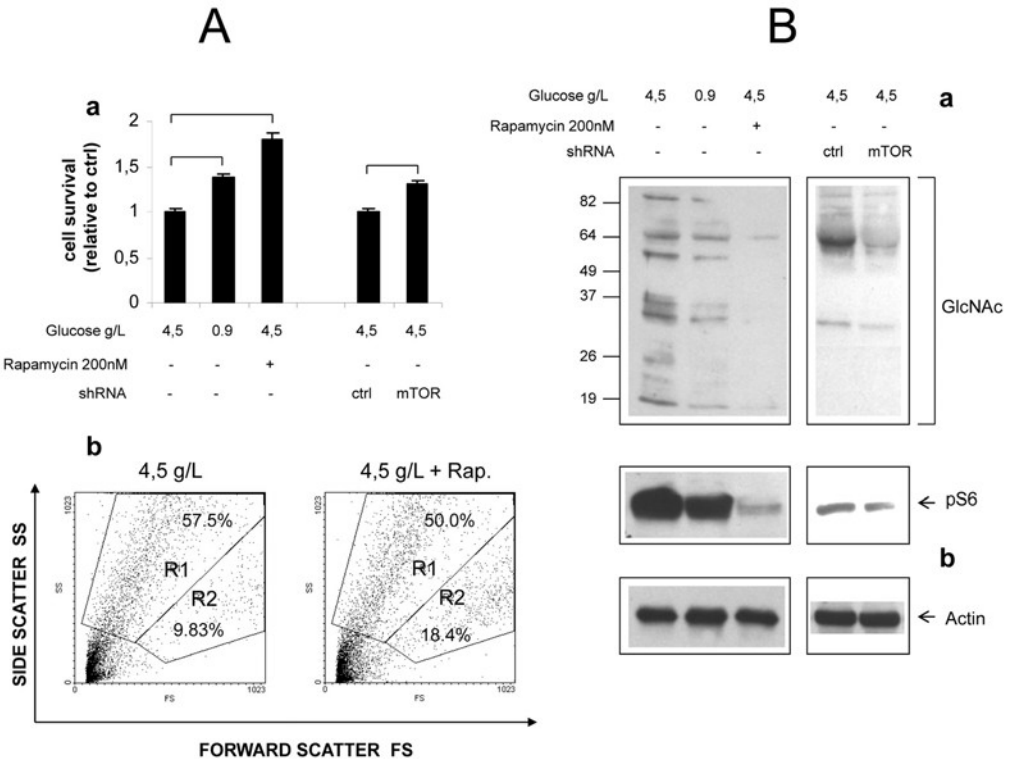

Figure 6. Role of mTOR in hyperglycemic damage of HUVEC cells. (**A**) ***a*** Effect of glucose, Rapamycin and mTOR knock-down on survival of growth factor-starved HUVECs. Values are relative to cell survival in high glucose (10-15% survival). Numbers are mean± SD of four samples from two independent experiments. All the indicated comparisons were significant by at least $p<0.05$ (two-tailed unpaired T-test). ***b*** Representative Forward/Side scatter plots of live (Region R2) and dead (Region R1) cells under high glucose and high glucose + Rapamycin. Raw numbers indicate percentages with respect to all the plotted events, including cell debris. Survivals were calculated on relevant regions only, according to the formula %survival= %R2/(%R1+%R2). (B) Western blot analysis of GlcNAcylated proteins in total lysates of HUVEC cells. Glucose, Rapamycin and mTOR knock-down were combined as indicated. Impact of treatments on mTOR signaling was evaluated by anti phospho S6 immunoblotting (***b***). Equal protein loading was verified by anti-actin staining. Blots representative of two independent experiments.

To further investigate the mechanistic role of the PI3K-AkT cascade in cell survival induced by nutrient deprivation, cells were treated with the PI3 kinase specific inhibitor LY294002, and exposed to normal or glucose-deprived media in the absence of serum. Surprisingly, the PI3K inhibitor failed to reverse cell protection by glucose withdrawal, but attenuated cell death in nutrient-repleted medium (Figure 6A, a), suggesting that residual AkT activity may be detrimental rather than protective in this culture condition. Interestingly, biochemical studies revealed that, while AkT/PKB phosphorylation was, as expected, decreased, also the serine phosphorylation of S6 was strongly downregulated. This is an evidence that inhibition of the mTOR cascade, a downstream target of AkT [10], accompanied PI3K blockade (Figure 6A, b).

In a complementary series of experiments, over-expression of a constitutively active form of AkT (myrAkT) in *Phoenix* cells failed to prevent cell death in nutrient rich medium, while slightly decreasing cell protection by glutamine withdrawal (Supplementary Figure S2).

Collectively, these data do not support a role for AkT in cell survival by nutrient restriction in our cell model, but rather indicate that protection operates also in the context of PI3K (and AkT) inhibition, provided that the mTOR cascade is also blocked. Conversely, AkT appears to increase cell death in the presence of abundant nutrients, and to negatively interfere with cell protection by Glutamine deprivation.

mTOR inhibition attenuates hyperglycemic damage in primary endothelial cells

In an attempt to verify that mTOR-dependent nutrient toxicity is not restricted to one single transformed cell line, we cultivated primary human endothelial cells (HUVEC) in high (4.5 g/L) ambient glucose, a well established model of endothelial hyperglycemic damage. Specific endothelial growth factors (EGF, FGF-B, VEGF and IGF-1), normally required for the optimal propagation of these cells, were omitted from the culture medium, while FBS (5%) was included to limit cellular stress. In these harsh conditions, a majority of cells detached from the plate and appeared dead after 48-60 hours of incubation, the percentage of live cells (quantified by flow cytometry as the percentage of cells with high forward scatter, low side scatter profile) ranging from 10 to 15%. Cell survival, however was significantly improved (nearly doubled) by Rapamycin, to an extent even larger than by cultivation in normal (0.9 g/L) glucose (Figure 6A, a). Importantly, these differences matched the phospho-rylation level of S6, an index of mTOR activity (Figure 6B). Likewise, mTOR knock-down by lentivirus-delivered shRNA consistently increased cell survival by about 20%, in accordance with the evident although incomplete inhibitory effect on mTOR signaling (Figures 6A, a and 6B).

Additionally, accumulation of O-GlcNacylated proteins, a biochemical hallmark of endothelial damage by high glucose [2, 32], was drastically reduced by Rapamycin and, although to a lesser extent, by mTOR knock-down (Figure 6B).

Thus, inhibition of the mTOR cascade partially rescues primary human endothelial cells from hyperglycemic damage under growth factor restriction, confirming and extending analogous findings obtained in *Phoenix* cells.

DISCUSSION

We describe here a novel mechanism for cell survival regulation by nutrients, our major conclusion being that activation of the mTOR signaling pathway is detrimental to cell survival in the context of growth factor scarcity. This conclusion is mainly based on mechanistic studies performed on a widely used tumor cell line, but has also been validated using a cell model (human primary endothelial cells) relevant to nutrient-related pathologies like vascular ageing and diabetic complications.

We have shown that, in the absence of exogenous growth factors, the 293-T "*Phoenix*" retrovirus packaging cell line undergoes massive cell death in a fashion strictly dependent on the availability of nutrients in the growth medium. In particular, with respect to a normally supplemented medium containing both glucose (either 4.5 g/l or 1 g/l), and glutamine + non essential aminoacids, withdrawal of either supplement exerts a remarkable protective effect with a nearly complete rescue of the culture, at least in the considered time frame (3-4 days). Importantly, although not investigated in detail, morphological data and flow cytometry evidence of subdiploid DNA accumulation and high side-scattering cell profiles (not shown) clearly suggest that nutrient-induced death of *Phoenix* cells largely occurs by apoptosis.

From a biochemical point of view, we have clearly demonstrated the involvement of the nutrient sensor mTOR in the protective cell response to nutrient restriction, and investigated its complex relation with the PI3 kinase/AkT signaling cascade. In view of the growing attention towards the mTOR/S6K cascade as a signaling module at the crossroad of multiple

pathogenic mechanisms from diabetes and ageing to cancer, the observation that mTOR inhibition mediates the cell protective effect of nutrient withdrawal adds special value to our observation.

Cell damage by excess nutrient contributes to important pathologic conditions including Metabolic Syndrome, insulin resistance and diabetic micro- and macro-angiopatic complications. In a current model for hyperglycemic vascular damage, multiple pathogenic mechanisms (including deregulation of the polyol and hexosamine pathways and hyperactivation of PKC) are triggered in endothelial cells by glucose-driven overproduction of reactive oxygen species [2]. Our results significantly diverge from this model: first of all, death of *Phoenix* cells in high nutrients does not seem to involve Reactive Oxygen Species, although mitochondrial inhibitors, but not antioxidants, provide a significant protective effect. Second, not only hyperglycemia, but also physiological (5 mM) concentrations of glucose appear "toxic" in our model, in presence of glutamine/aminoacids. On the other hand, removal of nutrients from the culture medium has no gross effect on cell energy balance, based on ATP measurements displayed in figure 1 D. We therefore favor the idea that a fine signaling mechanism, sensitive to physiological levels of both nutrients (glucose and aminoacids) as well as to mitochondrial dysfunction [33], regulates cell survival in our experimental setting; this mechanism has been identified in the activation of mTOR and his downstream cascade.

Experiments on HUVEC cells have been performed to test the relevance of the above mechanism in a more physiological context. These experiments have confirmed that the mTOR cascade contributes to endothelial damage by the combination of excess nutrients and growth factors scarcity, although with some differences between the two cell models. In particular, base-line mortality is higher and in part nutrient-insensitive in endothelial cells, and, as a consequence, effects of mTOR blockade on cell survival less dramatic. Conversely, drastic changes in GlcNAcylated protein accumulation in response to ambient glucose or mTOR functional status have been difficult to demonstrate in *Phoenix* cells (not shown). Notwithstanding these incongruencies, studies on endothelial cells strengthen, on one side, the role of mTOR in glycotoxicity, and underscore, on the other side, the potential of the *Phoenix* cell model in recapitulating important biochemical aspects of nutrient-related human pathology.

The downstream molecular events linking inhibition of mTOR (TORC1) to cell survival in the presented cell models needs further investigation. Although evidence of increased AkT phosphorylation/activation in cells deprived of nutrients or subdued to mTOR blockade represented an attractive candidate mechanism, our findings in *Phoenix* cells did not support this conclusion. In fact, a) cell survival by nutrient deprivation was not reverted by the PI3K inhibitor LY294002, and conversely, b) cell death in the presence of nutrients was actually attenuated by AkT/PKB blockade, while overexpression of AkT slightly decreased rescue by glutamine deprivation. Instead, since protection by Ly294002 in nutrient-rich medium (Figures 5B, a and S2) occurred in parallel with inactivation of the mTOR cascade (Figure 5B, b), these findings reinforce the idea that 1) mTOR signaling is absolutely critical for cell death in this experimental context, and 2) that beneficial effect of mTOR occurs also in the context of nearly complete AkT inhibition.

Interestingly, the detrimental action of the PI3K/AkT cascade on *Phoenix* cell survival, as suggested by data in figure 5 and S2, while rather unusual for a cancer cell line, is instead reminiscent of genetic evidence from model organisms, whereby PI3K inhibition promotes resistance to stress and longevity [34].

Other mechanisms for the protective effect of mTOR inhibition can be envisaged and deserve experimental verification.

First, inhibition of mTOR may protect cells by arresting cell cycle and preventing inappropriate G1/S transition, in the absence of growth/survival factors. Growth curves displayed in figure 1 B showing reduced but not arrested proliferation by nutrient restriction, partially support this possibility. P53, which is involved in a metabolic checkpoint induced by cell energy depletion [35], unlikely participates in cell cycle regulation in our model, since this tumor suppressor protein is functionally inactivated in *Phoenix* cells by the large T antigen. Instead, another metabolic checkpoint triggered by mitochondrial damage and accumulation of oxygen radicals, recently described in *Drosophila* [36], is compatible with our finding of increased ROS in glucose- deprived *Phoenix* cells (Figure 2).

Second, attenuation of ER stress [37], and induction of autophagy [38] may also contribute to cell protection by inhibition of the mTOR cascade in our cellular models. In fact, of the few reported examples of mTOR pro-apoptotic activity, most refer to conditions in which ER stress can be demonstrated or at least suspected [29-31, 37]. Along similar lines, autophagy exerts important antiageing effects in model organisms and prevents cell damage by accumulation of misfolded proteins or

damaged mitochondria [28]. Future work along the lines above outlined is therefore warranted.

Likewise, further effort is required to validate the above described, mTOR dependent circuitry of metabolic toxicity in tissues directly involved in nutrient-related pathology. While initial experiments performed on endothelial cells encouragingly point to this direction, (Fig 6), peripheral nerves and pancreatic beta cells definitely deserve to be investigated.

In conclusion, we have presented novel evidence for a negative regulation of cell survival by excess nutrients through the mTOR pathway. If confirmed, and extended, these observations may have important theorethical implications for the molecular understanding of the ageing process, and significant impact on the prevention and treatment of important nutrient- and aging-associated diseases like type II diabetes and its complications.

Additionally, we have shown that HEK-293T *Phoenix* cells, an easy-to-handle and highly genetically manipulable cell line, can represent a valuable tool for mechanistic studies and pharmacological screenings related to nutrient-dependent cell damage, and by extension to stem cell biology and ageing.

METHODS

Reagents, antibodies, plasmids and cell lines. Chemicals were purchased from Sigma-Aldrich (Milan, Italy) unless differently stated. Rapamycin was from LC Laboratories (Woburn, MA), LY294002 from Cayman Chemical Company (Ann Arbor, MI). The redox-sensitive dye H2-Dichlorofluorescein Diacetate (H2-DCF-DA) was obtained from Invitrogen s.r.l. (San Giuliano Milanese, Italy).

The following primary antibodies were used: anti sir2/Sirt1 (rabbit polyclonal, cat.# 09-844) and anti SOD2 (rabbit polyclonal, cat.# 06-984) from Upstate Biotechnology/Millipore (Vimodrone, Milan, Italy); anti-actin (goat polyclonal, cat #sc-1615 and sc-1616), anti S6 kinase 1 (rabbit polyclonal, C18, sc-230), and anti mTOR/FRAP (rabbit polyclonal, C19-R, cat.# sc-1550-R) from Santa Cruz Biotechnology Inc. (Heidelberg, Germany); anti p-S6K1, Thr 389 (cat# 9205); anti p-S6, Ser 235-236 (cat#2211); anti p-4EBP1, Thr 37-46, (cat# 2855P); anti p-AMPK α, Thr 172, (cat# 2531); anti phosho-(Ser 437) AkT, (cat# 9271); anti AkT, (cat# 9272); anti p-GSK3-β, Ser-9, (cat# 9336), all from Cell Signaling Technology (Danvers, MA). HRP-conjugated goat anti rabbit IgG antiserum was from BIORAD (Segrate, Milan, Italy).

The plasmid encoding the human Sirt-1 cDNA in the pBabe Puro vector backbone was kindly provided by Dr. Michael Greenberg (Harvard Medical School, Boston, MA). Expression constructs for rat mTOR (pcDNA3 vector, Invitrogen) and human Catalase (pLNCX vector, Clontech, Mountain View, CA) were a gift of Dr. Toren Finkel (NHLBI, NIH, Bethesda, MD). The construct encoding a myristoylated, constitutively active mutant of human AkT fused to the Estrogen Receptor ligand binding domain (Myr(⊗1-129)-AkT-HA-ER) in the pWZL-hygro retroviral vector [27] was provided by Dr. Barbara Bedogni (University of Stanford, CA).

The pcDNA3-based construct encoding human SOD2 was described elsewhere [39]. Mission™ shRNA clones constructed within the lentivirus plasmid vector pLKO.1-Puro were purchased from Sigma Aldrich (Milan, Italy).

293-T *Phoenix* cells, a retrovirus packaging line derived from E1A-transformed embryonic human kidney cells (HEK-293) carrying a temperature sensitive T antigen [40], were kindly provided by Dr. G. Nolan (University of Stanford, CA). A detailed description of this cell derivative can be found in the Nolan's Laboratory Home Page (http://www.stanford.edu/group/nolan/retroviral_systems/phx.html).

Cells were routinely maintained in Dulbecco's Modified Eagle's Medium (DMEM) containing 4.5 g/l glucose, 2 mM Glutamine, 1 mM Sodium Pyruvate, Non Essential Aminoacids and Penicillin-Streptomycin (EUROBIO, Les Ulis, France).

Human Umbilical Vein Endothelial Cells (HUVEC) were obtained from Lonza/Clonetics→ (Walkersville, MD, USA) and maintained in EBM-2 Basal Medium supplemented with hEGF, VEGF, B-FGF, IGF-1, Hydrocortisone, Heparin, Acorbic Acid, Gentamicin, Amphotericin B and 2% FBS (EGM-2 Bulletkit, Lonza, CC-3162). For experimental procedures cells between passages 4 and 7 were used.

Cell viability assay. *Phoenix* Cells were seeded at 10^5 cells/well, in 24-well plate in complete medium and incubated for 16 to 24 hours. Medium was then replaced with glucose-free/glutamine-free DMEM (Eurobio) (basic formulation as reported in supplemental table 1), 1 mM Pyruvate, Penicillin-Streptomycin and 1 mM HEPES pH 7.4. When necessary the medium was supplemented with serum (or Bovine Serum Albumin, BSA), glucose, glutamine and Non Essential Aminoacids (NEAA, formulation of the 50X solution in supplemental table 2). Pharmacological inhibitors were

also added at this stage, at the following concentrations: 2-deoxyglucose (2-DG), 10 mM; Rapamycin, 200 nM; Ly294002, 20 μM; Rotenone, 5 μM; 3-nitropropionic acid (3-NPA), 1 mM; 2,4 Dinitrophenol, DNP, 1 mM; N-Acetyl Cysteine (NAC) 10 mM. After 72-96 hours incubation (humidified incubator, 37°C, 5% CO_2) live and dead cells were collected by gentle pipetting and transferred into dedicated vials for flow cytometry (COULTER Epics, 480 nm Argon laser lamp). Immediately before analysis Propidium Iodide was added at 1 μg/ml. PI-positive cells (FL-3) were scored as dead cells after threshold definition with unstained cells; cell debris was gated out and excluded from the analysis [41].

HUVEC cells were seeded in 12 well plates at 10^5 cells/well in complete medium, and left to adhere for 12 hours. Medium was then replaced with glucose-free DMEM containing 5% FBS but no specific endothelial growth factor, and D-glucose was added from a 300 mM stock (in PBS) at the desired dilution. Rapamycin was added at 200 nM at this stage and 24 hours later, without medium change.

After 48-60 hours of incubation cells were trypsinized, pooled with floating cells and analysed by flow cytometry, as described in reference 21. Live and dead cells were identified based on the position on the forward scatter-side scatter plot, and the % of cell survival calculated by the formula live cells/(live cells+dead cells).

Cell proliferation assay. Cells were seeded at 10^4 cells/well, in 24-well plate in complete medium. 16-24 hours later medium was replaced with glucose or glutamine-free DMEM without FBS. Live cells from triplicate wells were counted at different time-points (0, 24, 48 and 72 hours) by an hemocytometer; dead cells were excluded based on morphology and trypan blue uptake.

Cell transfections. Transient transfections of *Phoenix* cells were made with the EFFECTENE reagent (QIAGEN, Hilden, Germany), directly in 24 well plate, using about 150 nanograms DNA/well. A master transfection mix for 6 wells typically contained 1 μg DNA, 4 μl of Enhancer and 10 μl of transfection reagent, according to the manufacturer's indications with minor changes. Transfection efficiency was routinely above 50% in these conditions, based on flow cytometry of cells transfected with a GFP expressing plasmid. After 24-36 hours cells were used for survival assay or biochemical analysis (see below).

Lentiviral-mediated RNA interference. Recombinant vesicular stomatitis virus (VSV)–pseudotyped lentiviral vectors were obtained by standard procedure, according to Tiscornia et al. [42]. Briefly, 293 T human embryonic kidney cells were co-transfected by calcium phosphate with the lentiviral packaging (pMDLg/RRE), envelope (pMD2.G), and rev-expressing (pRSV-REV) plasmids, together with the pLKO.1-based short hairpin constructs specific for ***mTOR*** (TRCN0000038677) or the Mission™ non-target control vector. Viral supernatants were collected 48 hours after transfection, filtered through 0.22-μm pore nitrocellulose filters, concentrated by ultracentrifugation at 50,000 x *g* for 140 min at RT and stored at –80 C until use. Target cells were transduced with the lentiviral vector stocks in presence of 6 μg/ml Polybrene and selected using puromycin-containing medium.

Confocal analysis of cell oxidation and intracellular NAD(P)H. Cells were seeded in 35 mm glass bottom dishes (Ibidi, Integrated Biodiagnostic, Martinsried, Germany) and transfected with 0.75 μg of a construct encoding the redox-sensitive Yellow Fluorescent Protein (mt-rxYFP). After 48 hours cells were deprived of serum and nutrients for additional 24 hours, and fluorescent cells imaged and quantified by confocal microscopy (Leica, DM-IRE2 Germany) as described in detail elsewhere [43]. Briefly, fluorescence signals of samples excited at 488 nm (F_{488}) and at 458 nm (F_{458}) were measured and the ratio ($\mathbf{F} = F_{488}/F_{458}$) calculated. Values of F for completely reduced (F_{red}) and completely oxidised (F_{ox}) rxYFP were obtained from literature [44]. Pseudocolor images were constructed based on ***R*** values, defined as

$$\boldsymbol{R = (F-F_{ox})/(F_{red}-F_{ox})}$$

and ranging between 0 (complete oxidation) and 1 (complete reduction), by means of a dedicated software generated through the Labview 7.1 interface [23]. For image quantitation, average *R* values were determined within multiple Regions of Interest (ROIs, single cells or small cell clusters) for each sample, and their Mean±SD (n = 7 to 9) determined and utilized for further statistical analysis (Student *t*-test). In some experiments, after initial cell imaging in nutrient-deficient medium, nutrients were added back and cell redox responses monitored for 30 minutes or longer.

Intracellular NAD(P)H was measured, in the same experimental settings as above, by two-photon confocal analysis of cell green autofluorescence after two-photon excitation at 366 nm, as described by Patterson et al. [44].

Biochemical studies. For protein phosphorylation studies *Phoenix* cells were plated at 1.5 x 10^5/well in 12-well plate and incubated for 16 to 24 hours in complete medium. The day after, cells were switched to DMEM without glucose, glutamine/NEAA and FCS, and these components were added back where necessary. Serum-free samples were given BSA 20 mg/ml (stock) at the same dilution as FCS (typically 10%, i.e. 2 mg/ml final concentration). Antioxidants and chemical inhibitors were also added at this stage of the experiment (see above, viability assay). After 24 hours supernatants were removed and cells lysed in 100 microliters of ice-cold lysis buffer (NaCl 150 mM, Tris-HCl 50 mM pH 8; 2 mM EDTA) containing 1% v/v Triton X-100, 0.1 % v/v SDS, 1:1000 Protease Inhibitor cocktail (Sigma), 1 mM Sodium Orthovanadate, 1 mM NaF; 2 mM β-glycerophosphate. After 15 minutes on ice with occasional vortexing cells were spun down at 14,000 rpm, 4°C to remove debris and unlysed cells, and supernatant quantified for protein content (DC Protein Assay, BIORAD), resuspended in 6X Laemmli buffer, boiled for 2 minutes and stored at –80°C or directly loaded onto denaturing discontinuous polyacrylamide gels for SDS-PAGE. Proteins were then electroblotted onto nitrocellulose membrane (PROTRAN®, Whatman, Dassel, Germany). After reversible Ponceau S staining to confirm protein transfer and equal loading throughout the lanes, membranes were blocked in TBS-T containing 5% skim milk. Antisera were added in 3% milk at the appropriate dilution and incubated for 16 hours on a rotating plate at 4°C. After extensive wash in TBS-T, immuno-complexes were visualized by incubation with HRP-conjugated secondary reagents (BIORAD) followed by enhanced chemoluminescence (ECL, GE Healthcare, Milan, Italy) and autoradiography. In some experiments autoradiograms were digitalized and band intensity (band volume, i.e. area x mean pixel intensity) quantified with a dedicated software (Quantity One, BIORAD). Quantitation was normally not performed when differences displayed were immediately evident. Occasionally membranes were stripped in 2% SDS at 60°C, washed, blocked and subdued to a second round of hybridization.

For protein O-glycation and phosphorylation studies on HUVEC, cells were handled as for viability assays, except that after 24 hours of incubation supernatants and floating cells were removed and adherent cells lysed as described above.

Accumulation of GlcNAcylated proteins was determined by immunoblotting using a specific anti O-GlcNAc monoclonal antibody (CTD 110.6, COVANCE [45]).

Catalase assay. As an indirect assessment of intracellular catalase activity, cells were switched to serum-free medium (without BSA), loaded for 30 minutes with the redox sensitive fluorescent dye H2-Dichlorofluorescein Diacetate (H2-DCF-DA) and challenged with 1 mM hydrogen peroxide for 15 minutes. Cells were then quickly transferred to tubes for flow cytometry and green fluorescence (Fl-1) quantified. Resistance to H_2O_2-induced cell oxidation was assumed to correlate with cell capacity to degrade hydrogen peroxide. Extracellular catalase and the catalase inhibitor Aminotriazol were used to validate this procedure.

Determination of intracellular ATP. ATP was quantified by chemiluminescence using a dedicated kit (ENLITEN® ATP Assay, PROMEGA, Milan, Italy) according to the manufacturer's recommendations. For each sample luminescent emission was normalized for total protein content, determined as described above.

Statistics. Data sets (usually triplicate culture wells) were compared by the two-tailed Student's *t*-test for independent samples. Threshold for statistical significance was set at $p<0.05$

ACKNOWLEDGEMENTS

The authors are grateful to Drs. Barbara Bedogni (Stanford, CA), Toren Finkel (NIH, Bethesda, MD), Michael Greenberg (Harvard, Boston, MA), and Gary Nolan (La Jolla, San Diego, CA) for the generous gift of expression constructs and cell lines.
The work was supported by the European Association for the Study of Diabetes (EASD), EFSD/GSK Programme for the Study of Metabolic Toxicity in Diabetes (to G.P) and the Italian Ministry of University and Research and Catholic University (MIUR ex 60% linea D1 to G.P.).

CONFLICT OF INTERESTS STATEMENT

The authors of this manuscript have no conflict of interests to declare.

REFERENCES

1. Um SH, D'Alessio D, Thomas G. Nutrient overload, insulin resistance, and ribosomal protein S6 kinase 1, S6K1. Cell Metab. 2006; 3:393-402.
2. Brownlee M. Biochemistry and molecular cell biology of diabetic complications. Nature. 2001;414:813-820.
3. Bordone L, Guarente L. Calorie restriction, SIRT1 and metabolism:understanding longevity. Nat Rev Mol Cell Biol. 2005; 6:298-305.

4. Firestein R, Blander G, Michan S, Oberdoerffer P, Ogino S, Campbell J, Bhimavarapu A, Luikenhuis S, de Cabo R, Fuchs C, Hahn WC, Guarente LP, Sinclair DA. The SIRT1 deacetylase suppresses intestinal tumorigenesis and colon cancer growth. PLoS ONE. 2008; 3:e2020.

5. Gao X, Zhang Y, Arrazola P, Hino O, Kobayashi T, Yeung RS, Ru B, Pan D. Tsc tumour suppressor proteins antagonize amino-acid-TOR signalling. Nat Cell Biol. 2002; 4:699-704.

6. Sarbassov DD, Ali SM, Sabatini DM. Growing roles for the mTOR pathway. Curr Opin Cell Biol. 2005; 17:596-603.

7. Wullschleger S, Loewith R, Hall MN. TOR signaling in growth and metabolism. Cell. 2006;124:471-484.

8. Inoki K, Zhu T, Guan KL. TSC2 mediates cellular energy response to control cell growth and survival. Cell. 2003; 115:577-590.

9. Sancak Y, Peterson TR, Shaul YD, Lindquist RA, Thoreen CC, Bar-Peled L, Sabatini DM. The Rag GTPases bind raptor and mediate amino acid signaling to mTORC1. Science. 2008; 320:1496-1501.

10. Inoki K, Li Y, Zhu T, Wu J, Guan KL. TSC2 is phosphorylated and inhibited by Akt and suppresses mTOR signalling. Nat Cell Biol. 2002; 4:648-57.

11. Kim DH, Sabatini DM. Raptor and mTOR: subunits of a nutrient-sensitive complex. Curr Top Microbiol Immunol. 2004; 279:259-270.

12. Sarbassov DD, Guertin DA, Ali SM, Sabatini DM. Phosphorylation and regulation of Akt/PKB by the rictor-mTOR complex. Science. 2005; 307:1098-1101.

13. Um SH, Frigerio F, Watanabe M, Picard F, Joaquin M, Sticker M, Fumagalli S, Allegrini PR, Kozma SC, Auwerx J, Thomas G. Absence of S6K1 protects against age-and diet-induced obesity while enhancing insulin sensitivity. Nature. 2004; 431**:**200-205.

14. Selman C, Tullet JM, Wieser D, Irvine E, Lingard SJ, Choudhury AI, Claret M, Al-Qassab H, Carmignac D, Ramadani F, Woods A, Robinson IC, Schuster E, Batterham RL, Kozma SC, Thomas G, Carling D, Okkenhaug K, Thornton JM, Partridge L, Gems D, Withers DJ. Ribosomal protein S6 kinase 1 signaling regulates mammalian life span. Science. 2009; 326:140-144.

15. Shah OJ, Wang Z, Hunter T. Inappropriate activation of the TSC/Rheb/mTOR/S6K cassette induces IRS1/2 depletion, insulin resistance, and cell survival deficiencies. Curr Biol. 2004; 14:1650-1656.

16. Harrington LS, Findlay GM, Gray A, Tolkacheva T, Wigfield S, Rebholz H,Barnett J, Leslie NR, Cheng S, Shepherd PR, Gout I, Downes CP, Lamb RF. The TSC1-2 tumor suppressor controls insulin-PI3K signaling via regulation of IRS proteins. J Cell Biol. 2004; 166: 213-223.

17. Ozcan U, Ozcan L, Yilmaz E, Düvel K, Sahin M, Manning BD, Hotamisligil GS. Loss of the tuberous sclerosis complex tumor suppressors triggers the unfolded protein response to regulate insulin signaling and apoptosis. Mol Cell. 2008; 29:541-551.

18. Demidenko ZN, Blagosklonny MV. Growth stimulation leads to cellular senescence when the cell cycle is blocked. Cell Cycle. 2008;7:3355-3361.

19. Blagosklonny MV. Aging: ROS or TOR. Cell Cycle. 2008: 7:3344-3354.

20. Lowe SW, Jacks T, Housman DE, Ruley HE. Abrogation of oncogene-associated apoptosis allows transformation of p53-deficient cells. Proc Natl Acad Sci U S A. 1994; 91:2026-2030.

21. Mazurek S, Eigenbrodt E. The tumor metabolome. Anticancer Res. 2003; 23:1149-1154.

22. Nahle Z, Polakoff J, Davuluri RV, McCurrach ME, Jacobson MD, Narita M, Zhang MQ, Lazebnik Y, Bar-Sagi D, Lowe SW. Direct coupling of the cell cycle and cell death machinery by E2F. Nat Cell Biol. 2002; 4:859-864.

23. Nemoto S, Takeda K, Yu ZX, Ferrans VJ, Finkel T. Role for mitochondrial oxidants as regulators of cellular metabolism. Mol Cell Biol. 2000;20:7311-7318.

24. Brunet A, Sweeney LB, Sturgill JF, Chua KF, Greer PL, Lin Y, Tran H, Ross SE, Mostoslavsky R, Cohen HY, Hu LS, Cheng HL, Jedrychowski MP, Gygi SP, Sinclair DA, Alt FW, Greenberg ME. Stress-dependent regulation of FOXO transcription factors by the SIRT1 deacetylase. Science. 2004; 303: 2011-2015.

25. McDaniel ML, Marshall CA, Pappan KL, Kwon G. Metabolic and autocrine regulation of the mammalian target of rapamycin by pancreatic beta-cells. Diabetes. 2002;51:2877-2885.

26. Corton JM, Gillespie JG, Hawley SA, Hardie DG. 5-aminoimidazole-4-carboxamide ribonucleoside. A specific method for activating AMP-activated protein kinase in intact cells? Eur J Biochem. 1995 ; 229:558-565.

27. Bedogni B, Welford SM, Cassarino DS, Nickoloff BJ, Giaccia AJ, Powell MB. The hypoxic microenvironment of the skin contributes to Akt-mediated melanocyte transformation. Cancer Cell. 2005;8:443-454.

28. Ravikumar B, Vacher C, Berger Z, Davies JE, Luo S, Oroz LG, Scaravilli F, Easton DF, Duden R, O'Kane CJ, Rubinsztein DC. Inhibition of mTOR induces autophagy and reduces toxicity of polyglutamine expansions in fly and mouse models of Huntington disease. Nat Genet. 2004; 36:585-595.

29. Castedo M, Ferri KF, Blanco J, Roumier T, Larochette N, Barretina J, Amendola A, Nardacci R, Métivier D, Este JA, Piacentini M, Kroemer G. Human immunodeficiency virus 1 envelope glycoprotein complex-induced apoptosis involves mammalian target of rapamycin/FKBP12-rapamycin-associated protein-mediated p53 phosphorylation. J Exp Med. 2001; 194:1097-1110.

30. Tirado OM, Mateo-Lozano S, Sanders S, Dettin LE, Notario V. The PCPH oncoprotein antagonizes the proapoptotic role of the mammalian target of rapamycin in the response of normal fibroblasts to ionizing radiation. Cancer Res. 2003; 63:6290-6298.

31. Peterson TR, Laplante M, Thoreen CC, Sancak Y, Kang SA, Kuehl WM, Gray NS, Sabatini DM. DEPTOR is an mTOR inhibitor frequently overexpressed in multiple myeloma cells and required for their survival. Cell. 2009; 137:873-886.

32. Du XL, Edelstein D, Rossetti L, Fantus IG, Goldberg H, Ziyadeh F, Wu J, Brownlee M. Hyperglycemia-induced mitochondrial superoxide overproduction activates the hexosamine pathway and induces plasminogen activator inhibitor-1 expression by increasing Sp1 glycosylation. Proc Natl Acad Sci U S A. 2000; 97:12222-12226.

33. Desai BN, Myers BR, Schreiber SL. FKBP12-rapamycin-associated protein associates with mitochondria and senses osmotic stress via mitochondrial dysfunction. Proc Natl Acad Sci U S A. 2002; 99:4319-4324.

34. Guarente L, Kenyon C. Genetic pathways that regulate ageing in model organisms. Nature. 2000;408:255-262.

35. Jones RG, Plas DR, Kubek S, Buzzai M, Mu J, Xu Y, Birnbaum MJ, Thompson CB. AMP-activated protein kinase induces a p53-dependent metabolic checkpoint. Mol Cell. 2005;18:283-293.

36. Owusu-Ansah E, Yavari A, Mandal S, Banerjee U. Distinct mitochondrial retrograde signals control the G1-S cell cycle checkpoint. Nat Genet. 2008; 40:356-361.

37. Xu C, Bailly-Maitre B, Reed JC. Endoplasmic reticulum stress: cell life and death decisions. J Clin Invest. 2005; 115:2656-2664.

38. Castedo M, Ferri KF, Kroemer G. Mammalian target of rapamycin (mTOR): pro- and anti-apoptotic. Cell Death Differ. 2002; 9:99-100.

39. Pani, G., Bedogni, B., Anzevino, R., Colavitti, R., Palazzotti, B., Borrello, S., and Galeotti, T. Deregulated manganese superoxide dismutase expression and resistance to oxidative injury in p53-deficient cells. Cancer Res. 2000; 60:4654-4660

40. Swift S, Lorens J, Achacoso P, Nolan GP. Rapid production of retroviruses for efficient gene delivery to mammalian cells using 293T cell-based systems. Curr Protoc Immunol. 2001;Chapter 10:Unit 10.17C.

41. Bedogni B, Pani G, Colavitti R, Riccio A, Borrello S, Murphy M, Smith R, Eboli ML, Galeotti T. Redox regulation of cAMP-responsive element-binding protein and induction of manganous superoxide dismutase in nerve growth factor-dependent cell survival. J Biol Chem. 2003; 278:16510-16519.

42. Tiscornia G, Singer O, Verma IM. Production and purification of lentiviral vectors. Nat Protoc. 2006; 1:241-245.

43. Maulucci G, Labate V, Mele M, Panieri E, Arcovito G, Galeotti T, Østergaard H, Winther JR, De Spirito M, Pani G. High-resolution imaging of redox signaling in live cells through an oxidation-sensitive yellow fluorescent protein. Sci Signal. 2008; 1:pl3.

44. Patterson GH, Knobel SM, Arkhammar P, Thastrup O, Piston DW. Separation of the glucose-stimulated cytoplasmic and mitochondrial NAD(P)H responses in pancreatic islet beta cells. Proc Natl Acad Sci U S A. 2000; 97:5203-5207.

45. Comer FI, Vosseller K, Wells L, Accavitti MA, Hart GW. Characterization of a mouse monoclonal antibody specific for O-linked N-acetylglucosamine. Anal Biochem. 2001; 293:169-177.

SUPPLEMENTAL DATA

Table 1. Formulation of Glucose-free/Glutamine-free DMEM.

Inorganic Salts	**mg/L**
Calcium Chloride anhydrous	200.00
Ferric(III)-Nitrate•9H_2O	0.10
Potassium Chloride	400.00
Magnesium Sulphate anhydrous	97.70
Sodium Chloride	6400.00
Sodium Dihydrogen Phosphate• H_2O	125.00
Carbonate	3700.00
Amino Acids	
L-Arginine• HCl	84.00
L-Cystine	48.00
L-Glutamine	0
Glycine	30.00
L-Histidine• HCl• H_2O	42.00
L-Isoleucine	105.00
L-Leucine	105.00
L-Lysine• HCl	146.00
L-Methionine	30.00
L-Phenylalanine	66.00
L-Serine	42.00
L-Threonine	95.00
L-Tryptophan	16.00
L-Tyrosine	72.00
L-Valine	94.00
Vitamins	
D-Calcium-Pantothenate	4.00
Choline Chloride	4.00
Folic Acid	4.00
Myo-Inositol	7.20
Nicotinamide	4.00
Pyridoxal• HCl	4.00
Riboflavin	0.40
Thiamine• HCl	4.00
Other Components	
D-Glucose	0
Phenol Red	15.00
Sodium Pyruvate	0

Table 2. Formulation of the DMEM Non essential aminoacids supplement solution (50x)

	mg/L (50x)
L-Arginine• HCl	6320.00
L-Cystine	1201.00
L-Histidine• HCl• H2O	2096.00
L-Isoleucine	2623.00
L-Leucine	2623.00
L-Lysine• HCl	3625.00
L-Methionine	755.00
L-Phenylalanine	1651.00
L-Threonine	2382.00
L-Tryptophan	510.00
L-Tyrosine	1811.00
L-Valine	2343.00

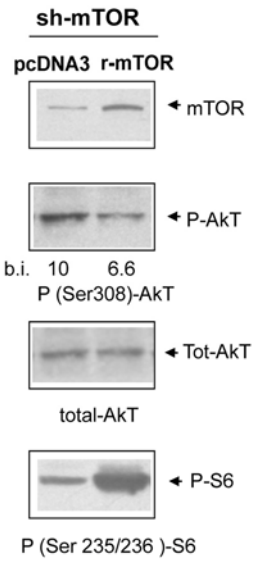

Figure S1. Inhibition of AkT phosphorylation by mTOR re-expression in sh-TOR *Phoenix* cells. Cells were analyzed as in figure 5A, after 24 hours of serum starvation, in the presence of nutrients. Densitometry of the phospho (Ser 308) AkT band is reported. Picture representative of two independent experiments.

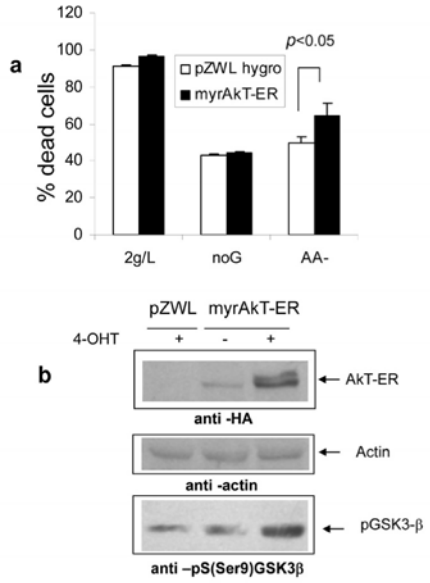

Figure S2. A constitutively active mutant of AkT (myrAkT-ER) fails to protect *Phoenix* cells from serum starvation and high nutrients. ***a***. Survival assay displaying a slight increase in mortality of glutamine-deprived cells expressing the myrAkT-ER mutant. All cultures were exposed to 1 mM 4-hydroxy-Tamoxifen (4-OHT) for the entire period of incubation (72 hours); note that transfection efficiency was 50% at most in this and other experiments. Values are Mean SD of triplicate samples. Significance was determined by unpaired, two-tailed Student t-test. Representative of two experiments with two independent transfections. ***b***. Western blot analysis confirming expression, responsiveness to 4-OHT and activity of the myrAkT mutant in cells grown in standard medium containing FCS. myrAkT-ER accumulates in response to 4-OHT as revealed by anti-tag (HA) immunoblot. Phosphorylation of the AkT substrate GSK3-β on Serine 9 was evaluated as an index of AkT activity (lower panel). Equal protein loading was confirmed by anti actin immunoblot (middle panel). Representative of two independent experiments.